8219

PRF

REACTING
FLUIDS
LABORATORY

N70 15079

NASA CR 107533

FINAL REPORT
ON
NASA GRANT NGR 19-001-016

EVALUATION OF THE ENERGY TRANSFER IN THE CHAR ZONE DURING ABLATION

Part I: Theoretical and Experimental Results for Heat Shield Surface Temperatures up to 3000°F

by
Ralph W. Pike, Associate Professor
Principal Investigator

Gary C. April, Research Associate

Eduardo G. del Valle, Research Associate

Department of Chemical Engineering

May 1, 1969

LOUISIANA STATE UNIVERSITY

PREFACE

This is Part I of two parts of a final report on NASA Grant NGR 19-001-016, Evaluation of the Energy Transfer in the Char Zone during Ablation. This part describes the theoretical and experimental results obtained for the energy absorbed by the nonequilibrium, equilibrium and frozen flow of pyrolysis gases in the char zone for heat shield surface temperatures up to 3000°F. In Part II of this final report research results will be presented for the analysis of the energy absorbed in the char zone and the decomposition zone. during ablation for heat shield surface temperatures up to 6000°F. Also the other topics specified in the research proposals will be included in this report. Part II will be completed by July 1, 1969.

This report, Part I, also serves as the Ph.D. dissertation of Gary C. April. Part II will also serve as the Ph.D. dissertation of Eduardo G. del Valle.

ENERGY TRANSFER IN THE CHAR ZONE OF A CHARRING ABLATOR

A Dissertation

Submitted to the Graduate Faculty of the
Louisiana State University and
Agricultural and Mechanical College
in partial fulfillment of the
requirements for the degree of
Doctor of Philosophy

in

The Department of Chemical Engineering

by

Gary Charles April
B.S., Louisiana State University, 1962
M.S., Louisiana State University, 1968
May, 1969

To Lynne for her Love,
Patience and Understanding

ACKNOWLEDGMENTS

This research was performed under the direction of Dr. Ralph W. Pike. His encouragement and guidance is gratefully acknowledged.

Appreciation is also expressed to the National Aeronautics and Space Administration's Langley Research Center which sponsored the research and, especially, to Robert T. Swann, Grant Monitor, whose interest and consultation gave an added sense of achievement to the research.

The author would also like to acknowledge the E. I. DuPont DeNemours Company for making possible, through an educational leave of absence, the opportunity to return to the university for an advanced degree; the Charles E. Coates Memorial Fund of the L.S.U. Foundation for funds to pay a portion of the typing cost of the dissertation, and, the L.S.U. Computer Research Center for the use of their facilities during the course of the study.

Special thanks are also given to Eduardo del Valle, co-worker during the research, John Balhoff, a very consciencious and adept

Chemical Engineering student who assisted with much of the experimental program, Marty Love who typed the manuscript, and many friends who contributed to the successful completion of this research.

TABLE OF CONTENTS

PAGE

LIST OF TABLES

Table No. Page No.

CHAPTER I

CHAPTER II

CHAPTER III

CHAPTER IV

CHAPTER VI

Table No. Page No.

APPENDIX A

Table No. Page No.

APPENDIX C

APPENDIX D

APPENDIX E

Table No. Page No.

APPENDIX F

LIST OF FIGURES

Figure No. Page No.

CHAPTER I

CHAPTER II

CHAPTER III

CHAPTER IV

CHAPTER V

CHAPTER VI

Figure No. Page No.

Figure No. Page No.

Figure No. Page No.

APPENDIX A

APPENDIX B

APPENDIX C

APPENDIX F

APPENDIX G

PROGRAM LISTINGS

ABSTRACT

The energy transfer associated with the reacting flow of pyrolysis products through the char layer of a low density nylon-phenolic resin charring ablator was studied experimentally and theoretically. It was found that a non-equilibrium flow model, employing finite reaction rate data for the important reactions among the pyrolysis products, was necessary to accurately describe the energy transport within the char. The important reactions and kinetic data for a temperature range of 500° to 3000°F, with experimental simulation to 2300°F, were determined and incorporated into the mathematical model, called the TEMPRE System. This model, in conjunction with experimental results obtained in a Char Zone Thermal Environment Simulator, were used to clearly show the shortcomings of the limiting cases of frozen and equilibrium flow in predicting the true behavior within the char layer.

A comparison of the experimental data obtained using low density, nylon-phenolic resin chars was made with the results obtained using graphite as a simulated char. The non-equilibrium flow model accurately predicted energy transport in the graphite medium using the same important reactions and kinetic data developed for flow through chars. This conclusion was needed to justify the use of graphite for the measurement of carbon

deposition from methane and phenol, and, in the catalyst evaluation studies.

Carbon deposition and decomposition product distributions were determined for methane and phenol using carbon-14 tracers. The product distributions were helpful in providing additional evidence that the chemical reactions included in the model were correct. The identified products of methane and phenol thermal decomposition were carbon monoxide, carbon dioxide, methane, ethylene, acetylene and phenol. Carbon deposition measurements within the char layer were used to locate the temperature where chemical reactions among the pyrolysis products became significant. In general, deposition was greatest near the front surface where the temperature varied between 1800 - 2300°F.

The above results were also used in the catalyst evaluation studies. The introduction of a catalyst into the pyrolysis product stream (homogeneous) or as a coating on the graphite (heterogeneous) was made in order to accelerate reaction rates and have them occur at lower temperatures. This resulted in a higher energy absorption by the pyrolysis products. Bromine (homogeneous) had an excellent activity for this by lowering the temperature at which reactions start from about 1900°F to about 1500°F. This effect was also measured by comparing the experimental exit gas compositions with the compositions calculated by the non-equilibrium flow model using conventional non-catalytic, kinetic data. The relative difference in these values was a good measure of the extent of chemical reaction resulting from the addition of the catalyst into the system.

Molybdenum and tungsten co-catalysts (heterogeneous) had essentially no effect in accelerating chemical reactions within the char. The slightly different carbon deposition profiles obtained were not within experimental accuracy to conclusively indicate a beneficial increase in the rate of chemical reactions. Platinum catalyst was also tested but it showed no activity for accelerating the chemical reactions. It is known that platinum is poisoned by carbon monoxide, and this is present in the pyrolysis products.

In addition to the above, the air oxidation of nylon-phenolic resin chars was studied to determine the rate of oxidation of the char with distance from the front surface. The maximum rate was obtained with air flowing from the heated front surface through the char and leaving the rear surface. There was no flow of pyrolysis products. With a front surface temperature of 2047°F and an air mass flux of 0.035 lb/ft^2sec an 81% conversion of oxygen was obtained. The gas leaving the back surface contained 4.0% O_2. This indicated that oxidation was taking place at all depths within the char, and this was confirmed with a non-equilibrium flow calculation.

I. INTRODUCTION

The Nature of Aerodynamic Heating During Planetary Reentry

One of the most serious problems encountered when space vehicles reenter a planetary atmosphere is aerodynamic heating. Typical reentry velocities for various Earth orbital missions are listed in Table 1-1. Before a manned spacecraft can land safely, these speeds must be reduced to conventional aircraft speeds. This can be accomplished by applying a reverse thrust or by taking advantage of the frictional resistance of the atmosphere. Since the return velocity is of the same magnitude as the launch velocity, the reverse thrust method requires the same quantity of fuel for the reentry phase. This doubles the fuel requirement for the mission and makes the added weight to the system prohibitive. Hence, it is more efficient to use the aerodynamic braking method to reduce the vehicle speed to a safe level (1,2,3).

A high speed orbiting vehicle possesses a large amount of kinetic energy (K.E. = $\frac{1}{2}mV^2$). In aerodynamic braking, this energy is converted to heat as the body descends through the resisting atmosphere. In Table 1-1 the kinetic energy (per unit weight) possessed by a vehicle at various orbital altitudes above the Earth is also listed. For example, a 5000 pound vehicle having an

Table 1-1. Initial Reentry Velocity and Kinetic Energy for Space Vehicles at Various Altitudes Above the Earth (1,2)

Orbital Altitude Nautical Miles	Velocity Ft/Sec	Kinetic Energy BTU/Lb
300	26,000	13,500
1000	27,000	14,600
20000	33,800	22,800
Circumlunar	36,000	26,000
Venus or Mars	37,200	27,600

initial reentry velocity of 26,000 feet per second must convert 67,500,000 BTU of kinetic energy to heat. Consider a vehicle that is constructed of structural steel having a specific heat of 0.117 BTU per pound per degree Fahrenheit. If a temperature increase of 1150°F is attained, the maximum amount of heat that is absorbed is 675,000 BTU, or one percent of the total heat generated. It is evident from this example that only a small fraction of the thermal energy can be permitted to reach the vehicle without causing destructive effects. The remaining large fraction (99 percent) must be transferred to the surrounding atmosphere by the proper selection of the vehicle shape and materials of construction (1,3).

There are two general classifications of body configuration used in ballistic reentry design (3,4,5,6): the slender body and blunt body configurations. The slender body shape causes a minimum aerodynamic drag condition with only slight disturbance of the air flow. A typical low drag, high speed shape is shown in Figure 1-1 with the associated flow field that results. This shape produces a weak, attached shock wave with a large percentage of the heat generated being absorbed by the body. The use of slender body configurations is best suited to ballistic missile and supersonic flow applications where low heating loads are experienced for short periods of time.

Since reentry of space vehicles requires a maximum amount of energy transfer to the atmosphere, the blunt or high drag configuration is more applicable. In Figure 1-2 the typical flow field characteristics for the blunt body is shown. An extremely strong, detached shock wave extends well beyond the body. A major portion of the energy is absorbed by the air flowing between the shock wave and vehicle surface and is carried away in the wake behind the craft. The shock layer becomes progressively hotter during the course of reentry causing dissociation and ionization of the air. This results in heat transfer by conduction, convection and radiation to the surface of the vehicle. Although the heat absorbed is a small portion of the heat generated, the relative amount is sufficient to produce surface temperatures in excess of 6000°F. Therefore, a thermal protection system must be employed to protect the vehicle from these high temperatures and heat fluxes.

One possible solution is to provide enough structural mass to safely absorb the heat (3,7). However, since most metals are poor heat sinks, this method would result in extreme weight penalties.

Transpiration cooling is a second method (8). This technique protects the vehicle by injecting a fluid through openings at the body surface into the boundary layer. The injected fluid blocks heat transfer into the material and maintains a safe temperature at the space cabin wall. This method

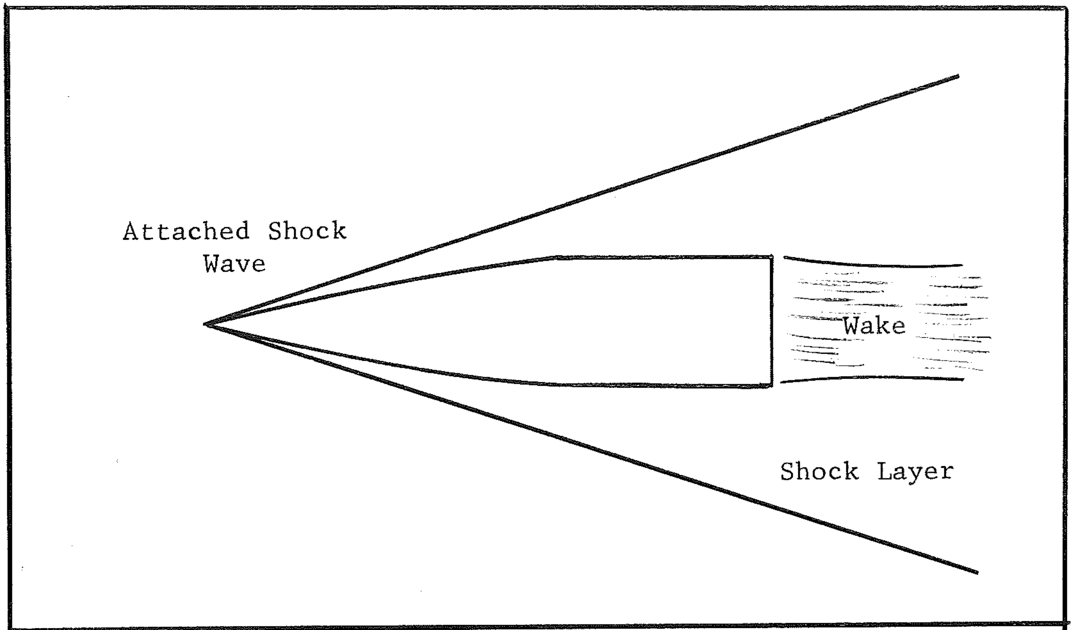

Figure 1-1. Slender Body Flow Field

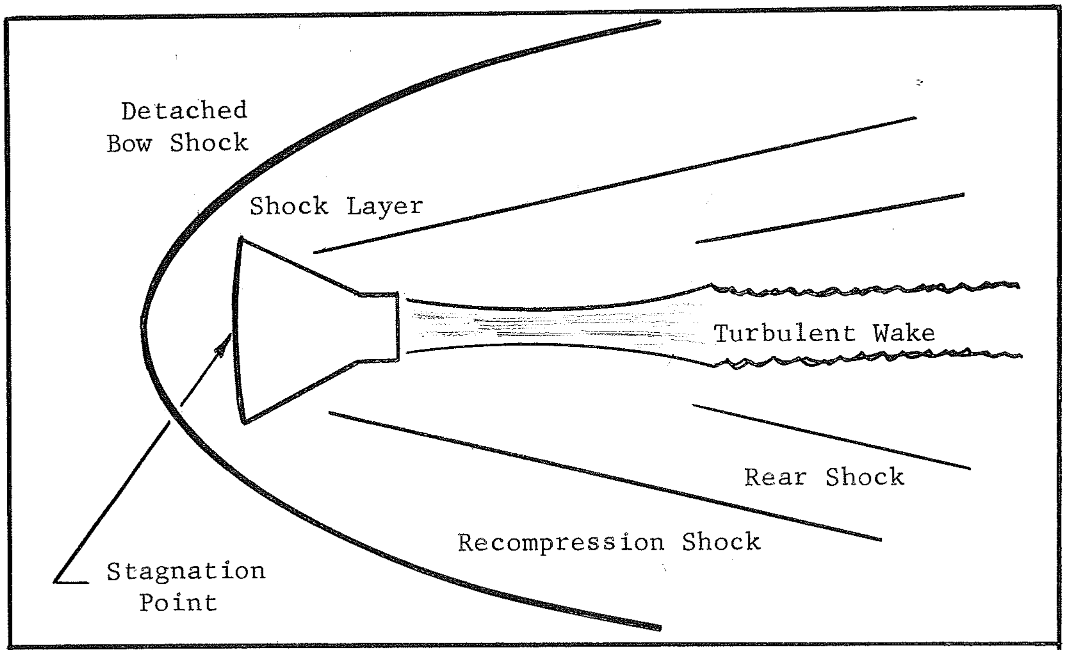

Figure 1-2. Blunt Body Flow Field

likewise requires additional weight such as equipment to pump and regulate the flow of coolant; and as a result, it is prohibitive in manned reentry applications.

Other methods of heat protection exist (i.e. convective, film and radiation cooling) but the most successful technique has been ablative cooling (7,9).

Ablative Thermal Protection of Planetary Reentry Vehicles

Ablative cooling is similar to heat sink and transpiration cooling in method, but it is drastically different in the mechanisms used to achieve the desired results. Ablation sacrifices structural stability to preserve thermal resistivity by melting, vaporizing and/or subliming relatively thin layers of the material at the surface. Although absorption of heat by phase change is the distinguishing feature of the process, energy dissipation by radiation, conduction, convection, transpiration and chemical reaction is likewise achieved (7,10).

Ideally, an ablative material must possess a low thermal conductivity, high heat capacity and large heat of degradation to effectively restrict the extreme temperatures to the surface of the vehicle. Success has been achieved employing compositions of nylon, phenolic resin, silicon elastomers and others. A partial list of the many different materials tested for use as ablative heat shields is presented in Table 1-2 (5,9,14).

There are two kinds of ablative protection systems. One

Table 1-2. List of Materials Tested for Heat Protection of Reentry Vehicles (14)

Plastics:	Ceramics:	Reinforced Systems:
Polytetrafluoroethylene (Teflon)	Fused Silica	Glass Fiber-reinforced Phenolics
Polyethylene	Zirconia	Metal Fiber-reinforced Ceramics
Polyamides	Magnesia	Organic Resin-filled Porous Ceramics
Phenolics	Foamed Ceramics	Ceramic-filled Metal Honeycombs
Modified Epoxies		Inorganic Particle-filled Refractory
Foamed Resins		
Carbonized Resins		

is non-charring, and the other is charring. A non-charring ablator is one in which the material vaporizes into gases and enters the boundary layer counter to the heat flow. This counter flow of mass effectively blocks heat transfer into the material and protects the vehicle. Teflon (polytetrafluoroethylene) is one such non-charring compound which undergoes chain shortening steps to form small polymer units that eventually vaporize. Extensive research with Teflon and other non-charring ablative materials have been reported over a wide range of applications (11,12).

The charring ablator, on the otherhand, has proven to be one of the most successful heat shields for reentry heat protection. Being a combination of plastics that decompose to a char of porous carbon and low molecular weight gases, it protects the vehicle by conduction, convection, plastic decomposition, transpiration, endothermic chemical reactions of the pyrolysis gases, reradiation from the char surface, and thickening of the boundary layer. The charring ablator is conveniently divided into three separate zones which include the plastic decomposition zone, the char zone or layer, and the boundary layer as shown in Figure 1-3.

In the decomposition zone the virgin plastic degrades to char and low molecular weight gases. These gases flow through the char zone and undergo chemical reactions such as cracking, free radical formation and ionization. A very large quantity

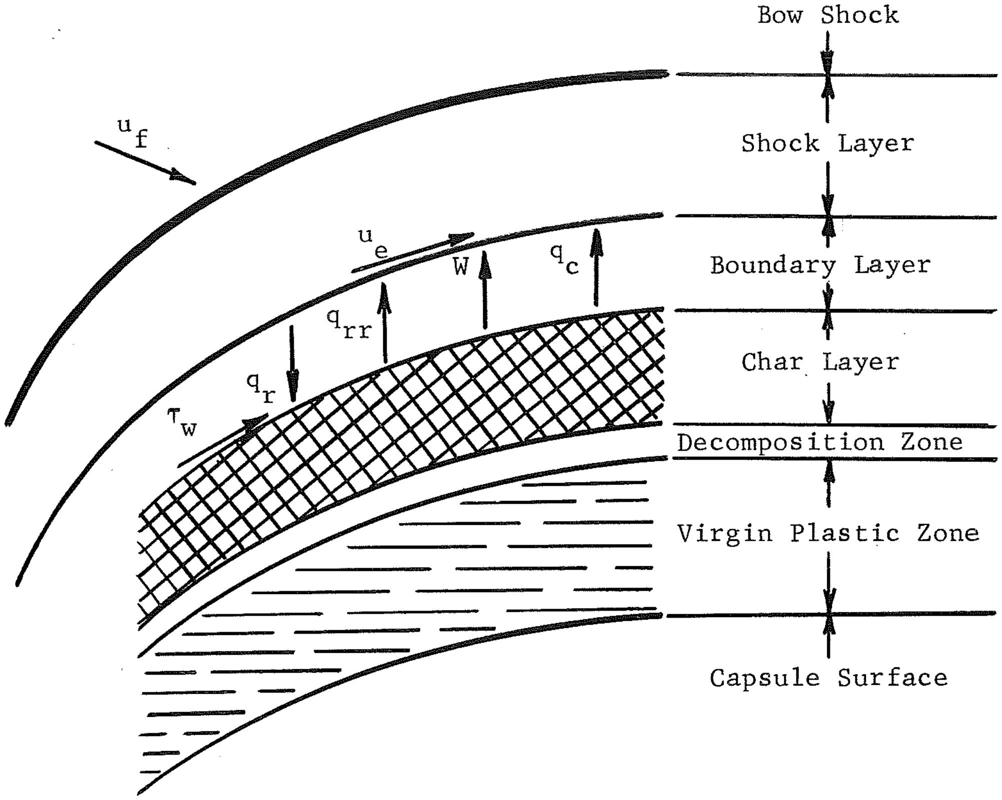

u_f - velocity of the flow field

u_e - velocity at the boundary layer edge

τ_w - shear force at the char surface

q_r - radiative heat transfer to the char surface

q_{rr} - reradiative heat transfer from the char surface

W - mass flux of pyrolysis gases leaving char surface

q_c - convective heat transfer to the char surface

Figure 1-3. Schematic Diagram of the Various Zones Developed During Reentry of a Capsule Protected by an Ablative Heat Shield.

of heat is absorbed by these predominantly endothermic reactions as the gas temperature increases from the decomposition zone to the char surface. These hot gases are then injected into the boundary layer with additional absorption of heat due to expansion and further chemical reactions (13,14,15).

Energy Transfer in the Char Zone of a Charring Ablator

Each of the above regions has been the subject of a sizeable research effort, and various types of mathematical models to describe the charring ablator process have been developed. Previous work on these regions is discussed in the susequent section on the State of the Art. In this dissertation an effort is made to obtain a better description of the phenomena taking place in the char zone. An accurate description is needed of the energy transfer in the char layer and the species compositions and fluxes entering the boundary layer. At present these variables are evaluated by considering the flow to be either frozen (no reaction) or in chemical equilibrium.

For frozen flow the lower limit on the energy transfer is computed since the energy absorbed by the pyrolysis products is just the change in sensible heat as these gases flow through the porous char. This is the simplest case to evaluate mathematically, and the classical transpiration cooling solution to the energy equation is applicable (16).

For equilibrium flow in the char zone the upper limit on the energy transfer is obtained since chemical reaction rates are infinitely fast, and the composition of the pyrolysis products only vary with the temperature as predicted by thermodynamic equilibrium. This approximation gives the maximum amount of heat that can be absorbed since the reactions occurring are predominantly endothermic. The mathematical description of this case is more detailed than for frozen flow since an additional term for heat absorption by chemical reaction must be included in the energy equation. Many investigators feel this model would more accurately describe the actual behavior in the char zone since the reaction rates should be very fast at the high temperatures encountered.

For a more accurate description of the reacting flow in the char zone the kinetics of the chemical reactions must be included in solving the energy equation. The solution is more complex than the limiting cases because compositions of the pyrolysis products must be calculated from the reaction rate expressions which are differential equations. Of all the possible reactions that could occur in the char zone within the temperature range encountered, the ones that actually occur must be selected and included in the analysis.

In addition, experiments must be conducted to assure the theoretical model accurately predicts the energy transfer in the char zone. This can be accomplished by flowing a mixture of compounds typical of the actual pyrolysis gases through chars formed in arc-jet heaters. The chars can be radiantly heated to simulate the surface heating during reentry. Gases entering and leaving the char zone can be analyzed to determine the extent of the reactions taking place in the char. Thus the accuracy of the mathematical computations can be assessed.

Furthermore, the results of the analysis, referred to as the non-equilibrium model, can be compared with the limiting cases. In this way the limitations incurred by assuming equilibrium or frozen flow are evaluated. A detailed investigation into the types of reactions occurring, the amount of carbon deposition taking place in the char layer, and ways to make the ablation of char forming materials more efficient is determined.

REFERENCES

1. Ely, Lawrence D., *Return from Space*, Charles C. Thomas, Publisher, Springfield, Illinois, 6-9 (1966).

2. Seifert, Howard S., and Kenneth Brown, *Ballistic Missile and Space Vehicle Systems*, John Wiley and Sons, Inc., New York, 448-9 (1961).

3. Ordway, Fredrick I., James P. Gardner, and Mitchell R. Sharpe, Jr., *Basic Astronautics*, Prentice-Hall, Inc., Englewood Cliffs, New Jersey, 346-9 (1962).

4. Duncan, Robert C., *Dynamics of Atmospheric Entry*, McGraw-Hill Book Co., Inc., New York, 117-9 (1962).

5. Martin, John J., *Atmospheric Reentry*, Prentice-Hall, Inc., Englewood Cliffs, New Jersey, 83-6 (1966).

6. Wingrove, Rodney C., "Flight Dynamics of Planetary Entry," *Recent Developments in Space Flight Mechanics*, *9*, 225 (1966).

7. Steverding, Bernard, and Vernon A. Nieberlein, "Ablation for Heat Shielding," *Chemical Engineering*, *72* (15), 163 (July 19, 1965).

8. Kelley, J. B., and M. R. L'Ecuyer, "Transpiration Cooling - Its Theory and Application," Report No. TM-66-5, Jet Propulsion Center, Purdue University, Contract NsG 592, N66-30856 (June 1966).

9. Abraham, Lewis H., Structural Design of Missiles and Spacecraft, McGraw-Hill Book Co., Inc., New York, 247-65 (1962).

10. Fein, M. M., S. J. Tunkel and M. S. Cohen, "New Developments in Ablative Cooling," CEP Symposium Series, 60 (52), 99 (1964).

11. Matting, Fred W. and Dean R. Chapman, "Analysis of Surface Ablation of Noncharring Materials with Description of Associated Computing Program," NASA TN D-3758 (December 1966).

12. Kuehn, Donald M. and Daryl J. Monson, "Attached and Separated Boundary Layers on Highly Cooled, Ablating and Nonablating Models at M = 13.8," NASA TN D-4041 (June 1967).

13. Diaconis, N. S., W. R. Warren, Jr. and T. E. Shaw, "The Hypervelocity Heat Protection Problem," Propulsion and Reentry, XVIth. International Astronautical Congress, Athens (1965).

14. Schmidt, Donald L., Engineering Design for Plastics, Chapter 13, Reinhold Publishing Co., Inc., New York (1962).

15. Freedman, S. I., _Developments in Heat Transfer_, Chapter 5, M. I. T. Press, Cambridge, Massachusetts (1962).

16. Bird, R. B., W. E. Stewart, and E. N. Lightfoot, _Transport Phenomena_, John Wiley & Sons, Inc., New York, 328-30 (1960).

II. STATUS OF PREVIOUS RESEARCH ON FLOW IN THE CHAR ZONE

Research and development of ablative heat shields for space vehicles can be placed into two broad catagories. The first involves detailed investigation of various isolated processes within the ablation mechanism. These studies include the flow of pyrolysis gases through porous media (1,2,3,4,5,6,7,8,9,10), plastic decomposition chemistry (11,12,13,14), boundary layer interaction with the char surface (15,16), and many others (17,18,19,20,21). The second category covers the analysis of the transient response during reentry of the combined heat and mass transfer mechanisms occurring between the heat shield and the flow field (15,16,23). Research in both areas is essential in the development of effective thermal protection systems. The former category improves the accuracy of the transient response calculations, while the latter allows for more efficient and economic design of the ablative heat shields.

This research describes the transport phenomena resulting from the flow of pyrolysis gas products through the char zone of a charring ablator. In particular, the pyrolysis products are those formed by the thermal degradation of nylon-phenolic resin composites. The nature and extent of chemical reaction between the pyrolysis products and the char zone, along with the energy absorbed by the flow in this zone, are of major interest. Likewise, knowledge of the extent of carbon deposition resulting from the various hydrocarbon cracking reactions that take place is important in developing a realistic model to predict ablator performance.

The following sections will discuss some of the typical transient response analyses briefly, and related work to flow in the char zone in detail. In particular, the transient analysis of Kratsch, *et. al.* (21), Kendall, *et. al.* (15) and Swann, *et. al.* (16) will be reviewed with emphasis on the analysis of the char zone. Subsequently, a detailed review of work pertinent to flow in porous media with and without chemical reactions is presented. These include the studies of Koh and del Casal (1,2,3) for transpiration cooling, of Clark (4) for high temperature experimental studies using methane flow through porous carbon and graphite, and of Weger, *et. al.* (5,6) for carbon deposition studies resulting from thermal cracking of hydrocarbon gases as they pass through heated char specimens.

Transient Models for the Analyses of Thermal Protection Systems

The need for accurate transient analyses of thermal protection systems of space vehicles is required to insure the safe return of the space craft and its occupants. The interaction of the shock heated gas and the ablative heat shield is extremely complex.

There is no single ground test facility where experiments can simulate the reentry of a space vehicle. Wind tunnel tests are used to study flow field characteristics, while radiant, induction and resistance heating facilities are used to simulate the thermal environment encountered during ablation. Therefore, an accurate mathematical model is essential to effectively predict the behavior of these thermal protection systems during reentry.

Almost all of the major aerospace firms and governmental organizations interested in reentry have modeled the transient response of ablative heat shields. It is impossible to discuss all of these various transient analyses; however, a brief history and a few typical models, namely those of Kratsch, *et. al.* (21), Kendall, *et. al.* (15) and Swann, *et. al.* (16) will be discussed. The weaknesses in these analyses will be pointed out, and it will be shown how this work will permit an improvement to present transient models.

One of the earliest theoretical studies of the ablation of a char forming plastic by Scala (17) "attempted to define the key physicochemical aspects of the problem and included a discussion of the importance and function of the char layer during the ablation process" (18). In a later study with Gilbert (18), they recognized the existance "of a complex mixture of low and high molecular weight gaseous species that interact chemically with the char and the gases in the boundary layer near the surface" (18). Although the complexity of chemical reactions within the char zone was discussed, the model of Scala and Gilbert (18) was for a gas mixture containing carbon monoxide, methane, hydrogen and ammonia which remained frozen as it transpired through the char. Similarly, the models of Barriault and Yos (19) and Meyers and Harmon (20) considered the flow to be frozen in the char zone.

The analysis of Kratsch _et_. _al_. (21) was a one dimensional, transient analysis that coupled the energy and mass transfer in char-forming ablative heat shields. Depolymerization kinetics of the ablative plastic was handled by an Arrhenius-type expression based on thermogravimetric analysis data. Chemical errosion of the carbonaceous medium by reactions occuring within and at the surface of the char were included. The receding surface boundary condition and aero-convective and gas-radiation heating boundary condition were specified input functions to the computer calculations.

The in-depth analysis of the char layer considered the pyrolysis gas products to be in thermodynamic equilibrium as they passed through the zone. Only gas phase reactions were included. This resulted in an overprediction of the carbon in the condensed phase as observed in experimental char analyses and was attributed to a shift in gas phase controlled reactions to gas-solid phase controlled reactions within the char. No provisions to include such chemical interactions of the pyrolysis gases with the solid carbon was made; however, an empirical adjustment based on experimental data was incorporated to correct for the overprediction of solid carbon.

This work was the first attempt to describe a rather complex system with a model that was not restricted by the over-simplification of frozen flow, constant physical properties, or omitted heat absorption terms.

The analysis of Kendall, *et*. *al*. (15) coupled a laminar, equilibrium boundary layer solution with a one dimensional, transient response of the ablative composite. The boundary layer solution was related to the shock layer by specifying edge boundary conditions. Similarly, the boundary layer solution was related to the transient response of the ablative composite by surface conditions. Four options were available to couple the ablating surface with the boundary layer. These included specifying (a) wall enthalpy, (b) pyrolysis gas species mass fluxes, (c) wall component mass flux with surface equilibrium or (d) coupled mass and energy balance at the wall as provided by a transient charring conduction solution.

The one dimensional, in-depth analysis considered the virgin plastic to pyrolyse to char and gaseous products and assumed thermal equilibrium and zero residence time of the pyrolysis products within the char layer. Char deposition and/or depletion was not considered in the analysis. A modified form of Darcy's law was used to calculate the pressure distribution after a temperature profile had been established.

The analysis of Swann, et. al. (16) was a one-dimensional, numerical analysis of the transient response of an ablative composite. The thermal protection system could contain as many as three layers of different materials and the first two could have moving boundaries. The material response was coupled to the flow field by an energy balance at the char surface where the convective heating rate was computed using either a linear or a quadratic approximation to the blocking effectiveness for a laminar boundary layer. The cold-wall convective heating rate and the radiant heating rate incident on the surface were specified functions of time. These values appeared as inputs to the computer solution. The surface was removed by vaporization at the sublimation temperature and by diffusion controlled chemical reactions of oxygen at the surface.

The energy equation applied to the char zone which was used by Swann, et. al. (16) can be put in the following form:

$$-\frac{\partial}{\partial x}\left(k\frac{\partial T}{\partial x}\right) + \left[\left(\frac{W}{W_o}\right)\bar{C}_p + \frac{\sum_{j=1}^{k} H_j R_j}{W_o\left(\frac{\partial T}{\partial x}\right)}\right] W_o \frac{\partial T}{\partial x} = -\rho C_p \frac{\partial T}{\partial x} \qquad (2\text{-}1)$$

where W is the mass flux of pyrolysis products at x and W_o is the mass flux of the pyrolysis products entering the char zone. The term in brackets is referred to as an effective reacting gas heat capacity which is computed considering the flow to be frozen ($\Sigma H_j R_j = 0$) or in thermodynamic equilibrium ($\Sigma H_j R_j \neq 0$).

The results of this research will permit the calculation of the non-equilibrium reacting gas heat capacity, i.e. the term in brackets of equation (2-1). The computation of the energy absorbed by chemical reactions for non-equilibrium flow will be discussed in the next chapter. This will permit the calculation of the non-equilibrium reacting gas heat capacity to be used with a simultaneous solution of the transient energy equation (2-1). With these results the transient response of a charring ablator can be predicted for non-equilibrium flow in the char zone.

Analysis of the Char Zone of a Charring Ablator

The analysis of the char zone of a charring ablator is in essence a study of flow through porous media accompanied by chemical reactions in the fluid and between the fluid and the medium. The porous medium is carbon, and the fluid is the pyrolysis products resulting from thermal degradation of the ablative composite.

Although there has been extensive work by the petroleum industry on flow through porous media for improving well performance (22), there has been little work describing the complex, non-equilibrium flow encountered in the char zone during ablation. However, there has been a significant amount of research in the aerospace field on transpiration cooling.

To describe flow in the char zone there have been two types of analyses. The first involves flow of fluids having constant physical properties with the gas and solid phases at different temperatures (thermal non-equilibrium). The second involves flow in porous media with variable physical properties but with thermal equilibrium between the solid and gas.

The studies of Koh and del Casal (1,2,3) were most directly related to this work and illustrate both analyses. In particular, the first paper presented analytical solutions to the one-dimensional energy equation for (a) constant physical properties with thermal non-equilibrium and (b) variable physical properties with thermal equilibrium between phases. The second study was for chemical non-equilibrium flow through porous matrices with thermal equilibrium. The third paper gave a summary of an experimental study used to verify the models proposed in the analytical studies.

Clark (4) extended the transpiration cooling analysis of Koh and del Casal (2) to simulated ablative chars. In this study methane-helium mixtures were passed through resistance heated porous carbon and graphite specimens in a temperature range from 2000° to 3500°F.

Weger, et. al. (4,5) used a chemical non-equilibrium analysis of gas flow through chars and carbon specimens to study the extent of carbon deposition resulting from hydrocarbon cracking reactions. The effect of carbon densification on the char and flow properties were analysed. An induction furnace was used to achieve uniformly high temperatures across the char specimens.

Transpiration Cooling Studies by Koh and del Casal: The works of Koh and del Casal (1,2,3) summarized the approach taken in both types of transpiration analyses described above. In their first paper analytical solutions to the one dimensional energy equation were presented. These included the special cases of (a) constant properties with thermal non-equilibrium between the gas and solid phases, and (b) variable properties with thermal equilibrium between the two phases. The equations used by the authors for a non-reacting (frozen), transpiration cooling analysis were (1):

$$\left[k_m \frac{dT_m}{dx}\right]_{T_f} = \int_{T_{f_i}}^{T_f} W\bar{C}_p \, dT_f \qquad (2\text{-}2)$$

Equation (2-2) is an overall energy balance for a fluid flowing in the porous matrix and equates the energy transfer by matrix conduction at the point x to the change in fluid enthalpy between an initial temperature, T_{f_i}, and the temperature at point x, T_f.

$$W\bar{C}_p \frac{dT_f}{dx} = h\,(T_m - T_f) \qquad (2\text{-}3)$$

Equation (2-3) is an energy balance for the coolant phase and equates the energy transfer from the coolant by convection to the energy transfer from the coolant to the solid phase.
The energy transfer by gas conduction was omitted from the equation as insignificant with respect to the gas convection.
Equations (2-2) and (2-3) were used to couple the coolant and solid phases of the system for the thermal non-equilibrium condition.

The pressure distribution within the matrix was determined using Darcy's Law as given below which neglects inertial effects.

$$\frac{dP}{dx} = -\frac{W\mu}{\gamma\rho} \tag{2-4}$$

The one-dimensional, steady state continuity equation was used and is:

$$W = \rho v = \text{constant} \tag{2-5}$$

The equation of state for the coolant phase was the following:

$$\rho = P/ZRT_f \tag{2-6}$$

The boundary conditions used to solve these equations were the pressure and matrix temperature at the rear (x=0) and front (x=L) surfaces of the matrix.

$$\left.\begin{array}{l} P = P_o \\ T_m = T_{m_o} \end{array}\right. \quad \text{at} \quad x = 0 \tag{2-7}$$

$$\left.\begin{array}{l} P = P_L \\ T_m = T_{m_L} \end{array}\right. \quad \text{at} \quad x = L \tag{2-8}$$

The results for the analysis were presented for two cases. The first considered the heat transfer coefficient and the physical and thermodynamic properties as constants, while the second was a variable properties solution.

In the solution for the first case, the equations were non-dimensionalized and an analytical solution was obtained. The approach used by the authors follows. Rewriting equations (2-2) and (2-3) in dimensionless form gave:

$$\frac{d\theta_m}{d\eta} = \frac{W\bar{C}_p L}{k_m}\,\theta_f = B\theta_f \tag{2-9}$$

and

$$\frac{d\theta_f}{d\eta} = \frac{hL}{W\bar{C}_p}\,(\theta_m - \theta_f) = A\,(\theta_m - \theta_f) \tag{2-10}$$

where

$$\theta_m = \frac{T_m - T_{f_i}}{T_{m_L} - T_{f_i}} \tag{2-11}$$

$$\theta_f = \frac{T_f - T_{f_i}}{T_{m_L} - T_{f_i}} \qquad (2\text{-}12)$$

$$A = \frac{hL}{W\bar{C}_p} \qquad (2\text{-}13)$$

$$B = \frac{W\bar{C}_p L}{k_m} \qquad (2\text{-}14)$$

$$\eta = x/L \qquad (2\text{-}15)$$

The boundary conditions in dimensionless form were:

$$\theta_m = \theta_{m_o} \quad \text{at} \quad \eta = 0 \qquad (2\text{-}16)$$

$$\theta_m = 1 \quad \text{at} \quad \eta = 1 \qquad (2\text{-}17)$$

Differentiation of equation (2-9) with respect to η and substituting the expressions for θ_f and $d\theta_f/d\eta$ into equation (2-10) gave a second order differential equation in terms of θ_m:

$$\frac{d^2\theta_m}{d\eta^2} + A\frac{d\theta_m}{d\eta} - AB\theta_m = 0 \qquad (2\text{-}18)$$

The general solution of this equation was:

$$\theta_m = C_1\mathrm{Exp}(r_1\eta) + C_2\mathrm{Exp}(r_2\eta) \tag{2-19}$$

where

$$r_1 = \frac{A}{2}\left[-1 + (1 + 4B/A)^{1/2}\right] \tag{2-20}$$

and

$$r_2 = \frac{A}{2}\left[-1 - (1 + 4B/A)^{1/2}\right] \tag{2-21}$$

Using the dimensionless boundary conditions to evaluate C_1 and C_2 in equation (2-19) resulted in the following dimensionless temperature distributions for the matrix (θ_m) and coolant (θ_f) as functions of the dimensionless matrix thickness (η):

$$\theta_m = \left[\frac{1-\theta_{m_o}\mathrm{Exp}(r_2)}{\mathrm{Exp}(r_1)-\mathrm{Exp}(r_2)}\right]\mathrm{Exp}(r_1\eta) - \left[\frac{1-\theta_{m_o}\mathrm{Exp}(r_1)}{\mathrm{Exp}(r_1)-\mathrm{Exp}(r_2)}\right]\mathrm{Exp}(r_2\eta) \tag{2-22}$$

$$\theta_f = \frac{1}{B}\left\{\left[\frac{1-\theta_{m_o}\mathrm{Exp}(r_2)}{\mathrm{Exp}(r_1)-\mathrm{Exp}(r_2)}\right] r_1\mathrm{Exp}(r_1\eta) - \left[\frac{1-\theta_{m_o}\mathrm{Exp}(r_1)}{\mathrm{Exp}(r_1)-\mathrm{Exp}(r_2)}\right] r_2\mathrm{Exp}(r_2\eta)\right\} \tag{2-23}$$

Results of the above analysis were presented in the form of graphs and will be discussed following the review of the variable properties analysis.

The variable properties analysis of Koh and del Casal (1) was made for the case of thermal equilibrium between the coolant and solid phases. A reduction in the complexity of the previous analysis resulted which permitted physical property data in the form of polynomial expressions to be incorporated into the equations obtained for the thermal equilibrium analysis. A summary of the approach used by the authors follows.

Once again the energy equation (2-2) was rewritten in dimensionless form as:

$$\phi_k \frac{d\phi}{d\eta} = \frac{W\bar{C}_p^* L}{k_m^*} \int_{\phi_i}^{\phi} \phi_{c_p}\, d\phi = \int_{\phi_i}^{\phi} \phi_{c_p}\, d\phi \qquad (2\text{-}24)$$

where:

$$\phi = T/T^* \qquad (2\text{-}25)$$

$$\phi_{c_p} = \bar{C}_p/\bar{C}_p^* \qquad (2\text{-}26)$$

$$\phi_k = k_m/k_m^* \qquad (2\text{-}27)$$

The thermal conductivity and heat capacity of the coolant were calculated by the usual polynomials where a and b were coefficients in the expressions:

$$\phi_k = \sum_{i=o}^{\varkappa} a_i \phi^i \qquad (2\text{-}28)$$

$$\phi_{c_p} = \sum_{j=o}^{\omega} b_j \phi^j \qquad (2\text{-}29)$$

Substitution of equations (2-28) and (2-29) into equation (2-24) followed by integration gave:

$$B\eta = \int_{\phi_o}^{\phi} \frac{\sum_{i=o}^{\varkappa} a_i \phi^i}{\left[\sum_{j=o}^{\omega} \left(\frac{b_i}{j+1}\right) \phi^{j+1}\right]_{\phi_i}^{\phi}} d\phi = I(\phi_o, \phi) \qquad (2\text{-}30)$$

The transformed boundary condition described by equation (2-7) was used to obtain (2-30), and this is:

$$\phi = \phi_o \quad \text{at} \quad \eta = 0 \qquad (2\text{-}31)$$

The inlet and outlet surface temperatures were related to B using the second transformed boundary condition (2-8) which was:

$$\phi = \phi_L \quad \text{at} \quad \eta = 1 \qquad (2\text{-}32)$$

The resulting equation, applying these boundary conditions, was:

$$B = \int_{\phi_o}^{\phi_L} \frac{\sum_{i=o}^{\varkappa} a_i \phi^i}{\left[\sum_{j=o}^{\omega} \left(\frac{b_j}{j+1}\right) \phi^{j+1}\right]_{\phi_i}^{\phi}} d\phi = I(\phi_o, \phi_L) \qquad (2\text{-}33)$$

The solution of Darcy's Equation for coolant flow was likewise given in dimensionless form as:

$$\frac{P_o^{\,2} - P^2}{P_o^{\,2} - P_L^{\,2}} = \frac{\int_o^{\eta} \phi_\mu \theta_f d\eta}{\int_o^{1} \phi_\mu \theta_f d\eta} \tag{2-34}$$

where the viscosity was evaluated using a polynomial expression.

$$\phi_\mu = \sum_{i=0}^{\nu} c_i \phi^i \tag{2-35}$$

The constant and variable properties models of Koh and del Casal (1) were compared with the experimental data of Turnacliff (23) in which one half inch diameter spheres were used as the flow medium. The fluids studied were air and helium.

Results of the comparison of the constant properties, thermal non-equilibrium solution (equations 2-19 and 2-23) with the experimental data were presented as dimensionless plots of temperature (matrix and fluid) as a function of matrix thickness for values of matrix porosity between 0.259 and 0.477 and fluid Reynolds number between 62 and 862. The physical properties of the fluid were evaluated at a mean temperature of 110°F at the back and front surfaces. These plots are reproduced in Figures 2-1, 2-2 and 2-3. As can be seen a very good agreement between the analytical and experimental results was obtained.

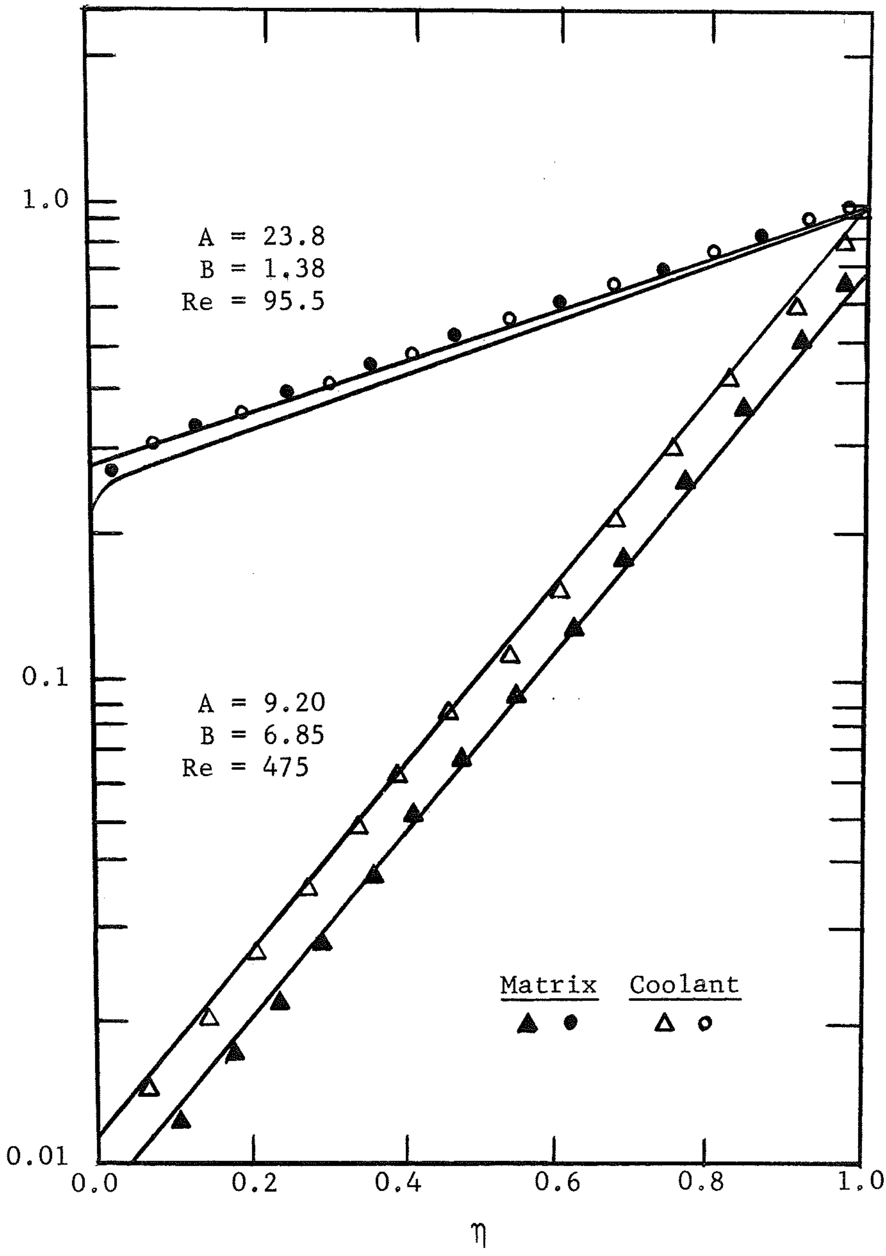

Figure 2-1. Comparison of Calculated and Measured Temperature Distributions, Porosity = 0.259.

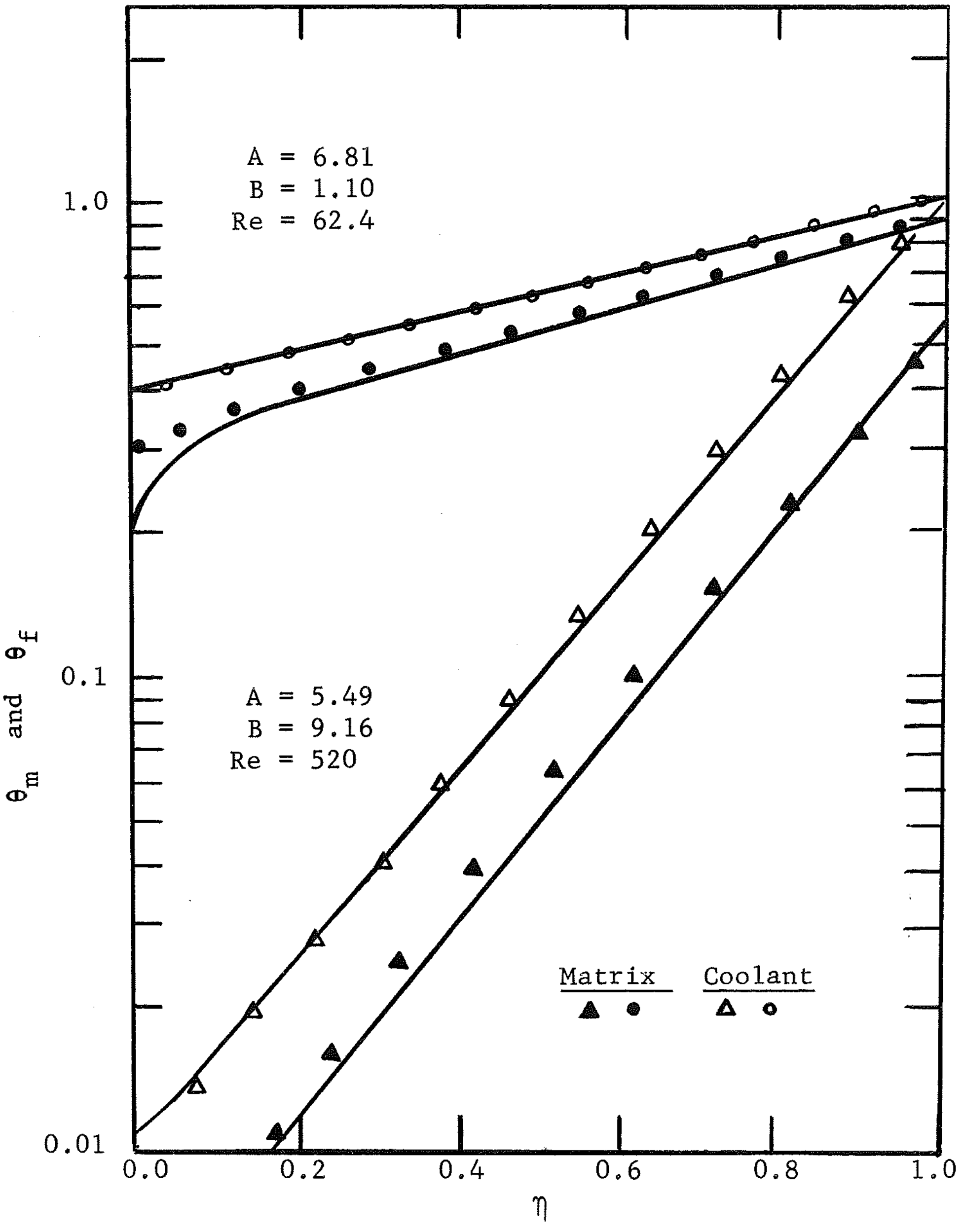

Figure 2-2. Comparison of Calculated and Measured Temperature Distributions, Porosity = 0.395.

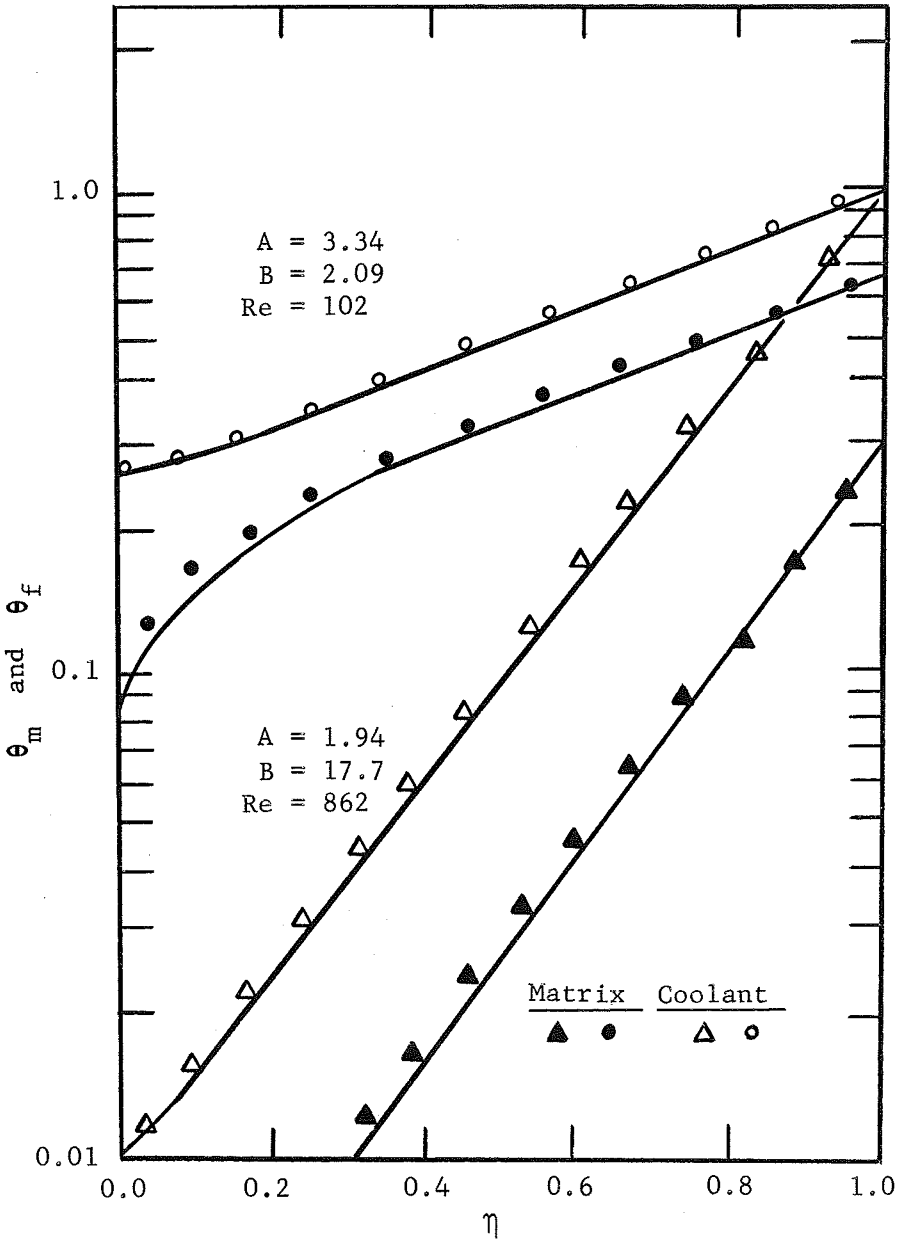

Figure 2-3. Comparison of Calculated and Measured Temperature Distributions, Porosity = 0.477.

Three important conclusions were drawn from the constant properties, thermal non-equilibrium analysis. First, a decrease in the Reynolds number at fixed porosity values decreased the difference between the matrix and fluid temperatures. The Reynolds number can be decreased by decreasing the fluid velocity, or, by decreasing the pore diameter of the matrix. In either case the mass flux of coolant to the matrix is reduced causing longer holdup of the fluid phase within the matrix. This additional holdup time favors thermal equilibrium between the solid and fluid phases. Secondly, a decrease in the Reynolds number at fixed porosity values increased the difference between the fluid reservoir temperature (the temperature of the fluid prior to entry into the matrix at the back surface) and the matrix back surface temperature for a constant front surface temperature. This is caused by reducing the net capacity of the fluid to absorb heat transferred to the back surface from the heated front surface. Thirdly, the results of Turnacliff can be extrapolated to transpiration cooling, where a matrix pore diameter is used that is several orders of magnitude smaller (for the same values of fluid velocity) than that used by Turnacliff (23). This showed that thermal equilibrium between the solid and fluid was a reasonable approximation for transpiration cooling.

For the variable properties, thermal equilibrium solution (equation 2-33), Koh and del Casal analysed air and helium flow through Nickel Foametal matrices having porosity values between 0.42 and 0.735. The inlet temperature of the coolant was 540°R and the matrix front surface temperature was 2700°R. The results, presented again as a dimensionless plot of temperature as a function of matrix thickness, are reproduced in Figure 2-4. Also shown were temperature profiles for the constant properties solution. A close approximation to the variable properties solution was obtained at a matrix porosity value of 0.42. However, as the porosity was increased (to 0.53 and 0.735), departure of the constant properties temperature distributions from those of the variable properties analysis was observed. This indicated the importance of a variable physical properties analysis in any realistic model of flow through media having moderate to high (>0.50) porosity.

In the above analyses, simplifying assumptions were made to obtain analytical solutions. Important modes of energy absorption, such as fluid conduction and chemical reaction, were omitted from the models. This greatly restricted the application of the models to a small class of problems (i.e., flow of an inert coolant through a porous medium in transpiration cooling). In order to extend their analyses to a broader area of application, Koh and del Casal in a second paper (2) proposed dissociation of the coolant within the porous matrix.

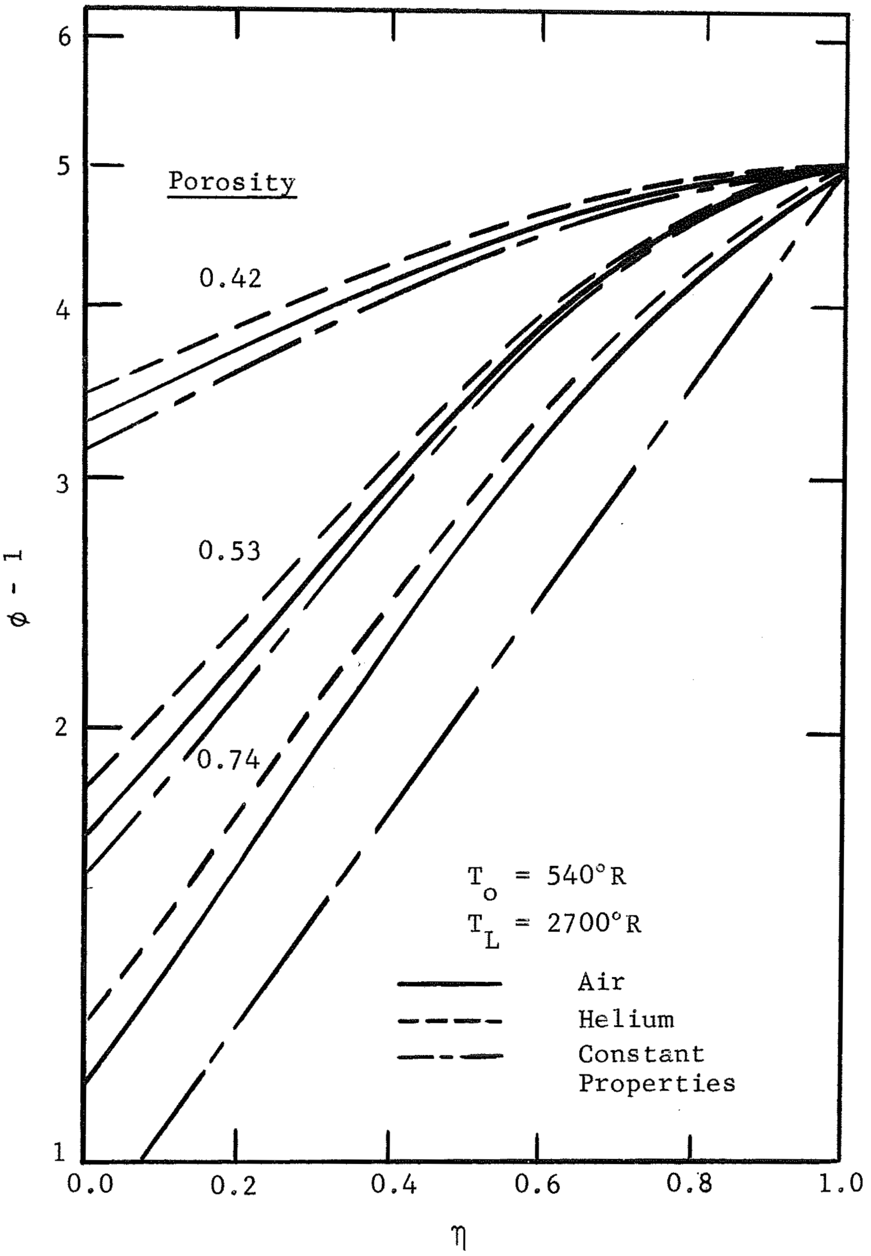

Figure 2-4. Temperature Distributions for Air and Helium Flows Through Nickel Foametal.

The dissociation of coolant to various products was represented by the general chemical reaction below.

$$S_o \rightleftarrows s_1S_1 + s_2S_2 + \dots + s_iS_i \qquad (2\text{-}36)$$

The energy absorbed by chemical dissociation of the coolant within the matrix was incorporated into the thermal equilibrium, energy balance equation (2-2) as:

$$k_m \frac{dT}{dx} = \sum_{i=0}^{S_n} \left[W_ih_i - (W_ih_i)_\infty \right] \qquad (2\text{-}37)$$

In equation (2-37), the term on the right hand side represented the local enthalpy flux resulting from the dissociation of the coolant to S_i species. The summation in equation (2-37) was made over S_n species to include additional species (S_{i+1} to S_n) that enter into the matrix from the fluid adjacent to the front surface by counter diffusion. The local enthalpy flux was equated to the energy absorbed by matrix conduction to complete the energy balance. Once again energy absorption by coolant conduction was omitted from the analysis.

In order to evaluate the local enthalpy flux needed in the energy equation (2-37), the following equations were solved simultaneously with the energy equation; the continuity equation (2-5) and the momentum equation (2-4). In addition the rate equation (2-38), which specified the rate of dissociation of the coolant, and the species continuity equation (2-39), were used.

$$\frac{dC_o}{dt} = -KF \tag{2-38}$$

$$N_i = Nn_i - \rho D_{im}\frac{dn_i}{dx} \tag{2-39}$$

The change in the molar concentration of species i was equated to the rate of chemical dissociation of the coolant by a differential material balance and is:

$$\frac{\partial N_o}{\partial x} = \frac{\partial C_o}{\partial t} \tag{2-40}$$

Rewriting equation (2-39) for the specific reaction (2-36) excluding the species (S_{i+1} to S_n) introduced into the matrix by diffusion from the boundary layer gave:

$$N_i = (Nn_i)_\infty + s_i\left[(Nn_o)_\infty - N_o\right] = \frac{W_i}{(MW)_i} \tag{2-41}$$

where the first term on the right hand side of the equation represented the mole flux of specie i at the reservoir, and the second term was the increase of mole flux of i due to the dissociation of "o" species. Substituting for W_i into the energy equation (2-37) gave:

$$k_m \frac{dT}{dx} = \sum_{i=o}^{S_n} \left\{ \left[(Nn_i)_\infty + s_i [(Nn_o)_\infty - N_o] \right] (MW)_i \, h_i - \left[N_i (MW)_i h_i \right]_\infty \right\} \tag{2-42}$$

Rearranging equation (2-42), with substitution for h_i by its defining equation ($h_i = \int_{T_{f_i}}^{T_f} C_{p_i} dT + h_i^{o}$), and, normalizing the parameters T and x using equations (2-12) and (2-15), gave the following dimensionless, first order, differential equation:

$$\frac{d\theta}{d\eta} = B \sum_{i=o}^{S_i} \frac{\bar{M}_i}{C_{p\infty}} \left\{ \left[n_{i\infty} + s_i (n_{o\infty} - R_o) \right] \left(\int_o^{\theta} C_{pi} d\theta + h_i^{\circ} \right) - (n_i h_i)_\infty \right\} \tag{2-43}$$

where B was defined in equation (2-14), $\bar{M}_i$ was the ratio of the molecular weights of species i to the molecular weight of the reservoir fluid, and h_i^{o} was the standard heat of formation of species i. The subscript ∞ referred to conditions at the reservoir.

To facilitate the solution of equation (2-43), the parameter R_o was defined as a dimensionless mole flux of species "o" using equations (2-39) and (2-40). A detailed derivation was presented in the original work (2) by the authors. The results of that derivation are presented below as equations (2-44) and (2-45):

$$R_o = \frac{[1 + w_\infty b]w - \frac{1}{\alpha_o}\frac{dw}{d\eta}}{1 + bw} \tag{2-44}$$

and

$$\frac{dR_o}{d\eta} = -\frac{KL}{N_\infty} F \tag{2-45}$$

These are two, first order, differential equations for the solution of R_o and w, the mole fraction of species "o". The boundary conditions for the above equations were the initial mole flux of species "o" in the reservoir,

$$R_o = w_\infty \quad \text{at} \quad \eta = 0 \tag{2-46}$$

and the final concentration of species "o" at the front surface,

$$w = w_L \quad \text{at} \quad \eta = 1 \tag{2-47}$$

The value of w_L was specified by an analysis of the boundary layer flow. Also, since the reaction rate parameters, F and K, were functions of temperature, the above equations (2-44) and (2-45) were solved simultaneously with the energy equation (2-37).

The pressure distribution was calculated from the momentum equation (2-4) using the gas equation of state given by equation (2-6). The resulting equation for the pressure drop at any point within the matrix was:

$$\frac{P_{\infty}^{2} - P^{2}}{2W\mu^{*}R\ T^{*}\ L} = \gamma \int_{0}^{\eta} \bar{z}\ \left(\frac{\mu}{\mu^{*}}\right)\ \left(\frac{T}{T^{*}}\right)\ d\eta \qquad (2\text{-}48)$$

where γ was the matrix permeability, R was the universal gas constant and μ, the viscosity.

The solution of equations (2-43), (2-44), (2-45), and (2-48) for the dissociation of air and ammonia within the porous matrices was obtained. The results were presented as plots of the dimensionless temperature as a function of matrix thickness for various values of the dissociation constant, K. These solutions are reproduced in Figures 2-5 and 2-6. The results showed the effect of the extent of dissociation on the value of the coolant temperature and energy absorbed within the matrix. For highly endothermic, dissociation reactions within the matrix, the local temperature was decreased due to the increased energy absorption by chemical reaction. This effect was illustrated in Figures 2-5 and 2-6 by the curves which fell below the K=0 (no chemical reaction) curve. As noted, in some cases, the non-equilibrium analyses ($K \neq 0$) produced results which indicated increased

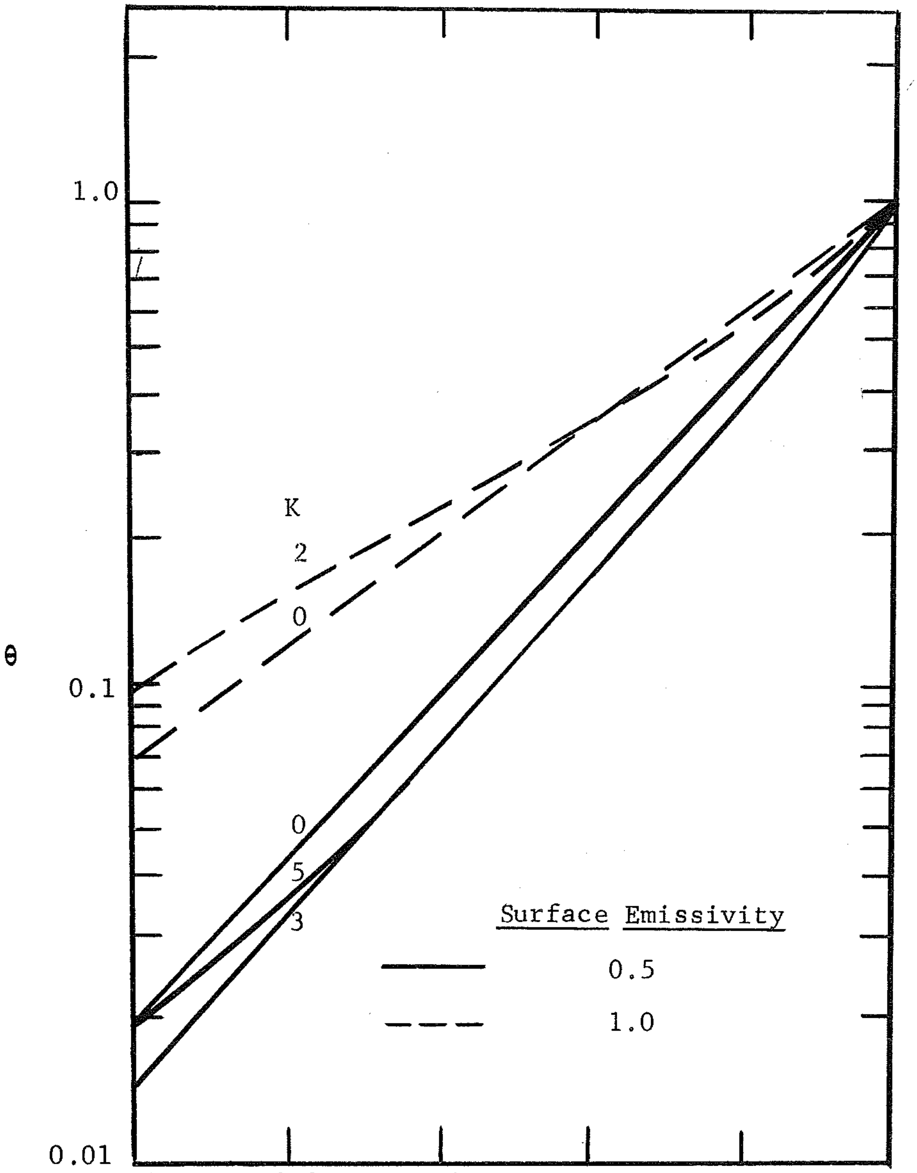

Figure 2-5. Temperature Distributions for NH_3 Flow Through a Porous Matrix as a Function of the Reaction Constant and Surface Emissivity.

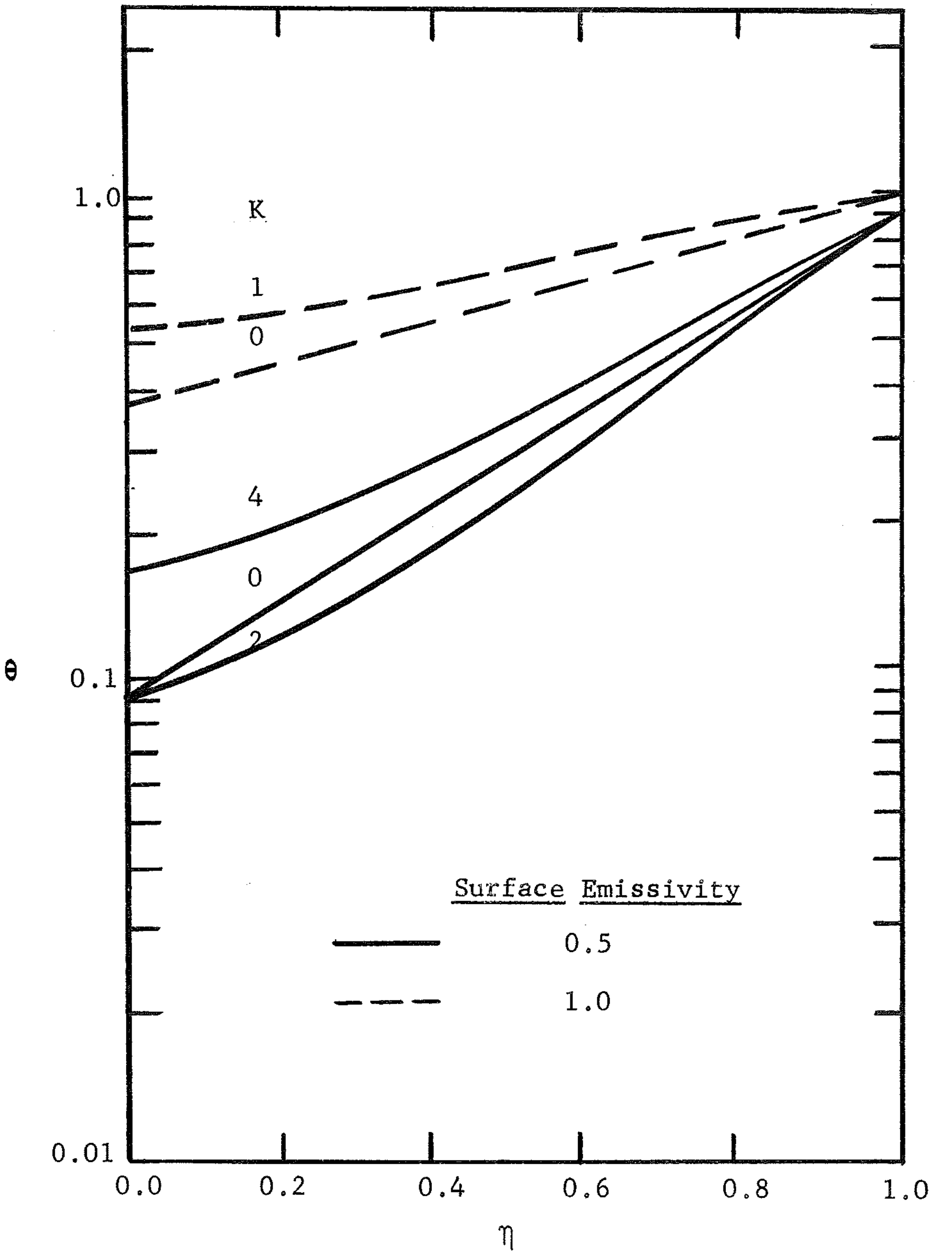

Figure 2-6. Temperature Distributions for NH_3 Flow Through a Porous Matrix as a Function of the Reaction Constant and Surface Emissivity.

temperature within the matrix. This resulted from the net decrease in the mass flux parameter, B, of equation (2-43) which was caused by the dissociation of the coolant. The dual effect of the rate of dissociation of the coolant on the mass and energy transfer within the matrix resulted in the intersection of the various curves in Figures 2-5 and 2-6.

The important conclusion drawn from this non-equilibrium flow analysis was that endothermic chemical (dissociation) reactions within the matrix reduced the total quantity of coolant required to maintain the surface temperature at a specified value.

The first and second papers by Koh and del Casal (1,2) neglected the effect of gas conduction on the energy transfer associated with flow through porous matrices for transpiration cooling. This was a valid assumption for high mass flux values ($\sim$ 0.1 lb./ft^2-sec) or for relatively small temperature gradients across the matrix (3000°R). However, at either low flow rates and/or high temperature gradients, as encountered in transpiration and ablative cooling applications, the effect of coolant conduction must be considered.

In order to develop a more generalized transpiration flow model Koh and del Casal (3) included coolant conduction in the non-equilibrium, constant properties model discussed previously (1). Also, an experimental study was conducted to test the reliability of this analytical model for predicting the temperature gradient and energy absorption within the porous matrix. Before the comparison is made, however, a brief discussion of the development of the governing equations of change and the analytical solutions will be made.

Once again the continuity (2-5), momentum (2-4) and equation of state (2-6) considered in Koh and del Casal's first paper (1) was used in this analysis. However, when energy absorption by coolant conduction was considered, the energy equation (2-2) relating the heat transfer by conduction from each phase and the increase in the fluid enthalpy from the reservoir temperature (T_{fi}) to a local temperature (T_f) was modified as follows:

$$\left[k_f \frac{dT_f}{dx}\right]_{T_f} + \left[k_m \frac{dT_m}{dx}\right]_{T_m} = \int_{T_{fi}}^{T_f} W\bar{C}_p dT_f \qquad (2\text{-}49)$$

Likewise, the energy balance relating the energy absorption by matrix conduction to the convective heat transfer from the matrix to the fluid at any cross-section within the matrix was:

$$\frac{d}{dx}\left(k_m \frac{dT_m}{dx}\right) = h(T_m - T_f) \qquad (2\text{-}50)$$

For constant properties, equation (2-50) reduced to:

$$k_m \frac{d^2T_m}{dx^2} = h(T_m - T_f) \qquad (2\text{-}51)$$

Rearranging equations (2-49) and (2-51) after normalization using the definitions of the dimensionless parameters in equations (2-11), (2-12), (2-13), (2-14), and (2-15), gave:

$$\frac{d\theta_m}{d\eta} + C\frac{d\theta_f}{d\eta} = B\theta_f \qquad (2\text{-}52)$$

and

$$\frac{d^2\theta_m}{d\eta^2} = AB\ (\theta_m - \theta_f) \qquad (2\text{-}53)$$

where C is the ratio of the fluid to matrix thermal conductivity:

$$C = \frac{k_f}{k_m} \qquad (2\text{-}54)$$

In order to solve the above equations for the dimensionless temperature distributions, θ_m and θ_f, three boundary conditions were required. These included, in normalized form, the back surface temperature of the matrix (x=0),

$$\theta_m = \theta_{m_o} \quad \text{at} \quad \eta = 0 \tag{2-55}$$

the front surface temperature of the matrix,

$$\theta_m = 1 \quad \text{at} \quad \eta = 1 \tag{2-56}$$

and, a local energy balance on the fluid phase at the back surface (x=0) relating the net increase in fluid enthalpy to the heat transfer by fluid conduction. In dimensionless form this was:

$$\frac{d\theta_f}{d\eta} = \frac{B}{C}\,\theta_f \quad \text{at} \quad \eta = 0 \tag{2-57}$$

Combining equations (2-52) and (2-53) gave a third order differential equation in θ_m:

$$\frac{d^3\theta_m}{d\eta^3} = \frac{B}{C}\,\frac{d^2\theta_m}{d\eta^2} - \left(\frac{AB}{C} + AB\right)\frac{d\theta_m}{d\eta} + \frac{AB^2}{C}\,\theta_m = 0 \tag{2-58}$$

A general solution to (2-58) was:

$$\theta_m = C_1\mathrm{Exp}[\Gamma_1\eta] + C_2\mathrm{Exp}[\Gamma_2\eta] + C_3\mathrm{Exp}[\Gamma_3\eta] \tag{2-59}$$

where Γ_1, Γ_2, and Γ_3 were the roots of the following auxiliary equation:

$$\Gamma^3 - \frac{B}{C}\Gamma^2 - AB\left(1 + \frac{1}{C}\right)\Gamma + \frac{AB^2}{C} = 0 \qquad (2\text{-}60)$$

Substitution of θ_m after differentiation into equation (2-52) resulted in a solution for the fluid temperature distribution, θ_f, as a function of η.

$$\theta_f = \left(1 - \frac{\Gamma_1^2}{AB}\right) C_1 \text{Exp}[\Gamma_1 \eta] + \left(1 - \frac{\Gamma_2^2}{AB}\right) C_2 \text{Exp}[\Gamma_2 \eta] + \left(1 - \frac{\Gamma_3^2}{AB}\right) C_3 \text{Exp}[\Gamma_3 \eta] \qquad (2\text{-}61)$$

where

$$C_1 = \frac{1}{\Delta_2}\left[(\theta_{m_o}\text{Exp}\Gamma_1 - 1)\left(1 - \frac{\Gamma_3^2}{AB}\right) + (1 - \theta_{m_o}\text{Exp}\Gamma_3)\left(1 - \frac{\Gamma_2^2}{AB}\right) + (\text{Exp}\Gamma_3 - \text{Exp}\Gamma_1)\,\theta_{f_o}\right] \qquad (2\text{-}62)$$

$$C_2 = \frac{1}{\Delta_2}\left[(1 - \theta_{m_o}\text{Exp}\Gamma_1)\left(1 - \frac{\Gamma_3^2}{AB}\right) + (\theta_{m_o}\text{Exp}\Gamma_3 - 1)\right.$$

$$(1 - \frac{\Gamma_1^2}{AB}) + (\mathrm{Exp}\Gamma_1 - \mathrm{Exp}\Gamma_3)\ \theta_{f_o}\Big] \tag{2-63}$$

$$C_3 = \frac{1}{\Delta_2}\Big[(\theta_{m_o}\mathrm{Exp}\Gamma_1 - 1)(1 - \frac{\Gamma_2^2}{AB}) + (1 - \theta_{m_o}\mathrm{Exp}\Gamma_2)(1 - \frac{\Gamma_1^2}{AB}) + (\mathrm{Exp}\Gamma_2 - \mathrm{Exp}\Gamma_1)\ \theta_{f_o}\Big] \tag{2-64}$$

and

$$\Delta_2 = (\mathrm{Exp}\Gamma_2 - \mathrm{Exp}\Gamma_1)(1 - \frac{\Gamma_3^2}{AB}) + (\mathrm{Exp}\Gamma_3 - \mathrm{Exp}\Gamma_2)(1 - \frac{\Gamma_1^2}{AB}) + (\mathrm{Exp}\Gamma_1 - \mathrm{Exp}\Gamma_3)(1 - \frac{\Gamma_1^2}{AB}) \tag{2-65}$$

For the special case of thermal equilibrium between the fluid and matrix ($T = T_f = T_m$), the temperature distribution was:

$$\frac{T - T_{f_i}}{T_L - T_{f_i}} = \mathrm{Exp}\Big[\frac{-W\bar{C}_p L}{k_m + k_f}(1 - \frac{x}{L})\Big] \tag{2-66}$$

Also a detailed development for flow of coolants through porous matrices with internal heat generation was presented. This topic will be discussed in a subsequent section which describes the research of Clark (4) in the area of ablative cooling.

In addition to the analytical development of the modified coolant conduction model, equation (2-61), Koh and del Casal presented experimental results to test the feasibility of the model under typical transpiration cooling conditions. These are summarized in Table 2-1. The fluids studied were water, air, carbon dioxide and methyl methacrylate. Metal matrices constructed of tungsten, poroloy, stainless steel and nickel were used. Porosity values varied from 0.20 to 0.75 for these media.

A radiant heat source was used to heat the front surface of the matrix to temperatures between 1820°F to 3200°F. Twenty-five infrared quartz lamps, staggered in two rows parallel to the front surface of the matrix, were used. The coolant flow passed through the matrix from the back to the front surface. The exit flow rate was measured with a pitot tube.

It is of interest to indicate the similarity in design of the apparatus of Koh and del Casal, _et_. _al_. (3) with the apparatus used in this study. Each was constructed without knowledge of the other, yet many of the major features (i.e., quartz heating lamps, specimen holder, etc.) were similar.

Table 2-1. Summary of Experimental Results for the Flow of Air, CO_2, H_2O, and Methyl Methacrylate Through Porous Matrices.

Coolant Fluid	Number of Tests	Temperature Range (°F)	Pressure (System) (psia)	Mass Flux (W) Coolant (lb_m/ft^2-sec)	Pressure Drop per Unit Mass Flux (Units)*
Air	15	70-2000°F	14.7 - 27.9	0 - 0.11	$(1.74 - 5.0)\times10^3$
CO_2	4	70-2000°F	14.7 - 15.0	$0 - 7.7\times10^{-5}$	Unsatisfactory Data
H_2O	10	70-1820°F	14.7 - 26.7	$0 - 2.7\times10^{-3}$	$(0.8 - 3.8)\times10^3$
Methyl Methacrylate	15	70-3200°F	14.7 - 25.7	$0 - 2.9\times10^{-2}$	$(0.07 - 4.3)\times10^5$

* Gas: Pressure Drop per Unit Mass Flux $= \frac{P_o - P_L}{W}$ $(lb_f\text{-sec}/lb_m)$

Liquid: Pressure Drop per Unit Mass Flux $= \frac{P_o^2 - P_L^2}{W}$ $(lb_f^2\text{-sec}/lb_m\text{-ft}^2)$

The experimental results obtained with the radiant heating apparatus by Koh and del Casal were compared to the results predicted by the constant property, thermal equilibrium solution including energy absorption by coolant conduction (equation 2-66). These comparisons were reproduced from the original paper and are presented as plots of dimensionless temperature as a function of matrix thickness in Figures 2-7, 2-8, and 2-9. As seen, very good agreement was obtained for all coolant species (water, air, carbon dioxide and methyl methacrylate) at matrix distances less than 0.5. However, in Figures 2-7 and 2-8, the results for air and carbon dioxide at matrix distance values greater than 0.5, differed from the predicted distributions as shown. This was caused, in part, by the experimental error; and, probably in part to the approximate solution obtained by considering the physical properties constant. It is reasonable to expect a better agreement near the back surface of the matrix where the coolant properties are not greatly influenced by the moderate temperature encountered (500°R - 1000°R). However, as the coolant approaches the front surface where temperatures increase rapidly from 700°R to 2200°R, the change in physical properties could certainly cause a poor correlation with the observed results. Once again, the importance of a variable properties analysis when temperature gradients greater than

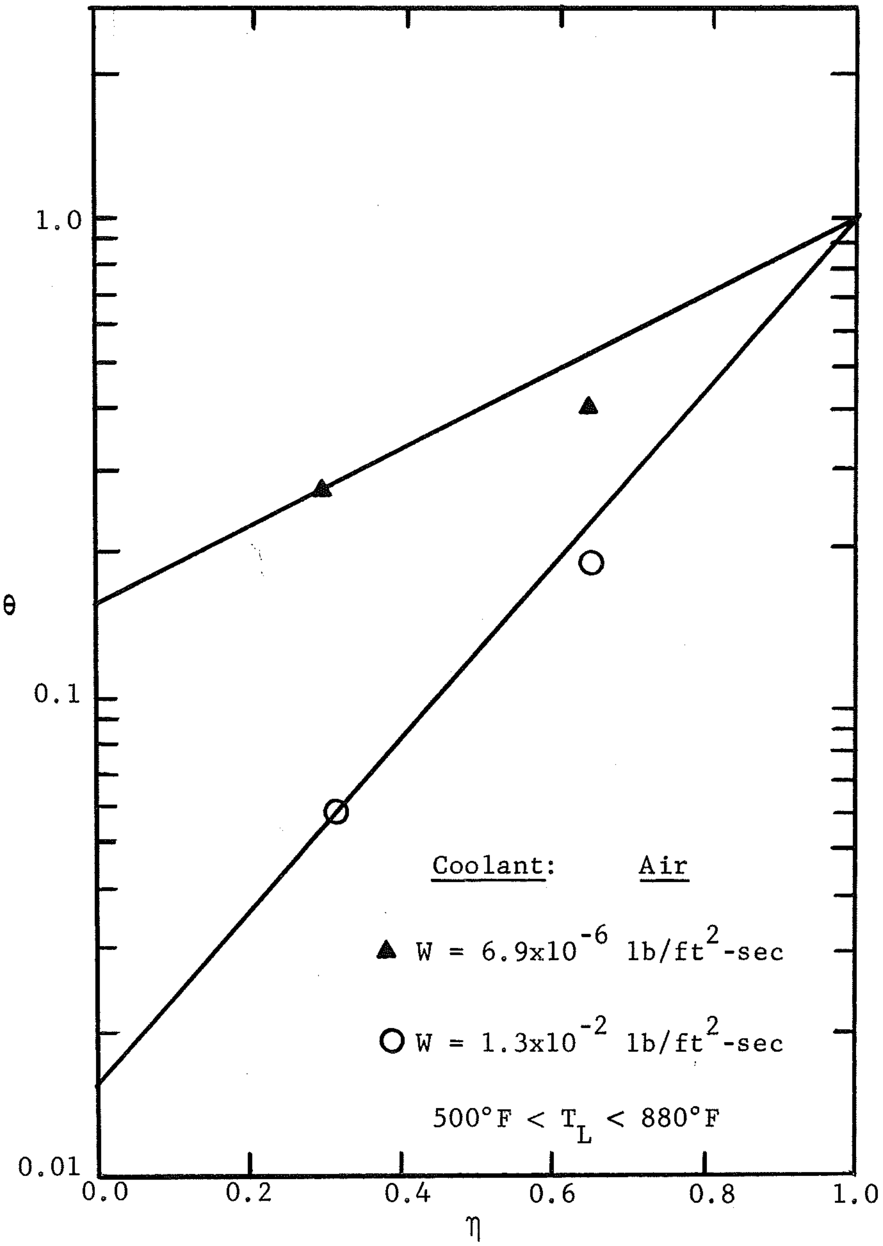

Figure 2-7. Temperature Distributions for Air Flow Through a Porous Matrix.

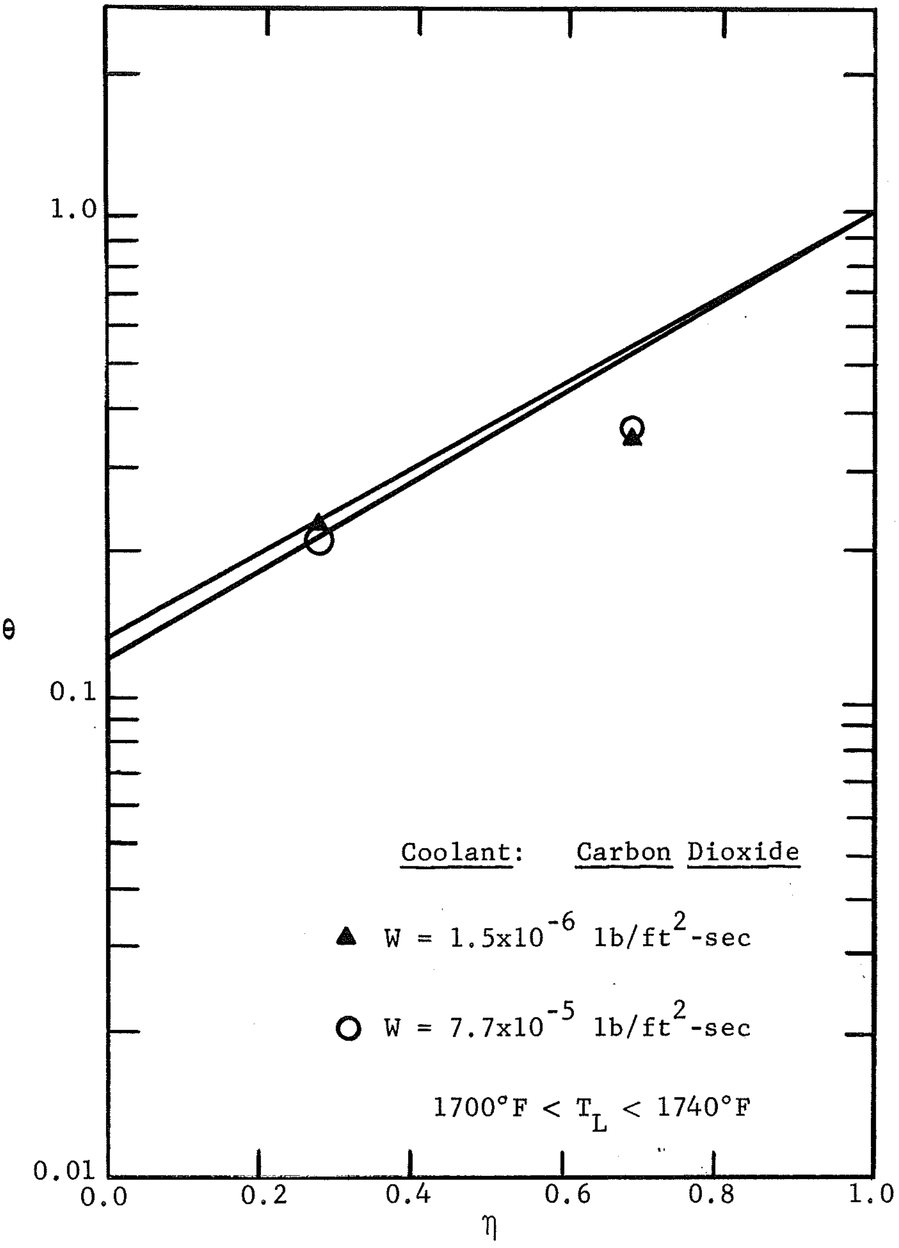

Figure 2-8. Temperature Distributions for CO_2 Flow Through a Porous Matrix.

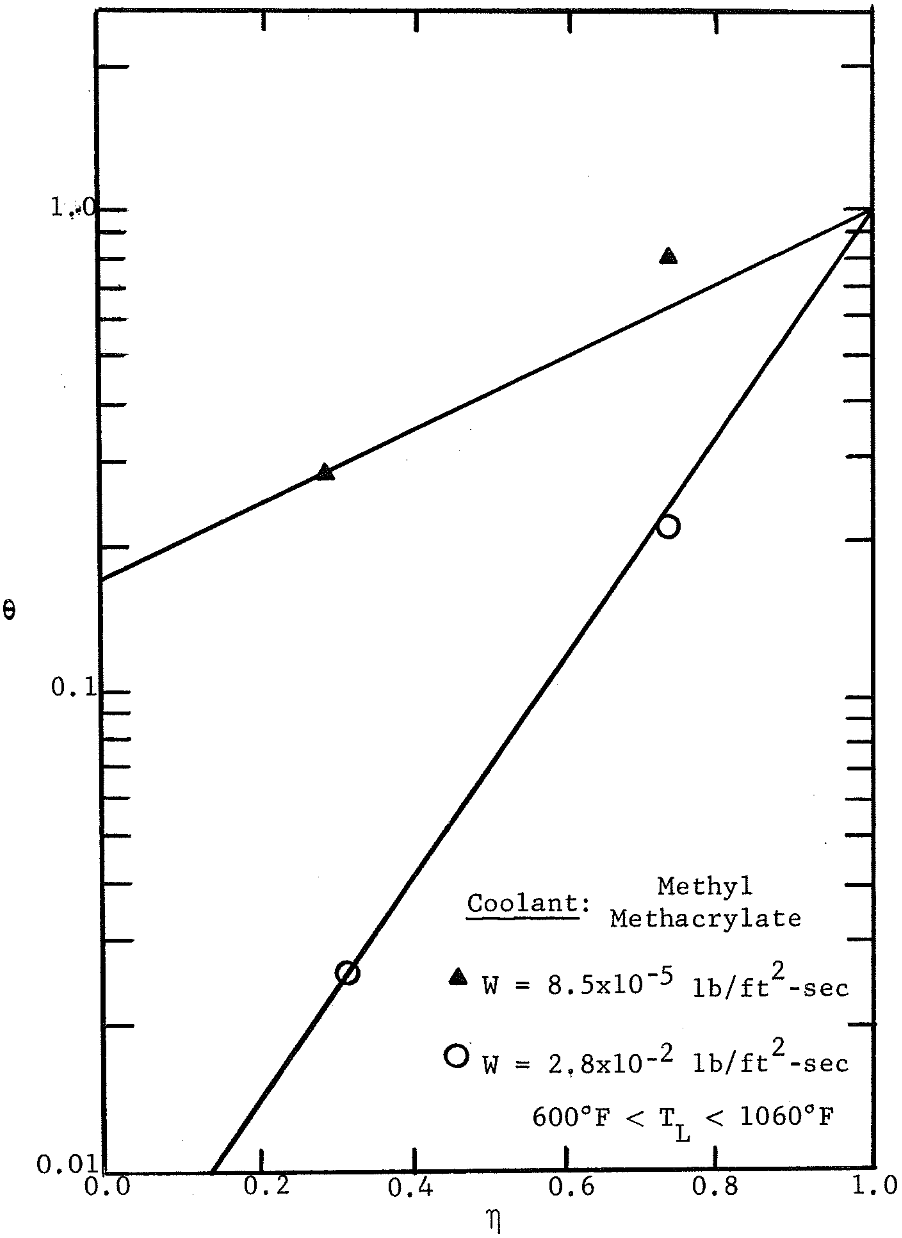

Figure 2-9. Temperature Distributions for Methyl Methacrylate Flow Through a Porous Matrix.

1000°R are encountered is illustrated for the accurate prediction of the actual behavior. No experimental results were presented for the chemical non-equilibrium analysis (2) of flow through porous matrices. However, carbon deposition was noted during the methyl methacrylate experiments resulting in serious plugging problems within the matrix. The carbon deposit was attributed to the thermal cracking of various hydrocarbons obtained as products from the depolymerization reactions of the methyl methacrylate.

The material in the three papers by Koh and del Casal (1,2,3) is summarized as follows. First, the simultaneous solutions of the continuity equation (2-5) and the momentum equation (2-4) with various forms of the energy equation were presented. The equations were for the flow of coolant through a one-dimensional porous matrix with:

(1) constant physical properties and thermal non-equilibrium between the coolant and solid phases,

(2) variable physical properties and thermal equilibrium between the coolant and the porous matrix,

(3) variable physical properties with thermal equilibrium between the phases accompanied by dissociation of the coolant within the matrix,

(4) constant properties with thermal non-equilibrium between the coolant and matrix and energy transfer by solid and matrix conduction, and,

(5) constant properties, thermal equilibrium flow with energy absorption by coolant and solid conduction.

In cases (1) and (5) experimental results by Turnacliff (23) and Koh and del Casal (3), respectively, were used to establish the accuracy of the solutions obtained; and, in general, the models predicted the observed results within experimental error. However, for the remaining cases, no experimental data were presented to establish the accuracy of the analytical results.

The contributions by the authors defining the effects of gas conduction, chemical reactions and internal heat generation on the fluid flow and heat transfer characteristics in high temperature porous matrices for transpiration cooling were indeed significant.

Quite naturally the results of Koh and del Casal (1,2,3) for transpiration cooling can be extended to ablation cooling for protection of space vehicles. The ablative cooling problem is more complex due to:

(1) the multicomponent nature of the pyrolysis gas phase,

(2) the chemical reactions of these gases with the carbonaceous layer formed during ablation, and,

(3) the extremely large temperature gradients existing between the back and front surfaces of the char

which require a variable physical properties solution to the equations of change.

However, the basic method of describing the energy and mass transfer for flow of fluids through porous media with chemical reaction is the same. In the next two sections the research of Clark (4) and Weger, et. al. (5,6) will be presented. They described the phenomena occurring in the char zone of a char forming ablator.

Clark (4) presented an analytical model for flow of methane and helium-methane mixtures through carbon and graphite matrices. The importance of thermal equilibrium between the gas and matrix was determined and the location and temperature within the porous specimens where methane underwent thermal decomposition to carbon and hydrogen was measured.

Weger, et. al. (5,6) formulated a kinetic model for predicting the physical property changes of the carbon layer resulting from carbon deposition. In particular, the effect of carbon densification on char porosity, and permeability, was discussed. Weger, et. al. (6) also postulated the reactions that contributed to carbon deposition and those that resulted in carbon depletion. The results were supported by an experimental program in which methane, aceylene, hydrogen, carbon monoxide and water were passed through carbon and graphite specimens individually and in mixtures.

Ablative Cooling Study by Clark: The research of Clark (4) extended, in part, the work of Koh and del Casal (3) to describe ablative cooling. Like Koh and del Casal (1), Clark studied the thermal non-equilibrium between a porous matrix and the gas flowing through the medium. More importantly, however, Clark investigated the thermal decomposition of methane as it passed through the carbon and graphite specimens and pinpointed the location and temperature where the decomposition occurred.

The analysis by Clark was for one-dimensional, methane and helium-methane mixtures flowing through porous carbon and graphite specimens. A heat generation term was included in the energy equation to describe the experimental results obtained using a resistance heated apparatus. The energy balance over the solid phase was:

$$k_m \frac{d^2 T_m}{dx^2} + q''' = h \, (T_m - T_f) \qquad (2\text{-}67)$$

where solid conduction and heat generation terms were equated to the convective heat transfer from the solid to the gas phase.

The energy balance relating the energy absorbed by gas convection to the convective heat transfer from the gas to the solid phase was:

$$W\bar{C}_p \frac{dT_f}{dx} = h\,(T_m - T_f) \qquad (2\text{-}68)$$

The continuity (2-5) and momentum equations (2-4) were in the form previously discussed. Heat conduction by the gas phase was considered small compared with gas convection and was omitted. Heat absorption by chemical reaction was, likewise, deleted from the energy equation.

The following summarizes the development of Clark to obtain a solution to the above equations. Combining equations (2-67) and (2-68) followed by integration resulted in equation (2-69):

$$k_m \frac{dT_m}{dx} + q''' x - W\bar{C}_p T_f + C_3 = 0 \qquad (2\text{-}69)$$

Substitution for $\frac{dT_m}{dx}$ obtained by differentiating equation (2-68) and rearranging gave a second order, non-homogeneous, linear, differential equation in T_f:

$$\frac{d^2T_f}{dx^2} + \frac{h}{W\bar{C}_p} \frac{dT_f}{dx} - \frac{h}{\bar{k}_m} T_f + \frac{h}{W\bar{C}_p k_m} q''' + C_3 = 0$$

(2-70)

The characteristic solution of equation (2-70) was given as:

$$T_c = A_1 \mathrm{Exp}[\Psi x] + B_1 \mathrm{Exp}[\xi x] \qquad (2\text{-}71)$$

where

$$\Psi = -\frac{1}{2}\frac{h}{W\bar{C}_p} + \frac{1}{2}\left[\left(\frac{h}{W\bar{C}_p}\right)^2 + 4\left(\frac{h}{k_m}\right)\right]^{1/2} \qquad (2\text{-}72)$$

and

$$\xi = -\frac{1}{2}\frac{h}{W\bar{C}_p} - \frac{1}{2}\left[\left(\frac{h}{W\bar{C}_p}\right)^2 + 4\left(\frac{h}{k_m}\right)\right]^{1/2} \qquad (2\text{-}73)$$

The particular solution of equation (2-70) was:

$$T_p = \frac{q'''x}{W\bar{C}_p} + \frac{k_m q'''}{(W\bar{C}_p)^2} + \frac{k_m C_3}{h} \qquad (2\text{-}74)$$

The general solution was the sum of equations (2-71) and (2-74):

$$T_f = A\ \mathrm{Exp}[\Psi x] + B\ \mathrm{Exp}[\xi x] + \frac{q'''}{W\bar{C}_p} + \frac{k_m q'''}{(W\bar{C}_p)^2} + \frac{k_m C}{h} \qquad (2\text{-}75)$$

Substituting for T_f into equation (2-69) followed by integration and rearrangement gave the temperature of the carbon matrix as a function of distance, x:

$$T_m = -\frac{W\bar{C}_p\xi}{h} A\ \mathrm{Exp}[\Psi x] - \frac{W\bar{C}_p\Psi}{h} B\ \mathrm{Exp}[\xi x]$$

$$+\ q'''\left[\frac{1}{h} + \frac{k_m}{(W\bar{C}_p)^2} + \frac{x}{W\bar{C}_p}\right] + \frac{k_m C}{h} \qquad (2\text{-}76)$$

Boundary conditions were required to evaluate the constants of integration, A, B, and C in equations (2-75) and (2-76). The gas temperature, radiative heat transfer and conductive heat transfer at the back surface were specified as:

$$T_f = T_{f_o}$$

$$-q_r = \sigma\bar{\epsilon}T_m^{\ 4}$$

$$-q_c = k_m\left(\frac{dT_m}{dx}\right) \quad \text{at } x = 0 \qquad (2\text{-}77)$$

and, the radiative and conductive heat transfer at the front surface were also specified:

$$q_r = \sigma\bar{\epsilon}T_m^{\ 4}$$

$$q_c = -\,k_m\left(\frac{dT_m}{dx}\right) \qquad \text{at } x = L \qquad (2\text{-}78)$$

The final equations for T_f and T_m obtained after substitution for the integration constants are given in Figure (2-10).

Figure 2-10. Equations for the Fluid and Matrix Temperatures for Flow Through Porous Media (Clark).

$$T_f = T_{f_o} + q'''\left\{\frac{x}{W\bar{C}_p} + \frac{h(\mathrm{Exp}[\Psi x] - 1)}{(W\bar{C}_p)^2\ \Psi\xi} + \frac{h(\mathrm{Exp}[\Psi L] - 1)(\mathrm{Exp}[\Psi x] - \mathrm{Exp}[\xi x])}{(W\bar{C}_p)^2\ \Psi\xi\ (\mathrm{Exp}[\xi L] - \mathrm{Exp}[\Psi L]}\right\} - \frac{(h\sigma\bar{\epsilon}T_m{}^4)_{x=0}}{k_m W\bar{C}_p \xi\Psi}$$

$$(\mathrm{Exp}[\Psi x] - 1) + \frac{h\sigma\bar{\epsilon}\left[(T_m{}^4)_{x=L} + (T_m{}^4)_{x=0}\ \mathrm{Exp}[\Psi L]\right]}{k_m W\bar{C}_p \Psi\xi\ (\mathrm{Exp}[\xi L] - \mathrm{Exp}[\Psi L])}\ (\mathrm{Exp}[\xi x] - \mathrm{Exp}[\Psi x]) \qquad (2\text{-}79)$$

$$T_m = T_{f_o} + q'''\left\{\frac{x}{W\bar{C}_p} + \frac{1}{h} + \frac{(\mathrm{Exp}[\Psi L] - 1)}{W\bar{C}_p(\mathrm{Exp}[\Psi L] - \mathrm{Exp}[\xi L]}\left(\frac{\mathrm{Exp}[\Psi x]}{\Psi} - \frac{\mathrm{Exp}[\xi x]}{\xi}\right) + \frac{h}{(W\bar{C}_p)^2\xi\Psi}\right.$$

$$\left.\left(\frac{1 + W\bar{C}_p\xi\mathrm{Exp}[\Psi x]}{h}\right)\right\} + \frac{(h\sigma\bar{\epsilon}T_m{}^4)_{x=0}}{k_m W\bar{C}_p \Psi\xi}\left(\frac{1 + W\bar{C}_p\xi\mathrm{Exp}[\Psi x]}{h}\right) +$$

$$\frac{\sigma\bar{\epsilon}\left[(T_m{}^4)_{x=L} + (T_m{}^4)_{x=0}\mathrm{Exp}[\Psi L]\right]}{k_m(\mathrm{Exp}[\xi L] - \mathrm{Exp}[\Psi L])}\left(\frac{\mathrm{Exp}[\Psi x]}{\Psi} - \frac{\mathrm{Exp}[\xi x]}{\xi}\right) \qquad (2\text{-}80)$$

A computer program was written to calculate the heat transfer coefficient, h, and the matrix and fluid temperatures, T_m and T_f, shown in equations (2-79) and (2-80).

The experimental data were used to measure the extent of thermal non-equilibrium between the gas and carbon phases. The experiments were also designed to determine whether helium-methane mixtures flowing in the carbon matrix were frozen, in chemical equilibrium or not in chemical equilibrium. Carbon deposition resulting from the cracking of methane was likewise measured.

A resistance heated apparatus was used by Clark to simulate the high temperatures ($\sim$5000°R) encountered during reentry flights. The test specimens were constructed of carbon or graphite with the facility to attach high voltage leads at either end. The center or test section of the material necked down to increase the current density and heating at that point. Flow tubes were mounted on either side of the test section with Saureisan cement. Methane and helium-methane mixtures were used to simulate the pyrolysis products formed by the thermal degradation of the plastic heat shield. Exit gas samples were obtained using a pitot tube and were analysed by gas chromatography to determine the extent of methane decomposition as the feed gas passed through the heated test section. Surface temperatures and gas stream temperatures were measured with a total radiation pyrometer and thermocouples. A pressure transducer was used to measure the pressure drop across the test section. Post-experimental investigations of the test section included density profile measurements using a mercury intrusion porosimeter and photomicrographic analyses to detect carbon deposition within the porous specimens.

The results, shown in Table 2-2 for pure methane flow, compare the solid and gas phase temperatures as a function of dimensionless thickness, η, over a range of mass fluxes and back surface temperatures. As seen, the greater the temperature gradient between the gas and solid at the inlet or back surface, the larger the temperature differences within the matrix. This is especially illustrated by comparing the values of the last column, the fractional reduction in the temperature difference from the initial condition ($\Delta T_\eta/\Delta T_o$). An increase in the mass flux from 0.003 to 0.03 $lb/ft^2 sec$ had little effect in reducing the temperature gradient compared with the effect noted for a back surface temperature decrease from 3000°R to 2000°R. In this particular investigation thermal non-equilibrium between the gas and solid is primarily caused by the resistance heating method for achieving temperature between 3000°R and 4000°R. In ablative heat protection applications the gas flowing from the pyrolysis zone into the char layer is at the local char temperature, and the abnormally

Table 2-2. Comparison of the Temperature Difference Between the Gas and Solid Phases for the Flow of Methane Gas Through Porous Matrices Having a Thickness of 0.025 to 0.033 Feet and a Porosity of 0.5.

Mass Flux lb/ft^2-sec	Back Surface Temperature °R	Inlet Gas Temperature °R	Temperature Difference, °R $\Delta T_\eta = T_s - T_g$					Fractional Reduction in the Temperature Difference $\Delta T_\eta/\Delta T_o$				
			$\eta=0$	0.25	0.50	0.75	1.00	$\eta=0$	0.25	0.50	0.75	1.00
0.039	2100	500	1600	450	250	100	- 50	1.0	0.28	0.16	0.06	-0.03
0.037	3200	500	2700	1200	600	300	-100	1.0	0.44	0.22	0.11	-0.04
0.003	3200	500	2700	1300	800	350	-100	1.0	0.48	0.30	0.13	-0.04

Note:

T_s = Solid Phase or Matrix Temperature

T_g = Gas Phase or Fluid Temperature

$\Delta T_\eta = (T_s - T_g)_\eta$

$\Delta T_o = (T_s - T_g)_{\eta=0}$

large temperature difference characteristic of the resistance heating apparatus is non-existent. Therefore, the assumption of thermal equilibrium between the gas and char in ablative cooling should be a very good approximation to the real behavior.

Clark also used this apparatus to determine whether methane thermally degraded within the heated carbonaceous specimen. The results shown as plots of methane conversion as a function of local temperature in Figures 2-11 and 2-12 indicated that frozen and equilibrium flow conditions existed at the low and high temperature ranges, respectively. The existence of a transition region between the above limiting conditions also occurred. This chemical non-equilibrium zone was found to occur between 2500°R and 3200°R for methane and helium-methane gas flow over a wide range of mass flux (0.018-0.07 lb/ft^2sec), char thickness (0.021-0.033 ft), and initial methane composition (12-100mole %) values. The following reactions were considered to take place within the carbon matrix.

$$\begin{aligned} 2CH_4 &\rightarrow C_2H_6 + H_2 \\ C_2H_6 &\rightarrow C_2H_4 + H_2 \\ C_2H_4 &\rightarrow C_2H_2 + H_2 \qquad (2\text{-}81) \end{aligned}$$

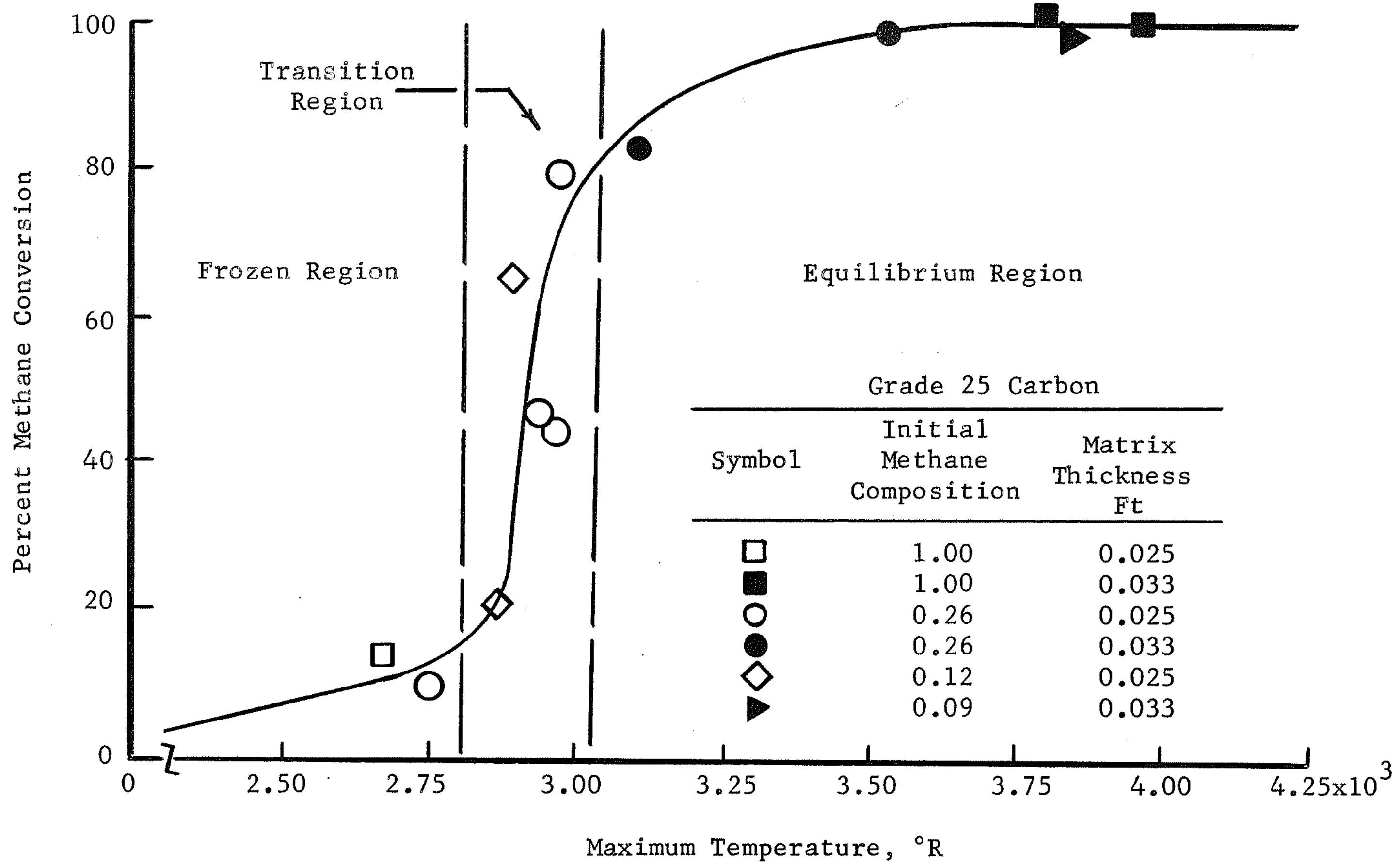

Figure 2-11. Frozen, Transition and Equilibrium Regions for the Thermal Decomposition of Methane to Carbon and Hydrogen in a Porous Carbon Matrix.

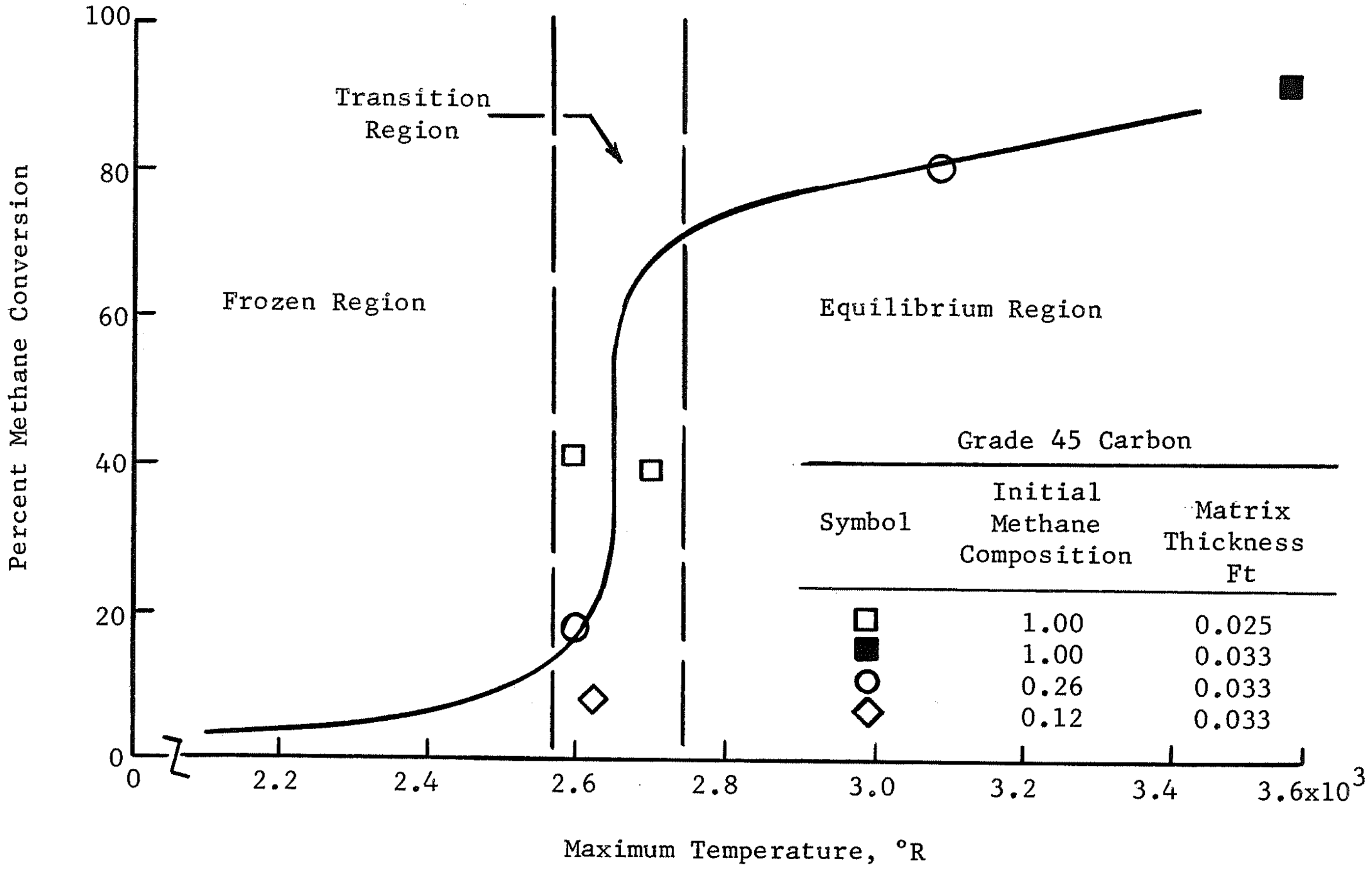

Figure 2-12. Frozen, Transition and Equilibrium Regions for the Thermal Decomposition of Methane to Carbon and Hydrogen in a Porous Carbon Matrix.

Comparison of the results for two grades of carbon were presented. These results were compared with gas chromatographic analyses of the exit gases as a function of temperature, and are presented in Figures 2-11 and 2-12. Some differences between the experimental and calculated results were attributed to differences in the internal pore structure which, according to the author, changed the thermal conductivity of the specimens.

The internal pore structure may certainly change from specimen to specimen. However, more importantly, were the changes resulting from carbon deposition. The densification effect resulted from the degradation of methane to hydrogen and carbon within the carbon and graphite specimens. This fact was also noted by pressure drop measurements and in post-experimental investigations of the specimens by photomicrographic analysis.

In order to summarize the research of Clark (4) presented in the foregoing sections, three important conclusions are stated.

(1) There was a noted temperature lag between the gas and solid phases within the porous, resistance heated matrices. These large differences were primarily a result of the high initial temperature gradient (2000-3000°R) at the back surface produced by the resistance heating technique to achieve high temperatures (3000-4000°R) within the

matrix. When using a radiant heating device where the initial temperature gradient is significantly smaller (gas = 600°R, back surface = 1200°R), the assumption of thermal equilibrium should be a very good approximation to the actual behavior for a one dimensional gas flow through a porous char.

(2) Although the choice of methane gas as a typical hydrocarbon pyrolysis product was an over simplification, the identification of a transition region within the porous matrix was very relevant. This region, defined when methane gas flow in the porous specimen changes from a frozen to a chemical equilibrium flow, occurred between 2500°R - 3200°R. Since ablative heat shields on reentering spacecraft experience temperatures between 1500°R and 5000°R across the char layer, this non-equilibrium, transition region could be an important mode of energy absorption.

(3) Carbon deposition in the pores of the various specimens was caused by the thermal cracking of methane to carbon and hydrogen. A noted increase in the amount of carbon deposited was observed for increases in temperature since the pyrolysis of methane became more pronounced at the higher temperatures. This latter conclusion supported the results of Weger, *et*. *al*. (5,6) discussed

in the following section.

Carbon Deposition Studies by Weger, et. al. (5,6): The basic objectives of Weger, et. al. (5,6) were to obtain reliable experimental data necessary for developing analytical models for predicting changes in the physical properties of the char zone during reentry. Emphasis was placed on the chemical reactions taking place between the pyrolysis gas products and the char resulting in either carbon deposition or depletion. This change in carbon density within the char produced variations in such properties as porosity, permeability and tortuosity.

In the first of two reports, Weger, et. al. (5) studied the flow of methane and nitrogen-methane mixtures within chars, and carbon or graphite specimens having porosities between 0.20 - 0.35. In the second report, (6), the investigations were extended to include such gases as acetylene, hydrogen, carbon monoxide, water, methane and mixtures of these to better simulate the pyrolysis products from nylon-phenolic resin composites.

In both studies an induction furnace was used to heat the porous specimens. The gas flow was passed radially through the cylindrical chars which were heated to temperatures between 2500°F and 4000°F. The exit gas stream was analysed by gas chromatography and, in the case of methane (5), compared with values calculated using reaction rate data. Photomicrographs and pressure drop measurements on the specimen were also made.

In order to describe the flow of gases through porous media, a modified form of Darcy's Law was used. This form included a term that accounted for inertial effects resulting from the relatively large mass flux values (0.01-0.04 lb/ft^2sec) studied. This equation is:

$$-\frac{dP}{dy} = \alpha\mu v_y + \beta\rho v_y^2 \tag{2-82}$$

where α and β were the viscous and inertial coefficients and μ, ρ and v_y were the viscosity, density, and radial component of the gas velocity. Integration of equation (2-82) over the specimen wall thickness resulted in an expression for the pressure distribution.

$$P = \left[P_2^2 - \frac{RT}{\pi L \Upsilon_o} \int_{y_2}^{y} \frac{\mu[QP/RT]}{(r_1 + y)M} dy\right]^{1/2} \tag{2-83}$$

In addition to the pressure distribution, Weger, et. al. developed an equation relating the change in permeability of the specimen as a function of experimental time. This value, called the mobility, was defined as the ratio of the permeability at any instant during the experiment to the permeability of the material prior to gas flow through the pores (γ/γ_o). It was a measure of the resistance to flow caused by carbon deposition and was derived for the first order decomposition of methane gas to carbon and hydrogen. In differential form, the mobility equation is:

$$\left.\frac{\partial M}{\partial t}\right|_y = \frac{C_1 M\left(\frac{P}{P_1}\right) \mathrm{Exp}\left[C_2 \int_o^y \frac{M^{\frac{1}{2}}(r_1+y)}{Q}\, dy\right]}{1 + \left(\frac{n_{CH4}}{n_T}\right)_1 \left[1 - \mathrm{Exp}\left[C_2 \int_o^y \frac{M^{\frac{1}{2}}(r_1+y)}{Q}\, dy\right]\right]} \tag{2-84}$$

where r_1, is the radius of the inside wall and the subscript 1 indicated evaluation of the parameter at the inside wall surface. A detailed derivation can be found in the original work by Weger, et. al. (5). No mobility calculations were presented in the second report (6) for the non-equilibrium flow of the other gases that were studied. However, a qualitative discussion of the various reactions and associated reaction rate expressions was presented.

In order to solve equations (2-83) and (2-84) for the pressure and mobility distributions within the specimen, the value of the total volumetric flow rate, Q, must be specified. This value was calculated for methane assuming the ideal gas equation of state:

$$Q = \frac{RT}{P}\left[(n_T)_o + (n_{CH_4})_o - n_{CH_4}\right] \qquad (2\text{-}85)$$

where n represented the total number of moles present and the subscript, o, indicated initial values.

The instantaneous value of the methane concentration was determined by:

$$n_{CH_4} = (n_{CH_4})_o \text{ Exp}\left[C_2 \int_o^y \frac{M^{\frac{1}{2}}(r_1+y)}{Q}\, dy\right] \qquad (2\text{-}86)$$

The constants C_1 and C_2 in the above equations were evaluated from methane decomposition data as:

$$C_1 = \frac{-2k^\circ \text{Exp}[-\frac{E}{RT}](\frac{n_{CH_4}}{n_T})_1\ P_1\ (MW)_d}{RT\rho_d} \qquad (2\text{-}87)$$

and

$$C_2 = -2k^\circ \text{Exp}\ [-\frac{E}{RT}]\ \pi L \epsilon_o \qquad (2\text{-}88)$$

where k° was the frequency factor in the reaction rate equation, E was the activation energy, $(M_w)_d$ was the molecular weight of the carbonaceous deposit and ρ_d was the density of the deposited carbon. The subscripts 1 and 2 referred to the inside and outside surfaces of the specimen in the above equations.

The simultaneous solution of equations (2-83), (2-84), (2-85) and (2-86) resulted in the desired values for the mobility, M; the flow rate, Q; the pressure, P; and the methane concentration, n_{CH_4}, as a function of experimental time. The comparison of the calculated mobility, and the experimental values are shown in Figure 2-13. As seen, very good agreement was obtained between the calculated values based on reaction kinetics data for methane and the experimental data.

Similar curves were presented for the other gases studied in the second part (6) of the investigation. With reference to Figures 2-13 and 2-14, methane and acetylene decomposition resulted in decreased values of mobility with time. This was due to carbon deposition as indicated by the following reactions:

$$CH_{4(g)} \rightleftarrows C_{(s)} + 2H_{2(g)} \tag{2-89}$$

$$C_2H_{2(g)} \rightleftarrows 2C_{(s)} + H_{2(g)} \tag{2-90}$$

The much sharper decrease in the mobility for acetylene was attributed to the formation of twice the amount of solid carbon per mole of gas as indicated in reactions (2-89) and (2-90).

Carbon monoxide and hydrogen flow did not effect a permeability change indicating no carbon deposition or depletion over the 2500°F - 4000°F temperature range studied. These results were supported by various literature sources (5 , 6) which indicated equations (2-91) and (2-92) to be

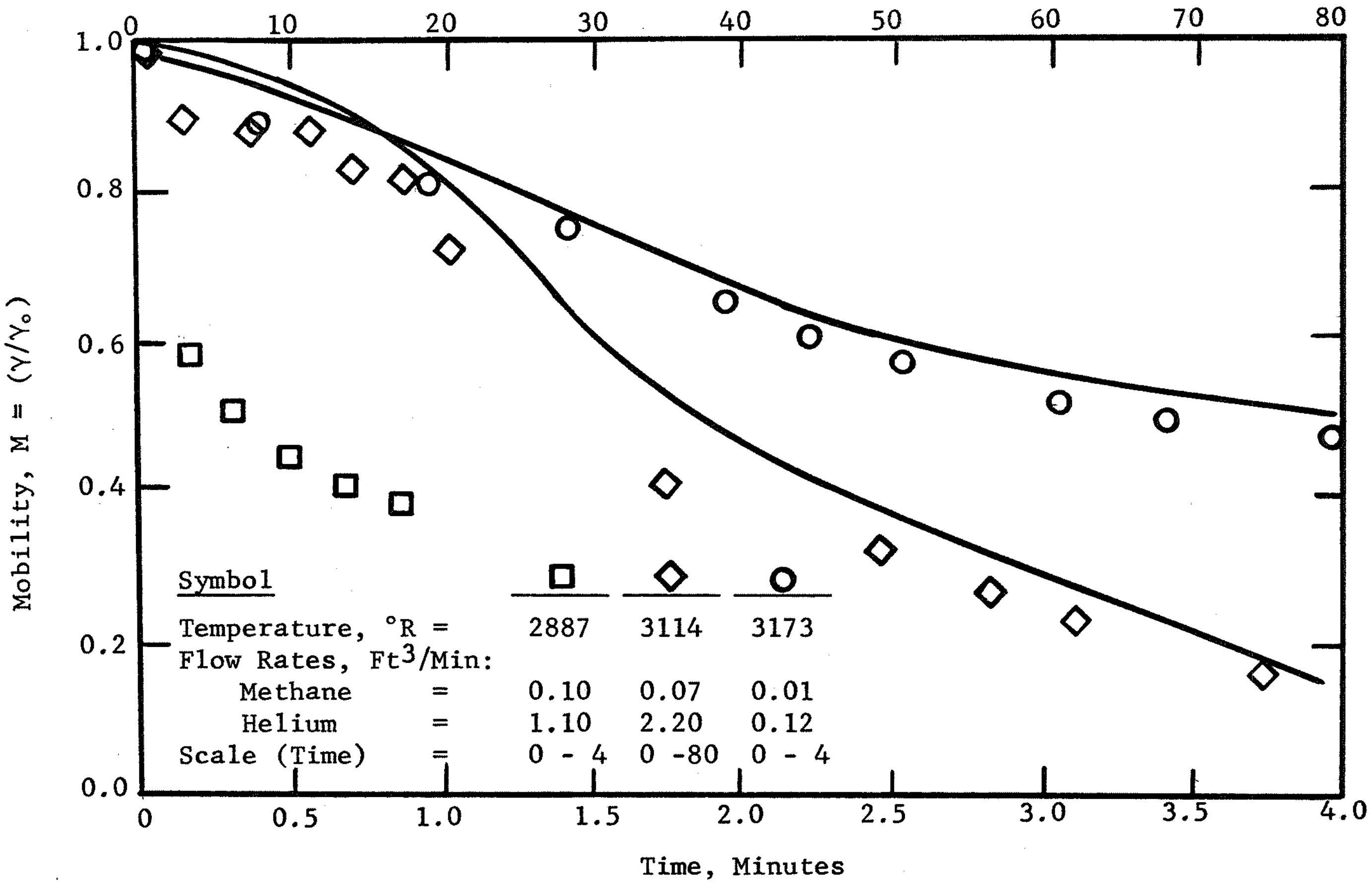

Figure 2-13. Experimental and Calculated Values of the Mobility for Methane-Helium Flow Through Porous Media.

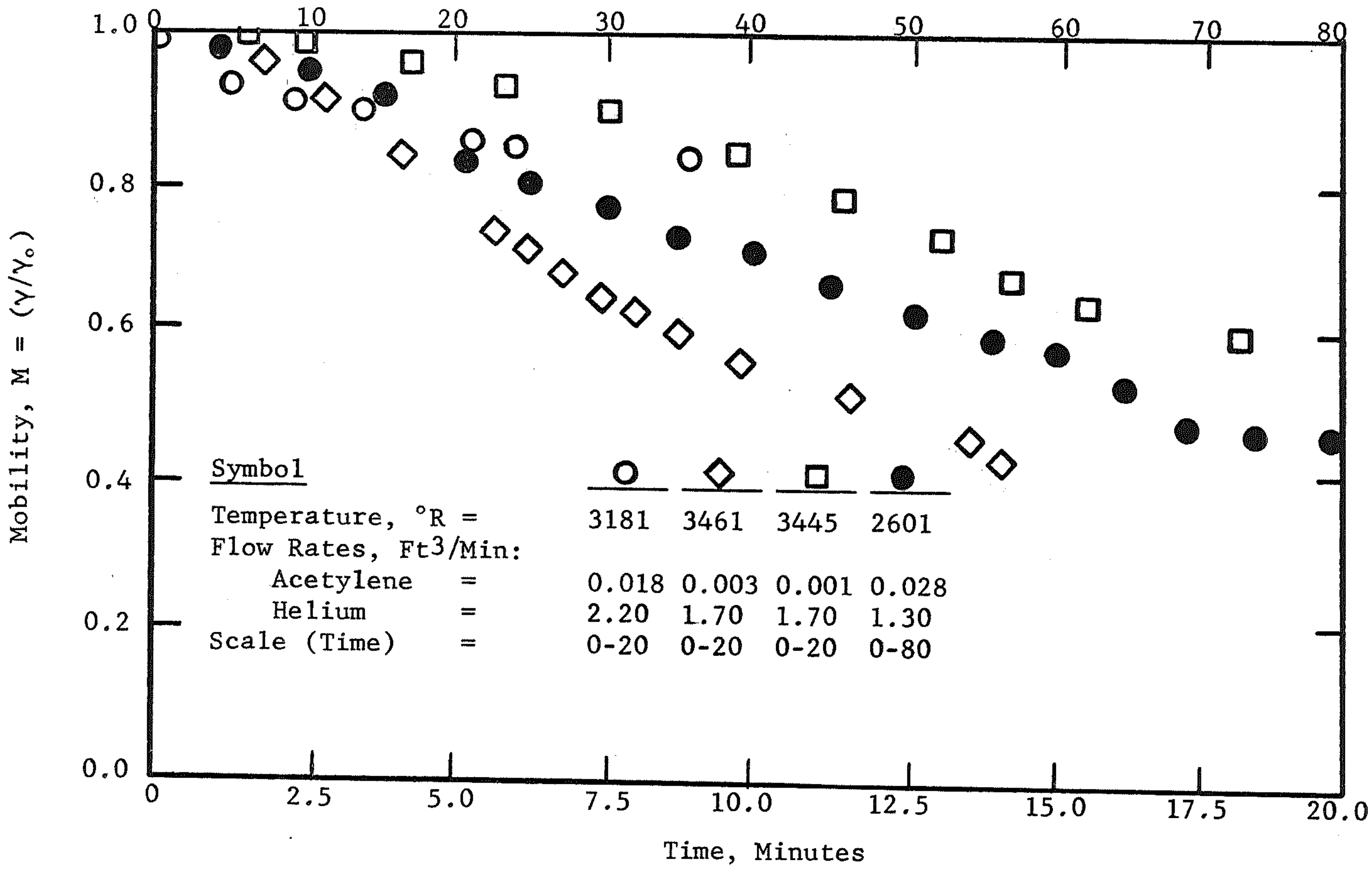

Figure 2-14. Experimental Values of the Mobility for Acetylene-Helium Flow Through Porous Media.

significant only above 4500°R.

$$2CO_{(g)} \rightleftarrows CO_{2(g)} + C_{(s)} \tag{2-91}$$

$$2H_{2(g)} + C_{(s)} \rightleftarrows CH_{4(g)} \tag{2-92}$$

Water, as steam, reacted with the porous specimen to deplete carbon. This fact was supported by a sharp increase in the mobility with time shown in Figure 2-15. The net reaction occurring was written as:

$$H_2O_{(g)} + C_{(f)} \rightleftarrows CO_{(g)} + H_{2(g)} \tag{2-93}$$

where $C_{(f)}$ was defined as a free active site on the specimen surface. A mechanism was presented relating the transition of interior carbon atoms to carbon at an active location. The water-gas shift reaction was also indicated to occur explaining the presence of carbon dioxide.

$$CO_{(g)} + H_2O_{(g)} \rightleftarrows CO_{2(g)} + H_{2(g)} \tag{2-94}$$

Results were also presented for various mixtures of the gases studied shown in Figures 2-16, 2-17 and 2-18. The most significant conclusion was that above 2200°F hydrogen

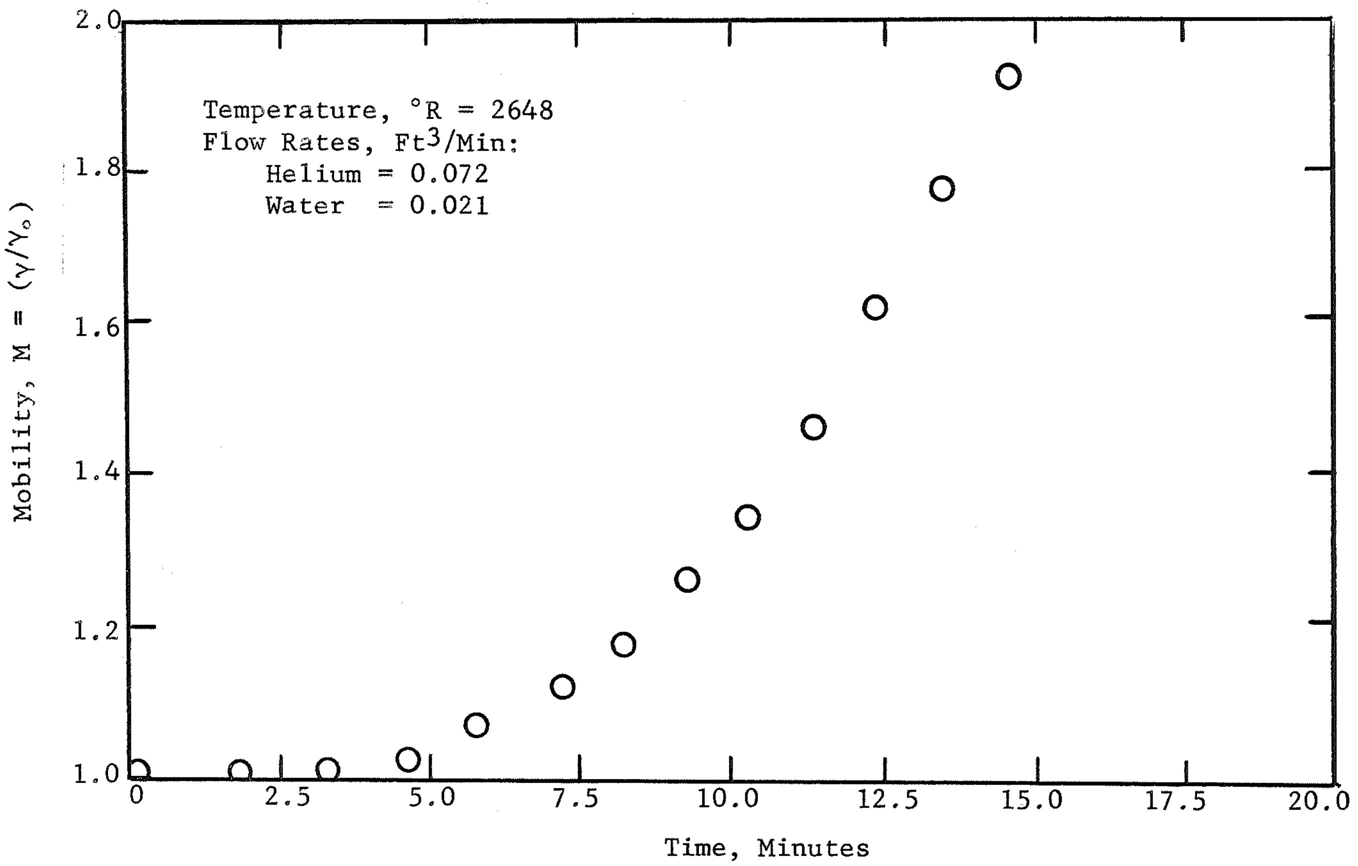

Figure 2-15. Experimental Values of the Mobility for Water-Helium Flow Through Porous Media.

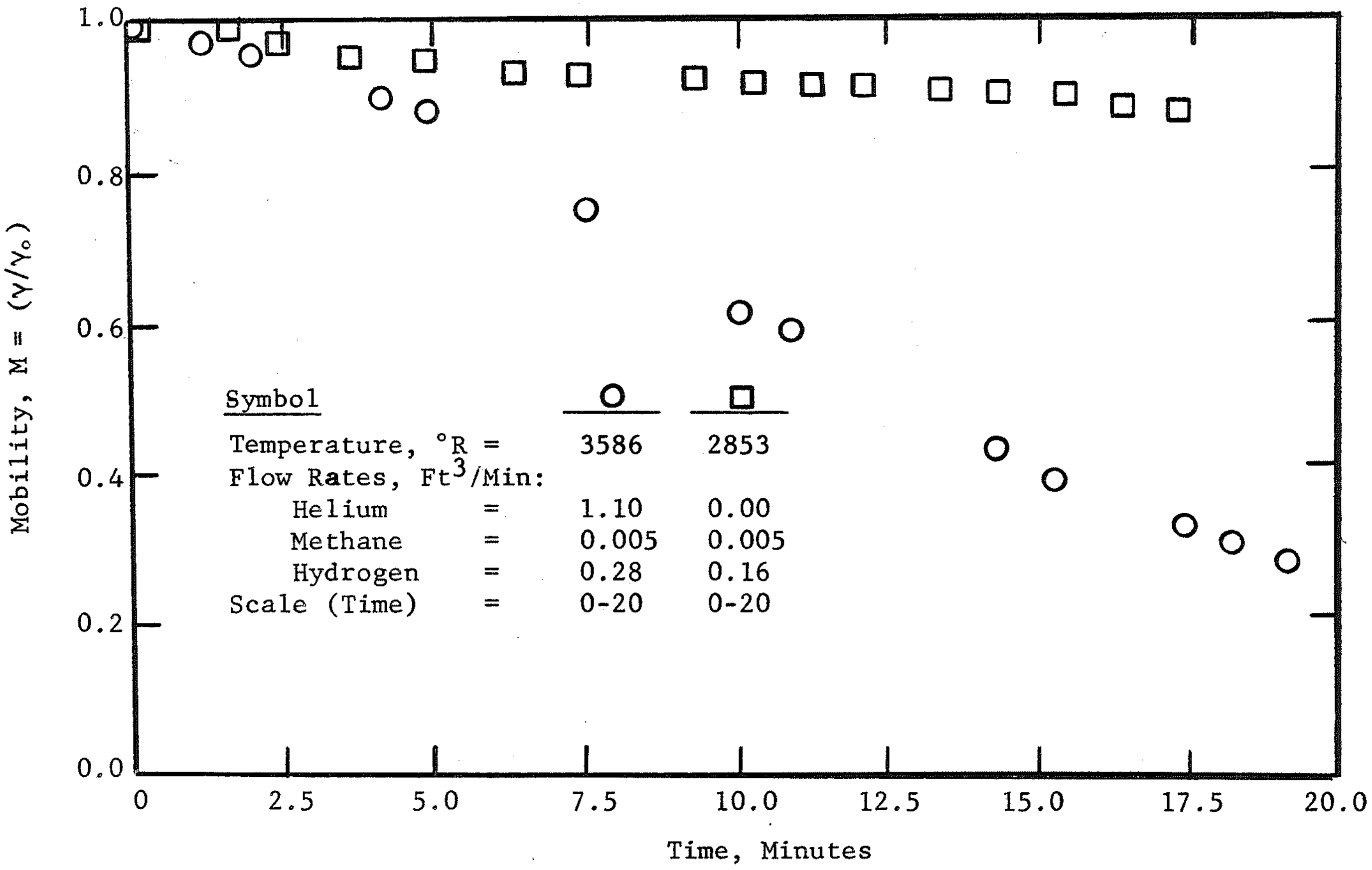

Figure 2-16. Experimental Values of the Mobility for Methane-Hydrogen-Helium Flow Through Porous Media.

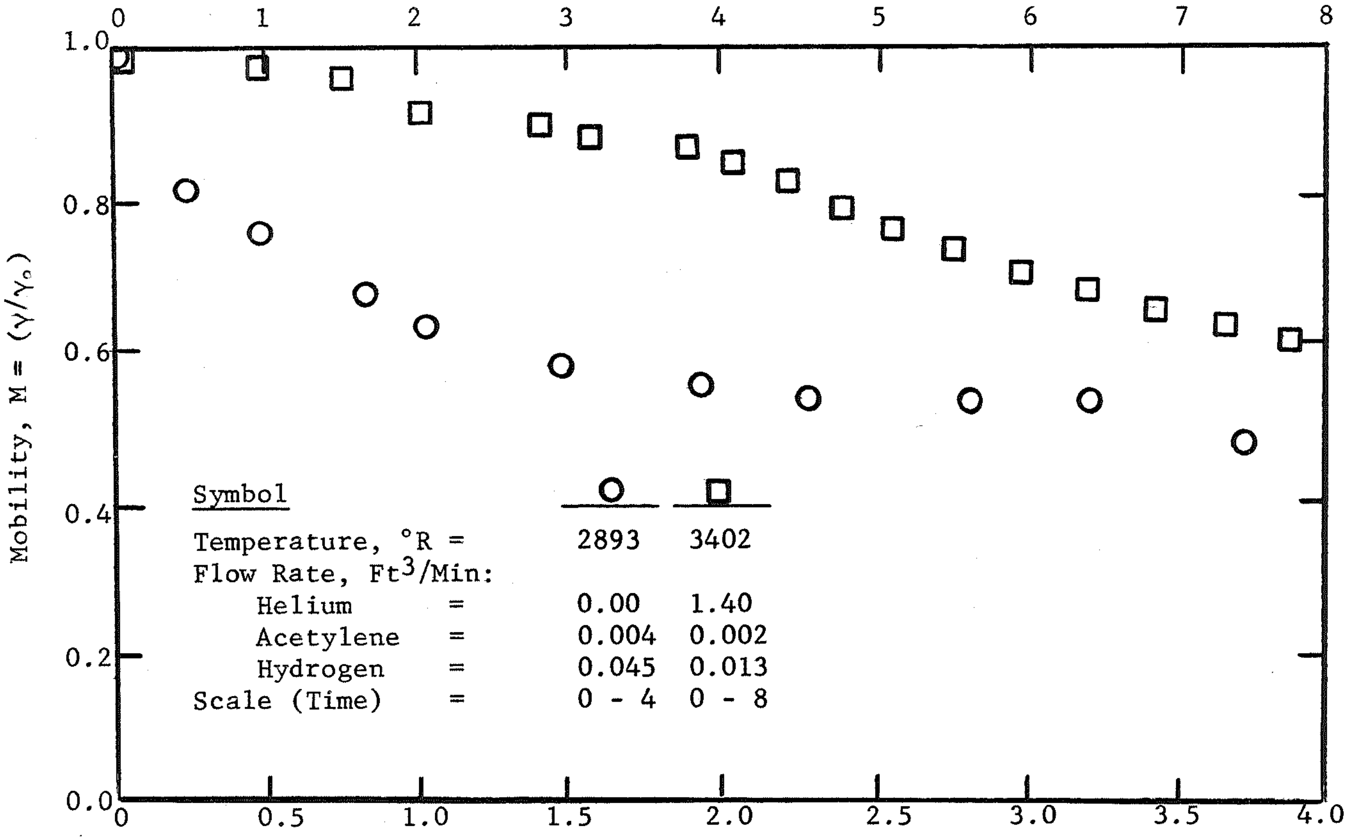

Figure 2-17. Experimental Values of the Mobility for Acetylene-Hydrogen-Helium Flow Through Porous Media.

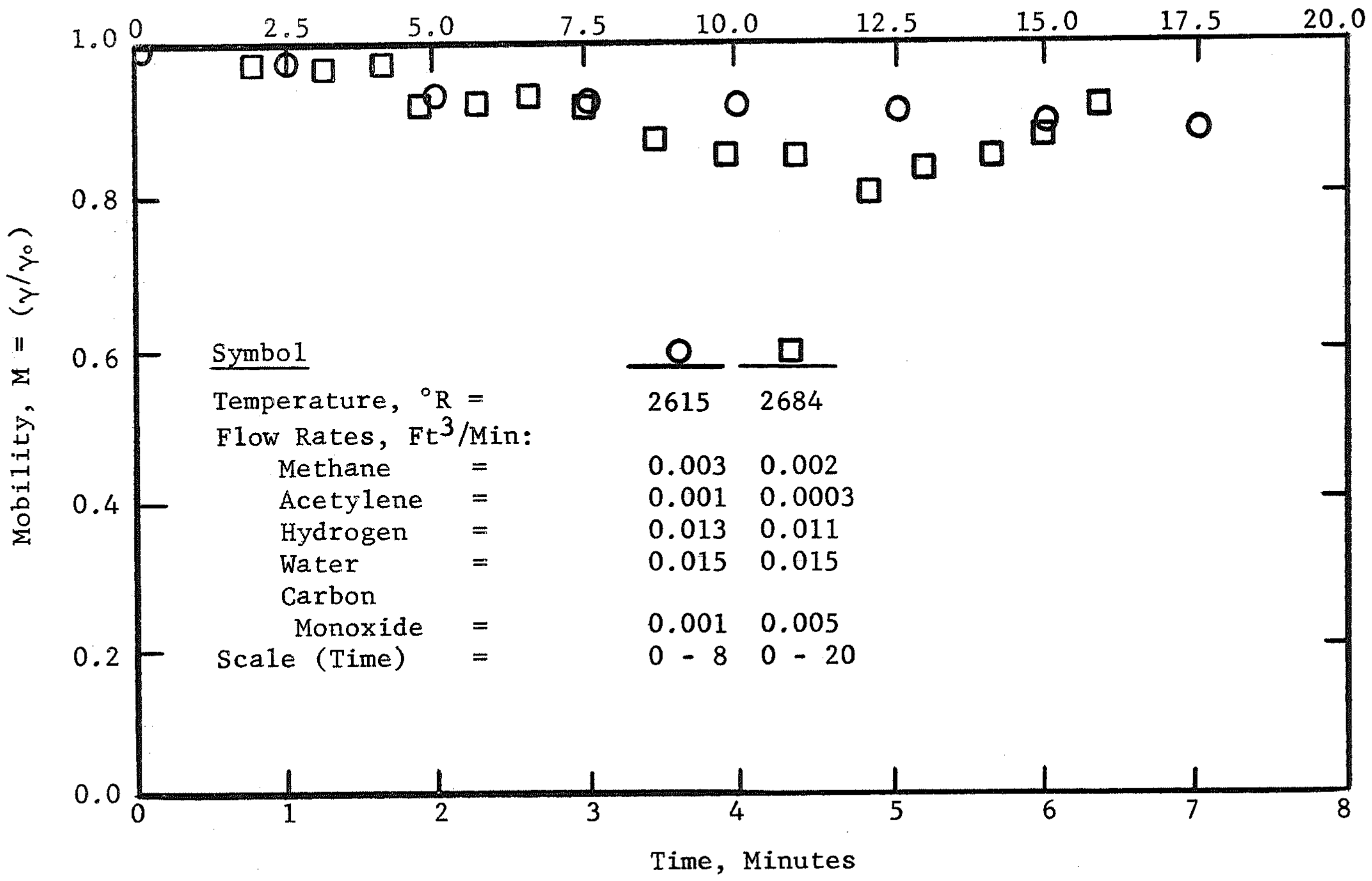

Figure 2-18. Experimental Values of the Mobility for the Flow of Various Gas Mixtures Through Porous Media.

did not affect the decomposition of methane. Below this temperature a noted decrease in the decomposition rate of methane was observed.

In summary, the research of Weger, et. al. was not only important in defining the types of reactions contributing to carbon deposition and depletion, but equally valuable in establishing a relationship between the non-equilibrium decomposition reactions (for methane) and the physical property changes within the char. In experiments where no carbon deposition or depletion resulted, the permeability of the porous materials was constant. However, sharp changes were measured when deposition or depletion of carbon occurred. The materials studied were low porosity specimens (0.20 - 0.35), and the effect of these changes in higher porosity chars (>0.5) was not determined. It was also found that the modified form of Darcy's law including inertial and viscous terms predicted the pressure drop across the porous specimens more accurately than the form neglecting inertial effects.

Summary of Previous Research on Flow in the Char Zone:

In the foregoing sections, several methods for analysing thermal and chemical non-equilibrium flow of fluids through porous media were reviewed. A considerable amount of information pertaining to the problems associated with the formulation of an accurate mathematical model for predicting energy transfer in the char layer was presented. These results are especially useful in evaluating the magnitude of the terms in the equations of change to develop a model of the energy transfer in the char zone. The important conclusions obtained from the discussed works by Koh and del Casal (1,2,3), Clark (4) and Weger, *et*. *al*. (5,6) are presented below with this idea in mind.

Thermal Equilibrium Between the Gas and Char: The existence of thermal equilibrium between the gas and solid phases greatly reduces the complexity of the equations of change required to describe the system (1). A slight difference in the local gas and solid temperatures is likely to exist; however, the effect on energy transfer within the char is small.

Clark (4) reported differences of 200°R to 800°R at the midpoint of 0.021 - 0.033 foot thick graphite and carbon matrices over a wide range of mass flux values, 0.018 to 0.07 $lb/ft^2 sec$. These large differences were a result of the initial gradient (2000-3000°R) between the gas and solid at the matrix back surface. This abnormally large gradient is produced by the resistance heating apparatus used to simulate high temperature reentry (~4000°R), and is not representative of the condition at the back surface of the char.

Instead, the pyrolysis gas and char back surface temperatures are approximately equal to the plastic decomposition temperature (~1500°R). Since no large initial gradient between the gas and solid phases exist, and, since the trend within the char layer is toward thermal equilibrium, this assumption should be valid.

Variable Physical Properties: The assumption of constant physical properties is only valid over a relatively small temperature range. However, in ablative cooling applications where the temperature gradient between the front and back surfaces exceeds 3000°R, changes in physical properties must be expected.

Koh and del Casal (1) noted a large difference in the results obtained between the constant and variable fluid physical properties models when considering solid matrices with porosities greater than 0.5. This was apparently attributed to the increasing importance of gas convective heat transfer in the high porosity materials. The only modes of energy transfer accounted for were gas convection and solid conduction. In ablative cooling using nylon-phenolic resin chars with porosities between 0.7 - 0.8, the gas convection term will be significant and hence properties must be considered variable over the large temperature range.

With regard to the solid or char properties, Weger, et. al.

(5,6) found that char porosity and permeability changed measureably when carbon deposition and/or depletion occurred within the region. However, these results were limited to methane flow through low porosity materials (0.2 - 0.35). The effect of these changes on the pressure drop and energy transfer for high porosity materials (0.7 - 0.8) was not determined. Until more pertinent data are obtained such that the permeability and porosity changes can be incorporated into the model, these values are taken as constant in high porosity chars. This is a very good approximation in any porous material if carbon deposition and/or depletion is negligible.

Modified Form of Darcy's Law: The momentum equation for flow through porous media takes the form of Darcy's empirical equation. This equation relates the fluid velocity to the pressure drop within the porous media. Weger, et. al. (5,6) found that a better prediction of the pressure drop across the porous specimens tested was obtained when a modified form of Darcy's Law including inertial effects was used. Inertial effects become significant for mass flux values exceeding (0.01 lb/ft^2sec). Since in ablative cooling applications, mass flux values as large as 0.05 lb/ft^2sec are encountered, the modified form of Darcy's Law should be used.

Various Modes of Energy Absorption: In all of the papers reviewed dealing with the prediction of temperature distributions within porous media, gas convection and solid conduction were included as the major modes of heat transfer. Heat transfer by gas conduction was usually neglected as small in comparison with the above mentioned modes.

Koh and del Casal (3) presented results which defined clearly when gas conduction could be neglected. This occurred at either high gas flow rates or small temperature gradients across the porous material. At low flow rates (<0.01 lb/ft^{2}sec) or large temperature gradients (>2500°R), energy absorption by gas conduction becomes important. Both of these conditions are evident in ablation cooling applications. Therefore, any realistic model should include gas heat conduction in the derived energy equation. Energy absorption by chemical reaction is also important and will be discussed in the following section.

Chemical Non-Equilibrium Flow: Koh and del Casal (2), Clark (4) and Weger, et. al. (5,6) recognized the importance of chemical reactions of the flowing gas phase within the porous medium. Koh and del Casal (2) and Clark (4) considered chemical reactions an important mode of energy absorption, while Weger, et. al. (5,6) used them to explain changes in physical properties of the porous specimens by deposition or depletion of carbon.

The identification of a non-equilibrium or transition region for methane gas flow in carbon (or graphite) specimens was made by Clark (4). This transition region occurred between 2500-3200°R which is well within the range of temperatures experienced during ablation (1500-5000°R). It is very likely that the more complex pyrolysis products obtained during reentry would undergo similar transitions from a frozen, through non-equilibrium to equilibrium flow over a wide range of temperatures. Therefore a non-equilibrium flow analysis is required to accurately predict the energy absorption within the char layer.

This fact was likewise reported by Weger, _et_. _al_. (6) who identified a variety of reactions among the gases thought to be a part of the pyrolysis gas stream. The existence of a chemical non-equilibrium reaction for methane was proven by experimental measurement of carbon deposition within the porous specimens.

Accurate Description of the Pyrolysis Products: In order to simulate the flow of gases resulting from the thermal decomposition of a nylon-phenolic resin composite, an accurate description of the various components must be available. In all of the previous research to date, simplified gases (helium, methane, etc.) or gas mixtures (methane, carbon monoxide, carbon dioxide, hydrogen, etc.) were used. While these constitute a portion of the decomposition products expected, they do not represent the entire pyrolysis product composition. Concurrent with this research is work being done by Nelson (11) and Sykes (12) at N.A.S.A.'s Langley Research Center to identify the products of pyrolysis. These and other results have been used continually through this study to achieve an accurate description of the pyrolysis product stream entering the back surface. A discussion of the methods of selecting the species composition in the pyrolysis gas entering the char zone is presented in Appendix G .

Proper Chemical Reactions and Associated Reaction Kinetic Data: Also essential to a correct prediction of the energy transfer in a char layer is the selection of the proper chemical reactions for describing the non-equilibrium flow of the gases. A continuous search and screening technique has been used during this study to update the reactions included in the model. Each reaction chosen for the model must be based on the pyrolysis products initially present and those gases leaving the char at the front surface. The temperature gradient across the char is also an important parameter.

More difficult than finding specific chemical reactions is the task of locating accurate kinetic data for those reactions considered. This problem covers the range of not finding any data to finding several sources of data which are contradictory in nature. In each case, a difficult solution to the problem results. Much of the technique used to screen this data is presented in Chapter III.

The above summary of previous research has illustrated some of the important considerations that must be included in any realistic model used for predicting the energy transfer in the char zone of a charring ablator. These results, along with other fundamental knowledge regarding the ablative cooling process, form a basis on which an accurate mathematical model can be formulated. This is the primary objective of this research.

In the following chapters, the equations of change will be developed subject to the restrictions defined by the previous research discussed in this chapter. Solutions of these equations for frozen, chemical equilibrium, and chemical non-equilibrium flow will be obtained using numerical methods of computation. Finally, these analytical results will be compared with each other and with experimental data to determine the reliability of the formulated flow model.

REFERENCES

1. Koh, J. C. Y. and E. P. del Casal, "Heat and Mass Flow Through Porous Matrices for Transpiration Cooling," Paper 16, Proceedings of the 1965 Heat Transfer and Fluid Mechanics Institute, Stanford University Press, Los Angeles, California, 263-81 (June 21-23, 1965).

2. Koh, J. C. Y. and E. P. del Casal, "Heat and Mass Transfer with Chemical Reactions for Fluid Flow Through a Porous Matrix in Re-Entry Thermal Protection," A.I.A.A. Fourth Aerospace Sciences Meeting, Los Angeles, California (June 27-29, 1966).

3. Koh, J. C. Y., E. P. del Casal, R. W. Evans, and V. Deriugin, "Fluid Flow and Heat Transfer in High-Temperature Porous Matrices for Transpiration Cooling," Technical Report AFFDL-TR-66-70, The Boeing Company, 207 pages (May 1966).

4. Clark, Ronald K., "Flow of Hydrocarbon Gases in Porous Media at Elevated Temperatures," M.S. Thesis, University of Virginia, 108 pages (August 1968).

5. Weger, Eric, Jere Brew and Roger Schwind, "An Investigation of Carbon Deposition in Chars," Report BSD-TR-66-385, Washington University, St. Louis, Missouri, 84 pages (1966).

6. Weger, Eric, Jere Brew and Ronald Servais, "An Investigation of Carbon Deposition in Chars - II," Report SAMSO-TR-68-123, Washington University, St. Louis, Missouri, 96 pages (January 1968).

7. April, G. C., R. W. Pike and E. G. del Valle, "Solution of the Frozen Flow Energy Equation," NASA-CR-77026 (July 1966).

8. April, G. C., R. W. Pike and E. G. del Valle, "Transport Phenomena in the Char Zone During Ablation. I: Evaluation of the Energy Transfer for Frozen and Equilibrium Flow," Paper 13d, 63rd National Meeting of the A.I.Ch.E., Salt Lake City, Utah (May 1967).

9. del Valle, E. G., R. W. Pike and G. C. April, "Transport Phenomena in the Char Zone During Ablation. II: Equilibrium Composition of Degradation Products of Ablation," Paper 13e, 63rd National Meeting of the A.I.Ch.E., Salt Lake City, Utah (May 1967).

10. April, G. C., R. W. Pike and E. G. del Valle, "Non-Equilibrium Flow and the Kinetics of Chemical Reactions in the Char Zone," Symposium on Ablative Plastics, 155th National A.C.S. Meeting, San Francisco, California (April 1968).

11. Nelson, James B., "Determination of Kinetic Parameters of Six Ablation Polymers by Thermogravimetric Analysis," NASA TN D-3919 (April 1967).

12. Sykes, George F., Jr., "Decomposition Characteristics of a Char-Forming Phenolic Polymer Used for Ablative Composites," NASA TN D-3810 (February 1967).

13. Ladacki, Michael, Janet V. Hamilton and Samuel N. Cohz, "Heat of Pyrolysis of Resin in Silica-Phenolic Ablator," AIAA Journal, 4 (10), 1798 (October 1966).

14. Freidman, Henry L., "Pyrolysis of Plastics in a High Vacuum Arc Image Furnace - II," Journal of Applied Polymer Science, 9, 1005-18 (1965).

15. Kendall, Robert M., Eugene P. Bartlett, and Ronald A. Rindal, "A Multi-component Boundary Layer Chemically Coupled to an Ablating Surface," AIAA Journal, 5 (6), 1063 (June 1967).

16. Swann, Robert T., Claud M. Pittman and James C. Smith, "One Dimensional Numerical Analysis of the Transient Response of Thermal Protection Systems," NASA TN D-2976 (September 1965).

17. Scala, S. M., "A Study of Hypersonic Ablation," General Electric Co., Missile and Space Vehicle Department, Report R59SD438 (September 1959).

18. Scala, S. M. and L. M. Gilbert, "Thermal Degradation of a Char-Forming Plastic During Hypersonic Flight," ARS Journal, 32 (6), 917-24 (June 1962).

19. Barriault, R. J. and J. Yos, "Analysis of the Ablation of Plastic Heat Shields that Form a Charred Surface Layer," ARS Journal, 30 (9), 823-9 (September 1960).

20. Myers, H. and D. B. Harmon, Jr., "Energy Transfer Processes in Decomposing Polymeric Systems," Douglas Aircraft Co., Missile and Space Systems Division, Report 1020 (September 1960).

21. Kratsch, K. M., L. F. Hearne and H. R. McChesney, "Thermal Performance of Heat Shield Composites During Planetary Entry," AIAA-NASA National Meeting, Palo Alto, California, 3 (September 30-October 1, 1963).

22. Green, D. W. and R. H. Perry, "Heat Transfer With a Flowing Fluid Through Porous Media," Heat Transfer, ed. by J. W. Westwater, Gas Chemical Engineering Symposium Series, 57 (32) (1961).

23. Turnacliff, R. D., *An Experimental Study of Local Convective Heat Transfer and Pressure Drop for Laminar and Turbulent Flow of Air Within a Uniformly Packed Bed of Spheres*, Ph.D. Dissertation, University of Minnesota (1957).

III. DEVELOPMENT OF THE MATHEMATICAL ANALYSIS FOR REACTING FLOW IN THE CHAR ZONE OF A CHARRING ABLATOR

Introduction

The momentum, energy and mass transfer associated with the flow of the pyrolysis products through the char layer of a char-forming ablative plastic is considered. The pyrolysis products, formed by the thermal degradation of the plastic heat shield, enter the char layer at the decomposition temperature of the plastic. The products experience a temperature increase as they flow through the char and undergo thermal cracking to lower molecular weight species which react with each other and with the carbonaceous char layer. These predominantly endothermic reactions are important modes of energy absorption and must be included in any realistic analysis of the energy transfer in the char layer.

One of the main objectives of this research is to develop an accurate and realistic mathematical model that describes the transport phenomena in the char zone. The description of the momentum, energy and mass transfer within the char will be obtained by reducing the general equations of change (continunity, momentum and energy) to forms applicable to non-equilibrium flow in the char. The resulting equations will also be simplified for the cases of frozen and equilibrium flow. Lastly, typical boundary conditions will be specified, followed by a discussion of the numerical solution of the equations.

Statement of the Problem

The mathematical model describing the transport phenomena taking place when pyrolysis products pass through the char zone of a charring ablator has the form of a one dimensional and steady flow. A schematic diagram showing the pyrolysis gas flowing through the porous char layer is depicted in Figure 3-1. As indicated, the pyrolysis products enter the char at the decomposition temperature, T_o, and exit at a higher front surface temperature, T_L. Changes in the mass flux of the various species within the char occur as a result of chemical reactions at finite reaction rates, R_j. A pressure drop $(P_o - P_L)$ across the char is also experienced.

The particular restrictions and assumptions made in the formulation of the model will be presented and justified in the following paragraphs. The use of these restrictions to simplify the general equations of change will follow. The solution of the resulting equations for frozen, equilibrium and non-equilibrium flow within the char zone will complete the chapter.

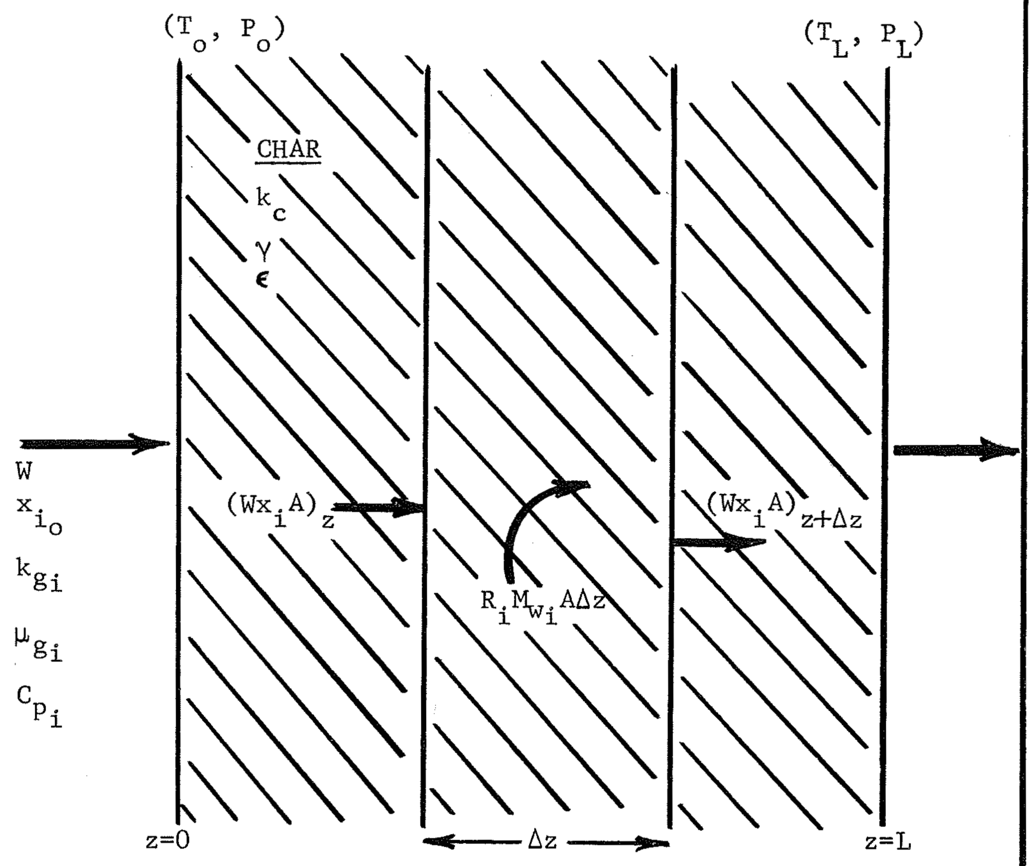

Figure 3-1. Schematic Diagram of the Char Zone.

Restrictions to the General Equations of Change for Flow in the Char Zone

To solve any realistic problem, certain simplifying assumptions and/or restrictions must be applied which reduce the complexity of the general equations of change. In the following sections, the various restrictions which apply to this particular problem are presented and justified.

One Dimensional, Steady Flow of Pyrolysis Products in the Char Zone: The flow of pyrolysis gases within the char zone is a steady state process since the char thickness is constant with respect to time after an initial short, transient period. During this short period the char layer builds up due to unequal rates of ablation and surface removal. The data of Peters and Wadlin (1) in Figure 3-2 for a 50:50 weight ratio nylon-phenolic resin ablative composite formed in a subsonic electric air arc jet shows this graphically. Also the residence time of a particle of pyrolysis gas fluid is very short compared to the rate of change of the char surfaces.

In addition to the above, the radius of curvature of reentering capsules (eg., Mercury, Gemini and Apollo spacecraft), is small in comparison with the char thickness such that flow is one dimensional and normal to the front surface. This restriction does not apply at the edge where flow in the radial

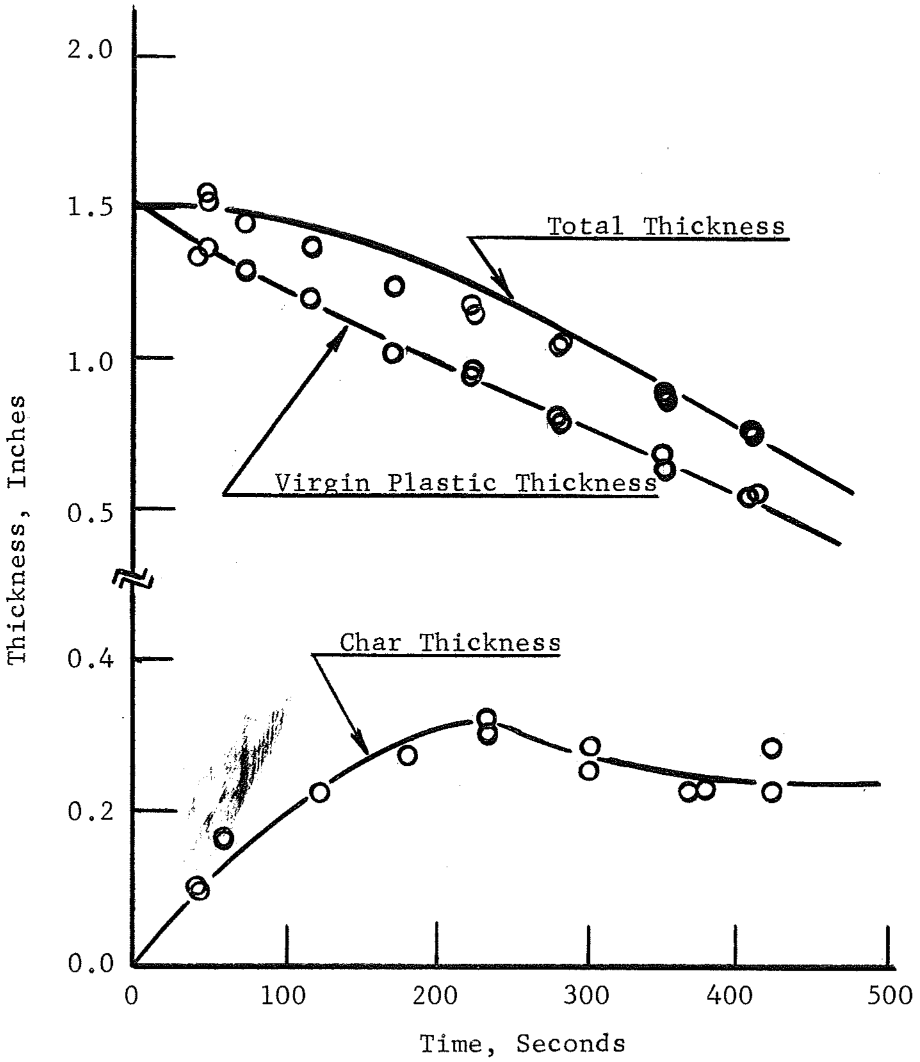

Figure 3-2. Thickness of the char and virgin plastic as a function of time (1).

direction becomes significant. However, this region is small in comparison with the stagnation region where the maximum heating occurs. Therefore the edge region can be neglected without serious error.

Ideal Pyrolysis Gas Mixtures: The pyrolysis gases are assumed to behave as an ideal gas mixture within the char layer. This is reasonable when considering the high temperatures (1500 - 5000°F) and low pressures ($\leq$ 1 atm.) encountered during reentry.

Gas and Char Physical Properties: Because of the large temperature gradient across the char, gas physical properties (heat capacity, thermal conductivity and viscosity) are considered variable with temperature. Variations with temperature in the char properties are not accounted for based largely on the absence of experimental data for low density nylon-phenolic resin chars. Weger, et.al. (2) reported variations in the permeability of low porosity (0.2 - 0.35) char specimens when significant amounts of carbon deposition and/or depletion occured at high temperatures (3000 - 4000°F). However, for the temperature range considered in this research (1500 - 3000°F), carbon deposition and/or depletion was small, and thus the permeability could be considered constant. Similarly, the char porosity was considered uniform and equal to 0.8 for low density nylon-phenolic resin chars (3) and 0.5 for graphite (4).

The variation of the char thermal conductivity with temperature was accounted for by fitting empirical curves to data reported by the Southern Research Institute (5) and the Jet Propulsion Laboratory (6) of the California Institute of Technology. These data are presented in Appendix C.

Thermal Equilibrium Between the Pyrolysis Products and the Char: The temperatures of the pyrolysis products and the char at any section normal to the flow were assumed equal. There is a difference between the gas and the char, but it is generally small. This is supported by data presented by Koh and del Casal (7) in which a maximum temperature difference of 300°F was determined for the flow of air and helium through packed beds of spheres. The maximum temperature of the matrix was 2700°F and the range of Reynold's Numbers and porosities were 62-862 and 0.2-0.35, respectively.

Clark (4) also investigated thermal equilibrium for methane and methane-helium flow through porous graphite. This work had very large temperature gradients (1600 - 2700°F) between the phases at the inlet surface, and showed a rapid approach to thermal equilibrium within the porous graphite. For example, a difference of 3200°R at the back surface was reduced to 600°R half way through the char and to 300°R at the three-quarters point.

Momentum Transfer in the Char Zone: The modified form of Darcy's Law was used to model the momentum transfer within the char zone. This was based on the research of Weger, et.al. (2). It was shown in this work that the modified form, including an inertial term, gave a more accurate prediction of the experimental data for mass flux values of the order of 0.05 lb/ft^2-sec.

PV Work and Viscous Dissipation: The pressure drop across a one-quarter inch thick, low density, nylon-phenolic resin char was experimentally measured to be approximately 15 lb/ft^2 for a pyrolysis gas mass flux of 0.05 lb/ft^2-sec. and a front surface temperature of 2000°F. The PV work contribution to the energy transport is 1.2 BTU/ft^3-sec. The convective energy term in the energy equation evaluated at the back surface where the temperature gradient is smallest, (about 40,000°F/ft) is 1000 BTU/ft^3-sec for an average gas heat capacity of 0.5 BTU/10°F. From this comparison energy dissipation by PV work can be omitted from the analysis without error.

Furthermore, since the velocity ($\sim$5 ft/sec) and the viscosity ($\sim$0.05 cp) of the gas mixture are small, energy generated by viscous dissipation is omitted from the energy equation.

Diffusional Transport: Energy or mass transport by diffusion is negligibly small in comparison with the bulk fluid transport. The average residence time of a gas particle in a one-quarter inch thick char layer is 0.01 seconds for a mass flux value of 0.05 lb/ft^2-sec.

Work Against Gravity: For horizontal flow of pyrolysis gases through the porous char, work against gravity is zero.

The application of the above restrictions to the general equations of change for flow of pyrolysis gases within the char zone of a charring ablator is discussed in the next section of this chapter.

Derivation of the Equations of Change for Flow in the Char Zone

Species Continuity Equation: With reference to Figure 3-1, the continuity equation for species i of a gas mixture flowing through a porous medium is (8):

$$\frac{D\rho_i}{Dt} = -\rho_i(\bar{\nabla}\cdot\bar{v}) - (\bar{\nabla}\cdot\bar{j}_i) + R_i \qquad (3\text{-}1)$$

where ρ_i is the concentration, $\bar{j}_i$, the mass flux, R_i, the rate of production by chemical reaction of species i and $\bar{v}$ is the velocity of the pyrolysis products within the pores.

For the one-dimensional, steady flow of pyrolysis gases through the char zone, neglecting mass transport by diffusion, equation (3-1) reduces to:

$$\frac{d}{dz}(\rho_i v) = R_i \qquad (3\text{-}2)$$

Summing the species continuity equations over all the gas species in the mixture gives the overall continuity equation:

$$\frac{d}{dz}(\rho v) = 0 \tag{3-3}$$

which assumes no mass loss or increase due to formation or depletion of the solid phase.

Integration between the back surface, z = 0, and any point, z, within the char results in equation (3-4):

$$\int_{(\rho v)_o}^{(\rho v)_z} d(\rho v) = \left[(\rho v)_z - (\rho v)_o\right] = 0 \tag{3-4}$$

This equation, defining the gas mass flux as the product of the gas density and velocity, is equivalent to the statement that the gas mass flux is constant through the char;

$$W_p = \rho v = \text{constant} \tag{3-5}$$

where W_p is the mass flux based on the cross sectional area of voids in the char (units of $\text{lb./ft}^2_{\text{voids}}\text{-sec}$). The mass flux based on the total area is given by the following equation:

$$W = \epsilon W_p \tag{3-6}$$

where W has the units lb/ft^2_{total}-sec.

In the above formulation the change in pyrolysis gas mass flux is considered small resulting from deposition and/or depletion by chemical reactions. In the event there is a significant change in the pyrolysis gas mass flux due to chemical reactions the appropriate form of the species continuity equations must be incorporated into the analysis as will be discussed subsequently.

Momentum Equation: The momentum equation for flow through porous media was formulated by H. P. G. Darcy in 1856 (7). Darcy observed during experiments with a one-dimensional packed bed that gas velocity at any point in the bed was directly proportional and in the same direction as the pressure gradient at that point. In vector notation, including the effect of body forces when considering a vertical flow direction, Darcy's Law is:

$$\bar{v} = -\left(\frac{\gamma}{\epsilon\mu}\right)\left(\bar{\nabla}P - \rho\bar{g}\right) \tag{3-7}$$

Applying this equation to a one-dimensional, horizontal flow through a porous char layer and solving for the pressure gradient gives:

$$-\frac{dP}{dz} = \left(\frac{\mu}{\gamma}\right)(v\epsilon) \qquad (3\text{-}8)$$

This equation is valid at low gas velocities within the porous medium. However, at high gas velocities the addition of a term to account for inertial effects is included. This additional term leads to a modified form of Darcy's law.

$$-\frac{dP}{dz} = \left(\frac{\mu}{\gamma}\right)(v\epsilon) + \beta\rho(v\epsilon)^2 \qquad (3\text{-}9)$$

Multiplying both sides of equation (3-9) by the gas density, ρ, followed by substitution of the ideal gas equation of state ($\rho = \frac{P(M_W)}{RT}$) on the left hand side of the equation results in equation (3-10):

$$-\left[\frac{(M_w)P}{RT}\right]\frac{dP}{dz} = \rho\left(\frac{\mu}{\gamma}\right)(v\epsilon) + \beta\rho^2(v\epsilon)^2 \qquad (3\text{-}10)$$

Substitution for the mass flux, W, with rearrangement gives:

$$-PdP = \left(\frac{RT}{M_w}\right)\left[\left(\frac{\mu}{\gamma}\right)(W) + \beta(W)^2\right] \qquad (3\text{-}11)$$

Integration of equation (3-11) between the front surface pressure ($P = P_L$ at $z = L$), and any point within the char layer, (P at z), results in an integral equation for the pressure distribution over the char.

$$P = \left\{ P_L^{\,2} + 2R \left[\int_z^L \left(\frac{\mu}{\gamma}\right) (W) \left(\frac{T}{M_w}\right) dz + \int_z^L \beta \left(\frac{T}{M_w}\right) (W)^2 dz \right] \right\}^{1/2} \tag{3-12}$$

In this equation all parameters that vary with temperature (hence, char distance) are left under the integral signs. These variations are calculated by polynomials in temperature and from the simultaneous solution coupled from the energy equation since the pressure changes are small (~ 15 lb_f/ft^2) compared to the total pressure (~ 2000 lb_f/ft^2).

Energy Equation: The form of the general energy equation for a gas mixture containing K species is (8):

$$\rho \bar{C}_p \frac{DT}{Dt} = -(\bar{\nabla} \cdot \bar{q}) - (\bar{\bar{T}} : \bar{\nabla} \bar{v}) + \sum_{i=1}^{K} (\bar{j}_i \cdot \bar{g}_i)$$

$$+ \left(\frac{\partial \ln \bar{\bar{V}}}{\partial \ln T}\right)_{P, x_i} \frac{DP}{Dt} + \sum_{i=1}^{K} H_i \left[(\bar{\nabla} \cdot \bar{J}_i) - R_i \right] \tag{3-13}$$

The above equation is applied to one dimensional, steady flow of gases in the char zone. Neglecting energy by viscous dissipation, work against gravity and energy transfer by diffusion, the result is:

$$\rho\bar{C}_p v\frac{dt}{dz} = \frac{d}{dz}(q_z) + \left(\frac{\partial \ln \bar{V}}{\partial \ln T}\right)_{P,x_i} v\frac{dP}{dz} - \sum_{i=1}^{K} H_i R_i \qquad (3\text{-}14)$$

Furthermore, for an ideal gas $\left(\frac{\partial \ln \bar{V}}{\partial \ln T}\right)_{P,x_i} = 1$, and neglecting the work by pressure forces across a high porosity char, equation (3-14) simplifies to:

$$\rho\bar{C}_p v\frac{dT}{dz} = \frac{d}{dz}(q_z) - \sum_{i=1}^{K} H_i R_i \qquad (3\text{-}15)$$

where q_z is given by Fourier's Law of heat conduction:

$$q_z = -k_g\frac{dT}{dz} \qquad (3\text{-}16)$$

Substitution for the mass flux, W, from equation (3-6) and multiplication of each side by the porosity, ϵ, to obtain the gas phase contribution to the total energy transfer in the char zone gives:

$$\epsilon\left(\frac{W}{\epsilon}\right)\bar{C}_p\frac{dT}{dz} = \epsilon\frac{d}{dz}\left(k_g\frac{dT}{dz}\right) - \epsilon\sum_{i=1}^{K} H_i R_i \qquad (3\text{-}17)$$

Similarly, for the solid porous medium, neglecting heat transfer by convection, the general energy equation reduces to the following form for one dimensional heat conduction with chemical reaction.

$$(1 - \epsilon) \frac{d}{dz} (k_c \frac{dT}{dz}) - (1 - \epsilon) H_c R_c = 0 \qquad (3\text{-}18)$$

The addition of equations (3-17) and (3-18) gives the equation for the total energy transfer in the char:

$$\epsilon \bar{C}_p W_p \frac{dT}{dz} = \frac{d}{dz} \left[k_e \frac{dT}{dz} \right] - \sum_{i=1}^{K+1} H_i \bar{R}_i \qquad (3\text{-}19)$$

where k_e represents an effective thermal conductivity defined as:

$$k_e = \epsilon k_g + (1 - \epsilon) k_c \qquad (3\text{-}20)$$

and

$$\sum_{i=1}^{K+1} H_i \bar{R}_i = \epsilon \sum_{i=1}^{K} H_i R_i + (1 - \epsilon) H_c R_c \qquad (3\text{-}21)$$

represents the energy absorption by chemical reactions based on the total volume of char. The solution of equation (3-19) will give the temperature distribution in the char layer. In addition to the equations of change just developed, one additional equation is considered. This is the equation for the net heat absorption within the char zone.

Heat Flux Equation: The heat flux equation determines the net heat transfer within the char layer of a charring ablator.

It is defined as the difference in the heat flux value at the back and front surfaces of the char.

$$q_{c_z} = (q_c - q_o) = (k_e \frac{dT}{dz})_L - (k_e \frac{dT}{dz})_o \tag{3-22}$$

Solving for $(k_e \frac{dT}{dz})$ from the energy equation (3-19) by integration between the front and back surface temperatures gives the equation needed to evaluate the net heat flux within the char.

$$q_{c_z} = (q_L - q_o) = \sum_{i=1}^{K} \int_{T_o}^{T_L} \epsilon W_p C_{p_i} x_i dT + \sum_{i=1}^{K+1} \int_{T_o}^{T_L} H_i \bar{R}_i dT \tag{3-23}$$

In equation (3-23), the first term represents heat absorbed by sensible enthalpy change and the second term accounts for heat absorption by chemical reaction.

In summary, the important differential equations for describing the flow of pyrolysis products in the char layer are shown in Table 3-1. The next sections will discuss these equations in terms of the various models used to describe the flow within the char (i.e., frozen, equilibrium, and non-equilibrium flow). Typical boundary conditions will be discussed for the solution of the equations. The development of the numerical solution techniques will complete the theo-

Table 3-1. Summary of the Important Equations Related to the Flow of Pyrolysis Products in the Char Zone.

Species Continuity Equation:	$\frac{d}{dz}(\rho_i v) = R_i$	(3-2)
Momentum Equation (Darcy's Law):	$P = \{P_L^2 + 2R \int_z^L (\frac{\mu}{\gamma})(W)(\frac{T}{M_w})\, dz + \int_z^L \beta(\frac{T}{M_w})(W)^2\, dz\}^{1/2}$	(3-12)
Energy Equation:	$\epsilon \bar{C}_p W_p \frac{dT}{dz} = \frac{d}{dz}[k_e \frac{dT}{dz}] - \sum_{i=1}^{K+1} H_i \bar{R}_i$	(3-19)
Heat Flux Equation:	$q_{c_z} = (q_L - q_o) = \sum_{i=1}^{K} \int_{T_o}^{T_L} \epsilon W_p C_{p_i} x_i\, dT + \sum_{i=1}^{K+1} \int_{T_o}^{T_L} H_i \bar{R}_i\, dT$	(3-23)

retical discussion.

Boundary Conditions for the Flow of Pyrolysis Products Through the Char Zone

There are two important sets of boundary conditions that can be specified to obtain solutions to the equations of change. The first set specifies the pressure and temperature at the front surface, and, the temperature and pyrolysis gas composition entering the back surface of the char. These are shown in statements (3-24) and (3-25).

$$\begin{aligned} T &= T_L \\ P &= P_L \qquad \text{at} \qquad z = L \end{aligned} \tag{3-24}$$

and

$$\begin{aligned} T &= T_o \\ x_i &= x_{i_o} \qquad (i = 1,2,3,\ldots, K) \qquad \text{at} \qquad z = 0 \end{aligned} \tag{3-25}$$

These conditions for mass flux, W, as a parameter make the solution of the energy equation a two point boundary value problem. This requires an iterative solution. Because PV work was negligible in the energy equation, the momentum equation (modified Darcy's law) can be used to compute the pressure distribution after a solution of the energy equation is obtained using an average pressure in the char. The heat flux at the char front surface is also calculated using equation (3-23). The computer program used for these solutions is called the Iterative TEMPRE System (IT) and is discussed in Appendix A.

The second set of boundary conditions specifies the temperature, initial pyrolysis gas composition and the sum of the heat of pyrolysis and the heat conducted in the virgin plastic at the back surface of the char, q_p.

$$\begin{aligned} T &= T_o \\ x_i &= x_{i_o} \ ; \ (i = 1,2,3,\ldots, K) \\ q_p &= -\left(k_e \frac{dT}{dz}\right) \quad \text{at} \quad z = 0 \end{aligned} \tag{3-26}$$

For mass flux, W, and q_p as parameters, the solution of the energy equation as an initial value problem can be obtained. This does not require an iterative solution as did the first case. To be useful, however, a parametric study of the mass flux and q_p is needed over the range of values expected during reentry.

In order to calculate the pressure distribution within the char, the front surface pressure is again specified.

$$P = P_L \quad \text{at} \quad z = L \tag{3-27}$$

The heat flux and pressure distribution calculations are the same as those made in the Iterative TEMPRE System. The computer program for this method of solution is called the Non-Iterative TEMPRE System (NIT).

Both systems are discussed in detail in Appendices A and B where a complete block flow diagram and program listing are presneted. The particular application of the equations of change and the above boundary conditions to frozen, equilibrium and non-equilibrium flow of pyrolysis gases within the char layer will be developed in the next section.

Application of the Transport Equations to Frozen, Equilibrium and Non-Equilibrium Flow in the Char

As mentioned in the Introduction, there are two limiting cases currently used to simplify the analysis of the flow of pyrolysis gases through the char zone. These are to consider the flow to be either frozen or in thermodynamic equilibrium. This research deals with the development of a third model, one for non-equilibrium flow, which will predict more accurately the actual behavior within the char layer. In this section the equations of continuity, momentum, energy and surface heat transfer will be applied to develop each of the three flow models. In a subsequent chapter, the solutions of the particular equations for each model will be compared with each other and with experimental data. In this way the accuracy of the analysis for non-equilibrium flow in the char zone can be evaluated and the extent to which the two limiting cases predict the behavior can be determined.

Frozen Flow: The frozen flow model is an idealization in which the pyrolysis products entering the char zone do not change in composition as they pass through the medium. Therefore, any benefit from the energy absorbed by the predominently endothermic chemical reactions which occur between the gases and char is not obtained. It specifies a lower limit on the amount of energy absorbed in the char zone. Of the three cases it is the simplest because the chemical reaction terms in the energy and heat flux equations are zero:

$$\sum_{i=1}^{K+1} H_i \bar{R}_i = 0$$

Applying this to the equations of change developed previously results in the following simplifications for frozen flow in the char layer.

Continuity Equation $W = W_p \epsilon = \text{constant}$ (3-6)

Momentum Equation

$$P = \left\{P_L^2 + 2R\int_Z^L \left(\frac{\mu}{\gamma}\right)(W)\left(\frac{T}{M_w}\right)dz + \int_Z^L \beta\left(\frac{T}{M_w}\right)(W)^2 dz\right\}^{1/2} \qquad (3\text{-}12)$$

Heat Flux Equation

$$q_{c_z} = (q_L - q_o) = \sum_{i=1}^{K}\int_{T_o}^{T_L} \epsilon W_p C_{p_i} X_i dT \qquad (3\text{-}28)$$

Energy Equation

$$\epsilon \bar{C}_p W_p \frac{dT}{dz} = \frac{d}{dz}\left[k_e \frac{dT}{dz}\right] \qquad (3\text{-}29)$$

The numerical solution of these equations will be discussed in a later section. Typical results for constant and variable physical properties are presented in Appendix A.

<u>Equilibrium Flow</u>: The equilibrium flow in the char zone gives an upper limit on the amount of heat that can be absorbed within the char zone. The reason is that the reactions occuring within the char are predominately endothermic. The set of equations used to describe flow for this case is the same as the equations developed previously: continuity (3-6), momentum (3-12), energy (3-19), and heat flux (3-23). The distinguishing feature lies in the method used to calculate the energy absorption by chemical reactions:

$$\sum_{i=1}^{K+1} H_i \bar{R}_i \neq 0$$

Rewriting the species continuity equation, (3-2), in terms of the mole flux of species i gives:

$$R_i = \frac{d}{dz}(\rho v) = \frac{d}{dT}(Wx_i)\frac{dT}{dz} \qquad (3\text{-}30)$$

Therefore, in order to evaluate the term, $\sum_{i=1}^{K+1} H_i\bar{R}_i$, the mass flux, W, and the mass fraction, x_i, of the species in the gas and solid phases must be known as a function of temperature. The species composition and molal ratio of gases to carbon are a function of temperature, pressure and elemental composition of the virgin plastic and can be calculated by one of the many approaches in the literature (10,11). In this study, the free energy minimization technique was used. The following section outlines the important points of this method.

Equilibrium Compositions by Free Energy Minimization: When several reactions occur between a number of species, the composition resulting at equilibrium depends on the simultaneous equilibrium for all separate reactions. The criteria for this equilibrium in a chemically reacting system at constant temperature and pressure is that the free energy change is zero or that the total free energy of the mixture is a minimum. The free energy change for a reaction is considered a driving force which makes the reaction approach equilibrium. It is also a measure of the departure of the reacting system from an equilibrium state.

Consider a mixture containing q chemical species (K gaseous species and K + 1 to q condensed species) formed from m chemical elements. The free energy function at constant temperature and pressure of species i (assuming ideal behavior) can be expressed as:

$$f_{i,gas} = n_i(\bar{F}^\circ_T/RT)_i + \ln P + \ln(\frac{n_i}{\bar{n}}) \ ; \ 1 \le i \le K \tag{3-31}$$

where $$\bar{n} = \sum_{i=1}^{K} n_i \tag{3-32}$$

and n_i is the moles of species i present and $\bar{n}$ is the total moles present in the reacting mixture. Assuming the activity coefficient of the pure condensed species is one, the free energy expressions for these become:

$$f_{i,condensed} = n_i(\bar{F}^\circ_T/RT)_i \ ; \ K + 1 \le i \le q \tag{3-33}$$

The total free energy of the mixture is obtained by summing (3-31) and (3-33) and is:

$$F(n) = \sum_{i=K+1}^{q} f_{i,condensed} \tag{3-34}$$

The mixture contains fixed amounts of each of the m elements, b_j; and the free energy equation is constrained by mass conservation equations of the form:

$$b_j = \sum_{i=1}^{K} a_{i_j} n_i + \sum_{i=K+1}^{q} a_{i_j} n_i \; ; \; j = 1,2,\ldots,m \qquad (3\text{-}35)$$

The a_{i_j} represents the formula number giving the amount of gram atoms of the j element in species i. For example, for CH_4, a_{i_j} is one for carbon, and four for hydrogen.

At a given temperature and pressure it is necessary to determine the amount of each chemical species present, n_i, that minimizes the free energy (3-34). This is subject to the specification of the total amount, b_j, of each element. Following the method of White, et.al. (12) the usual Lagrangian multiplier procedure of equating the partial derivatives with respect to the n_i's of the augmented function to zero and solving gives a complicated set of equations with the amount of each species, n_i, expressed implicitly. To obtain a simpler, but an iterative solution, a quadratic approximation to the free energy function is formed by a Taylor's series expansion about a point $\bar{y}$ $(y_1,y_2,\ldots y_K)$, and a neighboring point $\bar{n}$ $(n_1,n_2,\ldots n_K)$. This is:

$$Q(n) = F(y) + \sum_{i=1}^{K}\left[(\bar{F}^{\circ}_{T}/RT)_{i} + \ln P + \ln(\frac{y_{i}}{\bar{y}})\right]\Delta_{i}$$

$$+ 1/2 \sum_{i=1}^{K}\sum_{k=1}^{K}(\frac{\delta_{ik}}{y_{i}} - \frac{1}{\bar{y}})\Delta_{i}\Delta_{k} + \sum_{i=K+1}^{q}(\bar{F}^{\circ}_{T}/RT)_{i}\Delta_{i} \qquad (3\text{-}36)$$

To minimize $Q(\bar{n})$ subject to the mass balance constraints, the augmented function employing Lagrange multipliers, π_j, is formed.

$$G(n) = Q(\bar{n}) + \sum_{j=1}^{m}\pi_{j}(b_{j} - \sum_{i=1}^{K}a_{ij}n_{i} - \sum_{i=K+1}^{q}a_{ij}n_{i}) \qquad (3\text{-}37)$$

At this point the usual procedure would be to set partial derivatives of $G(\bar{n})$ with respect to the independent variables $(n_1, n_2, \ldots, n_q)$ and the Lagrangian multipliers $(\pi_1, \pi_2, \ldots, \pi_m)$ equal to zero and solve simultaneously the resulting set of $m + q$ equations for the minimum of the constrained quadratic approximation. Then the procedure would be repeated employing a convergence criteria to approach the point of minimum free energy. However, it is more convenient to use a different procedure which requires that only $m + 1 + s$ equations (where s is the total number of solid or condensed phases present) be solved simultaneously rather than $m + K + s$ equations. Since a quadratic approximation is used, the linear equations resulting from taking the partial derivatives with respect to the n_i's can be solved directly. Equating the partial derivatives with respect to the n_i's to zero for $i = 1,2,\ldots,K$ results in the following set of equations.

$$n_{i,gas} = -f_{i,gas}(y) + \left(\frac{y_i}{\bar{y}}\right)\bar{n} + \sum_{j=1}^{m} (\pi_j a_{i_j}) y_i \quad ; \quad i=1,2,\ldots,K \tag{3-38}$$

This gives K explicit equations for the moles of the gases in terms of the m + 1 unknowns, π_j's and $\bar{n}$. Equation (3-38) permits the elimination of n_i from the material balance equations (3-35). Note that in doing this, equation (3-35) is in terms of y_i's, which are the initial guesses used to start the iteration. Substituting equation (3-38) into equation (3-35) and defining:

$$r_{jk} = \sum_{i=1}^{K} (a_{i_j})(a_{i_k}) y_i \quad ; \quad j,k = 1,2,\ldots,m \tag{3-39}$$

After some manipulations the following result is obtained.

$$\sum_{j=1}^{m} r_{jk}\pi_j + c_k\bar{u} + \sum_{i=K+1}^{q} a_{i_k} n_i = b_k + \sum_{i=1}^{K} a_{i_k} f_i(y) \quad ; \quad k=1,2,\ldots,m \tag{3-40}$$

where:

$$c_k = \sum_{i=1}^{K} a_{i_k} y_i \tag{3-41}$$

and: $$\bar{u} = \bar{n}/\bar{y} \tag{3-42}$$

Equation (3-40) represents m equations in m + 1 unknowns, the π_j's and $\bar{u}$, which apply to gases only. An additional equation is obtained by summing the K equations given by equation (3-38).

$$\sum_{j=1}^{m} b_j \pi_j = \sum_{i=1}^{K} f_i(y) \tag{3-43}$$

The additional s equations needed to compute the amount of condensed phases present are obtained by equating the partial derivative of $G(\bar{n})$ with respect to the moles of the condensed species, n_i, to zero which gives:

$$(\bar{F}_T^\circ/RT)_i = \sum_{j=1}^{m} a_{ij} \pi_j \; ; \; K + 1 \leq i \leq q \tag{3-44}$$

These equations, which are to be solved simultaneously, are given in matrix form in Table 3-2. When the matrix is solved, values for the moles of condensed species are obtained directly. Also the values π_j's and $\bar{u}$ are obtained. These values are substituted in equation (3-38) to calculate the moles of the gas species, n_i. These calculated values, after appropriate adjustment to insure rapid convergence, are used as a starting value for the next iteration. This process is repeated until

Table 3-2. General Equations for the Solution of the Equilibrium Composition of Gas-Condensed Mixture by the Free Energy Minimization Technique*.

$$
\begin{aligned}
r_{11}\Pi_1 + r_{12}\Pi_2 + \dots r_{1m}\Pi_m + b_1'u + a_{K+1,1}x_{K+1} + \dots + a_{q,1}x_q &= b_1 + \sum_{i=1}^{K} a_{i1}f_i(Y) \\
r_{21}\Pi_1 + r_{22}\Pi_2 + \dots r_{2m} + b_2'u + a_{K+1,2}x_{K+1} + \dots + a_{q,2}x_q &= b_2 + \sum_{i=1}^{K} a_{i2}f_i(Y) \\
r_{31}\Pi_1 + r_{32}\Pi_2 + \dots r_{3m}\Pi_m + b_3'u + a_{K+1,3}x_{K+1} + \dots + a_{q,3}x_q &= b_3 + \sum_{i=1}^{K} a_{i3}f_i(Y) \\
r_{41}\Pi_1 + r_{42}\Pi_2 + \dots r_{4m}\Pi_m + b_4'u + a_{K+1}x_{K+1} + \dots + a_{q,4}x_q &= b_4 + \sum_{i=1}^{K} a_{i4}f_i(Y) \\
\vdots \\
r_{m,1}\Pi_1 + r_{m2}\Pi_2 + \dots r_{mm}\Pi_m + b_m'u + a_{K+1}x_{K+1} + \dots + a_{q,m}x_q &= b_m + \sum_{i=1}^{K} a_{im}f_i(Y) \\
b_1\Pi_1 + b_2\Pi_2 + \dots + b_m\Pi_m &= \sum_{i=1}^{K} f_i(Y) \\
a_{n+1,1}\Pi_1 + \dots + a_{n+q,m}\Pi_m &= (F^\circ/RT)_{K+1} \\
a_{n+2,1}\Pi_1 + \dots + a_{n+2,m}\Pi_m &= (F^\circ/RT)_{K+2} \\
\vdots \qquad & \qquad \vdots \\
a_{q1}\Pi_1 + a_{q,2}\Pi_2 + \dots + a_{q,m}\Pi_m &= (F^\circ/RT)_q
\end{aligned}
$$

* Note that equations have been written for more than a condensed phase.

the minimum free energy is reached.

Convergence Procedure: Normally in the iterative procedure, the amount of each species, n_i, which is calculated at the minimum of the constrained quadratic approximation, is used as the next estimate. To insure that oscillations and over-corrections will not occur, the following convergence scheme, similar to that of White (12), is used. The values of the moles of the gas species, $y_{i(new)}$, for the next iteration are obtained using the following expression:

$$y_{i(new)} = y_{i(old)} + \lambda\Delta_i \tag{3-45}$$

where

$$\Delta_i = n_i - y_{i(old)} \tag{3-46}$$

and λ is the parameter of the line through n_i and $y_{i(old)}$. Substituting equation (3-45) into (3-34) and taking the derivative with respect to λ gives the following:

$$\frac{dF(\lambda)}{d\lambda} = \sum_{i=1}^{K} \Delta_i \left\{ c_i + \ln[(y_i + \lambda\Delta_i)/(\bar{y} + \lambda\bar{\Delta})] \right\} + \sum_{i=K+1}^{q} \Delta_i (\bar{F}^\circ_T/RT)_i \tag{3-47}$$

where:

$$c_i = (\bar{F}^\circ_T/RT)_i + \ln P \tag{3-48}$$

and:

$$\bar{\Delta} = \sum_{i=1}^{K} \Delta_i \qquad (3\text{-}49)$$

The value of $dF/d\lambda$ must remain negative to insure convergence to the minimum free energy. Sometimes it becomes necessary to meet this requirement by reducing λ to a value less than one. Once this value is found, equation (3-45) is used to obtain the numerical value of each y_i for the next iteration. It turns out that as the minimum is approached large changes in λ are necessary which causes the value of $dF/d\lambda$ to become smaller. This allows for a controlled path of descent and convergence to the minimum free energy is obtained.

A typical free energy minimization solution giving the composition of the major components as a function of temperature at atmospheric pressure is shown in Figure 3-3. From this solution the species continuity equation (3-30) can be solved for R_i, and, the energy absorption by chemical reactions $(\sum_{i=1}^{K+1} H_i \bar{R}_i)$ can be calculated.

In non-equilibrium flow, the form of the energy equation remains the same as that for equilibrium flow. The difference in the two lies in the manner in which the energy absorption by chemical reaction must be calculated.

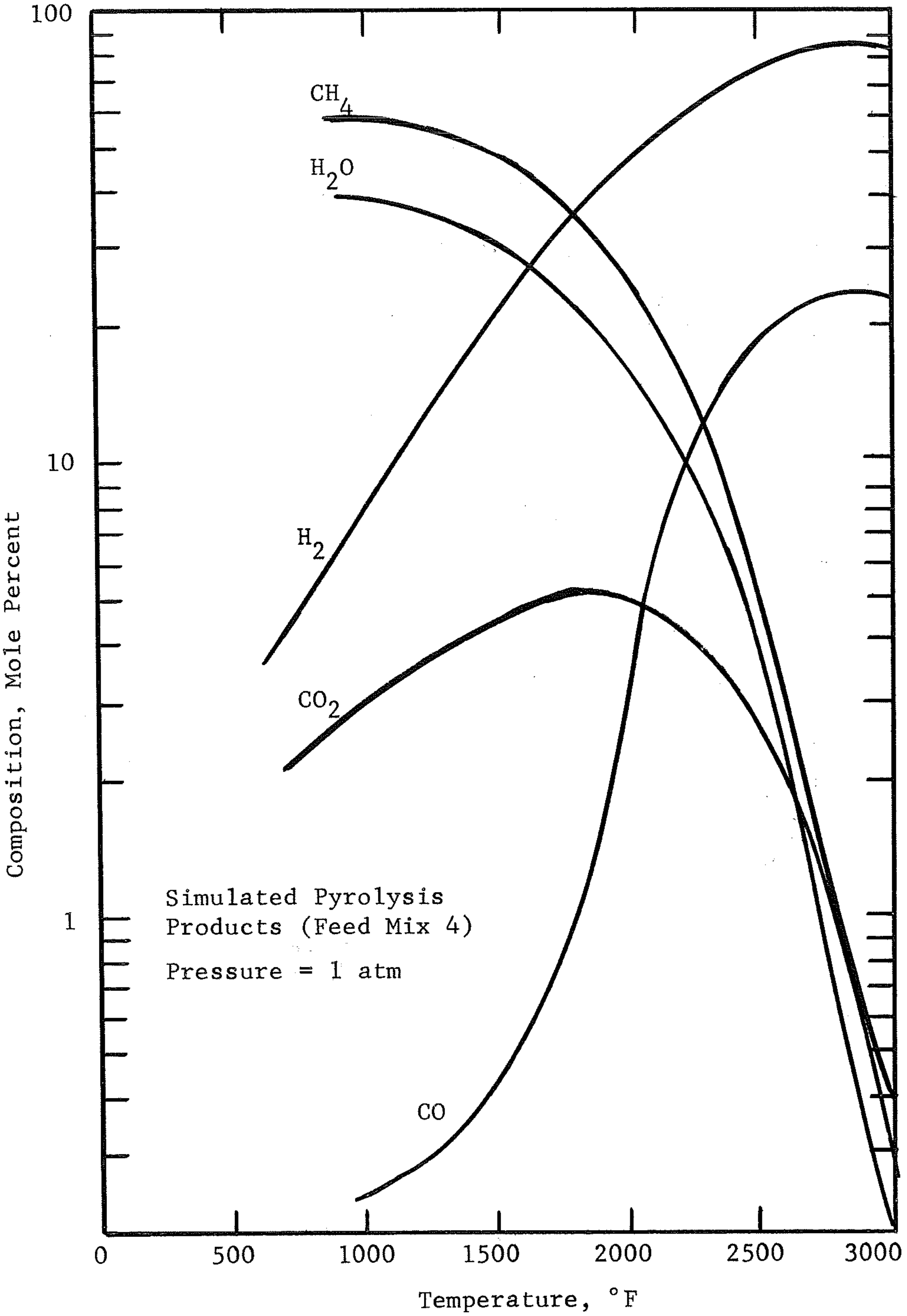

Figure 3-3. Equilibrium Composition of the Simulated Pyrolysis Products in Equilibrium with Solid Carbon (1:1 Ratio by weight of Phenolic Resin-Nylon Char).

Non-Equilibrium Flow: The equations of change for non-equilibrium flow are the same as those developed for equilibrium flow. The evaluation of the energy absorption by chemical reaction, however, is dependent on the finite reaction rates of each reaction occurring within the char zone. Therefore, in addition to temperature and pressure, the reaction rate, R_i, is also a function of the mass flux and composition entering the char layer. This requires a knowledge of the specific reactions taking place within the char and the associated kinetic data; i.e., frequency factor and activation energy. The following paragraphs will present a method for determining the important reactions and the technique for using the kinetic data to predict the actual behavior within the char zone.

Reaction Rate and Rate Constant Equation: In general, a chemical reaction can be written in the following form:

$$\sum_{i=1}^{q} r_{ij} A_i \rightleftarrows \sum_{i=1}^{q} p_{ij} A_i \; ; \; j = 1,2,3,\ldots,m \tag{3-50}$$

For this j-th chemical reaction, r_{ij} and p_{ij} are the stoichiometric coefficients of the reactants and products respectively for species A_i. There are a total of q chemical species and m chemical reactions in the system.

The rate of reaction of the i-th species, R_i, is given by the following equation for the m chemical reactions:

$$R_i = \sum_{j=1}^{m} (p_{ij} - r_{ij}) \left[k_{fj} \prod_{k=1}^{q} c_i^{r'_{ij}} - k_{rj} \prod_{k=1}^{q} c_i^{p'_{ij}} \right] ;$$

$$i = 1,2,3,\ldots,q \qquad (3\text{-}51)$$

where c_i is the concentration of component i and r'_{ij} and p'_{ij} represent the power on the concentrations. It is not necessary for these to be equal to r_{ij} and p_{ij}. The forward and reverse reaction rate constants are k_{fj} and k_{rj}. This is the equation for R_i that is used in the computer implemented numerical solution of the transport equations. Equation (3-51) is a very convenient and general formulation for the reaction rate of the j-th species in m simultaneous chemical reactions. The stoichiometric coefficients and the powers on the concentrations are each conveniently represented as a matrix.

In addition to the above, the reaction rate constants are also required. A general form for the rate constant of the i-th chemical reaction is:

$$k_j = A_j T^{s_j} \mathrm{Exp}\,(-E_j/RT) \; ; \; j = 1,2,3,\ldots,m \qquad (3\text{-}52)$$

where A_j is the frequency factor and E_j, the energy of activation.

With these mathematical generalizations the analysis is resolved to one of selecting the important chemical reactions taking place in the char zone along with precise values of the rate constants. These equations and associated rate constants can then be used in equation (3-48) to calculate the reaction rate, R_i, which is needed to solve the transport equations.

The non-equilibrium flow model is an order of magnitude more complex than the chemical equilibrium computations. The latter case involves the solution of a set of algebraic equations with the energy and momentum equations. The former requires the solution of a set of non-linear, ordinary differential equations (species continuity equations) simultaneously with the energy equation. There is also the additional difficulty of determining all of the important chemical reactions that take place in the system and the initial composition of pyrolysis products entering the char zone. For equilibrium flow, only the elemental composition is required. Finally, there is the laborious task of collecting and evaluating reaction kinetic data appearing in the literature.

Chemical Reactions in the Char Layer: The general nature of the reactions occurring in the char zone of a charring ablator has been qualitatively established (13). Between 500°F and 3000°F, the primary reactions occurring are hydrocarbon cracking reactions of high molecular weight species to lower molecular weight species (ultimately H_2, CO_2, CO, H_2O, etc.). From 3000°F to about 6000°F, free radical and recombination reactions take place, with ionization reactions beginning to appear at the upper end of this temperature region. This study is concerned with the reactions occurring below 3000°F; i.e., hydrocarbon cracking reactions, primarily. Free radical, recombination and ionization reactions are not considered as they do not take place. Fortunately, this greatly simplifies the already complex system of reactions that could occur. Establishing the fact that reacting flow in the char zone can be accurately described in the temperature range from 500° to 3000°F establishes the basis for extending the investigation to temperatures in the 3000°F to 6000°F range.

Pike (14), in an effort to condense the large assortment of reaction kinetic data available in the literature, has compiled a detailed listing of reactions and the corresponding kinetic data for the C-H-O-N system. In a subsequent report (15) this and other kinetic data were analysed. The calculation of the isothermal conversion for each reaction possible in the char zone over a wide range of temperatures was included. This formed one method for determining the important reactions taking place in the char zone as discussed below.

<u>Criterion for Reaction Selection</u>: The rate of a chemical reaction increases with temperature. For a particular reaction, if a significant conversion of reactants to products is obtained with the char at a uniform and specified temperature, then it can be assumed that there may be a significant conversion when

a temperature gradient exists in the char layer with the front surface at this specified temperature. Thus, this reaction is considered important. An example of this behavior is the reaction illustrated in Figure 3-4 as a plot of conversion versus temperature. For another reaction if there is no conversion in the char at a uniform higher temperature (3000°F), there will be no conversion when there is a temperature gradient in the char. Therefore, this reaction can be omitted when there is a temperature gradient in the char with a front surface temperature of 3000°F. However, the products formed by the reaction may indeed be included as important components subject to further reactions. This logic forms the basis of the isothermal analysis of reaction kinetics data in the literature (15).

Although the reactions postulated to take place over a given temperature range (500°F to 3000°F) could occur, they are also restricted by the components initially present in the pyrolysis gas stream. For example, the reaction of butane and oxygen forming carbon dioxide and water is a likely candidate between 500°F and 3000°F; however, the absence of either butane or oxygen eliminates the reaction from consideration. A considerable amount of caution must be exercised to make certain that the components are not formed at some time within the char, making the reaction an important part of the system.

Composition of Pyrolysis Products: As discussed above, the

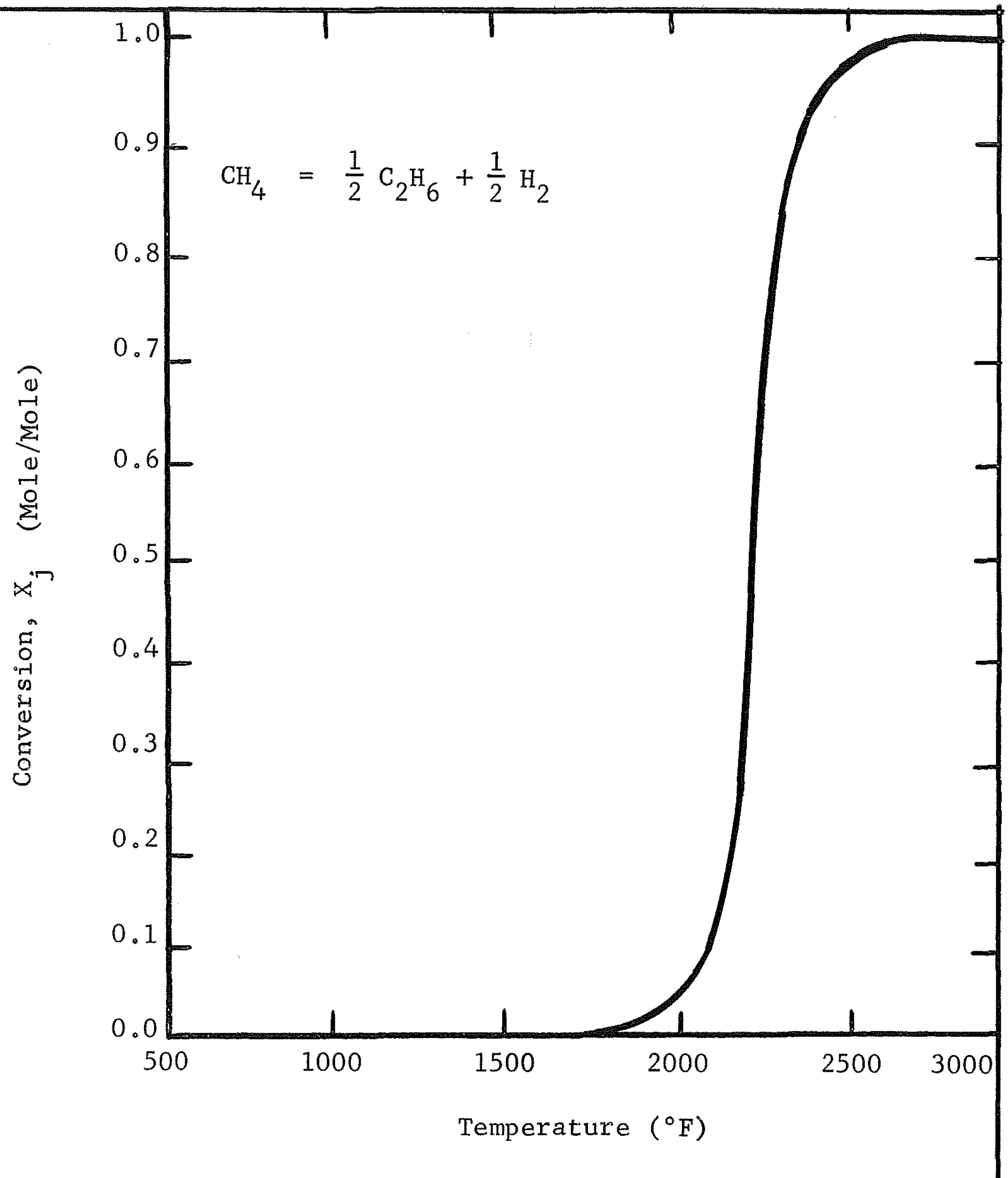

Figure 3-4. Isothermal Conversion of Methane to Hydrogen and Ethane Between 500 and 3000°F.

pyrolysis product composition at the back surface of the char is important in reducing the total possible reactions likely to occur within a specified temperature range. First attempts to study the non-equilibrium flow of pyrolysis products through a porous char layer relied on two separate sources for estimating the gas composition entering the char at the back surface. The first method which served as an order of magnitude analysis was the equilibrium compositions calculated by the free energy minimization method (10). The second was analyses of the degradation products of low density nylon-phenolic resin composites by pyrolysis gas chromatography (16,17). Table 3-3 lists the compositions obtained by each method. As noted, the unavailability of accurate analytical procedures and thermophysical data for the high molecular weight pyrolysis products (i.e., phenol, cresol, toluene, etc.) left a region of definite uncertainty. As a result, the major components of the pyrolysis products were identified as methane, hydrogen, carbon dioxide, carbon monoxide and nitrogen by many (18,19) with unknown quantities of water and high molecular weight residues completing the analysis.

Subsequent research by Sykes (20) confirmed the presence of phenol-based materials as primary constituents in the high molecular weight residues. Table 3-4 represents a more precise pyrolysis gas composition obtained in this work. Very good

Table 3-3. Pyrolysis Products Resulting From the Thermal Decomposition of a Nylon-Phenolic Resin Composite Excluding the High Molecular Weight Species.

Component	Computed Equilibrium Compositions Mole %					Experimentally Determined Compositions Mole %		
	Kratsch (19)			del Valle (10)		Freidman (24)	Shulman (25)	Beecher & Rosenweig (26)
	540°F	1540°F	2540°F	440°F	980°F	1290 °F	1470°F	2190 °F
Carb. Monoxide	23.8	31.6	20.4	0.0	1.9	11.5	4.0	12.0
Carb. Dioxide	4.5	0.0	0.0	1.5	3.4	2.3	0.3	0.0
Nitrogen	7.0	6.3	2.3	8.1	6.3	0.1	0.0	0.0
Hydrogen	0.0	5.6	47.4	1.5	43.2	25.2	13.0	54.0
Hydrogen Cyanide	0.0	1.0	4.1	0.0	0.0	0.0	30.0	0.0
Methane	57.4	45.4	3.0	56.4	26.2	4.3	1.5	12.0
Ammonia	0.0	0.0	0.0	0.0	0.0	4.3	13.0	0.0
Water	0.0	0.0	0.0	32.5	19.0	16.1	38.0	12.0
Diacetylene	0.0	0.0	0.0	0.0	0.0	1.0	0.0	0.0
Acetone	0.0	0.0	0.0	0.0	0.0	0.7	0.0	0.0
Acetylene	0.0	1.1	22.1	0.0	0.0	11.5	0.0	0.0
Cresol	0.0	0.0	0.0	0.0	0.0	0.0	0.9	2.5
Phenol	0.0	0.0	0.0	0.0	0.0	0.0	0.0	2.5
Ethane	0.6	0.1	0.0	0.0	0.0	0.2	0.0	5.0
Ethylene	0.0	4.4	0.6	0.0	0.0	14.7	0.0	
Benzene	6.7	4.4	0.0	0.0	0.0	1.0	0.0	
Toluene	0.0	0.0	0.0	0.0	0.0	0.5	0.0	
Xylene	0.0	0.0	0.0	0.0	0.0	0.3	0.0	
Propane	0.0	0.0	0.0	0.0	0.0	1.4	0.0	
Isopropanol	0.0	0.0	0.0	0.0	0.0	1.6	0.0	
Totals	100.0	100.0	100.0	100.0	100.0	100.0	100.0	100.0

Table 3-4. Pyrolysis Products Resulting From the Thermal Decomposition of Nylon-Phenolic Resin Composites Including the High Molecular Weight Species.

Component	Sykes (20) Mole% (Nylon-Phenolic Resin)		Sykes (17) Mole%
	By Flash Pyrolysis at 800°C	By Pyrolysis at 50°C Increments to 800-900°C	(Phenolic Resin Only)
Phenol	8.0	7.6	6.7
Methylphenol	4.0	4.0	2.1
Dimethylphenol	2.8	3.2	0.0
Trimethylphenol	2.4	2.7	0.0
Benzene	0.4	0.4	0.2
Toluene	0.0	0.2	0.4
Cyclopentanone	1.2	2.5	0.0
Hydrogen	30.2	32.2	47.1
Methane	3.8	4.0	9.4
Carbon Monoxide	5.3	3.6	5.2
Carbon Dioxide	12.1	6.8	1.5
Water	20.1	23.3	22.0
Ammonia	0.8	0.4	0.0
Unidentified	9.2	10.1	5.2
Totals	100.0	100.0	100.0

agreement was obtained by comparing the reported experimental results with an overall energy balance technique using heats of formation and heats of combustion data for the virgin plastic and the experimentally determined pyrolysis product composition. Typical composition data of the simulated pyrolysis products used in this research are presented in Table 4-3 of Chapter IV.

The remaining portion of this chapter shall discuss the pertinent physical and thermodynamic property relationships and the numerical techniques used to obtain a solution to the equations of change.

Physical and Thermodynamic Properties: In any real problem where the temperature gradient varies over a wide range (>1000°K), changes in the physical and thermodynamic properties as a function of temperature occur. For the multicomponent flow of a reacting gas within a porous char, composition change by chemical reaction is also important. The equations used in this research for calculating the variations in physical and thermodynamic properties with temperature will be discussed in two parts; the gas phase properties and the char or solid phase properties.

Gas Phase Physical Properties: The gas phase physical and thermodynamic properties required for the solution of the equations of change are the thermal conductivity, viscosity and heat capacity. The physical property equations are those presented by Sherwood and Reid (21) and the thermodynamic equations were obtained from McBride, *et.al.* (22).

The thermal conductivity of a pure gas is calculated using the equation shown below:

$$k_{g_i} = \frac{2.6693 \times 10^{-5} \left(\frac{T}{M_{w_i}}\right)^{\frac{1}{2}} (C_{v_i} + 4.47)}{\sigma^2 \Omega_v} \qquad (3\text{-}53)$$

For an ideal gas the heat capacity at constant volume is $C_{pi} - R$ and the collision diameter, σ, and collision integral, Ω_v, are tabulated for the individual gas components. The thermal conductivity of the gas mixture is calculated as:

$$\bar{k}_g = \sum_{i=1}^{K} n_i k_{g_i} \Big/ \sum_{i=1}^{K} n_i \qquad (3\text{-}54)$$

The viscosity of a pure gas is given by a similar equation:

$$\mu_{g_i} = \frac{2.6693 \times 10^{-3} \left[(M_{w_i})T\right]^{\frac{1}{2}}}{\sigma^2 \Omega_v} \qquad (3\text{-}55)$$

The viscosity of the gas mixture is calculated by an equation approximating the Chapman-Enskog Theory:

$$\bar{\mu} = \sum_{i=1}^{K} \mu_i \left[1 + \sum_{\substack{j=1 \\ j \neq i}}^{K} \phi_{i_j} (n_j/n_i)\right]^{-1} \qquad (3\text{-}56)$$

where the parameter, ϕ_{i_j}, is calculated by equation (3-57).

$$\phi_{i_j} = \left[1 + (\mu_i/\mu_j)^{\frac{1}{2}}(M_{w_i}/M_{w_j})^{\frac{1}{4}}\right]^2 \left[\sqrt{8}\left(1 + (M_{w_i}/M_{w_j})\right)^{\frac{1}{2}}\right]^{-1} \tag{3-57}$$

The thermodynamic properties are calculated by empirical curve fitting equations (23). These equations are:

(1) For the heat capacity,

$$C_{p_i}/R = a_i + b_i T + c_i T^2 + d_i T^3 + e_i T^4 \tag{3-58}$$

(2) For the free energy, and

$$\frac{F^\circ_{T_i}}{RT} = a_i(1 - \log_{10} T) - \frac{b_i}{2} T - \frac{c_i}{6} T^2 - \frac{d_i}{12} T^3 - \frac{e_i}{20} T^4 + \frac{f_i}{T} - g_i \tag{3-59}$$

(3) For the enthalpy.

$$\frac{H^\circ_{T_i}}{RT} = a_i + \frac{b_i}{2} T + \frac{c_i}{3} T^2 + \frac{d_i}{4} T^3 + \frac{e_i}{5} T^4 + \frac{f_i}{T} \tag{3-60}$$

The empirical constants for the above equations, along with typical data for the gas components studied in this research are presented in Appendix C.

Char Physical Properties (Thermal Conductivity, Porosity and Permeability): The char porosity and permeability values were assumed constant in this study. This assumption is valid when the temperature range is restricted to values where little carbon deposition or depletion is obtained. The porosity value was assumed equal to the average effective porosity of the materials; i.e., char porosity = 0.8 (3), graphite porosity = 0.5 (4). The permeability values were average values obtained by analysis of a variety of experimental data reported in Appendix C. A Carmen-Kozeny plot of the data was used to estimate the permeability coefficients, α and β, which were needed in the differential momentum equation (3-12).

Char thermal conductivity values were obtained from experimental data shown in Appendix C. The variation with temperature was determined by a linear least squares fit of the data. For the particular data used, the experimental conductivities were reported for an inert gas (nitrogen or argon) within the pores. These values are, therefore, more representative of an effective conductivity since the conductivity of the inert gases is approximately equal to the pyrolysis gas conductivity.

$$k_e = k_c \text{ (experimental)} \tag{3-61}$$

Provisions are made in the TEMPRE System for calculating the effective conductivity when char conductivities are measured with the pores evacuated. In this instance equation (3-62) must be used.

$$k_e = \epsilon \bar{k}_g + (1 - \epsilon) k_c \tag{3-62}$$

The use of the above physical and thermodynamics property equations in conjunction with the numerical integration methods gives the variable properties solutions to the equations of change.

Numerical Solution of the Equations of Change

Prior to the selection of a numerical method, the accuracy of the numerical solution desired must be specified. This determines the interval size needed in the analysis which effects the round-off errors associated with the calculation of the solution. If a relatively small interval size is used, the round-off errors may be intolerable. On the other hand, a very large interval size could produce large truncation errors which results in a solution that does not approach the true solution. One technique used to determine if a specific interval size is a reasonable choice involves the computation of the solution for the particular interval selected, and interval sizes reduced by a factor of one half of each preceeding value. Comparison of the solutions for each interval chosen should reveal when the approximate solution approaches the true solution or when round-off errors make the calculated solution invalid.

In general, increased accuracy requires increased complexity in (or order of) the numerical method used. Therefore, there is an optimum decision to be made between the nearness of the approximate solution to the real solution and the computational time required to obtain the solution. The best approach is obviously the one that minimizes truncation and round-off errors.

Numerical Solution of the Differential Energy Equation: The energy equation describing the flow of pyrolysis gases through the char zone of a charring ablator is a second order, non-linear differential equation with variable coefficients. In order to obtain a solution to this equation, a numerical integration technique must be used. This requires the equation to be transformed into a finite difference form which can be integrated stepwise on a digital computer. Of the various methods available, all require the specification of the order and stepsize to achieve the desired solution. Two general types of numerical integration schemes are commonly used; the self-starting methods, ranging from the Euler equation to the Runge-

Kutta series, and, the predictor-corrector methods which require the specification or calculation of several initial points to start the procedure. The number of points is proportional to the order of the particular equation used. Because of the accuracy and relatively straight forward nature of the self-starting methods, a fourth order Runge-Kutta formula was selected.

The general formulae, and the formulae as they apply to the differential energy equation are presented in Table 3-5. The truncation error is of the order $O(h^5)$ where h is the step size (23). The parameters A_1, A_2, A_3, and A_4 in equation (3-68) correspond to the Runge-Kutta constants generated by the numerical integration of the energy equation.

Therefore, in the non-equilibrium flow analysis, the solution of the energy and continuity equations are calculated simultaneously because of the interdependence of the temperature and the mole flux (composition).

Numerical Solution of the Species Continuity Equation: In the non-equilibrium flow analysis, the species continuity equation expressing the mole (or mass) flux of each species as a function of temperature must be solved simultaneously with the differential energy equation. Rewriting equation (3-30) in terms of the mole flux, N_i, of species i gives:

$$\frac{dN_i}{dT} = \left(\frac{R_i}{M_{w_i}}\right)\left(\frac{1}{dT/dz}\right) \qquad (3\text{-}69)$$

Table 3-5. Fourth Order Runge-Kutta Formulae for Solving the Differential Energy Equation for Flow of Pyrolysis Gases Through the Char Zone.

General Formulae

$$y_{M+1} = y_M + h\left[y'_M + \frac{1}{6}(A_1 + A_2 + A_3)\right] + 0\,(h^5) \tag{3-63}$$

$$y'_{M+1} = y'_M + \frac{1}{6}(A_1 + 2A_2 + 2A_3 + A_4) \tag{3-64}$$

$$\begin{aligned} A_1 &= h\,f(x_M,\ y_M,\ y'_M) \\ A_2 &= h\,f(x_M + \tfrac{1}{2}h,\ y_M + \tfrac{h}{2}y'_M + \tfrac{h}{8}A_1,\ y'_M + \tfrac{A1}{2}) \\ A_3 &= h\,f(x_M + \tfrac{1}{2}h,\ y_M + \tfrac{h}{2}y'_M + \tfrac{h}{8}A_2,\ y'_M + \tfrac{A2}{2}) \\ A_4 &= h\,f(x_M + h,\ y_M + hy'_M + \tfrac{h}{2}A_3,\ y'_M + A_3) \end{aligned} \tag{3-65}$$

Table 3-5. Fourth Order Runge-Kutta Formulae for Solving the Differential Energy Equation for Flow of Pyrolysis Gases Through the Char Zone (Continued).

Formulae for the Flow of Pyrolysis Gases Through Chars

$$T_{N+1} = T_N + h\left[T'_N + \frac{1}{6}(A_1 + A_2 + A_3)\right] \qquad (3\text{-}66)$$

$$T'_{N+1} = T'_N + \frac{1}{6}(A_1 + 2A_2 + 2A_3 + A_4) \qquad (3\text{-}67)$$

$$A_1 = h(T'_o)\left[\frac{W_p\bar{C}_p\epsilon}{k_e} - \frac{dk_e/dT}{k_e}(T'_o) + \frac{\Sigma H_i\bar{R}_i}{k_e}\right]_{T_o}$$

$$A_2 = h(T'_o+\tfrac{1}{2}A_1)\left[\frac{W_p\bar{C}_p\epsilon}{k_e} - \frac{dk_e/dT}{k_e}(T'_o + \tfrac{1}{2}A_1) + \frac{\Sigma H_i\bar{R}_i}{k_e}\right]_{T_o+\frac{h}{2}T'_o+\frac{h}{8}A_1}$$

$$A_3 = h(T'_o+\tfrac{1}{2}A_2)\left[\frac{W_pC_p\epsilon}{k_e} - \frac{dk_e/dT}{k_e}(T'_o+ \tfrac{1}{2}A_2) + \frac{\Sigma H_i\bar{R}_i}{k_e}\right]_{T_o+\frac{h}{2}T'_o+\frac{h}{8}A_2}$$

$$A_4 = h(T'_o + A_3)\left[\frac{W_pC_p\epsilon}{k_e} - \frac{dk_e/dT}{k_e}(T'_o+A_3) + \frac{\Sigma H_i\bar{R}_i}{k_e}\right]_{T_o+hT'_o+\frac{h}{2}A_3}$$

(3-68)

where the temperature gradient, dT/dz, is calculated in the energy equation solution. Substitution for R_i from equation (3-51) results in the final form of the equation used to calculate the species mole flux, N_i, in the TEMPRE system.

$$\left(\frac{dN_i}{dT}\right) = \sum_{j=1}^{m} \frac{(p_{ij} - r_{ij})}{M_{wi}} \left[k_{fj} \prod_{i=1}^{K+1} c_i^{r'_{ij}} - k_{rj} \prod_{i=1}^{K+1} c_i^{p'_{ij}} \right];$$

$$i = 1,2,3,\ldots, K + 1 \qquad (3\text{-}70)$$

The solution of the K+1 first order differential equations for the mole flux, N_i, is obtained by numerical integration using a fourth order Runge-Kutta formula (23).

$$N_{i_{M+1}} = N_{i_M} + \frac{1}{6} (B_{i,1} + 2B_{i,2} + 2B_{i,3} + B_{i,4}) \qquad (3\text{-}71)$$

where

$$B_{i,1} = hf\, (T_0, N_{1,0}, N_{2,0}, N_{3,0}, \cdots , N_{K+1,\ 0})$$

$$B_{i,2} = hf\, (T_0 + \frac{h}{2}T_0' + \frac{h}{8}A_i, N_{i,0} + \tfrac{1}{2}B_{2,1}, N_{I+1,0} + \tfrac{1}{2}B_{K+1,1})$$

$$B_{i,3} = hf\, (T_0 + \frac{h}{2} T_0' + \frac{h}{8} A_2, N_{1,0} + \tfrac{1}{2}B_{1,2}, N_{2,0} + \tfrac{1}{2}B_{2,2},$$

$$\ldots, N_{K+1,0} + \tfrac{1}{2}B_{K+1,2})$$

$$B_{i,4} = hf\,(T_0 + hT_0' + \frac{h}{2} A_3, N_{i,0} + B_{1,3}, N_{2,0} + B_{2,3},$$
$$\ldots, N_{K+1,0} + B_{K+1,3}) \qquad (3\text{-}72)$$

and M is a location within the char layer. The interdependence of the energy and species continuity equations can be seen by noting the presence of the A_j values in the above equations (3-72). These values are the Runge-Kutta parameters calculated for the energy equation solution at the same position within the char. A one-to-one correspondence between the A_j and $B_{i,j}$ values must exist to obtain a non-equilibrium flow solution. To start the integration, the initial composition, temperature and temperature gradient at the back surface are used to calculate the first intermediate temperature and Runge-Kutta parameter, A_1. These values are then used to estimate the mole flux of each species at the same intermediate position within the char zone. The intermediate flux values are then substituted into the energy equation for the calculation of the next intermediate temperature. This procedure is continued until the four (for a fourth order analysis) constants associated with each differential equation (continuity and energy) are calculated. At this point the temperature and concentration at a position advanced one interval unit into the char are calculated using equations (3-66) and (3-70).

This technique is repeated to the second boundary of the problem. If a non-iterative set of boundary conditions is specified (i.e., one boundary completely specified), the solution to the energy equation is obtained in one cycle and the calculation of the pressure and heat flux distributions can be started. If, however, a two point boundary value problem is being solved, a guessed value of the gradient must be used to start the solution. When the temperature at the front surface is calculated, it must be compared with the specified value. A calculated value which is too high or low requires an adjustment of the initial gradient and repetition of the entire procedure. Therefore, in addition to the Runge-Kutta logic, a convergence procedure to approach the known front surface temperature is also required.

Convergence Techniques for the Iterative Runge-Kutta Analysis: The specific convergence scheme used in the Iterative TEMPRE System is subdivided into three main parts. These include: (1) a gross correction procedure, (2) a fine correction procedure, and, (3) a limit or check procedure. Each method uses a simplified formula which bases the corrected adjustment on the relative overshoot or undershoot of the front surface temperature.

Gross Correction Procedure: This method is used when the absolute value of the difference in the calculated and true front surface temperature exceeds a specified tolerance limit (usually ≥ 5% of the specified front surface temperature). When this condition is met, adjustment of the initial slope is made using the following equation:

$$T'_{0_{new}} = T'_{0_{old}} \left(1 + \lambda \left[\frac{T_{L_{true}} - T_{L_{calculated}}}{T_{L_{true}}}\right]\right) \qquad (3\text{-}73)$$

where λ is an adjustable parameter from 0 to 1.

<u>Fine Correction Procedure</u>: This method is employed when the calculated front surface temperature falls between tolerance limits of $0.05 > 1 - T/T_L > 0.01$ of the specified value or when two complete cycles have been calculated. In this case a more precise adjustment is used taking advantage of the previous calculations to rapidly approach the specified front temperature and to prevent oscillations around that point. The specific equation used to adjust the initial gradient for the next iteration is:

$$T'_{0_{new}} = T'_{0_{old}} + \left[\frac{T_{L_{true}} - T_{L_{calc.\ this\ cycle}}}{T_{L_{calc.\ this\ cycle}} - T_{L_{calc.\ last\ cycle}}}\right] \left[T'_{0_{last\ cycle}} - T'_{0_{this\ cycle}}\right] \qquad (3\text{-}74)$$

Very good convergence is obtained with these simple equations over a range of front surface temperatures between 1500 - 3000°F and mass flux values between 0.00003 - 0.1 lb/ft^2-sec. Three iterations are required to obtain a solution within the stated tolerance range.

<u>Limit</u> <u>or</u> <u>Check</u> <u>Procedure</u>: A limit corresponding to a 20% overshoot of the front surface temperature is used to terminate the calculations at any point within the char where this condition is violated. A reduction in the initial gradient is made according to equation (3-73) and the procedure is restarted.

In addition to the above, several checks are included in the Runge-Kutta analysis to insure the calculated and/or adjusted values of the gradient remain non-negative and non-zero. The program logic includes an adjustment calculation similar to equation (3-73) which, on repeated violations, instructs the system to print pertinent information for diagnosis of the problem. With these simple adjustment equations, the iterative solution is obtained very quickly and with sufficient accuracy to insure a good approximation to the real solution.

A comparison of the temperature profiles obtained for the frozen flow energy equation (3-29) at various interval sizes is presented in Table 3-6. Based on the presented results, an interval size of one hundred units (or 1/400 ths of an inch for a one-quarter thick char) was used.

Table 3-6. Comparison of Various Runge-Kutta Increment Sizes for the Frozen Flow Variable Properties Model.

Dimensionless Char Distance (z/L)	Temperature (°F) Runge-Kutta Increment Sizes (A) 10	50	100	400
0.0	500.0000	500.0000	500.0000	500.0000
0.2	631.4212	625.6282	625.4788	625.4202
0.4	824.2823	819.5501	819.4515	819.3908
0.6	1106.1787	1102.8111	1102.7770	1102.7141
0.8	1494.5636	1492.8853	1492.8260	1492.7604
1.0	2000.0000	2000.0000	2000.0000	2000.0000

Conditions: $W = 0.05$ lb/ft^2-sec $L = 0.0208$ ft $\epsilon = 0.8$

Gas Composition: (Mole/Mole Gas)

$CO = 0.245$, $CO_2 = 0.046$, $N_2 = 0.073$, $CH_4 = 0.570$, $C_6H_6 = 0.068$

Numerical Solutions of the Heat Flux and Momentum Equations

The heat flux and momentum equations are solved after a valid temperature profile is calculated. Both heat flux and pressure are uncoupled from the energy equation by considering the energy dissapation by PV work small in comparison with other modes of energy transfer in the system. The equations for the heat flux and pressure are first order differential equations with variable coefficients.

$$q_{c_z} = \sum_{i=1}^{K} \int_{T_o}^{T_L} \epsilon W_p C_{P_i} x_i \, dT + \sum_{i=1}^{K+1} H_i \bar{R}_i dT \qquad (3\text{-}23)$$

$$P = \left\{P_L^2 + 2R \int_z^L \left(\frac{\mu}{\gamma}\right)(W)\left(\frac{T}{M_w}\right)dz + \int_z^L \beta\left(\frac{T}{M_w}\right)(W)^2 dz\right\}^{\frac{1}{2}} \qquad (3\text{-}12)$$

A Simpson's Rule integration technique is used to obtain solutions for the integral terms in these equations. The general formula for the Simpson's Rule analysis is (23):

$$\int_{z_o}^{z_{2n}} f dz = \frac{h}{3}\Big[f_o + 4\,(f_i + f_3 + \ldots + f_{2n-1})$$

$$+ 2(f_2 + f_4 + \ldots + f_{2n-2}) + f_{2n}\Big] - \frac{nh^5}{90} f^{(4)}$$

$$(3\text{-}75)$$

where $\frac{nh^5}{90} f^{(4)}$ represents the truncation error.

In terms of the heat flux and pressure equations, the

Simpson's Rule functions are:

$$\int f_{p_1} dz = \int (\frac{\mu}{\gamma})(W)(\frac{T}{M_w}) dz \qquad (3\text{-}76)$$

$$\int f_{p_2} dz = \int \beta (\frac{T}{M_w})(W)^2 dz \qquad (3\text{-}77)$$

$$\int f_{h_1} dz = \int \epsilon W_p C_p x_i dT \qquad (3\text{-}78)$$

$$\int f_{h_2} dz = \int H_i \bar{R}_i dT \qquad (3\text{-}79)$$

Once again the step-size is an important parameter that must be specified. A similar procedure as that described for the Runge-Kutta analysis to obtain the optimum value of the interval size was used. This minimizes the errors and maximizes the accuracy of the approximate solution. A comparison of the solutions for various step sizes as presented in Table 3-7. An interval size of twenty steps was used in this analysis. Calculation of the pressure profile within the char is made from the front surface where $P = P_L$ to the rear surface pressure. Results are reported as a pressure distribution and a surface heat flux which correspond to the total heat transferred within the char zone.

Summary of the Theoretical Development of the Equations of Change for Flow in the Char Zone

The equations of change (continuity, momentum, and energy)

Table 3-7. Comparison of Various Simpson's Rule Increment Sizes for the Frozen Flow, Variable Properties Model.

Dimensionless Char Distance	Pressure (lb/ft^2) Simpson's Rule Increment Sizes			
(z/L)	20	50	100	200
0.00	2175.5921	2175.5918	2175.5913	2175.5912
0.33	2173.4147	2173.4144	2173.4139	2173.4138
0.67	2168.7373	2168.7368	2168.7364	2173.7364
1.00	2160.0000	2160.0000	2160.0000	2160.0000

Conditions: $W = 0.05\ lb/ft^2$-sec $L = 0.0208$ ft $\epsilon = 0.8$

Gas Composition: (Mole/Mole Gas)

$CO = 0.245$, $CO_2 = 0.046$, $CH_4 = 0.570$, $N_2 = 0.073$, $C_6H_6 = 0.068$

were developed for modeling the reacting flow of pyrolysis gases through the char zone of a charring ablator. The particular application to frozen, equilibrium, and non-equilibrium flow were discussed along with methods for determining the heat absorption by chemical reaction for the latter two models. A free energy minimization technique was employed for calculating the composition and heat absorption resulting from chemical reactions assumed to occur at equilibrium.

For the non-equilibrium flow, a discussion of the importance of the particular reactions considered in the model, associated kinetic data and initial pyrolysis gas composition entering the char was presented.

Typical boundary conditions were presented which led to two separate solutions to the differential energy equation. These were:

(1) The iterative solution which resulted by specifying the front and back surface temperatures with the gradient unknown at either location, and,

(2) the non-iterative solution obtained by specifying the temperature and temperature gradient (heat of pyrolysis) at the rear surface of the char. A fourth order Runge-Kutta numerical integration method was used to achieve the solution as a temperature distribution across the char.

Similarly, the momentum and heat flux equations were integrated using Simpson's Rule. The solutions were presented as a pressure distribution across the char and a heat flux at the char front surface. A fourth order Runge-Kutta integration of the species continuity equation, coupled with the energy equation, produced concentration gradients for each pyrolysis gas species as a function of the char distance.

Specific values of the solutions will be presented and compared with experimental data obtained on the Char Zone Thermal Environment Simulator in Chapter VI. A detailed presentation of the experimental apparatus and procedure follows in Chapters IV and V, respectively.

REFERENCES

1. Peters, R. W. and K. L. Wadlin, "The Effect of Resin Composition and Fillers on the Performance of a Molded Charring Ablator," NASA TN D-2024, 9 (December 1963).

2. Weger, Eric, Jere Brew and Ronald Servais, "An Investigation of Carbon Deposition in Chars - II," Report SAMSO-TR-68-123, Washington University, St. Louis, Missouri, 96 pages (January 1968).

3. Wilson, R. Gale, "Thermophysical Properties of Six Charring Ablators from 140° to 700°K and Two Chars From 800° to 3000°K," NASA TN D-2991 (October 1965).

4. Clark, Ronald K., "Flow of Hydrocarbon Gases in Porous Media at Elevated Temperatures," M.S. Thesis, University of Virginia, 108 pages (August 1968).

5. Engelke, W. T., C. M. Pyron, Jr., and C. D. Pears, "Thermophysical Properties of a Low Density Phenolic-Nylon Ablation Material," NASA CR-809 (July 1967).

6. Nagler, R. G., "The Thermal Conduction Process in Carbonaceous Chars," JPL Technical Report 32-1010, Jet Propulsion Laboratory, California Institute of Technology, Pasadena, California (February 1967).

7. Koh, J. C. Y. and E. P. del Casal, "Heat and Mass Flow Through Porous Matrices for Transpiration Cooling," Paper 16, Proceedings of the 1965 Heat Transfer and Fluid Mechanics Institute, Stanford University Press, Los Angeles, California, 263-81 (June 21-23, 1965).

8. Bird, R. B., W. E. Stewart, and E. N. Lightfoot, Transport Phenomena, John Wiley & Sons, Inc., New York, 328-30 (1960).

9. Scheidegger, Adrian E., The Physics of Flow Through Porous Media, University of Toronto Press, 68-76 (1960).

10. del Valle, E. G., R. W. Pike and G. C. April, "Transport Phenomena in the Char Zone During Ablation. II: Equilibrium Composition of Degradation Products of Ablation," Paper 13e, 63rd National Meeting of the A.I.Ch.E., Salt Lake City, Utah (May 1967).

11. Zeleznik, F. J. and S. Gordon, "A General IBM 704 or 7090 Computer Program for Computation of Chemical Equilibrium Composition, Rocket Performance, and Chapman-Jouguet Detonation," NASA TN D-1454 (October 1962).

12. White, W. B., S. H. Johnson and G. B. Dantzig, "Chemical Equilibrium in Complex Mixtures," Journal of Chemical Physics, 28 (5), 751-5 (May 1958).

13. Schmidt, D., "Thermal Parameters of Re-Entry Ablative Plastics," WADD Technical Report 60-90, Wright-Patterson AFB, Ohio, Aeronautical Systems Division (1960).

14. Pike, R. W., "Evaluation of the Literature for Chemical Reactions and the Reaction Rates for the Decomposition Products from Charring Ablators," NASA LWP-181, Langley Research Center, Hampton, Virginia (January 1966).

15. Pike, R. W., Gary C. April and E. G. del Valle, "Non-Equilibrium Flow and the Kinetics of Chemical Reactions in the Char Zone," NASA CR-66455 (July 1967).

16. Nelson, James B., "Determination of Kinetic Parameters of Six Ablation Polymers by Thermogravimetric Analysis," NASA TN D-3919 (April 1967).

17. Sykes, George F., Jr., "Decomposition Characteristics of a Char-Forming Phenolic Polymer Used for Ablative Composites," NASA TN D-3810 (February 1967).

18. Scala, S. M. and L. M. Gilbert, "Thermal Degradation of a Char-Forming Plastic During Hypersonic Flight," <u>ARS Journal</u>, <u>32</u> (6), 917-24 (June 1962).

19. Kratsch, K. M., L. F. Hearne and H. R. McChesney, "Thermal Performance of Heat Shield Composites During Planetary Entry," AIAA-NASA National Meeting, Palo Alto, California, 3 (September 30-October 1, 1963).

20. Sykes, G. F., Private Communication to R. W. Pike (March 14, 1968).

21. Reid, R. C. and Sherwood, T. K., The Properties of Gases and Liquids, 2nd ed., McGraw-Hill Book Co., New York, 395-519 (1966).

22. McBride, Bonnie J., Sheldon Heimel, J. G. Ehbens, Sanford Gordon, "Thermodynamic Properties to 6000°K for 210 Substances Involving the First Eighteen Elements," NASA SP-3001 (1963).

23. Abramowitz, Milton and I. A. Stegun, editors, Handbook of Mathematical Functions with Formulas, Graphs, and Mathematical Tables, 3rd Printing, National Bureau of Standards Applied Mathematics Series 55, Washington, D.C., 886, 896-7 (1965).

24. Freidman, H. L., "Pyrolysis of Plastics in a High Vacuum Arc Image Furnace," Journal of Applied Polymer Science, 9, 1005 (1965).

25. Shulman, G. P., and H. W. Lochte, "Thermal Degradation of Polymers. II. Mass Spectrometric Thermal Analysis of Phenol-Formaldehyde Polycondensates," Journal of Applied Polymer Science, 10, 619-635 (1966).

26. Beecher, Norman, and Ronald E. Rosensweig, "Ablation Mechanisms in Plastics with Inorganic Reinforcement," ARS Journal, 31, 532-538 (1961).

IV. CHAR ZONE THERMAL ENVIRONMENT SIMULATOR

Introduction

The experimental data presented in this study were obtained using an apparatus that simulated the flow of pyrolysis gases through the char layer of a charring ablator during reentry. Low density nylon-phenolic resin chars, graphite and carbon were obtained from the National Aeronautics and Space Administration's Entry Structures Branch at the Langley Research Center. These specimens were placed in a metal holder with the front surface exposed to a bank of infrared quartz lamps used to simulate the high temperatures experienced by a reentering vehicle. Simulated pyrolysis gases were passed through the char from the rear surface to the heated front surface. The exit gases were sampled and analyzed for comparison with the inlet gas composition to determine whether chemical reactions had occurred within the char. These results were also compared with the calculated exit gas compositions for frozen, equilibrium and non-equilibrium flow conditions in the TEMPRE system. This was the method used to determine the accuracy of the non-equilibrium model for predicting the heat transfer for the flow of reacting pyrolysis products in the char zone.

A schematic diagram of the Char Zone Thermal Environment Simulator is shown in Figure 4-1. For convenience, the system

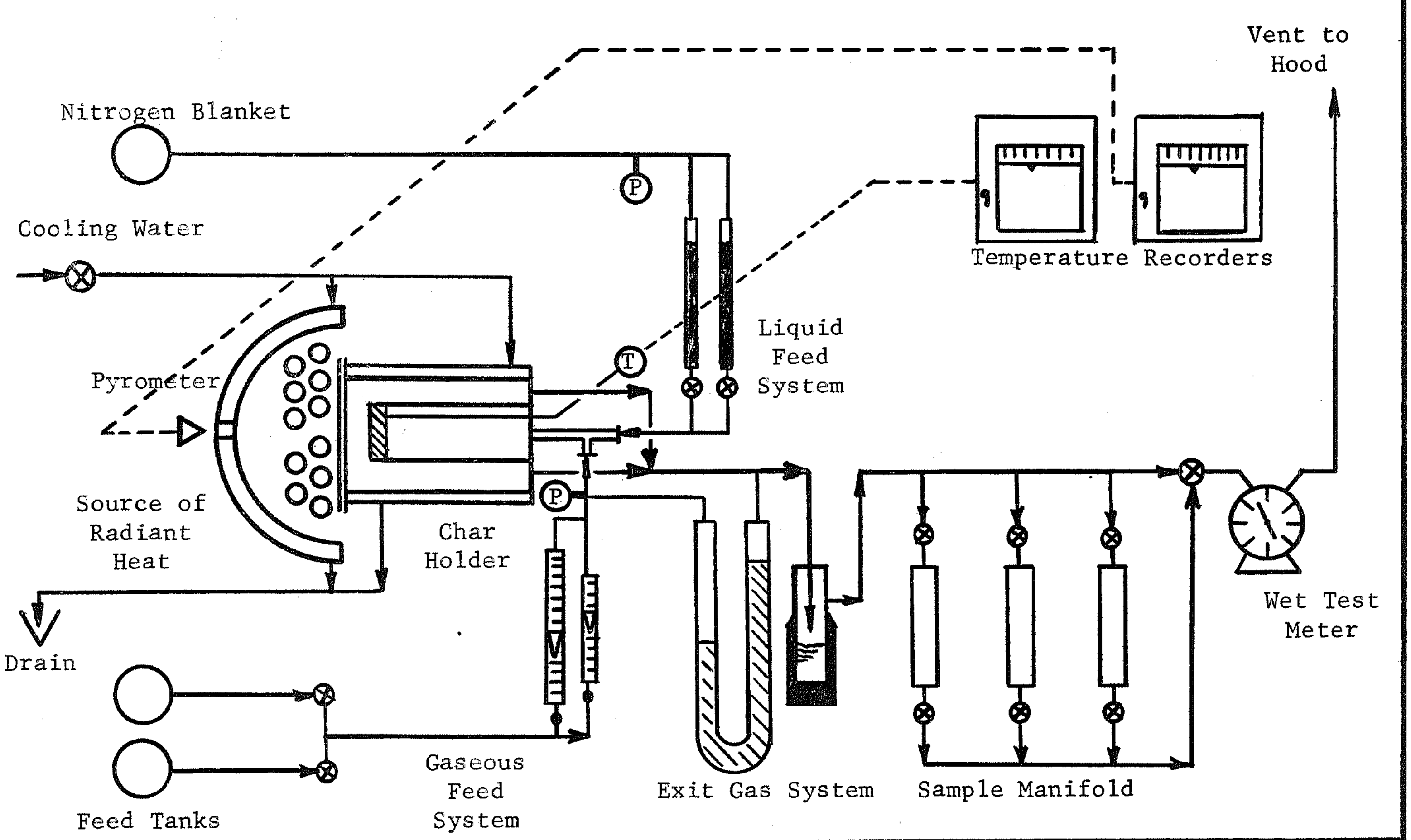

Figure 4-1. Schematic Diagram of the Char Zone Thermal Environment Simulator

has been divided into five sections. These are:

(1) The Char Holder

(2) The Radiant Heating System

(3) The Pyrolysis Gas Feed and Sampling System

(4) The Analytical and Measuring Equipment

(5) The Radioactive Tracer System

Each of the above will be discussed in the following paragraphs.

Char Holder

The most important part of the experimental apparatus is the char holder. It was constructed to permit the heating of one surface to produce the temperature gradient experienced during reentry, and, to flow simulated pyrolysis gases through the char with collection of the exit gases for chemical analysis. Comparison of the exit gas composition with the inlet values determined whether chemical reactions occurred within the char layer. Rapid cooling of the exit gases to prevent further thermal decomposition was another important feature of the design.

A sectional diagram of the holder is shown in Figure 4-2. It was constructed of two steel pipes arranged in a concentric pattern. The outer section was six inches in diameter (O.D.) and five inches long. A five and three-eighths inch diameter by one-eighths inch thick quartz glass cover plate was attached to the front surface by a flange plate and two asbestos gaskets.

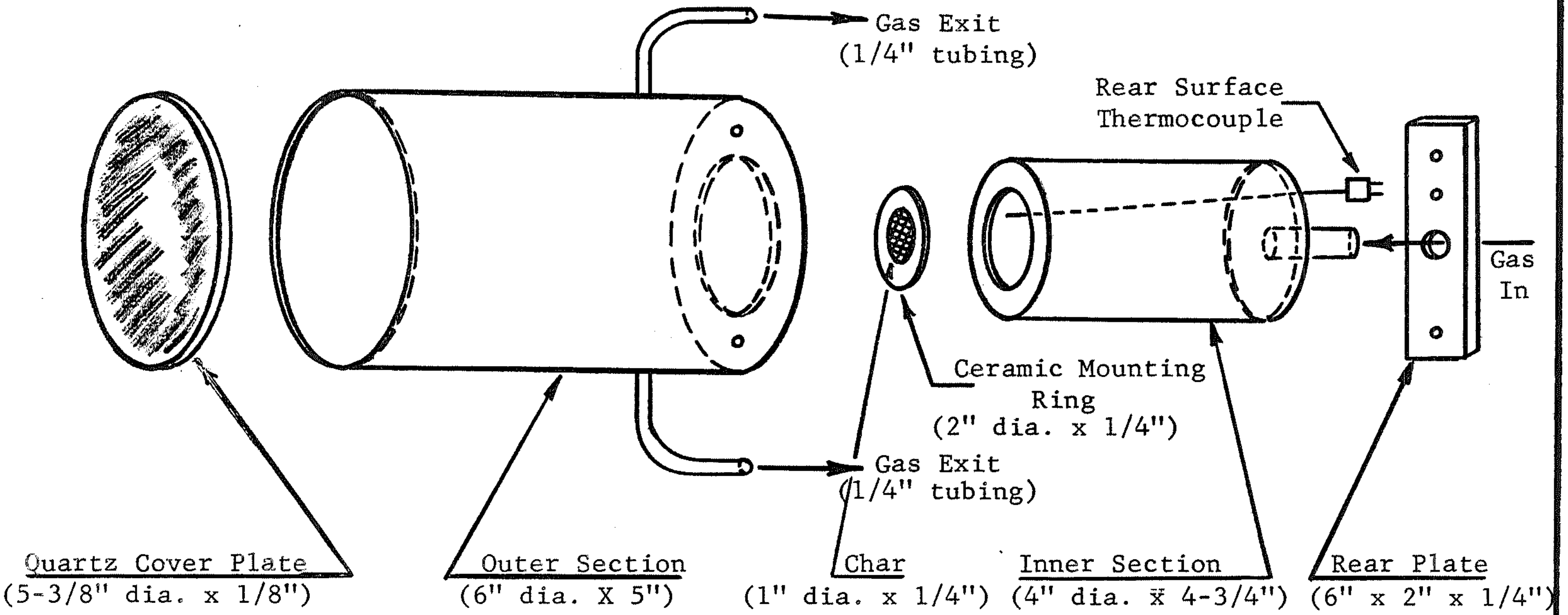

Note: Outer Section of Holder is coiled with 1/4" copper tubing and insulated (Thermon T-63).

Figure 4-2. Sectional Diagram of the Char Holder and Associated Parts.

The quartz glass plate sealed the holder on that face and was transparent to the radiant energy from the infrared lamps. A rear plate eight inches square was welded to the outer pipe. There was a four inch diameter (O.D.) slot cut in the center of this flange for mounting the inner pipe. Insertion of the inner section sealed the holder at the rear.

The outside portion of the larger pipe was coiled with one-quarter inch copper tubing and covered with Thermon T-63 high temperature cement for maximum heat exchange. Water was used as the coolant. Also two one-quarter inch lines were located at the base of the larger pipe for the pyrolysis gases to flow from the annular to the sampling system.

The inner pipe was four inches in diameter (O.D.) and four and three-quarters inches long. The front surface was machined to hold a two inch diameter char specimen which was cemented in place with Mullite No. 67-751 or Sauereisan No. 29 cement. The rear surface had a one quarter inch machined lip used to seal the inner and outer sections of the holder. A rectangular plate was used to hold the inner section firmly in place. Two one-quarter inch lines were located in the rear flange of the inner pipe sections for entry of the simulated pyrolysis gas flow and back surface temperature measurement.

The char specimens were made from low density nylon-phenolic resin composites which had been formed in the high voltage arc image furnaces at the Langley Research Center. They were about two and one-half inches in diameter by one-quarter inch thick. These specimens were cut to give a cross sectional area of 0.5 to 1.5 square inches, and were mounted in a two inch diameter mold using Mullite or Sauereisan cement. The cement was inert and very stable at the elevated temperatures experienced during experimentation. In Figure 4-3 the various steps in the molding procedure are illustrated. High density nylon-phenolic resin composite chars, graphite and carbon specimens were mounted in the same manner. A list of the various materials used is shown in Table 4-1.

Radiant Heating System

The radiant heating system was composed of several infrared, quartz heating elements (Figure 4-4) connected in delta on a three phase terminal block. A 220 volt (100 amp maximum current) power source was used to illuminate the lamps. The quantity, type and location of the elements from the specimen surface are listed in Table 4-2 for various ranges of front surface temperatures. The lamps were arranged in two staggered rows parallel to the specimen front surface. The terminal blocks were constructed of nylon and, along with the metal lamp tips, were cooled by forcing dry air across these areas from a Le Roi, Model RX1, two stage compressor.

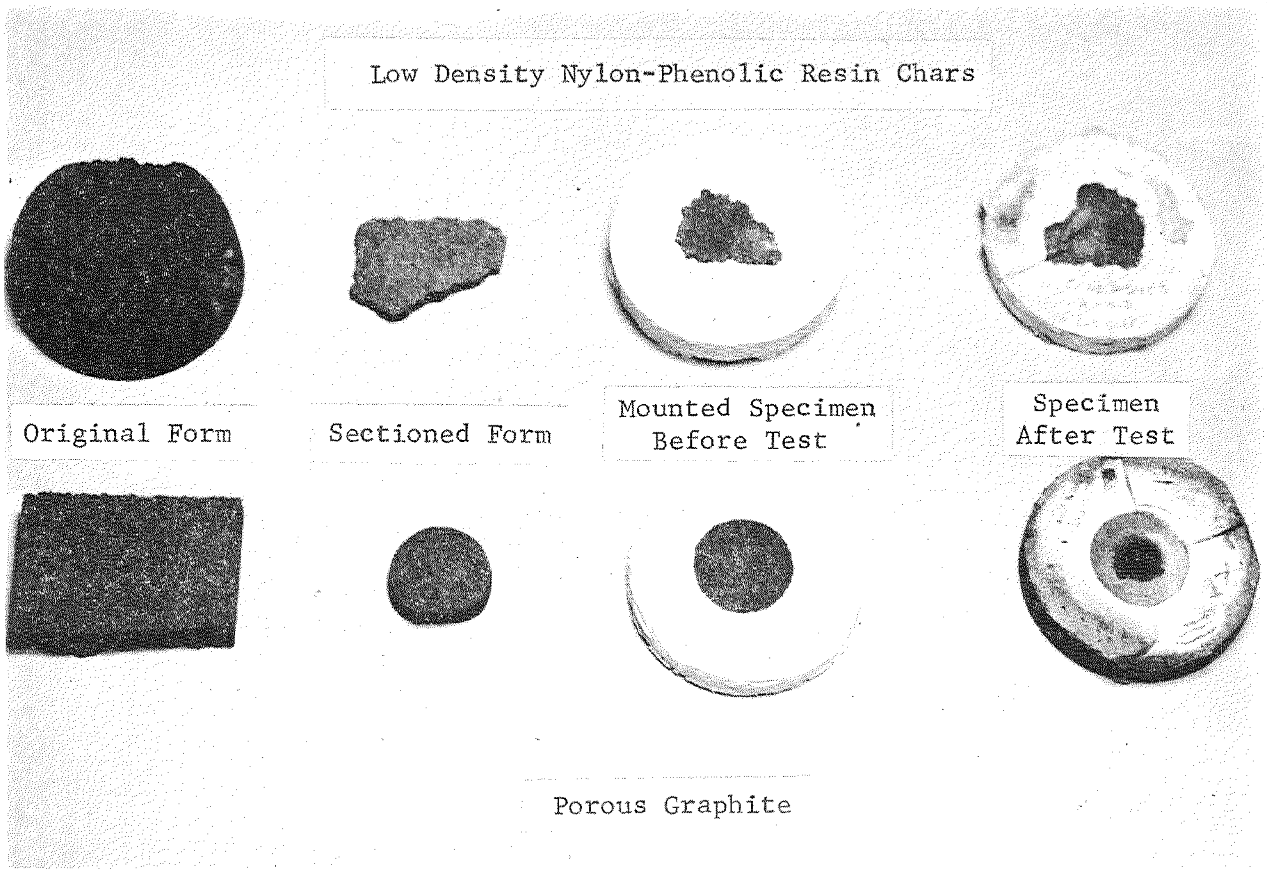

Figure 4-3. Various Steps in the Molding Procedure for Low Density Nylon-Phenolic Resin Chars and Graphite.

Photo by J. R. Langley

Table 4-1. Identification and Properties of the Char and Graphite Specimens Tested in the Char Zone Thermal Environment Simulator.

POROUS MEDIUM	CODE IDENTIFICATION	AVERAGE POROSITY	DENSITY, lb/ft^3		PORE DIAMETER, μm	THERMAL CONDUCTIVITY AT 70°F BTU/ft-sec-°R
			APPARENT	TRUE		
High Density Nylon-Phenolic Resin Char	LRC-HD-(xxx-xxxx)	0.75	22.4	91.7	24	0.5
Low Density Nylon-Phenolic Resin Char	LRC-LD-(xxx-xxxx)	0.86	13.1	92.9	8	0.4
High Pore Graphite - Grade 25	LRC-HP-GR(y)-25	0.47	-	64.4	119	1.0
Low Pore Graphite - Grade 45	LRC-LP-GR(y)-45	0.47	-	65.0	58	1.0

Notes:

(1) LRC indicates the supplier of the char and graphite specimens (Langley Research Center -NASA).

(2) HD = High Density, LD = Low Density, HP = High Pore, LP = Low Pore, GR = Graphite.

(3) The notation in (xxx-xxxx) is additional LRC identification; e.g. C9-S102.

(4) The notation (y) is a code for the catalyst(s) used in a particular test run;
a = Tungsten and Molybdenum Catalysts coated on the graphite specimen,
b = Bromine (Homogeneous) Catalyst fed with the pyrolysis gas mixture,
c = Platinum Catalyst coated on the graphite specimen.

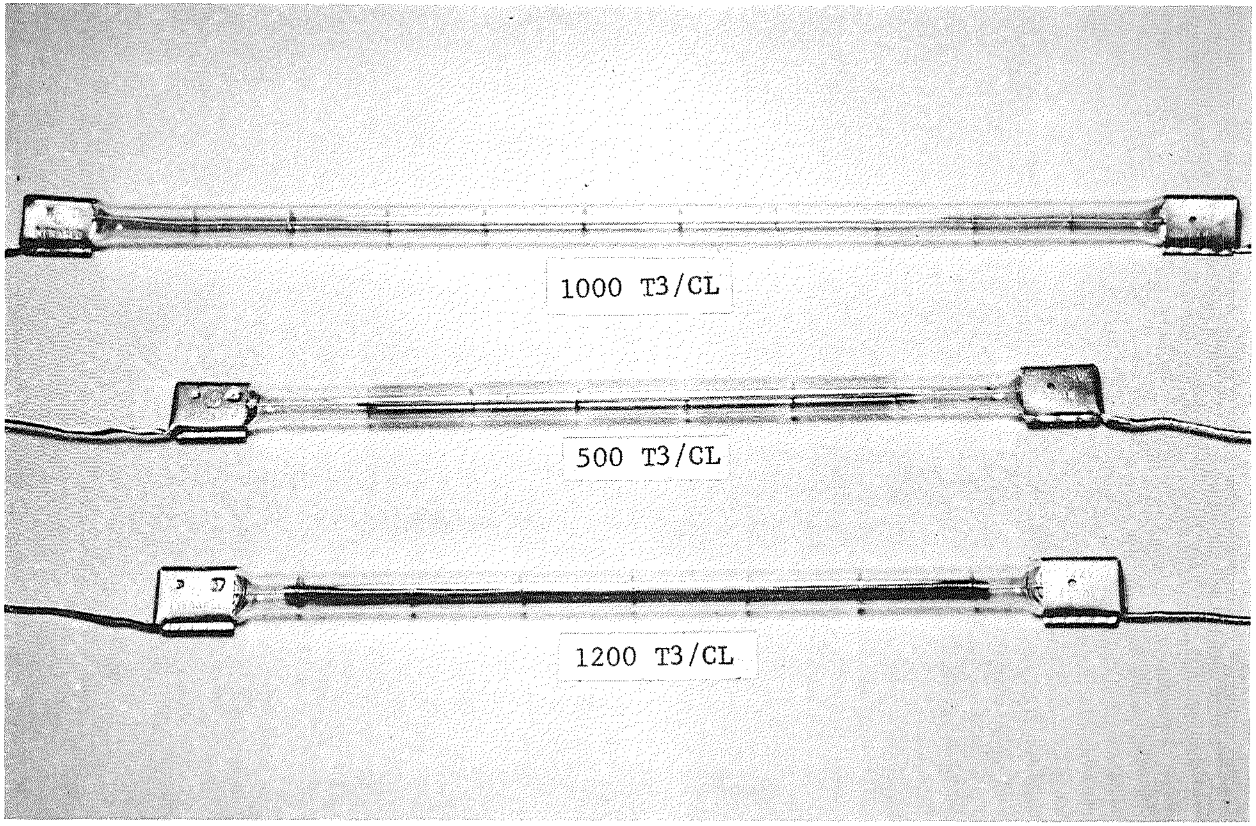

Figure 4-4. Intrared Quartz Heating Lamps.

Photo by J. R. Langley

Table 4-2. Heating Lamp Requirements and Description for Maintaining the Char Front Temperature at a Specific Value.

LAMP TYPE	DESIGN VOLTAGE	OPERATING VOLTAGE	FILAMENT	LENGTH, inches		LIFE hr	QUANTITY USED	TEMPERATURE RANGE, °F	INDEX TO RUNS
				OVERALL	FILAMENT				
1000T3/CL	240	204	Tungsten	13.81	10.0	9	15	1350-1750	I-XII
500T3/CL	120	204	Tungsten	8.81	5.0	9	15	1550-1800	XIII-XV
1200T3/CL	144	204	Tungsten	8.81	6.0	-	9	1800-2300	XVI-XXXII

Notes: (1) 500T3/CL lamps operated at double the rated voltage.

(2) 1200T3/CL lamps operated at one and one half the rated voltage.

(3) Temperature range is also a function of the air coolant flow rate. The above values are for an air flow rate that maintained the lamp terminals below 400°F.

Type THW 600 volt copper wire was used to connect the terminal leads to the main power supply switch. Figure 4-5 shows a complete electrical circuit diagram for the radiant heating system.

A reflector constructed of gold-plated aluminum was mounted on the rear, sides, top and bottom to concentrate the radiant energy on the specimen. The rear, top, and bottom sections were water cooled using three-eighths inch copper tubing with a Thermon T-63 cement coating for maximum heat exchange. A one half inch hole was located in the rear reflector for the purpose of measuring the front surface temperature with an optical pyrometer. A complete sectional diagram of the radiant heating system is shown in Figure 4-6.

Pyrolysis Gas Feed and Sampling System

The compositions of the simulated pyrolysis gas used in the experiments are listed in Table 4-3. Several of the earlier experimental runs reported were made with a simulated pyrolysis gas composed of methane, hydrogen, carbon monoxide, carbon dioxide and nitrogen (1,2). Later experiments included water and phenol in addition to the above mentioned gas species (3,4,5). This last mixture required the construction of a two phase feed system (liquid water and phenol at room temperature) with subsequent vaporization of the liquid

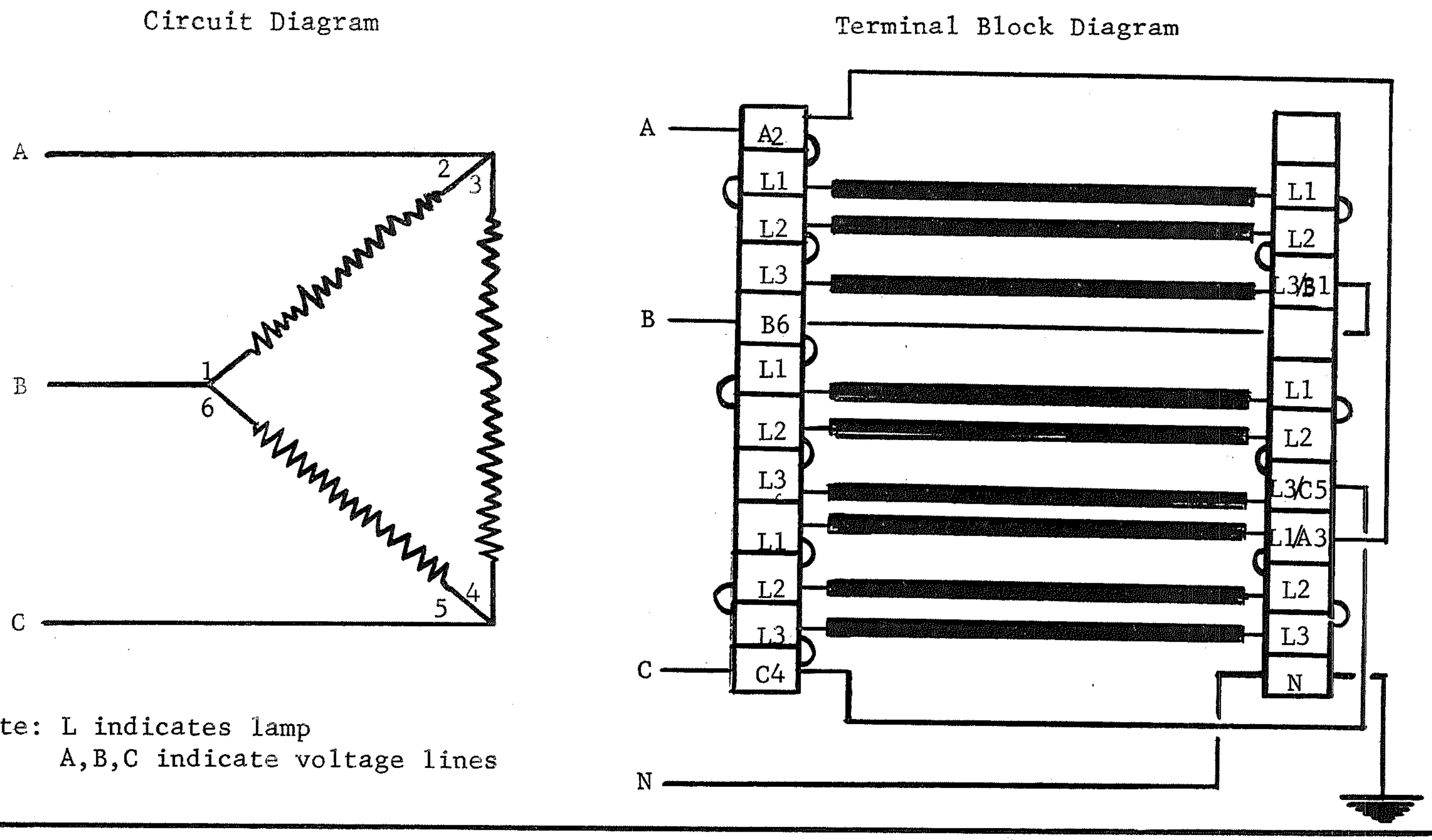

Circuit Diagram

Terminal Block Diagram

Note: L indicates lamp
A,B,C indicate voltage lines

Figure 4-5. Electrical Circuit Diagrams of the Radiant Heating System.

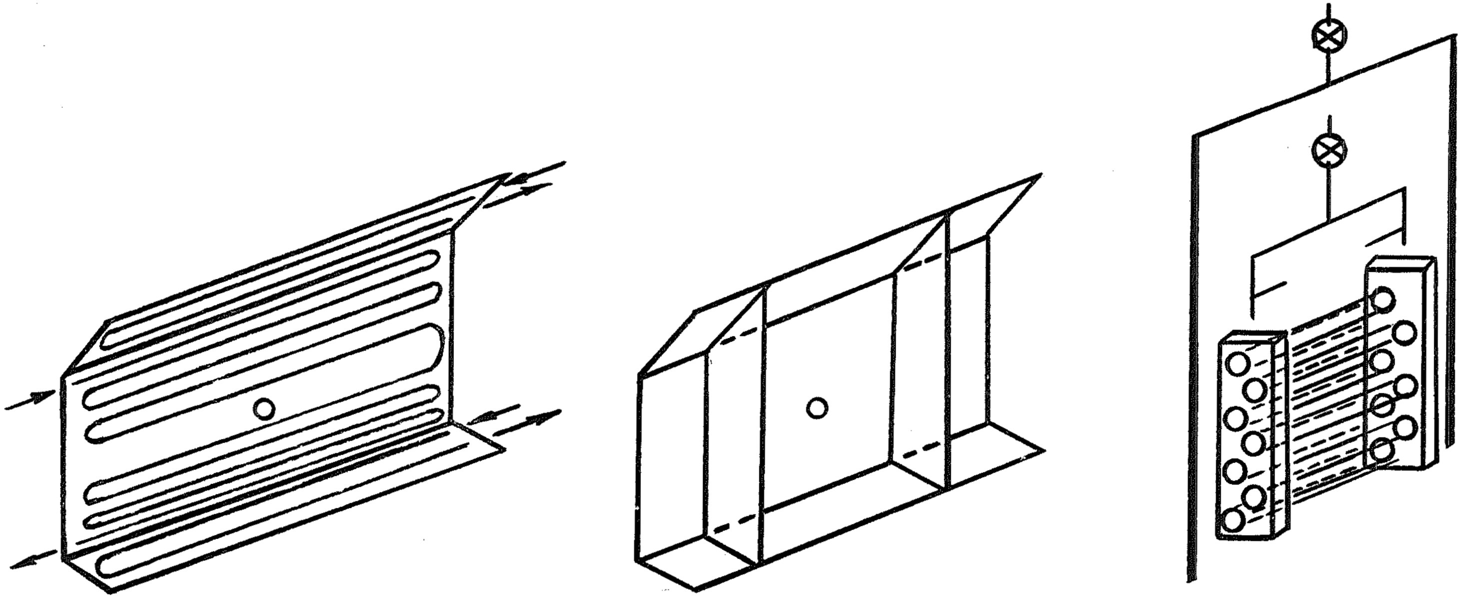

Reflector Back-up Plate
with 3/8" Copper Tubing for
Water Cooling

(Insulated with Thermon T-63)

Gold-Plated Reflector Plate
(Front Surface Only)

Lamp Supports with
Air Coolant Lines
for Lamp Terminal
Cooling

Figure 4-6. Sectional Diagram of the Radiant Heating System.

Table 4-3. Simulated Pyrolysis Gas Mixtures Used in Experiments on the Char Zone Thermal Environment Simulator.

COMPONENT	IDENTIFICATION		SIMULATED PYROLYSIS GAS COMPOSITIONS (Mole %)				
	SUPPLIER	GRADE	FEED MIX 1	FEED MIX 2	FEED MIX 3	FEED MIX 4	FEED MIX 5 (b)
CH_4	Matheson	99.9%	32.5	43.6	46.3	6.7	6.7
H_2	Matheson	99.95%	37.2	35.0	31.7	33.4	33.4
CO	Matheson	99.5%	8.2	4.9	5.5	3.7	3.7
CO_2	Matheson	99.5%	6.6	2.9	2.5	1.1	1.1
N_2	Airco	99.7%	15.5	13.6	14.0	0.0	0.0
(a) C_2H_6	Matheson	99.0%	-	-	-	-	-
(a) C_2H_4	Matheson	99.0%	-	-	-	-	-
(a) C_2H_2	Airco	99.6%	-	-	-	-	-
C_6H_6O	Merck	Reagent	0.0	0.0	0.0	6.2	6.2
H_2O	Distilled (CO_2 free)		0.0	0.0	0.0	48.9	48.9
INDEX OF EXPERIMENTS			I-IV	V-XII	XIII-XVIII	XIX-XXVI	XXVII-XXXII

Notes: (a) These gases were used to calibrate the gas chromatograph for analysis as products in the exit stream from the Char Zone Thermal Environment Simulator.

(b) This feed mix was purchased from the Matheson Company as a pre-mix (gases only) containing 250 μc of carbon-14 labeled methane (6μc per lb mole).

components prior to their entry into the char holder.

The gaseous portion of the pyrolysis products were premixed and stored in a two and one-half cubic foot gas cylinder at a pressure of 250-500 psig. The gas was pressure fed through a one-quarter inch copper tube to a rotameter located on the instrument board. The liquid components were likewise pressure fed from individually calibrated feed vessels. The liquid and gaseous streams entered the inner section of the char holder at a junction near the back of the apparatus. The temperature of the line and the holder were maintained above the boiling point of the liquid components.

The pyrolysis products flowed through the char and exited through the annular space. They then passed through an ice water-cooled gas-liquid separator where condensation of the unreacted water and phenol, as well as any liquid products, were collected and analyzed. The gaseous portion continued to a gas sampling manifold. This section was composed of a series of one hundred cubic centimeter pyrex sampling bombs mounted in parallel on the instrument board. A by-pass line was used to divert the exit gas flow around the sampling bombs, such that these containers could be removed during an experiment and replaced with empty bombs. A wet test meter was used to measure the volumetric flow rate of the exit gas stream. Figure 4-7 is a photograph of the feed, exit

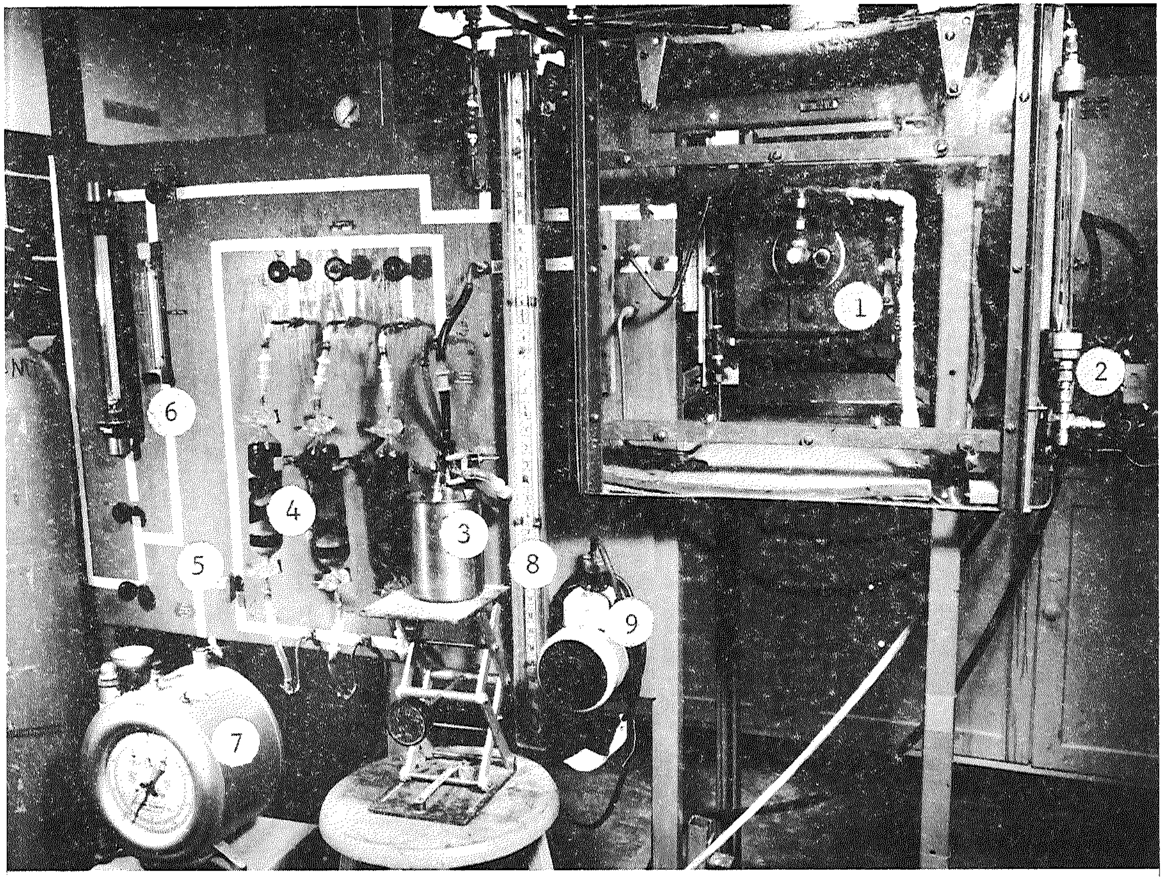

LEGEND

① Char Holder

② Liquid Feed Burets

③ Liquid-Gas Separator

④ Gas Sampling Container

⑤ By-Pass Valve

⑥ Rotameter

⑦ Exit Gas Wet Test Meter

⑧ Manometer

⑨ Powerstat to Heated Gas Inlet Lines

Figure 4-7. Photograph of the Char Zone Thermal Environment Simulator.

Photo by J. R. Langley

gas and sampling sections of the apparatus.

The char holder and radiant heating systems were totally enclosed in a transite (sides, top and bottom) and plexiglass (doors) box which was connected to the laboratory hood with a four inch diameter flexible pipe.

Analytical and Measuring Equipment

Temperature: There were several locations in the system where temperature measurements were made during an experiment. These are indicated in Figure 4-1. In all locations except the front char surface, iron-constantan thermocouples were used. The front surface char temperature was measured with a Leeds and Northrup Model 8891c Rayotube total radiation pyrometer. The pyrometer focused on a one-quarter inch diameter section of the front char surface at a distance of ten inches from the sighting element. A one-half inch hole was cut in the back section of the reflector plate to allow focusing on the char surface. A Leeds and Northrup Speedomax H recorder was used to monitor the front surface temperature. A Leeds and Northrup Model 1549172 Galvonometer was used to measure the temperature of the other locations. The accuracy of the thermocouple measurements were checked to ± 2%, and the optical pyrometer to ± 1% at a maximum temperature of 2500°F. Calibration of the temperature measuring equipment was made at various intervals prior to experimental runs.

Pressure: The pressure drop across the char was measured with a U-tube manometer. Water was used as a manometer fluid and readings of ± 0.05 inches (of water) were obtainable. Pressure gauges were located at the top of the liquid feed vessels and in the process feed line to make certain the pressure gradient was sufficient to maintain flow from the vessels. Figure 4-1 indicates the location of the various pressure measuring devices used.

Metering: The flow rate of the gaseous portion of the pyrolysis products was measured using one of two rotameters. A Fischer-Porter Model FP 1/2-21-G-10/83 (2.55 scfm air) rotameter tube was used for high flow conditions and a Schutte-Koernig Model SK 1/8-15-C-5 (0.5 scfm air) rotameter tube was used in low flow applications. Calibration of these meters were made with air and helium flow using an American 0.1 cubic foot per hour wet test meter. The rotameter values were readable to ± 2% of scale.

Liquid flow was metered using calibrated twelve inches long by one quarter inch diameter (I.D.) Fischer-Porter glass cylinders. These tubes were calibrated with water and were readable to ± 1% of scale. These vessels were rated at a 30 psig working pressure.

A 0.1 cubic foot per hour wet test meter was used to measure the volumetric flow rate of the gas portion of the total product stream. This was done to obtain a material balance on the system. Material balances for the experimental runs were within 95-102% unless otherwise indicated on the experimental data sheets in Appendix D .

Gas Analysis: The collected exit gases from the char layer were analyzed on a Packard Model 7800 gas chromatograph equipped with a Model 871 proportional temperature controller and a Model 836 power supply. A Model 802 dual column oven was also included in the chromatographic system. Figure 4-8 is a photograph of the analytical equipment.

Two columns were used to determine the composition of the sampled gases. A nine foot by one quarter inch diameter column packed with Hewlett-Packard BPL-20 activated charcoal was used to determine hydrogen, carbon monoxide and methane compositions. A typical scan of the various gas species is shown in Figure 4-9. Approximately fourteen minutes were required to obtain a complete scan.

The second column was a six foot by one quarter inch glass column packed with Porapak S manufactured by Waters Associates, Incorporated. This column separated methane, carbon dioxide, ethylene, acetylene and ethane. A typical scan for these species is shown in Figure 4-10. Approximately seventeen minutes were required to complete this analysis.

Duplicate and triplicate samples were used to obtain an

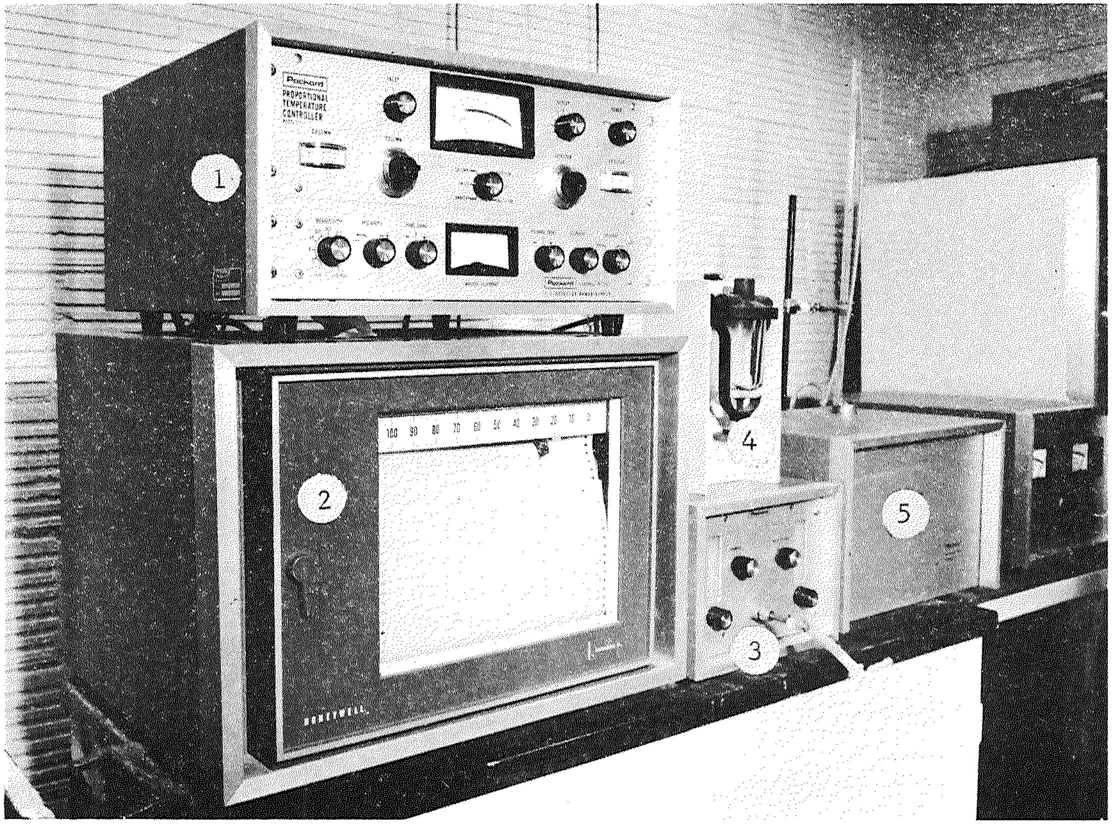

LEGEND

① Temperature Controller

② Recorder

③ Sampling Part

④ Sample Flow Indicators

⑤ Column Oven

Figure 4-8. Photograph of the Gas Chromatographic System.
Photo by J. R. Langley

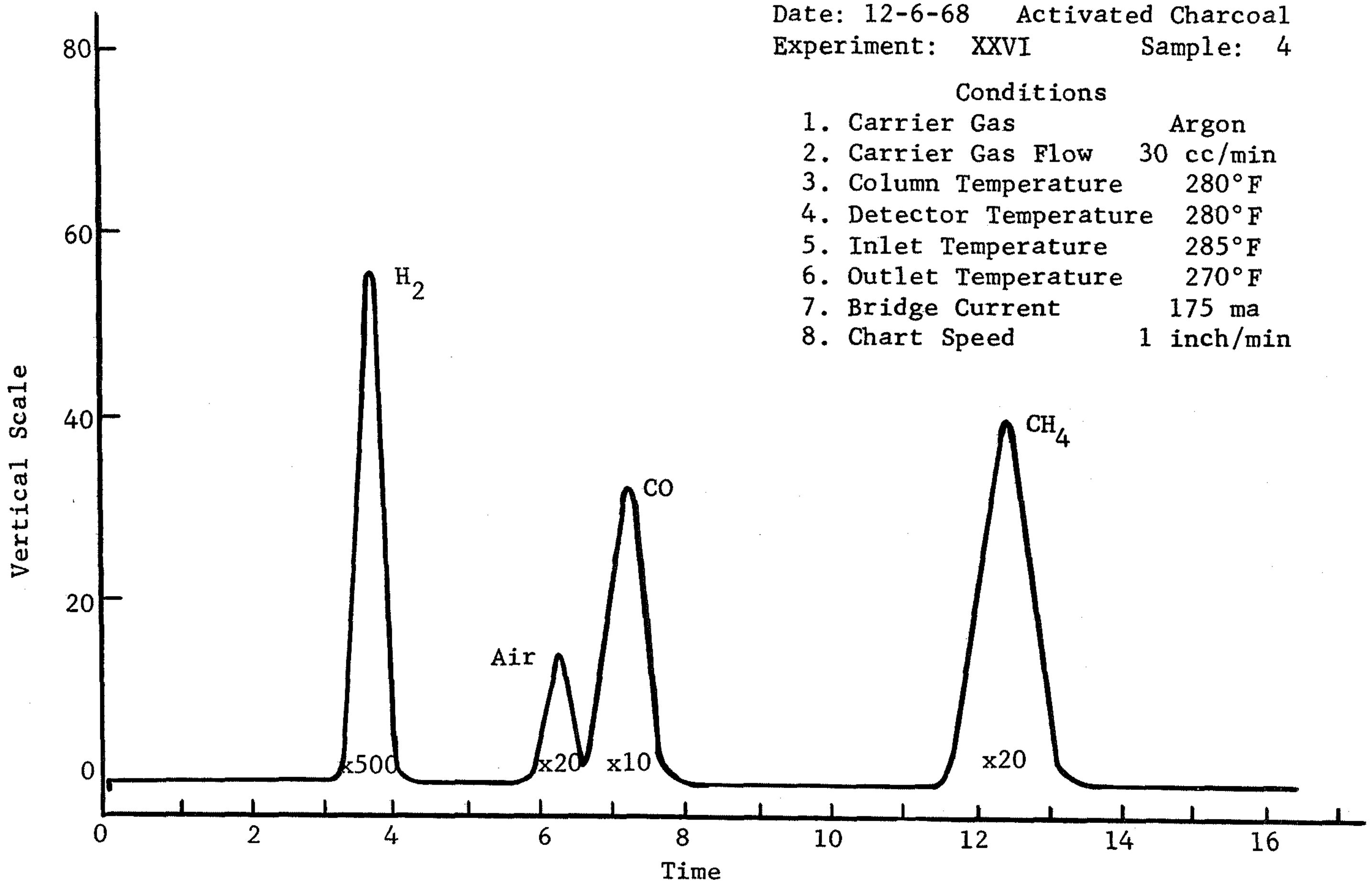

Date: 12-6-68 Activated Charcoal
Experiment: XXVI Sample: 4

Conditions

1. Carrier Gas	Argon
2. Carrier Gas Flow	30 cc/min
3. Column Temperature	280°F
4. Detector Temperature	280°F
5. Inlet Temperature	285°F
6. Outlet Temperature	270°F
7. Bridge Current	175 ma
8. Chart Speed	1 inch/min

Figure 4-9. Typical Gas Chromatographic Scan for Activated Charcoal Column.

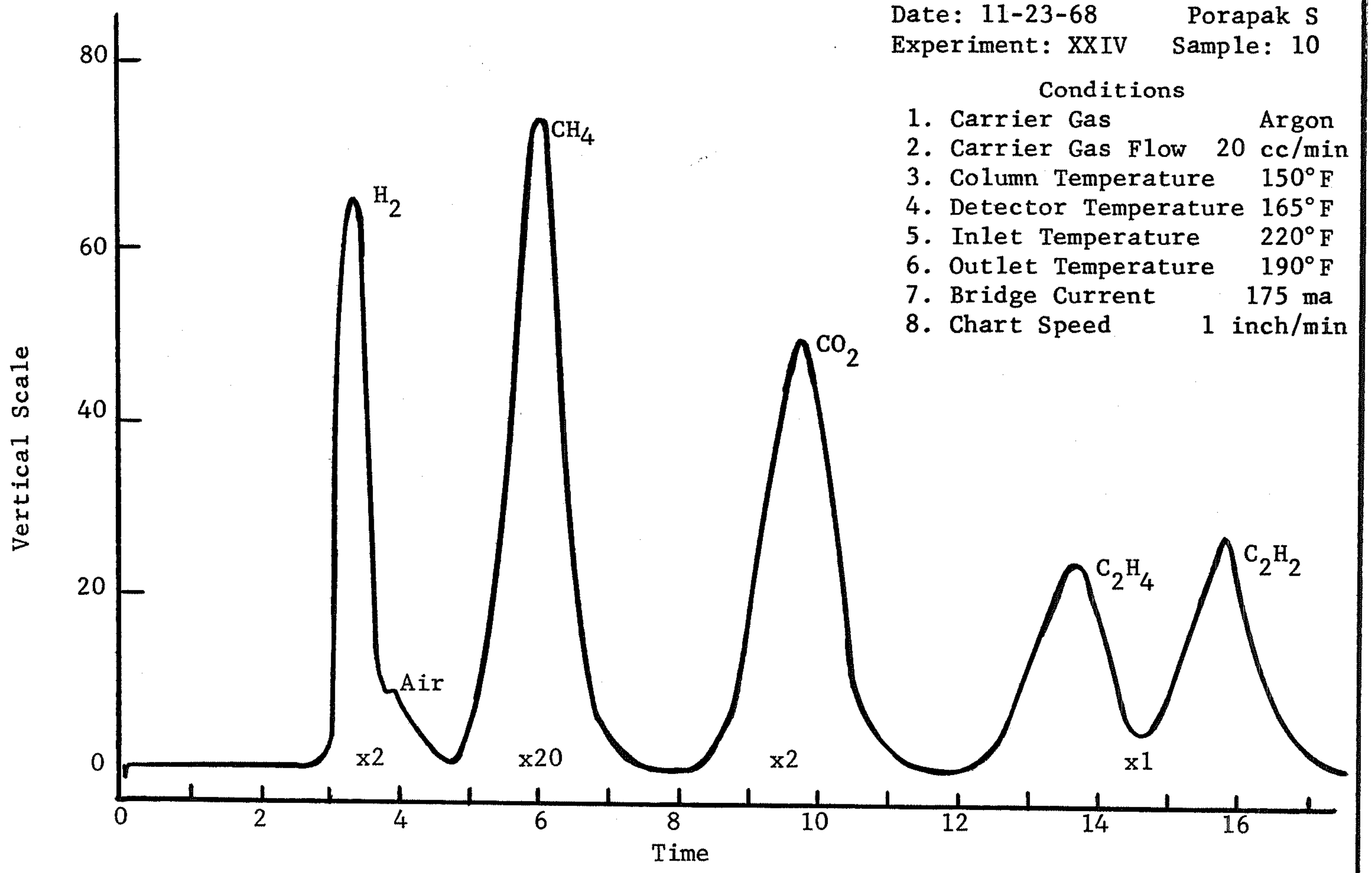

Date: 11-23-68 Porapak S
Experiment: XXIV Sample: 10

Conditions

1. Carrier Gas	Argon
2. Carrier Gas Flow	20 cc/min
3. Column Temperature	150° F
4. Detector Temperature	165° F
5. Inlet Temperature	220° F
6. Outlet Temperature	190° F
7. Bridge Current	175 ma
8. Chart Speed	1 inch/min

Figure 4-10. Typical Gas Chromatographic Scan for Porapak S Column.

average composition. Normalization of the results from the two columns was made using methane gas as a reference. A Honeywell Electronik 16 recorder was used to record the peaks from the gas chromatographic system.

The accuracy of the gas chromatographic analysis was reported as the standard deviation at a ninety-five per cent confidence limit. Two different deviations are listed in Table 4-4. These are the analytical deviation which determines the accuracy of the gas chromatographic analysis and the sampling plus analytical deviation which defines the overall accuracy of the system. The closeness of the two deviations indicates the reproduceability of the sampling procedure.

Liquid Analysis: The separated liquid phase from the exit stream was analysed for phenol content by a two-step titrametric analysis. This procedure, outlined in ASTM Bulletin D 2145 (6), involved the reaction of the aqueous phenol solution with excess bromine to form tribromophenol according to the following reaction:

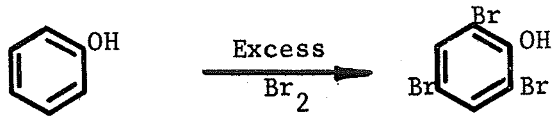

(4-1)

The excess bromine was then mixed with potassium iodide forming free iodine.

Table 4-4. Standard Deviation of the Gas Chromatographic Analyses.

GAS COMPONENT	RANGE OF COMPOSITIONS ANALYZED (Mole %)	STANDARD DEVIATION AT A 95% CONFIDENCE LIMIT	
		SAMPLING PLUS ANALYSIS	ANALYSIS ONLY
Hydrogen	34 - 71	± 1.64	± 1.31
Methane	12 - 45	± 1.34	± 1.33
Carbon Monoxide	3 - 17	± 1.14	± 0.92
Carbon Dioxide	2 - 9	± 0.82	± 0.58
Ethylene	0.2 - 1.1	± 0.20	-
Acetylene	0.2 - 1.5	± 0.18	-
Nitrogen	12 - 16	-	± 1.08
Overall Analysis	-	± 1.02	± 0.97

$$\underset{Br_2}{\text{excess}} \xrightarrow{KI} 2KBr + I_2 \qquad (4\text{-}2)$$

The free iodine was then titrated with a standard sodium thiosulfate solution to a starch indicator end point. The amount of bromine substitution to the phenol ring determined the phenol concentration in solution. Any polymerized or oxidized phenols were assumed to be present in small concentration and were accounted for as equivalent phenol. Results were accurate to ± 0.7 per cent at a 95% confidence limit for a range of concentrations from 2% to 70%.

Radioactive Tracer Analyses

In addition to the above analytical procedures, radioactive tracer analyses of the exit stream were made to determine:

(1) the gas and/or liquid products formed from the degradation of a certain carbon-14 labeled species in the simulated pyrolysis gas (i.e., methane and phenol), and,

(2) the extent of carbon deposition within the porous char. These analyses determined the degree of thermal decomposition of methane and/or phenol to carbon and lower molecular weight gases.

A Packard Instrument Company Model 2002 liquid scintillation spectrometer with a Model 280A precision ratemeter was used in the analysis. A Model 325 Tri-Carb combustion furnace was used to combust the separated gas components as they exited the gas chromatographic column to carbon dioxide and water. Facilities for counting carbon-14 (labeled CO_2 combustion products) and tritium (labeled H_2 obtained by reducing H_2O with iron at elevated temperatures) were available in this system. The equipment is shown in Figure 4-11.

<u>Radioactivity of the Separated Gas Chromatographic Effluent Stream</u>: The purpose of this analysis was to determine which gas products were formed from the thermal degradation of carbon-14 labeled methane and/or phenol contained in a simulated pyrolysis gas stream. The analysis involved the combustion of each separated gas component to carbon dioxide and water. Complete combustion was achieved by passing the gases over copper oxide pellets at a controlled temperature of 750°F. Water was removed by absorption in a six inch by one-quarter inch diameter tube packed with Aquasorb®. The dry carbon dioxide was then bubbled through three cubic centimeters of 1 molar hyamine hydroxide (in methanol) solution for absorption and eventual analysis in the liquid scintillation spectrometer. A static counting procedure was used for periods of twenty minutes or greater. Comparison of the radioactivity of each collected sample corresponding to a gas chromatographic peak produced the desired data identifying which species were formed from the labeled pyrolysis gas component. The relative

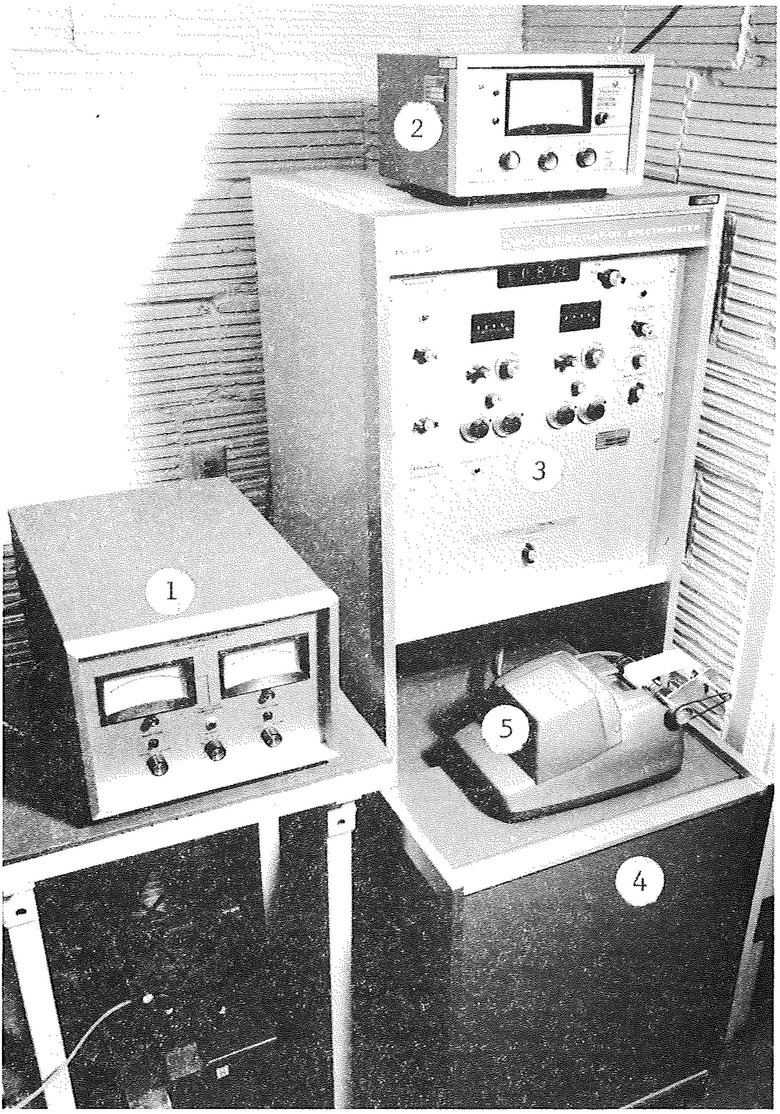

① Combustion Oven ② Rate Meter ③ Scintillator

④ Sample Compartment ⑤ Recorder

Figure 4-11. Photograph of the Liquid Scintillation Spectrometer.

Photo by J. R. Langley

intensity of the radioactive level of each sample gave a qualitative indication of its concentration with respect to the total concentration measured by the gas chromatographic analysis. Figure 4-12 is a typical radioactive analysis plot of the separated gas species.

Radioactivity of Solid Carbon and Liquid Products: It was also important in this research to determine the extent of carbon deposition within the char layer. One method to obtain this information involved the use of carbon-14 labeled methane and/or phenol which deposited radioactive carbon within the char as a result of thermal degradation of the simulated pyrolysis products. Analysis of the char specimen for radioactivity determined the extent of deposition.

Combustion of the char specimen in a muffle combustion furnace with dry air at 1400 - 1600°F produced carbon dioxide which was absorbed in a one molar hyamine hydroxide (in a methanol) solution. A diagram of the equipment is shown in Figure 4-13. Sectioning of the char prior to combustion was used as a means of determining deposition as a function of char depth. This information was used to locate the position (and thus temperature) where carbon deposition became significant. This also indicated the position where chemical reactions occur. A typical profile is shown in Figure 4-14.

Liquid product (or unreacted liquid pyrolysis components)

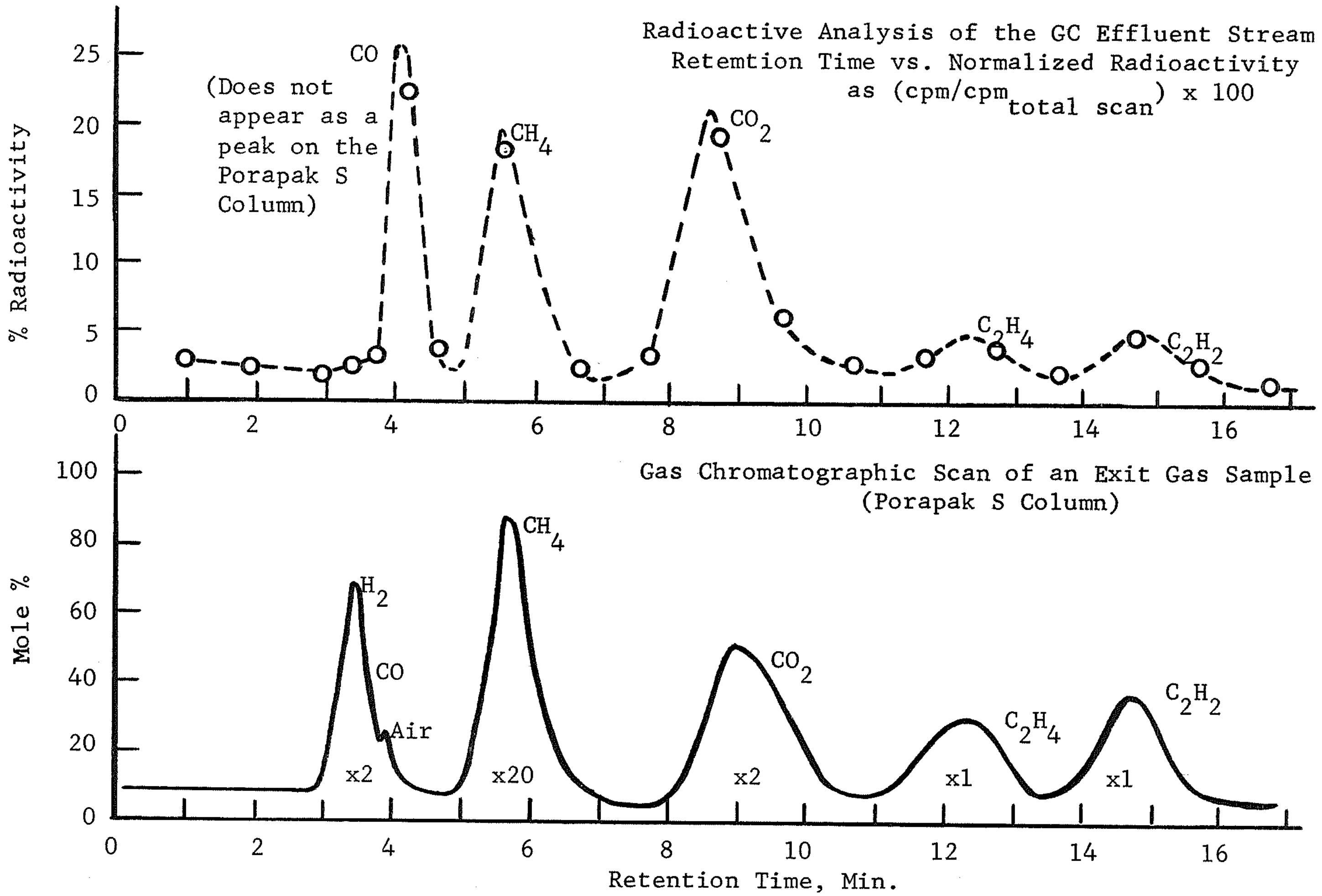

Figure 4-12. Plot of the Percent Radioactivity of Each Species in a Typical Exit Gas Sample from the Char Zone Thermal Environment Simulator.

Figure 4-13. Schematic Diagram of the Muffler Furnace System Used to Combust the Char Specimens from the Char Zone Thermal Environment Simulator to Water and Carbon Dioxide for Radioactivity Analysis.

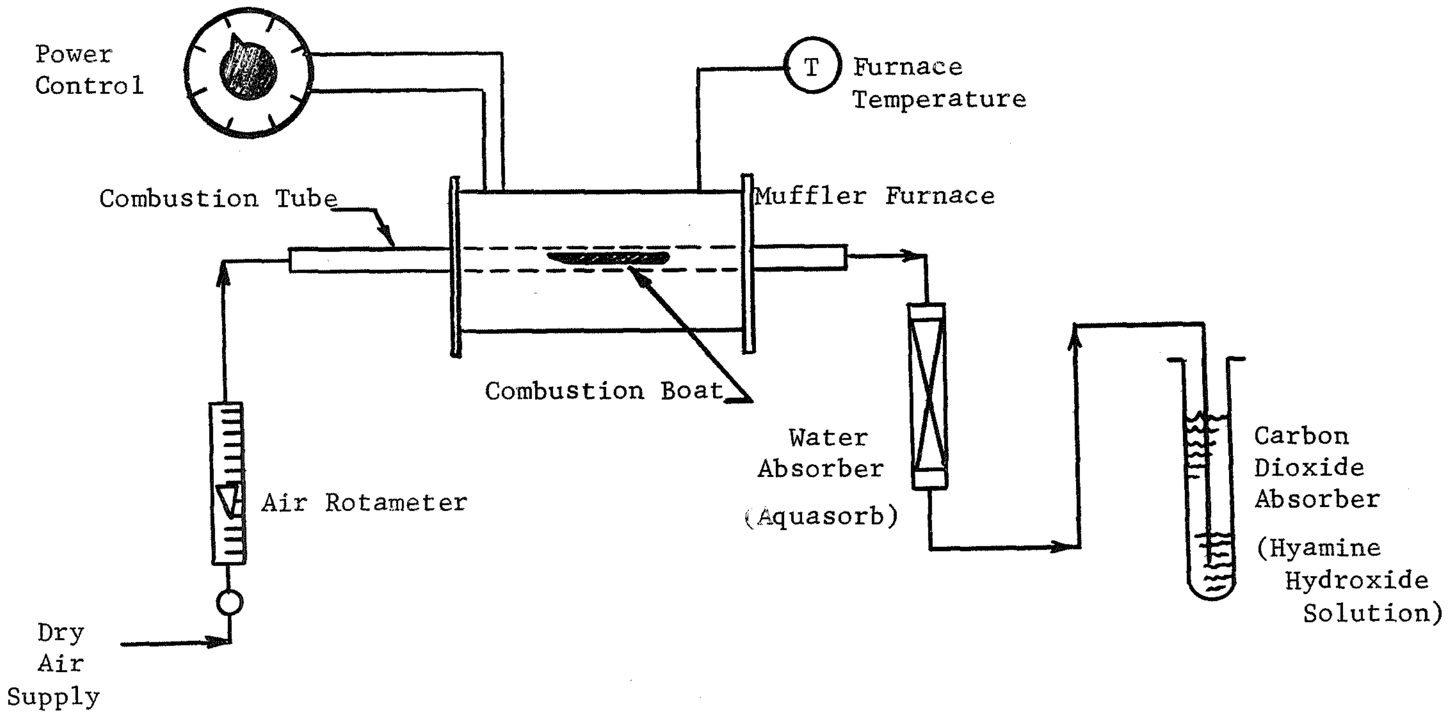

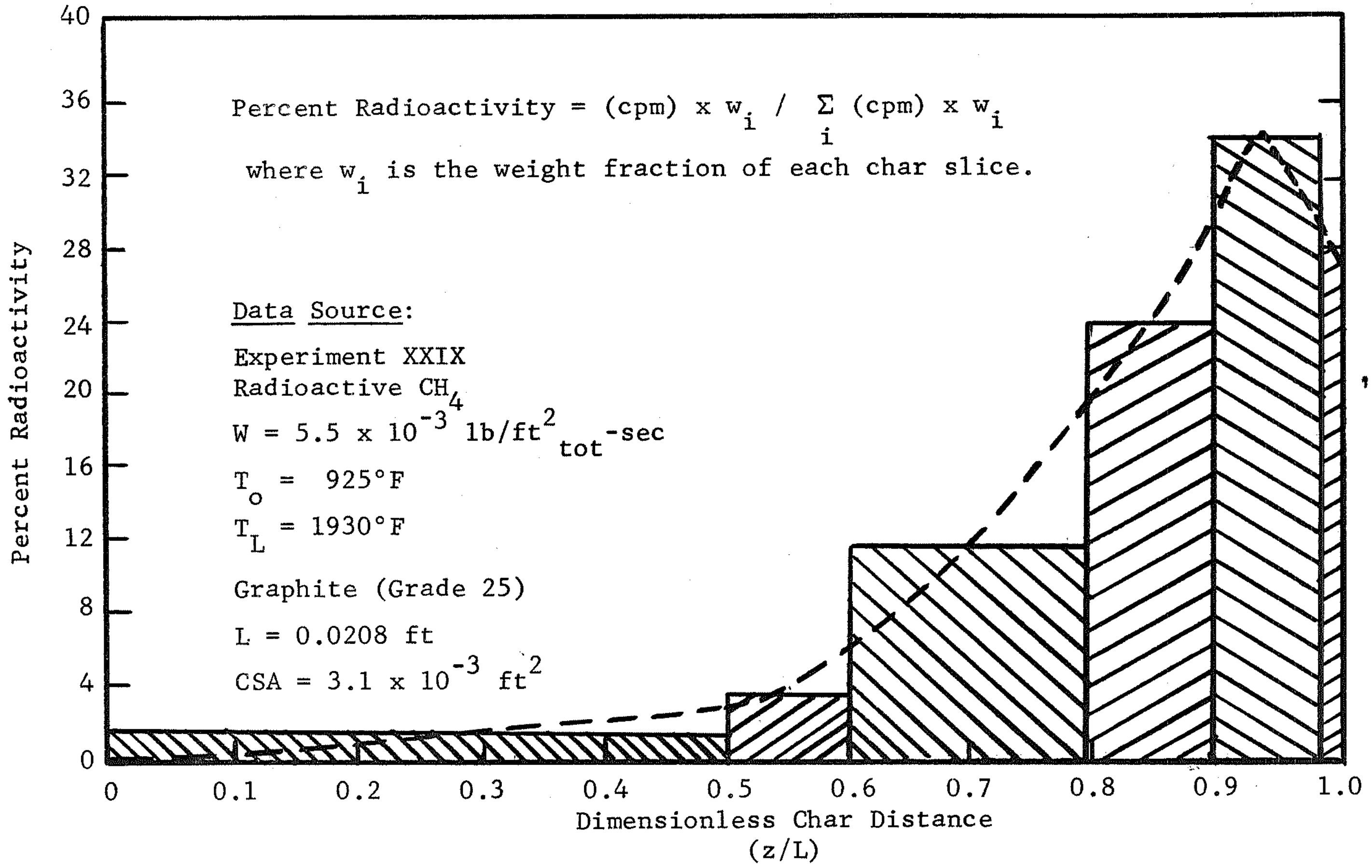

Figure 4-14. Plot of the Percent Radioactivity vs. the Dimensionless Char Distance Illustrating the Location of Carbon Deposition.

samples were also analysed for radioactivity to determine the extent of chemical reaction (conversion of the labeled pyrolysis component) within the char. Injection of the liquid sample into the inlet side of the Tri-Carb combustion furnace, with water absorption and CO_2 collection for radioactive monitoring was the technique used. In this way the effects of color and water quenching were eliminated (7).

Accuracy of the Radioactive Analyses: The accuracy of the liquid scintillation spectrometer is measured as a standard deviation and is approximately equal to the square root of the number of counts above background at a 68% confidence limit.

$$\sigma \cong N^{1/2} \qquad (4\text{-}3)$$

The percent error is calculated as the standard deviation divided by the number of counts times one hundred.

$$\%\ \text{error} = \left(\frac{\sigma}{N}\right) 100 \qquad (4\text{-}4)$$

The percent error is thus reduced by increasing the number of counts per sample. In the case of this research where a large system dilution was experienced, counting times up to 100 minutes were made to increase the counts, and thus reduced the error. The background count of the scintillation fluor solution used in the radioactive tracer analysis varied between 15-20 cpm. The background count for each vial was calculated as the average of six replicate measurements for a period of 100 minutes each. The smallest counts above background were approximately 20 cpm counted for 100 minutes giving 2000 counts. The percent error for this case would be:

$$\%\ \text{error} = \left(\frac{N^{1/2}}{N}\right)100 = \frac{(2000)^{1/2}}{2000} \times 100 = 2.2\% \qquad (4\text{-}5)$$

which is an unusually large value. However, these levels were encountered only in gas samples which had been collected after being separated by gas chromatographic analysis. For the purpose of indicating which products were produced from certain simulated pyrolysis products, the calculated error did not significantly affect the outcome of the analysis. This is indicated in Figure 4-12 in which the measured radioactivity of each separated species is plotted vs. retention time. The dotted lines indicate the standard deviation of the measured values.

For the case of solid and liquid samples, the counts obtained per sample were always in excess of 10,000 counts. The percent error at 10,000 counts is 1.0% and the standard deviation at the 68% confidence limit is ± 100 counts.

A more detailed discussion of the random error associated with materials undergoing radioactive decay can be found in the work of Wang and Willis (8).

REFERENCES

1. Kratsch, K. M., L. F. Hearne and H. R. McChesney, "Thermal Performance of Heat Shield Composites During Planetary Entry," AIAA-NASA National Meeting, Palo Alto, California, 3 (September 30-October 1, 1963).

2. Scala, S. M. and L. M. Gilbert, "Thermal Degradation of Char-Forming Plastic During Hypersonic Flight," *ARS Journal*, *32* (6), 917-24 (June 1962).

3. Ladacki, Michael, Janet V. Hamilton and Samuel N. Cohz, "Heat of Pyrolysis of Resin in Silica-Phenolic Ablator," *AIAA Journal*, *4* (10), 1798 (October 1966).

4. Nelson, James B., "Determination of Kinetic Parameters of Six Ablation Polymers by Thermogravimetric Analysis," NASA TN D-3919 (April 1967).

5. Sykes, George F., Jr., "Decomposition Characteristics of a Char-Forming Phenolic Polymer Used for Ablative Composites," NASA TN D-3810 (February 1967).

6. American Society for Testing Materials, "Phenol Content of Phenol-Water Mixtures," ASTM D 2145-63T, Part 20, 978-80 (January 1967).

7. Wang, C. H. and D. L. Willis, *Radiotracer Methodology in Biological Science*, Prentice Hall, Inc., Englewood Cliffs, New Jersey, 111-12 (1965).

8. *Ibid*., 186-206.

V. OPERATING PROCEDURES FOR THE CHAR ZONE THERMAL ENVIRONMENT SIMULATOR

The procedure used for all experiments with the Char Zone Thermal Environment Simulator considered safety as the prime requisite. The recommendations for safe handling of hazardous materials outlined in Dangerous Properties of Industrial Materials by N. I. Sax (1) and "Chemical Safety Data Sheets" by the Manufacturing Chemists' Association (2,3,4) were used as guides. Proper ventilation of the laboratory and various safety devices including exhaust hoods, eye wash basin, safety shower, fire extinguisher and self-contained breathing equipment were available and employed.

The experimental procedure for the operation of the Char Zone Thermal Environment Simulator is divided into five main portions for convenience. These are:

(1) Pre-startup phase
(2) Startup phase
(3) Experimental phase
(4) Shutdown phase
(5) Analytical phase

These will be discussed in the following paragraphs.

Pre-startup Phase

The pre-startup phase involved a one hour check period of the apparatus and auxiliary equipment. During this time the following items were checked:

(1) Insertion of the char holder section was made with proper allignment.

(2) Pressure and leak testing of all process lines, feed vessels and sampling containers were made.

(3) All recorders and other measuring devices were properly installed and tested.

(4) Coolant air and water lines were checked for proper operation and sufficient volumes.

(5) Vent system and safety equipment were operative.

After these items were satisfactorily checked, the second phase of the procedure was started.

Startup Phase

This phase of the procedure dealt with the final adjustments to the system prior to the experimental phase. During this period the equipment was subjected to full power with on-line checking of the recorders and process supply lines. The following items were checked during this phase:

(1) Helium (or Argon) gas at the experimental flow rate level was started.

(2) Temperature recorders and other measuring devices were turned on.

(3) Water flow to the reflector (and outer char holder section when needed) was turned on.

(4) Air flow to the terminal block cooling system was turned on.

(5) Sample bombs were evacuated and inserted into the sampling manifold.

(6) Hood vent system was adjusted to pull directly from the apparatus hood section with total exhaust through the vent stack.

(7) Heating lamps were turned on.

At this point a final check was made to make certain the pyrometer was focused on the char surface and the temperature was recording properly. Several on-line checks of the pressure drop, terminal block temperatures and flow rates were made to make certain that operation was normal. This phase of the procedure continued until the front and back surface temperatures were constant. At this point the experimental phase started.

Experimental Phase

The experimental phase began when simulated pyrolysis gas and liquid species were substituted for the helium (or Argon) flow in the system. An additional check period was made for temperatures to return to steady state (about 5-7 minutes). Data were recorded and sampling of the exit gases and liquids were made at three to five minute intervals during the run. The total time for a normal experimental run was from fifteen to twenty minutes in length.

Additional runs were made by changing conditions and allowing sufficient time for the system to again reach steady state. During this waiting period the exit gases were by-passed around the sampling manifold and the gas sampling containers from the previous run were exchanged with empty bombs. This procedure was continued for a maximum of one hour and thirty minutes total run time. This maximum was set to decrease the possibility of severe damage to the heating system and the char holder.

Shutdown Phase

The termination of the experimental phase was made by following the outlined procedure listed below:

(1) The pyrolysis gas flow was stopped and helium (or argon) flow was begun,

(2) The exit gas was by-passed around the sampling manifold.

(3) The lamps were turned off.

(4) All flows were left on until a temperature of 200°F or less was attained by the char holder.

(5) All recorders and other measuring devices were turned off.

(6) All flows were stopped.

(7) The hood system was placed in the normal operating condition with the apparatus hood isolated from the system.

(8) Equipment and recorder pens were cleaned and stored for the next experiment.

(9) The char holder, lamps and reflector were inspected for damage after removing and labeling the char specimens for char density analysis.

The entire experimental procedure required between three and four hours of preparation and run time, excluding the analytical phase of the operation. This part was done separately and usually required a one to two day period for a one hour experiment.

Analytical Phase

The analytical procedures are subdivided into four areas. These are the gas analysis, the liquid analysis, the char analysis and the radioactive analyses. Each procedure will be discussed separately in the following paragraphs.

Gas Analyses: In order to obtain accurate analyses of the gas collected from the Char Zone Thermal Environment Simulator, the gas chromatograph must be calibrated for the type and concentration of each gas component contained in the sample. Reagent grade gases (see Table 4-3) were used for this purpose and calibration by the peak area technique was employed.

Calibration Procedure: The equipment used to calibrate the gas chromatograph is shown in Figure 5-1. The method involved the introduction of a pure gas sample into the gas sampling valve of the chromatograph through valve A with all other valves closed. After a sufficient flow of gas was noted exiting the system through the water "bubbler", valve A was closed and valves B and C opened. A vacuum pump was used to evacuate the system to a specific pressure measured with the manometer. At that point the manometer reading was recorded and the sample injected. The mole percent of the pure gas in the sampling loop was calculated as:

$$\text{Mole \%} = \left(\frac{P_{\text{Barometer}} - P_{\text{Manometer}}}{P_{\text{Barometer}}}\right)100 \qquad (5\text{-}1)$$

A plot of the peak area as a function of the mole percent pure gas injected into the chromatograph gave the calibration curve desired. An example calibration curve for methane is shown in Figure 5-2. In order to cover the entire range of concentrations obtained during the experimental program, it was necessary, in some cases, to calibrate for the sample gas

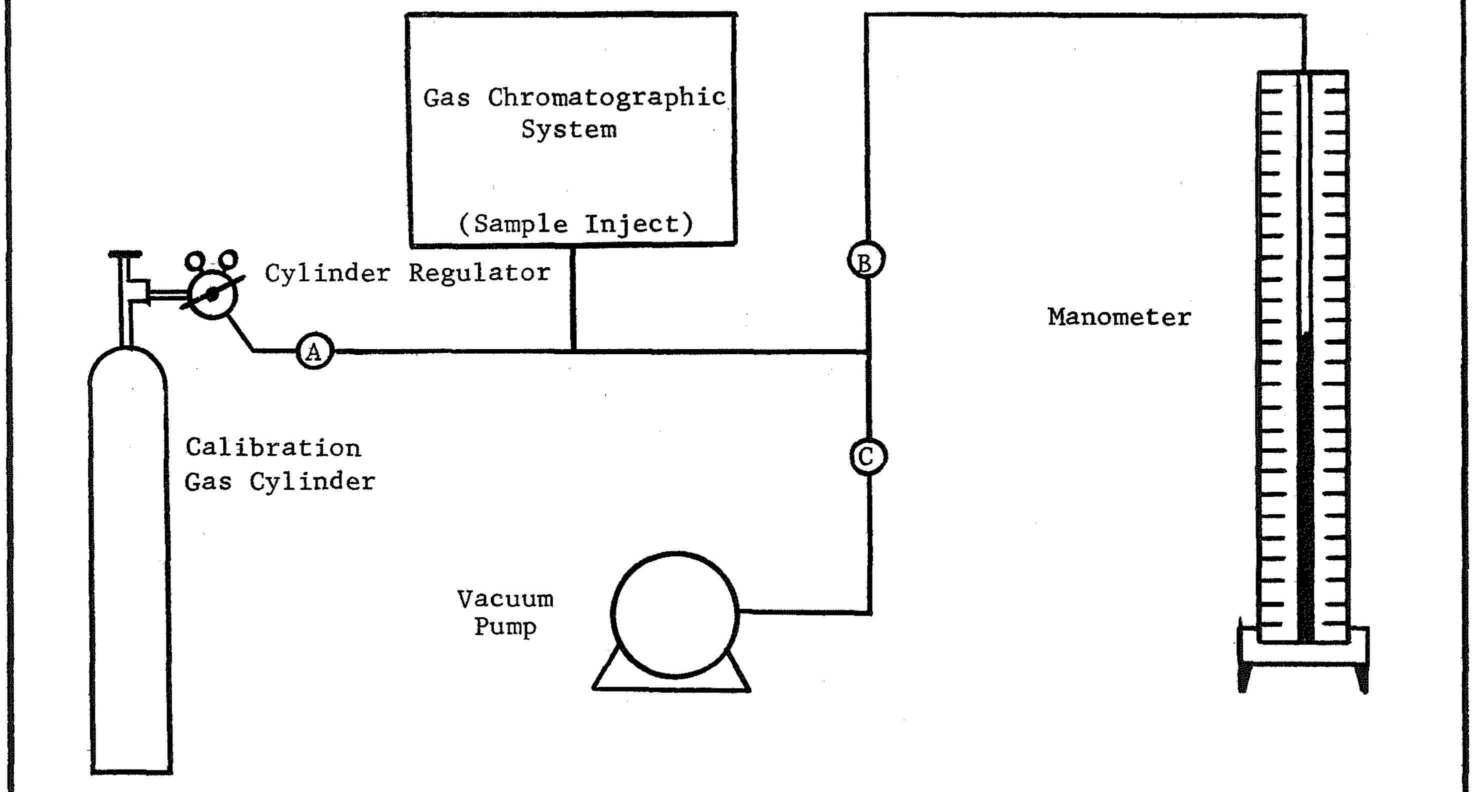

Figure 5-1. Equipment Used to Calibrate the Gas Chromatographic System.

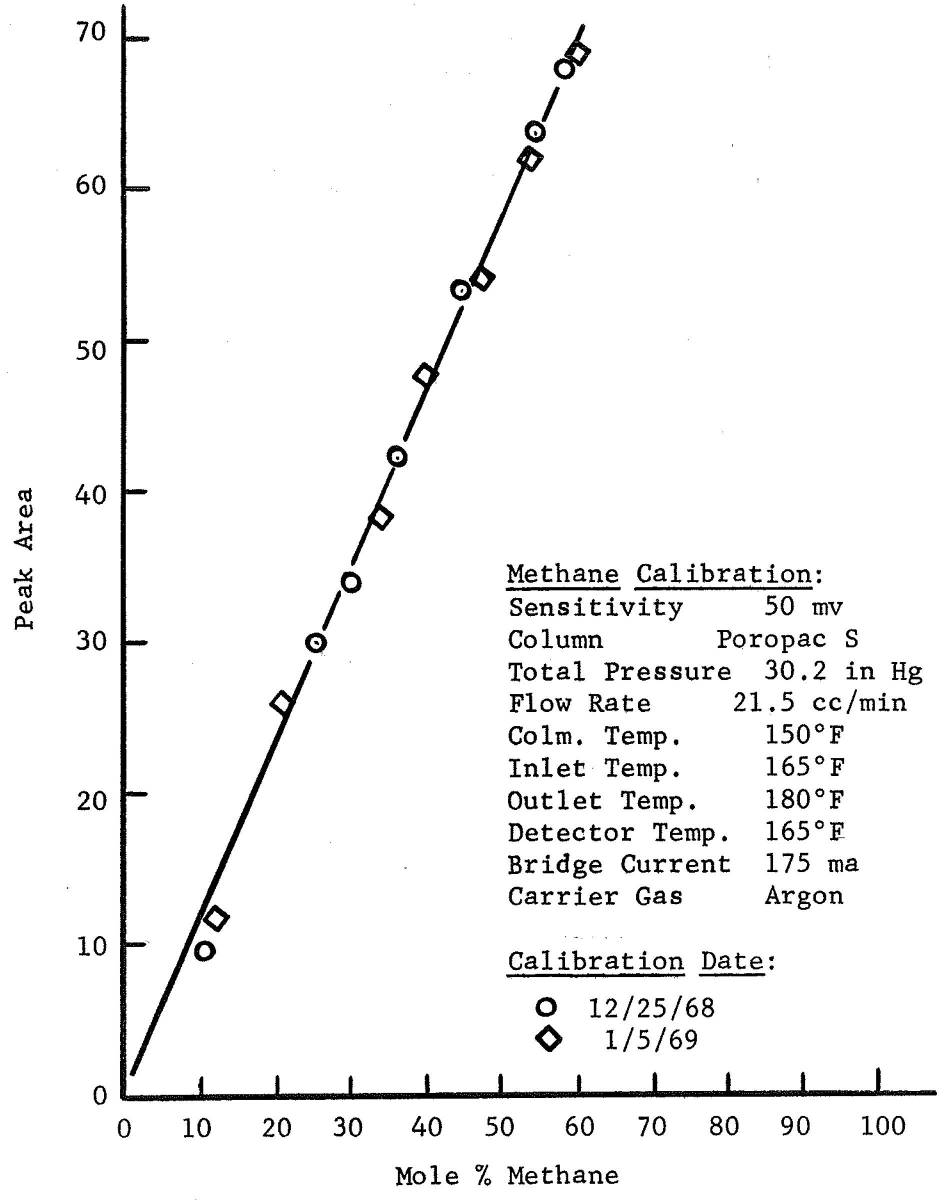

Figure 5-2. Typical Calibration Curve for Methane on the Poropac S Column.

component at various chromatograph sensitivities. Once these curves had been prepared, however, it was a simple procedure to calculate the composition of gas samples accurately and quickly.

Determination of Reproducibility: The gas analyses were regularly checked for reproducibility. One of two techniques were used. First, injection of a pure gas used to calibrate the instrument was made and the peak area vs. concentration was compared with the calibration curve. Agreement within the accuracy limitations of the system constituted a reproducible analysis.

Secondly, a standard sample, (i.e., one which contained all gas components at or near the expected concentrations in typical exit gas samples), was injected into the chromatograph with comparison against the actual composition of the mixture. Again, an analysis within the tolerable limits constituted a reproducible analysis.

Each of the above methods were used frequently to insure the proper and accurate operation of the instrument. Recalibration of the system was repeated when either of the above tests failed to reproduce the standard analyses.

Sampling Technique: In addition to errors caused by changes in the system, quite often changes in sampling technique produced non-reproducible analyses. The particular chromatographic system was equipped to minimize the error associated with varying sample size by using two one cubic centimeter sampling loops. These loops where connected by a Carle Sampling Valve, Model No. 2014, which alternately filled one loop with a gas sample while sweeping the other loop with carrier gas to the detector of the gas chromatograph for analysis.

Gas samples were introduced into the loops by forcing mercury into the containers from the bottom, This compressed the gases in the container such that flow into the sampling valve was obtained by opening the top stopcock. This method proved far superior to the gas bladder method of injection with regard to leaks and ease of handling. The operating procedure for the gas chromatograph is standard information and reference is made to Figures 4-9 and 4-10 for the operating conditions used in this research.

Liquid Analysis: The method for determining phenol in aqueous solutions is reported in ASTM Bulletin D 2145 (5). A summary of that procedure follows.

Preparation of Standard Solutions: The following standard solutions are required in the analysis for phenol in aqueous solutions.

1. Bromide-Bromate solution is made by dissolving 10.2 grams of KBr and 2.8 grams of $KBrO_3$ in water with dilution to one liter.

2. Hydrochloric acid solution is made by mixing an

equal volume of concentrated HCl (sp. gr. 1.19) with water.

3. Potassium Iodide solution is made by dissolving 150 grams of KI in water with dilution to 1 liter.

4. Sodium Thiosulfate standard solution is made by dissolving 25.0 grams of $Na_2S_2O_3 \cdot 5H_2O$ in boiling water. Add 0.1 gram of Na_2CO_3 to the cooled solution to stabilize and dilute to one liter. Standardize at frequent intervals to insure an accurate normality.

5. Starch solution is made by titrating 5 grams of soluble starch and five to ten milligrams of HgI_2 with three to five milliliters of water. Add the suspension to one liter of boiling water and boil for five to ten minutes. Decant the clear supernatant after cooling.

Analytical Procedure: The analytical procedure for phenol determination follows:

1. Accurately weigh 0.5 - 0.6 grams of the aqueous phenol solution into a five hundred milliliter volumeters flask. (Take larger samples if the concentration is less than 85%).

2. Mark two 250 ml. iodine flasks as "blank" and two as samples. Pipet 50 ml. of the sample solution into each flask marked "blank". Pipet 50 ml. of bromide-bromate solution into each flask. Measure 10 ml. of the HCl solution with a small graduate. Add the contents to one of the flasks all at once and stopper quickly sealing the top by pouring 5 mls. of KI solution

into the neck surrounding the glass stopper. Swirl vigorously for thirty seconds. Repeat for the remaining three flasks.

3. Allow each flask to stand undisturbed for ten minutes. Cool in an ice bath for one minute. Loosen the stopper and allow the first solution to flow into the flask. Shake for thirty seconds. Add KI in the neck, recool, allow the second to enter the flask and shake again for thirty seconds. Repeat once more. (A brown color in the vapor space of the flask after each treatment indicates free bromine. The addition of KI until the bromine color is no longer visible indicates successful reaction with KI.)

4. Rinse the stopper and flask walls with water. Titrate the solution with $Na_2S_2O_3$. When the color changes to pale yellow, add five ml. of starch solution. Continue titrating to a clear (from blue) end point.

5. The phenol concentration in the original sample is calculated using the following equation:

$$\text{Phenol (\% wt.)} = \left\{\begin{bmatrix}\text{ml. of } Na_2S_2O_3 \text{ soln.}\\ \text{req'd for blanks}\end{bmatrix} - \begin{bmatrix}\text{ml. of } Na_2S_2O_3 \text{soln.}\\ \text{req'd for samples}\end{bmatrix}\right\} \left[\frac{(\text{Normality of } Na_2S_2O_3) \times 1.569}{\text{grams of original sample}}\right] \qquad (5\text{-}2)$$

The standard deviation was calculated as 0.7% at a 95% confidence limit over a phenol concentration range of 2 - 70%.

<u>Char Analysis</u>: In order to analyze the char specimens

removed from the Char Zone Thermal Environment Simulator for radioactivity, combustion to water and CO_2 followed by absorption of the labeled (C^{14}) CO_2 was required. To do this, a muffler combustion furnace was used. Char specimens were placed in the combustion tube at 1500°F and dry air was passed over the carbon for 2 to 3 hours. The exit gas was passed through a water absorber and then a CO_2 absorber for subsequent radioactive monitoring.

In this study, the carbon deposition as a function of char depth was desired. To accomplish this experimentally, thin slices of the specimen were removed by lightly passing them over emery paper. The collected "fines" were placed in the combustion tube after recording the weight loss of the original char. This procedure was repeated for up to seven to ten sections with collection of the CO_2 (C^{14} labeled) exit gas after combustion of each section. The samples were then prepared for radioactive analysis.

Radioactive Analysis: All radioactive analyses were made using gases combusted in either the Tri-Carb Furnace (gas chromatographic systems) or the muffler combustion furnace (chars) for higher counting efficiencies (6). Samples were collected in 1 molar hyamine hydroxide (in methanol) solution with subsequent dilution in standard scintillation fluor. The following procedures were used for each analysis.

Preparation of the Scintillation Fluor: The concentrated liquid scintillation solution was made by dissolving 125 grams of 2,5-diphenyloxozole (PPO) and 2,5 grams of 1,4-bis-2(4-methyl-5-Phenyloxozolyl)-benzene in pure toluene diluted to one liter. Both compounds were obtained from the Packard Instrument Company.

The scintillation fluor used in the radioactive analysis was made by adding 1 ml. of the concentrated solution to twenty-four milliliters of toluene.

Radioactive Gas Analyses: The effluent stream from the gas chromatograph was monitored for radioactivity to ascertain the products and quantities of materials formed from the original C^{14} labeled species in the simulated pyrolysis gas. The effluent gas was passed through test tubes containing about 3 cc of 1 molar hyamine hydroxide (in methanol) solution. At 1/2 and/or 1 minute intervals, the test tubes were changed, thus producing a discrete sampling pattern of the effluent gas. This was continued for the entire length of the gas chromatogram. The contents of the test tube were emptied into the scintillation fluor solution for radioactive counting. Comparison of the radioactivity in each test tube with the gas chromatogram, produced the necessary identification of the components formed from reactions of the labeled species in the simulated pyrolysis gas. Repeated injection of the same gas sample was often done to concentrate the radioactive level in the separate test tubes. Approximately thirty minutes between injections were required to reduce the radioactivity in the system to a non-contamination level. Counting for 100 minutes was made to decrease the error of the analysis.

Radioactive Liquid and Char Analyses: The liquid and char radioactive analyses were identical to the gas analyses. The only exceptions were:

(1) the liquid sample was injected by syringe (1-10μl) into the gas chromatographic column instead of entering through the sampling loop,

(2) the entire combusted effluent stream from the liquid and char combustions were collected in only one container for radioactive counting,

(3) for the char samples, the muffler combustion furnace was used instead of the Tri-Carb furnace to combust the solid carbon or graphite.

Disposal of Radioactive Samples: All samples containing radioactive carbon in the gaseous state were disposed through the laboratory hood designed specifically for that purpose according to Handbook 53 of the U.S. Department of Commerce and approved by the university's health physicist. Liquid samples and samples in scintillator fluor were collected in a special container for disposal by the L.S.U. Nuclear Science Center. No solid samples were retained in that state. All char specimens were combusted to CO_2 and H_2O with complete absorption of the labeled carbon dioxide in 1 molar hyamine hydroxide (in methanol) solution.

REFERENCES

1. Sax, N. Irving, Dangerous Properties of Industrial Materials, 2nd. Ed., Reinhold Publishing Corp., New York (1963).

2. Manufacturing Chemists' Association, "Properties and Essential Information for Safe Handling and Use of Acetylene," SD-7, Washington, D. C. (1957).

3. Manufacturing Chemists' Association, "Properties and Essential Information for Safe Handling and Use of Phenol," SD-4, Washington, D. C. (1964).

4. Manufacturing Chemists' Association, "Properties and Essential Information for Safe Handling and Use of Cresol," SD-48, Washington, D. C. (1952).

5. American Society for Testing Materials, "Phenol Content of Phenol-Water Mixtures," ASTM D 2145-63T, Part 20, 978-80 (January 1967).

VI. RESULTS OF THE NON-EQUILIBRIUM ANALYSIS OF PYROLYSIS GAS FLOW IN THE CHAR ZONE

Introduction

The results of the non-equilibrium analysis for pyrolysis gas flow in the char zone are presented in this chapter. In order to obtain solutions to the equations of change, the important chemical reactions occurring within the char; and, the pyrolysis gas composition entering at the back surface must be specified. The first part of this discussion is, therefore, devoted to the methods of selecting the correct initial composition and important chemical reactions for non-equilibrium flow.

This is followed by the solutions of the energy, momentum, heat flux and species continuity equations with comparisons to the experimental data obtained in the Char Zone Thermal Enviornment Simulator. Low density nylon-phenolic resin chars formed under simulated reentry conditions in arc jets at the Langley Research Center were used in this phase of the research. In this way the accuracy of the non-equilibrium model for predicting the real behavior is determined. Further comparisons with the two limiting models of frozen and equilibrium flow are made to determine the relative accuracy of each model in predicting the energy transfer in the char layer. This is followed by a detailed parametric study in which the three flow models are compared over a wide range of mass flux, heat of pyrolysis and front surface temperature values.

In subsequent sections, the reacting flow of the simulated pyrolysis gases through porous graphite will be compared with data obtained using chars formed from low density nylon-phenolic resin composites. The ability of the non-equilibrium flow model to accurately predict the behavior in each medium will justify the study of carbon deposition and pyrolysis gas decomposition using radioactive tracer technology with the more readily available and workable simulated char specimens.

The effect of homogeneous and heterogeneous catalysts on the chemical reaction rates and product distributions will also be determined and compared with the non-catalytic data. In this way the feasibility of adding small quantities of compounds that catalytically affect the heat absorption at lower temperatures can be determined.

Finally, a study of the effect of air injection at the front char surface is discussed. This work was aimed at determining the extent of combustion of the porous media at temperatures between 1500 - 2000°F.

Non-Equilibrium Flow of Pyrolysis Gases in the Char Zone

The non-equilibrium flow analysis describes the actual behavior within the char zone in which pyrolysis gases and char react chemically at finite reaction rates. In order to accurately predict this behavior, the pyrolysis gas composition entering the char layer and the important chemical reactions and corresponding rate data must be available. The following sections discuss the development of this essential information.

Pyrolysis Products Entering the Char Zone: In order to simulate analytically and experimentally the char zone during ablation, a very accurate description of the pyrolysis products resulting from the thermal degradation of low density, nylon-phenolic resins must be known. Although this has been the topic of a great deal of research (1,2,3,4,5), the inability to determine the chemical composition of varying quantities of liquid residues prevented an accurate description needed in a non-equilibrium flow analysis. The gas species (near room temperature) were identified, however, and these formed the basis of early experimental and analytical studies of the char layer phenomena (6,7,8,9,10). Some typical analyses are shown in Table 6-1 for these studies.

Notable advances were made by Nelson (1) and Sykes (2,3) in which a large portion of the unidentified liquid residue was analysed. Their methods included pyrolysis gas chromatography, differential thermal analysis and thermogravimetric analysis of nylon-phenolic resin, silicone elastomers, and composites of these polymers. Typical analyses are presented in Table 6-2.

Table 6-1. Pyrolysis Product Composition Resulting From the Thermal Degradation of Nylon-Phenolic Resin Composites Excluding High Molecular Weight Species.

Component	Computed Equilibrium Composition Mole %					Experimentally Determined Composition Mole %		
	Kratsch (6)			del Valle (10)		Freidman (7)	Shulman (8)	Beecher and Rosenweig (9)
	540°F	1540°F	2540°F	440°F	980°F	1290 °F	1470 °F	2190 °F
Carbon Monoxide	23.8	31.6	20.4	0.0	1.9	11.5	4.0	12.0
Carbon Dioxide	4.5	0.0	0.0	1.5	3.4	2.3	0.3	0.0
Nitrogen	7.0	6.3	2.3	8.1	6.3	0.1	0.0	0.0
Hydrogen	0.0	5.6	47.4	1.5	43.2	25.2	13.0	54.0
Hydrogen Cyanide	0.0	1.0	4.1	0.0	0.0	0.0	30.0	0.0
Methane	57.4	45.4	3.0	56.4	26.2	4.3	1.5	12.0
Ammonia	0.0	0.0	0.0	0.0	0.0	4.3	13.0	0.0
Water	0.0	0.0	0.0	32.5	19.0	16.1	38.0	12.0
Diacetylene	0.0	0.0	0.0	0.0	0.0	1.0	0.0	0.0
Acetone	0.0	0.0	0.0	0.0	0.0	0.7	0.0	0.0
Acetylene	0.0	1.1	22.1	0.0	0.0	11.5	0.0	0.0
Cresol	0.0	0.0	0.0	0.0	0.0	0.0	0.9	2.5
Phenol	0.0	0.0	0.0	0.0	0.0	0.0	0.0	2.5
Ethane	0.6	0.1	0.0	0.0	0.0	0.2	0.0	5.0
Ethylene	0.0	4.4	0.6	0.0	0.0	14.7	0.0	
Benzene	6.7	4.4	0.0	0.0	0.0	1.0	0.0	
Toluene	0.0	0.0	0.0	0.0	0.0	0.5	0.0	
Xylene	0.0	0.0	0.0	0.0	0.0	0.3	0.0	
Propane	0.0	0.0	0.0	0.0	0.0	1.4	0.0	
Isopropanol	0.0	0.0	0.0	0.0	0.0	1.6	0.0	
Totals	100.0	100.0	100.0	100.0	100.0	100.0	100.0	100.0

Table 6-2. Pyrolysis Products Resulting From the Thermal Degradation of Nylon-Phenolic Resins Including the Identified High Molecular Weight Species.

Component	Sykes (3) Mole % (Nylon-Phenolic Resin)		Sykes (2) Mole % (Phenolic Resin Only)
	By Flash Pyrolysis at 800°C	By Pyrolysis at 50°C Increments to 800-900 °C	
Phenol	8.0	7.6	6.7
Methylphenol	4.0	4.0	2.1
Dimethylphenol	2.8	3.2	0.0
Trimethylphenol	2.4	2.7	0.0
Benzene	0.4	0.4	0.2
Toluene	0.0	0.3	0.4
Cyclopentanone	1.2	2.4	0.0
Hydrogen	30.2	32.2	47.1
Methane	3.8	4.0	9.4
Carbon Monoxide	5.3	3.6	5.2
Carbon Dioxide	12.1	6.8	1.5
Water	20.1	23.3	22.0
Ammonia	0.8	0.4	0.0
Unidentified	9.2	10.1	5.2
Totals	100.0	100.0	100.0

The identification of these previously unknown species (i.e., phenol, cresol, xylene, etc.) was valuable information in the formulation of an accurate non-equilibrium flow analysis for flow in the char zone.

In this research, the analyses of Sykes (2) were used with one modification. The identified cyclic compounds, e.g. cresol, xylene, which were 3% by weight of the total, were considered to be phenol. This was done to reduce the experimental difficulties encountered with the metering of liquid phases in the Char Zone Thermal Environment Simulator, and, to keep the total number of species in the system to a small, but representative size. In so doing, the composition was adjusted to the values listed in Table 6-3.

To determine whether this simulated gas represented the actual pysolysis products at the back surface, an energy balance was made using experimental heats of pyrolysis (1,2) and combustion (10) data for the virgin plastic materials, and the heats of formation of the simulated gas species (12). The results, presented in Table 6-4 and discussed in detail in Appendix G, indicate the reliability of the simulation. A calculated value of the heat of pyrolysis of 213 BTU/lb was within the experminetal accuracy of the reported value (200 ± 20 BTU/bl) as shown in Table 6-4. The various simulated pyrolysis product compositions used in the experimental studies

Table 6-3. Composition of the Simulated Pyrolysis Products as Compared with the Analyses of Sykes(2) for the Thermal Degradation of Low Density Nylon-Phenolic Resins.

Component	Composition (Mole %)	
	Analysis of Sykes (2)	Simulated Pyrolysis Products (This Research)
Dimethylphenol	1.2	6.2
Phenol	4.7	
Benzene	0.1	
Toluene	0.2	
Water	48.9	48.9
Carbon Dioxide	1.1	1.1
Carbon Monoxide	3.7	3.7
Methane	6.7	6.7
Hydrogen	33.4	33.4
Totals	100.0	100.0

Table 6-4. Comparison of the Experimental Heat of Pyrolysis with Calculated Values Based on Heats of Formation of the Reported Pyrolysis Gas Components. (3).

Component Name	Weight Fraction by:		Average Weight Fraction, x_i	$x_i \Delta H_{f_{pi}}$ BTU/lb	$x_i C_{p_{mean}} \Delta T$ BTU/lb
	Flash	50° Inc.			
Phenol	0.124	0.112	0.118	- 49	34
Methylphenol	0.067	0.061	0.063	- 33	18
Dimethylphenol	0.049	0.052	0.051	- 29	14
Trimethylphenol	0.040	0.042	0.041	- 25	12
Benzene	0.004	0.001	0.003	2	2
Toluene	0.000	0.002	0.001	1	1
Cyclopentanone	0.019	0.039	0.029	- 18	9
Hydrogen	0.010	0.010	0.010	0	34
Methane	0.010	0.010	0.010	- 20	10
Carbon Monoxide	0.025	0.016	0.021	- 18	6
Carbon Dioxide	0.087	0.047	0.067	- 36	5
Water	0.059	0.066	0.062	-258	23
Ammonia	0.002	0.001	0.002	- 2	2
Unidentified*	0.173	0.173	0.173	- 72	51
Carbon Residue	-	-	0.340	133	99
			1.000	-742	320

Reactants	Weight Fraction, x_j	$x_j \Delta H_{r_j}$ BTU/lb	$x_j C_{p_{mean}} \Delta T$ BTU/lb
Nylon	0.4	-384	250
Phenolic Resin	0.6	-501	
	1.0	-885	250

ΔH_{pyr}(Calculated) = 213 BTU/lb

ΔH_{pyr}(Experimental) = 200 ± 20 BTU/lb

*Unidentified materials considered phenol in calculations of ΔH_{pyr}.

are summarized in Table 6-5.

Important Chemical Reactions: The basis for selecting or omitting chemical reactions in the non-equilibrium flow model is the isothermal analysis discussed in Chapter III and developed in Appendix F. For the pyrolysis products listed in Table 6-5 over a temperature range of 500 - 3000°F., the reactions and corresponding kinetic data describing the non-equilibrium flow in the char zone are presented in Table 6-6. The numbers underlined in the reference column represent the more reliable sources of information with specific application to this research. The contribution and importance of each reaction is discussed in the following paragraphs:

(1) Light Hydrocarbon Cracking Reactions: The first order thermal decomposition of methane, ethane, ethylene and acetylene represented in reactions 6-1 through 6-4 in Table 6-6 is a very important and necessary set of reactions if non-equilibrium flow is to be accurately described. Although methane is the only major light hydrocarbon in the pyrolysis product stream entering the char, reactions of ethane, ethylene, and acetylene must be included to account for their formation and subsequent reaction within the char. This was observed experimentally in the Char Zone Thermal Environment Simulator in which small quantities (0.1 - 1.5 mole %) of ethylene and acetylene were identified in the exit gas stream. No noticeable quantities (< 0.1 mole %)

Table 6-5. Simulated Pyrolysis Gas Mixtures Used in Experiments on the Char Zone Thermal Environment Simulator.

Component	Simulated Pyrolysis Gas Composition, Mole%			
	Feed Mix 1	Feed Mix 2	Feed Mix 3	Feed Mix 4 and 5
Methane	32.5	43.6	46.3	6.7
Hydrogen	37.2	35.0	31.7	33.4
Carbon Monoxide	8.2	4.9	5.5	3.7
Carbon Dioxide	6.6	2.9	2.5	1.1
Nitrogen	15.5	13.6	14.0	0.0
Phenol	0.0	0.0	0.0	6.2
Water	0.0	0.0	0.0	48.9
Index of Experiments	I-IV	V-XII	XIII-XVIII	XIX-XXXII

Table 6-6. Important Reactions and Associated Kinetic Data for the Pyrolysis Product Species in the Char Zone Between 500-3000°F.

General Form of the Reactions: $aA + bB + \dots + \; = \; rR + sS + \dots +$

General Rate Constant Equation: $k \; = \; k^{\circ}T^{-s}\,\mathrm{Exp}(-E/RT)$

Reaction Number	Reaction	Rate Law	Activation Energy E, Kcal/gm-mole)	Frequency Factor	s	References
(6-1)	$CH_4 = 1/2\ H_2 + 1/2\ C_2H_6$	k_fA	95.0	$7.6\mathrm{x}10^{14}$ *	0	14,15,16,17 18,19
(6-2)	$C_2H_6 = C_2H_4 + H_2$	k_fA	70.0	$3.1\mathrm{x}10^{14}$ *	0	14,20,16,17 18,21
(6-3)	$C_2H_4 = C_2H_2 + H_2$	k_fA	40.0	$2.6\mathrm{x}10^{8}$ *	0	14, 16
(6-4)	$C_2H_2 = 2C + H_2$	k_fA^2	10.0	$2.1\mathrm{x}10^{10}$ **	0	14,22,28
(6-5)	$C + 2H_2 = CH_4$	k_f	17.0	$2.0\mathrm{x}10^{9}$ ***	0	30,31,23,24 25,26,32
(6-6)	$C_6H_6O + H_2 = H_2O + C_6H_6$	k_fA	45.0	$2.0\mathrm{x}10^{13}$ *	0	49
(6-7)	$C_6H_6 = 3\ C_2H_2$	k_fA	35.0	$1.4\mathrm{x}10^{9}$ *	0	33
(6-8)	$C + H_2O = CO + H_2$	k_fAB	82.0	$1.2\mathrm{x}10^{12}$ **	-1	42,47,35,36 38,39,40,43
(6-9)	$CO + H_2O = H_2 + CO_2$	k_fAB	30.0	$1.0\mathrm{x}10^{12}$ **	0	41,35,36,38 39,40,43,44
(6-10)	$C + CO_2 = 2\ CO$	$k_fA - k_rR^2$	50.0 61.0	$1.0\mathrm{x}10^{6}$ * $1.0\mathrm{x}10^{-9}$ **	-1 0	45,46,35,36 38,39,40,44

* 1st Order (sec^{-1}) ** 2nd Order (cm^3/gm-mole-sec) *** 0th Order (gm-mole/cm^3-sec)

of ethane were found even at relatively high methane conversion. The reaction of carbon with hydrogen (reaction 6-5) forming methane was also important over the tempreature range from 500°F to 3000°F.

(a) Methane Decomposition: The reaction rate constant for the thermal decomposition of methane to ethane and hydrogen was based on the reported research of Palmer and Hirt (13) and Kozlov and Knorre (14). The activation energy of 95 Kcal/mole and the frequency factor of 7.6×10^{14} sec^{-1} used in the non-equilibrium flow model agreed closely with the values reported by Kozlov and Knorre (14) who correlated the results of several investigators. Their values were 91 Kcal/mole and 4.5×10^{-13} sec^{-1}. The range of activation energies in the literature varied from a low value of 73 Kcal/mole to 103 Kcal/mole (15, 16, 17, 18, 19). Values between 4.5×10^{13} and $1.0 \times 10^{15} sec^{-1}$ were also reported for the frequency factor.

(b) Decomposition of Ethane: The ethane formed by reaction (6-1) reacts completely forming ethylene as observed by its total absence in the exit stream from the Char Zone Thermal Environment Simulator. This indicated a somewhat faster reaction rate than that for the decomposition of methane and required the combination of a low activation energy and/or a high frequency factor. Steacie and Shane (27) and Kozlov and Knorre (14) reported values of 69 Kcal/mole and 1 x 10^{14} sec^{-1} for the activation energy and frequency factor, respectively. The values used in the non-equilibrium flow analysis were 70 Kcal/mole and 3.1 x 10^{13} sec^{-1} and are in good agreement with the literature data. The range of activation energies and frequency factors reported (14,20,27) were 64-78 Kcal/mole and $10^{13.5}$ - 10^{14} sec^{-1}.

(c) Decomposition of Ethylene: The thermal degradation of ethylene to acetylene and hydrogen is given by reaction (6-3). Values of 40 Kcal/mole and 2.6 x 10^{8} sec^{-1} were used in the non-equilibrium flow model as the activation energy and frequency factor. These were the values reported by Kozlov and Knorre (14) who correlated data from several sources. Ethylene in small concentrations were observed in the exit porduct stream from the Char Zone Thermal Environment Simulator.

(d) Acetylene Decomposition: Like ethylene, acetylene was identified in small concentrations (but to a larger extent than ethylene) in the exit product stream. The reaction rate should be comparable to the rate for ethylene reaction or perhaps slightly faster due to formation of acetylene by benzene decomposition (reaction 6-7). An activation energy of 10 Kcal/mole and a frequency factor of 5.1 x 10^{10} sec^{-1} $mole^{-1}$ cm^{3} were used in the second order rate equation in the TEMPRE System. The range in the energy of activation reported in the literature varied from 7 - 50 Kcal/mole (14,22,28,29). A frequency factor of 5.1 x 10^{10} sec^{-1} $mole^{-1}$ cm^3 was reported by Happel and Kramer (28). Reaction (6-4) is the only major reaction of acetylene of importance in this system, due to the absence of the acetylene polymerization products, benzene, diacetylene and triacetylene, in the exit stream.

(e) Methane Formation from the Reaction of Hydrogen and Carbon: In addition to the above reactions involving the light hydrocarbon products, reaction (6-5) in Table 6-6 is also important. Breisacher and Marx (30) and Corney and Thomas (31) observed an inflection point in the rate of methane production when hydrogen was passed over graphite. This inflection occurred near 1200 - 1300°F and resulted in a reduction in the activation energy from 70 to 12 Kcal/mole. The order of the reaction varied between zero and one half as the temperature increased to 2000°F. The reaction kinetics data for hydrogen atoms with carbon films by King and Wise (32) indicate a zeroth order reaction and an activation energy of 7-9 Kcal/mole at 440°F. A value of 17 Kcal/mole for the activation energy and a frequency factor of 2 x 10^9 gm mole/cm^3-sec for the zeroth order reaction were used in the non-equilibrium flow model. The value of the frequency factor was estimated from the kinetic theory (57) since none was reported in the literature.

(2) Reactions of Aromatic Hydrocarbons: The presence of aromatic hydrocarbons in the pyrolysis products is a result of the basic phenolic resin structure of the virgin plastic heat shield. Sykes (2) reported such aromatic compounds as benzene, toluene, xylene, cresol and phenol in varying quantities when phenolic resin underwent thermal decomposition. Of these, phenol and the phenol-based materials form the major portion of the aromatic compounds with benzene and toluene contributing less than 1 mole percent to the total pyrolysis gas composition.

In order to account for the chemical interaction of these compounds, two reactions are included in the non-equilibrium flow analysis. These are the phenol hydrogenation reaction (6-6) and the benzene decomposition reaction (6-7). The absence of benzene in the exit product stream from the Char Zone Thermal Environment Simulator makes the important products formed by these reactions water, hydrogen and carbon; the latter two resulting from acetylene decomposition by reaction (6-4).

(a) Phenol Hydrogenation: The catalytic and non-catalytic hydrogenation of phenol has been studied extensively as early as the 1920's by many investigators (50,51,52,53,54). However, no kinetic data has been reported for this data. The products of low pressure, gas phase hydrogenation (50) are benzene and cyclohexanol in varying quantities. Liquid phase hydrogenation at high pressures produce cyclohexanol and in some cases cyclohexanone (50,51,52). The yield of cyclohexanol is enhanced when a Raney Nickel catalyst is used in the liquid or vapor phase hydrogenation.

In order to determine the activation energy for this reaction, a comparison with the heats of hydrogenation (49) for compounds related to phenol were examined. These included ethyl benzene (48.9 Kcal/mole), o-xylene (47.3 Kcal/mole), mesitylene (47.6 Kcal/mole) and hydrindol (45.8 Kcal/mole). The activation energy used in the non-equilibrium flow analysis was 45 Kcal/mole which agreed with the values reported in the literature for similar compounds. The frequency factor was calculated from the kinetic theory (55) to be 2×10^{13} cm^3/mole sec.

(b) <u>Benzene Decomposition</u>: The decomposition of benzene to acetylene,diacetylene, hydrogen and biphenyl at 2000 - 2400°F was reported by Slysh and Kinney (34) to be first order. Hou and Palmer (33) described a more complex behavior made up of a mixed first and second order rate equation. The first order behavior was used to describe acetylene formation and resulted in an activation energy of 52 Kcal/mole with a frequency factor of $10^{9.2}$ sec^{-1}. The second order contribution described biphenyl formation with an activation energy of 40 Kcal/mole and a frequency factor of 10^{14} $mole^{-1}$ sec^{-1} cm^3. A first order rate expression with an activation energy of 35 Kcal/mole and a frequency factor of 2×10^9 sec^{-1} were used in the non-equilibrium flow analysis.

(3) Water-Gas Reactions: The water gas reactions are a very complex set of reactions which are critically dependent on the experimental conditions at which they are studied. These reactions include the carbon-steam reaction (6-8), the water-gas shift reaction (6-9) and the carbon-carbon dioxide reaction (6-10).

The general rules of behavior for this system of reactions are summarized below (36,37,38):

(i) Increases in the water concentration increases the carbon consumption rate,

(ii) Increases in the hydrogen concentration decreases or retards carbon consumption, and

(iii) A fixed ratio exists between carbon dioxide and carbon monoxide.

The water gas shift reaction is considered by many (35, 39,40) to be at equilibrium and unaffected by concentration changes, temperature and pressure changes at reasonably low pressures (~1 ATM) and moderate temperature (1000 - 1500°F). Walker (41), on the otherhand, reported definite deviations from this supposed equilibrium below 2300°F. A detailed discussion of the water gas reactions is presented in reference (42). The reaction kinetic data used in the TEMPRE System for each of the above reactions are compared with the literature in the following sections.

(a) Carbon-Steam Reaction: The carbon-steam reaction has been extensively studied by many investigators (35,36,38,39, 40,43,44). The reaction is first order and activation energies have been reported over a wide range of values (26-90 Kcal/mole). The more applicable data for graphite-steam reaction (42) indicated an activation energy of 80 Kcal/mole. This is in agreement with the value of 83 Kcal/mole (47), and 82 Kcal/mole was used in the non-equilibrium flow analysis of this research. A frequency factor of 1×10^{12} $\sec^{-1}$ was employed in the non-equilibrium flow calculations (55).

(b) Water-Gas Shift Reaction: The water-gas shift reaction below 2300°F was considered to be governed by a finite reaction rate in the TEMPRE System. A value of 30 Kcal/mole activation energy and 1×10^{12} $\sec^{-1}$ frequency factor was used to describe the reaction of water with carbon monoxide. The deviation from equilibrium below 2300°F is reported by Walker (41) and attributed, in part, to a diffusion controlled mechanism.

(c) Carbon-Carbon Dioxide Reaction: The reaction of carbon with carbon dioxide is best described by a rate equation which is first order and reversible. Values of the forward and reverse activation energies were reported as 50 Kcal/mole and 60.6 Kcal/mole by Austin and Walker (45) and Glovina (46).

The frequency factors were 1 x 16^{6} sec^{-1} and 1 x 10^{-9} sec^{-1} for the forward and reverse reactions, respectively. These reported values were used in the non-equilibrium flow analysis.

Experimental Simulation of the Flow of Reacting Pyrolysis Products in the Char Zone

The purpose of the experimental program was to obtain sufficient data for comparison with the calculated results of the non-equilibrium flow model. Simulated pyrolysis products were passed through radiant heated chars maintained at a front surface temperature of 1600 - 2300°F. Mass flux rates were varied between 0.0001 - 0.10 lb/ft^2-sec, and the back surface temperature was measured as a function of the particular front surface temperature and mass flux rate studied. The back surface temperature range was from 500 to 1200°F. These values, along with the porosity, thickness and cross section area of the char were input parameters to the non-equilibrium flow model. The composition of the exit product stream was calculated using the kinetic data for the important reactions listed in Table 6-6 and compared with the experimentally determined compositions. The relative closeness of the two compositions determined the accuracy of the model in predicting the flow of pyrolysis products within the char over a temperature range from 500 - 2300°F and mass flux rates between 0.0001 -

0.10 lb/ft^2 sec. The following paragraphs discuss the results of these comparisons. A detailed summary of results for all experimental tests is presented in Appendix D.

<u>Comparison of the Non-Equilibrium Flow Results with Experimental Data Using Chars</u>: The basis for evaluating the non-equilibrium flow model as an accurate analysis of energy transfer in the char zone of a charring ablator is by comparison of the experimentally determined exit product composition from the Char Zone Thermal Environment Simulator to the calculated composition in the non-equilibrium flow analysis. This is done in Table 6-7 in which the non-equilibrium exit product composition, calculated using the chemical reactions and corresponding kinetic data in Table 6-6, is compared with experimental data for mass flux rates between 0.0013 and 0.108 lb/ft^2-sec and front surface temperatures of 1680°F to 2300°F. The simulated pyrolysis gas composition entering the char zone is also shown (frozen), along with the compositions predicted by the equilibrium flow model. This set of experiments was conducted with chars formed from nylon-phenolic resin composites under simulated reentry conditions in the electric air arc jets at the Langley Research Center (N.A.S.A.). As seen in Table 6-7, the experimental and calculated composition predicted by the non-equilibrium flow model agreed within the experimental accuracy of the methods used. A summary of all low

Table 6-7. Comparison of Calculated and Experimental Exit Gas Compositions from the Char Zone Thermal Environment Simulator for Mass Flux Rates Between 0.00133 and 0.108 lb/ft^2-sec and Front Surface Temperatures Between 1680° and 2300°F.

RUN NUMBER MASS FLUX FRONT TEMP BACK TEMP	FLOW MODEL	H_2 MOLE %	CH_4 MOLE %	CO MOLE %	CO_2 MOLE %	N_2 MOLE %	H_2O MOLE %	C_6H_6O MOLE %	C_2H_4 MOLE %	C_2H_2 MOLE %	MODEL	
											ΔP	q_{cz}
XVIII-56	FROZEN	28.9	6.4	3.3	0.8	0.0	53.3	6.9	0.0	0.0	0.4	0.93
0.00208	EQUILIBRIUM	59.7	3.3	26.7	4.0	0.0	6.3	0.0	0.0	0.0	0.4	15.93
1690°F	NON-EQUILIBRIUM	23.0	11.1	2.8	2.1	0.0	53.8	7.1	0.0	0.0	0.4	0.99
1030°F	EXPERIMENTAL	24.8	10.3	3.4	1.3	0.0	53.7	6.5	0.0	0.0	0.8	-
XVIII-57	FROZEN	30.6	6.1	3.5	0.9	0.0	52.1	6.8	0.0	0.0	2.0	4.92
0.0101	EQUILIBRIUM	60.2	3.2	27.1	3.7	0.0	5.9	0.0	0.0	0.0	1.8	55.43
1690°F	NON-EQUILIBRIUM	29.1	7.2	3.4	1.1	0.0	52.3	6.9	0.0	0.0	2.0	4.97
975°F	EXPERIMENTAL	28.7	7.5	3.4	1.2	0.0	51.7	7.5	0.0	0.0	2.6	-
XVIII-58	FROZEN	30.6	6.2	3.5	1.0	0.0	51.9	6.8	0.0	0.0	22.0	69.80
0.1080	EQUILIBRIUM	59.5	3.5	26.0	4.4	0.0	6.5	0.0	0.0	0.0	18.8	735.2
1680°F	NON-EQUILIBRIUM	30.6	6.2	3.5	1.0	0.0	51.9	6.8	0.0	0.0	22.0	69.81
690°F	EXPERIMENTAL	30.8	6.1	3.4	1.1	0.0	50.8	5.8	0.0	0.0	17.5	-
XIX-60	FROZEN	29.3	6.0	3.3	0.9	0.0	53.7	6.8	0.0	0.0	0.7	1.17
0.00248	EQUILIBRIUM	62.7	0.8	35.2	1.5	0.0	0.9	0.0	0.0	0.0	0.6	13.0
2030°F	NON-EQUILIBRIUM	38.2	17.2	25.2	8.8	0.0	4.9	5.1	0.0	0.5	0.6	2.42
1375°F	EXPERIMENTAL	41.3	18.2	23.4	7.6	0.0	5.0	4.6	0.0	0.0	0.7	-
XIX-61	FROZEN	28.7	5.4	3.4	1.0	0.0	53.9	7.6	0.0	0.0	0.5	1.61
0.00220	EQUILIBRIUM	63.1	0.5	35.7	0.2	0.0	0.5	0.0	0.0	0.0	0.5	27.3
2140°F	NON-EQUILIBRIUM	36.6	18.3	31.2	7.3	0.0	0.6	5.2	0.0	0.7	0.4	2.94
1100°F	EXPERIMENTAL	36.4	18.4	31.2	7.0	0.0	2.1	4.9	0.0	0.0	0.9	-
XX-63	FROZEN	28.6	5.5	3.4	1.0	0.0	53.8	7.7	0.0	0.0	0.6	1.79
0.00224	EQUILIBRIUM	63.1	0.3	36.4	0.1	0.0	0.2	0.0	0.0	0.0	0.5	51.37
2290°F	NON-EQUILIBRIUM	30.7	21.4	38.6	3.4	0.0	0.0	4.6	0.3	1.0	0.5	3.18
1180°F	EXPERIMENTAL	30.4	19.8	38.0	5.7	0.0	0.0	5.0	0.5	0.6	0.6	-
XX-64	FROZEN	28.4	5.4	3.4	1.0	0.0	46.0	15.8	0.0	0.0	0.2	1.05
0.00103	EQUILIBRIUM	65.9	0.3	33.6	0.0	0.0	0.2	0.0	0.0	0.0	0.3	32.45
2300°F	NON-EQUILIBRIUM	25.2	25.6	38.5	0.9	0.0	0.0	7.9	0.5	1.3	0.2	1.18
1190°F	EXPERIMENTAL	26.7	26.4	40.3	0.6	0.0	0.0	7.1	0.4	1.0	0.2	-

density nylon-phenolic resin char experiments are presented in Appendix D. The results in Table 6-7 will be discussed in detail in the following paragraphs.

The maximum temperature attainable in the Char Zone Thermal Environment Simulator was 2300°F. This restriction to the temperature was caused by the limited power supply (70 KVA) to the radiant heating system, and by material and economic factors governing the design of high temperature equipment.

At temperatures between 1600 - 2300°F, mass flux rates of 0.01 lb/ft^2-sec or greater did not allow sufficient residence time of the pyrolysis products in the char layer. Therefore, the extent of chemical reactions was less than 1% and the flow was essentially frozen. This frozen behavior of the pyrolysis gases is illustrated in Table 6-8 for mass flux rates of 0.0101 and 0.1080 lb/ft^2-sec at a front surface temperature of 1600°F. The exit gas composition calculated in the non-equilibrium flow model and the experimentally determined values are compared with the inlet composition (frozen) and the composition predicted by the equilibrium flow model.

Although the frozen flow condition was accurately described by the non-equilibrium flow model, the ability to predict energy transfer when chemical reactions occur remained untested.

Table 6-8. Pyrolysis Gas Flow Through Low Density Nylon-Phenolic Resin Chars. Frozen Flow Behavior at Mass Flux Rates Below 0.01 lb/ft^2-sec.

RUN NUMBER MASS FLUX FRONT TEMP BACK TEMP	FLOW MODEL	H_2 MOLE %	CH_4 MOLE %	CO MOLE %	CO_2 MOLE %	N_2 MOLE %	H_2O MOLE %	C_6H_6O MOLE %	C_2H_4 MOLE %	C_2H_2 MOLE %	MODEL	
											ΔP	q_{cz}
XVIII-57	FROZEN	30.6	6.1	3.5	0.9	0.0	52.1	6.8	0.0	0.0	2.0	4.92
0.0101	EQUILIBRIUM	60.2	3.2	27.1	3.7	0.0	5.9	0.0	0.0	0.0	1.8	55.43
1690°F	NON-EQUILIBRIUM	29.1	7.2	3.4	1.1	0.0	52.3	6.9	0.0	0.0	2.0	4.97
975°F	EXPERIMENTAL	28.7	7.5	3.4	1.2	0.0	51.7	7.5	0.0	0.0	2.6	-
XVIII-58	FROZEN	30.6	6.2	3.5	1.0	0.0	51.9	6.8	0.0	0.0	22.0	69.80
0.1080	EQUILIBRIUM	59.5	3.5	26.0	4.4	0.0	6.5	0.0	0.0	0.0	18.8	735.2
1680°F	NON-EQUILIBRIUM	30.6	6.2	3.5	1.0	0.0	51.9	6.8	0.0	0.0	22.0	69.81
690°F	EXPERIMENTAL	30.8	6.1	3.4	1.1	0.0	50.8	5.8	0.0	0.0	17.5	-

Therefore, in order to acheive conditions where chemical reactions would become an important mode of energy absorption, and, the non-equilibrium model could be tested, the residence time of gases within the char was increased by decreasing the mass flux. The effect of changing the mass flux rate at a constant temperature of 1690°F is shown in Table 6-9. At a mass flux of 0.108 lb/ft^2-sec, the exit composition is the same as the composition of the simulated pyrolysis products entering the char. Decreasing the mass flux to 0.00208 lb/ft^2-sec causes a small, but detectable composition change, particularly in hydrogen and methane resulting from chemical reactions between the species in the char layer. It should be pointed out that the reported changes in composition of the exit product stream are predicted by the non-equilibrium flow model within the accuracy of the experimental data. While the frozen flow model predicts the actual behavior at the higher mass flux rates, the equilibrium flow model does not accurately describe the energy transfer over these mass flux rates. It erroneously predicts large changes in composition of all of the species even at the high mass flux value of run XVIII-58 of 0.108 lb/ft^2-sec as shown in Table 6-9.

The changes in composition resulting from chemical reactions occurring in the char layer are better illustrated by increasing the front surface temperature. In Table 6-10

Table 6-9. Flow of Pyrolysis Gases Through Low Density Nylon-Phenolic Resin Chars. Effect of Decreasing the Mass Flow Rate at a Temperature of 1690°F.

RUN NUMBER MASS FLUX FRONT TEMP BACK TEMP	FLOW MODEL	H_2 MOLE %	CH_4 MOLE %	CO MOLE %	CO_2 MOLE %	N_2 MOLE %	H_2O MOLE %	C_6H_6O MOLE %	C_2H_4 MOLE %	C_2H_2 MOLE %	MODEL	
											ΔP	q_{cz}
XVIII-56	FROZEN	28.9	6.4	3.3	0.8	0.0	53.3	6.9	0.0	0.0	0.4	0.93
0.00208	EQUILIBRIUM	59.7	3.3	26.7	4.0	0.0	6.3	0.0	0.0	0.0	0.4	15.93
1690°F	NON-EQUILIBRIUM	23.0	11.1	2.8	2.1	0.0	53.8	7.1	0.0	0.0	0.4	0.99
1030°F	EXPERIMENTAL	24.8	10.3	3.4	1.3	0.0	53.7	6.5	0.0	0.0	0.8	-
XVIII-58	FROZEN	30.6	6.2	3.5	1.0	0.0	51.9	6.8	0.0	0.0	22.0	69.80
0.1080	EQUILIBRIUM	59.5	3.5	26.0	4.4	0.0	6.5	0.0	0.0	0.0	18.8	735.2
1680°F	NON-EQUILIBRIUM	30.6	6.2	3.5	1.0	0.0	51.9	6.8	0.0	0.0	22.0	69.80
690°F	EXPERIMENTAL	30.8	6.1	3.4	1.1	0.0	50.8	5.8	0.0	0.0	17.5	-

a comparison of the exit gas composition is given for a front surface temperature range of 1690 - 2300°F at an average mass flux rate of ~0.002 lb/ft^2-sec. The transition from a frozen or non-reactive state to a state where chemical reactions become significant is clearly indicated by the change in product concentrations leaving the Char Zone Thermal Environment Simulator. Again the experimental exit product compositions agree with those predicted by the non-equilibrium flow analysis within the accuracy of the experimental data. Again the equilibrium flow analysis erroneously predicted the extent of reactions to be much greater than occurred.

In most of the above discussion, the initial pyrolysis product composition entering the char varied over a small range, rather than being constant. These variations were a result of variations in feeding the gas (CH_4, CO, CO_2 and H_2) and liquid (phenol and H_2O) phases at the low mass flux rates required to get chemical reactions among the species. Also, in some cases the composition was varied purposely to test the ability of the non-equilibrium flow model in predicting the energy transfer in the char zone for a wide variety of temperatures, mass flux rates and simulated pyrolysis product compositions.

These compositions were reported in Table 6-5, and it shows how simulated product compositions were varied in the

Table 6-10. Flow of Pyrolysis Gases Through Low Density Nylon-Phenolic Resin Chars. Effect of Increasing the Front Surface Temperature at a Mass Flux Rate of 0.002 lb/ft^2-sec.

RUN NUMBER MASS FLUX FRONT TEMP BACK TEMP	FLOW MODEL	H_2 MOLE %	CH_4 MOLE %	CO MOLE %	CO_2 MOLE %	N_2 MOLE %	H_2O MOLE %	C_6H_6O MOLE %	C_2H_4 MOLE %	C_2H_2 MOLE %	MODEL	
											ΔP	q_{cz}
XVIII-56	FROZEN	28.9	6.4	3.3	0.8	0.0	53.8	6.9	0.0	0.0	0.4	0.93
0.00208	EQUILIBRIUM	59.7	3.3	26.7	4.0	0.0	6.3	0.0	0.0	0.0	0.4	15.93
1690°F	NON-EQUILIBRIUM	23.0	11.1	2.8	2.1	0.0	53.8	7.1	0.0	0.0	0.4	0.99
1030°F	EXPERIMENTAL	24.8	10.3	3.4	1.3	0.0	53.7	6.5	0.0	0.0	0.8	-
XIX-60	FROZEN	29.3	6.0	3.3	0.9	0.0	53.7	6.8	0.0	0.0	0.7	1.17
0.00248	EQUILIBRIUM	62.7	0.8	35.2	1.5	0.0	0.9	0.0	0.0	0.0	0.6	13.0
2030°F	NON-EQUILIBRIUM	38.2	17.2	25.2	8.8	0.0	4.9	5.1	0.0	0.5	0.6	2.42
1375°F	EXPERIMENTAL	41.3	18.2	23.4	7.6	0.0	5.0	4.5	0.0	0.0	0.7	-
XIX-61	FROZEN	28.7	5.4	3.4	1.0	0.0	53.9	7.6	0.0	0.0	0.5	1.61
0.00220	EQUILIBRIUM	63.1	0.5	35.7	0.2	0.0	0.5	0.0	0.0	0.0	0.5	27.3
2140°F	NON-EQUILIBRIUM	36.6	18.3	31.2	7.3	0.0	0.6	5.3	0.0	0.7	0.4	2.94
1100°F	EXPERIMENTAL	36.4	18.4	31.2	7.0	0.0	2.1	4.9	0.0	0.0	0.9	-
XX-63	FROZEN	28.6	5.5	3.4	1.0	0.0	53.8	7.7	0.0	0.0	0.6	1.79
0.00224	EQUILIBRIUM	63.1	0.3	36.4	0.1	0.0	0.2	0.0	0.0	0.0	0.5	51.37
2290°F	NON-EQUILIBRIUM	30.7	21.4	38.6	3.4	0.0	0.0	4.6	0.3	1.0	0.5	3.18
1180°F	EXPERIMENTAL	30.4	19.8	38.0	5.7	0.0	0.0	5.0	0.5	0.6	0.6	-

kind and amount of each species present. The phenol-water free compositions (feed mix 1, 2 and 3) were based on early studies of plastic decomposition in which the chemical analyses were limited to species that were gases at a particular (usually near ambient) temperature (4,5,6). The phenol-water-gas composition, which more accurately represented the composition entering the char, was obtained after this research was started (1,2,3). However, as will be discussed, the same conclusions regarding the phenol-water free systems apply to the latter systems.

In Table 6-11 the effect of changing temperature (1575 - 2300°F) at a constant mass flux rate (~ 0.001 lb/ft^2-sec) is shown, while Table 6-12 shows the effect of changing mass flux (0.00003 - 0.0170 lb/ft^2-sec) at a front surface temperature of ~ 2000°F. for the various simulated pyrolysis product compositions studied. In each table, the transition from frozen flow to non-equilibrium flow is clearly shown, as is the very excellent agreement between the predicted exit gas compositions of the non-equilibrium flow analysis with the experimental results. At high mass flux rates (> 0.01 lb/ft^2-sec) or low front surface temperatures (< 1800°F), the flow in the char zone is accurately described by the frozen flow model. Furthermore, as seen in Table 6-12 for experiment XVI-48, the equilibrium flow model is only applicable when the mass flux

Table 6-11. Flow of Pyrolysis Gases Through Low Density Nylon-Phenolic Resin Chars. Effect of Changing the Front Surface Temperature at a Mass Flux Rate of 0.001 lb/ft^2-sec and Varying Pyrolysis Gas Compositions.

RUN NUMBER MASS FLUX FRONT TEMP BACK TEMP	FLOW MODEL	H_2 MOLE %	CH_4 MOLE %	CO MOLE %	CO_2 MOLE %	N_2 MOLE %	H_2O MOLE %	C_6H_6O MOLE %	C_2H_4 MOLE %	C_2H_2 MOLE %	MODEL ΔP	MODEL q_{cz}
V-11	FROZEN	37.2	32.5	8.2	6.6	15.5	0.0	0.0	0.0	0.0	0.5	0.85
0.0014	EQUILIBRIUM	71.6	1.4	14.9	0.1	11.4	0.6	0.0	0.0	0.0	0.5	13.10
1575°F	NON-EQUILIBRIUM	37.2	32.5	8.2	6.6	15.5	0.0	0.0	0.0	0.0	0.5	0.85
730°F	EXPERIMENTAL	37.0	32.0	8.5	6.4	15.5	0.0	0.0	0.0	0.0	0.7	-
VII-19	FROZEN	35.0	43.6	4.9	2.9	13.6	0.0	0.0	0.0	0.0	0.3	0.65
0.00090	EQUILIBRIUM	81.8	1.4	7.2	0.0	9.4	0.2	0.0	0.0	0.0	0.3	11.55
1730°F	NON-EQUILIBRIUM	35.0	43.6	4.9	2.9	13.6	0.0	0.0	0.0	0.0	0.3	0.66
705°F	EXPERIMENTAL	37.2	42.5	4.2	2.6	13.5	0.0	0.0	0.0	0.0	0.4	-
XIV-42	FROZEN	31.7	46.3	5.5	2.5	14.0	0.0	0.0	0.0	0.0	0.4	0.69
0.00090	EQUILIBRIUM	82.5	0.9	7.0	0.0	9.5	0.1	0.0	0.0	0.0	0.4	17.33
1800°F	NON-EQUILIBRIUM	31.7	46.2	5.5	2.5	14.0	0.0	0.0	0.0	0.0	0.4	0.70
960°F	EXPERIMENTAL	30.9	45.2	6.1	3.7	13.9	0.0	0.0	0.0	0.0	0.4	-
XVI-50	FROZEN	31.7	46.3	5.5	2.5	14.0	0.0	0.0	0.0	0.0	0.3	0.46
0.00120	EQUILIBRIUM	83.2	0.3	7.1	0.0	9.4	0.1	0.0	0.0	0.0	0.4	8.84
2035°F	NON-EQUILIBRIUM	51.3	29.6	6.2	0.3	9.1	0.0	0.0	1.0	2.5	0.5	0.78
1162°F	EXPERIMENTAL	53.0	29.2	6.7	0.2	10.7	0.0	0.0	0.0	0.2	1.5	-
XX-64	FROZEN	28.4	5.4	3.4	1.0	0.0	46.0	15.8	0.0	0.0	0.2	1.05
0.0013	EQUILIBRIUM	65.9	0.3	33.6	0.0	0.0	0.2	0.0	0.0	0.0	0.3	32.14
2300°F	NON-EQUILIBRIUM	25.2	25.6	38.5	0.9	0.0	0.0	7.9	0.5	1.3	0.2	1.48
1190°F	EXPERIMENTAL	26.7	26.4	40.3	0.6	0.0	0.0	7.1	0.4	1.0	0.2	-

Table 6-12. Flow of Pyrolysis Gases Through Nylon-Phenolic Resin Chars. Effect of Changing the Mass Flux for a Front Surface Temperature of 2035°F and Varying Pyrolysis Gas Compositions.

RUN NUMBER MASS FLUX FRONT TEMP BACK TEMP	FLOW MODEL	H_2 MOLE %	CH_4 MOLE %	CO MOLE %	CO_2 MOLE %	N_2 MOLE %	H_2O MOLE %	C_6H_6O MOLE %	C_2H_4 MOLE %	C_2H_2 MOLE %	MODEL	
											ΔP	q_{cz}
XVI-48	FROZEN	31.7	46.3	5.5	2.5	14.0	0.0	0.0	0.0	0.0	0.0	0.01
0.00003	EQUILIBRIUM	83.1	0.4	7.0	0.0	9.4	0.1	0.0	0.0	0.0	0.0	0.25
2055°F	NON-EQUILIBRIUM	84.7	8.2	2.9	0.0	3.8	0.0	0.0	0.1	0.3	0.0	0.03
1260°F	EXPERIMENTAL	84.5	7.7	3.0	0.6	4.2	0.0	0.0	0.0	0.4	0.1	-
XVI-49	FROZEN	31.7	46.3	5.5	2.5	14.0	0.0	0.0	0.0	0.0	0.2	0.26
0.0003	EQUILIBRIUM	83.1	0.4	7.0	0.0	9.4	0.1	0.0	0.0	0.0	0.2	4.84
2015°F	NON-EQUILIBRIUM	36.1	38.9	9.6	2.3	12.8	0.0	0.0	0.1	0.2	0.2	0.28
1120°F	EXPERIMENTAL	36.8	37.9	9.2	4.3	14.0	0.0	0.0	0.0	0.0	0.4	-
XVI-50	FROZEN	31.7	46.3	5.5	2.5	14.0	0.0	0.0	0.0	0.0	0.3	0.59
0.0012	EQUILIBRIUM	83.2	0.3	7.1	0.0	9.4	0.1	0.0	0.0	0.0	0.4	8.84
2035°F	NON-EQUILIBRIUM	51.3	29.6	6.2	0.3	9.1	0.0	0.0	1.0	2.5	0.5	0.78
1162°F	EXPERIMENTAL	53.0	29.2	6.7	0.2	10.7	0.0	0.0	0.0	0.2	1.5	-
XIX-60	FROZEN	29.3	6.0	3.3	0.9	0.0	53.7	6.8	0.0	0.0	0.7	1.17
0.00248	EQUILIBRIUM	62.7	0.8	35.2	1.5	0.0	0.9	0.0	0.0	0.0	0.6	13.0
2030°F	NON-EQUILIBRIUM	38.2	17.2	25.2	8.8	0.0	4.9	5.3	0.0	0.5	0.5	2.42
1375°F	EXPERIMENTAL	41.3	18.2	23.4	7.6	0.0	5.0	4.5	0.0	0.0	0.7	-
XVI-51	FROZEN	31.7	46.3	5.5	2.5	14.0	0.0	0.0	0.0	0.0	4.7	8.40
0.0170	EQUILIBRIUM	83.3	0.3	7.0	0.0	9.4	0.1	0.0	0.0	0.0	6.7	99.85
2035°F	NON-EQUILIBRIUM	31.7	46.2	5.8	2.3	14.0	0.0	0.0	0.0	0.0	4.8	8.54
1000°F	EXPERIMENTAL	32.7	45.8	4.8	3.7	14.0	0.0	0.0	0.0	0.0	5.3	-

rates are very small (< 0.00003 lb/ft^2-sec) corresponding to very large residence times within the char layer.

In summary, results have been presented for the flow of simulated pyrolysis products through actual low density nylon-phenolic resin chars under conditions approximating the reentry of ablative heat shields. Using the non-equilibrium flow model comparison of the calculated and experimentally determined exit gas composition was made. In all cases, except those listed in Table D-1 of Appendix D in which unusual or erratic behavior was rated, the predicted values of the exit gas composition by the non-equilibrium flow analysis were within the experimental accuracy of the measured values. These results were reported for front surface temperatures between 1350 - 2300°F, mass flux rates of 0.00003 - 0.1080 lb/ft^2-sec and values of the simulated pyrolysis products entering the char zone shown in Table 6-5.

The non-equilibrium flow model is, therefore, a very accurate and useful analysis of the energy transfer in the char zone of a char-forming ablator. In cases for high mass flux values of the order of 0.01 lb/ft^2-sec the frozen flow model accurately described the energy transfer in the char zone. Only at extremely low mass flux values of the order of 0.00003 lb/ft^2-sec did the equilibrium flow model approximate the changes in composition of the pyrolysis products as they pass through the char zone.

Comparison of the Non-Equilibrium Flow Results with the Results of the Frozen and Equilibrium Flow Analyses

As discussed in Chapter III, the frozen and equilibrium flow models bracket the non-equilibrium case. Frozen flow corresponds to a system in which no chemical reactions occur, while equilibrium flow refers to a system of species undergoing chemical reactions which are at equilibrium (a function of temperature and pressure only). Since the non-equilibrium flow model predicts the actual behavior, comparison of the exit gas compositions, temperature and pressure distributions, and surface heat flux for each model will determine the accuracy of the two limited flow analyses in predicting the energy transfer within the char layer.

These results are presented in Figure 6-1 and Table 6-13 for a mass flux rate of 0.05 lb/ft^2-sec, a front surface temperature of 1500°F and a back surface temperature of 500°F. The char porosity is 0.8 and the char thickness is 0.25 inches. As seen the temperature profile of the non-equilibrium flow analysis is identical to the frozen flow temperature profile. The relative closeness of these two models is likewise seen by comparing the exit gas composition, pressure drop across the char and surface heat flux in Table 6-13. Therefore, at the above conditions there is little evidence of chemical reactions

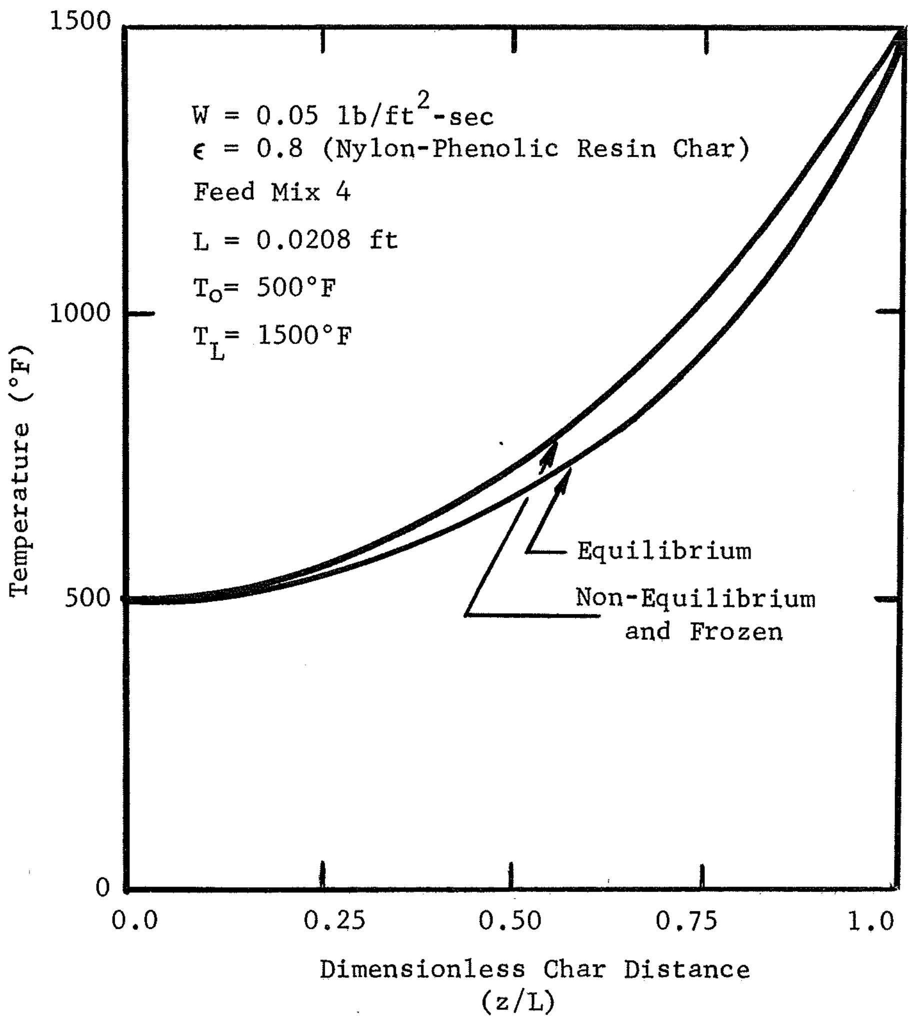

Figure 6-1. Temperature Profile for the Frozen, Equilibrium, and Non-Equilibrium Flow of Pyrolysis Gases Through the Char Zone of a Nylon-Phenolic Resin Ablator.

Table 6-13. Results of the Analyses of Frozen, Equilibrium and Non-Equilibrium Flow of Pyrolysis Gas Products Through a One-Quarter Inch Thick Low Density Nylon-Phenolic Resin Ablative Heat Shield Char at 1500°F.

Conditions: $W = 0.05$ lb/ft^2-sec $\epsilon = 0.8$ $T_o = 500$°F $L = 0.0208$ ft Feed Mix 4

Char Distance	Inlet	At z/L = 0.5			At z/L = 1.0		
Flow Model(s)	(All)	FF	EF	NEF	FF	EF	NEF
Mass Flux (lb/ft$^2_{voids}$-sec)	0.0625	0.0625	0.0626	0.0625	0.0625	0.0632	0.0625
Temperature (°F)	500.0	667.0	649.9	667.0	1500.0	1500.0	1500.0
Composition (Mole%):							
Hydrogen	33.4	33.4	2.9	33.4	33.4	9.2	33.4
Methane	6.7	6.7	35.4	6.7	6.7	33.3	6.7
Phenol	6.2	6.2	0.0	6.2	6.2	0.0	6.2
Water	48.9	48.9	54.8	48.9	48.9	48.4	48.9
Carbon Monoxide	3.7	3.7	0.0	3.7	3.7	0.1	3.7
Carbon Dioxide	1.1	1.1	6.9	1.1	1.1	8.9	1.1

Model	Pressure Drop Across Char lb/ft^2	Heat Flux at Surface BTU/ft^2-sec
Frozen Flow	6.9	32.56
Non-Equilibrium Flow	6.9	32.59
Equilibrium Flow	6.1	38.85

in the char and the energy transfer is closely predicted by the frozen flow model.

In Figure 6-2 and Table 6-14 the same results are presented for a front surface temperature of 2000°F. Although the reported non-equilibrium values are again very nearly equal to the frozen flow results, a noticeable change, especially in the concentration profile and surface heat flux is observed. This indicates chemical reactions among the species within the char layer.

A continuation of the analysis for a front surface temperature of 2500°F and 3000°F in Figures 6-3 and 6-4 and Tables 6-15 and 6-16, respectively, shows a more dramatic change which is reflected by a downward shift of the temperature profile toward the equilibrium curve and corresponding rapid changes in the concentration profile. Chemical reactions are obviously a very important mode of energy contribution under these last two sets of conditions.

It is not possible to extend the analysis to temperatures above 3000°F since the chemical behavior within the char will not be predicted by the chemical reactions of Table 6-6. In this event additional reactions must be included to accurately describe the energy transfer within the char zone. This extension is discussed by del Valle, et.al. (55).

In addition to the above comparisons, the temperature

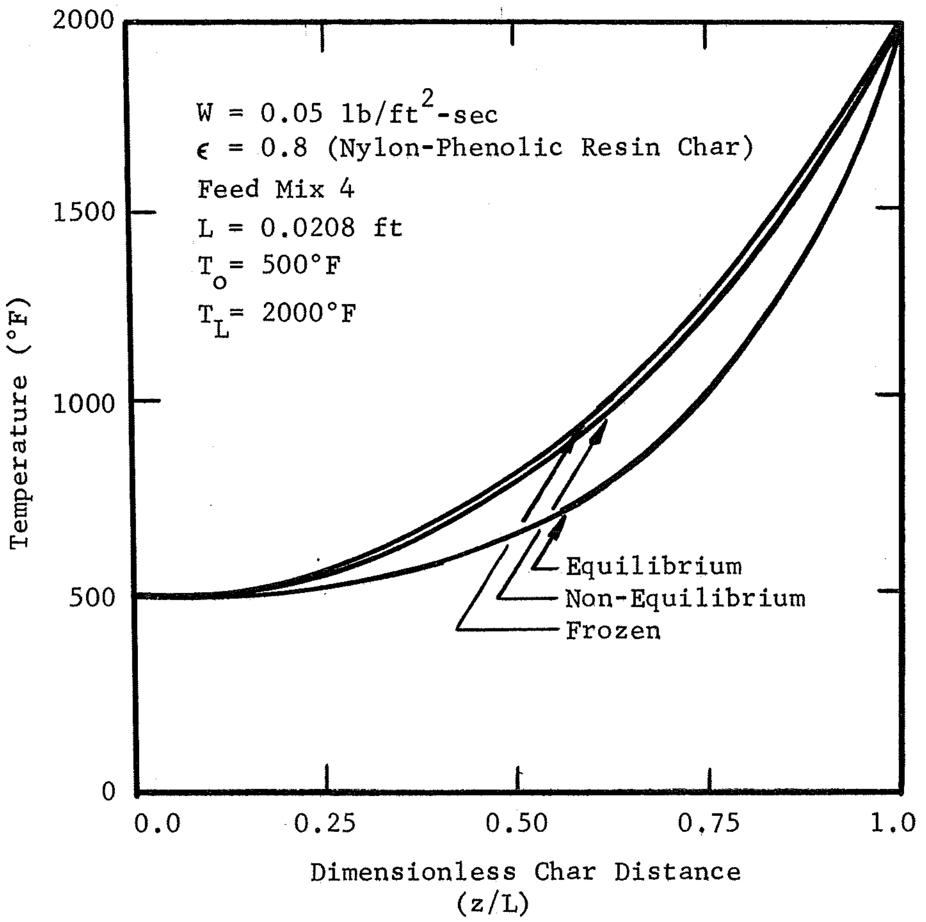

Figure 6-2. Temperature Profile for the Frozen, Equilibrium, and Non-Equilibrium Flow of Pyrolysis Gases Through the Char Zone of a Nylon-Phenolic Resin Ablator.

Table 6-14. Results of the Analyses of Frozen, Equilibrium and Non-Equilibrium Flow of Pyrolysis Gas Products Through a One-Quarter Inch Thick Low Density Nylon-Phenolic Resin Ablative Heat Shield Char at 2000°F.

Conditions: $W = 0.05\ \mathrm{lb/ft^2\text{-}sec}$ $\epsilon = 0.8$ $T_o = 500°F$ $L = 0.0208$ ft Feed Mix 4

Char Distance	Inlet	At z/L = 0.5			At z/L = 1.0		
Flow Model(s)	(All)	FF	EF	NEF	FF	EF	NEF
Mass Flux ($\mathrm{lb/ft^2_{voids}\text{-}sec}$)	0.0625	0.0625	0.0627	0.0625	0.0625	0.0628	0.0628
Temperature (°F)	500.0	794.4	720.7	794.0	2000.0	2000.0	2000.0
Composition (Mole%):							
Hydrogen	33.4	33.4	3.2	33.4	33.4	18.2	33.5
Methane	6.7	6.7	35.3	6.7	6.7	28.8	6.8
Phenol	6.2	6.2	0.0	6.2	6.2	0.0	6.2
Water	48.9	48.9	54.6	48.9	48.9	42.5	48.3
Carbon Monoxide	3.7	3.7	0.0	3.7	3.7	0.3	4.1
Carbon Dioxide	1.1	1.1	6.9	1.1	1.1	10.1	1.2

Model	Pressure Drop Across Char $\mathrm{lb/ft^2}$	Heat Flux at Char Surface $\mathrm{BTU/ft^2\text{-}sec}$
Frozen Flow	8.3	51.12
Non-Equilibrium Flow	8.2	51.53
Equilibrium Flow	6.9	71.64

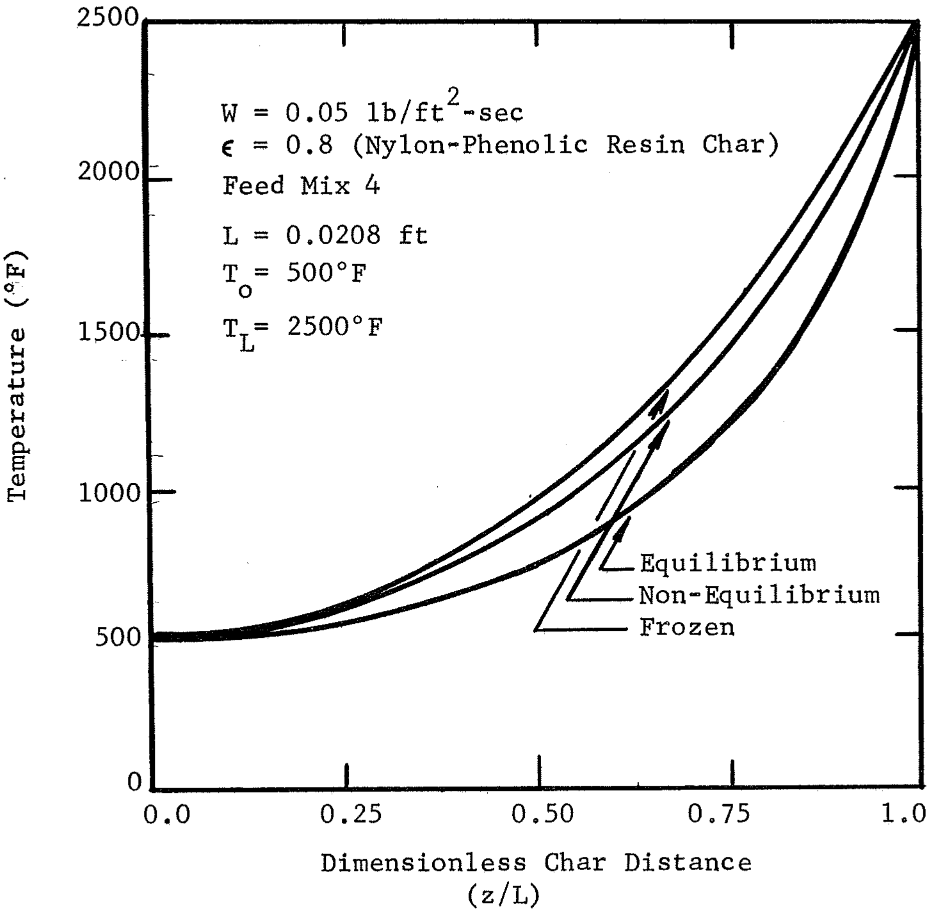

Figure 6-3. Temperature Profile for the Frozen, Equilibrium, and Non-Equilibrium Flow of Pyrolysis Gases Through the Char Zone of a Nylon-Phenolic Resin Ablator.

Table 6-15. Results of the Analyses of Frozen, Equilibrium and Non-Equilibrium Flow of Pyrolysis Gas Products Through a One-Quarter Inch Thick Low Density Nylon-Phenolic Resin Ablative Heat Shield Char at 2500°F.

<u>Conditions</u>: $W = 0.05$ lb/ft^2-sec $\epsilon = 0.8$ $T_o = 500$°F $L = 0.0208$ ft Feed Mix 4

Char Distance	Inlet	At z/L = 0.5			At z/L = 1.0		
Flow Model(s)	(All)	FF	EF	NEF	FF	EF	NEF
Mass Flux (lb/ft$^2_{\text{voids}}$-sec)	0.0625	0.0625	0.0628	0.0625	0.0625	0.0614	0.0771
Temperature (°F)	500.0	958.2	795.3	896.2	2500.0	2500.0	2500.0
<u>Composition</u> (<u>Mole %</u>):							
Hydrogen	33.4	33.4	3.3	33.4	33.4	36.5	51.1
Methane	6.7	6.7	35.4	6.7	6.7	18.8	5.3
Phenol	6.2	6.2	0.0	6.2	6.2	0.0	4.5
Water	48.9	48.9	54.1	48.9	48.9	31.4	8.3
Carbon Monoxide	3.7	3.7	0.0	3.7	3.7	1.9	29.4
Carbon Dioxide	1.1	1.1	7.1	1.1	1.1	11.5	1.2

Model	Pressure Drop Across Char lb/ft^2	Heat Flux at Char Surface BTU/ft^2-sec
Frozen Flow	9.8	71.50
Non-Equilibrium Flow	9.1	87.39
Equilibrium Flow	7.9	126.29

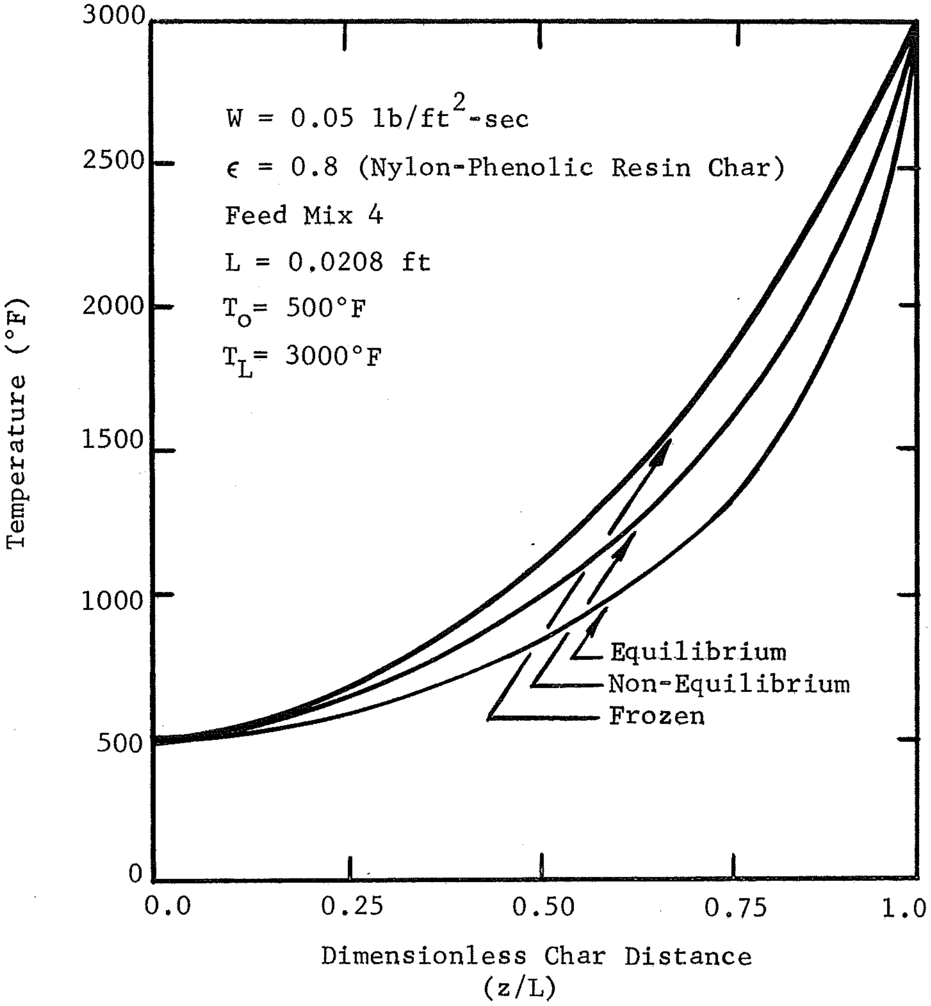

Figure 6-4. Temperature Profile for the Frozen, Equilibrium, and Non-Equilibrium Flow of Pyrolysis Gases Through the Char Zone of a Nylon-Phenolic Resin Ablator.

Table 6-16. Results of the Analyses of Frozen, Equilibrium and Non-Equilibrium Flow of Pyrolysis Gas Products Through A One-Quarter Inch Thick Low Density Nylon-Phenolic Resin Ablative Heat Shield Char at 3000°F.

Conditions: $W \doteq 0.05$ lb/ft^2-sec $\epsilon = 0.8$ $T_o = 500°F$ $L = 0.0208$ ft Feed Mix 4

Char Distance	Inlet	At z/L = 0.5			At z/L = 1.0		
Flow Model(s)	(All)	FF	EF	NEF	FF	EF	NEF
Mass Flux (lb/ft$^2_{voids}$-sec)	0.0625	0.0625	0.0628	0.0625	0.0625	0.0714	0.1096
Temperature (°F)	500.0	1150.0	843.3	990.8	3000.0	3000.0	3000.0
Composition (Mole %):							
Hydrogen	33.4	33.4	3.5	33.4	33.4	63.9	0.0$^{(a)}$
Methane	6.7	6.7	35.4	6.7	6.7	1.1	54.0
Phenol	6.2	6.2	0.0	6.2	6.2	0.0	2.4
Water	48.9	48.9	53.9	48.9	48.9	2.2	0.0
Carbon Monoxide	3.7	3.7	0.0	3.7	3.7	31.2	28.9
Carbon Dioxide	1.1	1.1	7.2	1.1	1.1	1.6	17.4

Model	Pressure Drop Across Char lb/ft^2	Heat Flux at Char Surface BTU/ft^2-sec
Frozen Flow	11.7	94.47
Non-Equilibrium Flow	10.4	149.26
Equilibrium Flow	8.6	230.37

Note: (a) Non-Equilibrium Flow Model Requires Additional Important Reactions and Associated Kinetics Data to Accurately Describe the Energy Transfer Near 3000°F.

profile, surface heat flux and pressure drop across the char are compared in Figures 6-3 and 6-5 for two pyrolysis product compositions. The results for the first simulated pyrolysis product composition, which was based on experimentally measured and computed equilibrium compositions excluding the high molecular weight cyclic compounds, is shown in Figure 6-5. The results in Figure 6-3 are for the more accurate composition based on pyrolysis gas chromatographic analyses of Sykes (2). A mass flux rate of 0.05 lb/ft^2-sec, front and back surface temperature of 2500°F and 500°F, respectively, and a one-quarter inch thick low density nylon-phenolic resin char ($\epsilon = 0.8$) were the conditions for each case presented.

Comparison of the temperature profiles for frozen and non-equilibrium flow show the same overall behavior; i.e., a downward shift by the non-equilibrium curves indicating a higher energy absorption due to chemical reactions between the pyrolysis products. On the otherhand, a noticeable difference in the equilibrium curves is observed. For the more accurate pyrolysis gas composition (Figure 6-3), the characteristically sharp downward shift of the equilibrium curve observed in Figure 6-5 does not occur.

The explanation for this difference will point out the inadequacy of the equilibrium flow model in predicting the true behavior within the char zone. Because the results of Figure 6-5

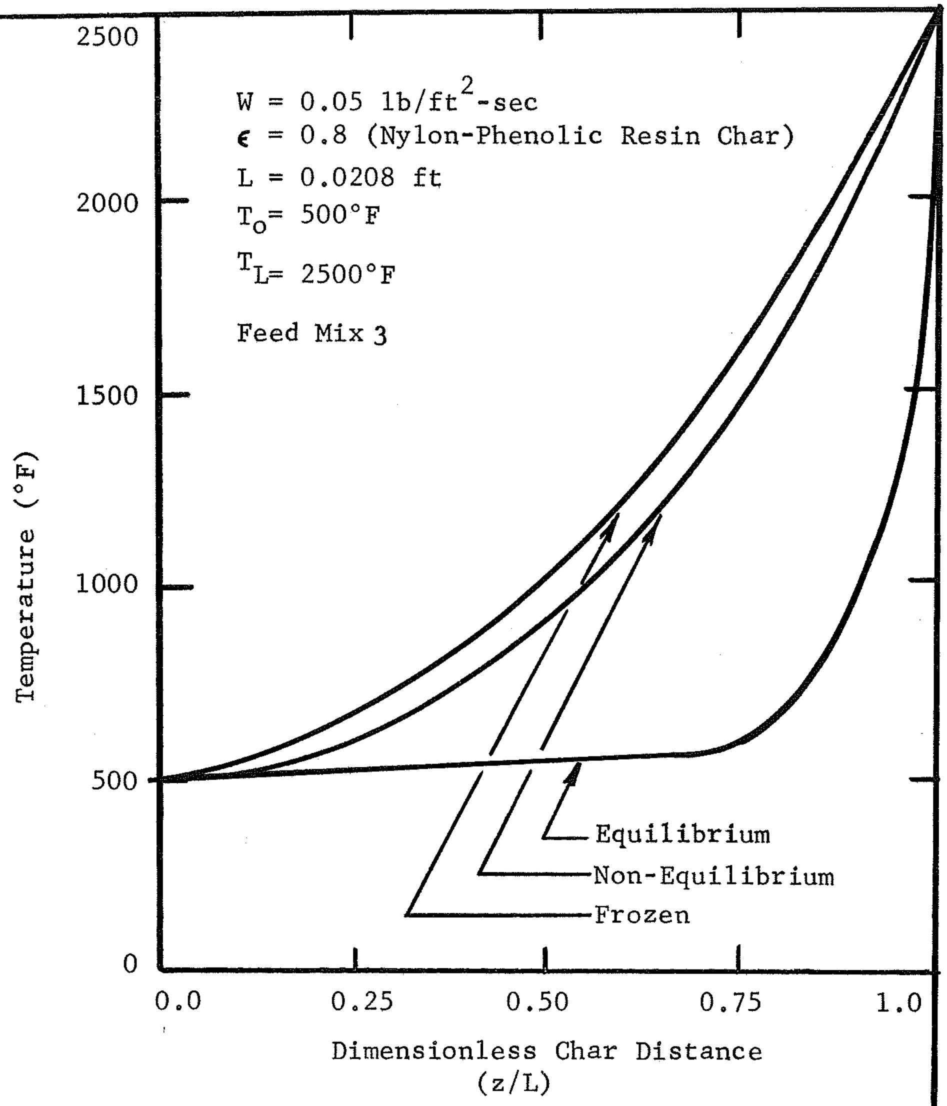

Model	Pressure Drop lb/ft^2	Surface Heat Flux BTU/ft^2-sec
Frozen Flow	12.97	52.20
Non-Equilibrium	12.45	107.64
Equilibrium Flow	9.75	271.25

Figure 6-5. Temperature Profile, Pressure Drop and Surface Heat Flux for the Flow of Pyrolysis Gases Through A One-Quarter Inch Thick Nylon-Phenolic Char.

were calculated for a pyrolysis product composition largely based on equilibrium calculated values, the inlet gas composition to the char were very nearly equal to the values calculated using the equilibrium flow model. As a result, very little energy absorption was omitted from the analysis due to the very small change in the inlet compositions which were already approximated as an equilibrium composition. This resulted in the relatively flat curve over nearly three quarters of the total char thickness.

On the otherhand, the more accurate pyrolysis product composition estimated from experimental data and dependent on finite reaction rates governing plastic decomposition, is far removed from the equilibrium calculated compositions. However, as these concentrations of gases are introduced into the equilibrium flow analysis, an abrupt adjustment to the equilibrium compositions calculated by minimizing the free energy is experienced. This is especially noted for phenol and methane which have initial compositions of 6.2 mole % and 6.7 mole %, respectively, but are immediately changed to 0.0 mole % and 35.3 mole % at the back surface temperature of 500°F. This erroneous adjustment results in the loss of energy absorption which results from phenol decomposition at finite reaction rates and causes the curve to more closely approach the frozen and non-equilibrium curves.

These same conclusions regarding the inability of the equilibrium flow model to accurately predict the true behavior is further shown in Table 6-17. Here, the surface heat flux values are compared for each model and for each simulated pyrolysis product composition. In comparing the relative values, i.e., the ratio of the heat flux of any model to the actual or non-equilibrium flow heat flux, the characteristic underpredictive nature of the frozen flow model (ratio = 0.818) and the extremely overpredictive behavior of the equilibrium flow model (ratio = 1.445) are shown. It further illustrates that although the frozen flow model can accurately describe the true behavior in some cases (low temperatures or high mass flux rates), the equilibrium flow model is totally inadequate over the temperature (500 - 3000°F) and mass flux (0.00003 - 0.10 lb/ft^2-sec) values studied in this research. Therefore, in order to obtain an accurate prediction of the energy transfer, a non-equilibrium flow model must be used within the transition region. This is only possible by considering chemical reactions between the species to occur at finite reaction rates as described by reliable kinetic data. Again the importance and application of the non-equilibrium flow model has been demonstrated and the limitations of the two ideal models shown. This discussion forms the basis for extending this research to higher temperatures involving more complex reactions and increased number of species.

Table 6-17. Comparison of the Surface Heat Flux Values for Each Flow Model and Two Pyrolysis Gas Compositions at a Front Surface Temperature of 2500°F.

Pyrolysis Gas Composition	Mole%	Flow Model	Surface Heat Flux BTU/ft^2-sec	Relative Heat Flux, ϕ_s
Hydrogen	31.7			
Methane	46.3	Frozen	52.20	0.485
Carbon Monoxide	5.5	Non-Equilibrium	107.64	1.000
Carbon Dioxide	2.5			
Nitrogen	14.0	Equilibrium	271.25	2.520
Water	0.0			
Phenol	0.0			
Hydrogen	33.4			
Methane	6.7	Frozen	71.50	0.818
Carbon Monoxide	3.7			
Carbon Dioxide	1.1	Non-Equilibrium	87.39	1.000
Nitrogen	0.0	Equilibrium	126.29	1.445
Water	48.9			
Phenol	6.2			

Note: The relative heat flux is defined as the ratio of the heat flux calculated by any model to the heat flux calculated by the non-equilibrium flow model. The relative closeness of this value, ϕ_s, to 1 determines the closeness with which the model (frozen or equilibrium) predicts the actual behavior. Values less than one show an underprediction, while values above one indicate an overprediction of the true state.

Parametric Study of the Flow of Pyrolysis Gases in the Char Zone

A comparison of the non-equilibrium flow results with the experimental data was important in determining the accuracy of the flow model. However, very little quantitative information, beyond the discrete sets of data for each experiment, was assembled regarding the effect of changing mass flux and/or temperature. As a result, a parametric study was undertaken to accurately relate the changes in these variables with variations in energy absorption within the char. To do this the non-iterative TEMPRE System (NIT) was used in which the back surface temperature and temperature gradient were specified as boundary conditions for various values of the mass flux. The results of the calculation were in the form of the net heat transfer at the surface, called the approximate aerodynamic heating, which was the sum of the surface heat flux and radiant heat flux resulting from the calculated front surface temperature:

$$q_a = \left[-k_e \frac{dT}{dz}\right]_{z=L} + \epsilon\sigma T_L^4 \qquad (6\text{-}11)$$

where a value of 0.95 was used for the emissivity. This information is shown in Figure 6-6 in which the mass flux is plotted against the aerodynamic heating for various heats of pyrolysis, q_p, (function of the temperature and gradient

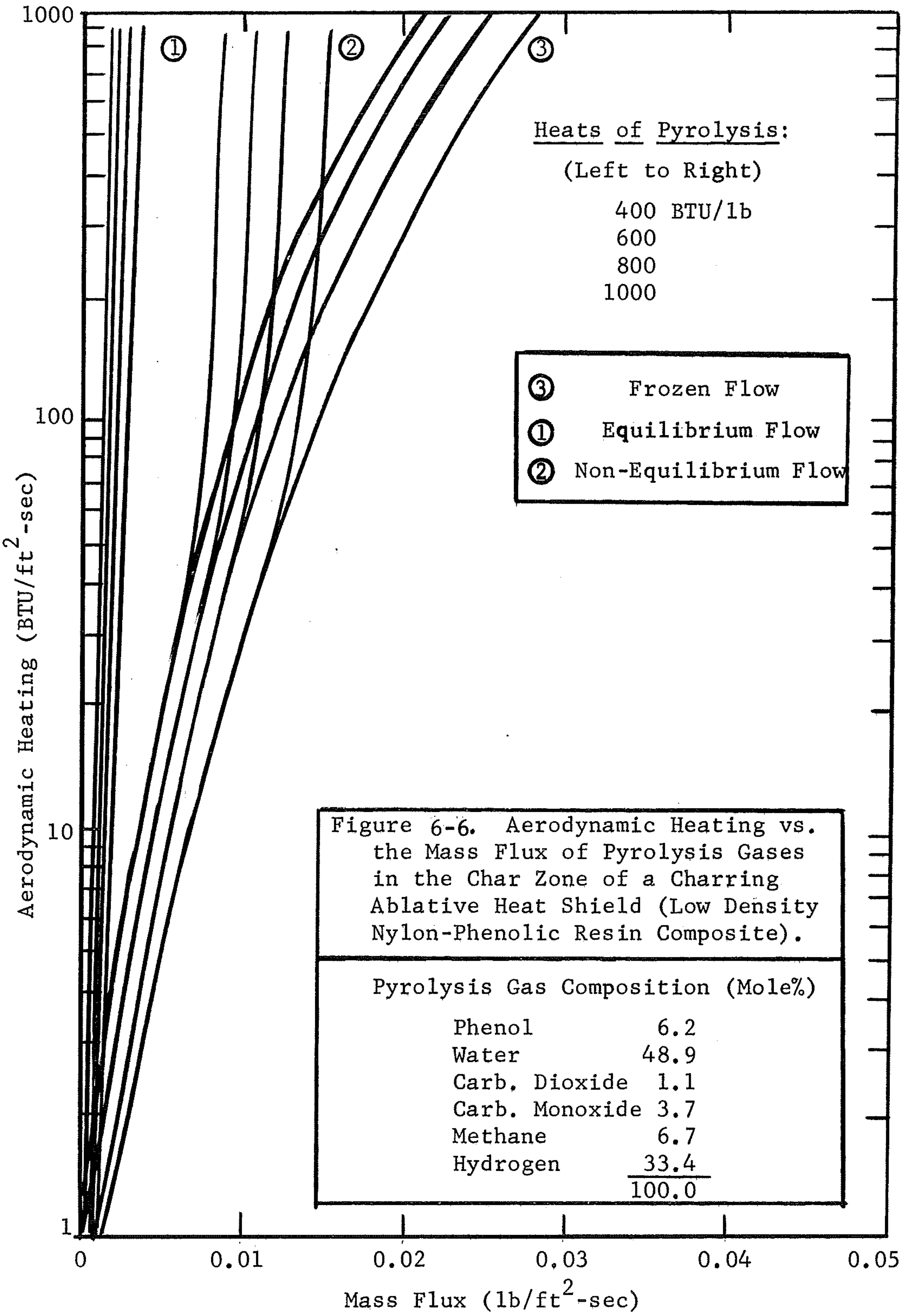

Figure 6-6. Aerodynamic Heating vs. the Mass Flux of Pyrolysis Gases in the Char Zone of a Charring Ablative Heat Shield (Low Density Nylon-Phenolic Resin Composite).

Pyrolysis Gas Composition (Mole%)

Phenol	6.2
Water	48.9
Carb. Dioxide	1.1
Carb. Monoxide	3.7
Methane	6.7
Hydrogen	33.4
	100.0

at the back surface):

$$q_p = -k_e \left. \frac{dT}{dz} \right|_{z=0} \tag{6-12}$$

where q_p is the sum of the energy absorbed by the decomposition of the polymer and the energy conducted through the virgin plastic. Results for the frozen, equilibrium and non-equilibrium flow models are presented. This form of presenting the results is a very convenient and informative method as will be seen.

In a reentry problem one of the important questions asked is what is the required heat shield weight for protection for a certain mission. Specification of the type of heat shield material to be used (e.g., nylon-phenolic resin) brackets the heat of pyrolysis value, while the trajectory calculations determine the amount of aerodynamic heating that can be expected. For example, an approximate aerodynamic heating rate of 500 BTU/ft^2-sec and a heat of pyrolysis of 400 BTU/lb locates three distinctive points on Figure 6-6; one for each of the frozen, equilibrium and non-equilibrium flow models. This corresponds to three distinctive values of the mass flux rate; 0.017 lb/ft^2-sec for frozen, 0.002 lb/ft^2-sec for equilibrium and 0.009 lb/ft^2-sec for non-equilibrium. The non-equilibrium flow model accurately predicted the behavior and would specify the exact heat shield weight (function of the mass flux) required. The frozen flow model shows an over-prediction because important endothermic reactions were omitted, and the equilibrium flow model shows an under-prediction, because reactions were assumed to occur at a greater extent than the actual behavior.

The results presented in Figure 6-6 also provide a way of determining at what point the non-equilibrium flow model changes from the frozen flow behavior to a truly non-equilibrium flow condition governed by finite reaction rates (50 BTU/ft^2-sec). This figure very graphically illustrates the differences in each model and permits the presentation of a large volume of information in a clear and readily accessible manner.

Calculation of the Reacting Gas Heat Capacity

In addition to the above information, the reacting gas heat capacity for the non-equilibrium flow of pyrolysis products through the char has been determined also. This term is very useful in the calculation of the one-dimensional, transient response of an ablative composite. The energy equation for the transient case can be put in the following form (56) for the char zone.

$$-\frac{\partial}{\partial z}\left(k\frac{\partial T}{\partial z}\right) + \left[\left(\frac{W}{W_o}\right)\bar{C}_p + \frac{\sum_{i=1}^{K+1} H_i \bar{R}_i}{W_o\left(\frac{\partial T}{\partial z}\right)}\right] W_o \frac{\partial T}{\partial z} = -\rho C_p \frac{\partial T}{\partial t} \qquad (6\text{-}13)$$

where W is the mass flux of pyrolysis products at z and W_o is the mass flux of pyrolysis products entering the char. The term in brackets is referred to as the effective reacting gas heat capacity. Hence, the flow within the char zone can be considered frozen ($\Sigma H_i\bar{R}_i \neq 0$) by introducing the reacting gas heat capacity as an input function to the transient calculations. In Figure 6-7 a plot of the reacting gas heat capacity as a function of temperature is shown for frozen, equilibrium and non-equilibrium flow within the char layer up to 3000°F. These curves were calculated for a mass flux of 0.05 $\mathrm{lb/ft^2}$-sec, a back surface temperature of 500°F, and, char porosity and thickness of 0.8 and 0.25 inches, respectively. The differences in the manner used to calculate the energy transfer by chemical reaction ($\Sigma H_i\bar{R}_i$) for equilibrium and non-equilibrium flow causes the curves to separate as shown.

Flow of Pyrolysis Products Through Porous Graphite

There are two important reasons for using porous graphite to simulate low density, nylon-phenolic resin chars used in ablative heat shield applications. These are availability and machinability of the graphite.

Nylon-phenolic resin chars were obtained from the National Aeronautics and Space Administration's Langley Research Center for use in the Char Zone Thermal Environment Simulator.

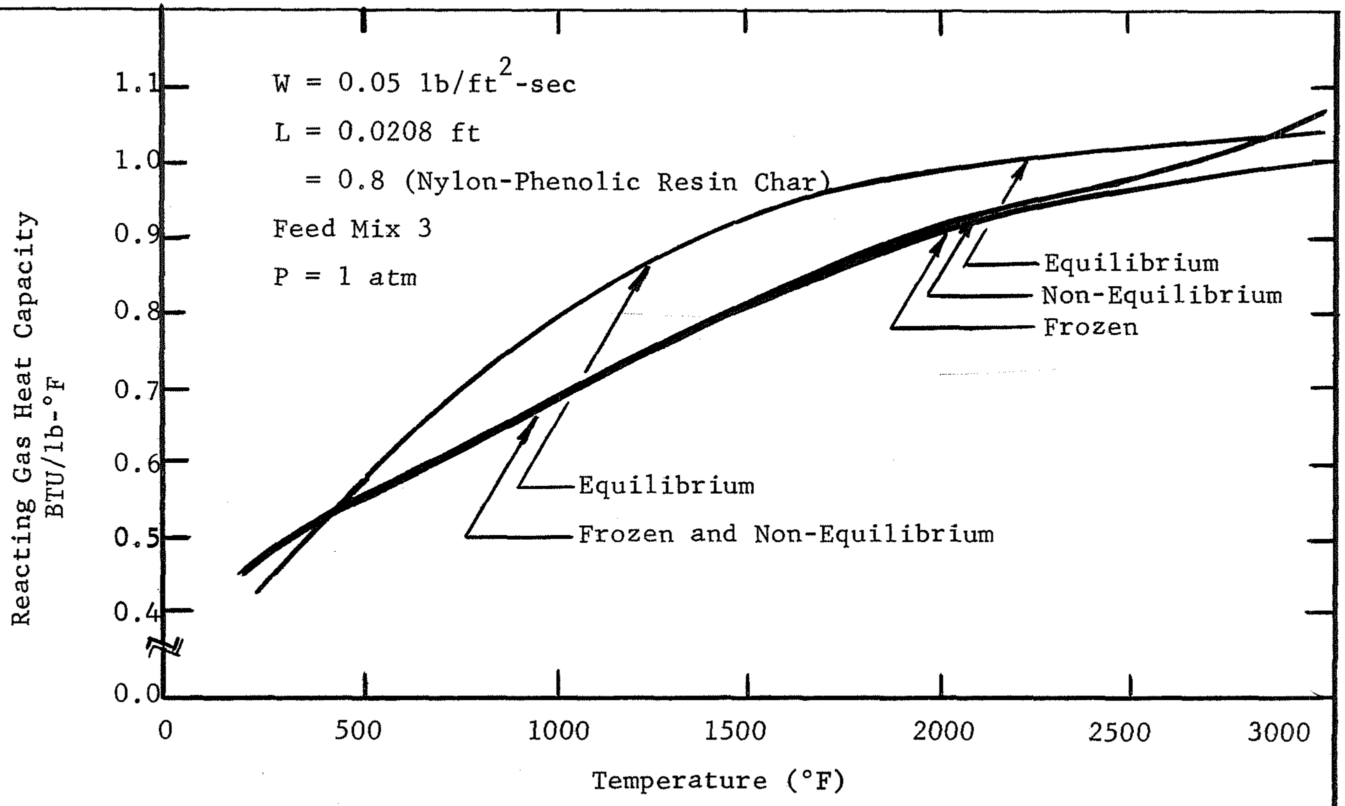

Figure 6-7. Plot of the Reacting Gas Heat Capacity for Frozen, Equilibrium and Non-Equilibrium Flow of Pyrolysis Gases Through the Char Zone.

Electric air arc jets were used to char the nylon-phenolic resins, and this represented a considerable effort in supplying just a few specimens for use in this research. Although two sections of char were usually obtained from each specimen, the demand for additional chars could not be met. In addition to the problem of obtaining the samples, the brittle nature of the chars caused serious problems in mounting on the char holder section. These complications led to the testing and use of graphite, expecially, for use in radioactive tracer and catalyst evaluation studies. However, for the successful substitution of graphite for the chars to be complete, the chemical behavior of the two must be essentially the same. This is to say that the same reactions and kinetic data important in predicting the energy transport within porous chars, must also do the same for energy transport in porous graphite. This will be shown in the following sections by comparing the exit gas compositions from the Char Zone Thermal Environment Simulator with the composition predicted by the non-equilibrium flow model, and, by direct comparison of char and graphite experimental results over a range of mass flux rates and front surface temperature common to both systems.

Comparison of Reacting Flow Through Chars and Graphite: Other than the differences in the structural properties of chars and graphite, the one most important consideration that must be accounted for is the change in mass flux rates caused by differences in material porosity. Therefore, to put the materials on a common basis for discussion, the mass flux rates previously discussed in terms of the total area ($\mathrm{lb/ft^2_{total}}$-sec) must be divided by the porosity to obtain rates within the pores ($\mathrm{lb/ft^2_{voids}}$-sec). Even though the superficial mass flux rates are different for each porous medium, the mass flux rate within the pores will be the same. Again, the porosity of the chars and graphite were 0.8 and 0.5, respectively.

The foregoing discussion is not intended to mean that chemical reactions will not be influenced by other structural properties beside the porosity (e.g., crystallidity, permeability, etc.). However, it emphasizes that the mass flux within the pore spaces must be equivalent for a valid comparison. Differences in the chemical reaction rates resulting from differences in structural makeup could eliminate graphite as a suitable substitute. However, this could only be determined by a comparison of experiments conducted over the range of conditions for which the proposed flow model is valid.

In Table 6-18 the exit gas composition from the Char Zone Thermal Environment Simulator for the flow of pyrolysis products through graphite are presented for mass flux rates of 0.0034 to 0.0059 $\mathrm{lb/ft^2}$-sec at a front surface temperature of approxi-

Table 6-18. Flow of Pyrolysis Gases Through Graphite. Effect of Changing Mass Flux Rates at a Front Surface Temperature of 1950°F.

RUN NUMBER MASS FLUX FRONT TEMP BACK TEMP	FLOW MODEL	H_2 MOLE %	CH_4 MOLE %	CO MOLE %	CO_2 MOLE %	N_2 MOLE %	H_2O MOLE %	C_6H_6O MOLE %	C_2H_4 MOLE %	C_2H_2 MOLE %	MODEL	
											ΔP	q_{cz}
XXVIII-93	FROZEN	25.8	7.2	4.3	1.3	0.0	50.1	11.3	0.0	0.0	0.2	1.92
0.0034	EQUILIBRIUM	62.7	1.3	33.5	0.8	0.0	1.7	0.0	0.0	0.0	0.2	28.4
1950°F	NON-EQUILIBRIUM	32.8	10.0	11.8	4.1	0.0	32.6	10.2	0.0	0.3	0.2	2.33
1110°F	EXPERIMENTAL	32.2	11.2	9.2	4.0	0.0	33.2	9.8	0.2	0.2	0.3	-
XXVIII-92	FROZEN	27.5	5.3	3.1	1.0	0.0	52.5	10.6	0.0	0.0	0.3	2.44
0.0044	EQUILIBRIUM	62.5	1.2	33.9	0.8	0.0	1.6	0.0	0.0	0.0	0.3	35.48
1920°F	NON-EQUILIBRIUM	29.3	7.7	8.0	2.5	0.0	42.2	10.1	0.0	0.2	0.3	2.75
1100°F	EXPERIMENTAL	30.0	8.7	8.0	3.4	0.0	39.9	9.6	0.2	0.2	0.4	-
XXIX-95	FROZEN	21.7	4.6	2.8	0.8	0.0	57.1	13.1	0.0	0.0	0.5	7.34
0.0059	EQUILIBRIUM	61.1	1.4	34.0	1.3	0.0	2.2	0.0	0.0	0.0	0.3	25.8
1935°F	NON-EQUILIBRIUM	22.9	5.1	4.7	1.2	0.0	53.1	12.9	0.0	0.1	0.5	7.65
930°F	EXPERIMENTAL	21.9	6.6	5.4	2.1	0.0	52.0	11.3	0.3	0.4	0.4	-

mately 1950°F. As in the case with chars, there is a significant amount of chemical reactions occurring in the porous medium for the lower mass flux rates (< 0.01 lb/ft^2-sec). More importantly, however, is the agreement within experiment error between the measured exit gas compositions and the predicted values by the non-equilibrium flow model using the same kinetic data employed for the char experiments.

A similar comparison is presented in Table 6-19 for an average mass flux rate of 0.0035 lb/ft^2-sec and front surface temperatures of 1950 and 2065°F. Again, excellent agreement within the experimental accuracy of the analyses was obtained between the non-equilibrium flow model compositions and the experimental values. However, a closer inspection of the graphite experiments in Table D-3 of Appendix D shows that the non-equilibrium predicted compositions do not agree in some cases with the experimental data. This is especially true for experiments XXI-66, XXIII-72, XXIII-73, and XXIV-76. These differences were a result of experimental difficulties associated with maintaining a steady liquid (water and phenol) feed rate as indicated in the experimental summary sheets of Table D-1; and, therefore, should not be interpreted as a failure of the model to predict the flow behavior in porous graphite.

In addition to these irregularities in the water-phenol-

Table 6-19. Flow of Pyrolysis Gases Through Graphite. Effect of Changing the Front Surface Temperature at a Mass Flux Rate of 0.0032 lb/ft^2-sec.

RUN NUMBER MASS FLUX FRONT TEMP BACK TEMP	FLOW MODEL	H_2 MOLE %	CH_4 MOLE %	CO MOLE %	CO_2 MOLE %	N_2 MOLE %	H_2O MOLE %	C_6H_6O MOLE %	C_2H_4 MOLE %	C_2H_2 MOLE %	MODEL ΔP	MODEL q_{cz}
XXVIII-93	FROZEN	25.8	7.2	4.3	1.3	0.0	50.1	11.3	0.0	0.0	0.2	1.92
0.0034	EQUILIBRIUM	62.7	1.3	33.5	0.8	0.0	1.7	0.0	0.0	0.0	0.2	28.4
1950°F	NON-EQUILIBRIUM	30.8	10.0	11.8	4.1	0.0	32.6	10.2	0.0	0.3	0.2	2.33
1110°F	EXPERIMENTAL	32.2	11.2	9.2	4.0	0.0	33.2	7.8	0.2	0.2	0.3	-
XXIII-71	FROZEN	25.8	4.9	2.9	0.9	0.0	54.7	10.8	0.0	0.0	0.2	2.02
0.0031	EQUILIBRIUM	62.6	0.7	35.8	0.3	0.0	0.7	0.0	0.0	0.0	0.2	31.85
2065°F	NON-EQUILIBRIUM	41.4	8.4	23.9	5.1	0.0	12.5	8.2	0.0	0.6	0.2	3.23
1108°F	EXPERIMENTAL	39.3	8.8	27.2	5.9	0.0	11.2	7.6	0.0	0.0	0.7	-

gas experiments, similar disagreement was also observed in several water-phenol free pyrolysis product investigations. In experiments IX and XI shown in Table 6-20, increased in methane and corresponding decreases in hydrogen concentrations clearly deviated from the predicted frozen flow behavior. These observations were attributed to problems associated with the fabrication of the graphite specimens. In the earlier experiments, the dust-like graphite "fines" which resulted from the milling process were not removed from the pore spaces within the plug. These "fines" provided additional surface area which made them highly susceptible to reaction with hydrogen to form methane. After complete reaction of the "fines" (about five to ten minutes), the hydrogen and methane concentrations in the exit stream returned to their initial compositions indicating frozen flow behavior. This is illustrated graphically in Figure 6-8 in which hydrogen and methane concentrations (in mole precent) are plotted against experimental run time (in minutes) for experiment IX.

Methane production of this kind was eliminated in subsequent experiments (XII, XIII, and XV in Table 6-21) by first passing nitrogen or helium through the graphite plugs prior to mounting in the char holder. This removed the "fines" from the pore spaces and eliminated the sharp increase in methane observed in Figure 6-8. The contrasting concentration profiles as a

Table 6-20. Flow of Pyrolysis Gases Through Porous Graphite. Effect of Having Graphite "Fines" in the Pore Spaces.

RUN NUMBER MASS FLUX FRONT TEMP BACK TEMP	FLOW MODEL	H_2 MOLE %	CH_4 MOLE %	CO MOLE %	CO_2 MOLE %	N_2 MOLE %	H_2O MOLE %	C_6H_6O MOLE %	C_2H_4 MOLE %	C_2H_2 MOLE %	MODEL	
											ΔP	q_{cz}
IX-25	FROZEN	35.0	43.6	4.9	2.9	13.6	0.0	0.0	0.0	0.0	0.5	0.41
0.0009	EQUILIBRIUM	76.7	5.6	5.8	0.2	10.0	1.7	0.0	0.0	0.0	0.5	4.91
1350°F	NON-EQUILIBRIUM	35.0	43.6	4.9	2.9	13.6	0.0	0.0	0.0	0.0	0.5	0.41
815°F	EXPERIMENTAL	20.2	55.2	8.0	3.5	13.6	0.0	0.0	0.0	0.0	0.9	-
IX-26	FROZEN	35.0	43.6	4.9	2.9	13.6	0.0	0.0	0.0	0.0	2.0	1.80
0.0039	EQUILIBRIUM	77.6	4.9	6.0	0.2	9.9	1.4	0.0	0.0	0.0	1.6	19.22
1370°F	NON-EQUILIBRIUM	35.0	43.6	4.9	2.9	13.6	0.0	0.0	0.0	0.0	2.0	1.80
800°F	EXPERIMENTAL	24.6	52.2	6.2	3.4	13.6	0.0	0.0	0.0	0.0	2.2	-
IX-27	FROZEN	35.0	43.6	4.9	2.9	13.6	0.0	0.0	0.0	0.0	39.0	28.25
0.0570	EQUILIBRIUM	77.0	5.2	5.9	0.2	10.0	2.7	0.0	0.0	0.0	24.8	89.50
1350°F	NON-EQUILIBRIUM	35.0	43.6	4.9	2.9	13.6	0.0	0.0	0.0	0.0	39.0	28.25
725°F	EXPERIMENTAL	27.0	51.5	5.5	2.9	13.6	0.0	0.0	0.0	0.0	28.2	-
XI-31	FROZEN	35.0	43.6	4.9	2.9	13.6	0.0	0.0	0.0	0.0	0.5	0.41
0.0009	EQUILIBRIUM	76.3	6.0	5.6	0.2	10.0	1.9	0.0	0.0	0.0	0.5	4.79
1335°F	NON-EQUILIBRIUM	35.0	43.6	4.9	2.9	13.6	0.0	0.0	0.0	0.0	0.5	0.41
805°F	EXPERIMENTAL	28.5	49.8	5.5	2.5	14.7	0.0	0.0	0.0	0.0	0.8	-
XI-32	FROZEN	35.0	43.6	4.9	2.9	13.6	0.0	0.0	0.0	0.0	2.1	1.68
0.0039	EQUILIBRIUM	78.1	4.6	6.1	0.1	9.8	1.3	0.0	0.0	0.0	1.81	18.78
1390°F	NON-EQUILIBRIUM	35.0	43.6	4.9	2.9	13.6	0.0	0.0	0.0	0.0	2.1	1.68
865°F	EXPERIMENTAL	29.8	49.2	4.9	2.9	13.6	0.0	0.0	0.0	0.0	2.0	-
XI-33	FROZEN	35.0	43.6	4.9	2.9	13.6	0.0	0.0	0.0	0.0	34.2	33.5
0.0570	EQUILIBRIUM	77.2	5.2	5.9	0.2	10.0	2.5	0.0	0.0	0.0	20.8	97.3
1355°F	NON-EQUILIBRIUM	35.0	43.6	4.9	2.9	13.6	0.0	0.0	0.0	0.0	34.2	33.5
595°F	EXPERIMENTAL	32.3	46.2	5.0	2.9	13.6	0.0	0.0	0.0	0.0	36.1	-

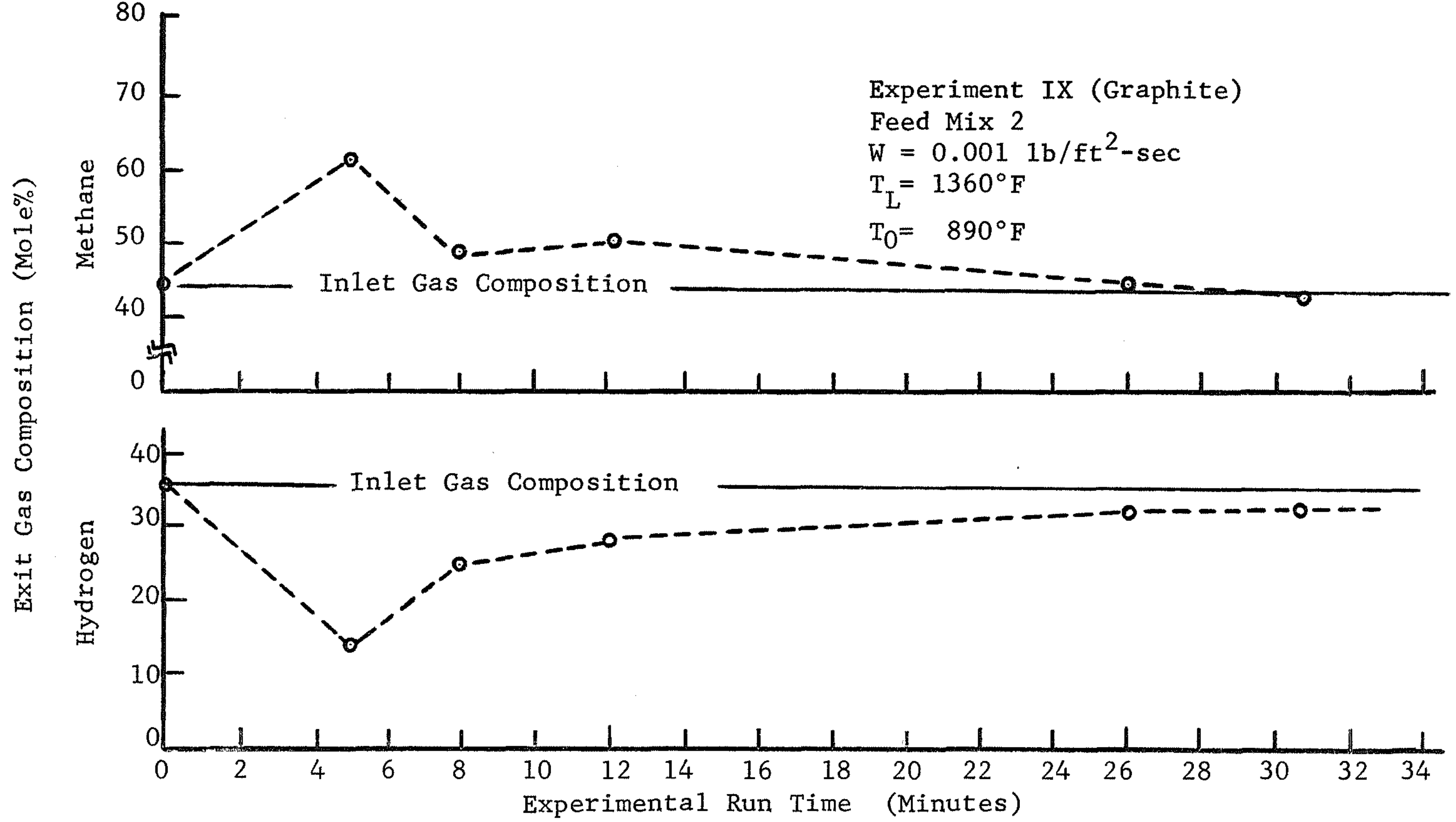

Figure 6-8. Typical Methane-Hydrogen Concentration Profile in the Exit Gas Stream from the Char Zone Thermal Environment Simulator for the Inclusion of Graphite "Fines" in the Pore Spaces.

Table 6-21. Flow of Pyrolysis Gases Through Porous Graphite. Exit Gas Compositions Resulting From Experiments In Which The "Fines" Were Cleared From The Pore Spaces By Passing Helium Through the Specimens.

RUN NUMBER MASS FLUX FRONT TEMP BACK TEMP	FLOW MODEL	H_2 MOLE %	CH_4 MOLE %	CO MOLE %	CO_2 MOLE %	N_2 MOLE %	H_2O MOLE %	C_6H_6O MOLE %	C_2H_4 MOLE %	C_2H_2 MOLE %	MODEL	
											ΔP	q_{cz}
XII-36	FROZEN	35.0	43.6	4.9	2.9	13.6	0.0	0.0	0.0	0.0	2.1	1.36
0.00390	EQUILIBRIUM	76.9	5.5	5.8	0.2	9.9	1.6	0.0	0.0	0.0	2.0	14.62
1350°F	NON-EQUILIBRIUM	35.0	43.6	4.9	2.9	13.6	0.0	0.0	0.0	0.0	2.1	1.36
920°F	EXPERIMENTAL	36.1	42.9	4.8	3.3	12.9	0.0	0.0	0.0	0.0	2.3	-
XIII-38	FROZEN	31.7	46.3	5.5	2.5	14.0	0.0	0.0	0.0	0.0	0.7	0.41
0.0009	EQUILIBRIUM	82.3	1.1	7.0	0.0	9.5	0.2	0.0	0.0	0.0	1.0	3.17
1690°F	NON-EQUILIBRIUM	31.7	46.3	5.5	2.5	14.0	0.0	0.0	0.0	0.0	0.7	0.41
1210°F	EXPERIMENTAL	32.6	41.3	8.9	5.2	14.0	0.0	0.0	0.0	0.0	0.5	-
XIII-39	FROZEN	31.7	46.3	5.5	2.5	14.0	0.0	0.0	0.0	0.0	2.9	1.74
0.0039	EQUILIBRIUM	82.4	1.0	7.0	0.0	9.5	0.1	0.0	0.0	0.0	4.2	13.01
1725°F	NON-EQUILIBRIUM	31.7	46.3	5.5	2.5	14.0	0.0	0.0	0.0	0.0	2.9	1.75
1220°F	EXPERIMENTAL	30.8	45.8	6.0	4.4	14.0	0.0	0.0	0.0	0.0	4.2	-
XIII-40	FROZEN	31.7	46.3	5.5	2.5	14.0	0.0	0.0	0.0	0.0	0.7	0.43
0.0009	EQUILIBRIUM	82.3	1.0	7.1	0.0	9.5	0.1	0.0	0.0	0.0	1.1	3.01
1750°F	NON-EQUILIBRIUM	31.7	46.3	5.5	2.5	14.0	0.0	0.0	0.0	0.0	0.7	0.42
1200°F	EXPERIMENTAL	30.8	45.7	5.9	3.6	14.0	0.0	0.0	0.0	0.0	1.5	-
XV-45	FROZEN	31.7	46.3	5.5	2.5	14.0	0.0	0.0	0.0	0.0	0.6	0.47
0.0009	EQUILIBRIUM	82.3	1.1	7.0	0.0	9.5	0.1	0.0	0.0	0.0	0.9	5.26
1710°F	NON-EQUILIBRIUM	31.7	46.3	5.5	2.5	14.0	0.0	0.0	0.0	0.0	0.6	0.47
1125°F	EXPERIMENTAL	31.7	46.8	4.5	3.0	14.0	0.0	0.0	0.0	0.0	1.2	-
XV-46	FROZEN	31.7	46.3	5.5	2.5	14.0	0.0	0.0	0.0	0.0	0.0	0.03
0.0001	EQUILIBRIUM	82.5	0.9	7.0	0.0	9.5	0.1	0.0	0.0	0.0	0.1	0.49
1755°F	NON-EQUILIBRIUM	31.7	46.3	5.6	2.4	14.0	0.0	0.0	0.0	0.0	0.0	0.03
1185°F	EXPERIMENTAL	32.5	43.7	6.2	4.6	13.0	0.0	0.0	0.0	0.0	0.2	-

function of run time are shown in Figure 6-9 for experiment XIII.

As a final comparison, several char and graphite experiments are examined in Table 6-22. To accomplish this the mass flux rates based on the void area were calculated and are shown in brackets. The listing in Table 6-22 is, also, made in order of increasing chemical reactions; i.e., low temperatures and high mass flux rates appear first. As seen, the char and graphite experiments are indeed compatible and behave, from the overall chemical viewpoint, as one material.

This permits the use of the more easily workable graphite materials in experiments designed to study carbon deposition and product distribution using Carbon-14 tracers, and, to investigate the effect of catalysts in accelerating the rates of chemical reactions within the char layer. Details of the results from these additional experimental investigations follow.

Radioactive Tracer Studies Using Porous Graphite

Radioactive methane and phenol were used in separate experiments to determine the specific products of decomposition from each labeled species. Also, the amount and location of carbon deposition in the char due to the thermal cracking of each species was determined.

The method used involved the sampling of the exit gas stream followed by gas chromatographic analysis. The frac-

Table 6-22. Flow of Pyrolysis Gases Through Graphite and Chars. Comparison of Results.

RUN NUMBER MASS FLUX: W (W_p) FRONT TEMP BACK TEMP	FLOW MODEL	H_2	CH_4	CO	CO_2	N_2	H_2O	C_6H_6O	C_2H_4	C_2H_2	MODEL	
		MOLE %	MOLE %	MOLE %	MOLE %	MOLE %	MOLE %	MOLE %	MOLE %	MOLE %	ΔP	q_{cz}
C-XVIII-56	FROZEN	28.9	6.4	3.3	0.8	0.0	53.3	6.9	0.0	0.0	0.4	0.93
0.00208	EQUILIBRIUM	59.7	3.3	26.7	4.0	0.0	6.3	0.0	0.0	0.0	0.4	15.93
(0.00260)	NON-EQUILIBRIUM	23.0	11.1	2.8	2.1	0.0	53.8	7.1	0.0	0.0	0.4	0.99
1690°F	EXPERIMENTAL	24.8	10.3	3.4	1.3	0.0	53.7	6.5	0.0	0.0	0.8	-
1030°F												
G-XXVIII-93	FROZEN	25.8	7.2	4.3	1.3	0.0	50.1	11.3	0.0	0.0	0.2	1.92
0.0034	EQUILIBRIUM	62.7	1.3	33.5	0.8	0.0	1.7	0.0	0.0	0.0	0.2	28.40
(0.0068)	NON-EQUILIBRIUM	28.8	10.0	11.8	4.1	0.0	32.6	10.2	0.0	0.3	0.2	2.33
1950°F	EXPERIMENTAL	32.2	11.2	9.2	4.0	0.0	33.2	9.8	0.2	0.2	0.4	-
1110°F												
C-XIX-60	FROZEN	29.3	6.0	3.3	0.9	0.0	53.7	6.8	0.0	0.0	0.7	1.17
0.00248	EQUILIBRIUM	62.7	0.8	35.2	1.5	0.0	0.9	0.0	0.0	0.0	0.6	13.00
(0.0031)	NON-EQUILIBRIUM	38.2	17.2	25.2	8.8	0.0	4.9	5.1	0.0	0.5	0.6	2.42
2030°F	EXPERIMENTAL	41.3	18.2	23.4	7.6	0.0	5.0	4.5	0.0	0.0	0.6	-
1375°F												
G-XXIII-71	FROZEN	25.8	4.9	2.9	0.9	0.0	54.7	10.8	0.0	0.0	0.2	2.02
0.0031	EQUILIBRIUM	62.6	0.7	35.8	0.3	0.0	0.7	0.0	0.0	0.0	0.2	31.85
(0.0062)	NON-EQUILIBRIUM	41.4	8.4	23.9	5.1	0.0	12.5	8.2	0.0	0.6	0.2	3.23
2065°F	EXPERIMENTAL	39.3	8.8	27.2	5.9	0.0	11.2	7.6	0.2	0.3	0.7	-
1108°F												
C-XX-63	FROZEN	28.6	5.5	3.4	1.0	0.0	53.8	7.7	0.0	0.0	0.6	1.79
0.00224	EQUILIBRIUM	63.1	0.3	36.4	0.1	0.0	0.2	0.0	0.0	0.0	0.5	51.37
(0.00280)	NON-EQUILIBRIUM	30.7	21.4	38.6	3.4	0.0	0.0	4.6	0.3	1.0	0.5	3.18
2290°F	EXPERIMANTAL	30.4	19.8	38.0	5.7	0.0	0.0	5.0	0.5	0.6	0.6	-
1180°F												

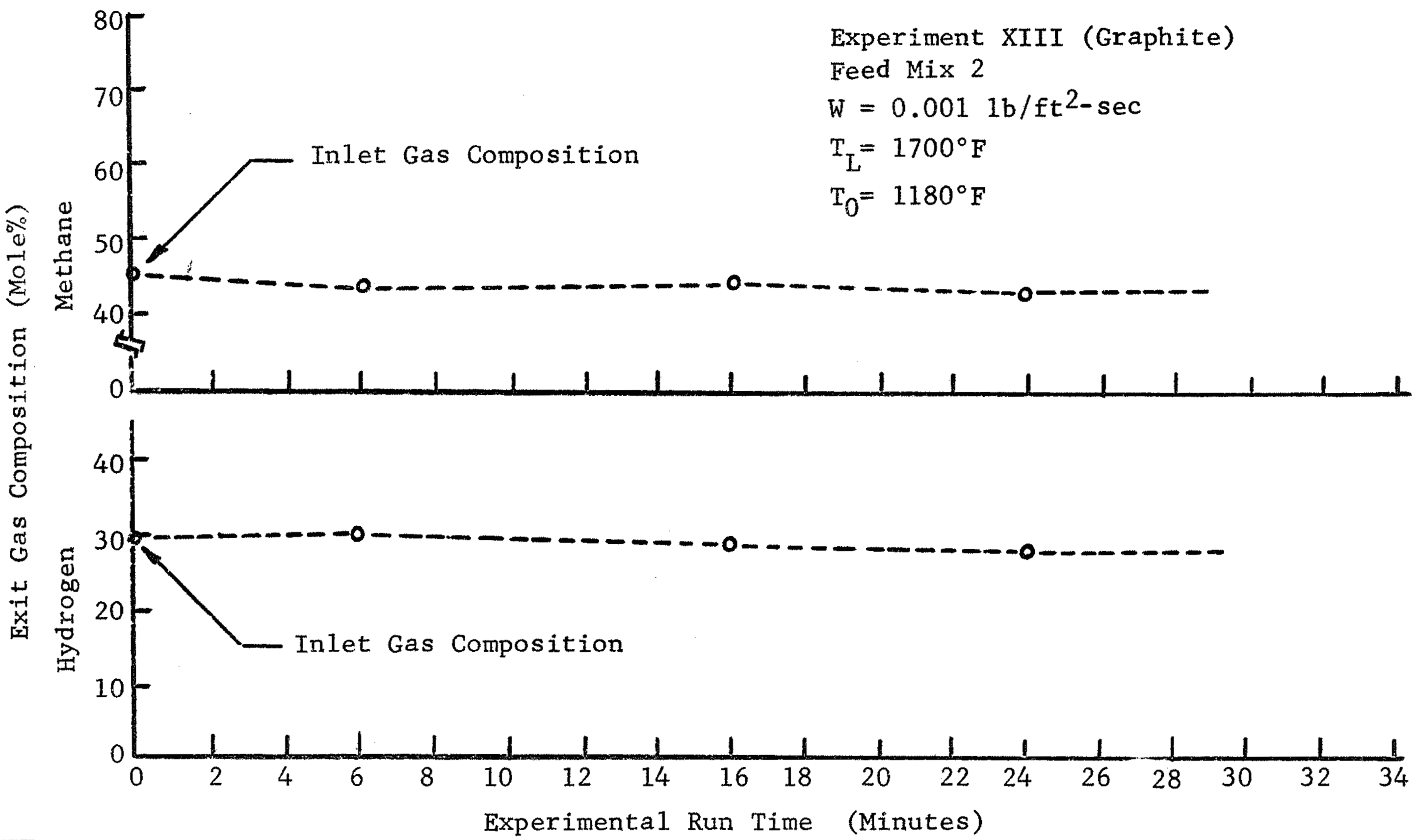

Figure 6-9. Typical Methane-Hydrogen Concentration Profiles in the Exit Gas Stream from the Char Zone Thermal Environment Simulator after Clearing the Pore Spaces of Graphite "Fines" with Helium or Nitrogen Flow.

tionated gas chromatographic effluent stream was then passed through a combustion furnace forming carbon dioxide and water. After trapping the water, the carbon dioxide was absorbed in a one molar hydroxide of hyamine (in methanol) solution. Collecting the carbon dioxide over small intervals (one half to one minute) produced radioactive concentrations corresponding to the separated gases indicated on the gas chromatogram. By comparing the two curves for identical retention times, the relative amount of each carbon-containing species formed from the thermal degradation of the labeled pyrolysis product entering the char was determined.

Typical results for Carbon-14 labeled methane are shown in Figure 6-10, in which the gas chromatogram(s) and corresponding radioactivity curve are presented. The particular results are for experiment XXIX in which the front surface temperature was 1935°F and the gas mass flux was 0.00591b/ft^2-sec. By comparing the two curves, the products of methane decomposition were found to be unreacted methane, carbon monoxide, carbon dioxide, ethylene and acetylene. These results for methane are very important in the light of predicting the manner in which energy can be absorbed by chemical reaction. Ethylene and acetylene, for example, are indirect products of methane decomposition predicted by reactions (6-1) through (6-4) in Table 6-7, while carbon monoxide and dioxide are formed by

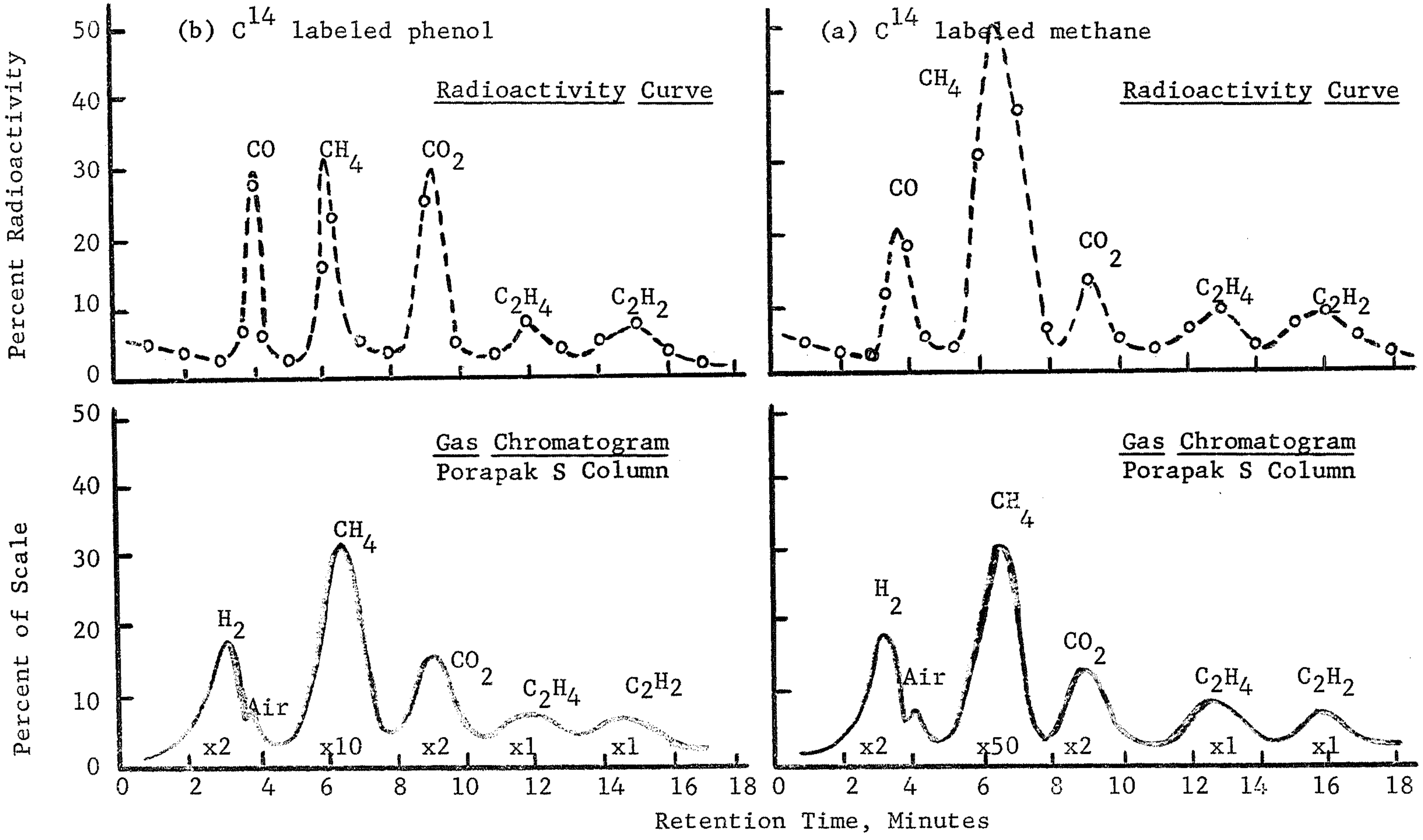

Figure 6-10. Gas Chromatograms and Radioactivity Curves of the Exit Product Stream from the Char Zone Thermal Environment Simulator; (a) C^{14} labeled methane, (b) phenol.

the reaction of steam with deposited carbon in reactions (6-8) through (6-10). This information established that the chemical reactions used to predict the phenomena occurring in any system are correct.

A similar discussion is presented for labeled phenol. These results are likewise shown in Figure 6-10. Conditions for the presented data were a front surface temperature of 1960°F and a mass flux rate of 0.0034 lb/ft^2-sec. The exit gas products for phenol degradation are methane, carbon monoxide, carbon dioxide, ethylene and acetylene, as well as unreacted phenol analysed in the liquid phase. Once again insight into the kind of reactions necessary to produce the products was obtained. The formation of hydrogen and carbon by reaction (6-6) and (6-7) is probable by the observed carbon deposition within the graphite. Hydrogenation of carbon by reaction (6-5) to form methane, followed by the steam-gas reactions (6-8, 6-9, 6-10) and the hydrocarbon cracking reactions (6-1, 6-2, 6-3, 6-4) accounts for each radioactive species observed.

In both methane and phenol degradation, thermal decomposition of the major species in the simulated pyrolysis product stream was described and accounted for by the reactions considered important between 500 - 3000°F.

In addition to the product distribution resulting from the thermal degradation of methane and phenol, deposited carbon was also observed to occur. The location of the carbon deposition within the char layer is important in defining the temperature at which reactions become significant. This topic is discussed in detail in the next section.

Carbon Deposition Studies by Radioactive Tracer Methods

The location and extent of carbon deposition resulting from methane and phenol decomposition was determined using Carbon-14 labeled methane and phenol. In the specific cases studied, labeled methane and phenol were fed separately as components in the simulated pyrolysis product stream entering the char. The char was removed after each experiment and sectioned by removing thin layers using emery paper. These layers varied between one and ten percent (by weight) of the total char and were combusted separately with collection of the carbon dioxide in one molar hydroxide hyamine (in methanol) solution. The radioactivity of each thin layer was determined and plotted as a function of char depth. In Figure 6-11 such a curve is shown for the thermal degradation of phenol and Figure 6-12 is a similar curve for the decomposition of radioactive labeled methane. The hashed-in rectangular blocks represent the total percent radioactivity of the thickness of the individual slices analysed, while the dotted curve represents the percent radioactivity per unit thick-

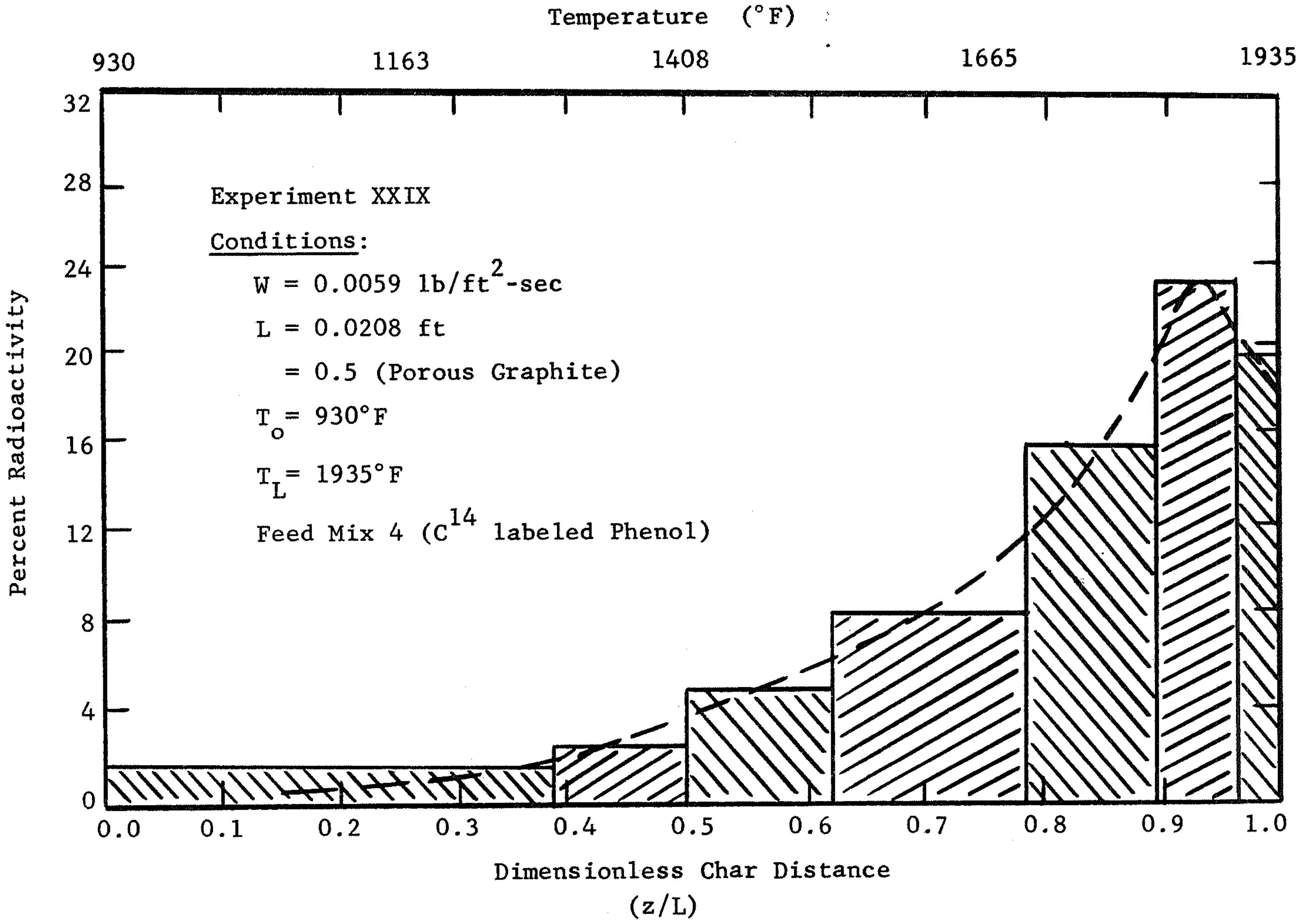

Figure 6-11. Carbon Deposition Profile for the Thermal Degradation of Phenol, a Major Component in the Pyrolysis Gas Stream.

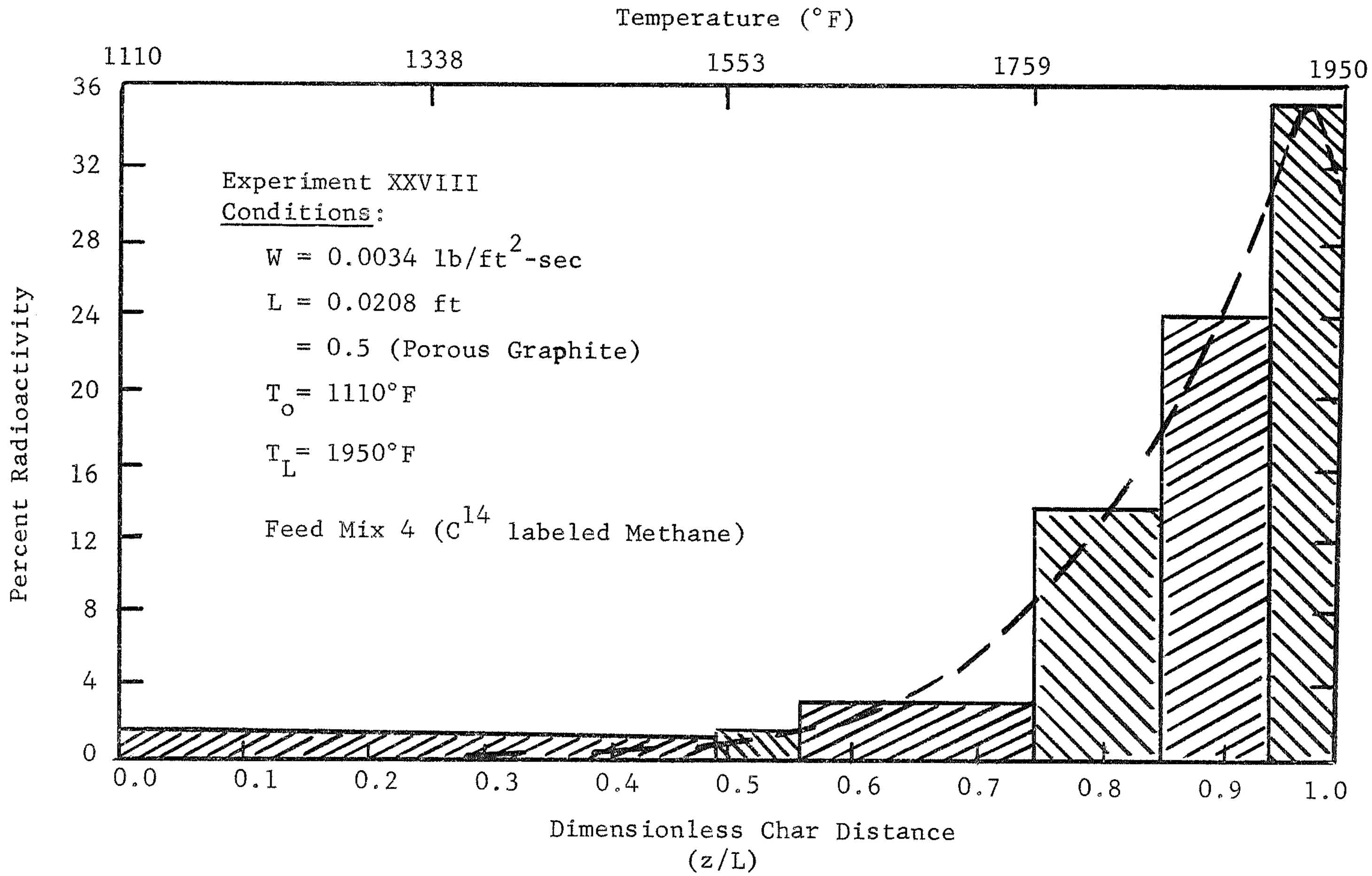

Figure 6-12. Carbon Deposition Profile for the Thermal Degradation of Methane, a Major Component in the Pyrolysis Gas Stream.

ness at a particular char depth. The results in Figure 6-11 are for phenol decomposition at a mass flux rate of 0.0059 lb/ft^2-sec and a front surface temperature of 1960°F. Deposition of carbon appears to start at a char depth of 0.38 corresponding to a temperature of 1300 °F, and continues uniformly to 0.925 where the temperature is 1925°F. At this point a rapid decrease is noted indicating either no further carbon deposition or disappearance of carbon by chemical reaction.

Similar results are observed for carbon deposition by methane decomposition in Figure 6-12. Since carbon deposition by methane and/or phenol degradation is an increasing function of temperature, and, since a substantial amount of phenol and methane is present in the exit gas stream, it is unlikely that carbon deposition reactions have terminated. Instead, the reaction of the deposited carbon with steam (or carbon dioxide) is a more probable explanation of the decline noted in Figure 6-12. This is also substantiated by the rapid decrease in water concentration at the same temperature where carbon deposition declines. Additionally, carbon was observed on the quartz cover plate and inside surfaces of the outer char holder section which indicated that the carbon deposition reactions were continuing after the gases had left the char surface. Therefore, a very comprehensive picture of carbon deposition with regard to its location, the causes for its appearance and disappearance, and its effect on the exit gas product distribution was obtained. This was one additional, important use of an accurate mathematical model in predicting phenomena very difficult and often impossible to determine with experimental techniques only.

The combination of the radioactive tracer techniques and the non-equilibrium flow analysis will be applied in evaluating various catalysts for accelerating the chemical reactions and, thereby, increasing the energy absorbed within the char zone. The effectiveness of each catalyst will be determined in the following section by comparing the results with data from non-catalytic experiments.

Catalytic Reactions of the Pyrolysis Products in the Char Zone

The discussion thus far has shown that chemical reactions within the char layer are very important modes of energy absorption. It was also pointed out that chemical non-equilibrium becomes important between 2000 - 2500 °F for a mass flux rate of 0.05 lb/ft^2-sec (Tables 6-13 through 6-16). Below this range, the flow of pyrolysis products through the char is essentially frozen, while above 2000 °F, the flow is best described by finite reaction rates for the important chemical reactions taking place within the char between the pyrolysis products.

In reentry applications where the temperature gradient across the ablator may vary from 500 - 5000°F, the frozen state (less than 2000 °F) can extend over nearly one third the entire thickness. Within this region heat absorption by conduction and convection are the only important modes of energy transfer. In order to increase the capacity of this region to absorb heat, and thus proportionately reduce the total heat shield weight requirement, the introduction of a catalyst to initiate chemical reactions in the lower temperature range ($<$ 2000 °F) was evaluated.

There are two types of catalyst systems: homogeneous and heterogeneous. The first involves the introduction of a chemical compound which is in the same phase as the pyrolysis product stream. The homogeneous catalyst effectively reduces the energy of activation by interacting with the various species present. To illustrate this interaction the catalytic chlorination of nitrous oxide in the presence of bromine is used as an example (58) of the action of a homogeneous catalyst. The direct chlorination occurs by reaction (6-14):

$$2NO + Cl_2 \rightarrow 2NOCl \qquad (6\text{-}14)$$

Introducing bromine results in a two reaction sequence as follows:

$$2NO + Br_2 \rightarrow 2NOBr \qquad (6\text{-}15)$$

$$2NOBr + Cl_2 \rightarrow 2NOCl + Br_2 \qquad (6\text{-}16)$$

The reaction with the greatest activation energy between (6-15) and (6-16) is the rate determining step for the sequence. Bromine is considered a catalyst if, and only if, the energy of activation of the rate determining step is smaller than the energy of activation of reaction (6-14). Such is the case for this example. Other homogeneous catalysts are iodine, hydrogen bromide, hydrogen fluoride, nitric oxide, chlorine and mercury (59,60,61,62,63).

In the case of the halogens, incorporation of an organic halide into the composite which thermal degrades at or near the temperature for the nylon-phenolic resin could be used to introduce the catalyst into the pyrolysis product stream. One example for bromine is tribromobutane which vaporizes at 225°C or 540°F (nylon-phenolic resin at 250°C) and forms HBr and cracked products of an olefin.

The second kind of catalyst system with application to flow of hydrocarbon products through porous media are the heterogeneous catalysts. These consist of a thin dispersion of an active metal on a porous solid, called a catalyst support. Gases are thus absorbed on the metal surfaces as they flow through the porous solid, undergo chemical reactions, and resorbed into the gas stream. The kind of solid supports used vary from clays and alumina to porous carbon.

Heterogeneous catalysts are widely used in the petroleum and chemical industries for accelerating hydrogenation and dehydrogenation reactions, hydrocracking reactions and hydroforming reactions. Some typical active metals used in these applications are platinum, tungsten, molybdenum, palladium, etc. (64). One example involves the catalytic hydrogenation of benzene to cyclohexane at room temperature with platinum on porous carbon supports (64). Cyclohexane is then cracked to lower molecular weight compounds at 840°F (65). Details for the catalytic cracking of numerous organic compounds are presented by Vogh (66).

In many cases the use of heterogeneous catalysts is restricted to applications which do not contain compounds that deactivate the metal surfaces. Some of these so called poisons are carbon monoxide, sulfur and deposits of carbon or coke. Although there is no sulfur in the pyrolysis product stream, carbon monoxide and deposited carbon are present requiring additional screening of the heterogeneous catalyst considered. The activity and selectivity of the catalyst chosen for this application is discussed in a subsequent section.

Because the heterogeneous catalyst exists in a different state, the solid phase, than the pyrolysis products, introduction into the system requires more detailed planning. There are two possible techniques that permit the placement of a finely dispersed metal catalyst on the char of a charring ablator. The first takes advantage of a nylon-platinum catalyst used to hydrogenate benzene to cyclohexane (67). The inclusion of this platinum impregnated nylon with nylon and phenolic resin during the molding process could be made. During ablation, the nylon would degrade and release the metal catalyst which would be distributed on the surface of the formed char layer. The presence of water and hydrogen at the lower temperatures (<900°F) would prevent coking, leaving the metal sites exposed to promote the pyrolysis reactions.

The second method is similar to the method used for introducing a homogeneous catalyst into the pyrolysis product stream. In this case an organo-metallic compound such as nickel stearate (68) could be included which would vaporize in the decomposition zone with deposition of nickel on the char surface. This action is commonly observed in vapor phase cracking processes (68,69) in which increased activity of the cracking catalyst results in excessive carbon and hydrogen formation. Other similar compounds are the carbonyl compounds of nickel, iron and cobalt (70). The combination of both catalysts systems may also be possible by using compounds containing both metal and halogen atoms, such as platinum iodide. The advantage of this type of co-catalyst would exist only if both groups were found to accelerate chemical reactions within the char layer.

The following sections will describe the results obtained in tests using the Char Zone Thermal Environment Simulator. Each catalyst system will be compared with non-catalytic data to determine the extent of chemical reaction due to the addition of the catalyst. The preparation of each catalyst and the procedure for introducing it into the experimental simulation will also be discussed.

Homogeneous Catalysis of the Pyrolysis Products: Unlike the heterogeneous catalysis systems, very little information regarding the activity of various homogeneous catalyst systems is contained in the literature. One source, however, reported the relative activity of several organic halides and halogen catalysts for the catalytic degradation of hydrocarbons to carbon monoxide, carbon dioxide and organic acids, aldehydes and ketones (71). A list of the relative activities of these catalysts are presented in Table 6-23 with iodine as a reference (relative activity of 100). No relative activities of nitrous oxide or mercury were found. Also hydrogen fluoride was omitted from the above list of relative activities.

Although the above may indeed be excellent homogeneous catalysts, certain aspects of the ablative process prohibit their use. For example, nitrous oxide, while exhibiting excellent

Table 6-23. Relative Activity of the Halogens and Organic Halides as Catalysts in the Thermal Degradation of Pyrolysis Gas Products.

Conditions: Oxidation of Aldehydhes and Ketones at 400-500°C and one Atmosphere.

Component Name	Relative Efficiency
Iodine (Reference)	100
Isopropyl Iodide	70
Ethyl Iodide	40
Methyl Iodide	30
Hydrogen Bromide	20
Isopropyl Bromide	5
Ethyl Bromide	4
Dibromoacetylene	3
Chlorides	0

catalytic activity for the thermal degradation of certain hydrocarbons requires a concentration too great to be practically included in the composite (59). Similarly, hydrogen fluoride and mercury are almost exclusively used as liquid phase catalysts (72,73). As a result, attention in this research was given to the halides which were not only reported as good catalysts in hydrocarbon decomposition and oxidation reactions (74), but also required in small enough concentrations to be conviently and economically feasible for ablative heat shield applications.

Experimental Results for Homogeneous Catalysis of the Pyrolysis Product Reactions with Bromine: As a matter of convenience in the experimental simulation apparatus, bromine was selected as a representative halide catalyst. It was convenient to dissolve bromine in the water and feed the resulting solution to the char holder with phenol and the gaseous pyrolysis products. The concentration of bromine in the water solution was varied from 1.0 to 4.0% by weight.

The selection of bromine as a suitable and typical catalyst was based on evidence of strong aromatic ring attack, such as with phenol, to form tribromophenol at ambient conditions. In addition it has excellent oxidative properties in decomposing hydrocarbons such as propane to carbon monoxide, carbon dioxide and other organic species such as organic acids, aldehydes and ketones (74). Furthermore, the formation of HBr from hydrogen and bromine occurs at moderate temperatures (200 - 300°C) by the following mechanism (75). This gives the additional catalytic benefit of HBr being present.

$$
\begin{aligned}
Br_2 &\rightarrow Br + Br \\
Br + H_2 &\rightarrow HBr + H \\
H + Br_2 &\rightarrow HBr + Br \\
H + HBr &\rightarrow H_2 + Br \\
Br + Br &\rightarrow Br_2^* \\
Br_2^* &\rightarrow Br + Br
\end{aligned}
\qquad (6\text{-}17)
$$

Also it established a reference to the remaining halide catalysts contained in Table 6-23 and thus makes an exhaustive investigation unnecessary if significant promotion of chemical reaction rates are found. The above mechanism is favored by low pressure and large surface area, both of which exist in the char zone during reentry.

Results of several experiments are shown in Table 6-24. The experimental exit gas compositions are no longer predicted by the non-equilibrium flow model within the experimental accuracy as observed for the non-catalytic experiments. Also the reactions are not at equilibrium as seen from the table.

The effect of bromine as a catalyst is better illustrated by comparing experiment XXVIII-92, in which the mass flux was

Table 6-24. Flow of Pyrolysis Gases Through Graphite. Effect of Bromine Catalyst on the Exit Gas Compositions.

RUN NUMBER MASS FLUX FRONT TEMP BACK TEMP	FLOW MODEL	H_2 MOLE %	CH_4 MOLE %	CO MOLE %	CO_2 MOLE %	N_2 MOLE %	H_2O MOLE %	C_6H_6O MOLE %	C_2H_4 MOLE %	C_2H_2 MOLE %	CATALYSTS
XXV-82	FROZEN	36.9	7.2	4.2	1.3	0.0	42.3	8.1	0.0	0.0	Bromine in Water 4% (by weight)
0.0065	EQUILIBRIUM	66.2	0.8	32.1	0.2	0.0	0.7	0.0	0.0	0.0	
2050°F	NON-EQUILIBRIUM	40.6	9.7	14.1	2.7	0.0	25.2	7.3	0.0	0.0	
1105°F	EXPERIMENTAL	41.6	11.8	18.9	3.4	0.0	16.4	7.1	0.3	0.5	
XXVII-87	FROZEN	2.3	3.4	0.4	0.1	0.0	0.0	93.8	0.0	0.0	Bromine in Water 1% (by weight)
0.00320	EQUILIBRIUM	73.7	1.5	24.1	0.3	0.0	0.4	0.0	0.0	0.0	
1980°F	NON-EQUILIBRIUM	2.8	3.6	0.5	0.1	0.0	0.0	91.3	0.0	0.6	
1060°F	EXPERIMENTAL	4.8	2.7	0.8	0.1	0.0	0.0	90.2	0.1	0.3	
XXVII-89	FROZEN	2.1	3.2	0.4	0.1	0.0	94.2	0.0	0.0	0.0	Bromine in Water 1% (by weight)
0.00508	EQUILIBRIUM	51.1	0.6	46.7	0.7	0.0	1.0	0.0	0.0	0.0	
2010°F	NON-EQUILIBRIUM	18.3	2.8	13.3	2.0	0.0	63.6	0.0	0.0	0.0	
1070°F	EXPERIMENTAL	28.2	3.4	21.5	6.0	0.0	40.8	0.0	0.4	0.5	
XXVI-84	FROZEN	34.3	6.6	3.9	1.1	0.0	45.4	8.7	0.0	0.0	Bromine in Water 2% (by weight)
0.0013	EQUILIBRIUM	65.0	1.0	32.5	0.4	0.0	1.0	0.0	0.0	0.0	
2020°F	NON-EQUILIBRIUM	39.5	10.7	16.6	3.8	0.0	21.5	7.5	0.0	0.4	
908°F	EXPERIMENTAL	37.8	15.3	21.0	4.8	0.0	14.2	6.3	0.2	0.4	

0.0044 lb/ft_2-sec, the front surface temperature of 1920°F and no bromine, with experiment XXV-81 (mass flux of 0.0038 lb/ft^2-sec, a front surface temperature of 1995°F and 4%(wt) bromine catalyst) in Table 6-25. The conditions are almost the same, and the extent of reaction is greater for the experiment with bromine present. The addition of bromine accelerated the chemical reactions as seen by the facts that significantly more of the water (17.6% rather than 25.4%) and phenol (7.2% rather than 9.5%) had been consumed than would have been if bromine had not been present. This is also seen by direct comparison of the experimental exit gas compositions from each of the similar experiments. A measured decrease in the water and phenol concentrations, with corresponding increases in methane, carbon monoxide, carbon dioxide, ethylene and acetylene are obtained in the bromine catalysed experiment. These same trends are observed in all investigations with bromine and are independent of the catalyst concentrations used(1.0 to 4.0% by weight).

The effect of the bromine catalysis is also seen by inspecting the carbon deposition profiles for the thermal decomposition of phenol in the simulated pyrolysis product stream. This is presented in Figures 6-13 and 6-14. The carbon deposition profile for the non-catalytic experiment is shown in Figure 6-13 for a mass flux of 0.0059 lb/ft^2-sec and 1935°F. Deposition

Table 6-25. Flow of Pyrolysis Gases Through Graphite. Comparison of Bromine Catalyzed and Non-Catalytic Exit Gas Compositions.

RUN NUMBER MASS FLUX FRONT TEMP BACK TEMP	FLOW MODEL	H_2 MOLE %	CH_4 MOLE %	CO MOLE %	CO_2 MOLE %	N_2 MOLE %	H_2O MOLE %	C_6H_6O MOLE %	C_2H_4 MOLE %	C_2H_2 MOLE %	COMMENTS
XXV-81	FROZEN	31.5	6.1	3.5	1.1	0.0	47.1	10.8	0.0	0.0	Bromine
0.0038	EQUILIBRIUM	64.7	0.9	33.2	0.4	0.0	0.9	0.0	0.0	0.0	in Water
1995°F	NON-EQUILIBRIUM	36.4	9.9	14.6	3.7	0.0	25.4	9.5	0.0	0.4	4%
1170°F	EXPERIMENTAL	40.2	11.9	15.1	7.0	0.0	17.6	7.2	0.3	0.7	(by weight)
XXVIII-92	FROZEN	27.5	5.3	3.1	1.0	0.0	52.5	10.6	0.0	0.0	No
0.0044	EQUILIBRIUM	62.5	1.2	33.9	0.8	0.0	1.6	0.0	0.0	0.0	Bromine
1920°F	NON-EQUILIBRIUM	29.3	7.7	8.6	2.5	0.0	42.2	10.1	0.0	0.2	
1100°F	EXPERIMENTAL	30.0	8.7	8.0	3.4	0.0	39.9	9.6	0.2	0.2	

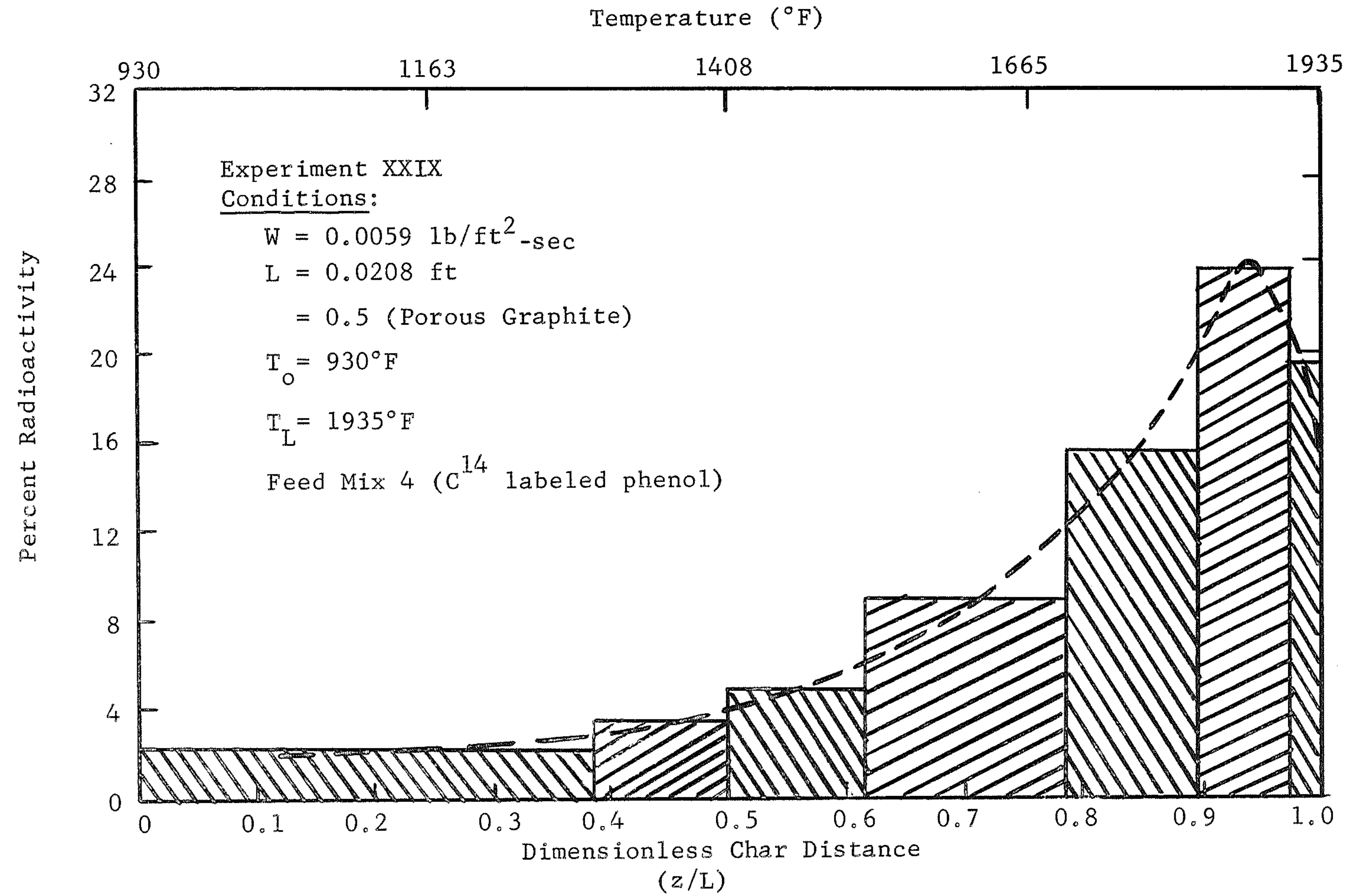

Figure 6-13. Carbon Deposition Profile for the Thermal Decomposition of Phenol, a Major Component in the Pyrolysis Gas Stream.

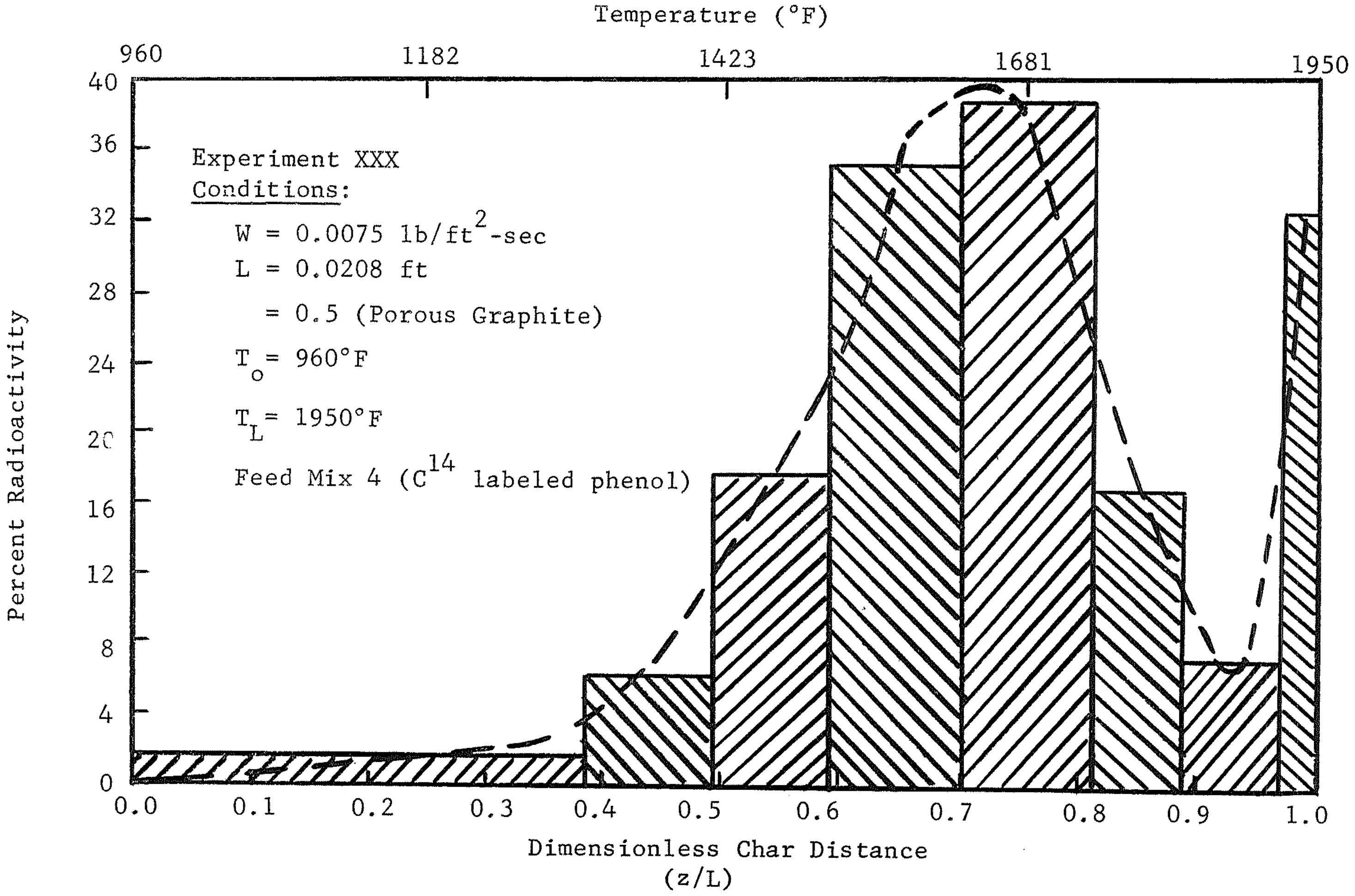

Figure 6-14. Carbon Deposition Profile for the Thermal Degradation of Phenol Catalyzed by Bromine in a Concentration of 4% (by weight).

begins at a distance of 0.38 in the char where the temperature is 1310 °F with a uniform increase to a maximum value at 0.925 or 1915°F. At this point the profile decreases. In contrast to this curve, Figure 6-14 represents the carbon deposition profile for the bromine catalysed experiment in which the mass flux was 0.0075 lb/ft^2-sec and 1900°F. There is a definite shift in the carbon deposition curve with the maximum value moving from 0.925 to 0.71 or from a temperature of 1915°F to 1630°F. Deposition again starts at a distance of 0.38 (1300°F). Also additional carbon deposition was noted near the front surface at a temperature of about 1925°F.

Similar profiles are shown in Figure 6-15 and 6-16 for carbon-14 labelled methane decomposition. Although the results are not as pronounced as the phenol data, a detectable shift in the carbon deposition pattern is again observed. Deposition begins at 0.48 (1555°F) for the non-catalytic experiment compared with 0.42 (1500°F) for the bromine catalyzed case. The point of maximum deposition is shifted away from the front surface to a position corresponding to 1893°F or 0.85. The peak for the bromine-free experiment is located at 0.98 (1930°F).

In summary these results show that bromine is an active catalyst for the catalytic cracking of phenol in the presence of hydrogen (hydrocracking) and to a lesser extent for the hydrocracking of methane. A similar discussion regarding the

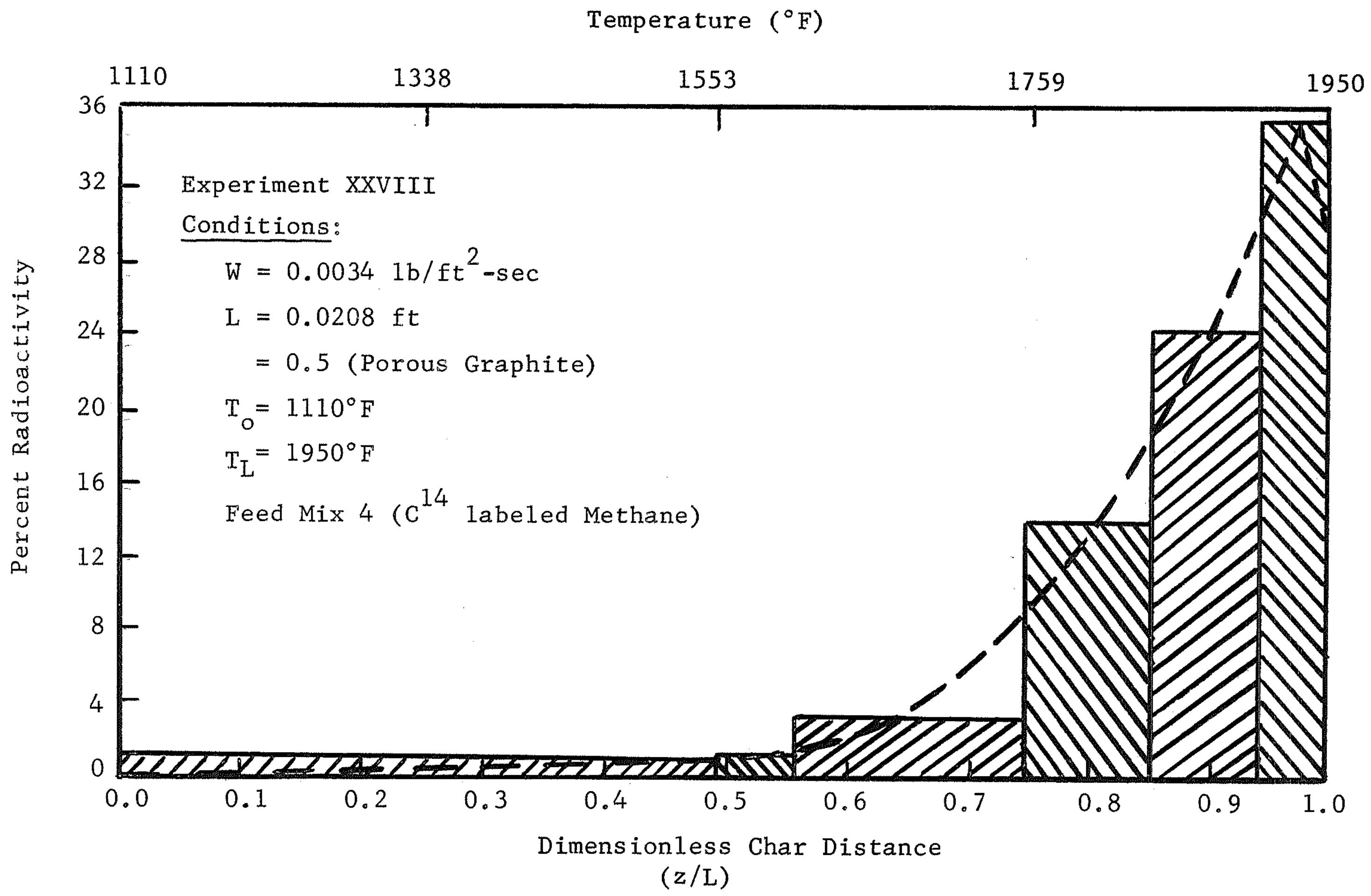

Figure 6-15. Carbon Deposition Profile for the Thermal Degradation of Methane, a Major Component in the Pyrolysis Gas Stream.

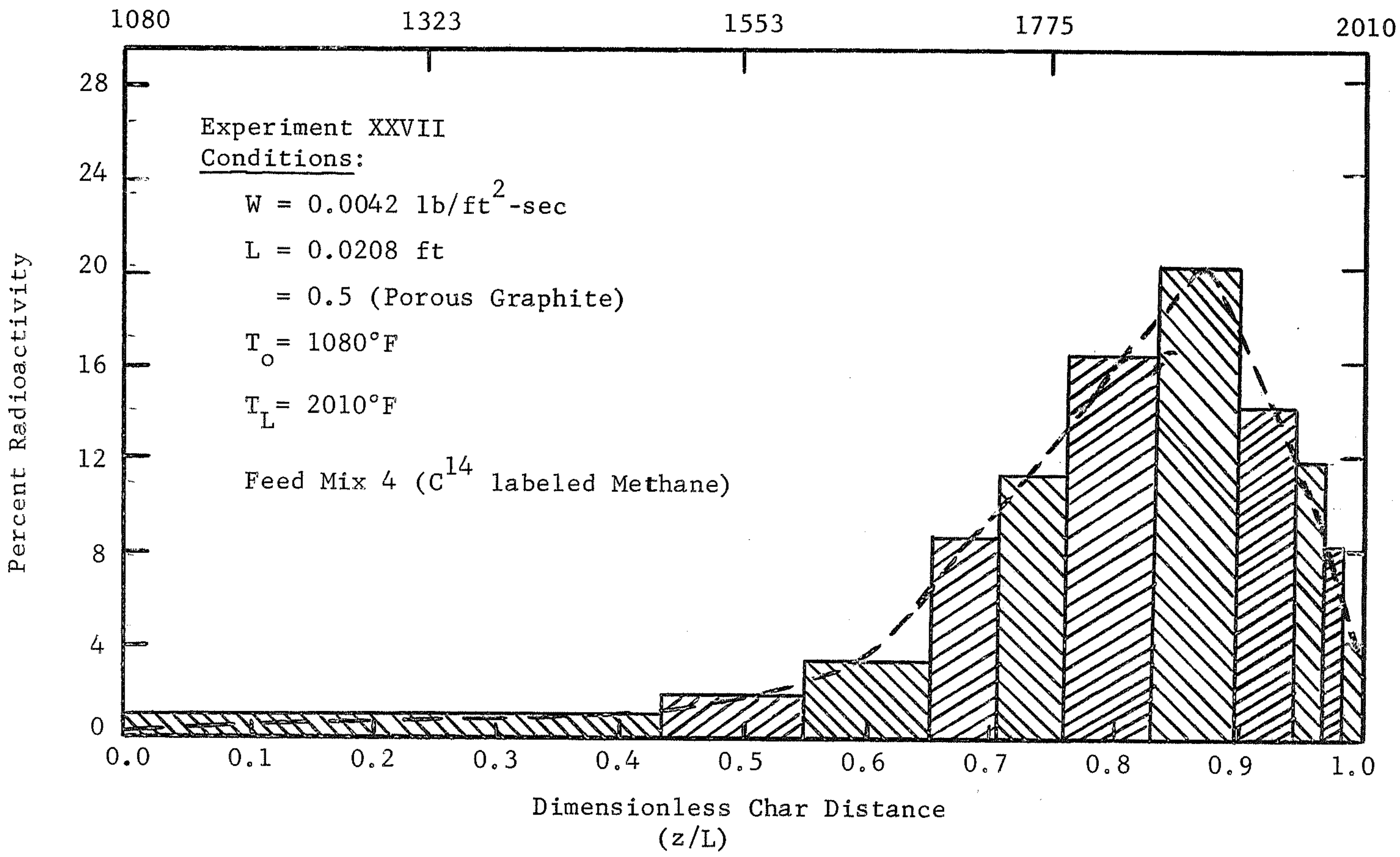

Figure 6-16. Carbon Deposition Profile for the Thermal Degradation of Methane Catalyzed by Bromine in a Concentration of 4% (by weight).

cracking of the pyrolysis products using heterogeneous catalyst is presented in the following section.

Heterogeneous Catalysis of the Pyrolysis Product Reactions Using a Tungsten-Molybdenum Co-Catalyst: A great deal of research into heterogeneous catalysts, their applications and activities has been reported in the literature (64,65,66,67). These catalyst are excellent hydrogenation accelerators for a number of hydrocarbons common to the petroleum and chemical industries. However, they are also susceptible to deactivation by reaction, adsorption or coating by several poisons. The two poisons which are present in the pyrolysis gases are carbon monoxide and coke (or carbon) formation. These two poisons are present in the char zone and must be considered when selecting possible heterogeneous catalysts. These poisons rule out the use of platinum, paladium, rhodium, nickel and selenium since these are all poisoned by carbon monoxide. In light of this discussion, tungsten, because of its relatively good activity in systems containing carbon monoxide, and molybdenum, because of its high selectivity in the thermal degradation of hydrocarbons, were selected as co-catalysts.

The method used to disperse these metals on the graphite specimens was the standard procedure to prepair heterogeneous catalysts and is as follows. First, the metals were obtained as metal acids (anhydrous) and added to hot (80°C) sulfuric acid.

Molybdenum was completely dissolved while tungsten formed a saturated solution. The graphite specimens were placed in the hot solution and stirred vigorously for thirty minutes. The second phase of the procedure involved the passing of carbon disulfide vapors through the graphite to convert the metal oxides to sulfides which increases the catalytic activity of the metals. The specimens were then dried at 110°F and reweighed to determine the weight of catalyst dispersed within the pores. The catalyst concentration varied from 5 to 6 percent (by weight) of the co-catalyst (50:50). This is typical of the dispersed (metal) phase composition of heterogeneous catalysts.

The effect of this catalyst on the reactions of the pyrolysis products in the char zone is shown in Table 6-26. Although there are noticeable differences between the experimentally measured exit gas compositions and the computed values for the uncatalyzed case, they are not as pronounced as the results for bromine. This is better indicated by comparing the results of non-catalytic experiments (XXVIII-92 and XXIX-94) with the values obtained in the heterogeneous co-catalyst systems (XXXII-99 and XXXI-98). The exit gas compositions are shown in Table 6-27 for an average mass flux rate of 0.0048 lb/ft^2-sec and a front surface temperature range of 1860° to 1945°F. No detectible difference between the four experiments is determined. Similarly,

Table 6-26. Flow of Pyrolysis Gases Through Graphite. Effect of Molybdenum-Tungsten Co-catalyst on the Exit Gas Composition.

RUN NUMBER MASS FLUX FRONT TEMP BACK TEMP	FLOW MODEL	H_2 MOLE %	CH_4 MOLE %	CO MOLE %	CO_2 MOLE %	N_2 MOLE %	H_2O MOLE %	C_6H_6O MOLE %	C_2H_4 MOLE %	C_2H_2 MOLE %	CATALYST
XXXI-97	FROZEN	20.0	4.2	2.1	0.6	0.0	62.1	11.0	0.0	0.0	Molybdenum & Tungsten 5-6% by weight as sulfides
0.0064	EQUILIBRIUM	59.4	1.7	33.7	2.0	0.0	3.1	0.0	0.0	0.0	
1875°F	NON-EQUILIBRIUM	20.4	4.6	3.0	0.9	0.0	60.1	10.9	0.0	0.0	
850°F	EXPERIMENTAL	21.6	5.6	4.1	1.3	0.0	58.0	9.0	0.2	0.3	
XXXI-98	FROZEN	26.2	5.5	2.9	0.8	0.0	52.7	11.9	0.0	0.0	as above
0.0048	EQUILIBRIUM	62.6	1.4	33.1	1.0	0.0	1.9	0.0	0.0	0.0	
1945°F	NON-EQUILIBRIUM	28.4	6.5	6.9	1.5	0.0	45.2	11.4	0.0	0.2	
950°F	EXPERIMENTAL	29.2	11.1	8.7	3.6	0.0	38.0	8.8	0.3	0.3	
XXXII-99	FROZEN	25.4	5.4	2.8	0.8	0.0	53.9	11.7	0.0	0.0	as above
0.0049	EQUILIBRIUM	62.6	1.4	33.1	1.0	0.0	1.9	0.0	0.0	0.0	
1860°F	NON-EQUILIBRIUM	26.3	6.3	5.0	1.4	0.0	49.6	11.5	0.0	0.1	
840°F	EXPERIMENTAL	27.6	7.2	6.6	2.6	0.0	45.2	10.2	0.2	0.4	
XXXII-100	FROZEN	14.0	2.3	1.5	0.4	0.0	69.4	12.4	0.0	0.0	as above
0.0098	EQUILIBRIUM	62.6	1.4	33.1	1.0	0.0	1.9	0.0	0.0	0.0	
1920°F	NON-EQUILIBRIUM	15.2	2.4	2.8	0.6	0.0	66.8	12.2	0.0	0.0	
900°F	EXPERIMENTAL	16.6	3.2	3.7	0.8	0.0	64.0	10.8	0.4	0.5	

Table 6-27. Flow of Pyrolysis Products Through Porous Graphite. Comparison of the Exit Gas Composition for Molybdenum-Tungsten Catalysed and Non-Catalyst Experiments.

RUN NUMBER MASS FLUX FRONT TEMP BACK TEMP	FLOW MODEL	H_2 MOLE %	CH_4 MOLE %	CO MOLE %	CO_2 MOLE %	N_2 MOLE %	H_2O MOLE %	C_6H_6O MOLE %	C_2H_4 MOLE %	C_2H_2 MOLE %	CATALYST
XXVIII-92	FROZEN	27.5	5.3	3.1	1.0	0.0	52.5	10.6	0.0	0.0	no catalyst
0.0044	EQUILIBRIUM	62.5	1.2	33.9	0.8	0.0	1.6	0.0	0.0	0.0	
1920°F	NON-EQUILIBRIUM	29.3	7.7	8.0	2.5	0.0	42.2	10.1	0.0	0.2	
1100°F	EXPERIMENTAL	30.0	8.7	8.0	3.4	0.0	37.9	11.6	0.2	0.2	
XXIX-94	FROZEN	25.6	4.1	2.9	0.8	0.0	55.2	11.5	0.0	0.0	no catalyst
0.0050	EQUILIBRIUM	61.8	1.1	34.9	0.7	0.0	1.5	0.0	0.0	0.0	
1925°F	NON-EQUILIBRIUM	28.1	5.8	7.8	2.1	0.0	45.1	10.9	0.0	0.3	
920°F	EXPERIMENTAL	25.5	5.8	10.5	2.7	0.0	42.7	12.2	0.2	0.2	
XXXI-98	FROZEN	26.2	5.5	2.9	0.8	0.0	52.7	11.9	0.0	0.0	Molybdenum Tungsten 5-6% (wt) as sulfide
0.0048	EQUILIBRIUM	62.6	1.4	33.1	1.0	0.0	1.9	0.0	0.0	0.0	
1945°F	NON-EQUILIBRIUM	28.4	6.5	6.9	1.5	0.0	45.2	11.4	0.0	0.2	
950°F	EXPERIMENTAL	29.2	11.1	8.7	3.6	0.0	38.0	8.8	0.3	0.3	
XXXII-99	FROZEN	25.5	5.3	2.8	0.8	0.0	53.9	11.7	0.0	0.0	Molybdenum Tungsten 5-6% (wt) as sulfide
0.0049	EQUILIBRIUM	62.6	1.4	33.1	1.0	0.0	1.9	0.0	0.0	0.0	
1860°F	NON-EQUILIBRIUM	26.3	6.3	5.0	1.4	0.0	49.6	11.5	0.0	0.1	
840°F	EXPERIMENTAL	27.6	7.2	6.6	2.6	0.0	45.2	10.2	0.2	0.4	

a comparison of the carbon deposition profiles for carbon-14 labeled phenol (XXVIII and XXXII) and methane (XXIX and XXXI) show no substantial shift in the position of the maximum deposition or the location where carbon deposition begins. These are shown in Figures 6-17 through 6-20. A slight difference in behavior near the front surface is observed. However, this represents no substantial change from the non-catalytic behavior.

A series of experiments with a platinum catalyst dispersed on the graphite specimens was also conducted using phenol-water free pyrolysis gases having a relatively low carbon monoxide concentration. These studies showed no catalytic activity over a temperature range of 1370° to 1755°F. The results of these tests are summarized in Table 6-28. The flow remained frozen in each experiment studied.

Summary of the Catalytic Studies to Increase Reactions in the Char Zone

Results for adding bromine to the pyrolysis product stream as a homogeneous catalyst indicated increased chemical reactions within the char zone. This acceleration was shown by comparison of the exit gas composition from non-catalytic and catalytic experiments with the calculated exit gas composition based on the non-equilibrium (non-catalysed) flow model. Furthermore,

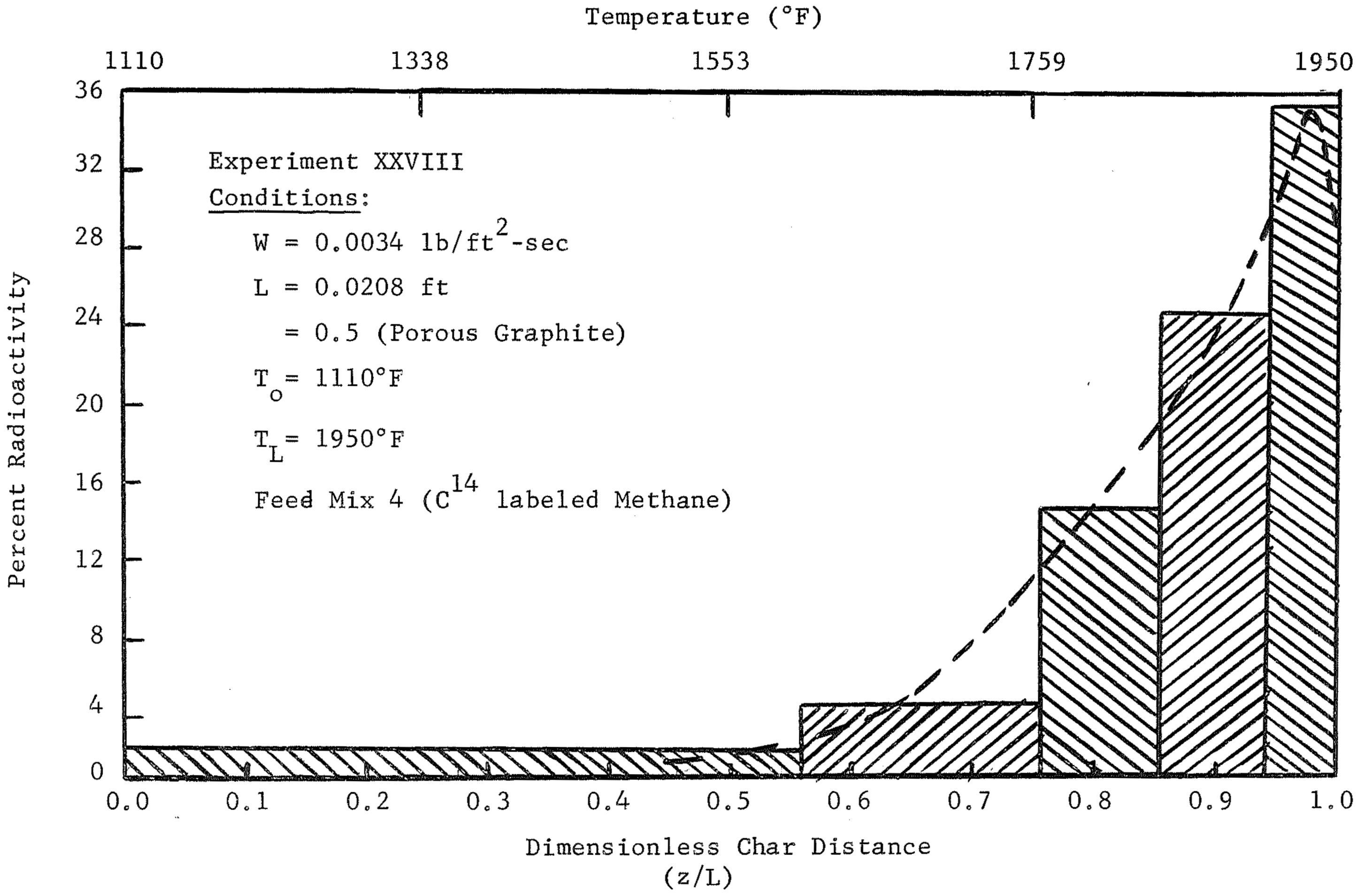

Figure 6-17. Carbon Deposition Profile for the Thermal Degradation of Methane, a Major Component in the Pyrolysis Gas Stream.

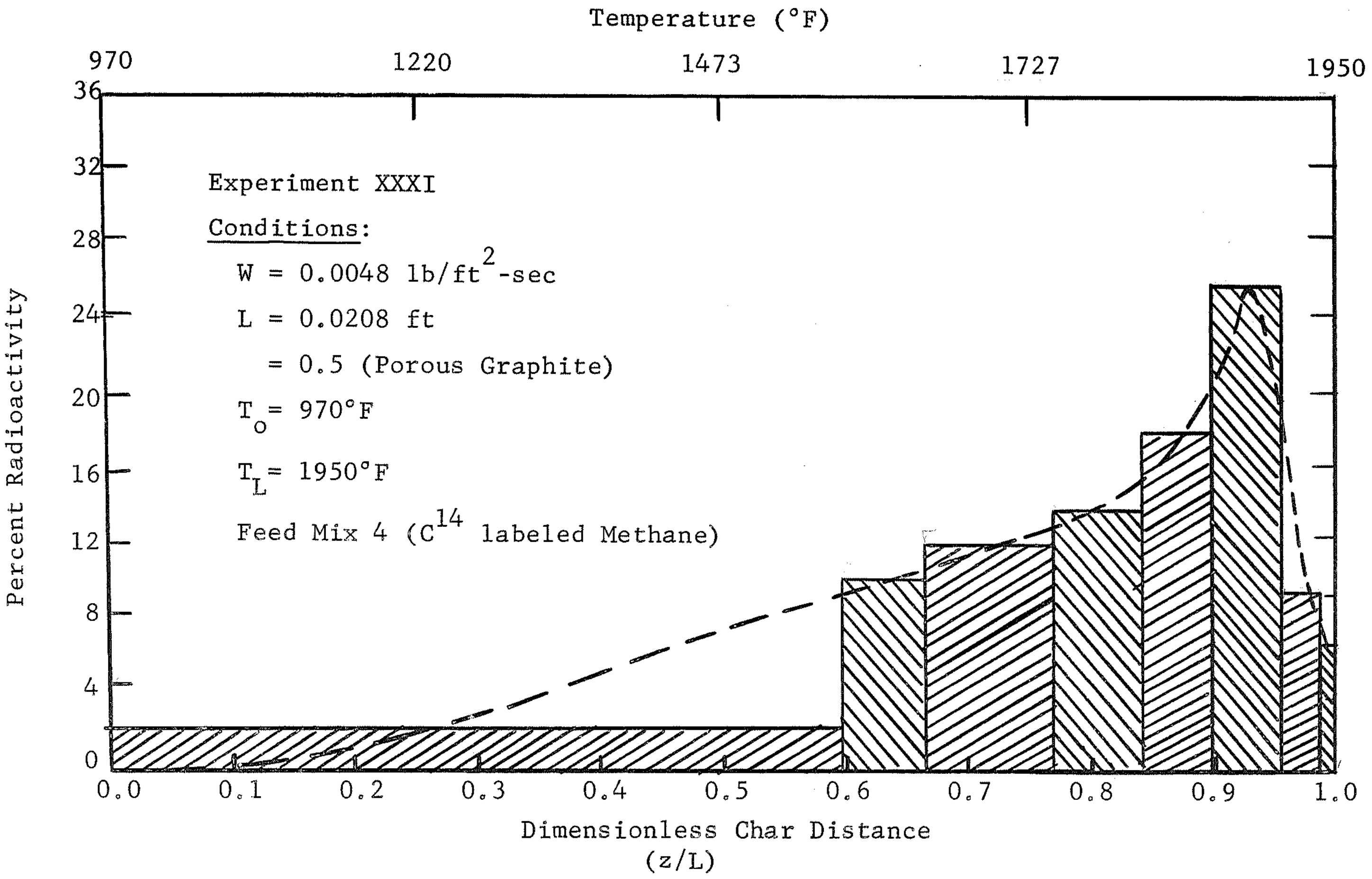

Figure 6-18. Carbon Deposition Profile for the Thermal Degradation of Methane Catalyzed with a Molybdenum-Tungsten Co-Catalyst Coating on the Graphite.

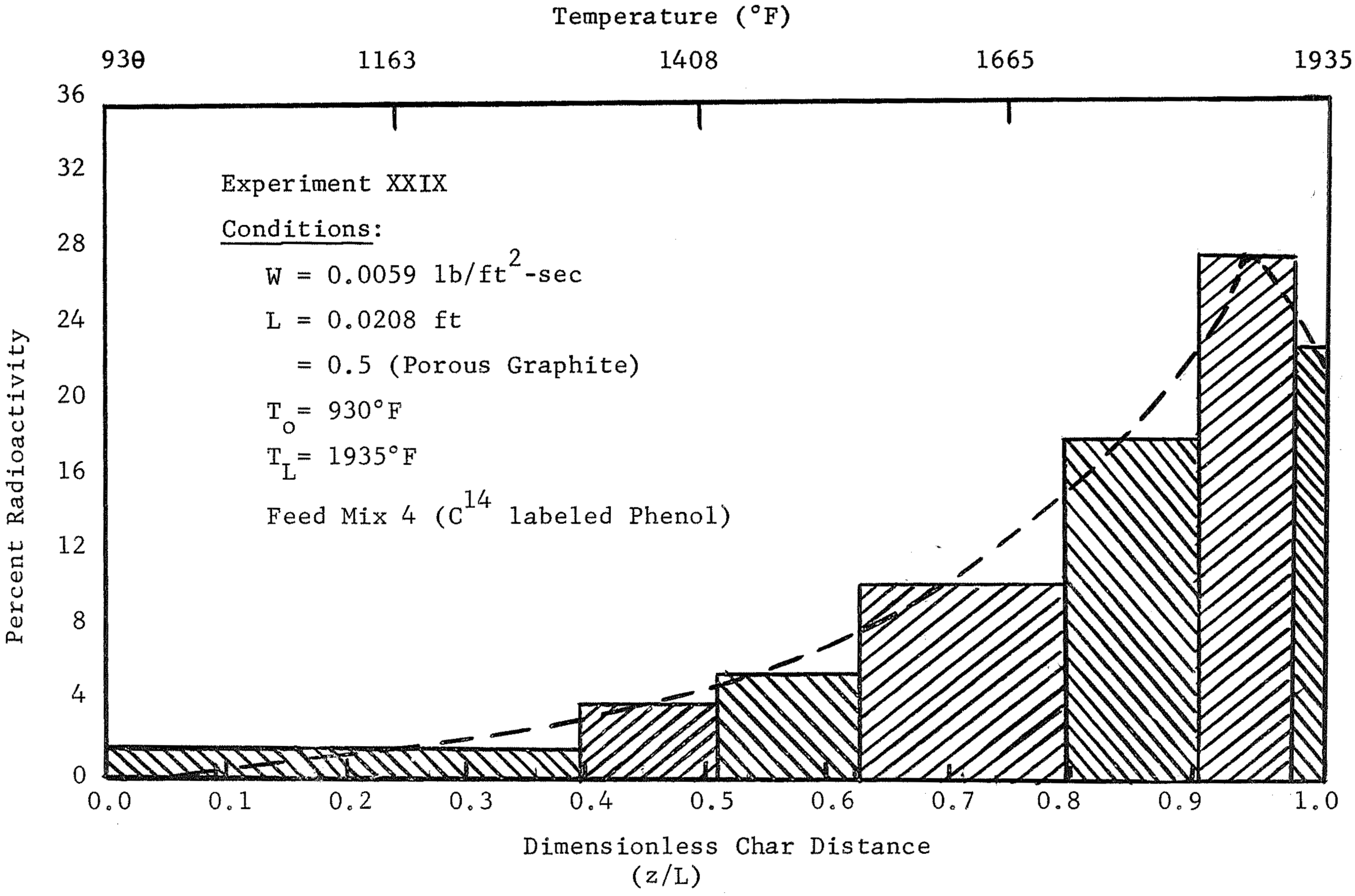

Figure 6-19. Carbon Deposition Profile for the Thermal Degradation of Phenol, a Major Component in the Pyrolysis Gas Stream.

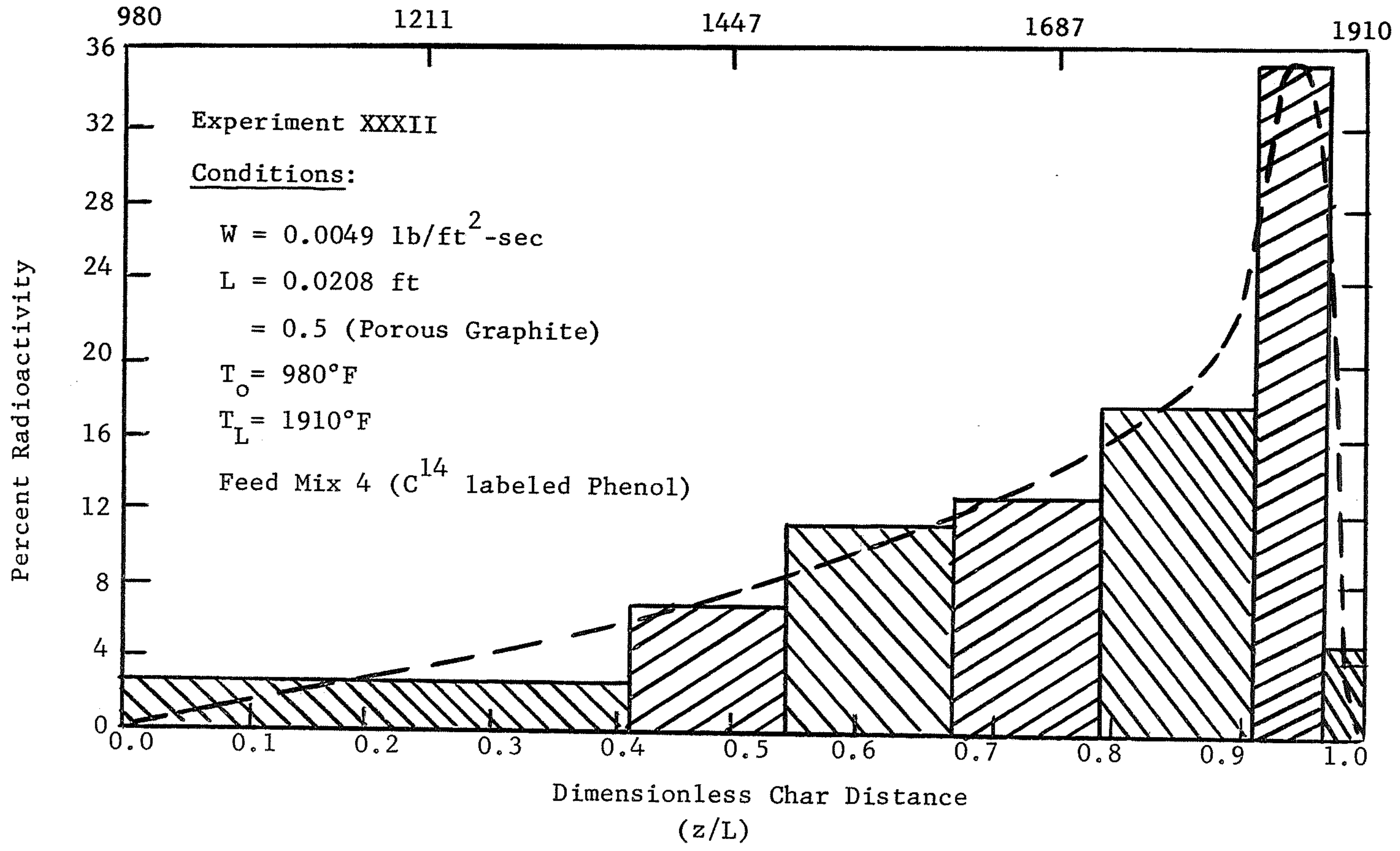

Figure 6-20. Carbon Deposition Profile for the Thermal Degradation of Phenol Catalyzed with a Molybdenum-Tungsten Co-Catalyst Coating on the Graphite.

Table 6-28. Flow of Pyrolysis Products Through Porous Graphite. Exit Gas Compositions of Platinum Catalysed Experiments.

RUN NUMBER MASS FLUX FRONT TEMP BACK TEMP	FLOW MODEL	H_2 MOLE %	CH_4 MOLE %	CO MOLE %	CO_2 MOLE %	N_2 MOLE %	H_2O MOLE %	C_6H_6O MOLE %	C_2H_4 MOLE %	C_2H_2 MOLE %	CATALYST
XIII-38	FROZEN	31.7	46.3	5.5	2.5	14.0	0.0	0.0	0.0	0.0	Platinum 5% (wt)
0.0009	EQUILIBRIUM	82.3	1.1	7.0	0.0	9.5	0.2	0.0	0.0	0.0	
1690°F	NON-EQUILIBRIUM	31.7	46.3	5.5	2.5	14.0	0.0	0.0	0.0	0.0	
1210°F	EXPERIMENTAL	32.6	41.3	8.9	5.2	14.0	0.0	0.0	0.0	0.0	
XIII-39	FROZEN	31.7	46.3	5.5	2.5	14.0	0.0	0.0	0.0	0.0	Platinum 5% (wt)
0.0039	EQUILIBRIUM	82.4	1.0	7.0	0.0	9.5	0.1	0.0	0.0	0.0	
1725°F	NON-EQUILIBRIUM	31.7	46.3	5.5	2.5	14.0	0.0	0.0	0.0	0.0	
1220°F	EXPERIMENTAL	30.8	45.8	6.0	4.4	14.0	0.0	0.0	0.0	0.0	
VIII-22	FROZEN	35.0	43.7	4.9	2.9	13.6	0.0	0.0	0.0	0.0	Platinum 5% (wt)
0.0038	EQUILIBRIUM	79.8	3.0	6.7	0.1	9.6	0.7	0.0	0.0	0.0	
1470°F	NON-EQUILIBRIUM	35.0	43.7	4.9	2.9	13.6	0.0	0.0	0.0	0.0	
739°F	EXPERIMENTAL	36.2	41.4	5.2	4.2	13.0	0.0	0.0	0.0	0.0	

carbon deposition profiles were used to locate the position and temperature where deposition resulting from methane and phenol thermal degradation occurred.

The use of bromine (or HBr) as a representative homogeneous catalyst made a detailed investigation unnecessary because of the relative activity of various halides to hydrogen bromide in Table 6-23. By comparison, iodine and organic iodides should have a greater influence on the pyrolysis product reactions, while chlorine or the organic chlorides should have a lesser influence.

No detectable change in the exit product composition, and, therefore, in the rates of chemical reaction of the pyrolysis products, were observed for tungsten and molybdenum co-catalysts and platinum over a temperature range of 1845° to 2300°F.

Oxidative Degradation of Low Density Nylon-Phenolic Resin Chars in an Air Stream at Elevated Temperatures

The oxidative degradation of low density nylon-phenolic resin chars is important in reentry applications as a result of the hot, shock heated air streams flowing adjacent to the char front surface. It is believed that a portion of this air stream penetrates the char front surface forming large cavities and irregular shaped, erroded areas on the surface of the heat shield during reentry or in models tested in arc jets.

In order to determine the extent of air oxidation, experiments were made in the Char Zone Thermal Environment Simulator in which air, at rates corresponding to reentry values, was injected into the char at the front surface. These experiments simulated a maximum air mass flux, because there is pyrolysis gas flow counter to the air during ablation.

To determine whether air reacted at the surface or in depth, samples of the exit gas stream were taken at short intervals to determine the oxygen conversion within the char. The result of these analyses for two separate experiments are shown in Figure 6-21. At an air mass flux of 0.0057 lb/ft^2-sec and a front surface temperature of 1485°F. The maximum conversion of oxygen at the back surface was 53% corresponding to an oxygen concentration of 10 mole percent leaving the back surface. A back surface temperature of 747°F was measured for the 1/8 inch thick char. Increasing the air flow rate to 0.035 lb/ft^2-sec and a front surface temperature of 2047°F, increased the maximum conversion at the rear surface to 81% or a concentration of four percent leaving the char back surface. The back surface temperature was measured at 304°F. The char thickness was 1/4 inch. The relatively low back surface temperatures indicate that the highly exothermic reaction probably occurs near the front surface. Although oxygen conversion at the back surface was never complete indicating the

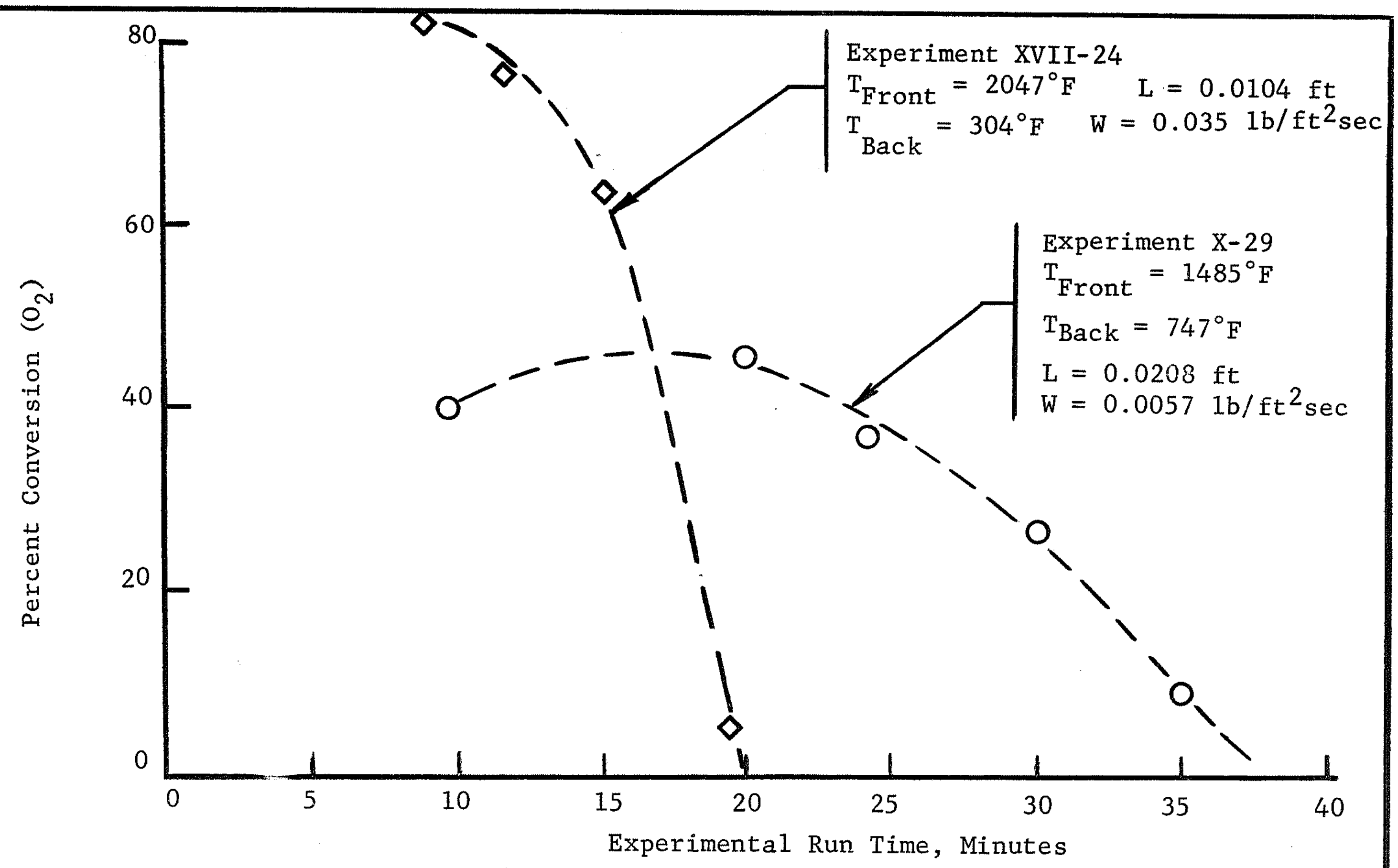

Figure 6-21. Conversion of Oxygen as a Function of Experimental Run Time for the Air Oxidation of Porous Graphite at High Temperatures.

presence of oxygen within the pores at all char depths, the extent of oxidation in depth appears small in comparison to the surface oxidation. A photograph of the front surface after 11 minutes exposure to an air mass flux of 0.035 lb/ft^2-sec and a temperature of 2047°F (Experiment XVII) is shown in Figure 6-22. The three large erroded areas indicate strong surface attack. The rounded edges near the errosions further support the concept that oxidation occurs where there is the least resistance to flow. The time for these holes to be formed can be estimated by comparing the length of time necessary to obtain near zero oxygen conversion at the back surface in Figure 6-21.

In addition to the experimental data, a modification to the isothermal analysis (Appendix F) was made by considering temperatures within the char to vary linearly with char distance. This approximation premits the calculation of the oxygen conversion for a given char depth (residence time) and front surface temperature. A comparison of the calculated and measured maximum conversions is shown in Table 6-29. The conversion of oxygen with char depth is also presented in Figure 6-23 for the linear approximation of the temperature and also the isothermal evaluations at the front and back surface temperatures. The data used to describe the air oxidation of graphite is presented in Table 6-29. Agreement of the calculated and experiment conversions at the back surface is within the experimental

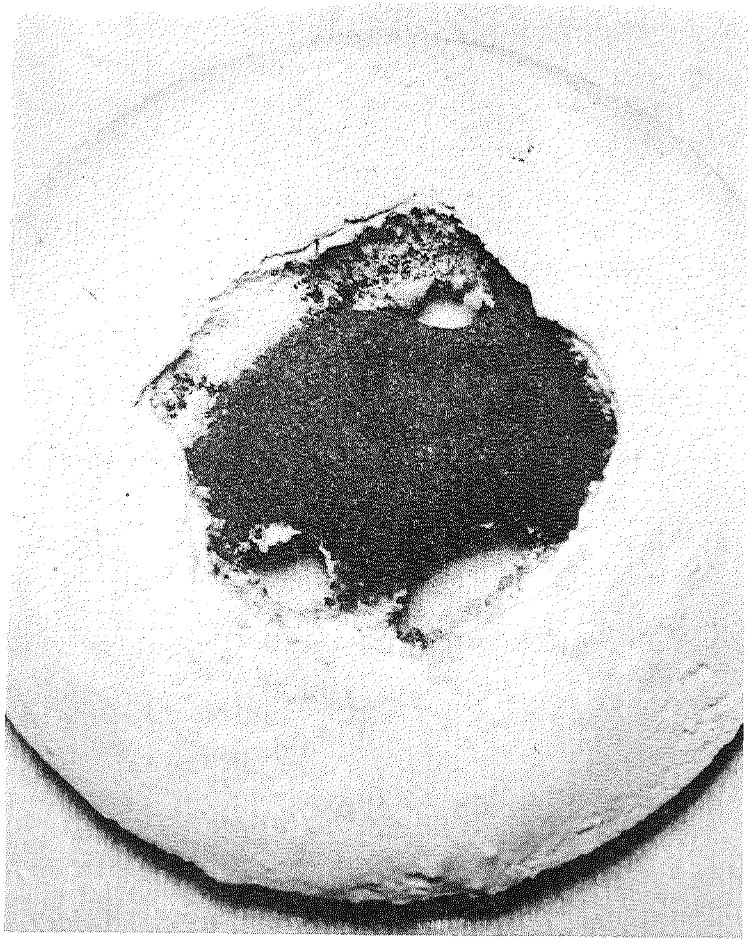

Experiment XVII

Low Density Nylon-
Phenolic Resin Char

LEGEND

① Ceramic Mounting Ring

② Erroded Areas

③ Ash Deposites

Figure 6-22. Photograph of the Char Front Surface after Eleven Minutes Exposure to Air Flowing at a Mass Flux of 0.035 lb/ft^2-sec and a Temperature of 2047°F.

Photo By J. R. Langley

Table 6-29. Air Oxidation of Low Density Nylon-Phenolic Resin Chars. A Detailed Comparison of the Calculated and Measured Oxygen Conversion at the Char Back Surface (Exit Surface).

Experiment Number:	X-29	XVII-54
Conditions:		
Mass Flux, lb/ft^2-sec	0.0057	0.0350
Front Temperature, °F	1485°F	2047°F
Back Temperature, °F	747°F	304°F
Char Thickness, ft	0.0104	0.0208
Experiment Run Time, Min.	35	25
Measured Maximum Conversion: (%)	43	83
Calculated Maximum Conversion:		
(1) at the Front Temperature	96	100
(2) at the Back Temperature	8	22
(3) at a Temperature which varied linearly with char depth	45	86
(4) at the Average Temperature	41	81

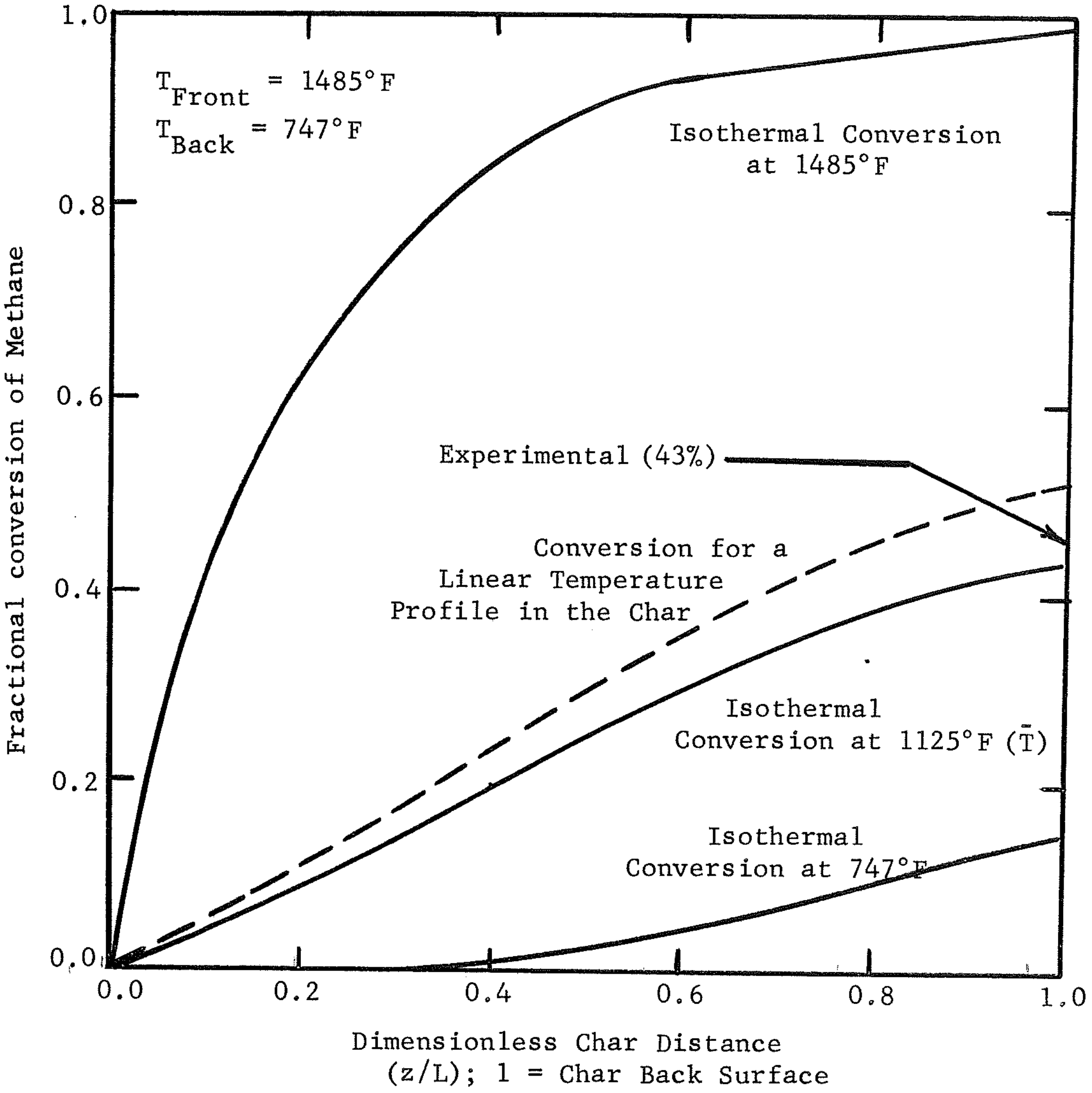

Figure 6-23. Conversion of Oxygen for the Flow of Air Through a Low Density Nylon-Phenolic Resin Char at a Mass Flux of 0.035 lb/ft^2-sec and a Temperature of 1485°F.

accuracy of the analyses. Values of 30Kcal/mole for the activation energy and 1 x 10^{17} sec^{-1} were used for the first order air oxidation of carbon. Energies of activation between 8 and 43 Kcal/mole, frequency factor between 10^{16} and 10^{18} and reaction orders of zero, one half and one are reported in the literature (42).

REFERENCES

1. Nelson, James B., "Determination of Kinetic Parameters of Six Ablation Polymers by Thermogravimetric Analysis", NASA TN D-3919 (April 1967).

2. Sykes, G. F., Private Communication to R. W. Pike (March 14, 1968).

3. Sykes, George F., Jr., "Decomposition Characteristics of a Char-Forming Phenolic Polymer Used for Ablative Composites," NASA TN D-3810 (February 1967).

4. Freidman, H. L., "Pyrolysis of Plastics in a High Vacuum Arc Image Furnace," Journal of Applied Polymer Science, 9, 1005 (1965).

5. Ladacki, Michael, Janet V. Hamilton and Samuel N. Cohz, "Heat of Pyrolysis of Resin in Silica-Phenolic Ablator," AIAA Journal, 4 (10), 1798 (October 1966).

6. Kratsch, K. M., L. F. Hearne and H. R. McChesney, "Thermal Performance of Heat Shield Composites During Planetary Entry," AIAA-NASA National Meeting, Palo Alto, California, 3, (September 30-October 1, 1963).

7. Scala, S. M. and L. M. Gilbert, "Thermal Degradation of a Char-Forming Plastic During Hypersonic Flight," ARS Journal, 32 (6), 917-24 (June 1962).

8. Shulman, G. P., and H. W. Lochte, "Thermal Degradation of Polymers. II. Mass Spectrometric Thermal Analysis of Phenol-Formaldehyde Polycondensates," Journal of Applied Polymer Science, 10, 619-635 (1966).

9. Beecher, Norman, and Ronald E. Rosensweig, "Ablation Mechanisms in Plastics with Inorganic Reinforcement," ARS Journal, 31, 532-538 (1961).

10. del Valle, E. G., R. W. Pike and G. C. April, "Transport Phenomena in the Char Zone During Ablation. II: Equilibrium Composition of Degradation Products of Ablation," Paper 13e, 63rd National Meeting of the A.I.Ch.E., Salt Lake City, Utah (May 1967).

11. April, Gary C., E. G. del Valle, Simon Hacker and R. W. Pike, "Comparison of Methods for Determining the Composition of Pyrolysis Products from the Degradation of Nylon-Phenolic Resin Ablative Composites," NASA-RFL-9, Louisiana State University, Baton Rouge, Louisiana (March 1969).

12. Perry, John H., ed., Chemical Engineers' Handbook, 3rd ed., New York: McGraw-Hill, 1950, pp. 236-243.

13. Palmer, H. B.; and Hirt, T. J.: "Thermal Decomposition Kinetics of Carbon Suboxide," J. Am. Chem. Soc., 84, 113-4 (Jan. 1962).

14. Kozlov, G. I.; and Knorre, V. G.: "Single Pulse Shock Tube Studies on the Kinetics of the Thermal Decomposition of Methane," Combustion and Flame, 6, 253-263 (Dec. 1962).

15. Hirt, T. J.; and Palmer, H. B.: "Kinetics of Deposition of Pyrolytic Carbon Films From Methane and Carbon Suboxide," Carbon, 1, 65-70 (1963).

16. Kozlov, G. I.; and Knorre, V. G. : "Kinetics of Thermal Decomposition of Methane by the Single-Pulse Shock Tube Method," Russian Jour. Phys. Chem., 37 (9), 1128-1130 (Sept. 1963).

17. Bradley, J. N.: Shock Waves in Chemistry and Physics, John Wiley, Inc., New York (1962).

18. Thon, N., ed.: Table of Chemical Kinetics Homogeneous Reactions, N.B.S. Circular 510 (Sept. 1958), Supplement 1 (Nov. 1956); N.B.S. Monograph 34, vol. 1 (Sept 1961), vol. 2 (July 1954).

19. Palmer, H. B.; and Hirt, T. J.: "The Activation Energy For the Pyrolysis of Methane," Journal Phys. Chem., 67 (3), 709-711 (March 1963).

20. Bartlit, J. R.; and Bliss, H.: "Kinetics of Ethane Pyrolysis," A.I.Ch.E. Journal, 11 (3), 562-572 (May 1965).

21. Quinn, C. P.: "The Thermal Dissociation amd Pyrolysis of Ethane," Proc. Roy. Soc., 275 1361 (Sept. 1963).

22. Cummings, G. A. McD.; Hall, A. R.; and Straker, R. A. M.: "Decomposition Flame of Acetylene and Methyl Acetylene," Eighth Int. Symp. on Combustion, Williams and Wilkins Co., Baltimore, 503-510 (1962).

23. Blair, J. D.; and Seschske, A.: "Graphite-Hydrogen Methane Kinetics Above 1600° K," A.E.C. Contract W-7405 ENG 36, LASL2896 (May 1962).

24. Hedden, K., Proceedings of the Fifth Conference on Carbon, Macmillan Co., New York, 125-31 (1962).

25. Gulbrasen, E. A.; Andrews, K. F.; and Brassert, F. A.: "The Reaction of Hydrogen With Graphite at 1200° to 1650°C," Jour. Electrochem. Soc., 112 (1), 49-52 (Jan. 1965).

26. King, A. B.; and Wise, H.: "Reaction Kinetics of Hydrogen Atoms With Carbon Films," Jour. Phys. Che., 67 (6), 1163-9 (June 1963).

27. Steacie, E. W. R., and Shane, Gerald, "The Kinetics of the Decomposition Reactions of the Lower Paraffins," Canadian Journal of Research, 18, 203-16 (1940).

28. Happel, John, and Kramer, Leonard, "Acetylene and Hydrogen from the Pyrolysis of Methane," Industrial and Engineering Chemistry, 59, 39-50 (Jan. 1967).

29. Chase, J. D., and Weinberg, F. J., "The Acetylene Decomposition Flame and the Deduction of Reaction Mechanism from 'Global' Flame Kinetics," Proc. Roy. Soc. A., 275, 411-429 (April 1963).

30. Breisacher, P., and Marx, P. C., "The Hydrogen-Graphite Reaction Between 360° and 800°," Jour. Am. Chem. Soc., 85, 3518-9 (Nov. 1963).

31. Carney, N. S., and R. B. Thomas, "Reactor of Carbon and Graphite Below 950° C.," British Report AERLE-C/R 2502 (June 1958).

32. King, Bruce A., and Henry Wise, "Reaction Kinetics of Hydrogen Atoms with Carbon Films," The Journal of Physical Chemistry, 67 (6), 1163-70 (June 1963).

33. Hou, K. C., and Palmer, H. B., "The Kinetics of Thermal Decomposition of Benzene in a Flow System," Jour. Phys. Chem., 69 (3), (March 1965).

34. Slysh, R. S., and C. R. Kinney, "Some Kinetics of the Carbonization of Benzene, Acetylene and Diacetylene at 1200°," The Journal of Physical Chemistry, 65, (June 1961).

35. Scott, G. S., "Mechanism of the Steam-Carbon Reaction," Industrial and Engineering Chemistry, 33, 1279-84 (1941).

36. Lewis, W. K., E. R. Gilliland, and Howard Hipkine, "Carbon-Steam Reaction at Low Temperatures," Industrial and Engineering Chemistry, 45, 1697-1703 (August 1953).

37. Haslam, R. T., F. L. Hitchcock, and E. W. Rudow, "The Water-Gas Reactions," Industrial and Engineering Chemistry, 15, 115-121 (February 1923).

38. Thiele, E. W., and R. T. Haslam, "Mechanism of the Steam-Carbon Reactions," Industrial and Engineering Chemistry, 19, 882-7 (August 1927).

39. Mayers, Martin A., "The Rate of Oxidation of Graphite by Steam," Journal of the American Chemical Society, 56, 1879-1884 (September 1934).

40. Warner, B. R., "Mechanism of the Steam-Carbon Reaction," Journal of the American Chemical Society, 60, 1447 (Aug. 1943).

41. Walker, P. L., Jr., Chemistry and Physics of Carbon, Volume 1, Marcel-Dekker, Inc., New York, 203-64 (1965).

42. Walker, P. L., Jr., F. Rusinko, Jr., and L. G. Austin, Gas Reactions of Carbon, Advances in Catalysis, 11, Academic Press, Inc., New York (1959).

43. Johnstone, H. F., C. Y. Chen, and Donald S. Scott, "Kinetics of the Steam-Carbon Reaction in Porous Graphite Tubes," Industrial and Engineering Chemistry, Volume 44, No. 7, 1564-69 (July 1952).

44. Binford, Jesse S., Jr., and Henry Eyring, "Kinetics of the Steam-Carbon Reaction," Journal of the American Chemical Society, 60, 486-491 (April 1956).

45. Austin, L. G., and P. L. Walker, Jr., "Effect of Carbon Monoxide in Causing Nonuniform Gasification of Graphite by Carbon Dioxide," A.I.Ch.E. Journal, 9 (3), 303-6 (May 1963).

46. Glovina, E. S., and G. P. Khaustovich, "The Interaction of Carbon with Carbon Dioxide and Oxygen at Temperatures Up to 3000°K," Eighth Int. Symp. on Combustion, Williams and Wilkins Co., Baltimore (1962).

47. Walker, P. L. Jr., Chemistry and Physics of Carbon, Volume 4, Marcel Dekker, Inc., New York, 287-383 (1965).

48. Maak, Robert O., "High Temperature Gas Reactions," MIT Office of Ordinance Research, Contract DA-19-020-ORD-4268 (June 1961).

49. Berkman, Sophia, J. C. Morrell and Gustov Egloff, Catalysis: Inorganic and Organic, Reinhold Publishing Co., New York, 572 (1940).

50. Carleton, Ellis, Hydrogenation of Organic Substances, 3rd Edition, D. Van Nostrand Co., Inc., New York (1930).

51. Augustine, R. L., Catalytic Hydrogenation, Marcel Dekker, Inc., New York (1965).

52. Sabatier, E. N. and J. H. Reid, Catalysis in Organic Chemistry, D. Van Nostrand Co., Inc., New York, 216 (1922).

53. Diwoky, F. F. and Homer Adkins, "Competitive Hydrogenation," *Journal of the American Chemical Society*, *53*, 1868 (1931).

54. Adkins, Homer and H. I. Cramer, "The Use of Nickel as a Catalyst for Hydrogenation," *Journal of the American Chemical Society*, *52*, 4349 (1930).

55. del Valle, E. G., R. W. Pike and G. C. April, "Modeling for a Set of Complex Chemical Reactions at High Temperatures," Sixty-First Annual Meeting (A.I.Ch.E.), Preprint 8F, Los Angeles, Calif. (1968).

56. Swann, R. T., Claud Pittman and J. C. Smith, "One Dimensional Numerical Analysis of the Transient Response of Thermal Protection Systems," NASA TN D-2976 (September 1965).

57. Benson, Sidney W., *Thermochemical Kinetics*, John Wiley and Sons, Inc., New York, 60 (1968).

58. Beekman, *op.cit.*, 166.

59. Laidler, K. J., *Chemical Kinetics*, 2nd Ed., McGraw Hill Book Co., New York, 484 (1965).

60. Kondrat'ev, V. N., *Chemical Kinetics of Gas Reactions*, Pergamon Press, New York, 36 (1964).

61. Laidler, *op.cit.*, 444.

62. Emmett, P. E., *Catalysis*, Reinhold Publishing Corp., Baltimore, Maryland, *5*, 388 (1957).

63. Minkoff, G. J. and C. F. H. Tipper, Chemistry of Combustion Reactions, Butterworths Publishing Co., Ltd., London, 249 (1962).

64. Emmett, op.cit., 5, 184.

65. Emmett, op.cit., 6, 427.

66. Emmett, op.cit., 6, 407.

67. Harrison, D. P. and H. F. Rase,"Nylon-Platinum Catalysts with Unusual Geometric and Selective Characteristics," Industrial and Engineering Chemistry - Fundamentals, 6 (2), 161 (May 1967).

68. Emmett, op.cit., 5, 217.

69. Emmett, op.cit., 6, 486.

70. Emmett, op.cit., 5, 98.

71. Schwab, Georg-Maria, H. S, Taylor and R. Spence, Catalysis, D. Van Nostrand Co., New York, 26-27 (1937).

72. Simons, J. H., Fluorine Chemistry, Volume V, Academic Press, New York, 2,78 (1964).

73. Laidler, op.cit., 8.

74. Jolles, Z. E., ed., Bromine and Its Compounds, Academic Press New York, 74, 102-3 (1966).

75. Schwab, op.cit., 58.

VII. CONCLUSIONS

Based on the experimental and theoretical results of this research the following conclusions are drawn:

Reacting Flow of Pyrolysis Products in the Char Zone

1. The reacting flow of pyrolysis products from nylon-phenolic resin composites in the char zone is accurately described by a non-equilibrium model employing reaction kinetic data of the important reactions occurring in the system. For the simulated pyrolysis product compositions in Table 6-5, mass flux values between 0.00003 - 0.10 lb/ft^2-sec and a front surface temperature range of 1350 - 2300°F, the reactions and associated kinetic data in Table 6-6 accurately describe the energy transfer in the char zone. These reactions are valid up to 3000°F. Above this temperature, additional reactions must be considered to accurately describe the reacting flow system.

2. Under conditions of high mass fluxes (> 0.01 lb/ft^2-sec) and/or low temperatures (< 2000°F), the flow of pyrolysis products is essentially frozen. These conditions define the upper limitation of the frozen flow model.

3. The equilibrium flow model erroneously predicts the behavior in the char for all conditions except those in which the mass flux rate is smaller than 0.0001 lb/ft^2-sec. Mass flux rates greater than this value require the use of a non-

equilibrium flow analysis to describe reactions occurring at finite rates.

Reacting Flow of Pyrolysis Products Through Porous Graphite

1. The same results are obtained for the reacting flow of pyrolysis products in porous graphite. The same important reactions and kinetic data that applied to the low density nylon-phenolic resin chars, likewise apply to the graphite between 1350 - 2300°F and 0.00003 - 0.10 lb/ft^2-sec. This permits the substitution of graphite for the brittle chars in studies requiring post-experimental analyses of the porous media; i.e., carbon deposition studies.

2. In order to compare the results from char and graphite experiments, the mass flux in the pores must be identical. This corrects for differences in the porosity of each material.

3. The inclusion of graphite "fines" in the pore spaces, during the fabrication procedure, results in reactions with hydrogen forming methane. Purging the graphite with helium or nitrogen prior to an experiment is sufficient to remove these dust-like particles from the pore spaces and eliminate the methane formed from this more reactive form of graphite.

Carbon Deposition Studies

1. The use of radioactive tracers is a very effective

method of determining the extent of carbon deposition within the char from the cracking of the pyrolysis gases. A plot of the percent radioactivity as a function of char depth very graphically determines the position where deposition starts, ends and is maximum.

2. Carbon is deposited as a result of the thermal degradation of methane and phenol. Deposition starts near the middle of the char ($z/L = 0.5$) where the temperature is 1400°F and increases uniformly to a maximum value near the front surface at a temperature of 1900 °F.

<u>Degradation Product Distribution</u>

1. The products of methane degradation were determined by comparing radioactive tracer concentration profiles with the gas chromatograms of the exit gases leaving the Char Zone Thermal Environment Simulator. The species identified were carbon monoxide, carbon dioxide, ethylene, acetylene and unreacted methane.

2. Similarly, the products of phenol degradation were determined. The species were identified as methane, carbon monoxide, carbon dioxide and unreacted phenol.

3. The above methods provided excellent supporting evidence that the reactions considered important in the mathematical model were correct.

Catalysts Evaluation Studies

1. The effect of adding homogeneous catalysts (such as bromine) to the pyrolysis product stream to accelerate chemical reactions and, therefore, the heat absorption in the system was determined. Bromine (and the organic halides and other halogens) produced a catalytic effect which reduced the temperature at which carbon deposition starts from 1400°F to 1200°F. The position of maximum deposition was likewise shifted 300°F. A sharp decline in the carbon deposition probably indicated rapid depletion of carbon by reactions with water and/or carbon dioxide.

The product concentrations of the exit gas stream is likewise different from the non-catalytic experiments and not predicted by the non-catalytic kinetic data.

2. Molybdenum and tungsten heterogeneous catalysts did not affect a measurable change in the behavior of the system. A slight shift in the carbon deposition profiles were observed; however, the results were outside the experimental accuracy of the analytical equipment. Platinum was used in earlier studies and, likewise, failed to produce a change.

Air Oxidation Studies

The effect of injecting air into low density nylon-phenolic resin chars at the front surface is rapid errosion near the edge regions of the chars. These experiments were conducted by passing air into the char from the front surface with no counter flow of pyrolysis products from the rear. The experimental results were bracketed by the isothermal analysis and values calculated using a linear description of the temperature profile within the char.

NOMENCLATURE

Symbol	Description	Units
A	area	L^2
	species identification in a general expression for a reaction	none
	Runge-Kutta parameter in the energy equation numerical solution method	T
	ratio of system parameter defined in equation (2-13)	none
a	formula number for chemical compounds	none
	coefficients in the polynomial defined in equation (2-28)	none
B	Runge-Kutta parameter in the species continuity numerical solution method	M/L^2t
	ratio of system parameter defined in equation (2-14)	none
b	mass of a chemical element	M
	coefficients in the polynomial defined in equation (2-29)	none
C	ratio of the fluid to matrix thermal conductivity	none
	molar concentration defined in equation (2-38)	$mole/L^3$
C_p	heat capacity of a pure component at constant pressure	L^2/t^2T
$\bar{C}_p$	heat capacity of a mixture at constant pressure	L^2/t^2T

Symbol	Description	Units
c	total number of atoms of a chemical element in the system defined by equation (3-41)	none
	coefficients in the polynomial defined in equation (2-35)	none
D	substantial derivative	none
	mass diffusivity	L^2/t
E	energy of activation	ML^2/t^2-mole
F	free energy	ML^2/t^2
F°	free energy at a standard state of 298°K and 1 atom	ML^2/t^2
f	free energy function defined in equations (3-31) and (3-33)	ML^2/t^2
	any mathematical function	none
G	augmented function of the quadratic approximation to the free energy function defined in equation (3-37)	ML^2/t^2
g	force of gravity	L/t^2
H	enthalpy	ML^2/t^2
H°	enthalpy at a standard state of 298°K and 1 atom	ML^2/t^2
h	heat transfer coefficient in equation (2-3)	M/t^3t
	numerical integration increment sizes	none

Symbol	Description	Units
J	molar flux	moles/tL^2
j	mass flux	M/tL^2
K	total number of gas species in the system	none
k	thermal conductivity	ML/t^3T
	reaction rate constant	*function of reaction order.
k°	frequency factor	
L	char thickness	L
M	mobility of a porous matrix defined in equation (2-84)	none
M_w	molecular weight	M/moles
m	total number of chemical reactions in the system	none
N	molar flux of species in the char zone	mole/tL^2
n	moles of species	moles
$\bar{n}$	mole fraction of species	none
P	pressure	M/Lt^2
p	stoichiometric coefficient of the products in a chemical reaction	none
p'	power on the concentration terms for products in a chemical reaction	none
Q	volumetric flow rate	L^3/t
	quadratic approximation of the free energy function (3-36)	ML^2/t^2
q'''	heat generation by chemical reaction	M/t^3

Symbol	Description	Units
q	number of gas plus solid (condensed) phases in the system	none
	energy transfer by conduction, convection or radiation	M/t^3
R	ideal gas constant	ML^2/t^2T mole
	chemical reaction rate	$mole/tL^3$
$\bar{R}$	effective chemical reaction rate for gas and solid species defined in equation (3-21)	$mole/tL^3$
R_e	Reynold's number	none
R_o	dimensionless mole flux defined in equation (2-43)	none
r	chemical reaction rate of a chemical species	$mole/tL^3$
	stoichiometric coefficient of the reactants in a chemical reaction	none
	radius of a cylindrical graphite test section included in equation (2-83)	L
r'	power on the concentration terms for reactants in a chemical reaction	none
s	power on the temperature in the rate equation (3-52)	none
T	temperature	T
T'	temperature gradient	T/L
t	time	t
$\bar{u}$	ratio of the actual to estimated mole fraction in the free energy minimization calculation (3-42)	none
V	volume	L^3

Symbol	Description	Units
v	velocity	L/t
W	mass flux based on the superficial velocity	M/L^2t
W_p	mass flux based on the velocity in the pores spaces of chars and graphite	M/L^2t
x	mass fraction of the species	none
	distance in the axial direction (Chapter II)	L
y	distance in the radial direction (2-82)	L
	estimated moles of species in the free energy minimization calculation	none
$\bar{y}$	estimated mole fraction in the free energy minimization calculation	none
z	distance in the axial direction (Chapter II and III)	L
$\bar{z}$	compressibility factor	none
Greek		
α_o	ratio of the mass flux to the mass diffusivity used in equation (2-44)	M/L^4
α	viscous coefficient in the modified Darcy's law equation (2-82)	L^{-2}
β	inertial coefficient in the modified Darcy's law equation (2-82)	L^{-1}
γ	permeability of a porous medium	L^2
δ	Kronecher Delta	none
Δ	a difference between two parameters	none
∇	del operator	none

Symbol	Description	Units
ϵ	porosity of a porous medium	none
$\bar{\epsilon}$	emissivity of a porous medium	none
η	dimensionless char distance defined in equation (2-15)	none
θ	dimensionless temperatures defined in equations (2-11) and (2-12)	none
λ	parameter of a straight line (0-1)	none
μ	viscosity	M/Lt
π	3.1416	none
ρ	density	M/L^3
$\bar{\sigma}$	Stefan-Boltzmann constant	M/t^3T^4
σ	collision diameter	L
τ	shear stress	M/t^2L
ϕ	dimensionless parameters defined in equations (2-25), (2-26) and (2-27)	none
	parameter used to calculate the viscosity of a gas mixture in equation (3-57)	none
Ω	collision integral	none
Π	Lagrangian multipliers in equation (3-37)	none

Subscripts

c	convection or conduction
d	carbonaceous deposit
e	effective or overall value
f	fluid or gas phase

Symbol	Description
g	gas phase
L	front surface of a char
m	matrix or solid phase
o	initial or inlet condition
P	pressure
	pyrolysis
	pores
r	radiation
s	solid phase
T	temperature
	total
y	distance in the radial direction
z	distance measured from the char back surface
∞	free stream condition
1	inside surface of a cylindrical tube
2	outside surface of a cylindrical tube
Superscripts	
*	a standard or reference condition
°	a standard or reference state
'	derivative

A. INTEGRITY OF THE CALCULATIONS IN THE TEMPRE SYSTEM

Introduction

The TEMPRE System is a general analysis implimented in FORTRAN IV for studying the energy transfer in the char zone of a charring ablator. Three separate flow models and two boundary condition options are contained in the system.

The Iterative TEMPRE System solves the two point boundary value problem obtained by specifying the back and front char surface temperatures. An iterative solution for the correct initial (or final) temperature gradient required to match the known front (or back) surface temperature is necessary.

The Non-Iterative TEMPRE System solves the energy equation with back surface temperature and heat of pyrolysis of the virgin plastic (and therefore the temperature gradient) specified. Since any front surface temperature is acceptable, a parametric study is necessary to investigate the wide range of back and front surface conditions on the system.

In both of the above options the type of flow can be specified as frozen, equilibrium, or non-equilibrium. These three models give the upper (equilibrium) and lower (frozen) limits on the system and the degree with which the actual (non-equilibrium) behavior differs from the two ideal cases.

A block flow diagram of the TEMPRE System is given in

Figure A-1. As indicated, the system is composed of one primary section and eight secondary sections. The function of each portion will be analyzed in detail in the following pages. Each section represents an independently tested unit of the entire system forming the basis for the overall integrity of the TEMPRE System.

Frozen Flow Model

The frozen flow model is the simplest and forms the basic structure of the TEMPRE System. A fourth order Runge-Kutta numerical integration scheme was used to solve the energy equation and is the important part of the primary section.

Solutions of the Energy Equation by a Fourth Order Runge-Kutta Analysis: The standard form for the solution of a second order differential equation using a fourth order Runge-Kutta analysis if shown below (1). The values of the next temperature and temperature gradient are given by equations (A-1) and (A-2).

$$T_{n+1} = T_n + h\left[T'_n + \frac{1}{6}(A_1 + A_2 + A_3)\right] \qquad \text{(A-1)}$$

and

$$T'_{n+1} = T'_n + \frac{1}{6}\left[A_1 + 2A_2 + 2A_3 + A_4\right] \qquad \text{(A-2)}$$

Figure A-1. Block Flow Diagram of the TEMPRE System.

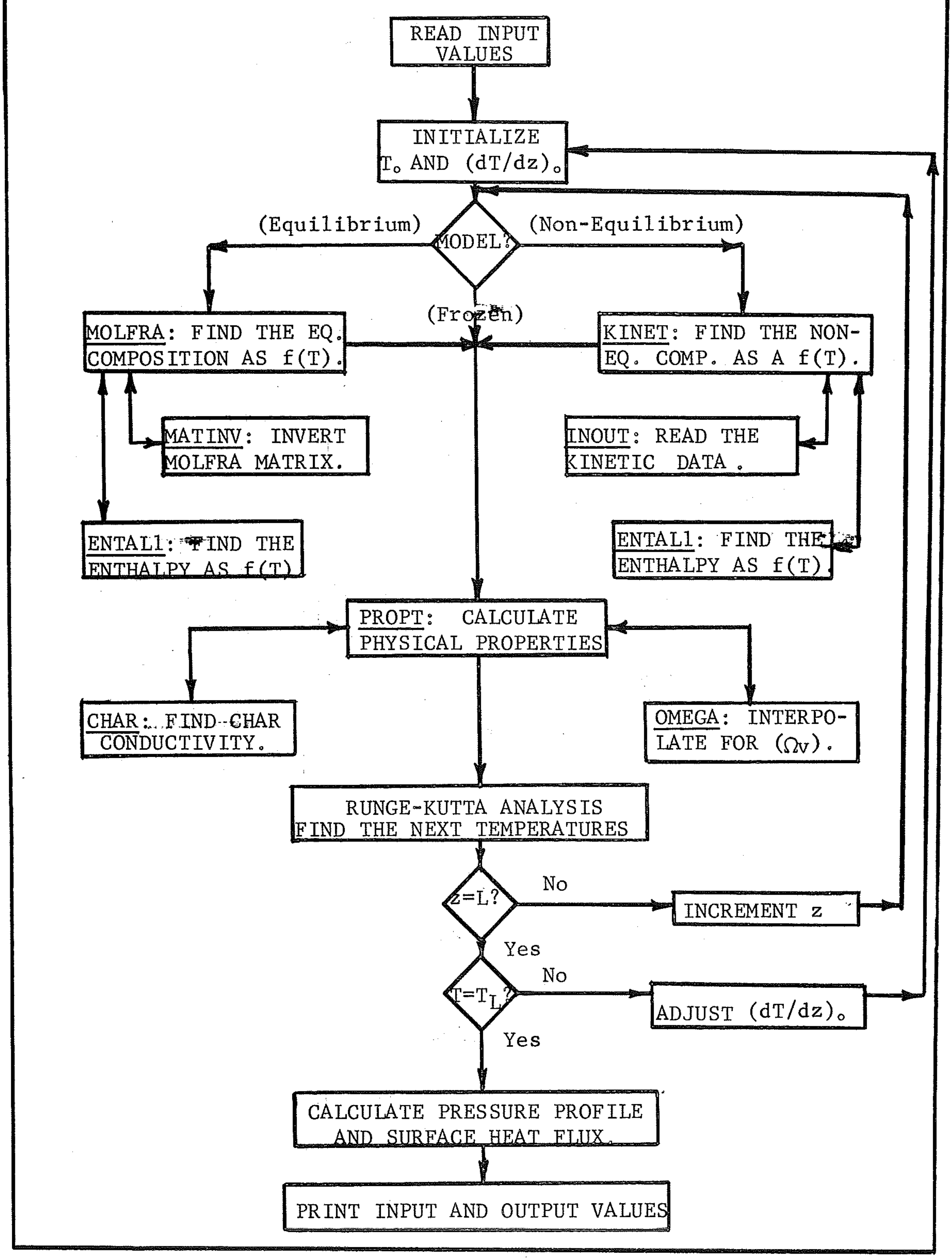

The values of A_i $(i = 1,2,3,4)$ are obtained by the following set of equations:

$$A_1 = h(T'_o)\left[\frac{W_p \bar{C}_p \epsilon}{k_c} - \frac{dk_e/dT}{k_e}(T'_o) + \frac{\Sigma H_i \bar{R}_i}{k_e}\right]_{T_o} \tag{A-3}$$

$$A_2 = h(T'_o + \tfrac{1}{2}A_1)\left[\frac{W_p \bar{C}_p \epsilon}{k_e} - \frac{dk_e/dT}{k_e}(T'_o + \tfrac{1}{2}A_1) + \frac{\Sigma H_i \bar{R}_i}{k_e}\right]_{T_o+\frac{h}{2}T'_o+\frac{h}{8}A_1} \tag{A-4}$$

$$A_3 = h(T'_o + \tfrac{1}{2}A_2)\left[\frac{W_p \bar{C}_p \epsilon}{k_e} - \frac{dk_e/dT}{k_e}(T'_o + \tfrac{1}{2}A_2) + \frac{\Sigma H_i \bar{R}_i}{k_e}\right]_{T_o+\frac{h}{2}T'_o+\frac{h}{8}A_2} \tag{A-5}$$

$$A_4 = h(T'_o + A_3)\left[\frac{W_p \bar{C}_p \epsilon}{k_e} - \frac{dk_e/dT}{k_e}(T'_o + A_3) + \frac{\Sigma H_i \bar{R}_i}{k_e}\right]_{T_o+hT'_o+\frac{h}{2}A_3} \tag{A-6}$$

Therefore, to begin the numerical solution, values of the temperature (T_n) and the temperature gradient (T'_n) must be specified at one surface of the char. This reduces the problem to a second order initial (or final) value problem.

In the Iterative TEMPRE System the temperature gradient at the surface must be guessed such that the temperature conditions at the back and front surfaces are satisfied. This requires an iterative solution accompanied by a suitable convergence scheme to insure effiecient and accurate approaches to the real solution. The Non-Iterative TEMPRE System is an initial (or final) value problem and requires no iterative scheme, and, therefore, no convergence logic.

Convergence Technique: The convergence technique in the TEMPRE System is purposely simple because of the rather complicated problem already existent with the numerical solution. It is composed of three main parts. The first or check portion limits the calculations made in the numerical analysis to values which are non-zero, non-negative and below an arbitrary ceiling on the desired (specified) front surface temperature. If either of the conditions mentioned above are violated, the temperature and gradient are printed for reference, the gradient is adjusted to correct the situation, and the analysis is restarted at the initial point.

The second type of logic within the convergence scheme is a gross correction to the gradient made when the final calculated temperature is greater than an arbitrary increment (100°F, for example) plus the desired final temperature. This involves taking the ratio of the actual to calculated final temperature and defining the new gradient as the product of this ratio and the old gradient value.

The third type involves a finer convergence scheme and is used when the final calculated temperature is within the arbitrary increment specified (100°F) or when two or more iterations have been made. This scheme involved the adjustment of the gradient by a linear interpolation using the final temperature ratio (actual to calculated), the ratio of the calculated temperatures for the last and next to last iteration, and the ratio of the gradients (initial) of the last and next to last iterations. This method converges in three to five iterations (30 seconds computer time) for frozen flow. Although there are many elaborate convergence techniques available to insure efficient and accurate approaches to the desired condition, no real incentive beyond the above simple scheme was justified in the Tempre System.

<u>Overall Runge-Kutta Stability and Accuracy</u>: A comprehensive investigation into the stability and accuracy of the Runge-Kutta analysis is essential to any program where that method is used to give numerical solutions to differential equations. Beyond the discussions by Ames (2) and Collatz (3) regarding the mathematical development of the Runge-Kutta equations, the most important question which must be answered is what increment size is necessary and sufficient to insure a stable, yet accurate solution. Results of an increment study made in the Frozen

Flow TEMPRE System for Constant Physical Properties and Variable Physical Properties are presented in Tables A-1 and A-2. A very large increment size is sufficient for the Constant Physical Properties case; however, a very critical decision arises for the Variable Physical Properties case. A value of 100 appears to be the point above which no real accuracy is gained for the investment of computer time. This value seems reasonable over the entire system, including the equilibrium and non-equilibrium flow cases.

Frozen Flow, Constant Physical Properties Analysis: For the case where gas and char physical properties are assumed independent of temperature, an analytical solution of the energy equation is obtained (4). This solution outlined in Table A-3 forms a basis for testing the accuracy and reliability of the numerical method. Since no subroutines are required to generate physical property data, a direct comparison of the Runge-Kutta analysis to the analytical solution is obtained. Table A-4 contains the values of the temperature for various dimensionless char depth values (z/L) for the analytical solution and two numerical solutions (step sizes of 10 and 100). Excellent agreement is noted at the smaller increment size as well as the larger.

Frozen Flow, Variable Physical Properties Analysis: In order to handle the variable physical properties (with temperature) option, three subroutines are added to the TEMPRE

Table A-1. Comparison of Various Runge-Kutta Increment Sizes for the Frozen Flow Constant Physical Properties Model

Dimensionless Char Distance (z/L)	Temperature (°F) Runge-Kutta Increment Size 10	50	100	400
0.0	500.0000	500.0000	500.0000	500.0000
0.2	609.4615	609.4597	609.4597	609.4597
0.4	775.9448	775.9413	775.9413	775.9414
0.6	1029.1543	1029.1497	1029.1497	1029.1498
0.8	1414.2683	1414.2642	1414.2643	1414.2643
1.0	2000.0000	2000.0000	2000.0000	2000.0000

Conditions: $W = 0.05$ lb/ft^2-sec $L = 0.0208$ ft $C_p = 0.7$ BTU/lb-°F

$k_e = 1.0$ BTU/ft-hr-°F $\epsilon = 0.8$

Table A-2. Comparison of Various Runge-Kutta Increment Sizes for the Frozen Flow Variable Physical Properties Model

Dimensionless Char Distance (z/L)	Temperature (°F) Runge-Kutta Increment Size 10	50	100	400
0.0	500.0000	500.0000	500.0000	500.0000
0.2	631.4212	625.6282	625.4788	625.4202
0.4	824.2823	819.5501	819.4515	819.3908
0.6	1106.1787	1102.8111	1102.7770	1102.7141
0.8	1494.5636	1492.8853	1492.8260	1492.7604
1.0	2000.0000	2000.0000	2000.0000	2000.0000

Conditions: W = 0.05 lb/ft^2-sec L = 0.0208 ft $\epsilon = 0.8$

Gas Composition (Mole/Mole Gas):

CO = 0.245, CO_2= 0.046, N_2= 0.073, CH_4= 0.570, C_6H_6= 0.068

Table A-3. Analytical Solution of the Energy Equation (3-29) for Constant Physical Properties

Form of the Energy Equation:

$$\frac{d^2T}{dz^2} = \frac{dT}{dz} (W\ C_p\ \epsilon\ /\ k_e) = \frac{dT}{dz} (N)$$

Form of the Solution:

$$\left(\frac{T - T_o}{T_L - T_o} \right) = \left[\frac{1 - \exp(Nz/L)}{1 - \exp(N)} \right]$$

For the specific solution presented in Table A-4, the values of the parameters are:

$W = 0.05$ lb/ft^2-sec
$L = 0.0208$ ft
$T_o = 500.0$ °F
$T_L = 2000.0$ °F
$C_p = 0.7$ BTU/lb-°F
$k_e = 1.0$ BTU/ft-hr-°F
$\epsilon = 0.8$

The analytical and numerical solutions are compared in Table A-4.

Table A-4. Comparison of the Analytical Solution of the Frozen Flow, Constant Physical Properties Model with the Runge-Kutta Solution for Two Increment Sizes

Dimensionless Char Distance (z/L)	Analytical Solution	Temperature (°F) Numerical Solutions 10 Increments	Temperature (°F) Numerical Solutions 100 Increments
0.0	500.0000	500.0000	500.0000
0.2	609.4597	609.4615	609.4597
0.4	775.9413	775.9448	775.9413
0.6	1029.1497	1029.1543	1029.1497
0.8	1414.2642	1414.2683	1414.2643
1.0	2000.0000	2000.0000	2000.0000

Conditions: $W = 0.05$ lb/ft^2-sec $L = 0.0208$ ft $C_p = 0.7$ BTU/lb-°F

$k_e = 1.0$ BTU/ft-hr-°F $(dT/dz)_o = 21180$ °F/ft $\epsilon = 0.8$

System. These are called PROPT, which calculates the physical properties of the gas mixture, the overall thermal conductivity and the conductivity gradient for specific values of temperature; CHAR, a curve fitting program used to estimate the char thermal conductivity from tabulated data; and OMEGA, a general Lagrangian interpolation program. Each will be discussed in detail in the following paragraphs.

In addition to the checks made on each individual subroutine, the overall Frozen Flow Variable Physical Properties Model is compared with solutions obtained in MIMIC (5), an analog-digital simulator. These techniques essentially represent two distinctive paths to the same solution and add confidence to the calculations made in the system. Table A-5 compares the temperature at various dimensionless char depths for the various numerical solutions. Copies of the MIMIC programs and solutions are given in Appendix H.

PROPT: The calculation of the gas and char physical properties are made in subroutine PROPT with assistance from OMEGA and CHAR. For a given temperature supplied from the main program, the heat capacity, thermal conductivity and viscosity of the pure gases and gas mixture are calculated. The equations used are described in Chapter III.

From subroutine CHAR, the thermal conductivity of the char is obtained and the effective conductivity (Equation 3-20) is calculated. The thermal conductivity gradient is likewise

Table A-5. Comparison of the Runge-Kutta Solution for the Frozen Flow, Variable Physical Properties with Two Solutions Obtained Using MIMIC (Analog-Digital Simulator)

Dimensionless Char Distance (z/L)	Temperature (°F) MIMIC (a) Solution	 MIMIC (b) Solution	 Runge-Kutta Solution
0.0	500.00	500.00	500.00
0.2	626.52	627.11	625.48
0.4	821.89	821.95	819.45
0.6	1105.76	1104.90	1102.78
0.8	1492.95	1494.89	1492.83
1.0	2000.00	2000.00	2000.00

Conditions: $W = 0.05\ \mathrm{lb/ft^2\text{-}sec}$ $L = 0.0208\ \mathrm{ft}$ $\epsilon = 0.8$ $(dT/dz)_o = 24172\ °\mathrm{F/ft}$

Gas Composition (Mole/Mole Gas):

$CO = 0.245$, $CO_2 = 0.046$, $N_2 = 0.073$, $CH_4 = 0.570$, $C_6H_6 = 0.068$

(a) Solution of Equation (H-1) (b) Solution of Equation (H-2) calculated in PROPT for use in the general energy equation. Subroutine OMEGA supplies the collision integral as a function of temperature for calculating the viscosity and conductivity of the pure gases. Figure A-2 is a comparison of the calculated values of the various physical properties and experimental values reported in the literature (6,7). Excellent agreement was found for a variety of gases over a wide range of temperatures.

OMEGA: The interpolation of input and calculated data is essential in the TEMPRE System. In the frozen flow analysis, interpolation for the collision integral as a function of temperature is performed for use in calculating the pure gas viscosity and conductivity. A standard Lagrangian interpolation formula is used. The degree of the formula and the size of the array are required input parameters. These may be varied over a wide range of values; however, the best combination must be determined for an accurate and efficient analysis.

In subsequent discussions, OMEGA is used to interpolate values of char distance as well as mass flux, molecular weight of the gas mixture, heat of reaction and concentration values as functions of temperature. Reliable values are obtained over a wide range of parameter values of large and small magnitude.

CHAR: This analysis can be any general curve fitting technique that best describes the available thermal conductivity

Figure A-2. Comparison of Calculated Physical Property Values with Experimental Values in the Literature. Part (a): Viscosity (Centipoise x 100)

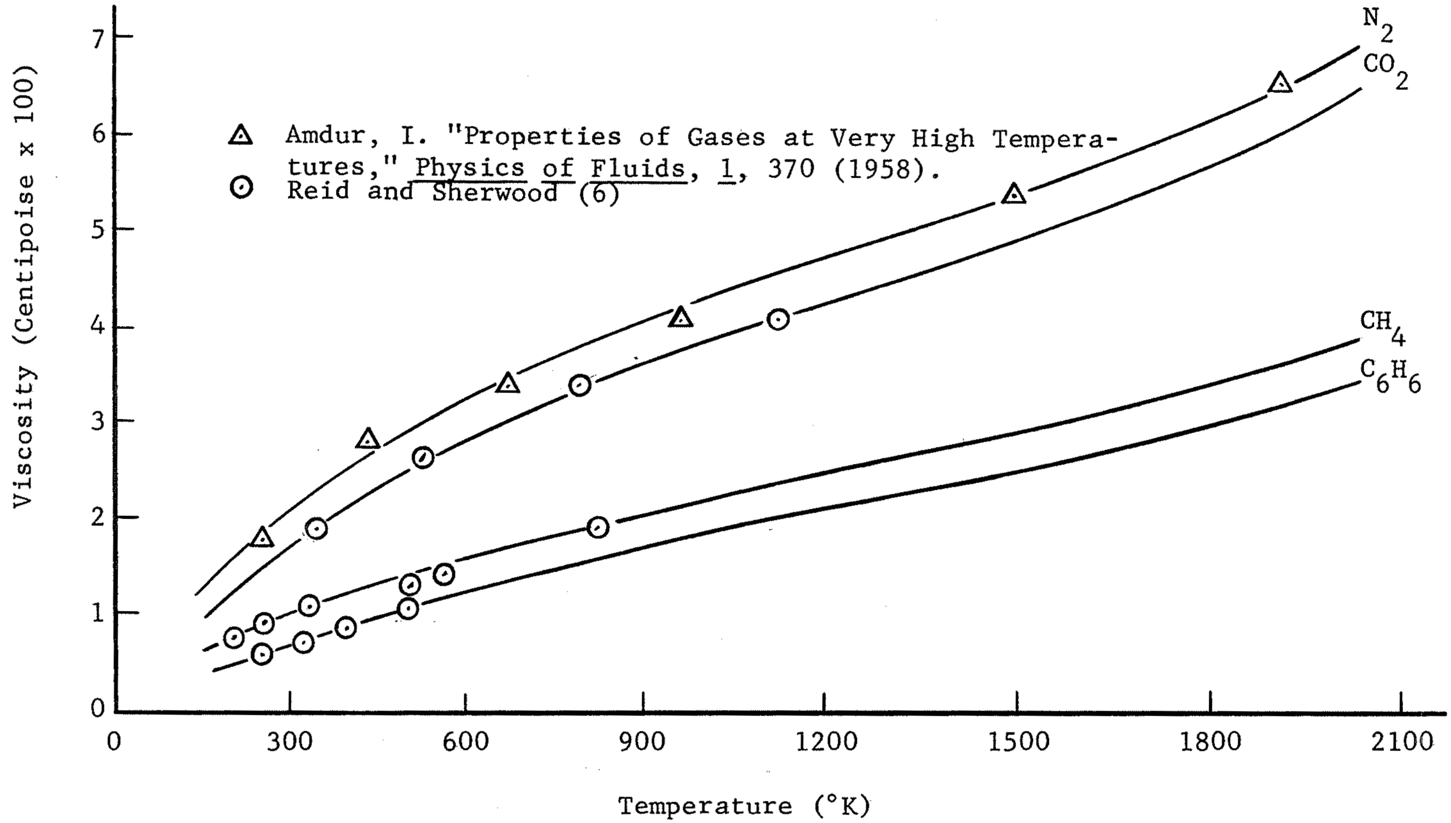

Figure A-2. Comparison of Calculated Physical Property Values with Experimental Values in the Literature. Part (b): Heat Capacity (Cal/gmmole-°K)

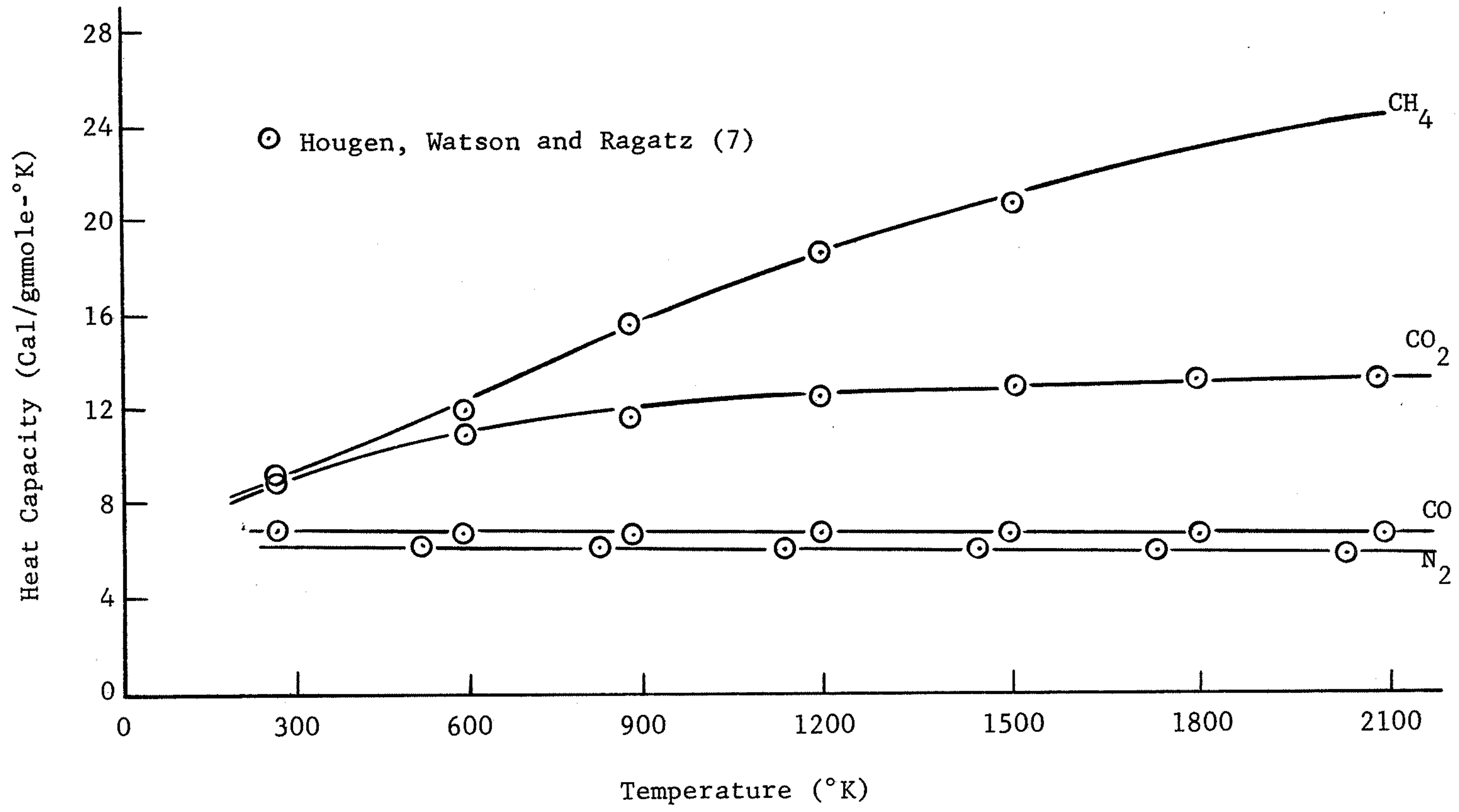

Figure A-2. Comparison of Calculated Physical Property Values with Experimental Values in the Literature. Part (c): Thermal Conductivity (Cal/cm-sec-°K)

Perry, J. H., ed., <u>Chemical Engineers' Handbook</u>, 2nd Edition, McGraw-Hill, New York, 461 (1950).

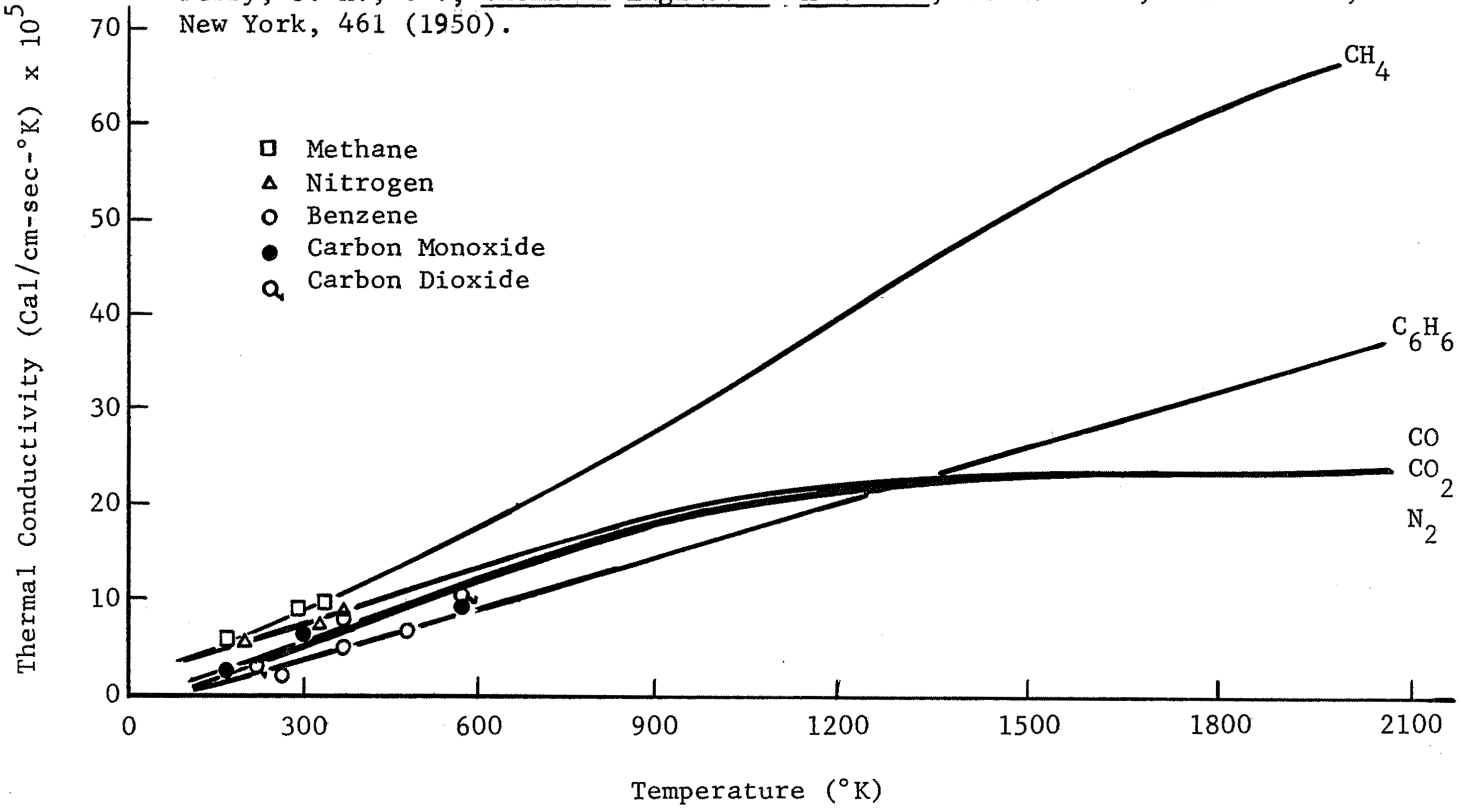

data of the char material. In the present analysis a linear least squares fit is used. Values of the correlation coefficient and standard deviation are 0.97169 and 0.000234 (at an average value of 0.0044) units respectively, indicating a very good fit of the data (8). A plot of the available char conductivity data vs. temperature (9) is shown in Figure A-3 with the corresponding least squares curve.

As more data becomes available at higher temperatures it is anticipated that higher order regression analyses might be necessary. Such changes are easily made by substituting the appropriate curve fitting technique as subroutine CHAR. From the slope and intercept (and other pertinent information for a multiple regression analysis) the conductivity and gradient are obtained for use in PROPT to calculate effective conductivity values.

Equilibrium Flow Model

The primary difference between the frozen flow and equilibrium flow models is the change in species concentrations with temperature in the later case. These changes, as calculated by a free energy minimization technique (10), are only a function of temperature and pressure and all pertinent results can be tabulated outside of the Runge-Kutta numerical procedure.

In addition to the subprograms required in the frozen flow

Figure A-3. Char Thermal Conductivity Data and the Associated Least Squares Curve.

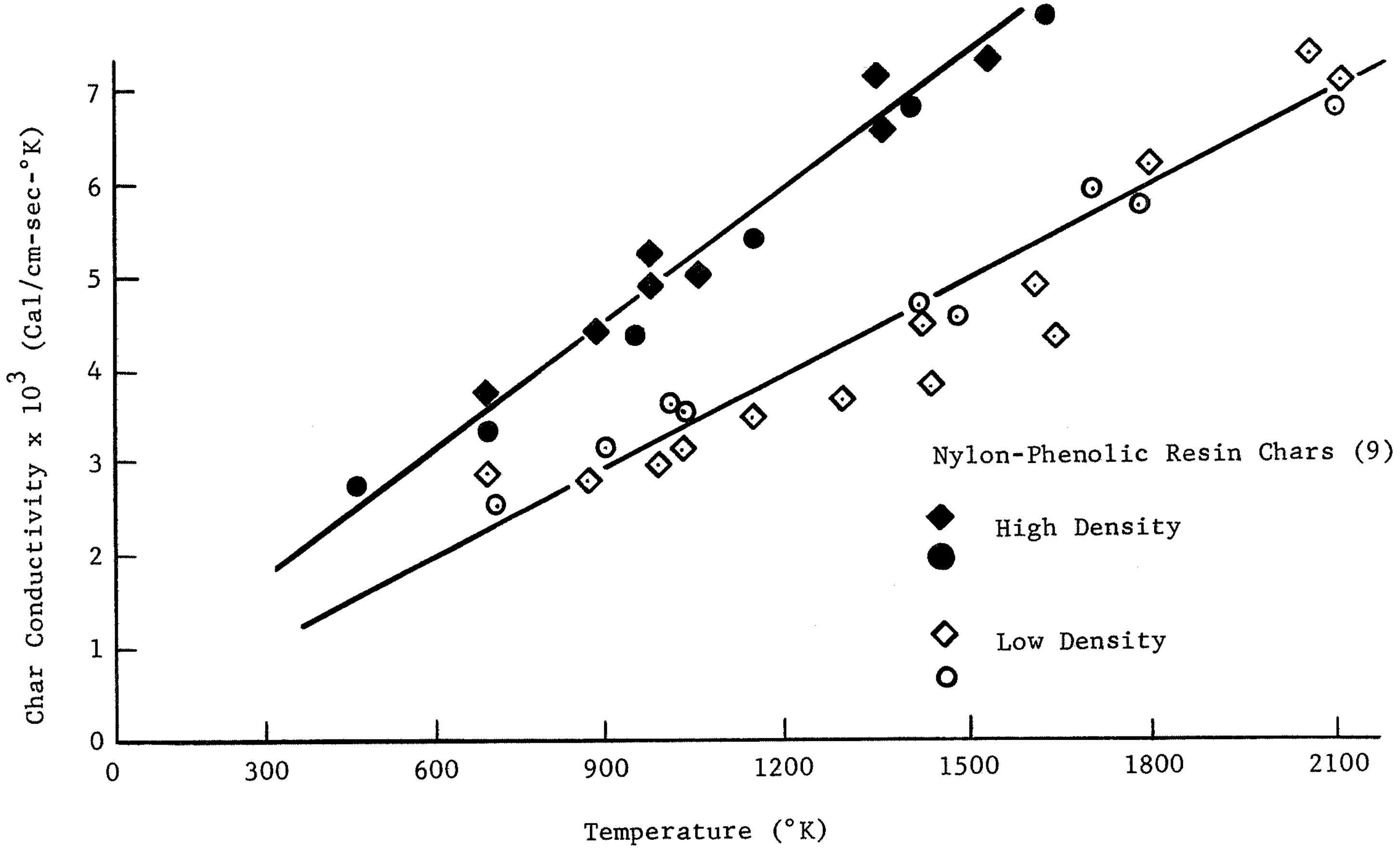

analysis (i.e., PROPT, CHAR, OMEGA) three additional operations must be added. MOLFRA performs the free energy minimization calculations and tabulates pertinent values to be transferred, as needed by the Runge-Kutta analysis, using OMEGA. ENTAL1 and MATINV are used to generate enthalpy data as a function of temperature and for matrix inversion, respectively. Once again each additional method will be discussed individually with emphasis on the accuracy and reliability of the calculations.

MOLFRA: The analysis contained in this subroutine uses the free energy minimization technique to predict the equilibrium composition of a reacting gas-solid mixture. It employs a search technique to compute the number of moles of each chemical species required to give the minimum free energy of the mixture. A detailed description is presented by del Valle (11).

To verify the calculations made by this program, several literature examples were used for comparison. Table A-6 indicates the reproducibility and accuracy with which the equilibrium model reproduced experimental and other numerical solutions. Once again reference to the work by del Valle (11) is made for detailed discussions of the results.

MATINV: This subroutine is a standard method for finding the inverse of a non-singular n x n matrix. The IBM Share Library is the source for this particular program (12). The inversion is performed iteratively by reducing the original matrix to an identity matrix by a series of row operations.

Table A-6. Comparison of the Equilibrium Composition of Ammonia and Unsymmetrical Dimethyl Hydrazine (UDNH) - Red Fuming Nitric Acid (RFNA) Propellant at 10 atm. Pressure.

Temperature °C	Ammonia Equilibrium at 10 atm. Calculated by:			UDNH-RFNA Equilibrium at 3000°K		
	Dodge	Haber	MOLFRA	Brandmair & Harnett		MOLFRA
325	10.38		11.59	H_2	3.6569	3.6567
350	7.35	8.04	8.21	H_2O	40.7310	40.7273
375	5.25		5.85	OH	9.5222	9.5216
400	3.85	4.12	4.21	CO	7.3355	7.3350
425	2.80		3.08	CO_2	10.4574	10.4563
450	2.04	2.21	2.28	N_2	23.2108	23.2170
475	1.61		1.71	NO	0.9386	0.9387
500	1.20	1.27	1.31	N	0.0021	0.0021
				H	0.9554	0.9553
				O	0.6136	0.6136
				O_2	2.5780	2.5780

The method is then repeated with the resulting identity matrix.

ENTAL1: The enthalpies of the various species as a function of temperature are calculated in subroutine ENTAL1. It is called by MOLFRA and KINET after the species compositions are calculated. Values of the enthalpy are calculated at a reference temperature of 298°K and modified by the heat capacity term as is usually done.

Non-Equilibrium Flow Model

Like the equilibrium flow model, the concentrations and heats of reaction vary with the temperature. However, in the non-equilibrium flow model, changes in the mole flux with temperature must be calculated as part of the Runge-Kutta analysis. That is, for each temperature generated in the Runge-Kutta analysis, a corresponding set of concentrations, heats of reaction, etc. must be calculated.

Because of the added complexity, a Runge-Kutta stability analysis, identical to those methods described for the frozen flow models, was made. The results shown in Table A-7 for step sizes of 100, 200, 400, 1000 show slightly higher differences in the various temperature profiles as compared with the frozen flow results in Tables A-1 and A-2. However, the results are within the convergence tolerance of 1% and the solution for 100 steps is valid. Over the temperature range from 500° to 3000°F, there is no incentive in a smaller increment for the added investment in computer time.

The substitution of KINET for MOLFRA and INOUT for MATINV completes the necessary transformations required to make the non-equilibrium flow calculatioms. KINET functions as MOLFRA, but uses

Table A-7. Comparison of Various Runge-Kutta Increment Sizes for the Non-Equilibrium Flow Model.

Dimensionless Char Distance (z/L)	Temperature °F Runge-Kutta Increment Size			
	100	200	400	1000
0.00	500.000	500.000	500.000	500.000
0.25	694.189	696.354	696.595	696.707
0.50	1053.285	1056.442	1056.760	1056.912
0.75	1615.478	1618.567	1618.779	1618.933
1.00	2500.000	2500.000	2500.000	2500.000

Conditions: $W = 0.05$ lb/ft^2-sec $L = 0.0208$ ft $\epsilon = 0.8$

Gas Composition (Mole/Mole Gas):

$C_6H_6O = 0.062$, $H_2O = 0.489$, $CO = 0.037$, $CO_2 = 0.011$, $CH_4 = 0.067$, $H_2 = 0.334$

a kinetic analysis instead of the equilibrium treatment for calculating the mole flux of each species. All pertinent kinetic data are entered through INOUT, a general input-output routine. A detailed discussion follows on each new addition to the TEMPRE system.

KINET: This program uses the kinetic data read into the system in INOUT for calculating the change in the species mole fluxes as a function of temperature. The new mole flux values are then used to calculate the heat of reaction, which for endothermic reactions, result in energy absorption.
This absorption is accounted for in the energy equation which solves for the next temperature based on the change in composition and heat of reaction values calculated. The interdependence between the mole flux and temperature requires a simultaneous solution of the differential energy and species continuity equations. KINET integrates the species continuity equation using a fourth order Runge-Kutta method.

INOUT: This subroutine contains the kinetic data needed to integrate the species continuity equation. The specific reactions, activation energies, frequency factors and stoichiometric coefficients are typical data read. The system is designed to handle any number of chemical reactions and chemical species.

In summary, the discussion thus far has been concerned with the development of a general computational system for analysing the energy transfer associated with the flow of pyrolysis gases through the char zone for frozen, equilibrium and non-equilibrium conditions. In addition to the solutions of the energy equation which results in a temperature distribution, the pressure distribution and surface heat flux areneeded to further describe the phenomena taking place within the char layer. This is the topic of the following sections.

Calculation of the Pressure Distribution and Surface Heat Flux

The pressure distribution across the char zone, and, the front surface heat flux are calculated by a Simpson's Rule integration of the differential momentum and heat flux equations, (3-12) and (3-23). Because these equations are uncoupled from the energy equation, their solutions are calculated after a valid temperature distribution has been obtained. Therefore, the integration method is the same in the iterative and non-iterative calculations. Interpolation using subprogram OMEGA of both char distance and collision integral as a function of the temperature distribution across the char is required. These operations allow the calculation of the gas mixture viscosity as a function of char distance. In addition the stored reaction rate and heat capacity data needed in the heat flux calculation are also interpolated for using OMEGA.

At the end of these calculations, all pertinent input and output information are printed for comparison with experimental or other analytical data.

Simpson's Rule Integration: As discussed in Chapter III, the Simpson's Rule formula is used to integrate the specific terms in the momentum and heat flux equations. As in the case of the Runge-Kutta analysis, a stepsize must be selected to produce an accurate, yet efficient, solution to the true solution. Table A-8 compares the solution of the momentum equation for various interval sizes. As noted, the solution becomes stable for a stepsize of twenty. A similar comparison for the heat flux calculation likewise indicated twenty units as a valid stepsize to insure accuracy. In the case of the pressure distribution, the solution for one case was compared with a graphical integration using a desk calculator and very good agreement was obtained.

Summary

This appendix introduced the TEMPRE System and discussed the various functions of each subprogram used in the analysis. More importantly, however, was the factual information presented which insured the calculations to be accurate, efficient and functioning as expected. This formed the basic proof of the integrity of the TEMPRE System.

In Appendix B a complete listing of the TEMPRE System will be presented with instructions regarding the use and interpretation of the input and output specifications. Specific examples will be illustrated for calculation of the temperature, pressure and concentration profiles within the char zone, the surface heat flux and change in mass flux for frozen, equilibrium and non-equilibrium flow of pyrolysis gases.

Table A-8. Comparison of Various Simpson's Rule Increment Sizes for the Frozen Flow, Variable Physical Properties Model

Dimensionless Char Distance (Z/L)	Pressure (lb/ft^2) Simpson's Rule Increment Size 20	 50	 100	 200
0.00	2175.5921	2175.5918	2175.5913	2175.5912
0.33	2173.4147	2173.4144	2173.4139	2173.4138
0.67	2168.7373	2168.7368	2168.7364	2168.7364
1.00	2160.0000	2160.0000	2160.0000	2160.0000

Conditions: $W = 0.05\ lb/ft^2\text{-sec}$ $L = 0.0208$ ft $\epsilon = 0.8$

Gas Composition (Mole/Mole Gas):

$CO = 0.245$, $CO_2 = 0.046$, $N_2 = 0.073$, $CH_4 = 0.570$, $C_6H_6 = 0.068$

REFERENCES

1. Abramowitz, Milton and I. A. Stegun, editors, Handbook of Mathematical Functions with Formulas, Graphs, and Mathematical Tables, 3rd Printing, National Bureau of Standards Applied Mathematics Series 55, Washington, D. C., 896-7 (1965).

2. Ames, W. F., Non-Linear Ordinary Differential Equations in Transport Processes, Academic Press, New York, 218-228 (1968).

3. Collatz, Lothar, The Numerical Treatment of Differential Equations, 3rd Edition, Springer-Verlag, New York, 61-78 (1966).

4. Pike, R. W., "Evaluation of the Literature for Chemical Reactions and the Reaction Rates for the Decomposition Products from Charring Ablators," NASA LWP-181, Langley Research Center, Hampton, Virginia (January 1966).

5. Petersen, H. E. and F. J. Sansom, "MIMIC - A Digital Simulator Program," SESCA INTERNAL MEMO 65-12 (May 1965).

6. Reid, R. C. and T. K. Sherwood, The Properties of Gases and Liquids, 2nd Edition, McGraw-Hill Book Co., New York, 395-519 (1966).

7. Hougen, R. A., K. M. Watson and R. A. Ragatz, Chemical Process Principles, Part I, John Wiley and Sons, Inc., New York, 250-258 (1959).

8. April, G. C., R. W. Pike and E. G. del Valle, "Solution of the Frozen Flow Energy Equation," NASA- CR-77026 (July 1966).

9. Wilson, R. Gale, "Thermophysical Properties of Six Charring Ablators from 140° to 700°K and Two Chars from 800° to 3000°K," NASA TN D-2991 (October 1965).

10. del Valle, E. G., R. W. Pike and G. C. April, "Thermodynamic Equilibrium of a Reacting Gas-Solid Mixture. I: Derivation of Equation and Convergence Procedure," NASA CR-79677 (October 1, 1966).

11. del Valle, E. G., R. W. Pike and G. C. April, "Thermodynamic Equilibrium of a Reacting Gas-Solid Mixture. II: Computer Implementation and Result," NASA CR-66309 February 1, 1967).

12. Sadaka, R. N., "Double Precision Matrix Inversion with Selective Pivot," IBM Share Library, No. 7090-F1, 3181 INV2 (1965).

B. ITERATIVE AND NON-ITERATIVE TEMPRE SYSTEMS

As discussed in Appendix A, the TEMPRE System is comprised of two main programs and eight subprograms. The iterative main program is for the analysis of a two point boundary value problem requiring an iterative solution technique, and the non-iterative main program is for an initial (or final) value problem which is non-repetitive in nature.

These two distinctive main programs are called "IT" and "NONIT" for obvious reasons. The complete analysis is thus generalized with the exception of the main programs which must be interchanged for a specific application. Figure B-1 graphically illustrates the complete TEMPRE System. The remaining sections of this appendix include a complete listing of the TEMPRE System with typical input and output formats for using and interpreting the system. The following outline will help locate the particular programs in the system.

Listing B-1	Iterative TEMPRE (Main) Program
Listing B-2	Non-Iterative TEMPRE (Main) Program
Listing B-3	TEMPRE Subprograms a - PROPT (Physical Properties) b - OMEGA (Interpolation) c - CHAR (Char Thermal Conductivity) d - MOLFRA (Free Energy Minimization) e - MATINV (Matrix Inversion) f - ENTAL1 (Enthalpy of Gas Mixtures) g - KINET (Chemical Reaction Rates) h - INOUT (Kinetic Data)
Listing B-4	Input Format
Listing B-5	Output Format

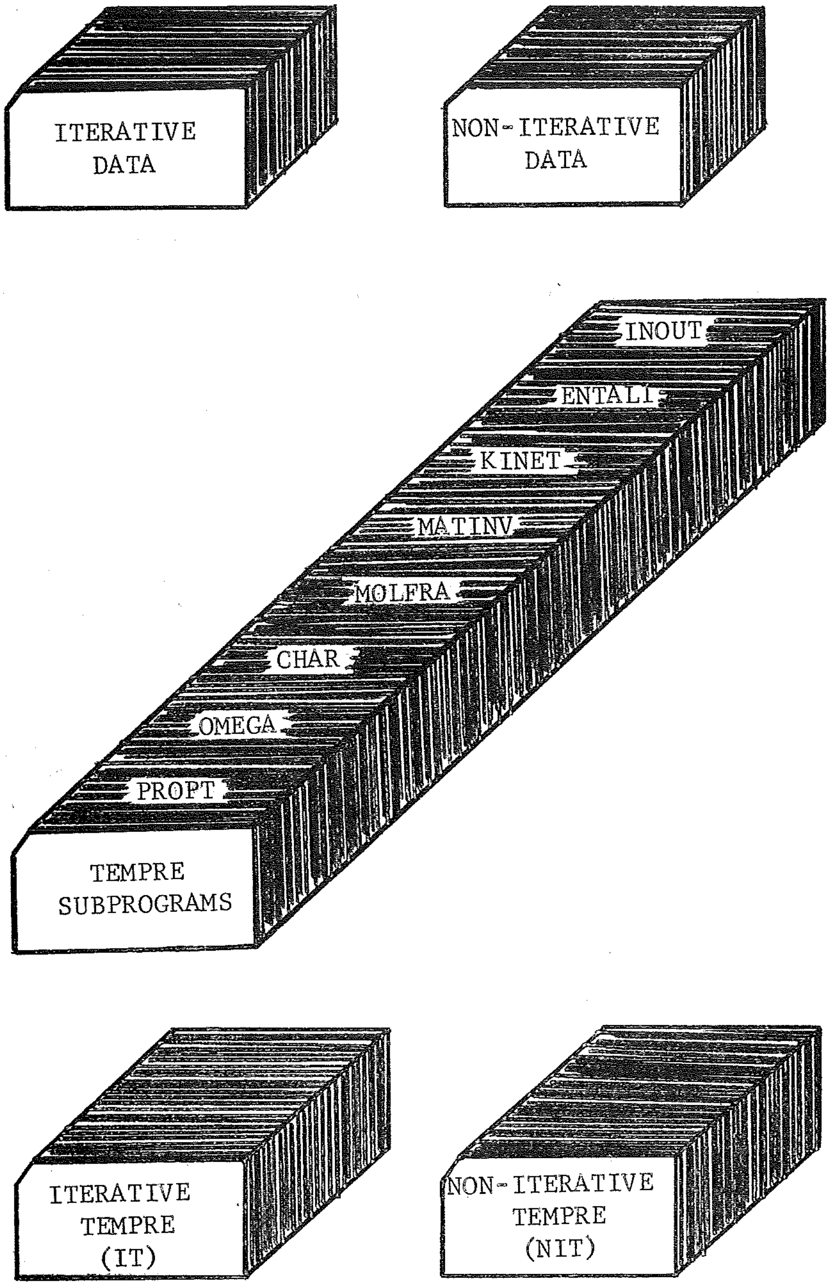

Figure B-1. TEMPRE System for Calculating the Energy Transfer in the Char Zone of a Charring Ablator.

Listing B-1. Iterative TEMPRE (Main) Program.

```
C
C
C        TEMPRE - GENERAL ITERATIVE SYSTEM ANALYSIS FOR STUDY OF THE
C        ENERGY AND MASS TRANSFER IN THE CHAR ZONE OF ABLATORS
C
C
      DIMENSION ICODE(20),ALPA(20),AA(20,6),
     1  S1(4),S2(4),S3(4),S4(4),S5(4),A11(4),A22(4),A33(4),A44(4),A55(4)
      DIMENSION AI(20),BI(20),CI(20),DI(20),EI(20),FI(20),GI(20),
     1  AII(20),BII(20),CII(20),DII(20),EII(20),FII(20),GII(20),FW(20),
     2   YI(20),EK(20),SIG(20),Y(20),DELH(20)
      DIMENSION RSC(15,15),PSC(15,15),NREX(15,15),NPEX(15,15),AF(30),
     1SF(20),AEF(20),AR(20),SR(20),AER(20),EQN(20,12),TABLE(70,20)
      DIMENSION T(300),DT(300),XTKE(100),ZOMGA(100),XN(300),FN(300),
     1  TT(300),TP(300),CP(20),COND(20),CV(20),VIS(20),XAXIS(300),
     2  YAXIS(300),QT(300),QDT(300),Z(300),PROD(300),CAPAC(300),
     3  PRODR(300),PRODCP(300),ZX(300),P(300),ZY(300)
      DIMENSION WFLUX(10),YCOMP(20,10)
      COMMON NC,NS,MM,WI,PL,RR,TZERO,DELTK,ICODE,ALPA,AA,S1,S2,S3,
     1   S4,S5,A11,A22,A33,A44,A55
      COMMON AI,BI,CI,DI,EI,FI,GI,AII,BII,CII,DII,EII,FII,GII,FW,YI
      COMMON EK,SIG,EPS,Y,DELH
      COMMON RSC,PSC,NREX,NPEX,AF,SF,AEF,AR,SR,AER,EQN,TABLE
C
C        READ INPUT PARAMETERS
C
C     NC=NO. OF GAS COMPONENTS
C     NS=NO. OF CONDENSED PLUS GAS COMPONENTS
C     MM=NO. OF ELEMENTS
C     KODE=1 CONDUCTIVITY OF CHAR WITH GAS IN PORES
C     KODE=2 CONDUCTIVITY OF CHAR WITH PORES EVACUATED
C
   10 READ11,NC,NS,MM,KODE
      DO15 J=1,MM
```

```
C
C     S1 THRU S5=EMPIRICAL CONSTANTS FOR HEAT CAPACITY OF ELEMENTS
C                                 (UP TO 1000 OK)
C
      READ14,S1(J),S2(J),S3(J),S4(J),S5(J)
C
C     A11 THRU A55=EMPIRICAL CONSTANTS FOR HEAT CAPACITY OF ELEMENTS
C                                 (ABOVE 1000 OK)
C
      READ14,A11(J),A22(J),A33(J),A44(J),A55(J)
   15 CONTINUE
      DO16 I=1,NS
C
C     AA=FORMULA NUMBER
C
      READ14,(AA(I,J),J=1,MM)
C
C     AI THRU GI=EMPIRICAL CONSTANTS FOR HEAT CAPACITY (ABOVE 1000 OK)
C
      READ14,AI(I),BI(I),CI(I),DI(I),EI(I),FI(I),GI(I)
C
C     AII THRU GII=EMPIRICAL CONSTANTS FOR HEAT CAPACITY (UP TO 1000 OK)
C
      READ14,AII(I),BII(I),CII(I),DII(I),EII(I),FII(I),GII(I)
   16 CONTINUE
C
C     EK=POTENTIAL PARAMETER/BOLTZMAN CONSTANT
C     SIG=COLLISION DIAMETER (OA)
C
      READ17,(EK(I),SIG(I),ALPA(I),I=1,NC)
   11 FORMAT(4I6)
   12 FORMAT(5F10.5)
   13 FORMAT(20X,2E10.4,2X,A4,I6,1E10.4)
   14 FORMAT(7E10.4)
   17 FORMAT(2F15.6,A4)
```

```
   18 FORMAT(F15.5)
C
C     ALPHA=VISCOUS COEFFICIENT IN DARCY EQUATION (1/FT)
C     BETA=INERTIAL COEFFICIENT IN DARCY EQUATION (1/FT2)
C
      READ22,ALPHA,BETA
C
C     NDATA=NO. OF XTKE VS. ZOMGA DATA POINTS
C     NDIM1=NO. OF DIMENSIONED LOCATIONS FOR EQUILIBRIUM PROGRAM CALCULA
C                             IN SUBPROGRAM OMEGA
C     NDIM2=NO. OF DIMENSIONED LOCATIONS FOR TEMPERATURE-DISTANCE CALCUL
C                             IN SUBPROGRAM OMEGA
C     NDIM3=NO. OF DIMENSIONED LOCATIONS FOR PHYSICAL PROPERTY CALCULATI
C                             IN SUBPROGRAM OMEGA
C        KEY = 1 (FROZEN FLOW)
C        KEY = 2 (EQUILIBRIUM FLOW)
C        KEY = 3 (NON-EQUILIBRIUM FLOW)
C        MTYPE = TYPE OF PROBLEM BEING CONSIDERED
C        1 = EXPERIMENTAL
C        2 = THEORETICAL
C
      READ23,NDATA,NDIM1,NDIM2,NDIM3,KEY,MTYPE
C
C     XTKE=PRODUCT OF TEMPERATURE AND 1/EK VALUE
C     ZOMGA=COLLISION INTEGRAL TABULATED VS XTKE
C
      READ24,(XTKE(I),ZOMGA(I),I=1,NDATA)
   22 FORMAT(2E15.5)
   23 FORMAT(6I6)
   24 FORMAT(2F15.5)
C
C        PRIMARY PARAMETERS INITIALIZED
C
      JCHAR=1
      K6=1
```

```
   30 Z(1)=0.0                                                          IT 105
      IJKL=1                                                            IT 106
C     EPS=CHAR POROSITY                                                 IT 107
C                                                                       IT 108
      READ18,EPS                                                        IT 109
C                                                                       IT 110
C     TL=TEMPERATURE AT Z=L (OF)                                        IT 111
C     T(1)=TEMPERATURE AT Z=0 (OF)                                      IT 112
C     DT(1)=TEMPERATURE GRADIENT AT Z=0 (OF/FT)                         IT 113
C     ZL=CHAR THICKNESS (FT)                                            IT 114
C     HI=RUNGE-KUTTA INCREMENT SIZE (FT)                                IT 115
C     HSIMPI=SIMPSON RULE INCREMENT SIZE (FT)                           IT 116
C                                                                       IT 117
   20 READ21,T(1),TL,DT(1),ZL,HI,HSIMPI,HS                              IT 118
   21 FORMAT(7F10.0)                                                    IT 119
C                                                                       IT 120
C     WI=INITIAL GAS MASS FLUX VALUE AT Z=0 (LB/FT2-SEC)                IT 121
C                                                                       IT 122
C     PL=PRESSURE AT Z=L (LB/FT2)                                       IT 123
C     RR=GAS CONSTANT (1.987 BTU/LB-MOLE/OR)                            IT 124
C     TZERO=REFERENCE TEMPERATURE (298.2 OK)                            IT 125
C     DELTK=TEMPERATURE INCREMENT USED TO CALCULATE DKC/DT (OK)         IT 126
C                                                                       IT 127
      READ12,WI,PL,RR,TZERO,DELTK                                       IT 128
C                                                                       IT 129
C     FW=MOLECULAR WEIGHT                                               IT 130
C     YI=INITIAL MOLE FRACTION OF GASES AT Z=0                          IT 131
C     ALPA=COMPONENT IDENTIFICATION                                     IT 132
C     ICODE=0 (GAS),    =1 (SOLID)                                      IT 133
C     DELH=ENTHALPY OF FORMATION AT 298 OK                              IT 134
C                                                                       IT 135
      READ13,(FW(I),YI(I),ALPA(I),ICODE(I),DELH(I),I=1,NS)              IT 136
      SUM=0.                                                            IT 137
      DO 126 I=1,NC                                                     IT 138
  126 SUM=SUM+YI(I)                                                     IT 139
```

```
      DO 127 I=1,NC
  127 YI(I)=YI(I)/SUM
      YI(NS)=YI(NS)/SUM
      RKSS=ZL/HI
      SRSS=HS/HSIMPI
      JRKSS=(RKSS*10.0+5.0)/10.0
      JSRSS=(SRSS*10.0+5.0)/10.0
C
C         INITIALIZATION OF PARAMETERS
C
      CALL ERRSET (207,256,-1,1)
      CALL ERRSET (208,256,-1,1)
      CALL ERRSET (209,256,-1,1)
      NO=1
      NN4=NC+4
      KOUNT=1
      TP1=T(1)
      K7=1
   40 N=1
      TEST=500.0
      W=WI/EPS
      DO31 I=1,NC
      Y(I)=YI(I)
   31 CONTINUE
      H=HI
      KN=1
      XAXIS(1)=0.0
      YAXIS(1)=0.0
   50 Z(1)=0.0
C
C         RUNGE-KUTTA ANALYSIS FOR TWO POINT BOUNDARY VALUE PROBLEM
C         (TO AND TL KNOWN, DT/DZ AT Z=0 ASSUMED) INVOLVING A NON-LINEAR
C         SECOND ORDER DIFFERENTIAL EQUATION (ENERGY BALANCE)
C         FIRST POINT ESTIMATED BY EULER METHOD
C
```

```
55    IF(N.GT.1)GO TO 101
   56 T(N+1)=H*DT(N)+T(N)
      DT(N+1)=DT(N)
      GO TO 138
  101 TC=T(N)
      TPREV=T(N-1)
      THETA=T(N)
  102 DTC=DT(N)
      DTHETA=DT(N)
      MX=1
      IF(DT(1).GT.0.0)GO TO103
 1109 DT(1)=DT(1)/((1.0+0.5*((TL-TCHECK)/TL))*2.0)
      GO TO 40
 103  ARK = H*DTC
  888 TNOW=TC
      RANKIN=TC+460.0
      TVAR=RANKIN/1.8
      DELZ=H
      GO TO (58,60,61),KEY
   58 AVGFW=0.0
      DO59 I=1,NC
      AVCFW=AVGFW+Y(I)*FW(I)
   59 CONTINUE
      GO TO 104
   60 IF(KOUNT.EQ.2)GO TO 710
C
C        USE MOLFRA TO GENERATE MOLE FRACTION, AVERAGE MOLECULAR WEIGHT
C        AND REACTION RATE EXPRESSION FOR USE IN TEMPRE
C        TRANSFER VALUES TABULATED IN MOLFRA FOR A SPECIFIC TEMPERATURE
C
      CALL MOLFRA(KOUNT,KPT3,K6,TP1)
      KOUNT=2
      KMAX=KPT3
      NN5=NN4+1
  710 DO 707 KL=2,NN5
```

```
      CALL OMEGA(TVAR,TABLE(1,1),TABLE(1,KL),KMAX,NDIM1,VARY)
                  IF(KL.GT.2)GO TO 704
                  REACT=VARY
                  GO TO 707
  704             IF(KL.GT.3)GO TO 705
                  AVGFW=VARY
                  GO TO 707
  705             IF(KL.GT.4)GO TO 708
                  W=VARY
                  GO TO 707
  708             Y(KL-4)=VARY
      GCAY=Y(KL-4)
      IF(GCAY.GT.0.0)GO TO 7070
  706             Y(KL-4)=1.0E-10
 7070 BRIAN1=ABS(TVAR-T(2))
      IF(BRIAN1.GT.1.0)GO TO 707
      KYCOMP=KL-4
      YCOMP(KYCOMP,1)=Y(KYCOMP)
  707 CONTINUE
      GOTO104
C
C         USE KINET TO GENERATE MOLE FRACTION, AVERAGE MOLECULAR WEIGHT
C         AND REACTION RATE EXPRESSION FOR USE IN TEMP
C         TRANSFER VALUES CALCULATED FOR A SPECIFIC TEMPERATURE
C
   61 DELZ=H
      CALL KINET(TP1,TVAR,DELZ,KN,K7,DTC,REACT,W,KPT3,AVGFW)
      KN=2
      KMAX=KPT3
      K7=2
      IF(BRIAN1.GT.1.0)GO TO 104
      DO1040 IOU=1,NS
      ICK=IOU+4
      YCOMP(IOU,1)=TABLE(1,ICK)
 1040 CONTINUE
```

```
C
C        USE PROPT TO GENERATE NEEDED PHYSICAL PROPERTY DATA
C        (HEAT CAPACITY,GAS AND CHAR CONDUCTIVITY AND DERIVATIVE OF
C        OVERALL THERMAL CONDUCTIVITY VALUES)
C
 104  CALL PROPT(TVAR,JCHAR,KODE,NDATA,XTKE,ZOMGA,NDIM3,CPMX,CDO,DCDO)
      JCHAR=2
      GASCP=(CPMX/AVGFW)*RR
      GCAAT=ABS(T(N)-TC)
      IF(GCAAT.GT.0.00001)GO TO 107
  106 CAPAC(N)=GASCP
      CAPAC(1)=CAPAC(2)
  107 GO TO(62,63,63),KEY
   62 GROUP=(W*EPS*GASCP/CDO)-(DCDO*DTC/CDO)
      GO TO 65
   63 GROUP=(W*EPS*GASCP/CDO)-(DCDO*DTC/CDO)+(REACT/CDO)
   65 DA=ARK*GROUP
      TPREV=TC
 105  GO TO (110,120,130,135),MX
C
C        CALCULATE PARAMETERS IN FORTH ORDER RUNGE-KUTTA ANALYSIS
C
 110  A1=ARK
      DA1=DA
      TC=THETA+0.5*A1+0.125*DA1*H
      DTC=DTHETA+0.5*DA1
      MX=2
C
C        IF TC BECOMES NEGATIVE READJUST ASSUMED VALUE OF DT/DZ AT Z=0
C        AND RETURN TO INITIALIZATION STEP
C
      IF(TC)133,133,103
 120  A2=ARK
      DA2=DA
      TC=THETA+0.5*A2+0.125*DA2*H
```

```
      DTC=DTHETA+0.5*DA2
      MX=3
      IF(TC)133,133,103
 130  A3=ARK
      DA3=DA
      TC=THETA+A3+0.5*DA3*H
      DTC=DTHETA+DA3
      MX=4
      IF(TC)133,133,103
 133  PRINT 2222,TC
 2222 FORMAT(1H0,3HTC=,1X,F15.6,8X,8HNEGATIVE)
      DT(1)=DT(1)*0.5
      GO TO 40
 135  A4=ARK
      DA4=DA
C
C        CALCULATE NEXT TEMPERATURE AND DERIVATIVE POINT USING FOURTH
C        ORDER RUNGE-KUTTA EQUATIONS
C
      T(N+1)=T(N)+(1.0/6.0)*(DA1+DA2+DA3)*H + A1
      DT(N+1)=DT(N)+(1.0/6.0)*(DA1+2.0*DA2+2.0*DA3+DA4)
C
C        TEST NEW TEMPERATURE POINT IF GREATER THAN  500 OF(2000-3000 OF
C        SURFACE TEMPERATURE) ADJUST DT/DZ AT Z=0 AND RETURN TO
C        INITIALTION STEP IF NEW TEMPERATURE POINT IS NAGATIVE RETURN TO
C        INITIALIZATION STEP. AFTER ADJUST DERIVATIVE (DT/DZ AT T=0)
C
      TLIMIT=TL+500.0
      ANDY1=T(N+1)
      IF(ANDY1.GT.TLIMIT)GO TO 6000
 5000 IF(ANDY1.GT.0.0)GO TO 138
 136  PRINT 137, T(N+1)
 137  FORMAT(1H0,7HT(N+1)=,1X,F15.6,8X,8HNEGATIVE)
      DT(1)=DT(1)*0.5
      GO TO 40
```

```
6000 PRINT 8000,T(N+1),TLIMIT
     PRINT8001,DT(N+1),N
8000 FORMAT(1H0,7HT(N+1)=,1X,F15.6,4X,8HEXCEEDED,1X,15HTLIMIT VALUE OF
    1,1X,F15.6)
8001 FORMAT(1H0,8HDT(N+1)=,1X,F20.5,8X,2HN=,1X,I6)
     IJKL=IJKL+1
     IF(IJKL.GE.10)GOTO30
     TRATIO=(TL-T(N+1))/TL
     DT(1)=DT(1)*(1.0+0.5*TRATIO)
     TCHECK=T(N+1)
     IF(DT(1))10,10,40
 138 Z(N+1)=Z(N)+H
     XAXIS(N+1)=Z(N+1)/ZL
     IF(N.EQ.201)GOTO140
     YAXIS(N+1)=(T(N+1)-T(1))/(TL-T(1))
     GOTO144
 140 DO141N=1,201
     PRINT142,N,XAXIS(N),T(N),CAPAC(N)
 142 FORMAT(1H0,I6,3F10.4)
 141 CONTINUE
     DT(1)=DT(200)
     T(1)=T(200)
     DT(2)=DT(201)
     T(2)=T(201)
     N=2
     GOTO101
C
C        IF NON-NEGATIVE AND LESS THAN  500 OF, TEST FOR CHAR DISTANCE
C
C        IF CHAR DISTANCE LESS THAN CHAR THICKNESS GO TO NEXT STEP IN
C        RUNGE-KUTTA ANALYSIS
C        IF CHAR DISTANCE EQUALS CHAR THICKNESS TEST FOR T-FINAL
C        (CALCULATED) VS (ACTUAL)
C
 144 ANDY2=ABS(ZL-Z(N+1))
```

```
      IF(ANDY2.LE.0.00001)GO TO 150
  145 N=N+1
      GO TO 101
  150 QT(NO)=T(N+1)
      QDT(NO)=DT(1)
      CAPAC(N+1)=CAPAC(N)
      PRINT 1501,DT(1),T(N+1)
 1501 FORMAT(1H0,14HINITIAL SLOPE=,F15.5,4X,18HFINAL TEMPERATURE=,F15.5)
      DIFF=ABS(TL-T(N+1))
      STEP=(10.0*(ZL/HI)+5.0)/10.0
      LSTEP=STEP
      LCHAR=LSTEP + 1
C
C        IF T-FINAL (CALCULATED) IS NOT EQUAL TO +,-1 OF T-FINAL
C        (ACTUAL) ADJUST INITIAL SLOPE AND RETURN TO INITIALIZATION STEP
C        IF T-FINAL (CALCULATED) IS +,-1 OF T-FINAL (ACTUAL),STORE THE
C        TEMPERATURE PROFILE
C
      IF(DIFF-25.)155,155,153
  152 TRATIO=(TL-T(N+1))/TL
      DT(1)=DT(1)*(1.0+0.9*TRATIO)
      TCHECK=T(N+1)
      NO=NO+1
      GO TO 40
  153 IF(NO.LE.1)GO TO 152
  154 RATIO=(TL-QT(NO))/(QT(NO-1)-QT(NO))
      RDASH=RATIO*(QDT(NO-1)-QDT(NO))
      DT(1)=DT(1)+RDASH
      NO=NO+1
      GO TO 40
C
C
C        CALCULATION OF PRESSURE PROFILE USING SIMPSON RULE INTEGRATION
C        OF MOMENTUM EQUATION (WITH RESULTS FROM ENERGY EQUATION)
C
```

```
C                                                                       IT 385
  155 DELTT=(TL-T(1))                                                   IT 386
C                                                                       IT 387
C        INITIALIZATION STATEMENTS. NOTE SINCE P' AT THE CHAR SURFACE IS  IT 388
C        SPECIFIED, INTEGRATION METHOD WILL PROCEED FROM Z=L TO Z=0.    IT 389
C                                                                       IT 390
      SIMP1=0.0                                                         IT 391
      SIMP2=0.0                                                         IT 392
      SIMP3=0.0                                                         IT 393
      SIMP4=0.0                                                         IT 394
      ZS=ZL/HS                                                          IT 395
C                                                                       IT 396
C        DEFINE JS AS THE TOTAL NO. OF SLICES IN THE CHAR               IT 397
C                                                                       IT 398
      JS=(10.0*ZS+5.0)/10.0                                             IT 399
      LS=JS+1                                                           IT 400
      WFLUX(1)=WI/EPS                                                   IT 401
      ZX(LS)=ZL                                                         IT 402
      TP(LS)=TL                                                         IT 403
      P(LS)=PL                                                          IT 404
      ACON1=2.6693*10.**(-3)                                            IT 405
      ACON5=2.42/3600.                                                  IT 406
      ACON7=778.16/32.2                                                 IT 407
      DO 260 N=1,JS                                                     IT 408
      NBAR=N-1                                                          IT 409
      HN=NBAR                                                           IT 410
      LO=LS-NBAR                                                        IT 411
      ZX(LO)=ZX(LS)-HN*HS                                               IT 412
      ZSIMP=HS/HSIMPI                                                   IT 413
      MS=(10.0*ZSIMP+5.0)/10.0                                          IT 414
C                                                                       IT 415
C        DEFINE MP AS THE TOTAL NO. OF POINTS OVER WHICH SIMPSON'S RULE IT 416
C        IS TO BE APPLIED                                               IT 417
C                                                                       IT 418
      MP=MS+1                                                           IT 419
```

```
      ZY(MP)=ZX(LO)
      DO 240 M=1,MP
      MBAR=M-1
      HM=MBAR
      MO=MP-MBAR
      ZY(MO)=ZY(MP)-HM*HSIMPI
      ZVAR=ZY(MO)
      ITEMP=LCHAR
C
C        FOR A SPECIFIED CHAR DISTANCE (STARTING AT Z=L AND PROCEEDING
C        BACK TO Z=0) OBTAIN THE CORRESPONDING TEMPERATURE FROM THE
C        TEMPERATURE PROFILE
C
      CALL OMEGA(ZVAR,Z,T,ITEMP,NDIM2,TVIS)
  205 TK=(TVIS+460.0)/1.8
  209 DO 216 I=1,NC
      TKE=(1.0/EK(I))*TK
        IMAX=NDATA
C
C        FOR THE VALUE OF THE TEMPERATURE FIND THE CORRESPONDING
C        COLLISION INTEGRAL TO CALCULATE THE PURE GAS VISCOSITY
C        CALCULATE VISCOSITY OF GAS MIXTURE USING METHOD OF WILKE-
C        JOHNSON
C
  211 CALL OMEGA(TKE,XTKE,ZOMGA,IMAX,NDIM3,OMGA)
      ACON2=FW(I)*TK
      VIS(I)=ACON1*SQRT(ACON2)/(SIG(I)**2)*OMGA
  216 CONTINUE
      IF(NC.LE.1)GOTO238
  220 GO TO(222,221,221),KEY
  221 TVAR=TK
      NN5=NN4+1
      DO217 KL=2,NN5
C
C        INTERPOLATE FOR DATA GENERATED IN MOLFRA AND/OR KINET FROM
```

```
C          STORED TABLE AT THE SPECIFIC CHAR DISTANCE IN QUESTION               IT 455
C                                                                               IT 456
      CALL OMEGA(TVAR,TABLE(1,1),TABLE(1,KL),KMAX,NDIM1,VARY)                   IT 457
                    IF(KL.GT.2)GO TO 214                                        IT 458
                    REACT=VARY                                                  IT 459
                    GO TO 217                                                   IT 460
  214               IF(KL.GT.3)GO TO 215                                        IT 461
                    AVGFW=VARY                                                  IT 462
                    GO TO 217                                                   IT 463
  215               IF(KL.GT.4)GO TO 219                                        IT 464
                    W=VARY                                                      IT 465
                    GO TO 217                                                   IT 466
  219               Y(KL-4)=VARY                                                IT 467
                    ANDY3=Y(KL-4)                                               IT 468
                    IF(ANDY3.GT.0.0)GO TO 2170                                  IT 469
  218               Y(KL-4)=1.0E-10                                             IT 470
 2170 IF(M.GT.1)GO TO 217                                                       IT 471
 2171 WFLUX(LO)=W                                                               IT 472
      KYCOMP=KL-4                                                               IT 473
      YCOMP(KYCOMP,LO)=Y(KYCOMP)                                                IT 474
  217 CONTINUE                                                                  IT 475
  222 VMIX=0.0                                                                  IT 476
      GO TO (2220,2221,2221),KEY                                                IT 477
 2220 WFLUX(LO)=WI/EPS                                                          IT 478
 2221 DO 237 J=1,NC                                                             IT 479
      TERM=1.0                                                                  IT 480
 223  DO 230 L=1,NC                                                             IT 481
      IF(L.NE.J)GO TO 226                                                       IT 482
 225  GO TO 230                                                                 IT 483
C                                                                               IT 484
C          CALCULATE THE VISCOSITY OF THE GAS MIXTURE                           IT 485
C                                                                               IT 486
  226 ACON4=VIS(J)/VIS(L)                                                       IT 487
      ACON20=SQRT(SQRT(FW(L)/FW(J)))                                            IT 488
      TOPV=(1.+SQRT(ACON4)*ACON20)**2                                           IT 489
```

```
  227 ACON8=1.+FW(J)/FW(L)                                                IT 490
      BOTV=2.*SQRT(2.)*SQRT(ACON8)                                        IT 491
 228  PHIV=TOPV/BOTV                                                      IT 492
      TERM=TERM+PHIV*(Y(L)/Y(J))                                          IT 493
 230  CONTINUE                                                            IT 494
      VMIX=VMIX+(VIS(J)/TERM)                                             IT 495
 237  CONTINUE                                                            IT 496
      GO TO 2380                                                          IT 497
  238 VISCOS=VIS(I)*ACON5                                                 IT 498
      GO TO 239                                                           IT 499
 2380 VISCOS=VMIX*ACON5                                                   IT 500
  239 TT(MO)=(TVIS/AVGFW)*W**2                                            IT 501
      PROD(MO)=TVIS*VISCOS*W/AVGFW                                        IT 502
      CALL OMEGA(TVIS,T,CAPAC,ITEMP,NDIM2,CPBAR)                          IT 503
      PRODCP(MO)=CPBAR*W                                                  IT 504
      GO TO(240,2401,2401),KEY                                            IT 505
 2401 PRODR(MO)=REACT                                                     IT 506
  240 CONTINUE                                                            IT 507
C                                                                         IT 508
C        STORE VALUES OF THE OUTPUT PARAMETERS AT INTERVALS SPECIFIED     IT 509
C        BY JS, THE GRID SIZE                                             IT 510
C                                                                         IT 511
      ZX(LO-1)=ZX(LO)-HS                                                  IT 512
      TP(LO-1)=TT(1)*AVGFW/W**2                                           IT 513
      DELTF=TP(LO)-TP(LO-1)                                               IT 514
C                                                                         IT 515
C        INTEGRATE USING SIMPSON RULE TO GET P AND QL                     IT 516
C                                                                         IT 517
      SUM1=0.0                                                            IT 518
      SUM2=0.0                                                            IT 519
      SUM3=0.0                                                            IT 520
      SUM4=0.0                                                            IT 521
      SUM5=0.0                                                            IT 522
      SUM6=0.0                                                            IT 523
      SUM7=0.0                                                            IT 524
```

```
      SUM8=0.0                                                          IT 525
      MEVEN=MP-1                                                        IT 526
      DO255 KP=2,MEVEN,2                                                IT 527
      SUM1=SUM1+4.0*PROD(KP)                                            IT 528
      SUM3=SUM3+4.0*TT(KP)                                              IT 529
 254  SUM5=SUM5+4.0*PRODCP(KP)                                          IT 530
      GO TO(255,2540,2540),KEY                                          IT 531
 2540 SUM7=SUM7+4.0*PRODR(KP)                                           IT 532
 255  CONTINUE                                                          IT 533
      MODD=MP-2                                                         IT 534
      DO256 KP=3,MODD,2                                                 IT 535
      SUM2=SUM2+2.0*PROD(KP)                                            IT 536
      SUM4=SUM4+2.0*TT(KP)                                              IT 537
 257  SUM6=SUM6+2.0*PRODCP(KP)                                          IT 538
      GO TO(256,2570,2570),KEY                                          IT 539
 2570 SUM8=SUM8+2.0*PRODR(KP)                                           IT 540
 256  CONTINUE                                                          IT 541
      SIMP1=((HSIMPI/3.0)*(PROD(1)+PROD(MP)+SUM1+SUM2)+SIMP1)*EPS**2    IT 542
      SIMP2=((HSIMPI/3.0)*(TT(1)+TT(MP)+SUM3+SUM4)+SIMP2)*EPS           IT 543
      P(LO-1)=SQRT(PL**2+(2.*RR)*(778.16/32.2)*(ALPHA*SIMP1+BETA*SIMP2))IT 544
      SIMP3=DELTF*HSIMPI/(HS*3.0)*(PRODCP(1)+PRODCP(MP)+SUM5+SUM6)+SIMP3IT 545
      GO TO(260,258,258),KEY                                            IT 546
  258 SIMP4=DELTF*HSIMPI/(HS*3.0)*(PRODR(1)+PRODR(MP)+SUM7+SUM8)+SIMP4  IT 547
  260 CONTINUE                                                          IT 548
      GO TO(2600,2601,2601),KEY                                         IT 549
 2600 QL=EPS*SIMP3                                                      IT 550
      GO TO 2603                                                        IT 551
 2601 QL=EPS*(SIMP3+SIMP4)                                              IT 552
C                                                                       IT 553
C        PRINT INPUT PARAMETERS                                         IT 554
C                                                                       IT 555
 2603 PRINT 597                                                         IT 556
 597  FORMAT(1H1/////////)                                              IT 557
      GO TO(5980,5981,5982),KEY                                         IT 558
 5980 PRINT598                                                          IT 559
```

```
598  FORMAT(11X,59H                                       FROZEN FLOW MODEL -  IT 560
    1 TEMPRE/)                                                                 IT 561
     GO TO 5989                                                                IT 562
5981 PRINT5983                                                                 IT 563
5983 FORMAT(11X,61H                                  EQUILIBRIUM FLOW MODEL    IT 564
    1 - TEMPRE/)                                                               IT 565
     GO TO 5989                                                                IT 566
5982 PRINT 5984                                                                IT 567
5984 FORMAT(11X,63H                             NON-EQUILIBRIUM FLOW MOD       IT 568
    1EL - TEMPRE/)                                                             IT 569
5989 GO TO(5985,5986),MTYPE                                                    IT 570
5985 PRINT 599                                                                 IT 571
 599 FORMAT(12X,51H                                           EXPERIMENTAL/    IT 572
    1/)                                                                        IT 573
     GO TO 5991                                                                IT 574
5986 PRINT 5990                                                                IT 575
5990 FORMAT(12X,51H                                            THEORETICAL/    IT 576
    1/)                                                                        IT 577
5991 PRINT600,T(1),NC                                                          IT 578
600  FORMAT(18X,26HINITIAL TEMPERATURE (OF) =,1X,F7.1,14X,26HNUMBER OF         IT 579
    1GAS COMPONENTS =,1X,I2/)                                                  IT 580
     PRINT601,DT(1)                                                            IT 581
601  FORMAT(18X,23HINITIAL SLOPE (OF/FT) =,1X,F10.1,14X,29HNO.  COMPONE        IT 582
    1NT  MOLE/MOLE GAS/)                                                       IT 583
     PRINT602,TL,ALPA(1),YI(1)                                                 IT 584
602  FORMAT(18X,24HFINAL TEMPERATURE (OF) =,1X,F9.1,15X,1H1,3X,A4,6X,F1        IT 585
    10.4/)                                                                     IT 586
     PRINT603,PL,ALPA(2),YI(2)                                                 IT 587
603  FORMAT(18X,25HFINAL PRESSURE (LB/FT2) =,1X,F8.1,15X,1H2,3X,A4,6X,F        IT 588
    110.4/)                                                                    IT 589
     PRINT604,WI,ALPA(3),YI(3)                                                 IT 590
604  FORMAT(18X,24HMASS FLUX (LB/FT2-SEC) =,1X,F9.4,15X,1H3,3X,A4,6X,F1        IT 591
    10.4/)                                                                     IT 592
     PRINT605,ZL,ALPA(4),YI(4)                                                 IT 593
605  FORMAT(18X,21HCHAR THICKNESS (FT) =,1X,F12.4,15X,1H4,3X,A4,6X,F10.        IT 594
```

```
     14/)
      PRINT606,EPS,ALPA(5),YI(5)
  606 FORMAT(18X,15HCHAR POROSITY =,1X,F18.2,15X,1H5,3X,A4,6X,F10.4/)
      PRINT607,ALPA(6),YI(6)
  607 FORMAT(18X,50H                                              6,3
     1X,A4,6X,F10.4/)
      PRINT6080,ALPA(7),YI(7)
 6080 FORMAT(18X,50HPERMEABILITY COEFFICIENTS                     7,3
     1X,A4,6X,F10.4/)
      PRINT608,ALPHA,ALPA(8),YI(8)
  608 FORMAT(18X,19H     ALPHA (FT-2) =,1X,E14.2,15X,1H8,3X,A4,6X,F10.4/
     1)
      PRINT609,BETA,ALPA(9),YI(9)
  609 FORMAT(18X,18H     BETA (FT-1) =,1X,E15.2,15X,1H9,3X,A4,6X,F10.4/)
      PRINT610,ALPA(10),YI(10)
  610 FORMAT(18X,50H                                             10,3
     1X,A4,6X,F10.4/)
      PRINT611,ALPA(11),YI(11)
  611 FORMAT(18X,50H                                             11,3
     1X,A4,6X,F10.4/)
      PRINT612,JRKSS,ALPA(12),YI(12)
  612 FORMAT(18X,23HRUNGE-KUTTA STEP SIZE =,1X,I10,14X,2H12,3X,A4,6X,F10
     1.4/)
      PRINT613,JSRSS,ALPA(13),YI(13)
  613 FORMAT(18X,25HSIMPSONS RULE STEP SIZE =,1X,I8,14X,2H13,3X,A4,6X,F1
     10.4/)
      PRINT586
  586 FORMAT(1H1)
C
C         PRINT OUTPUT PARAMETERS CORRESPONDING TO JS, GRID SIZE
C
      IKE=1
      MIKE=5
      LIKE=1
 2602 PRINT 597
```

```
      GO TO(2660,2661,2662),KEY
 2660 PRINT598
      GO TO 2663
 2661 PRINT5983
      GO TO 2663
 2662 PRINT 5984
 2663 GO TO(2664,2665),MTYPE
 2664 PRINT 599
      GO TO 261
 2665 PRINT 5990
  261 IF(LIKE.GT.1)GO TO 265
      PRINT2650,DELTT
 2650 FORMAT(35X,23HTEMPERATURE DROP (OF) =,1X,F20.1/)
      DELP=(P(1)-PL)
      PRINT2651,DELP
 2651 FORMAT(35X,24HPRESSURE DROP (LB/FT2) =,1X,F19.1/)
      PRINT2652,QL
 2652 FORMAT(35X,33HSURFACE HEAT FLUX (BTU/FT2-SEC) =,1X,F10.2//)
 265  PRINT2720,(ZX(KK),KK=IKE,MIKE)
 2720 FORMAT(14X,15HCHAR DEPTH (FT),6X,5F13.4)
      PRINT2721,(TP(KK),KK=IKE,MIKE)
 2721 FORMAT(14X,16HTEMPERATURE (OF),5X,5F13.1)
      PRINT2722,(P(KK),KK=IKE,MIKE)
 2722 FORMAT(14X,17HPRESSURE (LB/FT2),4X,5F13.1)
      PRINT2723,(WFLUX(KK),KK=IKE,MIKE)
 2723 FORMAT(14X,21HMASS FLUX(LB/FT2-SEC),5F13.4/)
      PRINT2724
 2724 FORMAT(14X,66H  GAS COMPONENT                        COMPOSITION (
     1MOLE/MOLE GAS)/)
      GO TO(2726,2727,2727),KEY
 2726 DO2728 KICK=1,LS
      DO2728LL=1,NS
      YCOMP(LL,KICK)=YI(LL)
 2728 CONTINUE
 2727 DO2729LL=1,NS
```

```
      YCOMP(LL,1)=YI(LL)                                               IT 665
      PRINT2725,ALPA(LL),(YCOMP(LL,KK),KK=IKE,MIKE)                    IT 666
 2725 FORMAT(18X,A4,11X,5E13.4)                                        IT 667
 2729 CONTINUE                                                         IT 668
      IF(MIKE.GE.LS)GO TO 2800                                         IT 669
      LIKE=LIKE+1                                                      IT 670
      MIKE=MIKE+5                                                      IT 671
      IKE=IKE+5                                                        IT 672
      GO TO 2602                                                       IT 673
 2800 PRINT 586                                                        IT 674
 278  GO TO 30                                                         IT 675
  300 STOP                                                             IT 676
      END                                                              IT 677
```

Listing B-2. Non-Iterative TEMPRE (Main) Program.

```
C
C
C        TEMPRE - GENERAL NON-ITERATIVE SYSTEM ANALYSIS FOR STUDY OF THE
C        ENERGY AND MASS TRANSFER IN THE CHAR ZONE OF ABLATORS
C
C
      DIMENSION ICODE(20),ALPA(20),AA(20,6),
     1  S1(4),S2(4),S3(4),S4(4),S5(4),A11(4),A22(4),A33(4),A44(4),A55(4)
      DIMENSION AI(20),BI(20),CI(20),DI(20),EI(20),FI(20),GI(20),
     1  AII(20),BII(20),CII(20),DII(20),EII(20),FII(20),GII(20),FW(20),
     2   YI(20),EK(20),SIG(20),Y(20),DELH(20)
      DIMENSION RSC(15,15),PSC(15,15),NREX(15,15),NPEX(15,15),AF(30),
     1SF(20),AFF(20),AR(20),SR(20),AFR(20),EQN(20,12),TABLE(70,20)
      DIMENSION T(300),DT(300),XTKE(100),ZOMGA(100),XN(300),FN(300),
     1  TT(300),TP(300),CP(20),COND(20),CV(20),VIS(20),XAXIS(300),
     2  YAXIS(300),Z(300),PROD(300),CAPAC(300),
     3  PRODR(300),PRODCP(300),ZX(300),P(300),ZY(300)
      DIMENSION WFLUX(10),YCOMP(20,10)
      COMMON NC,NS,MM,WI,PL,RR,TZERO,DELTK,ICODE,ALPA,AA,S1,S2,S3,
     1   S4,S5,A11,A22,A33,A44,A55
      COMMON AI,BI,CI,DI,EI,FI,GI,AII,BII,CII,DII,EII,FII,GII,FW,YI
      COMMON EK,SIG,EPS,Y,DELH
      COMMON RSC,PSC,NREX,NPEX,AF,SF,AFF,AR,SR,AFR,EQN,TABLE
C
C        READ INPUT PARAMETERS
C
C     NC=NO. OF GAS COMPONENTS
C     NS=NO. OF CONDENSED PLUS GAS COMPONENTS
C     MM=NO. OF ELEMENTS
C     KODE=1 CONDUCTIVITY OF CHAR WITH GAS IN PORES
C     KODE=2 CONDUCTIVITY OF CHAR WITH PORES EVACUATED
C
   10 READ11,NC,NS,MM,KODE
C
```

```
C     PL=PRESSURE AT Z=L (LB/FT2)                                        NIT 035
C     RR=GAS CONSTANT (1.987 BTU/LB-MOLE/OR)                             NIT 036
C     TZERO=REFERENCE TEMPERATURE (298.2 OK)                             NIT 037
C     DELTK=TEMPERATURE INCREMENT USED TO CALCULATE DKC/DT (OK)          NIT 038
C                                                                        NIT 039
      READ 12,PL,RR,TZERO,DELTK                                          NIT 040
      DO15 J=1,MM                                                        NIT 041
C     S1 THRU S5=EMPIRICAL CONSTANTS FOR HEAT CAPACITY OF ELEMENTS       NIT 042
C                                (UP TO 1000 OK)                         NIT 043
C                                                                        NIT 044
      READ14,S1(J),S2(J),S3(J),S4(J),S5(J)                               NIT 045
C                                                                        NIT 046
C     A11 THRU A55=EMPIRICAL CONSTANTS FOR HEAT CAPACITY OF ELEMENTS     NIT 047
C                                (ABOVE 1000 OK)                         NIT 048
C                                                                        NIT 049
      READ14,A11(J),A22(J),A33(J),A44(J),A55(J)                          NIT 050
   15 CONTINUE                                                           NIT 051
      DO16 I=1,NS                                                        NIT 052
C                                                                        NIT 053
C     AA=FORMULA NUMBER                                                  NIT 054
C                                                                        NIT 055
      READ14,(AA(I,J),J=1,MM)                                            NIT 056
C                                                                        NIT 057
C     AI THRU GI=EMPIRICAL CONSTANTS FOR HEAT CAPACITY (ABOVE 1000 OK)   NIT 058
C                                                                        NIT 059
      READ14,AI(I),BI(I),CI(I),DI(I),EI(I),FI(I),GI(I)                   NIT 060
C                                                                        NIT 061
C     AII THRU GII=EMPIRICAL CONSTANTS FOR HEAT CAPACITY (UP TO 1000 OK) NIT 062
C                                                                        NIT 063
      READ14,AII(I),BII(I),CII(I),DII(I),EII(I),FII(I),GII(I)            NIT 064
   16 CONTINUE                                                           NIT 065
C                                                                        NIT 066
C     EK=POTENTIAL PARAMETER/BOLTZMAN CONSTANT                           NIT 067
C     SIG=COLLISION DIAMETER (OA)                                        NIT 068
C                                                                        NIT 069
```

```
      READ17,(EK(I),SIG(I),ALPA(I),I=1,NC)                               NIT 070
C                                                                        NIT 071
C     EPS=CHAR POROSITY                                                  NIT 072
C                                                                        NIT 073
      READ18,EPS                                                         NIT 074
   11 FORMAT(4I6)                                                        NIT 075
   12 FORMAT(4F15.6)                                                     NIT 076
   14 FORMAT(7E10.4)                                                     NIT 077
   17 FORMAT(2F15.5,A4)                                                  NIT 078
   18 FORMAT(F15.5)                                                      NIT 079
C                                                                        NIT 080
C     ZL=CHAR THICKNESS (FT)                                             NIT 081
C     HI=RUNGE-KUTTA INCREMENT SIZE (FT)                                 NIT 082
C     HSIMPI=SIMPSON RULE INCREMENT SIZE (FT)                            NIT 083
C                                                                        NIT 084
   20 READ21,ZL,HI,HSIMPI,HS                                             NIT 085
C                                                                        NIT 086
C     ALPHA=VISCOUS COEFFICIENT IN DARCY EQUATION (1/FT)                 NIT 087
C     BETA=INERTIAL COEFFICIENT IN DARCY EQUATION (1/FT2)                NIT 088
C                                                                        NIT 089
      READ22,ALPHA,BETA                                                  NIT 090
C                                                                        NIT 091
C     NDATA=NO. OF XTKE VS. ZOMGA DATA POINTS                            NIT 092
C     NDIM1=NO. OF DIMENSIONED LOCATIONS FOR EQUILIBRIUM PROGRAM CALCULA NIT 093
C                             IN SUBPROGRAM OMEGA                        NIT 094
C     NDIM2=NO. OF DIMENSIONED LOCATIONS FOR TEMPERATURE-DISTANCE CALCUL NIT 095
C                             IN SUBPROGRAM OMEGA                        NIT 096
C     NDIM3=NO. OF DIMENSIONED LOCATIONS FOR PHYSICAL PROPERTY CALCULATI NIT 097
C                             IN SUBPROGRAM OMEGA                        NIT 098
C     KEY= 1 (FROZEN FLOW),  =2 (EQUILIBRIUM FLOW),  =3 (NON-EQUILIBRIUM NIT 099
C     MTYPE = TYPE OF PROBLEM                                            NIT 100
C        1 = EXPERIMENTAL                                                NIT 101
C        2 = THEORETICAL                                                 NIT 102
C                                                                        NIT 103
      READ23,NDATA,NDIM1,NDIM2,NDIM3,KEY,MTYPE                           NIT 104
```

```
C                                                                          NIT 105
C     XTKE=PRODUCT OF TEMPERATURE AND 1/EK VALUE                           NIT 106
C     ZOMGA=COLLISION INTEGRAL TABULATED VS XTKE                           NIT 107
C                                                                          NIT 108
      READ24,(XTKE(I),ZOMGA(I),I=1,NDATA)                                  NIT 109
C                                                                          NIT 110
C     EMIS=CHAR EMISSIVITY                                                 NIT 111
C     SIGMA=STEPHAN-BOLTZMAN CONSTANT (0.481 X 10-12 BTU/FT2-SEC-OF4)      NIT 112
C                                                                          NIT 113
      READ25,EMIS,SIGMA                                                    NIT 114
C                                                                          NIT 115
C     QPMIN=LOWER LIMIT ON THE HEAT OF PYROLYSIS(BTU/LB)                   NIT 116
C     QPINC=INCREMENT BY WHICH THE HEAT OF PYROLYSIS IS VARIED             NIT 117
C     QPMAX=UPPER LIMIT ON THE HEAT OF PYROLYSIS                           NIT 118
C                                                                          NIT 119
      READ26,QPMIN,QPINC,QPMAX                                             NIT 120
C                                                                          NIT 121
C     WIMIN=LOWER LIMIT ON THE GAS MASS FLUX(LBS/FT2-SEC)                  NIT 122
C     WIINC=INCREMENT BY WHICH THE GAS MASS FLUX IS VARIED                 NIT 123
C     WIMAX=UPPER LIMIT ON THE GAS MASS FLUX                               NIT 124
C                                                                          NIT 125
      READ26,WIMIN,WIINC,WIMAX                                             NIT 126
   21 FORMAT(4F10.0)                                                       NIT 127
   22 FORMAT(2F15.5)                                                       NIT 128
   23 FORMAT(6I6)                                                          NIT 129
   24 FORMAT(2F15.5)                                                       NIT 130
   25 FORMAT(F15.5,F20.5)                                                  NIT 131
   26 FORMAT(3F15.5)                                                       NIT 132
C                                                                          NIT 133
C     FW=MOLECULAR WEIGHT                                                  NIT 134
C     YI=INITIAL MOLE FRACTION OF GASES AT Z=0                             NIT 135
C     ALPA=COMPONENT IDENTIFICATION                                        NIT 136
C     ICODE=0 (GAS),    =1 (SOLID)                                         NIT 137
C     DELH=ENTHALPY OF FORMATION AT 298 OK                                 NIT 138
C                                                                          NIT 139
```

```
      READ27,(FW(I),YI(I),ALPA(I),ICODE(I),DELH(I),I=1,NS)                NIT 140
C                                                                         NIT 141
C     TO=TEMPERATURE AT THE SURFACE WHERE Z=0                             NIT 142
C                                                                         NIT 143
      READ 28,TO,TFMAX                                                    NIT 144
   27 FORMAT(20X,2E10.4,2X,A4,I6,1E10.4)                                  NIT 145
  28  FORMAT(2F15.5)                                                      NIT 146
C                                                                         NIT 148
C        INITIALIZATION OF PARAMETERS                                     NIT 149
C                                                                         NIT 150
      QP=QPMIN                                                            NIT 151
      WI=WIMIN                                                            NIT 152
      JCHAR=1                                                             NIT 153
      K6=1                                                                NIT 154
      K7=1                                                                NIT 155
 29   SUM=0.                                                              NIT 156
      DO 126 I=1,NC                                                       NIT 157
  126 SUM=SUM+YI(I)                                                       NIT 158
      DO 127 I=1,NC                                                       NIT 159
  127 YI(I)=YI(I)/SUM                                                     NIT 160
      YI(NS)=YI(NS)/SUM                                                   NIT 161
      T(1)=TO                                                             NIT 162
      RKSS = ZL/HI                                                        NIT 163
      SRSS = HS/HSIMPI                                                    NIT 164
      JRKSS=(RKSS*10.0+5.0)/10.0                                          NIT 165
      JSRSS=(SRSS*10.0+5.0)/10.0                                          NIT 166
   30 Z(1)=0.0                                                            NIT 167
      W=WI/EPS                                                            NIT 168
      QFLUX=QP*W                                                          NIT 169
      DO31 I=1,NC                                                         NIT 170
      Y(I)=YI(I)                                                          NIT 171
   31 CONTINUE                                                            NIT 172
      NN4=NC+4                                                            NIT 173
      KOUNT=1                                                             NIT 174
      TP1=T(1)                                                            NIT 175
```

```
   40 N=1
      H=HI
      KN=1
      XAXIS(1)=0.0
      YAXIS(1)=0.0
   50 Z(1)=0.0
C
C         RUNGE-KUTTA ANALYSIS FOR INITIAL SLOPE AND INITIAL TEMPERATURE
C         SPECIFIED AT THE BACK SURFACE.  NON-LINEAR, SECOND ORDER
C         DIFFERENTIAL EQUATION (ENERGY BALANCE).  FIRST POINT
C         ESTIMATED BY EULER METHOD
C
  101 TC=T(N)
      THETA=T(N)
      MX=1
  103 RANKIN=TC+460.0
      TVAR=RANKIN/1.8
C
C         USE PROPT TO GENERATE NEEDED PHYSICAL PROPERTY DATA
C         (HEAT CAPACITY,GAS AND CHAR CONDUCTIVITY AND DERIVATIVE OF
C         OVERALL THERMAL CONDUCTIVITY VALUES)
C
 104  CALL PROPT(TVAR,JCHAR,KODE,NDATA,XTKE,ZOMGA,NDIM3,CPMX,CDO,DCDO)
      JCHAR=2
 55   IF(N.GT.1)GO TO 1010
   56 DT(N)=QFLUX/CDO
      T(N+1)=H*DT(N)+T(N)
      DT(N+1)=DT(N)
      TPREV=T(1)
      GO TO 138
 1010 ARK = H*DTC
  888 TNOW=TC
      DELZ=H
      GO TO (58,60,61),KEY
C
```

```
   58 AVGFW=0.0
      AVGFW=AVGFW+Y(I)*FW(I)
   59 CONTINUE
      GO TO 1040
   60 IF(KOUNT.EQ.2)GO TO 710
C
C        USE MOLFRA TO GENERATE MOLE FRACTION, AVERAGE MOLECULAR WEIGHT
C        AND REACTION RATE EXPRESSION FOR USE IN TEMPRE
C        TRANSFER VALUES TABULATED IN MOLFRA FOR A SPECIFIC TEMPERATURE
C
      CALL MOLFRA(KOUNT,KPT3,K6,TP1)
      KMAX=KPT3
      NN5=NN4+1
  710 DO 707 KL=2,NN5
      CALL OMEGA(TVAR,TABLE(1,1),TABLE(1,KL),KMAX,NDIM1,VARY)
                  IF(KL.GT.2)GO TO 704
                  REACT=VARY
                  GO TO 707
  704             IF(KL.GT.3)GO TO 705
                  AVGFW=VARY
                  GO TO 707
  705             IF(KL.GT.4)GO TO 708
                  W=VARY
      GOTO707
  708             Y(KL-4)=VARY
      GCAY=Y(KL-4)
      IF(GCAY.GT.0.0)GO TO 7070
  706             Y(KL-4)=1.0E-10
 7070 BRIAN1=ABS(TVAR-T(2))
      IF(BRIAN1.GT.1.0)GO TO 707
      KYCOMP=KL-4
      YCOMP(KYCOMP,1)=Y(KYCOMP)
  707 CONTINUE
      GO TO 1040
C
```

```
C         USE KINET TO GENERATE MOLE FRACTION, AVERAGE MOLECULAR WEIGHT   NIT 246
C         AND REACTION RATE EXPRESSION FOR USE IN TEMP                     NIT 247
C         TRANSFER VALUES CALCULATED FOR A SPECIFIC TEMPERATURE            NIT 248
C                                                                          NIT 249
   61 DELZ=H                                                               NIT 250
      CALL KINET(TP1,TVAR,DELZ,KN,K7,DTC,REACT,W,KPT3,AVGFW)               NIT 251
      KN=2                                                                 NIT 252
      KMAX=KPT3                                                            NIT 253
      K7=2                                                                 NIT 254
      IF(BRIAN1.GT.1.0)GO TO 1040                                          NIT 255
      DO1045 IOU=1,NS                                                      NIT 256
      ICK=IOU+4                                                            NIT 257
      YCOMP(IOU,1)=TABLE(1,ICK)                                            NIT 258
 1045 CONTINUE                                                             NIT 259
 1040 GASCP=(CPMX/AVGFW)*RR                                                NIT 260
 3088 FORMAT(1H0,I2)                                                       NIT 261
      GCAAT=ABS(T(N)-TC)                                                   NIT 262
      IF(GCAAT.GT.0.00001)GO TO 107                                        NIT 263
  106 CAPAC(N)=GASCP                                                       NIT 264
      CAPAC(1)=CAPAC(2)                                                    NIT 265
  107 GO TO(62,63,63),KEY                                                  NIT 266
   62 GROUP=(W*EPS*GASCP/CDO)-(DCDO*DTC/CDO)                               NIT 267
      GO TO 65                                                             NIT 268
   63 GROUP=(W*EPS*GASCP/CDO)-(DCDO*DTC/CDO)+(REACT/CDO)                   NIT 269
   65 DA=ARK*GROUP                                                         NIT 270
      TPREV=TC                                                             NIT 271
  105 GO TO (110,120,130,135),MX                                           NIT 272
C                                                                          NIT 273
C         CALCULATE PARAMETERS IN FORTH ORDER RUNGE-KUTTA ANALYSIS         NIT 274
C                                                                          NIT 275
  110 A1=ARK                                                               NIT 276
      DA1=DA                                                               NIT 277
      TC=THETA+0.5*A1+0.125*DA1*H                                          NIT 278
      DTC=DTHETA+0.5*DA1                                                   NIT 279
      MX=2                                                                 NIT 280
```

```
      IF(TC)133,133,103                                                 NIT 281
  120 A2=ARK                                                            NIT 282
      DA2=DA                                                            NIT 283
      TC=THETA+0.5*A2+0.125*DA2*H                                       NIT 284
      DTC=DTHETA+0.5*DA2                                                NIT 285
      MX=3                                                              NIT 286
C                                                                       NIT 287
C        IF TC BECOMES NEGATIVE READJUST ASSUMED VALUE OF DT/DZ AT Z=0  NIT 288
C        AND RETURN TO INITIALIZATION STEP                              NIT 289
C                                                                       NIT 290
      IF(TC)133,133,103                                                 NIT 291
  130 A3=ARK                                                            NIT 292
      DA3=DA                                                            NIT 293
      TC=THETA+A3+0.5*DA3*H                                             NIT 294
      DTC=DTHETA+DA3                                                    NIT 295
      MX=4                                                              NIT 296
      IF(TC)133,133,103                                                 NIT 297
  133 PRINT 2222,TC                                                     NIT 298
 2222 FORMAT(1H0,3HTC=,1X,F15.6,8X,8HNEGATIVE)                          NIT 299
  135 A4=ARK                                                            NIT 300
      DA4=DA                                                            NIT 301
C                                                                       NIT 302
C        CALCULATE NEXT TEMPERATURE AND DERIVATIVE POINT USING FOURTH   NIT 303
C        ORDER RUNGE-KUTTA EQUATIONS                                    NIT 304
C                                                                       NIT 305
      T(N+1)=T(N)+(1.0/6.0)*(DA1+DA2+DA3)*H + A1                        NIT 306
      DT(N+1)=DT(N)+(1.0/6.0)*(DA1+2.0*DA2+2.0*DA3+DA4)                 NIT 307
C                                                                       NIT 308
C        TEST LAST TEMPERATURE CALCULATED AGAINST THE MAXIMUM VALUE.    NIT 309
C        IF TEMAX IS EXCEEDED,PRINT SUGGESTED ADJUSTMENT TO MASS FLUX   NIT 310
C        AND PROCEED TO NEXT JOB (OR CASE).  IF TEMAX IS NOT EXCEEDED   NIT 311
C        PROCEED TO CHAR DISTANCE CHECK TO SEE IF PROFILE IS COMPLETED. NIT 312
C                                                                       NIT 313
      IF(T(N+1)-TEMAX)138,136,136                                       NIT 314
  136 PRINT 586                                                         NIT 315
```

```
      PRINT 597
      PRINT 1361
 1361 FORMAT(14X,66HCALCULATED TEMPERATURE EXCEEDED THE ALLOWABLE LIMIT
     1FOR THIS MODEL/)
      PRINT 1362
 1362 FORMAT(16X,62HREDUCE THE MASS FLUX VALUE IN PROPORTION TO N DIVIDE
     1D BY JRKSS/)
      PRINT 1363,JRKSS,N
 1363 FORMAT(14X,23HRUNGE KUTTA STEP SIZE =,1X,I6,2X,27HLAST STEP IN ANA
     1LYSIS (N) =,1X,I6)
      PRINT 1364,TFMAX,T(N+1)
 1364 FORMAT(14X,21HMAXIMUM TEMPERATURE =,1X,F8.1,2X,24HLAST TEMPERATURE
     1 (N+1) =,1X,F9.1/)
      COR=(N+1)/JRKSS
      FLUXCO=COR*W
      PRINT 1365,FLUXCO
 1365 FORMAT(17X,50HSUGGESTED VALUE OF MASS FLUX TO COMPLETE PROFILE =,1
     1X,F9.3)
      GO TO 2722
 138  Z(N+1)=Z(N)+H
      ANDY2=ABS(ZL-Z(N+1))
      IF(ANDY2.LE.0.00001)GO TO 150
 145  N=N+1
      DTC=DT(N)
      DTHETA=DT(N)
      GO TO 101
  150 CAPAC(N+1)=CAPAC(N)
      TL=T(N+1)
      STEP=(10.0*(ZL/HI)+5.0)/10.0
      LSTEP=STEP
      LCHAR=LSTEP + 1
C
C         IF NON-NEGATIVE AND LESS THAN  500 OF, TEST FOR CHAR DISTANCE
C
C         IF CHAR DISTANCE LESS THAN CHAR THICKNESS GO TO NEXT STEP IN
```

```
C        RUNGE-KUTTA ANALYSIS                                             NIT 351
C        IF CHAR DISTANCE EQUALS CHAR THICKNESS, GO TO PRESSURE PROFILE   NIT 352
C      CALCULATION.                                                       NIT 353
C                                                                         NIT 354
C                                                                         NIT 355
C        CALCULATION OF PRESSURE PROFILE USING SIMPSON RULE INTEGRATION   NIT 356
C        OF MOMENTUM EQUATION (WITH RESULTS FROM ENERGY EQUATION)         NIT 357
C                                                                         NIT 358
C                                                                         NIT 359
      DELTT=(TL-T(1))                                                     NIT 360
C                                                                         NIT 361
C        INITIALIZATION STATEMENTS. NOTE SINCE P AT THE CHAR SURFACE IS   NIT 362
C        SPECIFIED, INTEGRATION METHOD WILL PROCEED FROM Z=L TO Z=0.      NIT 363
C        Z=L TO Z=0                                                       NIT 364
C                                                                         NIT 365
      SIMP1=0.0                                                           NIT 366
      SIMP2=0.0                                                           NIT 367
      SIMP3=0.0                                                           NIT 368
      SIMP4=0.0                                                           NIT 369
      ZS=ZL/HS                                                            NIT 370
C                                                                         NIT 371
C        DEFINE JS AS THE TOTAL NO. OF SLICES IN THE CHAR                 NIT 372
C                                                                         NIT 373
      JS=(10.0*ZS+5.0)/10.0                                               NIT 374
      LS=JS+1                                                             NIT 375
      WFLUX(1) = WI                                                       NIT 376
      ZX(LS)=ZL                                                           NIT 377
      TP(LS)=TL                                                           NIT 378
      P(LS)=PL                                                            NIT 379
      ACON1=2.6693*10.**(-3)                                              NIT 380
      ACON5=2.42/3600.                                                    NIT 381
      ACON7=778.16/32.2                                                   NIT 382
      DO 260 N=1,JS                                                       NIT 383
      NBAR=N-1                                                            NIT 384
      HN=NBAR                                                             NIT 385
```

```
      LO=LS-NBAR                                                        NIT 386
      ZX(LO)=ZX(LS)-HN*HS                                               NIT 387
      ZSIMP=HS/HSIMPI                                                   NIT 388
      MS=(10.0*ZSIMP+5.0)/10.0                                          NIT 389
C                                                                       NIT 390
C        DEFINE MP AS THE TOTAL NO. OF POINTS OVER WHICH SIMPSON'S RULE NIT 391
C        IS TO BE APPLIED                                               NIT 392
C                                                                       NIT 393
      MP=MS+1                                                           NIT 394
      ZY(MP)=ZX(LO)                                                     NIT 395
      DO 240 M=1,MP                                                     NIT 396
      MBAR=M-1                                                          NIT 397
      HM=MBAR                                                           NIT 398
      MO=MP-MBAR                                                        NIT 399
      ZY(MO)=ZY(MP)-HM*HSIMPI                                           NIT 400
      ZVAR=ZY(MO)                                                       NIT 401
      ITEMP=ICHAR                                                       NIT 402
C                                                                       NIT 403
C        FOR A SPECIFIED CHAR DISTANCE (STARTING AT Z=L AND PROCEEDING  NIT 404
C        BACK TO Z=0) OBTAIN THE CORRESPONDING TEMPERATURE FROM THE     NIT 405
C        TEMPERATURE PROFILE                                            NIT 406
C                                                                       NIT 407
      CALL OMEGA(ZVAR,Z,T,ITEMP,NDIM2,TVIS)                             NIT 408
  205 TK=(TVIS+460.0)/1.8                                               NIT 409
  209 DO 216 I=1,NC                                                     NIT 410
      TKE=(1.0/EK(I))*TK                                                NIT 411
      IMAX=NDATA                                                        NIT 412
C                                                                       NIT 413
C        FOR THE VALUE OF THE TEMPERATURE FIND THE CORRESPONDING        NIT 414
C        COLLISION INTEGRAL TO CALCULATE THE PURE GAS VISCOSITY         NIT 415
C        CALCULATE VISCOSITY OF GAS MIXTURE USING METHOD OF WILKE-      NIT 416
C        JOHNSON                                                        NIT 417
C                                                                       NIT 418
  211 CALL OMEGA(TKE,XTKE,ZOMGA,IMAX,NDIM3,OMGA)                        NIT 419
      ACON2=FW(I)*TK                                                    NIT 420
```

```
      VIS(I)=ACON1*SQRT(ACON2)/(SIG(I)**2)*OMGA                         NIT 421
  216 CONTINUF                                                          NIT 422
      IF(NC.LE.1)GOTO238                                                NIT 423
  220 GO TO(222,221,221),KEY                                            NIT 424
  221 TVAR=TK                                                           NIT 425
      NN5=NN4+1                                                         NIT 426
      DO217 KL=2,NN5                                                    NIT 427
C                                                                       NIT 428
C        INTERPOLATF FOR DATA GENFRATFD IN MOLFRA AND/OR KINET FROM     NIT 429
C        STORED TABLE AT THE SPECIFIC CHAR DISTANCE IN QUESTION         NIT 430
C                                                                       NIT 431
      CALL OMEGA(TVAR,TABLE(1,1),TABLE(1,KL),KMAX,NDIM1,VARY)           NIT 432
                      IF(KL.GT.2)GO TO 214                              NIT 433
                      REACT=VARY                                        NIT 434
                      GO TO 217                                         NIT 435
  214                 IF(KL.GT.3)GO TO 215                              NIT 436
                      AVGFW=VARY                                        NIT 437
                      GO TO 217                                         NIT 438
  215                 IF(KL.GT.4)GO TO 219                              NIT 439
                      W=VARY                                            NIT 440
                      GO TO 217                                         NIT 441
  219                 Y(KL-4)=VARY                                      NIT 442
                      ANDY3=Y(KL-4)                                     NIT 443
                      IF(ANDY3.GT.0.0)GO TO 2170                        NIT 444
  218                 Y(KL-4)=1.0F-10                                   NIT 445
 2170 IF(M.GT.1)GO TO 217                                               NIT 446
 2171 WFLUX(LO)=W                                                       NIT 447
      KYCOMP=KL-4                                                       NIT 448
      YCOMP(KYCOMP,LO)=Y(KYCOMP)                                        NIT 449
  217 CONTINUE                                                          NIT 450
  222 VMIX=0.0                                                          NIT 451
      GO TO (2220,2221,2221),KEY                                        NIT 452
 2220 WFLUX(LO)=WI                                                      NIT 453
 2221 DO 237 J=1,NC                                                     NIT 454
      TERM=1.0                                                          NIT 455
```

```
 223  DO 230 L=1,NC                                                    NIT 456
      IF(L.NE.J)GO TO 226                                              NIT 457
 225  GO TO 230                                                        NIT 458
C                                                                      NIT 459
C        CALCULATE THE VISCOSITY OF THE GAS MIXTURE                    NIT 460
C                                                                      NIT 461
  226 ACON4=VIS(J)/VIS(L)                                              NIT 462
      ACON20=SQRT(SQRT(FW(L)/FW(J)))                                   NIT 463
      TOPV=(1.+SQRT(ACON4)*ACON20)**2                                  NIT 464
  227 ACON8=1.+FW(J)/FW(L)                                             NIT 465
      BOTV=2.*SQRT(2.)*SQRT(ACON8)                                     NIT 466
 228  PHIV=TOPV/BOTV                                                   NIT 467
      TERM=TERM+PHIV*(Y(L)/Y(J))                                       NIT 468
 230  CONTINUE                                                         NIT 469
      VMIX=VMIX+(VIS(J)/TERM)                                          NIT 470
 237  CONTINUE                                                         NIT 471
      GO TO 2380                                                       NIT 472
  238 VISCOS=VIS(I)*ACON5                                              NIT 473
      GO TO 239                                                        NIT 474
 2380 VISCOS=VMIX*ACON5                                                NIT 475
  239 TT(MO)=(TVIS/AVGFW)*W**2                                         NIT 476
      PROD(MO)=TVIS*VISCOS*W/AVGFW                                     NIT 477
      CALL OMEGA(TVIS,T,CAPAC,ITEMP,NDIM2,CPBAR)                       NIT 478
      PRODCP(MO)=CPBAR*W                                               NIT 479
      GO TO(240,2401,2401),KEY                                         NIT 480
 2401 PRODR(MO)=REACT                                                  NIT 481
  240 CONTINUE                                                         NIT 482
C                                                                      NIT 483
C        STORE VALUES OF THE OUTPUT PARAMETERS AT INTERVALS SPECIFIED  NIT 484
C        BY JS, THE GRID SIZE                                          NIT 485
C                                                                      NIT 486
      ZX(LO-1)=ZX(LO)-HS                                               NIT 487
      TP(LO-1)=TT(1)*AVGFW/W**2                                        NIT 488
      DELTF=TP(LO)-TP(LO-1)                                            NIT 489
C                                                                      NIT 490
```

```
C          INTEGRATE USING SIMPSON RULE TO GET P AND QL                    NIT 491
C                                                                          NIT 492
      SUM1=0.0                                                             NIT 493
      SUM2=0.0                                                             NIT 494
      SUM3=0.0                                                             NIT 495
      SUM4=0.0                                                             NIT 496
      SUM5=0.0                                                             NIT 497
      SUM6=0.0                                                             NIT 498
      SUM7=0.0                                                             NIT 499
      SUM8=0.0                                                             NIT 500
      MEVEN=MP-1                                                           NIT 501
      DO255 KP=2,MEVEN,2                                                   NIT 502
      SUM1=SUM1+4.0*PROD(KP)                                               NIT 503
      SUM3=SUM3+4.0*TT(KP)                                                 NIT 504
  254 SUM5=SUM5+4.0*PRODCP(KP)                                             NIT 505
      GO TO(255,2540,2540),KEY                                             NIT 506
 2540 SUM7=SUM7+4.0*PRODR(KP)                                              NIT 507
  255 CONTINUE                                                             NIT 508
      MODD=MP-2                                                            NIT 509
      DO256 KP=3,MODD,2                                                    NIT 510
      SUM2=SUM2+2.0*PROD(KP)                                               NIT 511
      SUM4=SUM4+2.0*TT(KP)                                                 NIT 512
  257 SUM6=SUM6+2.0*PRODCP(KP)                                             NIT 513
      GO TO(256,2570,2570),KEY                                             NIT 514
 2570 SUM8=SUM8+2.0*PRODR(KP)                                              NIT 515
  256 CONTINUE                                                             NIT 516
      SIMP1=(HSIMPI/3.0)*(PROD(1)+PROD(MP)+SUM1+SUM2)+SIMP1                NIT 517
      SIMP2=(HSIMPI/3.0)*(TT(1)+TT(MP)+SUM3+SUM4)+SIMP2                    NIT 518
      P(LO-1)=SQRT(PL**2+(2.*RR)*(778.16/32.2)*(ALPHA*SIMP1+BETA*SIMP2))   NIT 519
      SIMP3=DELTF*HSIMPI/(HS*3.0)*(PRODCP(1)+PRODCP(MP)+SUM5+SUM6)+SIMP3   NIT 520
      GO TO(260,258,258),KEY                                               NIT 521
  258 SIMP4=DELTF*HSIMPI/(HS*3.0)*(PRODR(1)+PRODR(MP)+SUM7+SUM8)+SIMP4     NIT 522
  260 CONTINUE                                                             NIT 523
      GO TO(2600,2601,2601),KEY                                            NIT 524
 2600 QL=EPS*SIMP3                                                         NIT 525
```

```
      GO TO 261                                                         NIT 526
 2601 QL=EPS*(SIMP3+SIMP4)                                              NIT 527
 261  QR=EMIS*SIGMA*TL**4                                               NIT 528
      QA=QL+QR                                                          NIT 529
C                                                                       NIT 530
C     PRINT INPUT PARAMETERS                                            NIT 531
C                                                                       NIT 532
 2603 PRINT 597                                                         NIT 533
 597  FORMAT(1H1////////)                                               NIT 534
      GO TO(5980,5981,5982),KEY                                         NIT 535
 5980 PRINT598                                                          NIT 536
 598  FORMAT(11X,59H                                FROZEN FLOW MODEL - NIT 537
     1 TEMPRE/)                                                         NIT 538
      GO TO 5989                                                        NIT 539
 5981 PRINT5983                                                         NIT 540
 5983 FORMAT(11X,61H                              EQUILIBRIUM FLOW MODEL NIT 541
     1 - TEMPRE/)                                                       NIT 542
      GO TO 5989                                                        NIT 543
 5982 PRINT 5984                                                        NIT 544
 5984 FORMAT(11X,63H                           NON-EQUILIBRIUM FLOW MOD NIT 545
     1EL - TEMPRE/)                                                     NIT 546
 5989 GO TO(5985,5986),MTYPE                                            NIT 547
 5985 PRINT 599                                                         NIT 548
  599 FORMAT(12X,51H                                       EXPERIMENTAL/ NIT 549
     1/)                                                                NIT 550
      GO TO 5991                                                        NIT 551
 5986 PRINT 5990                                                        NIT 552
 5990 FORMAT(12X,51H                                        THEORETICAL/ NIT 553
     1/)                                                                NIT 554
 5991 PRINT600,T(1),NC                                                  NIT 555
 600  FORMAT(18X,26HINITIAL TEMPERATURE (OF) =,1X,F7.1,14X,26HNUMBER OF NIT 556
     1GAS COMPONENTS =,1X,I2/)                                          NIT 557
      PRINT 601,QP                                                      NIT 558
 601  FORMAT(18X,25HPYROLYSIS HEAT (BTU/LB) =,1X,F8.1,14X,29HNO.  COMPON NIT 559
     1ENT  MOLE/MOLE GAS/)                                              NIT 560
```

```
      PRINT 602,ALPA(1),YI(1)
 602  FORMAT(18X,50H                                                 1,3
     1X,A4,6X,F10.4/)
      PRINT603,PL,ALPA(2),YI(2)
 603  FORMAT(18X,25HFINAL PRESSURE (LB/FT2) =,1X,F8.1,15X,1H2,3X,A4,6X,F
     110.4/)
      PRINT604,WI,ALPA(3),YI(3)
 604  FORMAT(18X,24HMASS FLUX (LB/FT2-SEC) =,1X,F9.4,15X,1H3,3X,A4,6X,F1
     10.4/)
      PRINT605,ZL,ALPA(4),YI(4)
 605  FORMAT(18X,21HCHAR THICKNESS (FT) =,1X,F12.4,15X,1H4,3X,A4,6X,F10.
     14/)
      PRINT606,EPS,ALPA(5),YI(5)
 606  FORMAT(18X,15HCHAR POROSITY =,1X,F18.2,15X,1H5,3X,A4,6X,F10.4/)
      PRINT607,ALPA(6),YI(6)
 607  FORMAT(18X,50H                                                 6,3
     1X,A4,6X,F10.4/)
      PRINT6080,ALPA(7),YI(7)
 6080 FORMAT(18X,50HPERMEABILITY COEFFICIENTS                        7,3
     1X,A4,6X,F10.4/)
      PRINT608,ALPHA,ALPA(8),YI(8)
 608  FORMAT(18X,19H     ALPHA (FT-2) =,1X,E14.2,15X,1H8,3X,A4,6X,F10.4/
     1)
      PRINT609,BETA,ALPA(9),YI(9)
 609  FORMAT(18X,18H     BETA (FT-1) =,1X,E15.2,15X,1H9,3X,A4,6X,F10.4/)
      PRINT610,ALPA(10),YI(10)
 610  FORMAT(18X,50H                                                10,3
     1X,A4,6X,F10.4/)
      PRINT611,ALPA(11),YI(11)
 611  FORMAT(18X,50H                                                11,3
     1X,A4,6X,F10.4/)
      PRINT612,JRKSS,ALPA(12),YI(12)
 612  FORMAT(18X,23HRUNGE-KUTTA STEP SIZE =,1X,I10,14X,2H12,3X,A4,6X,F10
     1.4/)
      PRINT613,JSRSS,ALPA(13),YI(13)
```

```
 613  FORMAT(18X,25HSIMPSONS RULE STEP SIZE =,1X,I8,14X,2H13,3X,A4,6X,F1 NIT 596
     10.4/)                                                              NIT 597
      PRINT586                                                           NIT 598
 586  FORMAT(1H1)                                                        NIT 599
C                                                                        NIT 600
C        PRINT OUTPUT PARAMETERS CORRESPONDING TO JS, GRID SIZE          NIT 601
C                                                                        NIT 602
      IKE=1                                                              NIT 603
      MIKE=5                                                             NIT 604
      LIKE=1                                                             NIT 605
 2602 PRINT 597                                                          NIT 606
      GO TO(2660,2661,2662),KEY                                          NIT 607
 2660 PRINT598                                                           NIT 608
      GO TO 2663                                                         NIT 609
 2661 PRINT5983                                                          NIT 610
      GO TO 2663                                                         NIT 611
 2662 PRINT 5984                                                         NIT 612
 2663 GO TO(2664,2665),MTYPE                                             NIT 613
 2664 PRINT 599                                                          NIT 614
      GO TO 262                                                          NIT 615
 2665 PRINT 5990                                                         NIT 616
  262 IF(LIKE.GT.1)GO TO 265                                             NIT 617
      PRINT2650,DELTT                                                    NIT 618
 2650 FORMAT(35X,23HTEMPERATURE DROP (OF) =,1X,F20.1/)                   NIT 619
      DELP=(P(1)-PL)                                                     NIT 620
      PRINT2651,DELP                                                     NIT 621
 2651 FORMAT(35X,24HPRESSURE DROP (LB/FT2) =,1X,F19.1/)                  NIT 622
      PRINT2652,QL                                                       NIT 623
 2652 FORMAT(35X,33HSURFACE HEAT FLUX (BTU/FT2-SEC) =,1X,F10.2/)         NIT 624
      PRINT2653,QR                                                       NIT 625
 2653 FORMAT(35X,32HRADIANT HEAT FLUX BTU/FT2-SEC)=,1X,F11.2/)           NIT 626
      PRINT2654,QA                                                       NIT 627
 2654 FORMAT(35X,35HAERODYNAMIC HEAT FLUX(BTU/FT2-SEC)=,1X,F8.2//)       NIT 628
 265  PRINT2720,(ZX(KK),KK=IKE,MIKE)                                     NIT 629
 2720 FORMAT(14X,15HCHAR DEPTH (FT),6X,5F13.4)                           NIT 630
```

```
      PRINT2721,(TP(KK),KK=IKE,MIKE)                                    NIT 631
 2721 FORMAT(14X,16HTEMPERATURE (OF),5X,5F13.1)                         NIT 632
      PRINT2730,(P(KK),KK=IKE,MIKF)                                     NIT 633
 2730 FORMAT(14X,17HPRESSURE (LB/FT2),4X,5F13.1)                        NIT 634
      PRINT2723,(WFLUX(KK),KK=IKE,MIKE)                                 NIT 635
 2723 FORMAT(14X,21HMASS FLUX(LB/FT2-SFC),5F13.4/)                      NIT 636
      PRINT2724                                                         NIT 637
 2724 FORMAT(14X,66H  GAS COMPONENT                       COMPOSITION ( NIT 638
     1MOLE/MOLE GAS)/)                                                  NIT 639
      GO TO(2726,2727,2727),KEY                                         NIT 640
 2726 DO2728 KICK=1,LS                                                  NIT 641
      DO2728LL=1,NS                                                     NIT 642
      YCOMP(LL,KICK)=YI(LL)                                             NIT 643
 2728 CONTINUF                                                          NIT 644
 2727 DO2729LL=1,NS                                                     NIT 645
      YCOMP(LL,1)=YI(LL)                                                NIT 646
      PRINT2725,ALPA(LL),(YCOMP(LL,KK),KK=IKE,MIKE)                     NIT 647
 2725 FORMAT(18X,A4,11X,5E13.4)                                         NIT 648
 2729 CONTINUE                                                          NIT 649
      IF(MIKF.GF.LS)GO TO 2800                                          NIT 650
      LIKE=LIKF+1                                                       NIT 651
      MIKE=MIKF+5                                                       NIT 652
      IKE=IKE+5                                                         NIT 653
      GO TO 2602                                                        NIT 654
 2800 PRINT586                                                          NIT 655
  278 QP=QP+QPINC                                                       NIT 656
 9879 IF(QP-QPMAX)29,29,280                                             NIT 657
  280 QP=QPMIN                                                          NIT 658
      WI=WI+WIINC                                                       NIT 659
      IF(WI-WIMAX)29,29,2722                                            NIT 660
 2722 GO TO 20                                                          NIT 661
  300 STOP                                                              NIT 662
      END                                                               NIT 663
```

Listing B-3. TEMPRE Subprograms. (a) PROPT

```
C
C
C     SUBROUTINE PROPT  (HEAT CAPACITY AND CONDUCTIVITY VS. TEMPERATURE)
C
C
      SUBROUTINE PROPT(TVAR,JCHAR,KODE,NDATA,XTKE,ZOMGA,NDIM3,CPMX,CDO,
     1   DCDU)
      DIMENSION ICODE(20),ALPA(20),AA(20,6),
     1  S1(4),S2(4),S3(4),S4(4),S5(4),A11(4),A22(4),A33(4),A44(4),A55(4)
      DIMENSION AI(20),BI(20),CI(20),DI(20),EI(20),FI(20),GI(20),
     1  AII(20),BII(20),CII(20),DII(20),EII(20),FII(20),GII(20),FW(20),
     2   YI(20),EK(20),SIG(20),Y(20),DELH(20)
      DIMENSION RSC(15,15),PSC(15,15),NREX(15,15),NPEX(15,15),AF(30),
     1SF(20),AEF(20),AR(20),SR(20),AER(20),EQN(20,12),TABLE(70,20)
      DIMENSION CP(20),CV(20),COND(20),XTKE(100),ZOMGA(100)
      COMMON NC,NS,MM,WI,PL,RR,TZERO,DELTK,ICODE,ALPA,AA,S1,S2,S3,
     1   S4,S5,A11,A22,A33,A44,A55
      COMMON AI,BI,CI,DI,EI,FI,GI,AII,BII,CII,DII,EII,FII,GII,FW,YI
      COMMON EK,SIG,EPS,Y,DELH
      COMMON RSC,PSC,NREX,NPEX,AF,SF,AEF,AR,SR,AER,EQN,TABLE
      RANKIN=1.8*TVAR
      FAREN=RANKIN-460.0
      T=TVAR
      TC=T+DELTK
      AAA=2.6693*10.**(-5.)
      ACON=30.48/(252.*1.8)
      A1=TC
      A2=A1*TC
      A3=A2*TC
      A4=A3*TC
  500 DO516 I=1,NC
      TKE=(1.0/EK(I))*TC
      IMAX=NDATA
      GO TO(504,503),KODE
```

```
503  CALL OMEGA(TKE,XTKE,ZOMGA,IMAX,NDIM3,OMGA)
504  IF(TC.GT.1000.)GOTO506
 505 CP(I)=AII(I)+BII(I)*A1+CII(I)*A2+DII(I)*A3+EII(I)*A4
     GO TO 507
 506 CP(I)=AI(I)+BI(I)*A1+CI(I)*A2+DI(I)*A3+EI(I)*A4
507  CV(I)=RR*(CP(I)-1.0)
     GO TO(516,515),KODE
515  ACON1=TC/FW(I)
         TOP=AAA*SQRT(ACON1)*(CV(I)+4.47)
     BOT=SIG(I)**2*OMGA
         COND(I)=TOP/BOT
516  CONTINUE
         CPMX=0.0
         CDMX=0.0
     DO537 J=1,NC
     GO TO(535,536),KODE
536      SUMCD=COND(J)*Y(J)
         CDMX=CDMX+SUMCD
535      SUMCP=CP(J)*Y(J)
         CPMX=CPMX+SUMCP
537  CONTINUE
     GO TO (538,539),JCHAR
538  CALL CHAR(SLOPE,YINTCP,KODE)
539  SCHAR=SLOPE
     YCHAR=YINTCP
     CDCHAR=(SCHAR*TC)+YCHAR
     CHARK=CDCHAR*ACON
     GO TO(5400,5401),KODE
5400 CDO=CHARK
     GO TO 5402
5401 GASK=CDMX*ACON
     CDO=GASK*EPS + CHARK*(1.0-EPS)
5402 ANDY4=ABS(T-TC)
     IF(ANDY4.LT.0.00001)GO TO 560
540  IF(T.GE.TC)GO TO 550
```

```
541   CDOP=CDO
      TC=T-DELTK
      JCHAR=2
      GO TO 500
550   CDON=CDO
      DELTF=DELTK*1.8
      DCDO=(CDOP-CDON)/(DELTF*2.0)
      TC=T
      GO TO 500
560   RETURN
      END
```

Listing B-3. TEMPRE Subprograms. (b) OMEGA.

```
C
C
C        OMEGA - GENERAL INTERPOLATION SUBPROGRAM
C
C
      SUBROUTINE OMEGA (VAR,X,F,IMAX,NAME,SOM)
      DIMENSION X(NAME),F(NAME),XN(300),FN(300)
      NPTS=3
  607 XUP=1.E30
      DO611 I=1,IMAX
      T=VAR-X(I)
      IF(T.GE.0.0)GO TO 609
  608 T=-T
  609 IF(T.GE.XUP)GO TO 611
  610 IP=I
      XUP=T
  611 CONTINUE
      IN=1
      NPP=NPTS+1
      DO618I=1,NPP
      FN(I)=F(IP)
      XN(I)=X(IP)
      IF(IN.GT.0)GO TO 613
  612 IQ=IP-I
      GO TO 615
  613 IQ=IP+I
      IF(IMAX.GE.IQ)GO TO 615
  614 IP=IP-1
      GO TO 618
  615 IF(IQ.GT.0)GO TO 617
  616 IP=IP+1
      GO TO 618
  617 IP=IQ
      IN=-IN
```

```
  618 CONTINUE
      SOM=0.0
      FACT=1.0
      DO620 J=1,NPTS
      SOM=SOM+FACT*FN(1)
      DO619 I=J,NPTS
      IQ=I-J+1
  619 FN(IQ)=(FN(IQ+1)-FN(IQ))/(XN(I+1)-XN(IQ))
  620 FACT=FACT*(VAR-XN(J))
      RETURN
      END
```

Listing B-3. TEMPRE Subprogram. (c) CHAR

```
C
C
C        LEAST SQUARES FIT OF EXPERIMENTAL CHAR CONDUCTIVITY DATA
C
C
        SUBROUTINE CHAR(SLOPE,YINTCP,KODE)
      DIMENSION XCOND(100),YCOND(100)
C
C     MDATA=NO. OF XCOND VS. YCOND DATA POINTS
C     KODE= 1 (DATA WITH INERTS IN PORES)  = 2 (DATA WITH EVACUATED PORE
C
      READ700,MDATA,KODE
C
C     XCOND=TEMPERATURE (OK)
C     YCOND=CHAR CONDUCTIVITY TABULATED  VS TEMPERATURE (CAL/CM-SEC-OK)
C
      READ701,(XCOND(I),YCOND(I),I=1,MDATA)
  700 FORMAT(2I6)
  701 FORMAT(F15.0,E15.5)
          SUMX=0.0
          SUMY=0.0
          SUMXY=0.0
          SUMX2=0.0
          SUMY2=0.0
      TN=MDATA
      DO710 J=1,MDATA
          SUMX=SUMX+XCOND(J)
          SUMY=SUMY+YCOND(J)
          SUMXY=SUMXY+XCOND(J)*YCOND(J)
          SUMX2=SUMX2+XCOND(J)**2
          SUMY2=SUMY2+YCOND(J)**2
 710  CONTINUE
 720      SLOPE=(SUMXY-(SUMX*SUMY/TN))/(SUMX2-(SUMX**2  /TN))
 730     YINTCP=(SUMY-(SLOPE*SUMX))/TN
      RETURN
      END
```

Listing B-3. TEMPRE Subprograms. (d) MOLFRA

```
C
C     MOLFRA CALCULATES THE COMPOSITION,RATE,AND HEAT OF REACTION FOR
C     THE EQUILIBRIUM MODEL
C
C     CHEMICAL EQUILIBRIUM IN COMPLEX MIXTURE-METHOD OF WHITE-JOHNSON-DA
C     RAND METHOD(STEEPEST DESCENT),JOURNAL-CHEMICAL PHYSICS-VOL-28-NO5-
C
C
      SUBROUTINE MOLFRA(KOUNT,KPT3,K6,TP1)
      DIMENSION ICODE(20),ALPA(20),AA(20,6),
     1  S1(4),S2(4),S3(4),S4(4),S5(4),A11(4),A22(4),A33(4),A44(4),A55(4)
      DIMENSION AI(20),BI(20),CI(20),DI(20),EI(20),FI(20),GI(20),
     1  AII(20),BII(20),CII(20),DII(20),EII(20),FII(20),GII(20),FW(20),
     2   YI(20),EK(20),SIG(20),Y(20),DELH(20)
      DIMENSION RSC(15,15),PSC(15,15),NREX(15,15),NPEX(15,15),AF(30),
     1SF(20),AEF(20),AR(20),SR(20),AER(20),EQN(20,12),TABLE(70,20)
      DIMENSION XMW(20),X(20),FY(20),C(20),FORT(20),R(6,6),B(6,1),PI(6),
     1IPIVOT(6),BB(6),INDEX(6,2),BBP(6),DELT(20),ENT(20),DOTA(70,20),
     2DOTA1(70,20),CPDT(20),CPDT1(20),FSUM(20),YSUM(20),XY(20),XMASS(20)
     3,YX(20),PERC(20),HO(4),YPREV1(20),XLAM(20),YY(20)
      COMMON NC,NS,MM,WI,PL,RR,TZERO,DELTK,ICODE,ALPA,AA,S1,S2,S3,
     1   S4,S5,A11,A22,A33,A44,A55
      COMMON AI,BI,CI,DI,EI,FI,GI,AII,BII,CII,DII,EII,FII,GII,FW,YI
      COMMON EK,SIG,EPS,Y,DELH
      COMMON RSC,PSC,NREX,NPEX,AF,SF,AEF,AR,SR,AER,EQN,TABLE
      IF(K6.GT.1)GOTO3174
C
C     XT=INITIAL TEMPERATURE AT WHICH EQUILIBRIUM PROGRAM IS STARTED
C     TMAX=FINAL TEMPERATURE AT WHICH EQUILIBRIUM PROGRAM IS ENDED
C     TINC=TEMPERATURE INTERVAL IN EQUILIBRIUM PROGRAM CALCULATIONS
C     CRIT=CRITERION FOR CONVERGENCE IN EQUILIBRIUM PROGRAM
C
      READ 7,TMAX,TINC,CRIT
    7 FORMAT(10X,4E10.4)
```

```
      XT=(TP1+460.)/1.8                                                 MO  35
C                                                                       MO  36
C     NMAX=MAXIMUM SIZE OF THE SQUARE MATRIX                            MO  37
C     NFREQ=NO. AFTER WHICH TRACE COMPONENTS ARE CHECKED                MO  38
C                                                                       MO  39
      KEY=2                                                             MO  40
      READ2,NMAX,NFREQ                                                  MO  41
    2 FORMAT(2I6)                                                       MO  42
 3174 K6=2                                                              MO  43
      DO 3 I=1,NS                                                       MO  44
      Y(I)=YI(I)                                                        MO  45
      XMW(I)=FW(I)                                                      MO  46
    3 CONTINUE                                                          MO  47
      DEBAR=0.                                                          MO  48
      W=WI/EPS                                                          MO  49
      NN=NC                                                             MO  50
      NQ=NS                                                             MO  51
      MA=1                                                              MO  52
      NA=MM+1+NQ-NN                                                     MO  53
      P=PL/2160.0                                                       MO  54
      KPT=0                                                             MO  55
      KPT1=0                                                            MO  56
      MAXNT=100                                                         MO  57
      KCODE=0                                                           MO  58
      KREAD=0                                                           MO  59
      T=XT                                                              MO  60
      KOS=NN+4                                                          MO  61
      LL=NN+1                                                           MO  62
      M=MA                                                              MO  63
      N=NA                                                              MO  64
      KX=0                                                              MO  65
      XBETA=CRIT                                                        MO  66
 1000 DO320J=1,MM                                                       MO  67
      BB(J)=0.0                                                         MO  68
      DO 320 I=1,NQ                                                     MO  69
```

```
      BB(J)=BB(J)+AA(I,J)*Y(I)
  320 CONTINUE
 500  DO 433 I=1,NQ
      IF(ICODE(I).EQ.0)GOTO433
      KCODE=1
  433 CONTINUE
   45 NTEST=NFREQ
      NT=1
C
C
      IF(T.GT.1000.)GOTO6205
      DO 41  I=1,NQ
       FORT(I)=AII(I)*(1.-ALOG(T))-BII(I)*T/2.-CII(I)*(T**2)/6.
     1         -DII(I)*(T**3)/12.-EII(I)*(T**4)/20.+FII(I)/T-GII(I)
   41 CONTINUE
      GOTO1020
 6205 DO 6206 I=1,NQ
       FORT(I)=AI(I)*(1.-ALOG(T))-BI(I)*T/2.0-CI(I)*(T**2)/6.0
     1         -DI(I)*(T**3)/12.0-EI(I)*(T**4)/20.0+FI(I)/T-GI(I)
 6206 CONTINUE
 1020 CONTINUE
  300 YBAR=0.0
      DO50I=1,NN
   50 YBAR=YBAR+Y(I)
      DO10I=1,NN
      C(I)=FORT(I)+ALOG(P)
      FAC=Y(I)/YBAR
      IF(FAC.LT.1.E-38)FAC=1.E-38
      FY(I)=Y(I)*(C(I)+ALOG(FAC))
   10 CONTINUE
      IF(KCODE.EQ.0)GOTO111
      DO 11 I=LL,NQ
      FY(I)=Y(I)*FORT(I)
   11 CONTINUE
  111 DO30J=1,MM
```

```
      DO30K=1,MM                                                        MO 105
      ASUM=0.0                                                          MO 106
      DO20I=1,NN                                                        MO 107
      WAY=AA(I,J)*AA(I,K)*Y(I)                                          MO 108
   20 ASUM=ASUM+WAY                                                     MO 109
      R(J,K)=ASUM                                                       MO 110
   30 CONTINUE                                                          MO 111
      GSUM1=0.                                                          MO 112
      DO 1022 I=1,NQ                                                    MO 113
      GSUM1=GSUM1+FY(I)                                                 MO 114
 1022 CONTINUE                                                          MO 115
      DO70K=1,MA                                                        MO 116
      DO70J=1,MM                                                        MO 117
      SUM=0.                                                            MO 118
      DO130I=1,NN                                                       MO 119
  130 SUM=SUM+AA(I,J)*FY(I)                                             MO 120
      BSUM=SUM+BB(J)                                                    MO 121
      B(J,K)=BSUM                                                       MO 122
   70 CONTINUE                                                          MO 123
      CSUM=0.0                                                          MO 124
      DO80I=1,NN                                                        MO 125
   80 CSUM=CSUM+FY(I)                                                   MO 126
      JJ=MM+1                                                           MO 127
      DO91J=1,MA                                                        MO 128
   91 B(JJ,J)=CSUM                                                      MO 129
      DO 103 K=1,MM                                                     MO 130
      DSUM=0.0                                                          MO 131
      DO 101 I=1,NN                                                     MO 132
  101 DSUM=DSUM+AA(I,K)*Y(I)                                            MO 133
      BBP(K)=DSUM                                                       MO 134
  103 CONTINUE                                                          MO 135
      DO90J=1,MM                                                        MO 136
   90 R(J,JJ)=BBP(J)                                                    MO 137
      DO94K=1,MM                                                        MO 138
   94 R(JJ,K)=R(K,JJ)                                                   MO 139
```

```
      KK=MM+1                                                           MO 140
      KL=JJ                                                             MO 141
      IF(KCODE.EQ.0)GOTO1050                                            MO 142
      DO 29 I=LL,NQ                                                     MO 143
      KK=KK+1                                                           MO 144
      DO 29 J=1,MM                                                      MO 145
      R(J,KK)=AA(I,J)                                                   MO 146
   29 CONTINUE                                                          MO 147
      KL=NQ-NN+JJ                                                       MO 148
      KK=MM+2                                                           MO 149
      DO 95 K=KK,KL                                                     MO 150
      DO97 J=1,MM                                                       MO 151
   97 R(K,J)=R(J,K)                                                     MO 152
   95 CONTINUE                                                          MO 153
      KM=MM+1                                                           MO 154
      DO 1052 J=1,MA                                                    MO 155
      DO 1053 I=LL,NQ                                                   MO 156
      KM=KM+1                                                           MO 157
 1053 B(KM,J)=FORT(I)                                                   MO 158
 1052 CONTINUE                                                          MO 159
 1050 CONTINUE                                                          MO 160
      DO 1044 J=JJ,KL                                                   MO 161
      DO 1045 K=JJ,KL                                                   MO 162
 1045 R(J,K)=0.0                                                        MO 163
 1044 CONTINUE                                                          MO 164
      N=NA                                                              MO 165
      M=MA                                                              MO 166
      CALL MATINV(R,N,B,M,NMAX,IPIVOT,INDEX,ISCALE,DETERM)              MO 167
      DO100I=1;JJ                                                       MO 168
      PI(I)=B(I,M)                                                      MO 169
  100 CONTINUE                                                          MO 170
      U=PI(JJ)                                                          MO 171
      XBAR=U*YBAR                                                       MO 172
      IF(KCODE.EQ.0)GOTO59                                              MO 173
      KK=MM+2                                                           MO 174
```

```
      LW=LL                                                             MO 175
      DO 1002 J=KK,KL                                                   MO 176
      X(LW)=B(J,M)                                                      MO 177
 1002 LW=LW+1                                                           MO 178
   59 DO60I=1,NN                                                        MO 179
   60 FSUM(I)=-FY(I)+(Y(I)/YBAR)*XBAR                                   MO 180
      DO110I=1,NN                                                       MO 181
      PSUM=0.                                                           MO 182
      DO120J=1,MM                                                       MO 183
  120 PSUM=PSUM+PI(J)*AA(I,J)                                           MO 184
      YSUM(I)=PSUM*Y(I)                                                 MO 185
  110 X(I)=FSUM(I)+YSUM(I)                                              MO 186
      XLAMBD=1.0                                                        MO 187
  310 DO 86 I=1,NQ                                                      MO 188
      DELT(I)=X(I)-Y(I)                                                 MO 189
      IF(DELT(I).GE.0.)GOTO86                                           MO 190
      IF(X(I).GT.0.)GOTO86                                              MO 191
      X(I)=1.E-25                                                       MO 192
      XLAM(I)=-Y(I)/DELT(I)                                             MO 193
      XLAMBD=AMIN1(XLAMBD,XLAM(I))                                      MO 194
      XLAMBD=0.99*XLAMBD                                                MO 195
   86 CONTINUE                                                          MO 196
      DEBAR=0.                                                          MO 197
      DO87I=1,NN                                                        MO 198
   87 DEBAR=DEBAR+DELT(I)                                               MO 199
   93 DFDL=0.                                                           MO 200
      DO88I=1,NQ                                                        MO 201
      IF(ICODE(I).EQ.1)GOTO83                                           MO 202
   96 FAC=(Y(I)+XLAMBD*DELT(I))/(YBAR+XLAMBD*DEBAR)                     MO 203
   98 IF(FAC.GT.0.)GOTO82                                               MO 204
  991 XLAMBD=.9*XLAMBD                                                  MO 205
      IF(XLAMBD.GT.1.0E- 6)GOTO96                                       MO 206
   82 DFDL=DFDL+DELT(I)*(C(I)+ALOG(FAC))                                MO 207
      GOTO88                                                            MO 208
   83 DFDL=DFDL+DELT(I)*FORT(I)                                         MO 209
```

```
   88 CONTINUE                                                          MO 210
      IF(DFDL.LT.0.01)GOTO8081                                          MO 211
      XLAMBD=.9*XLAMBD                                                  MO 212
      IF(XLAMBD.GT.1.0E- 6)GOTO93                                       MO 213
 8081 IF(DFDL.LT.0.)GOTO89                                              MO 214
      PRINT2222,DFDL,NT                                                 MO 215
 2222 FORMAT(///1X,1E20.8,1X,1I6)                                       MO 216
   89 DO76I=1,NQ                                                        MO 217
      Y(I)=Y(I)+XLAMBD*DELT(I)                                          MO 218
      IF(Y(I).LT.1.E-25)Y(I)=1.E-25                                     MO 219
 76   CONTINUE                                                          MO 220
      SUMY=0.                                                           MO 221
      DO370I=1,NN                                                       MO 222
  370 SUMY=SUMY+Y(I)                                                    MO 223
      DO340I=1,NQ                                                       MO 224
  340 PERC(I)=(Y(I)/SUMY)*100.                                          MO 225
  350 BETA=0.                                                           MO 226
      DO85I=1,NQ                                                        MO 227
   85 BETA=BETA+ABS(DELT(I))                                            MO 228
      IF(BETA.LT.XBETA)GOTO800                                          MO 229
  560 IF(NT.GE.MAXNT)GOTO600                                            MO 230
      NT=NT+1                                                           MO 231
      IF(NT.GT.51)GOTO801                                               MO 232
      GOTO300                                                           MO 233
  600 XBETA=XBETA+0.001                                                 MO 234
      MAXNT=MAXNT+10                                                    MO 235
      NT=NT+1                                                           MO 236
      GOTO300                                                           MO 237
  800 NN=NC                                                             MO 238
      KX=KX+1                                                           MO 239
      IF(KX.LT.2)GOTO300                                                MO 240
      NT=NT+1                                                           MO 241
      DO 321 J=1,MM                                                     MO 242
      PRINT 322,BB(J)                                                   MO 243
  322 FORMAT(1X,6HBB(J)=,F12.8)                                         MO 244
```

```
  321 CONTINUE
 801  XSUMY=0.
      DO580I=1,NN
      XSUMY=XSUMY+Y(I)
 580  CONTINUE
      XMWGAS=0.0
      DO81I=1,NN
      XMWGAS=XMWGAS+XMW(I)*Y(I)
   81 CONTINUE
      DO 191I=1,NQ
      XMASS(I)=Y(I)*XMW(I)/XMWGAS
  191 CONTINUE
C
C     YSUM IS BEING SENT AS A DUMMY NUMBER TO ENTAL1,SINCE IN MOLFRA
C     THE RATE AND THE HEAT OF REACTION IS COMPUTED LATER IN THE PRO -
C     GRAM.
C
      CALL ENTAL1(T,HEAT1,ENT,ENTALP,YSUM,KEY)
      XMWGAS=XMWGAS/XSUMY
      XBETA=CRIT
      KPT=KPT+1
  171 TABLE(KPT,1)=T
      TABLE(KPT,3)=XMWGAS
C
C     REDIFINE MOLE BASIS
C
      IF(T.NE.XT)GOTO823
      SUM1=0.
      DO 822 I=1,NN
      Y(I)=(W/XMWGAS)*PERC(I)/100.
  822 SUM1=SUM1+Y(I)
      Y(NQ)=PERC(NQ)*SUM1/100.
      RIN=PERC(NQ)/100.*XMW(NQ)/XMWGAS
      ROUT=RIN
      DO 79 J=1,MM
```

```
      BB(J)=0.0                                                         MO 280
      DO79I=1,NQ                                                        MO 281
      BB(J)=BB(J)+AA(I,J)*Y(I)                                          MO 282
   79 CONTINUE                                                          MO 283
      GOTO1711                                                          MO 284
  823 WG=W                                                              MO 285
      ROUT=PERC(NQ)/100.*XMW(NQ)/XMWGAS                                 MO 286
      RATIO=(1.+RIN)/(1.+ROUT)                                          MO 287
      W=WG*RATIO                                                        MO 288
      RIN=ROUT                                                          MO 289
 1711 TABLE(KPT,4)=W                                                    MO 290
C                                                                       MO 291
C     CALCUALTION OF THE INDIVIDUAL MASS FLUXES                         MO 292
C                                                                       MO 293
      DO 1712 I=1,NN                                                    MO 294
      FLUX=W/XMWGAS*PERC(I)/100.*XMW(I)                                 MO 295
 1712 DOTA(KPT,I)=FLUX                                                  MO 296
      FLUX=W*ROUT                                                       MO 297
      DOTA(KPT,NQ)=FLUX                                                 MO 298
      DO 444 I=5,KOS                                                    MO 299
      TABLE(KPT,I)=PERC(I-4)/100.                                       MO 300
  444 CONTINUE                                                          MO 301
      NY=KOS+1                                                          MO 302
      TABLE(KPT,NY)=PERC(NQ)/100.                                       MO 303
      IF(T.GE.TMAX)GOTO333                                              MO 304
       T=T+TINC                                                         MO 305
      KX=0                                                              MO 306
      GOTO500                                                           MO 307
  333 KPT3=KPT-3                                                        MO 308
      KOUNT=2                                                           MO 309
      DO 8000 J=1,KPT3                                                  MO 310
      IF(J.GT.1)GOTO 732                                                MO 311
      DO 8001 I=1,NQ                                                    MO 312
      YPRIME=(1./(60.*TINC))*(-137.*DOTA(J,I)+300.*DOTA(J+1,I)-300.*DOTA MO 313
     1(J+2,I)+200.*DOTA(J+3,I)-75.*DOTA(J+4,I)+12.*DOTA(J+5,I))         MO 314
```

```
      DOTA1(J,I)=YPRIME
 8001 CONTINUE
      GOTO 8004
  732 IF(J.GT.2)GOTO733
      DO 8002 I=1,NQ
      YPRIME=(1./(60.*TINC))*(-12.*DOTA(J-1,I)-65.*DOTA(J,I)+120.*DOTA(J
     1+1,I)-60.*DOTA(J+2,I)+20.*DOTA(J+3,I)-3.*DOTA(J+4,I))
      DOTA1(J,I)=YPRIME
 8002 CONTINUE
      GOTO 8004
  733 DO 8071 I=1,NQ
      YPRIME=(1./(60.*TINC))*(3.*DOTA(J-2,I)-30.*DOTA(J-1,I)-20.*DOTA(J,
     1I)+60.*DOTA(J+1,I)-15.*DOTA(J+2,I)+2.*DOTA(J+3,I))
      DOTA1(J,I)=YPRIME
 8071 CONTINUE
 8004 CONTINUE
 8000 CONTINUE
      SUM2=0.
      DO 8007 J=1,KPT3
      T=TABLE(J,1)
      CALL ENTAL1(T,HEAT1,ENT,ENTALP,YSUM,KEY)
      DO 8006 I=1,NQ
      IF(I.LT.NQ)GO TO 8005
      SUM2=SUM2+DOTA1(J,I)*ENT(I)*(1.0-EPS)/XMW(I)
      GO TO 8006
 8005 SUM2=SUM2+DOTA1(J,I)*ENT(I)*EPS/XMW(I)
 8006 CONTINUE
      TABLE(J,2)=SUM2
 8007 CONTINUE
      RETURN
      END
```

Listing B-3. TEMPRE Subprograms. (e) MATINV

```
C
C
C     MATRIX INVERSION WITH ACCOMPANYING SOLUTION OF LINEAR EQUATIONS
C
C
      SUBROUTINE MATINV(A,N,B,M,NMAX,IPIVOT,INDEX,ISCALE,DETERM)
      DIMENSION A(NMAX,N),B(NMAX,M),IPIVOT(N),INDEX(NMAX,2)
      EQUIVALENCE (IROW,JROW), (ICOLUM,JCOLUM), (AMAX,T,SWAP)
C
C     INITIALIZATION
C
    5 ISCALE=0
    6 R1=10.0**18
    7 R2=1.0/R1
   10 DETERM=1.0
   15  DO 20 J=1,N
   20 IPIVOT(J)=0
   30 DO 550 I=1,N
C
C     SEARCH FOR PIVOT FLEMENT
C
   40 AMAX=0.0
   45 DO 105 J=1,N
   50 IF (IPIVOT(J)-1)60,105,60
   60 DO 100 K=1,N
   70 IF (IPIVOT(K)-1)80,100,740
   80 IF (ABS(AMAX)-ABS(A(J,K)))85,100,100
   85 IROW=J
   90 ICOLUM=K
   95 AMAX=A(J,K)
  100 CONTINUE
  105 CONTINUF
      IF (AMAX)110,106,110
  106 DETERM=0.0
```

```
      ISCALE=0
      GO TO 740
  110 IPIVOT(ICOLUM)=IPIVOT(ICOLUM)+1
C
C     INTERCHANGE ROWS TO PUT PIVOT ELEMENT ON DIAGONAL
C
  130 IF (IROW-ICOLUM)140,260,140
  140 DETERM=-DETERM
  150 DO 200 L=1,N
  160 SWAP=A(IROW,L)
  170 A(IROW,L)=A(ICOLUM,L)
  200 A(ICOLUM,L)=SWAP
  205 IF(M)260,260,210
  210 DO 250 L=1,M
  220 SWAP=B(IROW,L)
  230 B(IROW,L)=B(ICOLUM,L)
  250 B(ICOLUM,L)=SWAP
  260 INDEX(I,1)=IROW
  270 INDEX(I,2)=ICOLUM
  310 PIVOT=A(ICOLUM,ICOLUM)
C
C     SCALE THE DETERMINANT
C
 1000 PIVOTI=PIVOT
 1005 IF(ABS(DETERM)-R1)1030,1010,1010
 1010 DETERM=DETERM/R1
      ISCALE=ISCALE+1
      IF(ABS(DETERM)-R1)1060,1020,1020
 1020 DETERM=DETERM/R1
      ISCALE=ISCALE+1
      GO TO 1060
 1030 IF(ABS(DETERM)-R2)1040,1040,1060
 1040 DETERM=DETERM*R1
      ISCALE=ISCALE-1
      IF(ABS(DETERM)-R2)1050,1050,1060
```

```
 1050 DETERM=DETERM*R1                                                    MA  70
      ISCALE=ISCALE-1                                                     MA  71
 1060 IF(ABS(PIVOTI)-R1)1090,1070,1070                                    MA  72
 1070 PIVOTI=PIVOTI/R1                                                    MA  73
      ISCALE=ISCALE+1                                                     MA  74
      IF(ABS(PIVOTI)-R1)320,1080,1080                                     MA  75
 1080 PIVOTI=PIVOTI/R1                                                    MA  76
      ISCALE=ISCALE+1                                                     MA  77
      GO TO 320                                                           MA  78
 1090 IF(ABS(PIVOTI)-R2)2000,2000,320                                     MA  79
 2000 PIVOTI=PIVOTI*R1                                                    MA  80
      ISCALE=ISCALE-1                                                     MA  81
      IF(ABS(PIVOTI)-R2)2010,2010,320                                     MA  82
 2010 PIVOTI=PIVOTI*R1                                                    MA  83
      ISCALE=ISCALE-1                                                     MA  84
  320 DETERM=DETERM*PIVOTI                                                MA  85
C                                                                         MA  86
C     DIVIDE PIVOT ROW BY PIVOT ELEMENT                                   MA  87
C                                                                         MA  88
  330 A(ICOLUM,ICOLUM)=1.0                                                MA  89
  340 DO 350 L=1,N                                                        MA  90
  350 A(ICOLUM,L)=A(ICOLUM,L)/PIVOT                                       MA  91
  355 IF(M) 380,380,360                                                   MA  92
  360 DO 370 L=1,M                                                        MA  93
  370 B(ICOLUM,L)=B(ICOLUM,L)/PIVOT                                       MA  94
C                                                                         MA  95
C     REDUCE NON-PIVOT ROWS                                               MA  96
C                                                                         MA  97
  380 DO 550 L1=1,N                                                       MA  98
  390 IF(L1-ICOLUM)400,550,400                                            MA  99
  400 T=A(L1,ICOLUM)                                                      MA 100
  420 A(L1,ICOLUM)=0.0                                                    MA 101
  430 DO 450 L=1,N                                                        MA 102
  450 A(L1,L)=A(L1,L)-A(ICOLUM,L)*T                                       MA 103
  455 IF(M) 550,550,460                                                   MA 104
```

```
  460 DO 500 L=1,M
  500 B(L1,L)=B(L1,L)-B(ICOLUM,L)*T
  550 CONTINUE
C
C       INTERCHANGE COLUMNS
C
  600 DO 710 I=1,N
  610 L=N+1-I
  620 IF(INDEX(L,1)-INDEX(L,2))630,710,630
  630 JROW=INDEX(L,1)
  640 JCOLUM=INDEX(L,2)
  650 DO 705 K=1,N
  660 SWAP=A(K,JROW)
  670 A(K,JROW)=A(K,JCOLUM)
  700 A(K,JCOLUM)=SWAP
  705 CONTINUE
  710 CONTINUF
  740 RETURN
      END
```

Listing B-3. TEMPRE Subprograms. (f) ENTAL 1

```
C
      SUBROUTINE ENTAL1(T,HEAT1,ENT,SUM7,RATE,KEY)
C
C     SUBROUTINE ENTAL1 CALCUALTES THE HEAT OF REACTION OF THE MIXTURE,
C     THE HEAT OF FORMATION OF EACH INDIVIDUAL COMPONENT,AND THE SEN-
C     SIBLE ENTHALPY GAIN OF THE GASES AS THE TEMPERATURE INCREASES.
C
      DIMENSION ICODE(20),ALPA(20),AA(20,6),
     1  S1(4),S2(4),S3(4),S4(4),S5(4),A11(4),A22(4),A33(4),A44(4),A55(4)
      DIMENSION AI(20),BI(20),CI(20),DI(20),EI(20),FI(20),GI(20),
     1  AII(20),BII(20),CII(20),DII(20),EII(20),FII(20),GII(20),FW(20),
     2   YI(20),EK(20),SIG(20),Y(20),DELH(20)
      DIMENSION RSC(15,15),PSC(15,15),NREX(15,15),NPEX(15,15),AF(30),
     1SF(20),AEF(20),AR(20),SR(20),AER(20),EQN(20,12),TABLE(70,20)
      DIMENSION CPDT(20),CPDT1(20),ENT(20),RATE(20)
      COMMON NC,NS,MM,WI,PL,RR,TZERO,DELTK,ICODE,ALPA,AA,S1,S2,S3,
     1   S4,S5,A11,A22,A33,A44,A55
      COMMON AI,BI,CI,DI,EI,FI,GI,AII,BII,CII,DII,EII,FII,GII,FW,YI
      COMMON EK,SIG,EPS,Y,DELH
      COMMON RSC,PSC,NREX,NPEX,AF,SF,AEF,AR,SR,AER,EQN,TABLE
      A1=T-TZERO
      A2=(T**2-TZERO**2)/2.
      A3=(T**3-TZERO**3)/3.
      A4=(T**4-TZERO**4)/4.
      A5=(T**5-TZERO**5)/5.
      TZERO=298.15
      RR=1.987
      NQ=NS
      SUM7=0.
      HEAT1=0.
      DO 78I=1,NQ
      IF(T.LT.1000.0)GOTO6207
C
C     CALCULATE THE SENSIBLE ENTHALPY OF THE CHEMICAL
```

```
C     SPECIES FOR TEMPERATURES GREATER THAN 1000(OK).
C
      CPDT(I)=(AI(I)*A1+BI(I)*A2+CI(I)*A3+DI(I)*A4+FI(I)*A5)*RR
C
C     CALCULATE THE SENSIBLE ENTHALPY OF THE CONSTITUENT
C     ELEMENTS FOR TEMPERATURES GREATER THAN 1000(OK)
C
      IF(I.GT.1)GOTO6291
      DO 296J=1,MM
      CPDT1(J)=(S1(J)*A1+S2(J)*A2+S3(J)*A3+S4(J)*A4+S5(J)*A5)*RR
  296 CONTINUE
      GOTO6291
C
C     CALCULATE THE SENSIBLE ENTHALPY OF THE CHEMICAL
C     SPECIES FOR TEMPERATURES LESS THAN 1000(OK)
C
 6207 CPDT(I)=(AII(I)*A1+BII(I)*A2+CII(I)*A3+DII(I)*A4+EII(I)*A5)*RR
C
C     CALCULATE THE SENSIBLE ENTHALPY OF THE CONSTITUENT
C     ELEMENTS FOR TEMPERATURES LESS THAN 1000(OK).
C
      IF(I.GT.1)GOTO6291
      DO297J=1,MM
      CPDT1(J)=(A11(J)*A1+A22(J)*A2+A33(J)*A3+A44(J)*A4+A55(J)*A5)*RR
  297 CONTINUE
C
C     RSUM IS THE SENSIBLE ENTHALPY OF THE ELEMENTS OF THE ITH SPECIF
C     AT TEMPERATURE T(OK),WITH RESPECT TO THE STANDARD STATE(P=1ATM,
C     TZERO=298.15OK)
C
 6291 RSUM=0.
      DO 398 J=1,MM
      IF(ICODE(I).EQ.1)GOTO393
      RSUM=RSUM+0.5*AA(I,J)*CPDT1(J)
      GO TO 398
```

```
  393 RSUM=RSUM+AA(I,J)*CPDT1(J)                                              EN  70
  398 CONTINUE                                                                EN  71
      ENT(I)=DELH(I)+CPDT(I)-RSUM                                             EN  72
      IF(KEY.NE.3)GOTO787                                                     EN  73
      IF(I.GE.NO)GO TO 8005                                                   EN  74
      HEAT1=HEAT1+RATE(I)*EPS*ENT(I)                                          EN  75
      GO TO 787                                                               EN  76
 8005 HEAT1=HEAT1+RATE(I)*(1.0-EPS)*ENT(I)                                    EN  77
  787 IF(ICODE(I).EQ.1)GO TO 78                                               EN  78
      SUM7=SUM7+Y(I)*(DELH(I)+CPDT(I))                                        EN  79
   78 CONTINUE                                                                EN  80
      RETURN                                                                  EN  81
      END                                                                     EN  82
```

Listing B-3. TEMPRE Subprograms. (g) KINET.

```
C
C     KINET CALCULATES THE COMPOSITION ,RATE,AND HEAT OF REACTION FOR
C     THE KINETICS MODEL
C
C        SUBPROGRAM FOR THE KINETIC ANALYSIS OF THE CHAR SYSTEM
C
C
      SUBROUTINE KINET(TP1,TVAR,DELZ,KN,K7,DTC,HEAT,WNEW,KPT3,AVGFW)
      DIMENSION ICODE(20),ALPA(20),AA(20,6),
     1  S1(4),S2(4),S3(4),S4(4),S5(4),A11(4),A22(4),A33(4),A44(4),A55(4)
      DIMENSION AI(20),BI(20),CI(20),DI(20),EI(20),FI(20),GI(20),
     1  AII(20),BII(20),CII(20),DII(20),EII(20),FII(20),GII(20),FW(20),
     2   YI(20),EK(20),SIG(20),Y(20),DELH(20)
      DIMENSION RSC(15,15),PSC(15,15),NREX(15,15),NPEX(15,15),AF(30),
     1SF(20),AEF(20),AR(20),SR(20),AER(20),EQN(20,12),TABLE(70,20),
     2FLUXMO(20),FLUXMA(20),C(20),FK(20),RK(20),RATE(20),Y1(20),XFW(20)
      DIMENSION    PERCE(20),YTEMP(20),ENT(20),CPDT(20),CPDT1(20)
      DIMENSION FLUXI(20),FLUX1(20),FLUX2(20),FLUX3(20),FLUX4(20)
      DIMENSION TEST(50)
      DIMENSION RATER(30),NSTORE(30)
      COMMON NC,NS,MM,WI,PL,RR,TZERO,DELTK,ICODE,ALPA,AA,S1,S2,S3,
     1   S4,S5,A11,A22,A33,A44,A55
      COMMON AI,BI,CI,DI,EI,FI,GI,AII,BII,CII,DII,EII,FII,GII,FW,YI
      COMMON EK,SIG,EPS,Y,DELH
      COMMON RSC,PSC,NREX,NPEX,AF,SF,AEF,AR,SR,AER,EQN,TABLE
      KEY=3
      KSP1=NS
      KSP=NC
      IF(KN.EQ.1)K1=0
      IF(K1.EQ.0)K2=0
      IF(K1.EQ.0)W=WI
      T2=(TP1+459.)/1.8
      IF(K1.EQ.0)T1=T2
      IF(K1.EQ.0)DIF=10.
```

```
      IF(K7.EQ.1)GOTO88
      IF(K1.NE.0)GOTO74
      DO128 I=1,KSP1
  128 Y1(I)=YTEMP(I)
      W=WI/EPS
      IF(K7.GT.1)GOTO74
   88 KSP2=KSP1+1
      DO 83 J=1,KSP2
      DO 82 I=1,KSP2
      RSC(I,J)=0.
      PSC(I,J)=0.
      NREX(I,J)=0
      NPEX(I,J)=0
   82 CONTINUE
   83 CONTINUE
C
C     CONVERT TO KINET UNITS
C
       DO 127 I=1,KSP1
      XFW(I)=FW(I)
      Y1(I)=YI(I)
  127 YTEMP(I)=Y1(I)
      CALL INOUT(KSP1,NEQ,TINC,Y1,XFW)
   74 K1=K1+1
      P=PL/2160.
      R=82.06
      RR=1.987
      H=DELZ*30.48
   75 FORMAT(1X,I6)
      IF(K1.GT.1)GOTO3
C
C     INITIAL AVERAGE MOLECULAR WEIGHT
C
      SUM=0.
      DO1J=1,KSP
```

```
      SUM=SUM+XFW(J)*Y1(J)
    1 CONTINUE
      AVGFW=SUM
C
C     INITIAL MOLAL FLUX OF SPECIE J(GM-MOLES/CM2-SEC)
C
      ACON4=923.03/454.
      ACON1=(W/AVGFW)*454./923.03
      DO2J=1,KSP1
      FLUXMO(J)=ACON1*Y1(J)
C
C     INITIAL MASS FLUX OF SPECIE J(GRAMS/CM2-SEC)
C
      FLUXMA(J)=FLUXMO(J)*XFW(J)
 2    FLUXI(J)=FLUXMA(J)
      MX=1
C
C     CALCULATION OF C(J)
C
      IF(K1.GT.1)GOTO3
      WNEW=W
      TZERO=298.16
      T=(TP1 +460.)/1.8
      GOTO4
 3    T=TVAR
 4    SUM1=0.
      RRR=1000./(RR*T)
      ACON9=R*T/P
   73 DO5J=1,KSP
    5 SUM1=SUM1+FLUXMO(J)*ACON9
      SUM=0.
      DO6J=1,KSP
      C(J)=FLUXMO(J)/SUM1
    6 SUM=SUM+C(J)
      C(KSP1)=SUM*Y1(KSP1)
```

```
C
C     CALCULATE REACTION RATE CONSTANT
C
      DO7I=1,NEQ
      IF(SF(I).EQ.0.)GOTO900
      FK(I)=AF(I)*T**(-SF(I))*EXP(-AEF(I)*RRR)
      GOTO901
  900 FK(I)=AF(I)*EXP(-AEF(I)*RRR)
  901 IF(KN.EQ.1)GOTO902
  902 IF(SR(I).EQ.0.)GOTO903
      RK(I)=AR(I)*T**(-SR(I))*EXP(-AER(I)*RRR)
      GOTO7
  903 RK(I)=AR(I)*EXP(-AER(I)*RRR)
    7 CONTINUE
C
C     CALCULATION OF REACTION RATE OF SPECIE(J)
C
      DO12J=1,KSP1
      SUM2=0.
      DO11I=1,NEQ
      XMULTR=1.0
      XMULTP=1.0
      DO10K=1,KSP1
      IF(C(K).LT.1.E-37)C(K)=1.E-37
      NEW=NREX(I,K)
      IF(NEW.EQ.0)GOTO920
      XMULTR=XMULTR*(C(K)**NEW)
  920 NEW=NPEX(I,K)
      IF(NEW.EQ.0)GOTO10
      XMULTP=XMULTP*(C(K)**NEW)
   10 CONTINUE
      RATER(I)=FK(I)*XMULTR-RK(I)*XMULTP
      XNEW1=PSC(I,J)
      XNEW2=RSC(I,J)
      IF(XNEW1.EQ.XNEW2)GOTO11
```

```
      SUM2=SUM2+(XNEW1-XNEW2)*RATER(I)
   11 CONTINUE
      RATE(J)=SUM2
      TEST(J)=FLUXMA(J)
   12 CONTINUE
      DO 13 J=1,KSP1
      N=0
      SUM=0.0
      GO TO(7001,7002,7003,7004),MX
 7001 FLUX1(J)=H*RATE(J)*XFW(J)
      FLUXMA(J)=FLUXI(J)+0.5*FLUX1(J)
      GO TO 7000
 7002 FLUX2(J)=H*RATE(J)*XFW(J)
      FLUXMA(J)=FLUXI(J)+0.5*FLUX2(J)
      GO TO 7000
 7003 FLUX3(J)=H*RATE(J)*XFW(J)
      FLUXMA(J)=FLUXI(J)+FLUX3(J)
      GO TO 7000
 7004 FLUX4(J)=H*RATE(J)*XFW(J)
      FLUXMA(J)=FLUXI(J)+(1./6.)*(FLUX1(J)+2.*FLUX2(J)+2.*FLUX3(J)+
     1FLUX4(J))
      FLUXI(J)=FLUXMA(J)
 7000 IF(FLUXMA(J).GT.0.)GOTO 13
      DO 16 I=1,NEQ
      XTEST1=RSC(I,J)
      IF(XTEST1.EQ.0.)GO TO 16
      N=N+1
      NSTORE(N)=I
      SUM=SUM+RATER(I)
   16 CONTINUE
      IF(N.EQ.0)GOTO161
      IF(SUM.EQ.0.)GOTO161
      DO160II=1,N
      I=NSTORE(II)
      RA=RATER(I)/SUM
```

```
      DO 18 K=1,KSP1
      XTEST2=PSC(I,K)
      IF(XTEST2.EQ.O.)GOTO 18
      FLUXMA(K)=FLUXMA(K)+FLUXMA(J)/XFW(J)*PSC(I,K)/PSC(I,J)*XFW(K)*RA
      IF(FLUXMA(K).GT.O.)GOTO 18
      FLUXMA(K)=1.0E-37
 18   CONTINUE
      DO 171 L=1,KSP1
      XTEST=RSC(I,L)
      IF(XTEST.EQ.O.)GOTO 171
      IF(L.EQ.J)GOTO 171
      FLUXMA(L)=TEST(L)-FLUXMA(J)/XFW(J)*RSC(I,L)/RSC(I,J)*XFW(L)*RA
 171  CONTINUE
 160  CONTINUE
      RATE(J)=-TEST(J)/(DELZ*XFW(J))
  161 FLUXMA(J)=1.E-76
 13   CONTINUE
      MX=MX+1
      IF(MX.EQ.5)MX=1
      WNEW=0.
      SUM3=0.
      DO 19 J=1,KSP1
      FLUXMO(J)=FLUXMA(J)/XFW(J)
      IF(J.EQ.KSP1)GOTO 19
      SUM3=SUM3+FLUXMO(J)
      WNEW=WNEW+FLUXMA(J)*ACON4
 19   CONTINUE
      DO14J=1,KSP
      Y1(J)=FLUXMO(J)/SUM3
   14 PERCE(J)=Y1(J)*100.
C
C     CALCULATION OF THE RATIO OF THE MOLES OF THE
C     SOLID SPECIE TO THE MOLES OF GASES.
C
      Y1(KSP1)=FLUXMO(KSP1)/SUM3
```

```
      SUM=0.                                                            KI 210
      DO 111 I=1,KSP                                                    KI 211
      SUM=SUM+XFW(I)*Y1(I)                                              KI 212
  111 CONTINUE                                                          KI 213
      AVGFW=SUM                                                         KI 214
      DO6606 IK=1,NC                                                    KI 215
      Y(IK)=Y1(IK)                                                      KI 216
 6606 CONTINUE                                                          KI 217
      CALL ENTAL1(T,HEAT1,ENT,SUM7,RATE,KEY)                            KI 218
C                                                                       KI 219
C     CONVERT THE UNITS OF THE HEAT OF REACTION TERM                    KI 220
C     TO THOSE NEEDED IN GROUP                                          KI 221
C                                                                       KI 222
      HEAT=(HEAT1/252.)*(30.48**3)/DTC                                  KI 223
      KPT3=K2                                                           KI 224
      IF(T.LT.T1)GOTO37                                                 KI 225
      T1=T1+TINC                                                        KI 226
      KOS=KSP+4                                                         KI 227
      K2=K2+1                                                           KI 228
      DO17 I=5,KOS                                                      KI 229
      TABLE(K2,I)=Y1(I-4)                                               KI 230
   17 CONTINUE                                                          KI 231
      NY=KOS+1                                                          KI 232
      TABLE(K2,NY)=Y1(KSP1)                                             KI 233
 6021 TABLE(K2,1)=T                                                     KI 234
      TABLE(K2,2)=HEAT                                                  KI 235
      TABLE(K2,3)=AVGFW                                                 KI 236
      TABLE(K2,4)=WNEW                                                  KI 237
      TF=T*1.8-460.0                                                    KI 238
   37 SUM=0.                                                            KI 239
  112 CONTINUE                                                          KI 240
      RETURN                                                            KI 241
      END                                                               KI 242
```

Listing B-3. TEMPRE Subprogram. (h) INOUT

```
C
C
C      GENERAL INPUT-OUTPUT SUBPROGRAM FOR KINETIC ANALYSIS
C
C
      SUBROUTINE INOUT(KSP1,NEQ,TINC,Y1,XFW)
      DIMENSION ICODE(20),ALPA(20),AA(20,6),
     1  S1(4),S2(4),S3(4),S4(4),S5(4),A11(4),A22(4),A33(4),A44(4),A55(4)
      DIMENSION AI(20),BI(20),CI(20),DI(20),EI(20),FI(20),GI(20),
     1  AII(20),BII(20),CII(20),DII(20),EII(20),FII(20),GII(20),FW(20),
     2   YI(20),EK(20),SIG(20),Y(20),DELH(20)
      DIMENSION RSC(15,15),PSC(15,15),NREX(15,15),NPEX(15,15),AF(30),
     1SF(20),AEF(20),AR(20),SR(20),AER(20),EQN(20,12),TABLE(70,20),
     2Y1(20),XFW(20)
      COMMON NC,NS,MM,WI,PL,RR,TZERO,DELTK,ICODE,ALPA,AA,S1,S2,S3,
     1.  S4,S5,A11,A22,A33,A44,A55
      COMMON AI,BI,CI,DI,EI,FI,GI,AII,BII,CII,DII,EII,FII,GII,FW,YI
      COMMON EK,SIG,EPS,Y,DELH
      COMMON RSC,PSC,NREX,NPEX,AF,SF,AEF,AR,SR,AER,EQN,TABLE
C     READ EQN 1 CH4 = H2 + 0.5C2H6
      J=1
      READ 21,(EQN(J,I),I=1,12)
C
C     READ THE STOCHIOMETRIC COEFICIENTS OF THE EQUATION
C
      READ 22,RSC(1,2),PSC(1,1),PSC(1,3)
C
C     READ THE EXPONENTS OF THE RATE EQUATION
C
      READ 25,NREX(1,2),NPEX(1,1),NPEX(1,3)
C
C     READ THE COEFECIENTS OF THE FORWARD AND REVERSE REACTION RATE CONS
C     UNITS OF AF AND AR ARE IN GM-MOLES,CUBIC-CM,AND SECONDS
C     UNITS OF AEF AND AER ARE IN KCAL PER GM-MOLE
```

```
C
      READ23,AF(1),SF(1),AEF(1)
      READ23,AR(1),SR(1),AER(1)
C
C     READ EQN 2 C2H6 = H2 + C2H4
C
      J=J+1
      READ 21,(EQN(J,I),I=1,12)
      READ22,RSC(2,3),PSC(2,1),PSC(2,4)
      READ25,NREX(2,3),NPEX(2,1),NPEX(2,4)
      READ23,AF(2),SF(2),AEF(2)
      READ23,AR(2),SR(2),AER(2)
 21   FORMAT(12A4)
 22   FORMAT(6F4.0)
 23   FORMAT(E8.0,1X,2F6.0)
C
C     READ EQN 3 C2H4 = H2 + C2H2
C
      J=J+1
      READ 21,(EQN(J,I),I=1,12)
      READ22,RSC(3,4),PSC(3,1),PSC(3,5)
      READ25,NREX(3,4),NPEX(3,1),NPEX(3,5)
      READ23,AF(3),SF(3),AEF(3)
      READ23,AR(3),SR(3),AER(3)
C
C     READ EQN 4 C2H2 = 2C + H2
C
      J=J+1
      READ 21,(EQN(J,I),I=1,12)
      READ 22,RSC(4,5),PSC(4,13),PSC(4,1)
      READ25,NREX(4,5),NPEX(4,13),NPEX(4,1)
      READ23,AF(4),SF(4),AEF(4)
      READ23,AR(4),SR(4),AER(4)
C
C     READ EQN 5 C6H6 = 3C2H2
```

```
C                                                                       IN  70
      J=J+1                                                             IN  71
      READ 21,(EQN(J,I),I=1,12)                                         IN  72
      READ22,RSC(5,6),PSC(5,5)                                          IN  73
      READ25,NREX(5,6),NPEX(5,5)                                        IN  74
      READ23,AF(5),SF(5),AEF(5)                                         IN  75
      READ23,AR(5),SR(5),AER(5)                                         IN  76
C                                                                       IN  77
C     READ EQN 6 NH3 = 0.5N2 +1.5H2                                     IN  78
C                                                                       IN  79
      J=J+1                                                             IN  80
      READ 21,(EQN(J,I),I=1,12)                                         IN  81
      READ22,RSC(6,8),PSC(6,7),PSC(6,1)                                 IN  82
      READ25,NREX(6,8),NPEX(6,7),NPEX(6,1)                              IN  83
      READ23,AF(6),SF(6),AEF(6)                                         IN  84
      READ23,AR(6),SR(6),AER(6)                                         IN  85
C                                                                       IN  86
C      READ EQN 7 C6H6O + H2 = H2O + C6H6                               IN  87
C                                                                       IN  88
      J=J+1                                                             IN  89
      READ21,(EQN(J,I),I=1,12)                                          IN  90
      READ22, RSC(7,9),RSC(7,1),PSC(7,13),PSC(7,6)                      IN  91
      READ25,NRFX(7,9),NREX(7,1),NPEX(7,13),NPEX(7,6)                   IN  92
      READ23,AF(7),SF(7),AFF(7)                                         IN  93
      READ23,AR(7),SR(7),AER(7)                                         IN  94
C                                                                       IN  95
C     READ EQUATION 8 C + H2O = CO + H2                                 IN  96
C                                                                       IN  97
      J=J+1                                                             IN  98
      READ 21,(EQN(J,I),I=1,12)                                         IN  99
      READ 22,RSC( 8,13),RSC( 8,12),PSC( 8,11),PSC( 8,1)                IN 100
      READ25,NREX(8,13),NRFX(8,12),NPEX(8,11),NPEX(8,1)                 IN 101
      READ23,AF(8),SF(8),AFF(8)                                         IN 102
      READ23,AR(8),SR(8),AER(8)                                         IN 103
C                                                                       IN 104
```

```
C     READ EQN 9  C+CO2=CO                                              IN 105
C                                                                       IN 106
      J=J+1                                                             IN 107
      READ 21,(EQN(J,I),I=1,12)                                         IN 108
      READ 22,RSC(9,13),RSC(9,10),PSC(9,11)                             IN 109
      READ 25,NREX(9,13),NREX(9,10),NPEX(9,11)                          IN 110
      READ23,AF(9),SF(9),AEF(9)                                         IN 111
      READ23,AR(9),SR(9),AER(9)                                         IN 112
C                                                                       IN 113
C     READ EQN 10 C + 2H2 = CH4                                         IN 114
C                                                                       IN 115
      J=J+1                                                             IN 116
      READ21,(EQN(J,I),I=1,12)                                          IN 117
      READ 22,RSC(10,13), RSC(10,1),PSC(10,2)                           IN 118
      READ25,NREX(10,13),NREX(10,1),NPEX(10,2)                          IN 119
      READ23,AF(10),SF(10),AEF(10)                                      IN 120
      READ23,AR(10),SR(10),AER(10)                                      IN 121
C                                                                       IN 122
C     READ EQN 11 H2O + CO = H2 + CO2                                   IN 123
C                                                                       IN 124
      J=J+1                                                             IN 125
      READ21,(EQN(J,I),I=1,12)                                          IN 126
      READ22,RSC(11,12),RSC(11,11),PSC(11,1),PSC(11,10)                 IN 127
      READ25,NREX(11,12),NREX(11,11),NPEX(11,1),NPFX(11,10)             IN 128
      READ23,AF(11),SF(11),AEF(11)                                      IN 129
      READ23,AR(11),SR(11),AER(11)                                      IN 130
   25 FORMAT(6I2)                                                       IN 131
      READ 24,NEQ,TINC                                                  IN 132
   24 FORMAT(I6,1X,1F10.8)                                              IN 133
      RETURN                                                            IN 134
      END                                                               IN 135
```

Listing B-4. Iterative TEMPRE Input Format. (a) Non-equilibrium flow.

```
   12    13     4      1
1.36325E001.85605E-3-7.6675E-71.5104E-10-1.139E-14                      C H
-7.1244E-17.34065E-3-5.5262E-6 1.514E-09-2.382E-14                      C L
3.04369E00 6.1187E-4 -7.399E-9 -2.03E-11 2.459E-15                      H2 H
2.846085E04.1932E-03-9.6119E-69.5123E-09-3.309E-12                      H2 L
2.854576E0 1.5976E-3-6.2566E-71.1316E-10-7.69E- 15                      N2 H
3.691615E0-1.3333E-32.65031E-6-9.769E-10-9.977E-14                      N2 L
3.597613E07.81456E-4-2.2387E-74.2490E-11-3.346E-15                      O2 H
3.718995E0-2.5167E-38.58374E-6-8.2999E-92.7082E-12                      O2 L
0.000000E0 2.00000E0 0.00000E0 0.00000E0                                H2
3.04369E00 6.1187E-4 -7.399E-9 -2.03E-11 2.459E-15-8.5491E02 -1.648E00  H2 H
2.846085E04.1932E-03-9.6119E-69.5123E-09-3.309E-12-9.67254E2 -1.4118E0  H2 L
 1.00000E0 4.0000E00 0.0000E00 0.0000E00                                CH4
 1.18000E0 1.0950E-2-4.0620E-6 7.137E-10-4.749E-14-9.8556E03 1.2506E01  CH4 H
4.249768E0-6.9127E-3 3.1602E-5-2.9715E-89.5103E-12-1.01866E4-9.1755E-1  CH4 L
 2.00000E0 6.00000E0 0.00000E0 0.00000E0                                C2H6
1.43080E001.88898E-2-7.0441E-61.18720E-9-7.450E-14 0.0000E001.450804E1  C2H6 H D
2.882036E01.03220E-21.19144E-5-1.4833E-84.4750E-12 0.0000E007.589057E0  C2H6 L D
 2.00000E0 4.00000E0 0.00000E0 0.00000E0                                C2H4
 3.5023E00 1.159E-02-4.4745E-6 7.945E-10-5.323E-14 4.5439E03 2.4667E00  C2H4 H
1.120244E0 1.3906E-2 2.6568E-6-1.1560E-85.2387E-125.332889E3 1.58378E1  C2H4 L
 2.00000E0 2.00000E0 0.00000E0 0.00000E0                                C2H2
 4.4966E00 5.2698E-3-1.840E-063.1054E-10-2.000E-142.5637E004-3.14481E0  C2H2 H
7.90333E-1 2.3466E-2-3.5542E-5 2.7951E-8-8.448E-12 2.6255E04 1.4005E01  C2H2 L
 6.00000E0 6.00000E0 0.00000E0 0.00000E0                                C6H6
4.619872E02.88096E-2-1.1245E-51.95763E-9-1.258E-13 0.00000E0-1.16780E0  C6H6 H D
3.51119E-13.75399E-2-7.9472E-6-7.5090E-93.0385E-12 0.00000E01.986012E1  C6H6 L D
0.000000E0 0.00000E0 2.00000E0 0.00000E0                                N2
2.854576E0 1.5976E-3-6.2566E-71.1316E-10-7.69E- 15-8.90174E2 6.39029E0  N2
3.691615E0-1.3333E-32.65031E-6-9.769E-10-9.977E-14-1.06283E3 2.28750E0  N2 L
0.00000E00 3.00000E0 1.00000E0 0.00000E0                                NH3
2.149399E06.49285E-3-2.2695E-63.7394E-10-2.361E-14-6.40196E3 9.23891E0  NH3 H
3.77162E00-4.8621E-49.8742E-06-9.5679E-93.1313E-12-6.72810E3 1.4654E00  NH3 L
6.00000E00 6.00000E0 0.00000E0 1.00000E0                                C6H6O
```

```
-3.93169E06.93818F-2-5.2106E-51.24967E-82.0915E-12-1.33038E44.187817E1  C6H6O
-3.93169E06.93818E-2-5.2106E-51.24967E-82.0915E-12-1.33038F44.187817F1  C6H6O
 1.00000F0 0.00000E0 0.00000E0 2.00000E0                                CO2
 4.4129F003.1923E-03 -1.298E-6 2.415E-10-1.674E-14-4.8944E04-7.2876E-1  CO2 H
2.170100E0 1.0378E-2-1.0734E-56.34592E-9-1.628E-12-4.83526E4 1.06644E1  CO2 L
 1.00000E0 0.00000E0 0.00000E0 1.00000E0                                CO
 2.9512E00 1.5526E-3-6.1911E-7 1.135E-10-7.788E-15-1.4232E04 6.5314E00  CO H
3.787133E0-2.171E-035.07573E-6-3.4738F-97.7217E-13-1.43635E4 2.63355E0  CO L
0.000000E0 2.00000E0 0.00000E0 1.00000F0                                H2O
 2.67075E0 3.0317F-3 -8.535E-7 1.179E-10-6.197E-15-2.9889E04 6.88383E0  H2O H
4.15650F00-1.7244E-35.6982E-06-4.5930F-91.4234E-12-3.02888E4-6.8616E-1  H2O L
 1.0000E00 0.00000E0 0.0000E00 0.0000E00                                C
1.36325E001.85605E-3-7.6675E-71.5104E-10-1.139E-14-6.4967F02-7.9890E00  C H
-7.1244E-17.34065E-3-5.5262E-6 1.514E-09-2.382E-14-6.80533E1 2.79326E0  C L
           33.3           2.986    H2
          136.5           3.822   CH4
          230.0           4.418  C2H6
          205.0           4.232  C2H4
          185.0           4.221  C2H2
          440.0           5.270  C6H6
           91.5           3.681    N2
          312.0           3.432   NH3
         400.0            5.000 C6H6O
          190.0           3.996   CO2
          110.0           3.590    CO
          356.0           2.649   H2O
     050000F&09     050000E&05
    34     70   300    100      3     1
    0.30              2.785
    0.35              2.628
    0.40              2.492
    0.45              2.368
    0.50              2.257
    0.55              2.156
    0.60              2.065
```

```
  0.65           1.982
  0.70           1.908
  0.75           1.841
  0.80           1.780
  0.85           1.725
  0.90           1.675
  0.95           1.629
  1.00           1.587
  1.10           1.514
  1.20           1.452
  1.30           1.399
  1.50           1.314
  1.70           1.248
  1.90           1.197
  2.2            1.138
  2.6            1.081
  3.2            1.022
  4.0            0.9700
  5.0            0.9269
  7.0            0.8727
 10.0            0.8242
 20.0            0.7432
 40.0            0.6718
 70.0            0.6194
100.0            0.5882
200.0            0.5320
400.0            0.4811
         0.5
1185.0      1755.0   31176.0    0.0208  0.000208  0.000260   0.00520  XV-46G
 0.00011    2160.0     1.987    298.16      50.0                      XV-46G
                   2.00000E0 31.700E00    H2     0 0.00000E0          EXP XIII
                   1.6000E01 46.4000E0   CH4     0 -17889.E0          EXP XIII
                   30.0000E0 1.000E-18  C2H6     0-20316.6E0          EXP XIII
                  28.00000E0 1.000E-18  C2H4     0 12496.0E0          EXP XIII
                   2.6000E01 1.000E-18  C2H2     0 54194.0E0          EXP XI&&
```

```
                      78.00000E0 1.000E-18  C6H6      0 19778.8F0          EXP XIII
                       28.0000F0 14.000E00    N2      0 0.00000E0          EXP XIII
                       17.0000E0 1.000E-18   NH3      0 -11040.F0          EXP XIII
                       94.0000F0 1.000E-18  PHOH      0-23500.0E0          EXP XIII
                       44.0000E0 2.50000F0   CO2      0-94051.8E0          EXP XIII
                       2.8000E01 5.50000E0    CO      0-26415.7E0          EXP XIII
                       18.0000E0 1.000E-18   H2O      0-57797.9E0          EXP XIII
                       12.000F00 155.060F0     C      1 0.00000E0          FXP XIII
 CH4 = H2 & 0.5C2H6   1000-2500-0K
 1.0 1.0 0.5
 1 0 0
7.60E&14     0.0  95.0
 1.0E-32   0.0   0.0
 C2H6 = H2 & C2H4  970-1580-0K
 1.0 1.0 1.0
 1 0 0
3.14E&13   0.0  64.1
 1.0E-32   0.0   1.0
 C2H4 = H2 & C2H2  1500-2100-0K
 1.0 1.0 1.0
 1 0 0
2.57E&08   0.0  40.0
 1.0E-32   0.0   1.0
 C2H2 = 2C & H2   650-2500-0K
 1.0 2.0 1.0
 2 0 0
2.14E&10   0.0  10.0
 1.0E-32   0.0   1.0
 C6H6=3C2H2  1173-1523-0K
 1.0 3.0
 1 0
 1.4E&09   0.0  52.0
 1.0F-32   0.0   1.0
 NH3 = 0.5N2 & 1.5H2  1200-2650-0K
 1.0 0.5 1.5
```

```
 1 0 0
2.86E&06   0.0  60.8
 1.0E-30   0.0   1.8
 C6H6O & H2 = H2O & C6H6
 1.0 1.0 1.0 1.0
 1 1 0 0
2.00E&13   0.0   50.
 1.0E-30   0.0   1.0
 C & H2O = CO & H2
1.0 1.0 1.0 1.0
 0 1 0 0
1.20E&12  -1.0   85.
1.00E-30   0.0    1.
 C(S) & CO2 =  2CO
 1.0 1.0 2.0
 0 1 0
1.20E&12  -1.0   85.
1.00E-30   0.0    0.
 CO & H2O = CO2 & H2
 1.0 1.0 1.0 1.0
 1 1 0 0
2.00E&13   0.0   20.
 1.0E-30   0.0   1.0
    10  20.
     9      1
         698.0     244000E-03
         909.0     298000E-03
        1001.0     356000F-03
        1073.0     356000E-03
        1346.0     451000E-03
        1515.0     470000F-03
        1709.0     575000F-03
        1848.0     559000F-03
        1998.0     616000F-03
```

Listing B-4. Iterative TEMPRE Input Format. (b) Equilibrium flow.

```
    12    13     4     1
1.36325E001.85605E-3-7.6675E-71.5104E-10-1.139E-14                      C H
-7.1244E-17.34065E-3-5.5262E-6 1.514E-09-2.382E-14                      C L
3.04369E00 6.1187E-4 -7.399E-9 -2.03E-11 2.45 E-15                      H2 H
2.846085E04.1932E-03-9.6119E-69.5123E-09-3.309E-12                      H2 L
2.854576E0 1.5976E-3-6.2566E-71.1316E-10-7.69E- 15                      N2 H
3.691615E0-1.3333E-32.65031E-6-9.769E-10-9.977E-14                      N2 L
3.597613E07.81456E-4-2.2387E-74.2490E-11-3.346E-15                      O2 H
3.718995E0-2.5167E-38.58374E-6-8.2999E-92.7082E-12                      O2 L
0.000000E0 2.00000E0 0.00000E0 0.00000E0                                H2
3.04369E00 6.1187E-4 -7.399E-9 -2.03E-11 2.459E-15-8.5491E02 -1.648E00  H2 H
2.846085E04.1932E-03-9.6119E-69.5123E-09-3.309E-12-9.67254E2 -1.4118E0  H2 L
 1.00000E0 4.0000E00 0.0000E00 0.0000E00                                CH4
 1.18000E0 1.0950E-2-4.0620E-6 7.137E-10-4.749E-14-9.8556E03 1.2506E01  CH4 H
4.249768E0-6.9127E-3 3.1602E-5-2.9715E-89.5103E-12-1.01866E4-9.1755E-1  CH4 L
 2.00000E0 6.00000E0 0.00000E0 0.00000E0                                C2H6
1.43080E001.88898E-2-7.0441E-61.18720E-9-7.450E-14 0.0000E001.450804E1  C2H6 H D
2.882036E01.03220E-21.19144E-5-1.4833E-84.4750E-12 0.0000E007.589057E0  C2H6 L D
 2.00000E0 4.00000E0 0.00000E0 0.00000E0                                C2H4
 3.5023E00 1.159E-02-4.4745E-6 7.945E-10-5.323E-14 4.5439E03 2.4667E00  C2H4 H
1.120244E0 1.3906E-2 2.6568E-6-1.1560E-85.2387E-125.332889E3 1.58378E1  C2H4 L
 2.00000E0 2.00000E0 0.00000E0 0.00000E0                                C2H2
 4.4966E00 5.2698E-3-1.840E-063.1054E-10-2.000E-142.5637E004-3.14481E0  C2H2 H
7.90333E-1 2.3466E-2-3.5542E-5 2.7951E-8-8.448E-12 2.6255E04 1.4005E01  C2H2 L
 6.00000E0 6.00000E0 0.00000E0 0.00000E0                                C6H6
4.619872E02.88096E-2-1.1245E-51.95763E-9-1.258E-13 0.00000E0-1.16780E0  C6H6 H D
3.51119E-13.75399E-2-7.9472E-6-7.5090E-93.0385E-12 0.00000E01.986012E1  C6H6 L D
0.000000E0 0.00000E0 2.00000E0 0.00000E0                                N2
2.854576E0 1.5976E-3-6.2566E-71.1316E-10-7.69E- 15-8.90174E2 6.39029E0  N2
3.691615E0-1.3333E-32.65031E-6-9.769E-10-9.977E-14-1.06283E3 2.28750E0  N2 L
0.00000E00 3.00000E0 1.00000E0 0.00000E0                                NH3
2.149399E06.49285E-3-2.2695E-63.7394E-10-2.361E-14-6.40196E3 9.23891E0  NH3 H
3.77162E00-4.8621E-49.8742E-06-9.5679E-93.1313E-12-6.72810E3 1.4654E00  NH3 L
6.00000E00 6.00000E0 0.00000E0 1.00000E0                                C6H6O
```

```
-3.93169E06.93818E-2-5.2106E-51.24967E-82.0915E-12-1.33038E44.187817E1   C6H6O
-3.93169E06.93818E-2-5.2106E-51.24967E-82.0915E-12-1.33038E44.187817E1   C6H6O
 1.00000E0 0.00000E0 0.00000E0 2.00000E0                                 CO2
 4.4129E003.1923E-03 -1.298E-6 2.415E-10-1.674E-14-4.8944E04-7.2876E-1   CO2 H
2.170100E0 1.0378E-2-1.0734E-56.34592E-9-1.628E-12-4.83526E4 1.06644E1   CO2 L
 1.00000E0 0.00000E0 0.00000E0 1.00000E0                                 CO
 2.9512E00 1.5526E-3-6.1911E-7 1.135E-10-7.788E-15-1.4232E04 6.5314E00   CO H
3.787133E0-2.171E-035.07573E-6-3.4738E-97.7217E-13-1.43635E4 2.63355E0   CO L
0.000000E0 2.00000E0 0.00000E0 1.00000E0                                 H2O
 2.67075E0 3.0317E-3 -8.535E-7 1.179E-10-6.197E-15-2.9889E04 6.88383E0   H2O H
4.15650E00-1.7244E-35.6982E-06-4.5930E-91.4234E-12-3.02888E4-6.8616E-1   H2O L
 1.0000E00 0.00000E0 0.0000E00 0.0000E00                                 C
1.36325E001.85605E-3-7.6675E-71.5104E-10-1.139E-14-6.4967E02-7.9890E00   C H
-7.1244E-17.34065E-3-5.5262E-6 1.514E-09-2.382E-14-6.80533E1 2.79326E0   C L
          33.3           2.986  H2
         136.5           3.822 CH4
         230.0           4.418C2H6
         205.0           4.232C2H4
         185.0           4.221C2H2
         440.0           5.270C6H6
          91.5           3.681  N2
         312.0           3.432 NH3
        400.0            5.000PHOH
         190.0           3.996 CO2
         110.0           3.590  CO
         356.0           2.649 H2O
      050000E+09      050000E+05
    34     70    300     100      2      1
    0.30              2.785
    0.35              2.628
    0.40              2.492
    0.45              2.368
    0.50              2.257
    0.55              2.156
    0.60              2.065
```

```
  0.65           1.982
  0.70           1.908
  0.75           1.841
  0.80           1.780
  0.85           1.725
  0.90           1.675
  0.95           1.629
  1.00           1.587
  1.10           1.514
  1.20           1.452
  1.30           1.399
  1.50           1.314
  1.70           1.248
  1.90           1.197
  2.2            1.138
  2.6            1.081
  3.2            1.022
  4.0            0.9700
  5.0            0.9269
  7.0            0.8727
 10.0            0.8242
 20.0            0.7432
 40.0            0.6718
 70.0            0.6194
100.0            0.5882
200.0            0.5320
400.0            0.4811
         0.5
  920.0     1350.0   19682.0    0.0208  0.000208  0.000260   0.00520  XII-36G
 0.00390    2160.0     1.987    298.16      50.0                      XII-36G
                   2.00000E0 35.000E00    H2     0 0.00000E0          EXP VIII
                   1.6000E01 43.7000E0   CH4     0 -17889.E0          EXP VIII
                   30.0000E0 1.000E-18  C2H6     0-20316.6E0          EXP VIII
                  28.00000E0 1.000E-18  C2H4     0 12496.0E0          EXP VIII
                   2.6000E01 1.000E-18  C2H2     0 54194.0E0          EXP VIII
```

```
               78.00000E0 1.000E-18  C6H6    0 19778.8E0         EXP VIII
                28.0000E0 13.600E00    N2    0 0.00000E0         EXP VIII
                17.0000E0 1.000E-18   NH3    0 -11040.E0         EXP VIII
                94.0000E0 1.000E-18 C6H6O    0-23500.0E0         EXP VIII
                44.0000E0 2.90000E0   CO2    0-94051.8E0         EXP VIII
                2.8000E01 4.90000E0    CO    0-26415.7E0         EXP VIII
                18.0000E0 1.000E-18   H2O    0-57797.9E0         EXP VIII
                12.000E00 155.060E0     C    1 0.00000E0         EXP VIII
500.0    1600.0      20.0      0.01
6    25
9     1
     698.0     244000E-03
     909.0     298000E-03
    1001.0     356000E-03
    1073.0     356000E-03
    1346.0     451000E-03
    1515.0     470000E-03
    1709.0     575000E-03
    1848.0     559000E-03
    1998.0     616000E-03
```

Listing B-4. Iterative TEMPRE Input Format (c) Frozen Flow

```
   12     13      4       1
1.36325E001.85605E-3-7.6675E-71.5104E-10-1.139E-14                    C H
-7.1244E-17.34065E-3-5.5262E-6 1.514E-09-2.382E-14                    C L
3.04369E00 6.1187E-4 -7.399E-9 -2.03E-11 2.45 E-15                    H2 H
2.846085E04.1932E-03-9.6119E-69.5123E-09-3.309E-12                    H2 L
2.854576E0 1.5976E-3-6.2566E-71.1316E-10-7.69E- 15                    N2 H
3.691615E0-1.3333E-32.65031E-6-9.769E-10-9.977E-14                    N2 L
3.597613E07.81456E-4-2.2387E-74.2490E-11-3.346E-15                    O2 H
3.718995E0-2.5167E-38.58374E-6-8.2999E-92.7082E-12                    O2 L
0.000000E0 2.00000E0 0.00000E0 0.00000E0                              H2
3.04369E00 6.1187E-4 -7.399E-9 -2.03E-11 2.459E-15-8.5491E02 -1.648E00 H2 H
2.846085E04.1932E-03-9.6119E-69.5123E-09-3.309E-12-9.67254E2 -1.4118E0 H2 L
 1.00000E0 4.0000E00 0.0000E00 0.0000E00                              CH4
 1.18000E0 1.0950E-2-4.0620E-6 7.137E-10-4.749E-14-9.8556E03 1.2506E01 CH4 H
4.249768E0-6.9127E-3 3.1602E-5-2.9715E-89.5103E-12-1.01866E4-9.1755E-1 CH4 L
 2.00000E0 6.00000E0 0.00000E0 0.00000E0                              C2H6
1.43080E001.88898E-2-7.0441E-61.18720E-9-7.450E-14 0.0000E001.450804E1 C2H6 H D
2.882036E01.03220E-21.19144E-5-1.4833E-84.4750E-12 0.0000E007.589057E0 C2H6 L D
 2.00000E0 4.00000E0 0.00000E0 0.00000E0                              C2H4
 3.5023E00 1.159E-02-4.4745E-6 7.945E-10-5.323E-14 4.5439E03 2.4667E00 C2H4 H
1.120244E0 1.3906E-2 2.6568E-6-1.1560E-85.2387E-125.332889E3 1.58378E1 C2H4 L
 2.00000E0 2.00000E0 0.00000E0 0.00000E0                              C2H2
 4.4966E00 5.2698E-3-1.840E-063.1054E-10-2.000E-142.5637E004-3.14481E0 C2H2 H
7.90333E-1 2.3466E-2-3.5542E-5 2.7951E-8-8.448E-12 2.6255E04 1.4005E01 C2H2 L
 6.00000E0 6.00000E0 0.00000E0 0.00000E0                              C6H6
4.619872E02.88096E-2-1.1245E-51.95763E-9-1.258E-13 0.00000E0-1.16780E0 C6H6 H D
3.51119E-13.75399E-2-7.9472E-6-7.5090E-93.0385E-12 0.00000E01.986012E1 C6H6 L D
0.000000E0 0.00000E0 2.00000E0 0.00000E0                              N2
2.854576E0 1.5976E-3-6.2566E-71.1316E-10-7.69E- 15-8.90174E2 6.39029E0 N2
3.691615E0-1.3333E-32.65031E-6-9.769E-10-9.977E-14-1.06283E3 2.28750E0 N2 L
0.00000E00 3.00000E0 1.00000E0 0.00000E0                              NH3
2.149399E06.49235E-3-2.2695E-63.7394E-10-2.361E-14-6.40196E3 9.23891E0 NH3 H
3.77162E00-4.8621E-49.8742E-06-9.5679E-93.1313E-12-6.72810E3 1.4654E00 NH3 L
6.00000E00 6.00000E0 0.00000E0 1.00000E0                              C6H60
```

```
-3.93169E06.93818E-2-5.2106E-51.24967E-82.0915E-12-1.33038E44.187817E1  C6H6O
-3.93169E06.93818E-2-5.2106E-51.24967E-82.0915E-12-1.33038E44.187817E1  C6H6O
 1.00000E0 0.00000E0 0.00000E0 2.00000E0                                CO2
 4.4129E003.1923E-03 -1.298E-6 2.415E-10-1.674E-14-4.8944E04-7.2876E-1  CO2 H
2.170100E0 1.0378E-2-1.0734E-56.34592E-9-1.628E-12-4.83526E4 1.06644E1  CO2 L
 1.00000E0 0.00000E0 0.00000E0 1.00000E0                                CO
 2.9512E00 1.5526E-3-6.1911E-7 1.135E-10-7.788E-15-1.4232E04 6.5314E00  CO H
3.787133E0-2.171E-035.07573E-6-3.4738E-97.7217E-13-1.43635E4 2.63355E0  CO L
0.000000E0 2.00000E0 0.00000E0 1.00000E0                                H2O
 2.67075E0 3.0317E-3 -8.535E-7 1.179E-10-6.197E-15-2.9889E04 6.88383E0  H2O H
4.15650E00-1.7244E-35.6982E-06-4.5930E-91.4234E-12-3.02888E4-6.8616E-1  H2O L
 1.0000E00 0.00000E0 0.0000E00 0.0000E00                                C
1.36325E001.85605E-3-7.6675E-71.5104E-10-1.139E-14-6.4967E02-7.9890E00  C H
-7.1244E-17.34065E-3-5.5262E-6 1.514E-09-2.382E-14-6.80533E1 2.79326E0  C L
           33.3          2.986  H2
          136.5          3.822 CH4
          230.0          4.418C2H6
          205.0          4.232C2H4
          185.0          4.221C2H2
          440.0          5.270C6H6
           91.5          3.681  N2
          312.0          3.432 NH3
         400.0           5.000PHOH
          190.0          3.996 CO2
          110.0          3.590  CO
          356.0          2.649 H2O
     050000E&09     050000E&05
    34    70   300   100       1     2
    0.30           2.785
    0.35           2.628
    0.40           2.492
    0.45           2.368
    0.50           2.257
    0.55           2.156
    0.60           2.065
```

```
    0.65           1.982
    0.70           1.908
    0.75           1.841
    0.80           1.780
    0.85           1.725
    0.90           1.675
    0.95           1.629
    1.00           1.587
    1.10           1.514
    1.20           1.452
    1.30           1.399
    1.50           1.314
    1.70           1.248
    1.90           1.197
    2.2            1.138
    2.6            1.081
    3.2            1.022
    4.0            0.9700
    5.0            0.9269
    7.0            0.8727
   10.0            0.8242
   20.0            0.7432
   40.0            0.6718
   70.0            0.6194
  100.0            0.5882
  200.0            0.5320
  400.0            0.4811
          0.5
     500.0     3000.0     5047.0     0.0208  0.000208  0.000260    0.00520  CONTROL
    0.05       2160.0      1.987     298.16      50.0                        CONTROL
                      2.00000E0 133.40E00     H2      0 000000.E0
                      16.0000E0 6.7000E00    CH4      0 -17889.E0
                      30.0000E0  1.00E-18   C2H6      0 -20317.E0
                      28.0000E0  1.00E-18   C2H4      0  12496.E0
                      26.0000E0  1.00E-18   C2H2      0  54194.E0
```

```
                78.0000E0  1.00E-18  C6H6     0  19779.E0
                28.0000E0  1.00E-18    N2     0  00000.E0
                17.0000E0  1.00E-18   NH3     0 -11040.E0
                94.0000E0 6.2000F00  PHOH     0 -23500.E0
                44.0000E0  1.1000F0   CO2     0 -94052.E0
                28.0000E0  3.7000E0    CO     0 -26416.E0
                18.0000E0 48.9000F0   H2O     0 -57798.E0
                12.000E00 155.060E0     C     1 0.00000E0
9     1
    698.0      244000E-03
    909.0      298000E-03
   1001.0      356000E-03
   1073.0      356000E-03
   1346.0      451000E-03
   1515.0      470000E-03
   1709.0      575000E-03
   1848.0      559000E-03
   1998.0      616000E-03
```

Listing B-5. Iterative TEMPRE Output Format for Non-Equilibrium Flow.

```
                        NON-EQUILIBRIUM FLOW MODEL - TEMPRE

                                  EXPERIMENTAL

INITIAL TEMPERATURE (OF)  =       920.0         NUMBER OF GAS COMPONENTS  =  12

INITIAL SLOPE (OF/FT)  =        21359.9         NO.  COMPONENT  MOLE/MOLE GAS

FINAL TEMPERATURE (OF)  =        1350.0          1       H2        0.3497

FINAL PRESSURE (LB/FT2)  =       2160.0          2      CH4        0.4366

MASS FLUX (LB/FT2-SEC)  =        0.0039          3     C2H6        0.0000

CHAR THICKNESS (FT)  =           0.0208          4     C2H4        0.0000

CHAR POROSITY  =                   0.50          5     C2H2        0.0000

                                                 6     C6H6        0.0000

PERMEABILITY COEFFICIENTS                        7       N2        0.1359

     ALPHA (FT-2)               0.50E 09         8      NH3        0.0000

     BETA (FT-1)                0.50E 05         9    C6H60        0.0000

                                                10      CO2        0.0290

                                                11       CO        0.0490

RUNGE-KUTTA STEP SIZE  =            100         12      H2O        0.0000

SIMPSONS RULE STEP SIZE  =           20         13        C        1.5491
```

```
                    NON-EQUILIBRIUM FLOW MODEL - TEMPRE

                               EXPERIMENTAL

               TEMPERATURE DROP (OF)      =             930.0

               PRESSURE DROP (LB/FT2)      =              1.0

               SURFACE HEAT FLUX (BTU/FT2-SEC)      =      0.69


CHAR DEPTH (FT)             0.0000       0.0052       0.0104       0.0156       0.0208
TEMPERATURE (OF)             920.0       1030.0       1138.1       1244.6       1350.0
PRESSURE (LB/FT2)           2161.0       2160.8       2160.6       2160.3       2160.0
MASS FLUX (LB/FT2-SEC)      0.0039       0.0039       0.0039       0.0039       0.0039

 GAS COMPONENT                          COMPOSITION (MOLE/MOLE GAS)

       H2               0.3497E 00   0.3497E 00   0.3497E 00   0.3497E 00   0.3497E 00
      CH4               0.4366E 00   0.4366E 00   0.4366E 00   0.4366E 00   0.4366E 00
     C2H6               0.5084E-16   0.3661E-13   0.1547E-11   0.3831E-10   0.1687E-09
     C2H4               0.9990E-20   0.5288E-19   0.1638E-16   0.2837E-14   0.1394E-13
     C2H2               0.9990E-20   0.9991E-20   0.1066E-19   0.4033E-18   0.1969E-17
     C6H6               0.9990E-20   0.9990E-20   0.9990E-20   0.9990E-20   0.9990E-20
       N2               0.1359E 00   0.1359E 00   0.1359E 00   0.1359E 00   0.1359E 00
      NH3               0.9990E-20   0.9990E-20   0.9990E-20   0.9990E-20   0.9990E-20
    C6H6O               0.9990E-20   0.9990E-20   0.9990E-20   0.9990E-20   0.9990E-20
      CO2               0.2897E-01   0.2897E-01   0.2897E-01   0.2897E-01   0.2897E-01
       CO               0.4895E-01   0.4895E-01   0.4895E-01   0.4895E-01   0.4895E-01
      H2O               0.9990E-20   0.9990E-20   0.9990E-20   0.9990E-20   0.9990E-20
        C               0.1549E 01   0.1549E 01   0.1549E 01   0.1549E 01   0.1549E 01
```

C. PHYSICAL AND THERMODYNAMIC PROPERTIES

This appendix contains a series of tables, figures and charts relating physical and thermodynamic data necessary for the calculations in the TEMPRE system. In all cases, the information presented represents abstracted data applicable to this research. References to the original and more complete sources of information are provided. The following outline will be helpful in locating the particular data contained in this appendix.

Table C-1. Empirical Constants for Calculating the Heat Capacity of Elements to 1000°K

$$C_{p_i}/R = a + b(T) + c(T^2) + d(T^3) + e(T^4)$$

Element Name	Molecular Weight, M_w	Constants for C_p to 1000°K a	b x 10^3	c x 10^7	d x 10^{10}	e x 10^{15}
C	12	-0.71244	7.34068	-55.262	15.140	-2.382
H_2	2	2.84617	4.19321	-96.1193	95.1226	-330.934
N_2	28	3.69161	-1.33326	26.5031	-9.7688	-9.9772
O_2	32	3.71899	-2.51671	85.8374	-82.9987	270.8218

McBride, B. J., Sheldon Himel, J. G. Ehlers, Sanford Gordon, *Thermodynamic Properties to 6000°K for 210 Substances Involving the First 18 Elements*, NASA SP-3001 (1963).

Table C-2. Empirical Constants for Calculating the Heat Capacity of Elements Above 1000°K

$$C_{p_i}/R = a + b(T) + c(T^2) + d(T^3) + e(T^4)$$

Element Name	Molecular Weight, M_w	Constants for C_p Above 1000°K				
		a	b x 10^3	c x 10^7	d x 10^{10}	e x 10^{15}
C	12	1.36325	1.85605	-7.6675	1.5104	-1.139
H_2	2	3.04369	0.61187	-0.0740	-0.2033	0.2459
N_2	28	2.85458	1.59763	-6.2566	1.13158	-0.76897
O_2	32	3.59761	0.78146	-2.23867	0.42490	-0.33460

McBride, B. J., Sheldon Himel, J. G. Ehlers, Sanford Gordon, *Thermodynamic Properties to 6000°K for 210 Substances Involving the First 18 Elements*, NASA SP-3001 (1963).

Table C-3. Empirical Constants for Heat Capacity and Free Energy Calculation to 1000°K.

$$C_{p_i}/R = a + b(T) + c(T^2) + d(T^3) + e(T^4)$$

$$F^\circ_T/RT = a(1-\log_e T) - b(\frac{T}{2}) - c(\frac{T^2}{6}) - d(\frac{T^3}{12}) - e(\frac{T^4}{20}) - f(\frac{1}{T}) - g$$

Species Name	Molecular Weight, M_w	a	b x 10^3	c x 10^7	d x 10^{10}	e x 10^{14}	f	g
CH_4	16	4.2498	-6.9126	316.0213	-297.1543	951.0358	-10186.632	-0.9175
C_2H_6	30	2.8820	10.3220	119.1441	-148.3300	447.5010	0.000	7.5890
C_2H_4	28	1.1202	13.9057	26.5684	-115.6027	523.8693	5332.889	15.8377
C_2H_2	26	0.7903	23.4661	-355.4193	279.5055	-844.8413	26254.844	14.0052
C_6H_6	78	0.3511	37.5399	-79.4720	-75.0901	303.8520	0.000	19.8601
C_6H_6O	94	-3.9317	69.3818	-521.0600	124.9670	209.1500	-13303.800	41.8782
CO_2	44	2.1701	10.3781	-107.3394	63.4592	-162.8070	-48352.602	10.6640
CO	28	3.7871	-2.1709	50.7573	-34.7377	77.2168	-14363.508	2.6335
C	12	-0.7124	7.3406	-55.2618	15.1399	-2.3815	-68.053	2.7932
H_2	2	2.8461	4.1932	-96.1193	95.1227	-330.9342	-967.254	-1.4117
H_2O	18	4.1565	-1.7244	56.9823	-45.9300	142.3365	-30288.770	-0.6861
HCN	27	2.1681	10.7290	-150.8809	119.3302	-370.0445	14682.900	9.2810
NH_3	17	3.7716	-0.4862	98.7423	-95.6789	313.1324	-6728.093	1.4654
N_2	28	3.6916	-1.3332	26.5031	-9.7688	-9.9772	-1062.834	2.2875
O_2	32	3.7189	-2.5167	85.8374	-82.9987	270.8218	-1057.671	3.9080

McBride, B. J., Sheldon Heimel, J. G. Ehlers, Sanford Gordon, Thermodynamic Properties to 6000°K for 210 Substances Involving the First 18 Elements, NASA SP-3001 (1963).

Table C-4. Empirical Constants for Heat Capacity and Free Energy Calculation Above 1000°K.

$$C_{Pi}/R = a + b(T) + c(T^2) + d(T^3) + e(T^4)$$

$$F^\circ_T/RT = a(1-\log_e T) - b(\frac{T}{2}) - c(\frac{T^2}{6}) - d(\frac{T^3}{12}) - e(\frac{T^4}{20}) - f(\frac{1}{T}) - g$$

Species Name	Molecular Weight, M_w	a	b x 10^3	c x 10^7	d x 10^{10}	e x 10^{14}	f	g
CH_4	16	1.1795	10.9505	-40.6221	7.1370	-4.7490	-9855.66	12.5059
C_2H_6	30	1.4308	18.8898	-70.4410	11.8720	-7.4500	0.00	14.5080
C_2H_4	28	3.5023	11.5921	-44.7452	7.9452	-5.3235	4454.40	2.4667
C_2H_2	26	4.4965	5.2698	-18.4026	3.1054	-2.0004	25637.19	-3.1448
C_6H_6	78	4.6198	28.8096	-112.4510	19.5763	-12.5810	0.00	-1.1678
C_6H_6O	94	-3.9317	69.3818	-521.0600	124.9670	209.1500	-13303.800	41.8782
CO_2	44	4.4129	3.1923	-12.9782	2.4147	-1.6743	-4894.400	-0.7288
CO	28	2.9511	1.5525	-6.1911	1.1350	-0.7788	-14231.830	6.5314
C	12	1.3633	1.8560	-7.6675	1.5104	-1.1389	-649.670	-7.9890
H_2	2	3.0437	0.6119	-73.9936	-0.2033	0.2459	-854.910	-1.6481
H_2O	18	2.6707	3.0317	-8.5352	1.1791	-0.6197	-29888.994	6.8839
HCN	27	3.6538	3.4436	-12.5851	2.1692	-1.4296	14421.804	2.3726
NH_3	17	2.1494	6.4929	-22.6952	3.7394	-2.3606	-6401.962	9.2389
N_2	28	2.8546	1.5976	-6.2566	1.1316	-0.7690	-890.175	6.3903
O_2	32	3.5976	0.7815	-2.2387	0.4249	-0.3346	-1192.792	3.7493

McBride, B. J., Sheldon Heimel, J. G. Ehlers, Sanford Gordon, Thermodynamic Properties to 6000°K for 210 Substances Involving the First 18 Elements, NASA SP-3001 (1963).

Table C-5. Lennard-Jones Potentials[a] and Enthalpy of Formation[b] for the Compounds

Component Name	Molecular Weight, M_{w_i}	Collision Diameter, σ A°	Potential Parameter ÷ Boltzmann Constant $E^\circ/\bar{k}$, °K	Enthalpy of Formation (290°K) cal/gram mole
CH_4	16	3.822	136.5	-17889.0
C_2H_6	30	4.418	230.0	-20316.6
C_2H_4	28	4.232	205.0	12496.0
C_2H_2	26	4.221	185.0	54194.0
C_6H_6	78	5.270	440.0	19778.8
C_6H_6O	94	5.000	400.0	-23500.0
CO_2	44	3.996	190.0	-94052.0
CO	28	3.590	110.0	-26416.0
H_2	2	2.986	33.3	0.0
H_2O	18	2.649	356.0	-57797.9
HCN	27	3.630	569.1	31100.0
NH_3	17	3.432	312.0	-11040.0
N_2	28	3.681	91.5	0.0
O_2	32	3.433	113.0	0.0

[a] Reid, Robert C. and Thomas K. Sherwood, The Properties of Gases and Liquids, 2nd ed., New York: McGraw-Hill, pp. 632-633. (1966)

[b] Perry, John H., ed., Chemical Engineers' Handbook, 3rd ed., New York: McGraw-Hill, 1950, pp. 236--243.

Table C-6. Values of the Collision Integral Based on Lennard-Jones Potential for Calculating Pure Component Conductivity and Viscosity

$\bar{k}T/E^\circ$	Ω_v	$\bar{k}T/E^\circ$	Ω_v
0.30	2.785	1.30	1.399
0.35	2.628	1.50	1.314
0.40	2.492	1.70	1.248
0.45	2.368	1.90	1.197
0.50	2.257	2.2	1.138
0.55	2.156	2.6	1.081
0.60	2.065	3.2	1.022
0.65	1.982	4.0	0.9700
0.70	1.908	5.0	0.9269
0.75	1.841	7.0	0.8727
0.80	1.780	10.0	0.8242
0.85	1.725	20.0	0.7432
0.90	1.675	40.0	0.6718
0.95	1.587	70.0	0.6194
1.00	1.629	100.0	0.5882
1.10	1.514	200.0	0.5320
1.20	1.452	400.0	0.4811

Reid, Robert C. and Thomas K. Sherwood, The Properties of Gases and Liquids, 2nd ed., New York: McGraw-Hill, 1966, p. 399.

Figure C-1. Cornell-Katz Plot for a Low Density Nylon-Phenolic Resin Char.

Smyly, E. D. and C. M. Pyron, The Permeability of an Elastomer, a Low Density Epoxy and a Low Density Nylon-Phenolic Resin Char, Contract NAS1-5448, Task Order 6, Southern Research Institute (June 30, 1967).

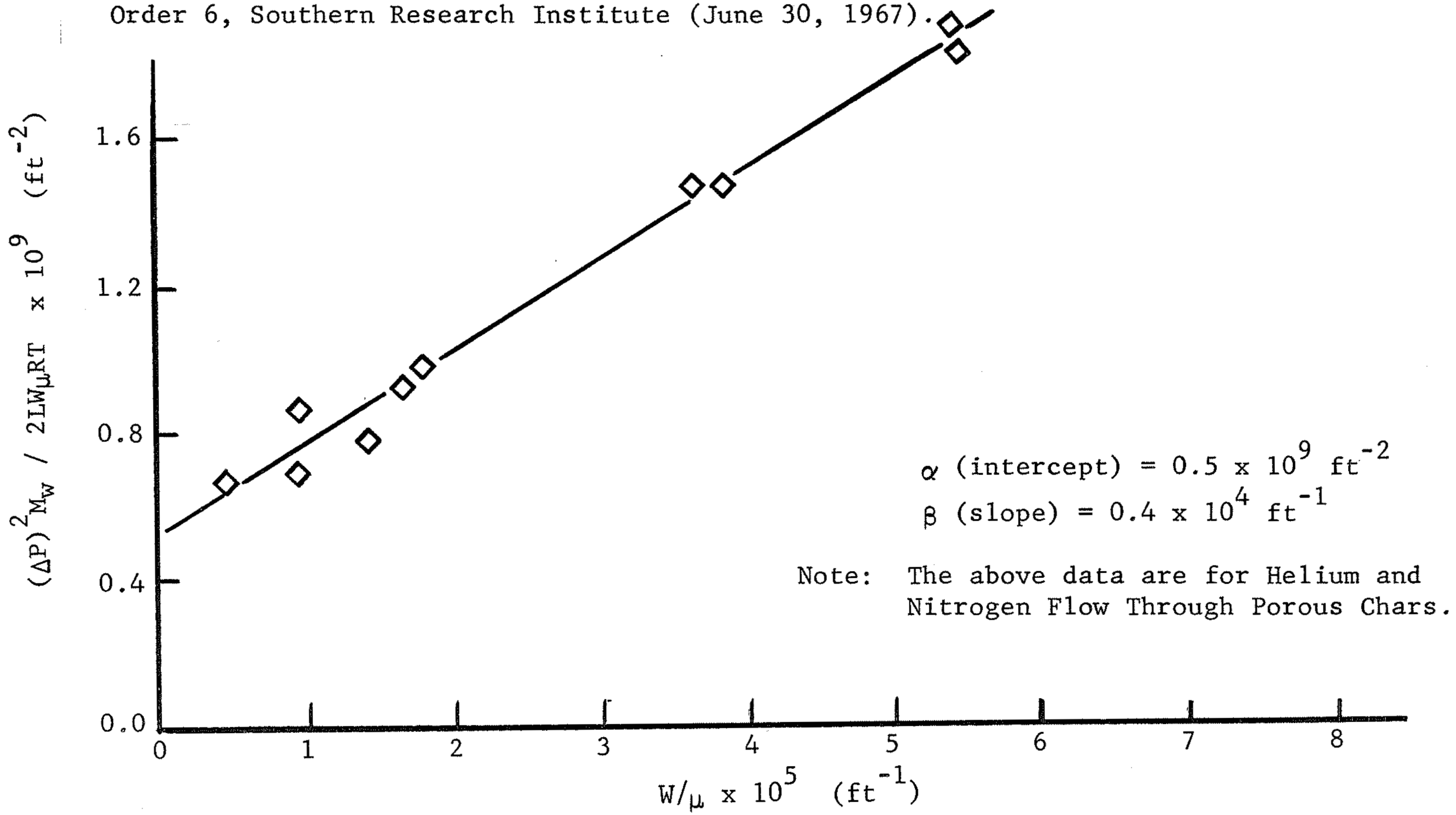

α (intercept) = $0.5 \times 10^9\ ft^{-2}$

β (slope) = $0.4 \times 10^4\ ft^{-1}$

Note: The above data are for Helium and Nitrogen Flow Through Porous Chars.

Figure C-2. Thermal Conductivity of a High and a Low Density Nylon-Phenolic Resin Char.

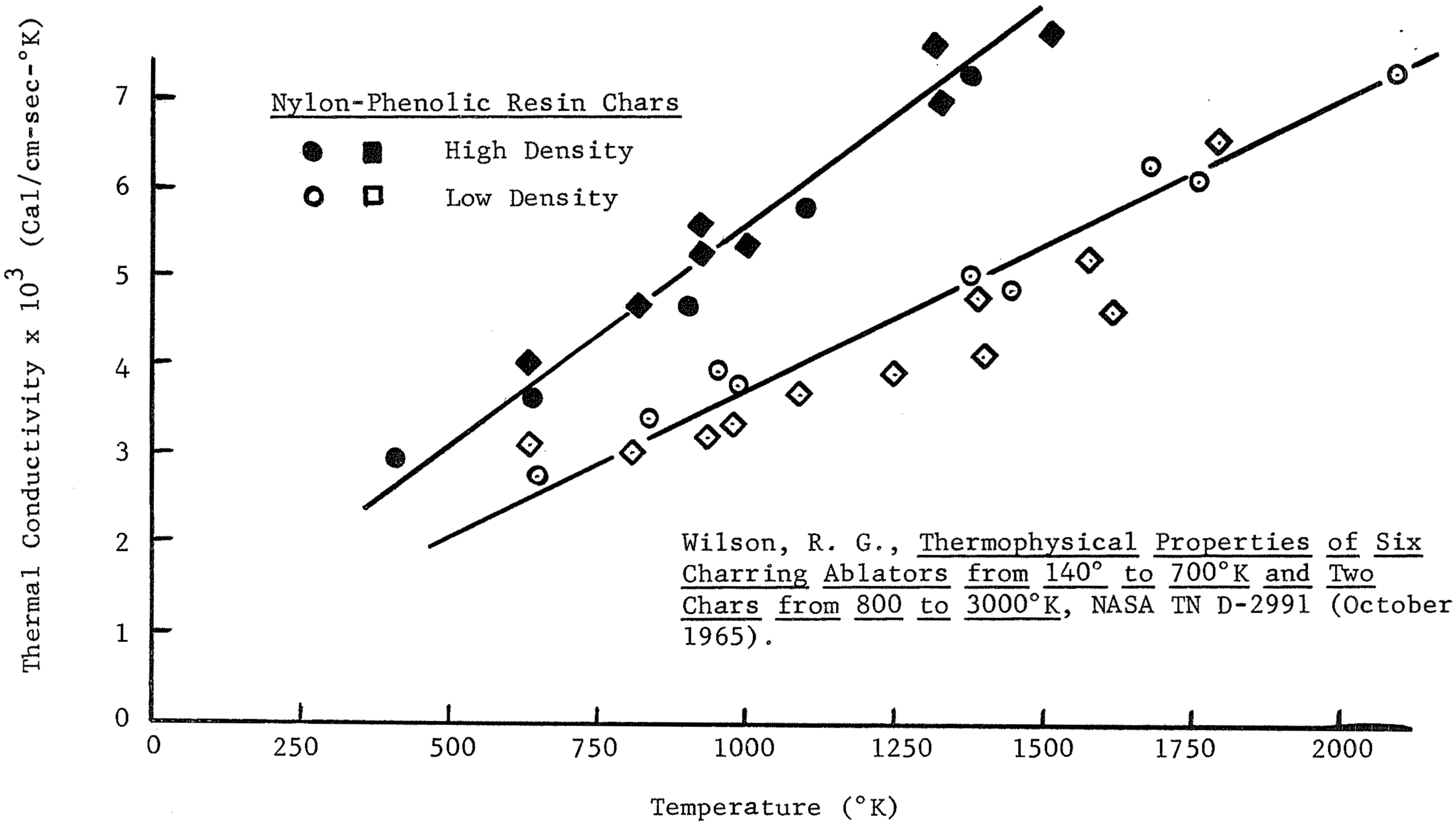

Wilson, R. G., Thermophysical Properties of Six Charring Ablators from 140° to 700°K and Two Chars from 800 to 3000°K, NASA TN D-2991 (October 1965).

D. SUMMARY OF EXPERIMENTAL AND ANALYTICAL RESULTS

This appendix contains a detailed summary of the experimental and analytical results determined in this research. The Char Zone Thermal Environment Simulator exit gas composition data listed in Tables D-2 through D-11 should be used in conjunction with Table D-1, a complete summary of the experiment conditions with comments on the overall behavior of the system for each case studied.

The following list of Tables will be helpful in locating the specific information contained in this section.

Table D-1. Summary of Test Data for Simulated Pyrolysis Gas Flow Through Porous Chars and Graphite in the Char Zone Thermal Environment Simulator.

RUN NUMBER	LAMP SYSTEM	PYROLYSIS GAS BLEND	DESCRIPTION OF POROUS MEDIUM			PYROLYSIS GAS MASS FLUX	EXPERIMENTAL ΔP, lb/ft^2	
			I.D. NO.	THICK. ft	C. S. A. ft^2	lb/ft^2_{tot}-sec	CHAR+LINES	CHAR
I-1	1000T3	HELIUM	LRC-LD C9-S46	0.0208	0.0127	0.00001-0.0002	-	-
II-2	1000T3	HELIUM	LRC-LD	0.0208	0.0127	0.00001-0.0005	0.50	0.40
3		FEED MIX 1	C9-S46			0.00154	0.39	0.25
4						0.00058	0.22	0.15
III-5	1000T3	HELIUM	LRC-LD	0.0208	0.0035	0.031-0.012	82-25	59.0
6		FEED MIX 1	C10-S52			0.0375	12.4	11.5
7						0.0205	6.2	5.8
IV-8	1000T3	HELIUM	LRC-LD	0.0208	0.0035	0.0017	1.3	0.9
9		FEED MIX 1	C10-S52			0.0051	2.4	1.7
V-10	1000T3	HELIUM	LRC-LD	0.0208	0.0035	0.00037	0.52	0.48
11		FEED MIX 2	C10-S52			0.00144	1.56	0.70
12						0.00072	0.78	0.20
13						0.00635	2.08	1.30
14						0.035-0.087	12.55	6.75
VI-15	1000T3	HELIUM	LRC-LD	0.0208	0.0049	0.00134	4.2	2.38
16		AIR	C10-S52			0.00970	2.6	1.78
17		HELIUM				0.00134	-	-
VII-18	1000T3	HELIUM	LRC-LD	0.0208	0.0049	0.00027	1.04	0.54
19		FEED MIX 2	C10-S52			0.00095	0.78	0.40

Table D-1. Summary of Test Data (Continued)

RUN NUMBER	TEMPERATURE (°F)			RUN TIME (Min)		OVERALL MATERIAL BALANCE (%)	REMARKS
	FRONT SURFACE	BACK SURFACE	CHAMBER INLET 1/4" FROM BACK	PER RUN	TOTAL TIME		
I-1	1300-1345	960-995	-	10	10	-	Leak around quartz cover plate. Thermocouple wire severed.
II-2	1250	890	-	6	6	92.4	System response to changes fast. Helium to Feed Mix change-over good. Leak around cover plate. No samples taken of exit gas.
3	1275-1285	790	-	9	15		
4	1295-1300	820-892	-	6	21		
III-5	1140-1175	80-115	-	8	8	89.0	Small leak in system-ΔP loss. Leak around inlet line and plate. Fire. No samples taken of exit gas.
6	1175-1275	170-335	-	21	29		
7	1340-1440	410-490	-	5	34		
IV-8	1250-1360	490-620	-	5	5	98.3	No noticeable leaks (New cement). No samples of exit gas taken.
9	1450-1645	630-895	-	23	28		
V-10	1365-1560	705-735	490-650	14	14	100.2	Samples of exit gas collected. Manometer blew near end of run 14. Lamp burnout, insulation melted. Short in high voltage line resulted
11	1560-1590	705-750	650-750	10	24		
12	1590-1618	750-818	750	14	38		
13	1610	760-780	700	13	51		
14	1530-1580	460-485	465	5	56		
VI-15	1500-1560	820-840	650-760	10	10	86.7	ΔP drop caused by char oxidation. Air injected through exit line. Gas samples collected through inlet line. Fire terminated experiment.
16	1590-1600	775-810	760-785	4	14		
17	1600	830-1150	800-1050	2	16		
VII-18	1520-1640	570-685	-	17	17	62.5	Cover plate cracked resulting in a fire and the poor material balance.
19	1680-1770	690-720	-	10	27		

Table D-1. Summary of Test Data (Continued).

RUN NUMBER	LAMP SYSTEM	PYROLYSIS GAS BLEND	DESCRIPTION OF POROUS MEDIUM			PYROLYSIS GAS MASS FLUX	EXPERIMENTAL ΔP, lb/ft^2	
			I.D. NO.	THICK. ft	C. S. A. ft^2	lb/ft$^2_{tot}$-sec	CHAR+LINES	CHAR
VIII-20	1000T3	HELIUM FEED MIX 2	LRC-HP GRc-25	0.0208	0.0055	0.00027	-	-
21						0.00095	57.2	0.8*
22						0.00375	57.4	1.7*
23						0.05200	-	-
IX-24	1000T3	HELIUM FEED MIX 2	LRC-HP GRc-25	0.0208	0.0055	0.00027	1.04	0.8
25						0.00095	1.04	0.9
26						0.00390	2.08	2.2*
27						0.05700	26.05	28.2*
X-28	1000T3	HELIUM AIR	LRC-HD CHAR	0.0104	0.0081	0.0008	2.08	2.05
29						0.0057	2.60	2.45
XI-30	1000T3	HELIUM FEED MIX 2	LRC-LP GR-45	0.0208	0.0055	0.00027	0.84	0.76
31						0.00095	1.04	0.80
32						0.00390	2.08	2.00
33						0.05700	34.04	36.18*
XII-34	1000T3	HELIUM FEED MIX 2	LRC-LP GR-45	0.0208	0.0055	0.00027	0.52	0.46
35						0.00095	0.72	0.60
36						0.00390	2.48	2.30
XIII-37	500T3	HELIUM	LRC-HP GR-25	0.0208	0.0055	0.00027	0.80	0.67
38						0.00095	1.04	0.55
39						0.00390	5.10	4.20
40						0.00095	1.75	1.56

* Estimated From Previous Experiments.

Table D-1. Summary of Test Data (Continued)

RUN NUMBER	TEMPERATURE (°F)			RUN TIME (Min)		OVERALL MATERIAL BALANCE (%)	REMARKS
	FRONT SURFACE	BACK SURFACE	CHAMBER INLET 1/4" FROM BACK	PER RUN	TOTAL TIME		
VIII-20	1250-1270	370-390	277-309	7	7	-	Wet test meter plugged. No material balance calculated. High ΔP caused by leak in exit gas line. Manometer out.
21	1330-1410	475-590	353-548	11	18		
22	1440-1500	673-805	600-785	13	31		
23	1440-1460	560-580	674-703	7	38		
IX- 24	1320-1350	770	-	8	8	-	Wet test meter being repaired, no material balance made. H_2O line to holder jacket broke; experiment terminated.
25	1330-1370	770-860	-	15	23		
26	1370	740-860	-	2	25		
27	1340-1360	710-740	-	10	35		
X-28	1370-1430	640-690	-	5	5	-	Air injected at front surface. Red glow at back surface. Run terminated when ΔP was zero.
29	1450-1520	705-790	-	52	57		
XI-30	1150-1280	450-750	-	5	5	95.0	Increased air coolant flow to lamp terminals. Nylon blocks melted. Crack in cover plate terminated experiment. Fire.
31	1280-1390	750-861	-	29	34		
32	1380-1400	863-865	-	12	46		
33	1350-1360	562-635	-	7	53		
XII-34	1250-1360	562-874	-	4	4	93.7	Red glow at back surface noted through quartz covered sighting tube.
35	1380-1420	897-953	-	26	30		
36	1340-1360	886-953	-	22	52		
XIII-37	1500-1635	888-1163	-	10	10	98.7	Red glow at back surface. Front surface temperature increased by reducing the air coolant flow across lamp banks
38	1660-1725	1205-1218	-	15	25		
39	1725	1218-1220	-	13	38		
40	1725-1770	1227-1260	-	9	47		

Table D-1. Summary of Test Data (Continued).

RUN NUMBER	LAMP SYSTEM	PYROLYSIS GAS BLEND	DESCRIPTION OF POROUS MEDIUM			PYROLYSIS GAS MASS FLUX lb/ft^2_{tot}-sec	EXPERIMENTAL ΔP, lb/ft^2	
			I.D. NO.	THICK. ft	C. S. A. ft^2		CHAR+LINES	CHAR
XIV-41	500T3	HELIUM FEED MIX 3	LRC-LD C22-S106	0.0208	0.0049	0.00027	2.5	1.7
42						0.00095	1.3	0.4
43						0.00390	5.2	1.3
XV-44	500T3	HELIUM FEED MIX 3	LRC-HP GR-25	0.0208	0.0055	0.00027	2.2	1.8
45						0.00095	1.9	1.2
46						0.00011	0.7	0.2
XVI-47	1200T3	HELIUM FEED MIX 3	LRC-LD CHAR	0.0208	0.0167	0.00009	0.05	0.0
48						0.00031	0.20	0.1
49						0.00003	0.55	0.4
50						0.00120	2.44	1.5
51						0.01700	15.62	5.3
52						0.00480	1.51	
XVII-53	1200T3	HELIUM AIR	LRC-LD CHAR	0.0208	0.0167	0.00502	52.0	37.8
54						0.03500	25.2	16.7
XVIII-55	1200T3	ARGON FEED MIX 4	LRC-LD CHAR	0.0104	0.0050	0.0182	28.0	7.9
56						0.0208	3.5	0.8
57						0.0101	3.5	2.6
58						0.1080	56.1	17.5
XIX-59	1200T3	HELIUM FEED MIX 4	LRC-LD CHAR	0.0208	0.0120	0.00013	2.4	1.6
60						0.00248	3.0	0.7
61						0.00220	3.4	0.9

Table D-1. Summary of Test Data (Continued)

RUN NUMBER	TEMPERATURE (°F)			RUN TIME (Min)		OVERALL MATERIAL BALANCE (%)	REMARKS
	FRONT SURFACE	BACK SURFACE	LAMP TERMINAL	PER RUN	TOTAL TIME		
XIV-41	1780-1800	708-977	-	15	15	99.3	Wire insulation burned. Short in power supply terminated experiment. Increased heating from new lamps.
42	1795-1800	945-977	-	22	37		
43	1800	895-913	-	14	51		
XV-44	1520-1665	698-1065	-	8	8	101.7	Red glow noted at back surface through sighting tube. Lamp cooling system modified.
45	1670-1750	1065-1180	-	26	34		
46	1750-1760	1180-1188	-	7	41		
XVI-47	1795-1965	607-874	-	5	5	97.5	Increased heating capability by using 1200T3 lamp (1.5 rated voltage). Air coolant flow effects front surface temperature. Red glow noted at back surface.
48	1985-2045	974-1264	-	20	25		
49	2055-2060	1259-1262	-	8	33		
50	2035	1262	-	6	39		
51	2025-2040	1002	-	17	56		
52	2030-2040	985-996	-	5	61		
XVII-53	1990-2005	295-337	-	8	8	101.2	ΔP large due to leak in exit gas line. Run terminated when ΔP dropped to zero.
54	2030-2065	289-337	-	8	16		
XVIII-55	1500-1680	630-1020	-	14	14	101.8	Liquid feed system tested with water. Liquid-gas separator tested in exit gas line.
56	1680-1695	923-1020	-	16	30		
57	1680-1700	993-1046	-	18	48		
58	1680	640-737	-	10	58		
XIX-59	2000-2055	1070-1270	300	6	6	84.5	Tested water-phenol feed system. Cooling line to holder ruptured terminating experiment.
60	2095-2165	1340-1410	450	22	28		
61	2100-2175	1000-1200	460	14	42		

Table D-1. Summary of Test Data (Continued).

RUN NUMBER	LAMP SYSTEM	PYROLYSIS GAS BLEND	DESCRIPTION OF POROUS MEDIUM			PYROLYSIS GAS MASS FLUX lb/ft^2_{tot}-sec	EXPERIMENTAL ΔP, lb/ft^2	
			I.D. NO.	THICK. ft	C. S. A. ft^2		CHAR+LINES	CHAR
XX-62	1200T3	ARGON FEED MIX 4	LRC-LD CHAR	0.0208	0.0085	0.00018	3.2	0.7
63						0.00224	2.1	0.6
64						0.00133	1.2	0.2
XXI-65	1200T3	ARGON FEED MIX 4	LRC-LP GR-45	0.0208	0.0055	0.00215	5.0	0.2
66						0.00297	7.1	-
67						0.00436	14.9	-
XXII-68	1200T3	ARGON FEED MIX 4	LRC-LP GR-45	0.0208	0.0055	0.00226	4.3	-
69						0.00334	2.4	-
XXIII-70	1200T3	ARGON FEED MIX 4	LRC-LP GR-45	0.0208	0.0055	0.00269	5.2	1.7
71						0.00309	2.2	0.7
72						0.00241	2.1	0.4
73						0.00230	1.4	0.2
74						0.00200	1.0	0.1
XXIV-75	1200T3	ARGON FEED MIX 4	LRC-LP GR-45	0.0208	0.0031	0.00450	-	-
76						0.00280	-	-
77						0.00142	-	-
78						0.00425	-	-
XXV-79	1200T3	ARGON FEED MIX 4	LRC-LP GRb-45	0.0208	0.0031	0.00137	5.2	1.8
80						0.00356	4.7	1.3
81						0.00376	4.5	1.1
82						0.00648	6.1	2.4

Table D-1. Summary of Test Data (Continued)

RUN NUMBER	TEMPERATURE (°F)			RUN TIME (Min)		OVERALL MATERIAL BALANCE (%)	REMARKS
	FRONT SURFACE	BACK SURFACE	LAMP TERMINAL	PER RUN	TOTAL TIME		
XX-62	2235-2280	1030-1148	210	6	6	89.9	Air supply to lamps cut off; run terminated. High ΔP caused by H_2O-phenol vaporization in feed lines.
63	2280-2295	1150-1210	350	18	24		
64	2295-2300	1180-1200	375	11	35		
XXI-65	1800-2030	720-980	310	7	7	81.0	Fire terminated experiment. H_2O-phenol vaporization in feed burets due to high temperature in box.
66	2030-2140	810-980	460	11	18		
67	2135	880-950	485	3	21		
XXII-68	1820-1930	1090-1150	375	11	11	81.5	Severe evaporation of H_2O and phenol caused termination of experiment.
69	1920	1150-1225	460	3	14		
XXIII-70	1810-2040	440-900	235	3	3	92.0	Modified H_2O-phenol feed system by placing burets outside box. Tested new liquid feed system with no gas flow. New system okay.
71	2040-2090	900-1315	375	24	27		
72	2092-2114	1200-1315	410	18	45		
73	2114-2123	1150-1200	420	9	54		
74	2112	1150	425	6	60		
XXIV-75	1760-1810	760-830	230	3	3	96.5	Manometer blew at high argon flow rate. Operated without ΔP measurement.
76	1810-2000	830-950	450	27	30		
77	2000-2020	880	510	24	54		
78	2010-2020	910-895	515	4	58		
XXV-79	1980-2040	700-900	235	3	3	98.9	Bromine water used as H_2O feed (4%wt) Wet test meter plugged during run 82.
80	2000-2080	900-1270	355	27	30		
81	1990-2000	1130-1210	357	18	48		
82	1990-2100	1080-1130	375	12	60		

Table D-1. Summary of Test Data (Continued).

RUN NUMBER	LAMP SYSTEM	PYROLYSIS GAS BLEND	DESCRIPTION OF POROUS MEDIUM			PYROLYSIS GAS MASS FLUX	EXPERIMENTAL ΔP, lb/ft^2	
			I.D. NO.	THICK. ft	C. S. A. ft^2	lb/ft^2_{tot}-sec	CHAR+LINES	CHAR
XXVI-83	1200T3	ARGON FEED MIX 4	LRC-LP GR-45	0.0208	0.0031	0.00098	-	-
84						0.00313	3.5	
85						0.01010	-	-
XXVII-86	1200T3	ARGON FEED MIX 4	LRC-LP GR-45	0.0208	0.0031	0.00110	8.5	4.2
87						0.00320	3.9	1.7
88						0.00421	2.5	1.1
89						0.00514	1.4	0.7
90						0.00490	-	-
XXVIII-91	1200T3	ARGON FEED MIX 4	LRC-LP GR-45	0.0208	0.0031	0.00400	3.0	1.8
92						0.00438	2.3	1.1
93						0.00338	3.5	2.2
XXIX-94	1200T3	FEED MIX 4	LRC-LP GR-45	0.0208	0.0031	0.00503	4.2	2.6
95						0.00591	5.7	3.5
XXX-96	1200T3	FEED MIX 4	LRC-LP GRb-45	0.0208	0.0031	0.00753	14.3	8.5
XXXI-97	1200T3	FEED MIX 4	LRC-LP GRa-45	0.0157	0.0031	0.00638	14.8	10.3
98						0.00478	8.2	6.8
XXXII-99	1200T3	FEED MIX 4	LRC-LP GRa-45	0.0157	0.0031	0.00490	-	-
100						0.00979	-	-

Table D-1. Summary of Test Data (Continued)

RUN NUMBER	TEMPERATURE (°F)			RUN TIME (Min)		OVERALL MATERIAL BALANCE (%)	REMARKS
	FRONT SURFACE	BACK SURFACE	LAMP TERMINAL	PER RUN	TOTAL TIME		
XXVI-83	1800-1980	820-890	235	7	7	90.5	Manometer blew during run 84. Bromine added to water in experiment XXV diluted to 2% wt.
84	1980-2060	890-925	295	36	43		
85	2055	881	325	13	56		
XXVII-86	1780-1840	800-880	235	5	5	99.2	Radioactive phenol fed to system. Manometer blew during run 90. Possible leak in exit gas line.
87	1840-2010	880-1080	340	24	29		
88	2010	1080	340	9	38		
89	2010	1040-1080	340	15	53		
90	2010	1065	345	7	60		
XXVIII-91	1910	480	160	3	3	98.6	Radioactive phenol fed to system. Gas samples checked for radioactivity and product distribution.
92	1910-1930	660-1125	220	35	38		
93	1930-1960	1080-1135	225	22	60		
XXIX-94	1850-1930	580-944	215	33	33	101.5	Radioactive methane fed to system. Possible leak in exit gas line.
95	1930-1940	852-944	230	16	49		
XXX-96	1640-1930	781-958	225	48	48	99.6	Radioactive methane fed to system. Bromine water fed as 4% wt.
XXXI-97	1800-1940	763-922	210	27	27	96.3	Radioactive methane fed to system. Coated char with 3% wt. Mo and 3% wt. W for catalyst experiment.
98	1940-1950	922-982	215	17	44		
XXXII-99	1800-1920	730-980	235	48	48	97.9	Radioactive phenol fed to system. Coated char with 3% wt. Mo and 3% wt. W for catalyst experiment.
100	1920	950-861	275	12	60		

Table D-2. Flow of Simulated Pyrolysis Products Through Low Density Nylon-Phenol Resin Chars. Comparison of the Experimental Exit Gas Composition (Mole Percent) with the Frozen, Equilibrium and Non-Equilibrium Flow Models.

RUN NUMBER MASS FLUX FRONT TEMP BACK TEMP	FLOW MODEL	H_2 MOLE %	CH_4 MOLE %	CO MOLE %	CO_2 MOLE %	N_2 MOLE %	H_2O MOLE %	C_6H_6O MOLE %	C_2H_4 MOLE %	C_2H_2 MOLE %	MODEL	
											ΔP	qcz
V-11	FROZEN	37.2	32.5	8.2	6.6	15.5	0.0	0.0	0.0	0.0	0.5	0.85
0.0014	EQUILIBRIUM	71.6	1.4	14.9	0.1	11.4	0.6	0.0	0.0	0.0	0.5	13.10
1575°F	NON-EQUILIBRIUM	37.2	32.5	8.2	6.6	15.5	0.0	0.0	0.0	0.0	0.5	0.85
730°F	EXPERIMENTAL	37.0	32.0	8.5	6.4	15.5	0.0	0.0	0.1	0.5	0.7	-
V-12	FROZEN	37.2	32.5	8.2	6.6	15.5	0.0	0.0	0.0	0.0	0.2	0.33
0.0007	EQUILIBRIUM	71.7	1.4	14.9	0.1	11.4	0.5	0.0	0.0	0.0	0.2	5.58
1604°F	NON-EQUILIBRIUM	37.2	32.5	8.2	6.6	15.5	0.0	0.0	0.0	0.0	0.2	0.33
784°F	EXPERIMENTAL	37.6	32.4	8.3	6.2	15.5	0.0	0.0	0.0	0.0	0.2	-
V-13	FROZEN	37.2	32.5	8.2	6.6	15.5	0.0	0.0	0.0	0.0	1.8	3.00
0.0064	EQUILIBRIUM	71.8	1.2	15.0	0.1	11.4	0.5	0.0	0.0	0.0	1.4	42.69
1610°F	NON-EQUILIBRIUM	37.2	32.5	8.2	6.6	15.5	0.0	0.0	0.0	0.0	1.8	3.00
770°F	EXPERIMENTAL	38.2	32.2	7.8	6.1	15.5	0.0	0.0	0.1	0.1	1.3	-
VII-19	FROZEN	35.0	43.6	4.9	2.9	13.6	0.0	0.0	0.0	0.0	0.3	0.65
0.0009	EQUILIBRIUM	81.8	1.4	7.2	0.0	9.4	0.2	0.0	0.0	0.0	0.3	11.55
1730°F	NON-EQUILIBRIUM	35.0	43.6	4.9	2.9	13.6	0.0	0.0	0.0	0.0	0.3	0.66
705°F	EXPERIMENTAL	37.2	42.5	4.2	2.6	13.5	0.0	0.0	0.0	0.0	0.4	-
XIV-42	FROZEN	31.7	46.3	5.5	2.5	14.0	0.0	0.0	0.0	0.0	0.4	0.69
0.0009	EQUILIBRIUM	82.5	0.9	7.0	0.0	9.5	0.1	0.0	0.0	0.0	0.4	17.33
1800°F	NON-EQUILIBRIUM	31.7	46.2	5.5	2.5	14.0	0.0	0.0	0.0	0.1	0.4	0.70
960°F	EXPERIMENTAL	30.9	45.2	6.1	3.7	13.9	0.0	0.0	0.0	0.2	0.4	-

Table D-2. Flow of Simulated Pyrolysis Products Through Chars (Continued).

RUN NUMBER MASS FLUX FRONT TEMP BACK TEMP	FLOW MODEL	H_2 MOLE %	CH_4 MOLE %	CO MOLE %	CO_2 MOLE %	N_2 MOLE %	H_2O MOLE %	C_6H_6O MOLE %	C_2H_4 MOLE %	C_2H_2 MOLE %	MODEL	
											ΔP	q_{cz}
XIV-43	FROZEN	31.7	46.3	5.5	2.5	14.0	0.0	0.0	0.0	0.0	1.6	2.99
0.0039	EQUILIBRIUM	82.6	0.8	7.0	0.0	9.5	0.1	0.0	0.0	0.0	1.3	67.70
1800°F	NON-EQUILIBRIUM	31.7	46.3	5.5	2.5	14.0	0.0	0.0	0.0	0.0	1.6	2.99
900°F	EXPERIMENTAL	32.6	43.9	5.8	3.7	14.0	0.0	0.0	0.0	0.0	1.3	-
XVI-48	FROZEN	31.7	46.3	5.5	2.5	14.0	0.0	0.0	0.0	0.0	0.0	0.01
0.00003	EQUILIBRIUM	83.1	0.4	7.0	0.0	9.4	0.1	0.0	0.0	0.0	0.0	0.25
2055°F	NON-EQUILIBRIUM	84.7	8.2	2.9	0.0	3.8	0.0	0.0	0.1	0.3	0.0	0.03
1260°F	EXPERIMENTAL	84.5	7.7	3.0	0.6	4.2	0.0	0.0	0.0	0.4	0.1	-
XVI-49	FROZEN	31.7	46.3	5.5	2.5	14.0	0.0	0.0	0.0	0.0	0.2	0.26
0.0003	EQUILIBRIUM	83.1	0.4	7.0	0.0	9.4	0.1	0.0	0.0	0.0	0.2	4.84
2015°F	NON-EQUILIBRIUM	36.1	38.9	9.6	2.3	12.8	0.0	0.0	0.1	0.2	0.2	0.28
1120°F	EXPERIMENTAL	36.8	37.9	9.2	4.3	14.0	0.0	0.0	0.0	0.0	0.4	-
XVI-50	FROZEN	31.7	46.3	5.5	2.5	14.0	0.0	0.0	0.0	0.0	0.3	0.46
0.0012	EQUILIBRIUM	83.2	0.3	7.1	0.0	9.4	0.1	0.0	0.0	0.0	0.4	8.84
2035°F	NON-EQUILIBRIUM	51.3	29.6	6.2	0.3	9.1	0.0	0.0	1.0	2.5	0.5	0.78
1162°F	EXPERIMENTAL	53.0	29.2	6.7	0.2	10.7	0.0	0.0	0.0	0.2	1.5	-
XVI-51	FROZEN	31.7	46.3	5.5	2.5	14.0	0.0	0.0	0.0	0.0	4.7	8.40
0.0170	EQUILIBRIUM	83.3	0.3	7.0	0.0	9.4	0.1	0.0	0.0	0.0	6.7	99.85
2035°F	NON-EQUILIBRIUM	31.7	46.2	5.8	2.3	14.0	0.0	0.0	0.0	0.0	4.8	8.54
1000°F	EXPERIMENTAL	32.7	45.8	4.8	3.7	14.0	0.0	0.0	0.0	0.0	5.3	-

Table D-2. Flow of Simulated Pyrolysis Products Through Chars (Continued).

RUN NUMBER MASS FLUX FRONT TEMP BACK TEMP	FLOW MODEL	H_2 MOLE %	CH_4 MOLE %	CO MOLE %	CO_2 MOLE %	N_2 MOLE %	H_2O MOLE %	C_6H_6O MOLE %	C_2H_4 MOLE %	C_2H_2 MOLE %	MODEL	
											ΔP	q_{cz}
XVIII-56	FROZEN	28.9	6.4	3.3	0.8	0.0	53.8	6.9	0.0	0.0	0.4	0.93
0.00208	EQUILIBRIUM	59.7	3.3	26.7	4.0	0.0	6.3	0.0	0.0	0.0	0.4	15.9
1690°F	NON-EQUILIBRIUM	23.0	11.1	2.8	2.1	0.0	53.8	7.1	0.0	0.0	0.4	0.99
1030°F	EXPERIMENTAL	24.8	10.3	3.4	1.3	0.0	53.7	6.5	0.0	0.0	0.8	-
XVIII-57	FROZEN	30.6	6.1	3.5	0.9	0.0	52.1	6.8	0.0	0.0	2.0	4.92
0.0101	EQUILIBRIUM	60.2	3.2	27.1	3.7	0.0	5.9	0.0	0.0	0.0	1.8	55.4
1690°F	NON-EQUILIBRIUM	29.1	7.2	3.4	1.1	0.0	52.3	6.9	0.0	0.0	2.0	4.97
975°F	EXPERIMENTAL	28.7	7.5	3.4	1.2	0.0	51.7	7.5	0.0	0.0	2.6	-
XVIII-58	FROZEN	30.6	6.2	3.5	1.0	0.0	51.9	6.8	0.0	0.0	22.0	69.8
0.1080	EQUILIBRIUM	59.5	3.5	26.0	4.4	0.0	6.5	0.0	0.0	0.0	18.8	735.2
1680°F	NON-EQUILIBRIUM	30.6	6.2	3.5	1.0	0.0	51.9	6.8	0.0	0.0	22.0	69.8
690°F	EXPERIMENTAL	30.8	6.1	3.4	1.1	0.0	50.8	5.8	0.0	0.0	17.5	-
XIX-60	FROZEN	29.3	6.0	3.3	0.9	0.0	53.7	6.8	0.0	0.0	0.7	1.17
0.00248	EQUILIBRIUM	62.7	0.8	35.2	1.5	0.0	0.9	0.0	0.0	0.0	0.6	13.0
2030°F	NON-EQUILIBRIUM	38.2	17.2	25.2	8.8	0.0	4.9	5.1	0.0	0.5	0.5	2.42
1375°F	EXPERIMENTAL	41.3	18.2	23.4	7.6	0.0	5.0	4.5	0.0	0.0	0.7	-
XIX-61	FROZEN	28.7	5.4	3.4	1.0	0.0	53.9	7.6	0.0	0.0	0.5	1.61
0.00220	EQUILIBRIUM	63.1	0.5	35.7	0.2	0.0	0.5	0.0	0.0	0.0	0.5	27.3
2140°F	NON-EQUILIBRIUM	36.6	18.3	31.2	7.5	0.0	0.5	5.3	0.0	0.7	0.4	2.94
1100°F	EXPERIMENTAL	36.4	18.4	31.2	7.0	0.0	2.1	4.9	0.0	0.0	0.9	-

Table D-2. Flow of Simulated Pyrolysis Products Through Chars (Continued).

RUN NUMBER MASS FLUX FRONT TEMP BACK TEMP	FLOW MODEL	H_2 MOLE %	CH_4 MOLE %	CO MOLE %	CO_2 MOLE %	N_2 MOLE %	H_2O MOLE %	C_6H_6O MOLE %	C_2H_4 MOLE %	C_2H_2 MOLE %	MODEL	
											ΔP	q_{cz}
XX-63	FROZEN	28.6	5.5	3.4	1.0	0.0	53.8	7.7	0.0	0.0	0.6	1.79
0.00224	EQUILIBRIUM	63.1	0.3	36.4	0.1	0.0	0.2	0.0	0.0	0.0	0.5	51.4
2290°F	NON-EQUILIBRIUM	30.7	21.4	38.6	3.4	0.0	0.0	4.6	0.3	1.0	0.4	3.18
1180°F	EXPERIMENTAL	30.4	19.8	38.0	5.7	0.0	0.0	5.0	0.5	0.6	0.6	-
XX-64	FROZEN	28.4	5.4	3.4	1.0	0.0	46.0	15.8	0.0	0.0	0.2	1.05
0.00133	EQUILIBRIUM	65.9	0.3	33.6	0.0	0.0	0.2	0.0	0.0	0.0	0.3	32.1
2300°F	NON-EQUILIBRIUM	25.2	25.6	38.5	0.9	0.0	0.0	7.9	0.5	1.3	0.2	1.18
1190°F	EXPERIMENTAL	26.7	26.4	40.3	0.6	0.0	0.0	7.1	0.4	1.0	0.2	-

Table D-3. Flow of Simulated Pyrolysis Products Through Graphite Specimens. Comparison of the Exit Gas Composition (Mole Percent) with the Frozen Equilibrium and Non-Equilibrium Flow Models.

RUN NUMBER MASS FLUX FRONT TEMP BACK TEMP	FLOW MODEL	H_2 MOLE %	CH_4 MOLE %	CO MOLE %	CO_2 MOLE %	N_2 MOLE %	H_2O MOLE %	C_6H_6O MOLE %	C_2H_4 MOLE %	C_2H_2 MOLE %	MODEL	
											ΔP	q_{cz}
VIII-21	FROZEN	35.0	43.6	4.9	2.9	13.6	0.0	0.0	0.0	0.0	0.4	0.61
0.0009	EQUILIBRIUM	77.5	5.0	6.0	0.2	9.9	1.4	0.0	0.0	0.0	0.4	0.87
1370°F	NON-EQUILIBRIUM	35.0	43.6	4.9	2.9	13.6	0.0	0.0	0.0	0.0	0.4	0.62
530°F	EXPERIMENTAL	30.8	45.9	6.0	3.7	13.6	0.0	0.0	0.0	0.0	0.8	-
VIII-22	FROZEN	35.0	43.6	4.9	2.9	13.6	0.0	0.0	0.0	0.0	2.0	2.23
0.0038	EQUILIBRIUM	79.8	3.0	6.7	0.1	9.6	0.5	0.0	0.0	0.0	1.5	26.07
1470°F	NON-EQUILIBRIUM	35.0	43.6	4.9	2.9	13.6	0.0	0.0	0.0	0.0	2.0	2.22
740°F	EXPERIMENTAL	36.0	41.6	5.2	3.6	13.6	0.0	0.0	0.0	0.0	1.7	-
VIII-23	FROZEN	35.0	43.6	4.9	2.9	13.6	0.0	0.0	0.0	0.0	30.6	35.90
0.0520	EQUILIBRIUM	79.4	3.4	6.6	0.1	9.7	0.8	0.0	0.0	0.0	27.8	166.82
1450°F	NON-EQUILIBRIUM	35.0	43.6	4.9	2.9	13.6	0.0	0.0	0.0	0.0	30.6	35.90
570°F	EXPERIMENTAL	35.2	43.4	4.8	3.1	13.5	0.0	0.0	0.0	0.0	-	-
IX-25	FROZEN	35.0	43.6	4.9	2.9	13.6	0.0	0.0	0.0	0.0	0.5	0.41
0.0009	EQUILIBRIUM	76.7	5.6	5.8	0.2	10.0	1.7	0.0	0.0	0.0	0.5	4.91
1350°F	NON-EQUILIBRIUM	35.0	43.6	4.9	2.9	13.6	0.0	0.0	0.0	0.0	0.5	0.41
815°F	EXPERIMENTAL	20.2	55.2	8.0	3.5	13.6	0.0	0.0	0.0	0.0	0.9	-
IX-26	FROZEN	35.0	43.6	4.9	2.9	13.6	0.0	0.0	0.0	0.0	2.0	1.80
0.0039	EQUILIBRIUM	77.6	4.9	6.0	0.2	9.9	1.4	0.0	0.0	0.0	1.6	19.22
1370°F	NON-EQUILIBRIUM	35.0	43.6	4.9	2.9	13.6	0.0	0.0	0.0	0.0	2.0	1.80
800°F	EXPERIMENTAL	24.6	52.2	6.2	3.4	13.6	0.0	0.0	0.0	0.0	2.2	-

Table D-3. Flow of Simulated Pyrolysis Products Through Graphite Specimens (Continued).

RUN NUMBER MASS FLUX FRONT TEMP BACK TEMP	FLOW MODEL	H_2 MOLE %	CH_4 MOLE %	CO MOLE %	CO_2 MOLE %	N_2 MOLE %	H_2O MOLE %	C_6H_6O MOLE %	C_2H_4 MOLE %	C_2H_2 MOLE %	MODEL	
											ΔP	q_{cz}
IX-27	FROZEN	35.0	43.6	4.9	2.9	13.6	0.0	0.0	0.0	0.0	39.0	28.25
0.0570	EQUILIBRIUM	77.0	5.2	5.9	0.2	10.0	2.7	0.0	0.0	0.0	24.8	89.50
1350°F	NON-EQUILIBRIUM	35.0	43.6	4.9	2.9	13.6	0.0	0.0	0.0	0.0	39.0	28.25
725°F	EXPERIMENTAL	27.0	51.5	5.5	2.9	13.6	0.0	0.0	0.0	0.0	28.2	-
XI-31	FROZEN	35.0	43.6	4.9	2.9	13.6	0.0	0.0	0.0	0.0	0.5	0.41
0.0009	EQUILIBRIUM	76.3	6.0	5.6	0.2	10.0	1.9	0.0	0.0	0.0	0.5	4.79
1335°F	NON-EQUILIBRIUM	35.0	43.6	4.9	2.9	13.6	0.0	0.0	0.0	0.0	0.5	0.41
805°F	EXPERIMENTAL	28.5	49.8	5.5	2.5	14.7	0.0	0.0	0.0	0.0	0.8	-
XI-32	FROZEN	35.0	43.6	4.9	2.9	13.6	0.0	0.0	0.0	0.0	2.1	1.68
0.0039	EQUILIBRIUM	78.1	4.6	6.1	0.1	9.8	1.3	0.0	0.0	0.0	1.8	18.78
1390°F	NON-EQUILIBRIUM	35.0	43.6	4.9	2.9	13.6	0.0	0.0	0.0	0.0	2.1	1.68
865°F	EXPERIMENTAL	29.8	49.2	4.9	2.9	13.6	0.0	0.0	0.0	0.0	2.0	-
XI-33	FROZEN	35.0	43.6	4.9	2.9	13.6	0.0	0.0	0.0	0.0	34.2	33.47
0.0570	EQUILIBRIUM	77.2	5.2	5.9	0.2	10.0	2.5	0.0	0.0	0.0	20.8	97.34
1355°F	NON-EQUILIBRIUM	35.0	43.6	4.9	2.9	13.6	0.0	0.0	0.0	0.0	34.2	33.47
595°F	EXPERIMENTAL	32.3	46.2	5.0	2.9	13.6	0.0	0.0	0.0	0.0	36.1	-
XII-35	FROZEN	35.0	43.6	4.9	2.9	13.6	0.0	0.0	0.0	0.0	0.5	0.37
0.0009	EQUILIBRIUM	78.3	4.3	6.3	0.1	9.8	1.2	0.0	0.0	0.0	0.5	4.62
1400°F	NON-EQUILIBRIUM	35.0	43.6	4.9	2.9	13.6	0.0	0.0	0.0	0.0	0.5	0.37
930°F	EXPERIMENTAL	35.8	42.5	5.5	3.4	12.8	0.0	0.0	0.0	0.0	0.6	-

Table D-3. Flow of Pyrolysis Products Through Graphite Specimens (Continued).

RUN NUMBER MASS FLUX FRONT TEMP BACK TEMP	FLOW MODEL	H_2 MOLE %	CH_4 MOLE %	CO MOLE %	CO_2 MOLE %	N_2 MOLE %	H_2O MOLE %	C_6H_6O MOLE %	C_2H_4 MOLE %	C_2H_2 MOLE %	MODEL	
											ΔP	q_{cz}
XII-36	FROZEN	35.0	43.6	4.9	2.9	13.6	0.0	0.0	0.0	0.0	2.1	1.36
0.0039	EQUILIBRIUM	76.9	5.5	5.8	0.2	9.9	1.6	0.0	0.0	0.0	2.0	14.62
1350°F	NON-EQUILIBRIUM	35.0	43.6	4.9	2.9	13.6	0.0	0.0	0.0	0.0	2.1	1.36
920°F	EXPERIMENTAL	36.1	42.9	4.8	3.3	12.9	0.0	0.0	0.0	0.0	2.3	-
XIII-38	FROZEN	31.7	46.3	5.5	2.5	14.0	0.0	0.0	0.0	0.0	0.7	0.41
0.0009	EQUILIBRIUM	82.3	1.1	7.0	0.0	9.5	0.2	0.0	0.0	0.0	1.0	3.17
1690°F	NON-EQUILIBRIUM	31.7	46.3	5.5	2.5	14.0	0.0	0.0	0.0	0.0	0.7	0.41
1210°F	EXPERIMENTAL	32.6	41.3	8.9	5.2	14.0	0.0	0.0	0.0	0.0	0.5	-
XIII-39	FROZEN	31.7	46.3	5.5	2.5	14.0	0.0	0.0	0.0	0.0	2.9	1.74
0.0039	EQUILIBRIUM	82.4	1.0	7.0	0.0	9.5	0.1	0.0	0.0	0.0	4.2	13.01
1725°F	NON-EQUILIBRIUM	31.7	46.3	5.5	2.5	14.0	0.0	0.0	0.0	0.0	2.9	1.75
1220°F	EXPERIMENTAL	30.8	45.8	6.0	4.4	14.0	0.0	0.0	0.0	0.0	4.2	-
XIII-40	FROZEN	31.7	46.3	5.5	2.5	14.0	0.0	0.0	0.0	0.0	0.7	0.43
0.0009	EQUILIBRIUM	82.5	0.9	7.0	0.0	9.5	0.1	0.0	0.0	0.0	1.1	3.01
1750°F	NON-EQUILIBRIUM	31.7	46.3	5.5	2.5	14.0	0.0	0.0	0.0	0.0	0.7	0.42
1200°F	EXPERIMENTAL	30.8	45.7	5.9	3.6	14.0	0.0	0.0	0.0	0.0	1.5	-
XV-45	FROZEN	31.7	46.3	5.5	2.5	14.0	0.0	0.0	0.0	0.0	0.6	0.47
0.0009	EQUILIBRIUM	82.3	1.1	7.0	0.0	9.5	0.1	0.0	0.0	0.0	0.9	5.26
1710°F	NON-EQUILIBRIUM	31.7	46.3	5.5	2.5	14.0	0.0	0.0	0.0	0.0	0.6	0.47
1125°F	EXPERIMENTAL	31.7	46.8	4.5	3.0	14.0	0.0	0.0	0.0	0.0	1.2	-

Table D-3. Flow of Pyrolysis Products Through Graphite Specimens (Continued).

RUN NUMBER MASS FLUX FRONT TEMP BACK TEMP	FLOW MODEL	H_2 MOLE %	CH_4 MOLE %	CO MOLE %	CO_2 MOLE %	N_2 MOLE %	H_2O MOLE %	C_6H_6O MOLE %	C_2H_4 MOLE %	C_2H_2 MOLE %	MODEL	
											ΔP	q_{cz}
XV-46	FROZEN	31.7	46.3	5.5	2.5	14.0	0.0	0.0	0.0	0.0	0.0	0.03
0.0001	EQUILIBRIUM	82.5	0.9	7.0	0.0	9.5	0.1	0.0	0.0	0.0	0.1	0.49
1755°F	NON-EQUILIBRIUM	31.7	46.3	5.6	2.4	14.0	0.0	0.0	0.0	0.0	0.0	0.03
1185°F	EXPERIMENTAL	32.5	43.7	6.2	4.6	13.0	0.0	0.0	0.0	0.0	0.2	-
XXI-66	FROZEN	23.5	4.5	2.7	0.8	0.0	61.8	6.7	0.0	0.0	0.3	3.18
0.0040	EQUILIBRIUM	60.2	0.6	38.1	0.3	0.0	0.7	0.0	0.0	0.0	0.2	44.22
2085°F	NON-EQUILIBRIUM	39.4	5.9	21.1	3.8	0.0	24.2	5.3	0.0	0.3	0.3	4.78
895°F	EXPERIMENTAL	35.5	12.2	22.2	10.6	0.0	13.3	5.8	0.2	0.2	-	-
XXI-67	FROZEN	51.2	9.9	5.8	1.7	0.0	29.2	2.2	0.0	0.0	0.4	4.60
0.0040	EQUILIBRIUM	71.5	0.7	27.2	0.1	0.0	0.4	0.0	0.0	0.0	0.3	50.90
2135°F	NON-EQUILIBRIUM	50.6	14.6	17.1	2.9	0.0	12.6	2.0	0.0	0.2	0.4	5.80
915°F	EXPERIMENTAL	48.5	11.8	20.7	2.3	0.0	14.8	1.4	0.2	0.3	-	-
XXIII-71	FROZEN	25.8	4.9	2.9	0.9	0.0	54.7	10.8	0.0	0.0	0.2	2.02
0.0031	EQUILIBRIUM	62.6	0.7	35.8	0.3	0.0	0.7	0.0	0.0	0.0	0.2	31.85
2065°F	NON-EQUILIBRIUM	41.4	8.4	23.9	5.1	0.0	12.5	8.2	0.0	0.6	0.2	3.23
1108°F	EXPERIMENTAL	39.3	8.8	27.2	5.9	0.0	11.2	7.6	0.0	0.0	0.7	-
XXIII-72	FROZEN	13.9	2.5	1.6	0.5	0.0	72.2	9.3	0.0	0.0	0.2	1.34
0.0024	EQUILIBRIUM	57.9	0.4	41.0	0.2	0.0	0.5	0.0	0.0	0.0	0.2	19.72
2105°F	NON-EQUILIBRIUM	37.4	13.0	33.2	9.1	0.0	0.8	5.8	0.0	0.7	0.2	2.65
1257°F	EXPERIMENTAL	43.1	10.0	30.4	6.9	0.0	2.1	6.7	0.3	0.5	0.4	-

Table D-3. Flow of Simulated Pyrolysis Products Through Graphite Specimens (Continued).

RUN NUMBER MASS FLUX FRONT TEMP BACK TEMP	FLOW MODEL	H_2 MOLE %	CH_4 MOLE %	CO MOLE %	CO_2 MOLE %	N_2 MOLE %	H_2O MOLE %	C_6H_6O MOLE %	C_2H_4 MOLE %	C_2H_2 MOLE %	MODEL P	MODEL q_{cz}
XXIII-73	FROZEN	6.6	1.3	0.8	0.3	0.0	78.9	12.1	0.0	0.0	0.2	1.37
0.0023	EQUILIBRIUM	56.7	0.4	42.2	0.2	0.0	0.5	0.0	0.0	0.0	0.2	18.93
2120°F	NON-EQUILIBRIUM	35.8	11.8	35.0	9.1	0.0	0.3	7.2	0.0	0.8	0.2	1.45
1175°F	EXPERIMENTAL	39.5	10.4	31.2	8.9	0.0	1.3	6.6	0.4	1.7	0.2	
XXIV-76	FROZEN	37.8	7.4	4.3	1.4	0.0	40.3	8.9	0.0	0.0	0.2	2.03
0.0028	EQUILIBRIUM	65.7	1.8	29.3	1.1	0.0	2.2	0.0	0.0	0.0	0.2	28.79
1905°F	NON-EQUILIBRIUM	34.0	12.6	7.7	3.1	0.0	33.5	8.8	0.0	0.3	0.2	2.13
890°F	EXPERIMENTAL	37.0	12.0	8.3	4.2	0.0	28.2	9.7	0.4	0.7	-	-
XXIV-78	FROZEN	2.0	4.1	2.4	0.7	0.0	89.1	1.7	0.0	0.0	0.3	2.76
0.0043	EQUILIBRIUM	51.5	0.6	46.0	0.8	0.0	1.1	0.0	0.0	0.0	0.2	45.96
2015°F	NON-EQUILIBRIUM	30.8	3.7	20.8	6.2	0.0	37.2	1.3	0.0	0.3	0.3	2.91
903°F	EXPERIMENTAL	26.5	6.8	16.8	9.5	0.0	37.3	1.6	0.6	0.9	-	-
XXVIII-92	FROZEN	27.5	5.3	3.1	1.0	0.0	52.5	10.6	0.0	0.0	0.3	2.44
0.0044	EQUILIBRIUM	62.5	1.2	33.9	0.8	0.0	1.6	0.0	0.0	0.0	0.3	35.48
1920°F	NON-EQUILIBRIUM	29.3	7.7	8.0	2.5	0.0	42.2	10.1	0.0	0.2	0.3	2.75
1100°F	EXPERIMENTAL	30.0	8.7	8.0	3.4	0.0	37.9	11.6	0.2	0.2	0.4	-
XXVIII-93	FROZEN	25.8	7.2	4.3	1.3	0.0	50.1	11.3	0.0	0.0	0.2	1.92
0.0034	EQUILIBRIUM	62.7	1.3	33.5	0.8	0.0	1.7	0.0	0.0	0.0	0.2	28.40
1950°F	NON-EQUILIBRIUM	30.8	10.0	11.8	4.1	0.0	32.6	10.2	0.0	0.3	0.2	2.33
1110°F	EXPERIMENTAL	32.2	11.2	9.2	4.0	0.0	33.2	9.8	0.2	0.2	0.3	-

Table D-3. Flow of Simulated Pyrolysis Products Through Graphite Specimens (Continued).

RUN NUMBER MASS FLUX FRONT TEMP BACK TEMP	FLOW MODEL	H_2 MOLE %	CH_4 MOLE %	CO MOLE %	CO_2 MOLE %	N_2 MOLE %	H_2O MOLE %	C_6H_6O MOLE %	C_2H_4 MOLE %	C_2H_2 MOLE %	MODEL	
											P	q_{cz}
XXIX-94	FROZEN	25.6	4.1	2.9	0.8	0.0	55.2	11.5	0.0	0.0	0.3	3.33
0.0050	EQUILIBRIUM	61.8	1.1	34.9	0.7	0.0	1.5	0.0	0.0	0.0	0.3	25.77
1925°F	NON-EQUILIBRIUM	28.1	5.8	7.8	2.1	0.0	45.1	10.9	0.0	0.3	0.3	3.68
920°F	EXPERIMENTAL	25.5	5.8	10.5	2.7	0.0	42.7	12.2	0.2	0.2	0.4	-
XXIX-95	FROZEN	21.7	4.6	2.8	0.8	0.0	57.1	13.1	0.0	0.0	0.5	7.34
0.0059	EQUILIBRIUM	61.1	1.4	34.0	1.3	0.0	2.2	0.0	0.0	0.0	0.3	49.85
1935°F	NON-EQUILIBRIUM	22.9	5.1	4.7	1.2	0.0	53.1	12.9	0.0	0.1	0.5	7.65
930°F	EXPERIMENTAL	21.9	6.6	8.4	2.1	0.0	52.0	11.3	0.3	0.4	1.0	-

Table D-4. Flow of Simulated Pyrolysis Products Through Graphite Specimens in the Presence of Heterogeneous Catalysts Coated on the Specimen Surface.

RUN NUMBER MASS FLUX FRONT TEMP BACK TEMP	FLOW MODEL	H_2 MOLE %	CH_4 MOLE %	CO MOLE %	CO_2 MOLE %	N_2 MOLE %	H_2O MOLE %	C_6H_6O MOLE %	C_2H_4 MOLE %	C_2H_2 MOLE %	CATALYST
VIII-21	FROZEN	35.0	43.7	4.9	2.9	13.6	0.0	0.0	0.0	0.0	Platinum
0.00100	EQUILIBRIUM	77.5	5.0	6.0	0.2	9.9	1.4	0.0	0.0	0.0	1%(wt)
1370°F	NON-EQUILIBRIUM	35.0	43.7	4.9	2.9	13.6	0.0	0.0	0.0	0.0	as $PtCl_4$
532°F	EXPERIMENTAL	25.9	48.7	5.2	4.2	13.0	0.0	0.0	0.0	0.0	
VIII-22	FROZEN	35.0	43.7	4.9	2.9	13.6	0.0	0.0	0.0	0.0	"
0.00380	EQUILIBRIUM	79.8	3.0	6.7	0.1	9.6	0.7	0.0	0.0	0.0	
1470°F	NON-EQUILIBRIUM	35.0	43.7	4.9	2.9	13.6	0.0	0.0	0.0	0.0	
739°F	EXPERIMENTAL	36.2	41.4	5.2	4.2	13.0	0.0	0.0	0.0	0.0	
IX-25	FROZEN	35.0	43.7	4.9	2.9	13.6	0.0	0.0	0.0	0.0	"
0.00100	EQUILIBRIUM	76.8	5.6	5.8	0.2	10.0	1.7	0.0	0.0	0.0	
1350°F	NON-EQUILIBRIUM	35.0	43.7	4.9	2.9	13.6	0.0	0.0	0.0	0.0	
815°F	EXPERIMENTAL	25.1	50.5	7.5	3.5	13.4	0.0	0.0	0.0	0.0	
IX-26	FROZEN	35.0	43.7	4.9	2.9	13.6	0.0	0.0	0.0	0.0	"
0.00390	EQUILIBRIUM	77.5	5.0	6.0	0.2	9.9	1.4	0.0	0.0	0.0	
1370°F	NON-EQUILIBRIUM	35.0	43.7	4.9	2.9	13.6	0.0	0.0	0.0	0.0	
800°F	EXPERIMENTAL	24.6	52.2	6.2	3.4	13.6	0.0	0.0	0.0	0.0	
IX-27	FROZEN	35.0	43.7	4.9	2.9	13.6	0.0	0.0	0.0	0.0	"
0.05700	EQUILIBRIUM	79.8	3.0	6.7	0.1	9.6	0.7	0.0	0.0	0.0	
1350°F	NON-EQUILIBRIUM	35.0	43.7	4.9	2.9	13.6	0.0	0.0	0.0	0.0	
725°F	EXPERIMENTAL	26.9	51.2	5.5	2.8	13.6	0.0	0.0	0.0	0.0	

Table D-4. Flow of Pyrolysis Products Through Graphite in the Presence of Heterogeneous Catalysts (Continued).

RUN NUMBER MASS FLUX FRONT TEMP BACK TEMP	FLOW MODEL	H_2 MOLE %	CH_4 MOLE %	CO MOLE %	CO_2 MOLE %	N_2 MOLE %	H_2O MOLE %	C_6H_6O MOLE %	C_2H_4 MOLE %	C_2H_2 MOLE %	CATALYST
XIII-38	FROZEN	31.7	46.4	5.5	2.5	14.0	0.0	0.0	0.0	0.0	Platinum 1%(wt) as Pt-Cl_4
0.0010	EQUILIBRIUM	82.3	1.1	7.0	0.0	9.5	0.2	0.0	0.0	0.0	
1693°F	NON-EQUILIBRIUM	31.6	46.5	5.5	2.5	14.0	0.0	0.0	0.0	0.0	
1211°F	EXPERIMENTAL	31.2	40.2	9.4	5.4	14.8	0.0	0.0	0.0	0.0	
XIII-39	FROZEN	31.7	46.4	5.5	2.5	14.0	0.0	0.0	0.0	0.0	"
0.0039	EQUILIBRIUM	82.4	1.0	7.0	0.0	9.5	0.1	0.0	0.0	0.0	
1725°F	NON-EQUILIBRIUM	31.7	46.4	5.5	2.5	14.0	0.0	0.0	0.0	0.0	
1219°F	EXPERIMENTAL	30.5	45.0	6.1	4.4	14.0	0.0	0.0	0.0	0.0	
XIII-40	FROZEN	31.7	46.4	5.5	2.5	14.0	0.0	0.0	0.0	0.0	"
0.0010	EQUILIBRIUM	82.5	0.9	7.0	0.0	9.5	6.1	0.0	0.0	0.0	
1747°F	NON-EQUILIBRIUM	31.7	46.4	5.5	2.5	14.0	0.0	0.0	0.0	0.0	
1242°F	EXPERIMENTAL	27.8	45.7	6.9	5.6	14.0	0.0	0.0	0.0	0.0	
XV-45	FROZEN	31.7	46.4	5.5	2.5	14.0	0.0	0.0	0.0	0.0	"
0.0010	EQUILIBRIUM	82.3	1.1	7.0	0.0	9.5	0.1	0.0	0.0	0.0	
1710°F	NON-EQUILIBRIUM	31.7	46.4	5.5	2.5	14.0	0.1	0.0	0.0	0.0	
1123°F	EXPERIMENTAL	25.9	51.8	4.6	2.9	14.8	0.0	0.0	0.0	0.0	
XV-46	FROZEN	31.7	46.4	5.5	2.5	14.0	0.0	0.0	0.0	0.0	"
0.0001	EQUILIBRIUM	82.5	0.9	7.0	0.0	9.5	0.1	0.0	0.0	0.0	
1755°F	NON-EQUILIBRIUM	31.7	46.3	5.7	2.4	14.0	0.0	0.0	0.0	0.0	
1185°F	EXPERIMENTAL	21.5	53.8	6.2	4.6	14.0	0.0	0.0	0.0	0.0	

Table D-4. Flow of Pyrolysis Products Through Graphite in the Presence of Heterogeneous Catalysts (Continued).

RUN NUMBER MASS FLUX FRONT TEMP BACK TEMP	FLOW MODEL	H_2 MOLE %	CH_4 MOLE %	CO MOLE %	CO_2 MOLE %	N_2 MOLE %	H_2O MOLE %	C_6H_6O MOLE %	C_2H_4 MOLE %	C_2H_2 MOLE %	CATALYSTS
XXXI-97	FROZEN	20.0	4.2	2.1	0.6	0.0	62.1	11.0	0.0	0.0	Molybdenum
0.0064	EQUILIBRIUM	59.4	1.7	33.7	2.0	0.0	3.1	0.0	0.0	0.0	& Tungsten
1875°F	NON-EQUILIBRIUM	20.4	4.6	3.0	0.9	0.0	60.1	10.9	0.0	0.0	5-6%(wt)
850°F	EXPERIMENTAL	21.6	5.6	4.1	1.3	0.0	58.0	9.0	0.2	0.3	as sulfide
XXXI-98	FROZEN	26.2	5.5	2.9	0.8	0.0	52.7	11.9	0.0	0.0	"
0.0048	EQUILIBRIUM	62.6	1.4	33.1	1.0	0.0	1.9	0.0	0.0	0.0	
1945°F	NON-EQUILIBRIUM	28.4	6.5	6.9	1.5	0.0	45.2	11.4	0.0	0.2	
950°F	EXPERIMENTAL	29.2	11.1	8.7	3.6	0.0	38.0	8.8	0.3	0.3	
XXXII-99	FROZEN	25.5	5.3	2.8	0.8	0.0	53.9	11.7	0.0	0.0	"
0.0049	EQUILIBRIUM	62.6	1.4	33.1	1.0	0.0	1.9	0.0	0.0	0.0	
1860°F	NON-EQUILIBRIUM	26.3	6.3	5.0	1.4	0.0	49.6	11.5	0.0	0.1	
840°F	EXPERIMENTAL	27.6	7.2	6.6	2.6	0.0	45.2	10.2	0.2	0.4	
XXXII-100	FROZEN	14.0	2.3	1.5	0.4	0.0	69.4	12.4	0.0	0.0	"
0.0098	EQUILIBRIUM	62.6	1.4	33.1	1.0	0.0	1.9	0.0	0.0	0.0	
1920°F	NON-EQUILIBRIUM	15.2	2.4	2.8	0.6	0.0	66.8	12.2	0.0	0.0	
900°F	EXPERIMENTAL	16.6	3.2	3.7	0.8	0.0	64.0	10.8	0.4	0.5	

Table D-5. Flow of Simulated Pyrolysis Products Through Graphite Specimens in the Presence of Homogeneous Catalysts Contained in the Inlet Stream.

RUN NUMBER MASS FLUX FRONT TEMP BACK TEMP	FLOW MODEL	H_2 MOLE %	CH_4 MOLE %	CO MOLE %	CO_2 MOLE %	N_2 MOLE %	H_2O MOLE %	C_6H_6O MOLE %	C_2H_4 MOLE %	C_2H_2 MOLE %	CATALYSTS
XXV-80	FROZEN	32.6	6.1	3.6	1.1	0.0	46.6	10.1	0.0	0.0	Bromine 4%(wt) in water
0.0016	EQUILIBRIUM	64.9	0.8	33.2	0.3	0.0	0.8	0.0	0.0	0.0	
2040°F	NON-EQUILIBRIUM	40.3	10.0	19.0	4.1	0.0	17.7	8.4	0.0	0.5	
1085°F	EXPERIMENTAL	41.3	10.9	21.5	8.4	0.0	11.8	5.4	0.1	0.6	
XXV-81	FROZEN	31.5	6.1	3.5	1.1	0.0	47.1	10.8	0.0	0.0	"
0.0018	EQUILIBRIUM	64.7	0.9	33.2	0.4	0.0	0.9	0.0	0.0	0.0	
1995°F	NON-EQUILIBRIUM	36.4	9.9	14.6	3.7	0.0	25.4	9.5	0.0	0.4	
1170°F	EXPERIMENTAL	40.2	11.9	15.1	7.0	0.0	17.6	7.2	0.3	0.7	
XXV-82	FROZEN	36.9	7.2	4.2	1.3	0.0	42.3	8.1	0.0	0.0	"
0.0065	EQUILIBRIUM	66.2	0.8	32.1	0.2	0.0	0.7	0.0	0.0	0.0	
2050°F	NON-EQUILIBRIUM	40.6	9.7	14.1	2.7	0.0	25.2	7.3	0.0	0.3	
1105°F	EXPERIMENTAL	41.6	11.8	18.9	3.4	0.0	16.4	7.1	0.3	0.5	
XXVI-84	FROZEN	34.3	6.6	3.9	1.1	0.0	45.4	8.7	0.0	0.0	Bromine 2% (wt) in water
0.0013	EQUILIBRIUM	65.0	1.0	32.5	0.4	0.0	1.0	0.0	0.0	0.0	
2020°F	NON-EQUILIBRIUM	39.5	10.7	16.6	3.8	0.0	21.5	7.5	0.0	0.4	
908°F	EXPERIMENTAL	37.8	15.3	21.0	4.8	0.0	14.2	6.3	0.2	0.4	
XXVI-85	FROZEN	50.0	9.6	5.6	1.6	0.0	28.0	5.2	0.0	0.0	"
0.0110	EQUILIBRIUM	71.6	1.0	26.5	0.2	0.0	0.7	0.0	0.0	0.0	
2055°F	NON-EQUILIBRIUM	48.5	11.7	8.2	2.0	0.0	24.4	5.1	0.0	0.1	
881°F	EXPERIMENTAL	44.5	15.0	12.0	2.3	0.0	20.6	5.1	0.2	0.3	

Table D-5. Flow of Pyrolysis Gases Through Graphite in the Presence of Homogeneous Catalysts. (Continued)

RUN NUMBER MASS FLUX FRONT TEMP BACK TEMP	FLOW MODEL	H_2 MOLE %	CH_4 MOLE %	CO MOLE %	CO_2 MOLE %	N_2 MOLE %	H_2O MOLE %	C_6H_6O MOLE %	C_2H_4 MOLE %	C_2H_2 MOLE %	CATALYSTS
XXVII-87	FROZEN	2.3	3.4	0.4	0.1	0.0	0.0	93.8	0.0	0.0	Br_2 1.0%
0.00320	EQUILIBRIUM	73.7	1.5	24.1	0.3	0.0	0.4	0.0	0.0	0.0	
1980°F	NON-EQUILIBRIUM	2.8	3.5	0.4	0.1	0.0	0.0	92.7	0.0	0.4	
1060°F	EXPERIMENTAL	4.8	2.7	0.8	0.1	0.0	0.0	90.2	0.1	0.3	
XXVII-88	FROZEN	1.8	2.6	0.3	0.1	0.0	0.0	95.2	0.0	0.0	"
0.00420	EQUILIBRIUM	73.8	1.3	24.3	0.2	0.0	0.3	0.0	0.0	0.0	
2010°F	NON-EQUILIBRIUM	3.1	2.7	0.4	0.1	0.0	0.0	93.2	0.0	0.6	
1080°F	EXPERIMENTAL	3.6	2.0	0.8	0.1	0.0	0.0	92.0	0.1	0.4	
XXVII-89	FROZEN	2.1	3.2	0.4	0.1	0.0	94.2	0.0	0.0	0.0	"
0.00508	EQUILIBRIUM	51.1	0.6	46.7	0.7	0.0	1.0	0.0	0.0	0.0	
2010°F	NON-EQUILIBRIUM	18.3	2.8	13.3	2.0	0.0	63.6	0.0	0.0	0.0	
1070°F	EXPERIMENTAL	28.2	3.4	21.5	6.0	0.0	40.8	0.0	0.4	0.5	
XXVII-90	FROZEN	1.4	2.1	0.3	0.1	0.0	96.1	0.0	0.0	0.0	"
0.00492	EQUILIBRIUM	50.4	0.5	47.4	0.7	0.0	1.0	0.0	0.0	0.0	
2010°F	NON-EQUILIBRIUM	15.9	1.9	11.7	1.8	0.0	68.8	0.0	0.0	0.0	
1065°F	EXPERIMENTAL	28.2	3.4	21.5	6.0	0.0	40.0	0.0	0.4	0.5	
XXX-96	FROZEN	17.7	3.8	2.1	0.6	0.0	63.6	12.2	0.0	0.0	Br_2 4%
0.0075	EQUILIBRIUM	60.1	0.8	37.5	0.5	0.0	1.0	0.0	0.0	0.0	
1900°F	NON-EQUILIBRIUM	19.7	4.1	4.5	1.0	0.0	58.8	11.9	0.0	0.1	
950°F	EXPERIMENTAL	46.4	15.1	15.2	5.5	0.0	8.8	8.4	0.4	0.4	

Table D-6. Air Oxidation of Porous Graphite Specimens Between 1485°F and 2047°F.

RUN NUMBER AIR MASS FLUX FRONT TEMP BACK TEMP	COMPOSITION AT THE BACK SURFACE FOR THE MAXIMUM OBSERVED OXIDATION RATE			TIME VS. CONCENTRATION CURVES FOR O_2 AND CO_2 IN THE EXIT GAS STREAM FROM THE CHAR ZONE THERMAL ENVIRONMENT SIMULATOR (Time in Minutes, O_2 and CO_2 in Mole %)
	MOLE % O_2	MOLE % N_2	MOLE % CO_2	
X-29 0.0057 1485°F 747°F 0.0104ft (Char Thickness)	11.4	79.5	8.6	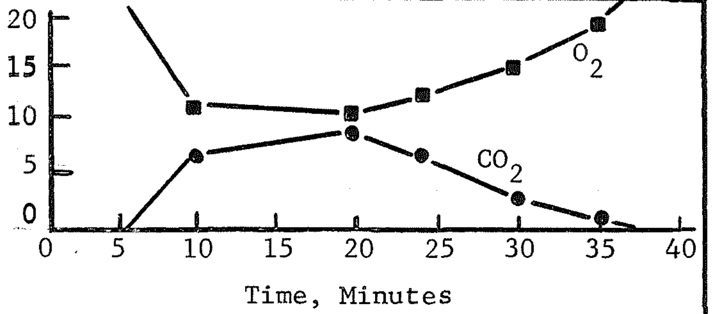
XVII-54 0.0350 2047°F 304°F 0.0108ft (Char Thickness)	4.3	79.0	16.7	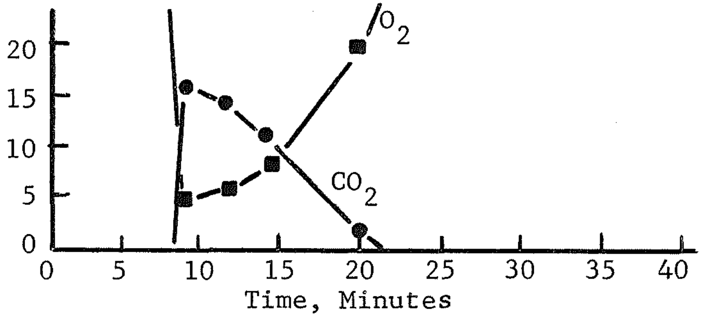
VI-16 0.00970 1595°F 792°F	(No Analysis Made - Air Contamination After Run Terminated)			

Table D-7. Summary of Radioactive Tracer Analyses of the Various Exit Product Streams From the Char Zone Thermal Environment Simulator.

Experiment XXVIII (C^{14} labeled phenol)

Radioactivity Fed to the System (Total), cpm = 18,900,000
Radioactivity in Gas Samples (6 Samples), cpm = 1,707
Radioactivity of the Liquid Phase, cpm = 16,000,000
Radioactivity of the Carbon Deposit, cpm = 17,564
Radioactivity of the Vent Gas (by difference) = 1,980,729
Dilution Factor (Total Radioactivity/Gas Activity) = 11,000

Gas Analysis:

Retention Time Minutes	Radioactivity cpm	% Radioactivity
1	4.8	1.7
2	2.5	0.9
3	3.9	1.4
4	76.7	27.1
5	74.4	26.3
6	13.3	4.7
7	3.7	1.3
8	11.3	4.0
9	42.9	15.2
10	5.3	1.9
11	3.1	1.1
12	13.9	4.9
13	12.9	4.6
14	4.4	1.6
15	4.0	1.4
16	5.5	1.9
Total	282.6	100.0

Char Analysis: Weight of Char = 1.326 gm

Slice	Weight	Weight %	Radioactivity	% R
1	0.0215	1.7	1062.4	6.0
2	0.0841	6.5	5076.0	28.9
3	0.1059	8.1	4325.1	24.6
4	0.0737	5.7	2684.9	15.3
5	0.1071	8.2	1608.0	9.2
6	0.1226	9.5	1208.0	6.9
7	0.7115	60.3	1600.0	9.1
	1.3264	100.0	17564.4	100.0

Table D-8. Summary of Radioactive Tracer Analyses of the Various Exit Product Streams From the Char Zone Thermal Environment Simulator.

Experiment XXIX (C^{14} labeled methane)

Radioactivity Fed into the System (Total), cpm = 874,000
Radioactivity in Gas Samples (5 Samples), cpm = 3,989
Radioactivity of the Liquid Phase, cpm = 1,848
Radioactivity as Carbon Deposit, cpm = 4,390
Radioactivity in Vent Gas (by difference), cpm = 863,773
Dilution Factor (Total Radioactivity/Gas Activity) = 219

Gas Analysis:

Retention Time Minutes	Radioactivity cpm	% Radioactivity
1	15.0	1.9
2	7.0	0.9
3	3.7	0.5
4	3.7	0.5
5	235.9	29.6
6	228.3	28.6
7	108.4	13.6
8	59.3	7.4
9	4.7	0.6
10	7.1	0.9
11	45.8	5.7
12	6.8	0.9
13	4.2	0.5
14	30.3	3.8
15	30.0	3.8
16	7.7	1.0
Total	797.8	100.0

Char Analysis: Weight of Char = 0.9812 gm

Slice	Weight	Weight %	Radioactivity	% R
1	0.0215	2.2	265.5	6.0
2	0.0841	8.6	1269.0	28.9
3	0.1059	10.7	1081.3	24.6
4	0.1737	17.7	671.3	15.3
5	0.1071	10.8	402.0	9.2
6	0.1226	12.3	302.1	6.9
7	0.3663	37.7	399.2	9.1
	0.9812	100.0	4390.4	100.0

Table D-9. Summary of Radioactive Tracer Analyses of the Various Exit Product Streams From the Char Zone Thermal Environment Simulator.

Experiment XXX (C^{14} labeled phenol)

Radioactivity Fed into System (Total), cpm	=	29,575,000
Radioactivity in Gas Samples (6 Samples), cpm	=	4,290
Radioactivity in the Liquid Phase, cpm	=	18,973,000
Radioactivity as Carbon Deposit, cpm	=	27,978
Radioactivity in Vent Gas (by difference), cpm	=	10,569,732
Dilution Factor (Total Radioactivity/Gas Activity)	=	7,400

Gas Analysis:

Retention Time Minutes	Radioactivity cpm	% Radioactivity
1	5.0	1.7
2	5.6	1.9
3	3.5	1.2
4	5.3	1.8
4.5	7.0	2.4
5	66.6	23.1
5.5	15.9	5.5
6	51.4	17.8
7	3.5	1.2
8	5.1	1.8
9	58.5	20.3
10	16.6	5.7
11	4.6	1.7
12	4.3	1.5
13	9.5	3.3
14	5.3	1.8
15	2.9	1.0
16	6.5	2.3
17	7.6	2.6
18	3.7	1.3
Total	715.0	100.0

Char Analysis: Weight of Char = 0.4818

Slice	Weight	Weight %	Radioactivity	% R
1	0.0145	3.1	1810.8	6.5
2	0.0414	8.6	1211.1	4.3
3	0.0331	6.9	2194.2	7.8
4	0.0555	11.5	8485.8	30.3
5	0.0565	11.7	7791.3	27.8
6	0.0484	10.0	3729.6	13.3
7	0.0565	11.7	1254.3	4.5
8	0.1759	36.5	1500.5	5.4
	0.4818	100.0	27977.6	100.0

Table D-10. Summary of the Radioactive Tracer Analyses of the Various Exit Product Streams From the Char Zone Thermal Environment Simulator.

Experiment XXXI (C^{14} labeled methane)

Radioactivity in System (Total), cpm = 774,000
Radioactivity in Gas Samples (7 Samples), cpm = 2,464
Radioactivity in Liquid Phase, cpm = 3,626
Radioactivity in Carbon Deposit, cpm = 1,625
Radioactivity in Vent Gas (by difference), cpm = 766,285
Dilution Factor (Total Radioactivity/Gas Activity) = 310

Gas Analysis:

Retention Time Minutes	Radioactivity cpm	% Radioactivity
1	6.5	1.8
2	4.7	1.3
3	6.4	1.8
4	6.3	1.8
4.5	31.2	8.9
5	122.4	34.8
5.5	78.2	22.2
6	2.9	0.8
7	1.8	0.5
8	29.3	8.3
9	11.2	3.2
10	3.4	1.0
11	5.5	1.6
12	6.0	1.7
13	5.8	1.7
14	10.3	2.9
15	11.2	3.2
16	4.4	1.3
17	4.0	1.1
Total	351.5	100.0

Char Analysis: Weight of Char = 1.1869 gm

Slice	Weight	Weight %	Radioactivity	% R
1	0.0111	0.9	206.4	5.7
2	0.0373	3.1	310.8	8.6
3	0.0792	6.7	867.0	23.9
4	0.0783	6.5	606.8	16.7
5	0.0853	7.2	135.2*	3.7*
6	0.1015	8.6	483.0	13.3
7	0.0822	6.9	403.9	11.1
8	0.7420	60.1	613.2	16.9
	1.1869	100.0	3626.0	100.0

* Sample Spilled.

Table D-11. Summary of Radioactive Tracer Analyses of the Exit Product Streams From the Char Zone Thermal Environment Simulator.

Experiment XXXII (C^{14} labeled phenol)

Radioactivity Fed into System (Total), cpm = 33,645,000
Radioactivity in Gas Samples (6 Samples), cpm = 2,280
Radioactivity in Liquid Phase, cpm = 27,654,000
Radioactivity in the Carbon Deposit, cpm = 19,829
Radioactivity in the Vent Gas, cpm (by difference) = 5,968,891
Dilution Factor (Total Radioactivity/Gas Activity) = 14,967

Gas Analysis:

Retention Time Minutes	Radioactivity cpm	% Radioactivity
1	5.7	1.5
2	2.6	0.7
3	3.2	0.8
4	64.2	16.9
4.5	110.9	29.2
5	21.3	5.6
5.5	10.2	2.7
6	2.8	0.7
7	4.7	1.2
8	14.3	3.8
9	4.3	1.1
10	3.0	0.8
11	12.1	3.2
12	4.1	1.1
13	9.3	2.4
14	15.1	4.0
15	5.2	1.4
Total	380.0	100.0

Char Analysis: Weight of Char = 1.2369 gm

Slice	Weight	Weight %	Radioactivity	% R
1	0.0374	3.0	1031.0	5.2
2	0.0736	5.9	7296.5	36.8
3	0.1526	12.3	3824.2	19.3
4	0.1550	12.6	2305.2*	11.6
5	0.1490	12.0	2512.3	12.7
6	0.1480	11.9	1644.3	8.3
7	0.5211	42.2	1215.0	6.1
	1.2367	100.0	19828.5	100.0

* Sample Spilled.

E. INTEGRITY OF THE ANALYTICAL METHODS

The accuracy and integrity of the analytical methods used in this research were determined by calculating the standard deviation from a mean value at a 95% confidence limit. This technique was used for analyses by chromatographic and liquid scintillation spectrometric methods on replicate samples. From these measurements an average was calculated by equation (E-1).

$$\bar{x} = \sum_{i=1}^{N} x_i / N \qquad \text{(E-1)}$$

From these averages the variance, s_x^2, of any measured value, x_i, from the average value, $\bar{x}$, can be calculated.

$$s_x^2 = \frac{\sum_{i=1}^{N} (\bar{x} - x_i)^2}{N - 1} \qquad \text{(E-2)}$$

The standard deviation was calculated by applying the t test at the 95% confidence limit for the stated degrees of freedom (N - 1).

$$\text{std.dev.}_{95\%,N-1} = (s_x^2)^{1/2} (t_{95\%,N-1}) \qquad \text{(E-3)}$$

Therefore, the measured quantities were expected to be $\bar{x} \pm (s_x^2)^{1/2} t$.

Obviously, the lower the range about $\bar{x}$ the more accurate the method for determining x_i.

For the cases where analytical measurement of values varied over a wide range, a weighted variance based on the number of degrees of freedom in each subgroup was calculated.

$$(s_x^2)_{net} = \frac{(N_1-1)(s_x^2)_1 + (N_2-1)(s_x^2)_2 + \dots + (N_i-1)(s_x^2)_i}{(N_1-1) + (N_2-1) + \dots + (N_i-1)} \tag{E-4}$$

The standard deviation was calculated as before (equation E-3). The following pages present typical data and results of this method for determining the integrity of the analytical procedures used.

Determination of the Accuracy of the Gas Chromatographic Analyses

The gaseous portion of the exit stream from the Char Zone Thermal Environment Simulator was sampled in one hundred cubic centimeter containers and analysed by gas chromatography. The particular gases contained in the samples were methane, carbon monoxide, carbon dioxide, ethylene, acetylene and nitrogen in varying quantities. In order to determine the accuracy of the analytical method, the data in Table E-1 were obtained. The variance in each subgroup was calculated in Table E-2 and the standard deviation at 95% for each gas species in the system and the overall or net standard deviation were calculated in Table E-3. The range for these analyses was ± 0.97% (net).

Table E-1. Measured Compositions of the Gas Species in the Feed Stream to the Char Zone Thermal Environment Simulator

Stream Identification		Composition, x_i (Mole %)				
		N_2	CO	CH_4	CO_2	H_2
Feed Mix 1		12.0	4.5	42.0	5.7	35.8
		12.8	4.9	40.7	6.3	37.7
		14.0	3.6	40.9	5.3	36.8
	Σx	38.8	13.0	123.6	17.3	110.3
	$\bar{x}$	12.93	4.33	41.20	5.43	36.77
	N-1	2	2	2	2	2
Feed Mix 2		15.8	8.6	33.0	6.8	36.5
		16.1	8.7	34.0	6.78	37.5
		16.0	8.1	33.5	6.75	36.5
		16.0	8.4	34.0		
	Σx	63.9	33.8	134.5	20.33	110.5
	$\bar{x}$	15.97	8.45	33.83	6.78	36.83
	N-1	3	3	3	2	2
Feed Mix 3		14.0	4.95	45.0	3.0	35.0
		14.0	5.0	43.9	2.6	35.0
		13.6	4.95	45.0	2.5	35.0
		14.0	4.9	45.0	3.0	33.9
		13.7	5.0	45.2	2.6	35.0
		14.6	5.9	44.1	3.0	35.2
		14.6	4.6	43.5	3.0	35.0
		13.5	4.5		2.4	34.1
		13.95	5.5		2.7	
					3.0	
	Σx	125.95	45.30	311.7	27.3	278.2
	$\bar{x}$	13.99	5.03	44.52	2.73	34.78
	N-1	8	8	6	9	7
Feed Mix 4		-	7.5	12.8	1.9	66.3
		-	7.5	12.8	1.8	66.25
	Σx	-	15.0	25.6	3.7	132.55
	$\bar{x}$	-	7.5	12.8	1.85	66.275
	N-1	-	1	1	1	1

Table E-2. Calculation of the Variances for Each of the Gas Species Listed in Table E-1.

Stream Identification		Square of the Differences $(\bar{x} - x_i)^2$				
		N_2	CO	CH_4	CO_2	H_2
Feed Mix 1		0.8704	0.0289	0.6400	0.0044	0.9409
		0.0176	0.3249	0.2500	0.2180	0.8649
		1.1384	0.5329	0.0900	0.2840	0.0009
	Σ	2.0264	0.8867	0.9800	0.5064	1.8067
	s_x^2	1.0132	0.4434	0.4900	0.2532	0.9034
Feed Mix 2		0.0306	0.0225	0.3906	0.0005	0.0900
		0.0156	0.0625	0.1406	0.0001	0.4900
		0.0006	0.1225	0.0156	0.0007	0.0900
		0.0006	0.0025	0.1406		
	Σ	0.0474	0.2100	0.6874	0.0013	0.6700
	s_x^2	0.0158	0.0700	0.2291	0.0007	0.3350
Feed Mix 3		0.0001	0.0002	0.2304	0.0707	0.0484
		0.0001	0.0010	0.3844	0.0179	0.0484
		0.1552	0.0002	0.2304	0.0547	0.0484
		0.0001	0.0176	0.2304	0.0707	0.7784
		0.0864	0.0010	0.4624	0.0179	0.0484
		0.3672	0.7516	0.1764	0.0707	0.1764
		0.2440	0.2840	1.0404	0.0707	0.0484
		0.3672	0.1874		0.1115	0.5624
		0.0019	0.2180		0.0001	
					0.0547	
	Σ	1.2222	1.4610	2.5748	0.5396	1.7552
	s_x^2	0.1527	0.1826	0.4591	0.0599	0.2507
Feed Mix 4		-	0.0000	0.0000	0.0025	0.0006
		-	0.0000	0.0000	0.0025	0.0006
	Σ	-	0.0000	0.0000	0.0050	0.0012
	s_x^2	-	0.0000	0.0000	0.0050	0.0012

Table E-3. Calculation of the Net Variances, Standard Deviation of Each Species and the Overall Standard Deviation.

Components	N_2	CO	CH_4	CO_2	H_2	Overall Gas Analysis
$\sum_{i=1}^{N}(N_i-1)(s_x^2)_i$	3.2960	2.5577	4.4222	1.0523	4.2331	-
$\sum_{i=1}^{N}(N_i-1)$ = d.f.	13	14	12	14	12	65
$(s_x^2)_{net}$	0.2535	0.1827	0.3685	0.0752	0.3528	0.24
$(s_x)_{net}$	0.503	0.428	0.607	0.274	0.594	0.485
$t_{95\%,\ d.f.}$	2.160	2.145	2.179	2.145	2.179	1.995
$(t_{95\%,\ d.f.})(s_x)$	1.086	0.918	1.323	0.588	1.294	0.97
Composition Range	12-16	3.6-8.7	33-45.2	2.4-6.8	34.1-37.7	2.4-45.2

Combined Accuracy of the Sampling and Analytical Methods for the Gas Phase

The accuracy of the sampling plus analytical technique was determined by taking replicate samples of the exit gas stream from the Char Zone Thermal Environment Simulator. These samples were analysed for each gas species (methane, hydrogen, carbon monoxide, carbon dioxide, ethylene and acetylene) with tabulation of the average compositions, variances and standard deviations in Tables E-4 and E-5. Comparison of the overall standard deviation for sampling plus analytical technique with the value for analytical technique only, indicated the reproducible nature of the sampling system. These values are 0.97% for the analytical standard deviation and 1.03% for the sampling plus analytical standard deviation. All of the data in Table E-4 were compiled for a simulated pyrolysis gas composition described by Feed Mix 4 (or 5) in Table 4-3.

Accuracy of the Liquid Analysis for Phenol in Aqueous Solutions

The standard deviation of the liquid analysis over a range of phenol compositions from 2 to 70% (by weight) was ± 0.71%. This compares well with the results reported in ASTM Bulletin D 2145 which was ± 0.5% for concentrations near 85% (by weight). The variance and standard deviation calculations for this analysis are presented in Table E-6.

Table E-4. Measured Compositions of Replicate Exit Gas Samples From the Char Zone Thermal Environment Simulator.

Sample Identification		Composition, x_i (Mole %)					
		H_2	CH_4	CO	CO_2	C_2H_4	C_2H_2
Experiment XXVI Samples 10, 2 and 7		61.6	16.7	16.0	4.9	0.7	0.8
		60.0	17.1	16.1	5.4	0.8	0.6
		61.4	15.6	16.7	5.0	0.7	0.7
	Σx	183.0	49.4	48.8	15.3	2.2	2.1
	$\bar{x}$	61.0	16.47	16.27	5.1	0.73	0.7
	N-1	2	2	2	2	2	2
Experiment XXVI Samples 4 & 13		70.8	15.3	10.5	3.0	0.23	0.22
		69.6	15.3	11.6	2.8	0.34	0.34
	Σx	140.4	30.6	22.1	5.8	0.57	0.56
	$\bar{x}$	70.2	15.3	11.05	2.9	0.285	0.28
	N-1	1	1	1	1	1	1
Experiment XXV Samples 5 & 7		65.2	15.4	10.2	8.4	0.7	0.12
		65.7	15.2	9.6	8.7	0.7	0.16
	Σx	130.9	30.6	19.8	17.1	1.4	0.28
	$\bar{x}$	65.45	15.3	9.9	8.55	0.7	0.14
	N-1	1	1	1	1	1	1
Experiment XXIII Samples 10,4 and11		58.7	20.4	13.6	7.3		
		57.7	20.2	14.6	7.6		
		56.9	21.5	14.1	7.6		
	Σx	173.3	62.1	42.3	22.5		
	$\bar{x}$	57.77	20.7	14.1	7.5		
	N-1	2	2	2	2		
Experiment XXIV Samples 15, 1 and 4		54.9	15.6		4.7	0.63	1.07
		56.2	15.1		4.7	0.81	0.92
		56.7	15.3		5.6	0.74	0.93
	Σx	167.8	46.0		15.0	2.18	2.92
	$\bar{x}$	55.93	15.33		5.0	0.727	0.973
	N-1	2	2		2	2	2
Experiment XX Samples 1 & 4		63.3	16.7	11.0	6.2	0.7	0.34
		63.1	15.7	10.8	7.1	0.8	0.40
	Σx	126.4	32.4	21.8	13.3	1.5	0.74
	$\bar{x}$	63.2	16.2	10.9	6.65	0.75	0.37
	N-1	1	1	1	1	1	1

Table E-4. Measured Compositions of Replicate Exit Gas Samples From the Char Zone Thermal Environment Simulator (Continued).

Sample Identification	Composition, x_i (Mole %)					
	H_2	CH_4	CO	CO_2	C_2H_4	C_2H_2
Experiment XXIII	54.6	13.5				
	54.1	12.5				
	53.7	11.9				
Samples 5, 9 and 10	Σx 162.4	37.9				
	$\bar{x}$ 54.13	12.63				
	N-1 2	2				

Table E-5. Calculation of the Net Variance, Standard Deviation for Each Group of Samples and the Overall Standard Deviation.

	H_2	CH_4	CO	CO_2	C_2H_4	C_2H_2	Over-all
$\sum_{i=1}^{N}(N_i-1)(s_x^2)_i$	6.092	4.146	1.592	1.210	0.048	0.043	-
$\sum_{i=1}^{N}(N_i-1)$ = d.f.	11	11	7	9	7	7	50
$(s_x^2)_{net}$	0.55	0.37	0.23	0.13	0.007	0.006	0.26
$(s_x)_{net}$	0.74	0.61	0.48	0.36	0.084	0.077	0.51
$t_{95\%,\ d.f.}$	2.201	2.201	2.365	2.262	2.365	2.365	2.00
$(t_{95\%,d.f.})(s_x)$	1.64	1.34	1.14	0.82	0.20	0.18	1.03
Composition Range	54-71	12-20	9.6-17	2.8-9	0.23-0.81	0.16-1.1	-

Table E-6. Variances and Standard Deviation for the Analysis of Phenol in Water.

Sample Number	1	2	3	4
Run 1	16.2	12.2	8.3	63.82
2	16.4	13.0	8.4	63.75
3	16.1	12.7		62.98
4	15.9			63.59
5				63.62
Σx	64.6	37.9	16.7	317.76
$\bar{x}$	16.1	12.6	8.35	63.55

Tabulated Standard Deviation of the Overall Analysis

$\sum_{i=1}^{N} (N_i-1)(s_x^2)_i \quad (i = 1, 2, 3, 4)$	0.920
$\sum_{i=1}^{N} (N_i-1) = \text{d.f.}$	10

$(s_x^2)_{net} = 0.092$	$(s_x) = 0.304$	$t_{95\%,\ 10} = 2.350$	$(t_{95\%,10})(s_x) = 0.71$

Accuracy of the Liquid Scintillation Counting Analyses

The accuracy of the radioactive analyses were determined in the same way as the gas chromatographic analyses. Replicate samples of the effluent stream from the gas chromatograph were collected as carbon dioxide after first passing through a combustion furnace. In general the radioactive level of the gas samples were very low because of the large dilution factor associated with the Char Zone Thermal Environment Simulator. Typical values for samples collected at one minute intervals are presented in Table E-7. The varying radioactive concentrations correspond to the location where a decomposition product separated in the gas chromatograph. By comparing the chromatogram with a plot of the radioactive concentrations (vs. time), the identification of the important products of decomposition of a particular radioactive labeled pyrolysis gas can be made.

The standard deviation of the reported values are listed in Table E-8. Very good agreement was obtained with the value of the deviation estimated by equation (4-4). These values were ± 1.03 cpm calculated by the usual procedure and ± 0.90 cpm estimated for an average count of 2070 and an average radioactive level of 40.9 cpm over the samples listed in Table E-7.

The standard deviation and percent error of the liquid and solid samples were estimated by equation (4-4) for counting levels exceeding 10000.

Table E-7. Measured Radioactivity of Gas Species in the Effluent Stream of the Gas Chromatographic System.

Experiment XXVIII Sample No.	Counts per Minute (cpm)									
	A2	A3	A4	A5	A6	A7	A8	A9	A10	A15
	22.70	19.57	21.08	97.53	94.32	31.09	21.21	28.30	62.50	21.80
	22.81	19.57	21.04	97.58	94.33	31.15	21.60	29.15	59.05	21.90
	20.80	21.50	22.20	95.65	90.50	30.70	21.24	28.30	62.50	21.45
	20.95	21.50	22.15	95.80	90.55	30.65	21.65	29.05	59.10	21.45
	23.60	20.50	20.25	96.00	92.10	31.50	20.90	27.90	61.50	22.35
	23.60	20.75	20.30	96.05	92.30	31.40	20.90	27.90	61.50	22.45
$\bar{x}$	22.41	20.57	21.17	96.10	92.35	31.08	21.25	28.43	61.04	21.90
Background	17.65	18.09	17.30	19.41	17.94	17.82	17.59	17.10	18.10	17.55
Net Count	4.76	2.48	3.87	76.69	74.41	13.26	3.66	11.33	42.94	4.35

Note: The background count is an average of ten values counted for 100 minutes. The small values for the Net Count are caused by the large dilution factor introduced in the gas sampling and analytical system. Radioactivity levels of the liquid and solid samples discussed in Chapter V are several orders of magnitude greater.

Table E-8. Determination of the Standard Deviation of Radioactive Gas Samples of the Effluent Stream from the Gas Chromatograph.

Experiment XXVIII Sample No.	A2	A3	A4	A5	A6	A7	A8	A9	A10	A15
	0.0841	1.0000	0.0081	2.0449	3.8809	0.0001	0.0016	0.0169	2.1316	0.0100
	0.1600	1.0000	0.0169	2.1904	3.9204	0.0049	0.0001	0.0169	2.1316	0.0000
	0.1521	0.8649	1.0609	0.2025	3.4225	0.1444	0.1225	0.5184	4.0401	0.2025
	0.2916	0.8649	0.9604	0.0900	3.2400	0.1849	0.1600	0.3844	4.2436	0.2025
$\boxed{N_i = 5}$	1.4161	0.0049	0.8464	1.2100	0.0625	0.1764	0.1225	0.2809	0.3136	0.2025
	1.4161	0.0324	0.7569	0.9025	0.0025	0.1024	0.1225	0.2809	0.2116	0.3025
$\Sigma(\bar{x} - x_i)^2$	3.5200	3.7671	3.6496	6.6403	14.5288	0.6131	0.5292	1.4984	13.0721	0.9200
(s_x^2)	0.7040	0.7534	0.7299	1.3281	2.9058	0.1226	0.1058	0.2997	2.6144	0.1840

$(s_x^2)_{net} = 0.9748$	$(s_x)_{net} = 0.9875$	$t_{95\%,50} = 2.00$	$t_{68\%,50} = 1.05$
$(t_{xx\%,50})(s_x)$	95% ± 1.97 cpm	68% ± 1.03 cpm	68%* ± 0.90 cpm

* Calculated as $\left[(N)^{1/2}/N\right] \times 100$ for N (Number of Counts) = 2070.

F. ISOTHERMAL FLOW ANALYSIS (1)

There is a sizeable number of possible reactions that can occur in the char layer as was discussed in Chapter III. To attempt to include all of these reactions in the solution of the energy equation to predict the energy absorbed within the char for non-equilibrium flow would be very difficult. Consequently it was necessary to devise a screening procedure to eliminate from consideration the reactions that were not important in the temperature range of current interest (500°F to 3000°F). The following reasoning was applied.

The rate of reaction increases with temperature. For a particular reaction, if a significant conversion of reactants to products was obtained with the char at a uniform and high temperature, then it was assumed that there could be a significant conversion when the char was subjected to a temperature gradient between 500°F and 3000°F. Thus these reactions should be considered in any analysis of the char zone.

Conversely if there was essentially no conversion at a high temperature (3000°F) for the char at this uniform temperature, there would be no conversion for a temperature gradient with 3000°F the maximum temperature. Thus these reactions were eliminated from consideration. Correspondingly if there is complete conversion within the char at a low temperature, there would be complete conversion for the case of a temperature gradient. Thus this kind of reaction would also be eliminated from the analysis, although the products of such a reaction may indeed be present as important species in the pyrolysis products entering the char at 500°F.

To determine the important chemical reactions in the temperature range from 500°F to 3000°F, the conversion of an equal molal mixture of the reactants flowing in the char was determined using the kinetic data reported in reference (2) for each reaction. The mass flux rates used for the reactants were 0.01 and 0.05 lb/ft^2-sec and the char was 0.25 inches thick with a porosity of 0.8. These results are presented in Tables F-1 through F-4 for the temperature range considered at 500°F intervals and a mass flux of 0.01 lb/ft^2-sec. The lower mass flux rate gave a longer residence time of the species in the char layer, and consequently a higher conversion. However, in comparing the conversions there was only a relatively small decrease in conversion due to the five-fold increase in the mass flux rate.

In Figure F-1 the conversion for two reactions are presented as a function of temperature. These are the thermal decomposition of ethylene and acetylene. It can be concluded by examining this figure that there would be no conversion of ethylene within the char for temperatures less than 1000°F and no conversion of acetylene for temperatures less than 2000°F. However the thermal cracking of ethylene would be important for temperatures above 1000°F and for acetylene above 2000°F.

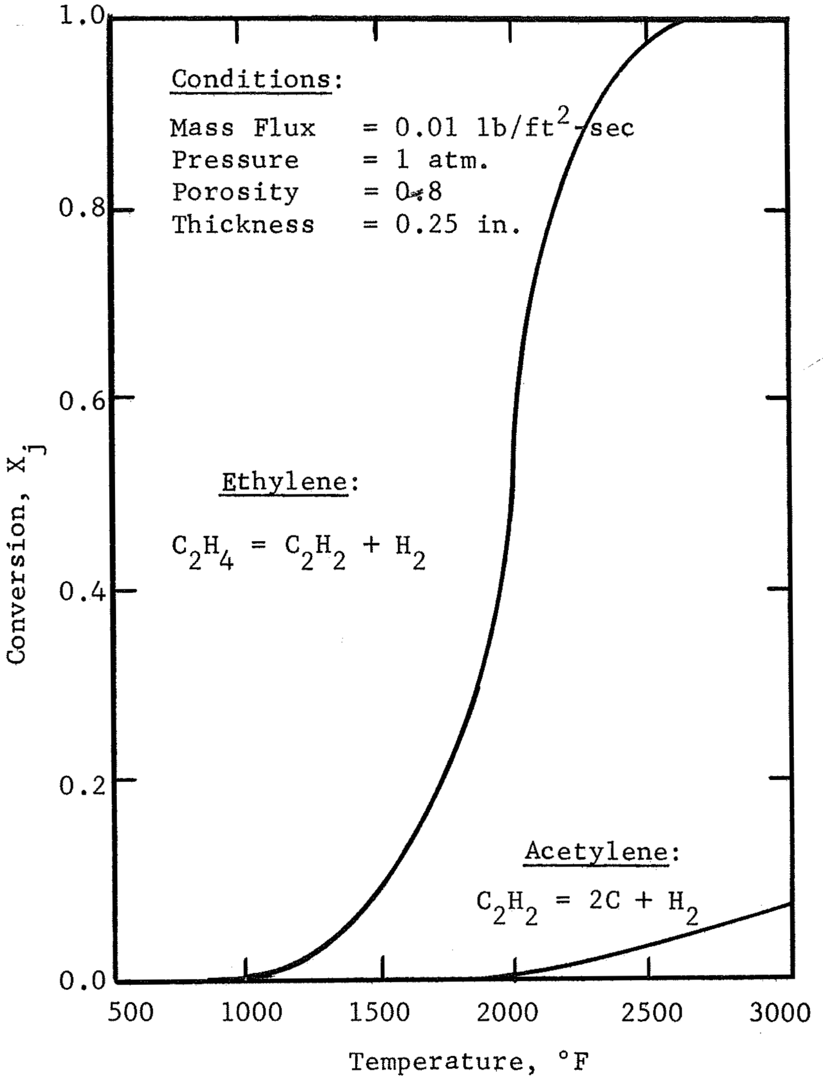

Figure F-1. Conversion of Pure Ethylene and Pure Acetylene at Isothermal Conditions (500°F-3000°F).

To make the discussion quantitative, the conversion of a reactant is defined as the ratio of the amount consumed by reaction to the amount initially present. To determine the conversion of a chemical reaction of the form:

$$aA + bB + cC = nN + oO + pP \qquad \text{(F-1)}$$

a material balance is made on component j flowing through a volumetric section of the char having a cross sectional area, A, and a width, Δz, as shown in Figure F-2. If N_j is the molal flux of component j at z, the material balance on component j for steady flow in the z direction is:

$$(N_j M_{w_j} A)_z + R_j M_{w_j} A \Delta z - (N_j M_{w_j} A)_{z+\Delta z} = 0 \qquad \text{(F-2)}$$

where R_j is the rate of formation of component j by chemical reaction. Rearranging the above equation and taking the limit as z approaches zero gives:

$$\frac{dN_j}{dz} = R_j \qquad \text{(F-3)}$$

The fractional conversion X_j of component j is defined as:

$$X_j = (N_{j_o} - N_j) / N_{j_o} \qquad \text{(F-4)}$$

where N_{j_o} is the molal flux of component j entering the char zone.

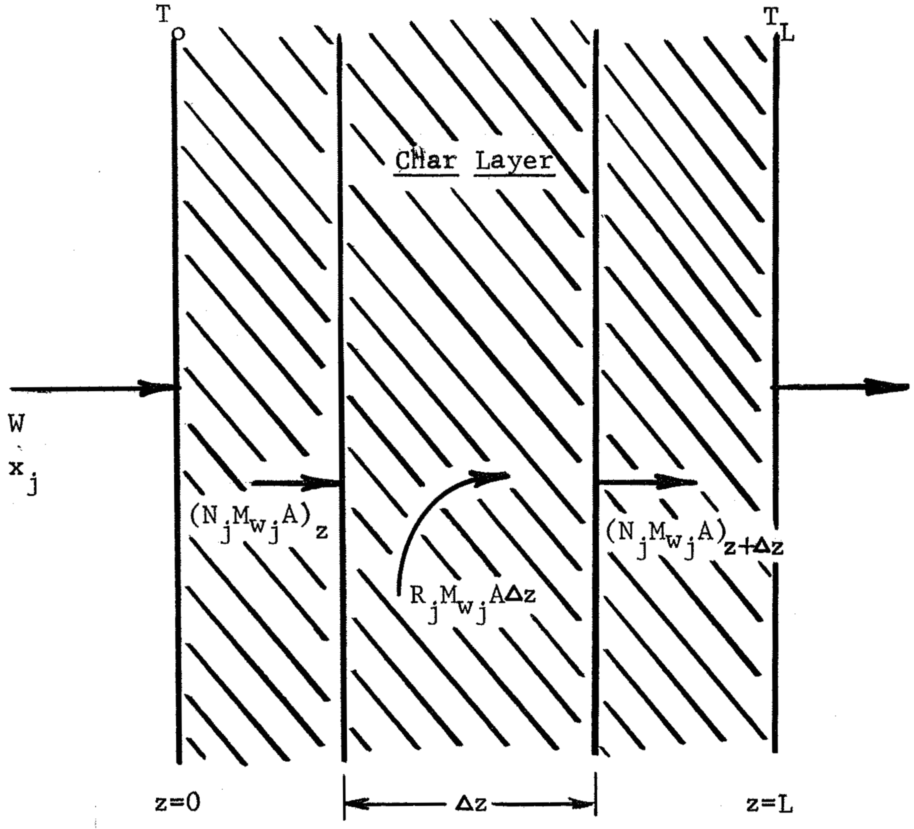

Figure F-2. Schematic Diagram of the Char Layer.

Differentiating the above equation with respect to z gives:

$$N_{jo}\left(\frac{dX_j}{dz}\right) = -\frac{dN_j}{dz} \qquad \text{(F-5)}$$

The continunity equation in terms of the volumetric flow rate, Q, of a gas entering the char is:

$$Q = (N_{jo}/x_{jo})\,\bar{M}_{w_o}A/\rho \qquad \text{(F-6)}$$

Equation (F-3) using equations (F-5) and (F-6) becomes:

$$\left(\frac{\rho x_{jo}}{\bar{M}_{w_o}}\right)\left(\frac{dX_j}{-R_j}\right) = \frac{A}{Q}\,dz \qquad \text{(F-7)}$$

This equation can be integrated from the back surface of the char where X_j and z are zero to the front surface where $X_j = X_{jL}$ (z=L) and the result is:

$$\frac{\rho x_{jo}}{\bar{M}_{wo}} \int_{o}^{X_{jL}} \frac{dX_j}{-R_j} = \frac{AL}{Q} = \frac{V}{Q} = S_t \qquad \text{(F-8)}$$

where S_t is the average residence time or space time; i.e., the average time a molecule stays within the char.

The reaction rate, R_j, for component A of reaction (F-1) is:

$$R_A = \left(-k_f\left[c_A^a\ c_B^b\ c_C^c\right] + k_r\left[c_N^n\ c_O^o\ c_P^p\right]\right) a \qquad \text{(F-9)}$$

Equation (F-9) is needed in order to perform the indicated integration in equation (F-8). A trial an error solution of the above integral equation is necessary to determine the final conversion, X_{jL}, since the average residence time, S_t, is known for a given char depth and decomposition product mass flux.

A computer program was written to calculate the solution of equation (F-8). The final conversion was varied in the solution technique until the calculated value of S_t corresponded to the known average residence time. A tolerance limit of $\pm$ 0.1% of the known value was specified. A Simpson's Rule integration was used to evaluate the integral in equation (F-8). A listing of the Fortran IV program is presented in Listing F-1.

The results of the computations using this program are presented in Tables F-1 through F-4. This includes the conversion for each reaction as a function of temperature from 500°F to 3000°F in intervals of 500°F. As seen there are a number of reactions which have a significant conversion in this temperature range. Excluding any other logical reasons which would eliminate a particular reaction from consideration in the non-equilibrium flow analysis, these reactions must be considered if a realistic mathematical model is to be formulated.

Listing F-1. Computer Program for Calculating the Conversion of a Reaction at Isothermal Conditions.

```
C
C     CALCULATION OF THE CONVERSION FOR CHEMICAL REACTIONS
C     THAT POSSIBLY OCCUR IN THE DECOMPOSITION ZONE OF
C     CHARRING ABLATORS. THE RESULTS COMPUTED ARE FOR THE
C     ISOTHERMAL FLOW IN THE CHAR ZONE AT TEMPERATURES
C     FROM 500.0-OF TO 3000.0-OF
C
C     EVALUATION OF THE ENERGY TRANSFER IN THE CHAR ZONE DURING ABLATION
C
C
      DIMENSION Y(150), EQN(150)
C
C     READ THE EQUATION R1&R2&R3=P1&P2&P3
      CALL FPTRAP(-3)
 1111 READ729,(EQN(I),I=1,12)
 729  FORMAT(12A6)
C
C     READ THE STOCHIOMETRIC COEFFICIENTS OF THE RATE EQUATION
 1112 READ730,R1,R2,R3,P1,P2,P3
C
C     READ EXPONENTS ON THE COMPOSITIONS OF THE RATE EQUATION
      READ 730,R4,R5,R6,P4,P5,P6
 730  FORMAT(6F4.0)
C
C     READ THE MOL WGT OF THE COMPONENTS
      READ731,FWR1,FWR2,FWR3,FWP1,FWP2,FWP3
 731  FORMAT(6F5.0)
C
C     READ THE INITIAL COMPOSITION OF THE REACTANTS IN MOLE FRACTION
      READ5,XR1,XR2,XR3,XP1,XP2,XP3
 5    FORMAT(6F10.0)
C
C     READ THE COEFFICIENTS OF THE FORWARD REACTION RATE CONSTANT
C     UNITS OF AF ARE IN CUBIC-CM,GM-MOLES AND SEC
```

```
C     UNITS OF AEF ARE IN KCAL PER GM-MOLE
      READ733,AF,SF,AEF
 733  FORMAT(E8.0,2F6.0)
C
C     READ THE COEFFICIENTS OF THE REVERSE REACTION RATE CONSTANT
C     UNITS OF AR ARE IN CUBIC-CM,GM-MOLES AND SEC
C     UNITS OF AER ARE IN KCAL PER GM-MOLE
      READ733,AR,SR,AER
C
 828  PRINT829,(EQN(I),I=1,12)
 829  FORMAT(1H1,12A6)
      PRINT 830
 830  FORMAT( 1X,35HINITIAL COMPOSITION (MOLE FRACTION))
      PRINT 833,XR1,XR2,XR3,XP1,XP2,XP3
C
      PRINT 831
 831  FORMAT(1H0,105HFINAL COMPOSITION (MOLE FRACTION)
     1 TEMP  FRACTIONAL  SP.TIME(CC-SEC/MOL) REACTION RATE  )
      PRINT 8311
 8311 FORMAT(1H ,105H    R1       R2      R3      P1      P2      P3
     1 (OF)  CONVERSION  COMPUTED  SPECIFIED (MOL/CC-SEC)   )
C
C     MASS FLUX OF DECOMPOSITION PRODUCTS, W, IN LB/FT2-SEC
      W=0.01
C
C     INITIAL VALUE OF TEMPERATURE,T,IS 500-OF
      T=500.
C     INITIAL VALUE OF THE PRESSURE ,P, IS 1.0 ATMS
      P=1.0
C     GAS CONSTANT,R,IN CALORIES/GMMOLE-OK
      R=1.987
C
C     CALCULATION OF THE AVERAGE MOL WGT OF THE GAS,FWA
C     ENTERING THE CHAR ZONE
      FWAR=FWR1*XR1&FWR2*XR2&FWR3*XR3
```

```
      FWAP=FWP1*XP1&FWP2*XP2&FWP3*XP3
      FWA=FWAR&FWAP
C
C     CALCULATION OF THE MOLAL FLOW RATE OF THE GAS,FTO
C     FTO HAS UNITS OF GMMOLES PER FT-FT SEC
      FTO=(454.0*W)/FWA
C
C     CALCULATION OF MOLAL FLUX OF THE INDIVIDUAL COMPONENTS
C     MOLAL FLUX UNITS ARF GMMOLES PER FT-FT SEC
      FR10=XR1*FTO
      FR20=XR2*FTO
      FR30=XR3*FTO
      FP10=XP1*FTO
      FP20=XP2*FTO
      FP30=XP3*FTO
C
C     CALCULATION OF THE SPACE TIME,ST,IN CUBIC-CM SEC/GMMOLES
      ST=(0.25*144.0)/(FTO*0.06103)
C
C     CONVERSION OF 100 PERCFNT IS ASSUMED INITIALLY
C     XCAF IS THE CONVERSION OF COMPONFNT A, INITIALLY 1.0
      XCAF=1.0
C     NO CONVERSION OF PRODUCTS INITIALLY
      XCA=0.0
C     INITIAL INCREMENTAL CHANGE,SA,OF THE CONVERSION XCAF
      SA=0.1
C
C     CALCULATION OF SPACE TIME FOR AN ASSUMED CONVERSION,XCAF.
C     REPFAT CALCULATIONS UNTIL CALCULATFD SPACE TIME IS EQUAL
C     TO THE KNOWN VALUE. THIS DETERMINES THE CORRECT VALUE
C     OF THE FINAL CONVERSION
C
C     FIRST
C     DETERMINE CONCENTRATION OF COMPONENTS FOR VARIOUS
C     INTERMEDIATE CONVERSIONS,XCA.CONCENTRATION ARE
```

```
C      IN GM-MOLES/CUBIC-CM
C      INCREMENTAL CHANGE IN XCA IS HI
 2222  HI=XCAF/100.0
       XCA=0.0
C
       DO1 I=1,101
C
C      F/S ARE MOLAL FLUXES CORRESPONDING TO CONVERSION XCA
C      MOLAL FLUXES HAVE UNITS OF GMMOLES/FT-FT SEC
C
       FR1=(1.0-XCA)*FR10
       FR2=FR20-(FR10*XCA*R2)/R1
       FR3=FR30-(FR10*XCA*R3)/R1
       FP1=FP10&(FR10*XCA*P1)/R1
       FP2=FP20&(FR10*XCA*P2)/R1
       FP3=FP30&(FR10*XCA*P3)/R1
C
C      THE TOTAL MOLAL FLUX CORRESPONDING TO CONVERSION XCA IS FT
C      FT HAS UNITS OF GM-MOLES/FT-FT-SEC
       FT=FT0&(FR10*XCA)*(P1&P2&P3-R1-R2-R3)/R1
C
C      CALCULATION OF THE COMPOSITION OF THE REACTING MIXTURE
C      C/S ARE CONCENTRATIONS IN GMMOLES/CUBIC-CM
       RR=82.054
       TOK=(T&460.0)/1.8
       H=P/(RR*TOK*FT)
       CR1=ABS(FR1*H)
       CR2=ABS(FR2*H)
       CR3=ABS(FR3*H)
       CP1=ABS(FP1*H)
       CP2=ABS(FP2*H)
       CP3=ABS(FP3*H)
C
C      CALCULATION OF RATE CONSTANTS FOR FORWARD AND REVERSE REACTIONS
C      RATE CONSTANT UNITS ARE IN CUBIC CM,GMMOLES AND SEC
```

```
C
C     FORWARD REACTION RATE CONSTANT, FK
      FK=AF*TOK**(-SF)*EXP((-AEF*1000.0)/(R*TOK))
C     REVERSE REACTION RATE CONSTANT, RK
C
      RK=AR*TOK**(-SR)*EXP((-AER*1000.0)/(R*TOK))
C
C     CALCULATION OF REACTION RATE,RA,OF COMPONENT A
C     RA HAS UNITS OF GMMOLES/CUBIC-CM SEC
      RA=FK*(CR1**R4)*(CR2**R5)*(CR3**R6)-RK*(CP1**P4)*(CP2**P5)*
     1(CP3**P6)
C
C     CALCULATION OF FUNCTION UNDER INTEGRAL-1/RA=Y(I)
      Y(I)=1.0/RA
C
C
 1    XCA=XCA&HI
C     STEP XCA TO GENERATE 101 VALUES OF Y(I)
C     CALCULATION OF FINAL COMPOSITION (MOLE FRACTION)
      YR1=FR1/FT
      YR2=FR2/FT
      YR3=FR3/FT
      YP1=FP1/FT
      YP2=FP2/FT
      YP3=FP3/FT
C
C     CALCULATION OF SPACE TIME FOR THE SPECIFIED CONVERSION,XCAF
C     INTEGRATION IS PERFORMED USING SIMPSONS RULE
      SUM1=0.0
      SUM2=0.0
      DO2 I=2,100
 2    SUM1=2.0*Y(I)&SUM1
      DO3 I=2,100,2
 3    SUM2=2.0*Y(I)&SUM2
C     INTEGRAL VALUE IS VINT-UNITS ARE CUBIC-CM SEC/GMMOLES OF A
```

```
      VINT=(HI/3.0)*(Y(1)&SUM1&SUM2&Y(101))
C     SPACE TIME CALCULATED IS VFTO-UNITS ARE CUBIC-CM SEC/GMMOLES
      VFTO=XR1*VINT
C
C
C     COMPUTATION STOPS IF SA IS LESS THAN 1.0E-10
      IF(SA.GT.1.0E-10)GO TO 777
      GO TO 123
 777  CONTINUE
C     DETERMINE IF THE DIFFERENCE BETWEEN THE SPECIFIED AND
C     CALCULATED SPACE TIME IS WITHIN 0.1. IF YES INCREASE THE
C     TEMPERATURE BY 500-OF
      CALL SSWTCH(1,JOB)
      GO TO (1111,778),JOB
 778  IF(ABS(ST-VFTO).LT.0.1) GO TO 123
C
C     DETERMINE IF VFTO IS GREATER THAN ST
      IF(VFTO.GT.ST)GOTO1234
C
C     VFTO IS LESS THAN ST
C
C     IS VFTO NEGATIVE
C     YES-REDUCE XCAF
C     NO-CONTINUE
      IF(VFTO.LT.0.0) GO TO 1321
C
C     THE CALCULATION STOPS IF THE CONVERSION IS GREATER THAN 99.99  PER
      IF(XCAF.GT.0.9999)GO TO 321
C
C     THE PREVIOUS VALUE OF VFTO IS RECALCULATED BY INCREASING
C     XCAF BY THE AMOUNT OF SA
C     THEN CHANGE SA TO 0.5*SA
      XCAF=XCAF&SA
      SA=0.5*SA
      GOTO 2222
```

```
C
C     CHECK TO INSURE XCAF IS LESS THAN 1.0
  321 IF(XCAF.GT.0.9999999)GO TO 112
      GOTO123
  112 SA=0.5*SA
      XCAF = XCAF - SA
      GO TO 2222
C
C     VFTO IS GREATER THAN ST
C
C     THE CALCULATION STOPS IF THE CONVERSION IS LESS THAN 0.05 PERCENT
 1234 IF(XCAF.LE.0.01)GOTO123
C
C
C     A CHECK TO PREVENT XCAF - SA = 0
 1321 IF(XCAF.GT.SA) GO TO 4321
      SA = 0.5*SA
C
C     THE VALUE OF XCAF IS REDUCED BY THE VALUE OF SA
 4321 XCAF=XCAF-SA
C
C     THEN THE CALCULATION IS REPEATED TO DETERMINE A
C     NEW SPACE TIME FOR COMPARISON
C
      GO TO  2222
C
C     VFTO IS ESSENTIALLY EQUAL TO ST (WITHIN 0.1)
C                          OR
C     CONVERSION, XCAF, IS LESS THAN 0.5 PERCENT
C                          OR
C     CONVERSION, XCAF, IS GREATER THAN 99.99  PERCENT
C     PRINT THE RESULTS
  123 PRINT 833,YR1,YR2,YR3,YP1,YP2,YP3,T,XCAF,VFTO,ST,RA
  833 FORMAT(1H0,6F8.4,F9.1,F8.4,3F12.5)
C
```

```
C     READ NEW DATA IF THE CONVERSION IS 100 PERCENT
C     CONVERSION WILL BE 100 PERCENT FOR ALL HIGHER TEMPERATURES
      IF(XCAF.GT.0.99) GO TO 2208
C
C     THEN REPEAT THE CALCULATIONS AT THE NEW TEMPERATURE
C
C     INCREASE THE TEMPERATURE BY 500-OF
      T=T&500.
C
C     RESET XCAF AND SA
      SA = 0.1
      XCAF=1.0
C
C     IF THE TEMPERATURE IS LESS THAN OR EQUAL TO 7000-OF
C     CONTINUE THE CALCULATION
      IF(T.LE.7000.0)GOTO 2222
C
C
C     PRINT DATA
 2208 PRINT 2209,W
 2209 FORMAT(1H0,25H MASS FLUX(LB/FT2-SEC) = , F8.4)
      PRINT2210,AF,SF,AEF
 2210 FORMAT(1H0,3HAF=,E9.2,5H  SF=,F6.2,6H  AEF=,F6.1)
      PRINT2211,AR,SR,AER
 2211 FORMAT(1H0,3HAR=,E9.2,5H  SR=,F6.2,6H  AER=,F6.1)
      PRINT2212
 2212 FORMAT(1H0,29HFWR1 FWR2 FWR3 FWP1 FWP2 FWP3)
      PRINT2213,FWR1,FWR2,FWR3,FWP1,FWP2,FWP3
 2213 FORMAT(1X,6F6.1)
      PRINT 2218
 2218 FORMAT(1H0,28H  STOCHIOMETRIC COEFFICIENTS)
      PRINT2214
 2214 FORMAT(1H0,24H  R1  R2  R3  P1  P2  P3)
      PRINT2215,R1,R2,R3,P1,P2,P3
 2215 FORMAT(1X,6F4.1)
```

```
      PRINT 2219
 2219 FORMAT(1H0,45H  EXPONENTS ON THE COMP. OF THE RATE EQUATION)
      PRINT 2216
 2216 FORMAT(1H0,24H  R4   R5   R6   P4   P5   P6)
      PRINT 2217,R4,R5,R6,P4,P5,P6
 2217 FORMAT(1X,6F4.1)
C     READ IN NEW DATA FOR CALCULATIONS OF NEXT EQUATION
      GOTO1111
   24 STOP
      END
```

```
                    ISOTHERMAL FLOW ANALYSIS - INPUT-OUTPUT DATA


C  +  CO2  =  2CO
INITIAL COMPOSITION (MOLE FRACTION)
 0.5000  0.5000  0.0000  0.0000  0.0000  0.0000

FINAL COMPOSITION (MOLE FRACTION)                    TEMP  FRACTIONAL  SP.TIME(CC-SEC/MOL)  REACTION RATE
   R1      R2      R3      P1      P2      P3        (OF)  CONVERSION  COMPUTED  SPECIFIED  (MOL/CC-SEC)

 0.4969  0.4969  0.0000  0.0062  0.0000  0.0000   500.0   0.0062     0.14E 23   0.36E 04    0.22E-24

 0.4969  0.4969  0.0000  0.0062  0.0000  0.0000  1000.0   0.0062     0.17E 11   0.36E 04    0.19E-12

 0.4969  0.4969  0.0000  0.0062  0.0000  0.0000  1500.0   0.0062     0.24E 05   0.36E 04    0.13E-06

 0.0000  0.0000  0.0000  1.0000  0.0000  0.0000  2000.0   1.0000     0.13E 04   0.36E 04    0.38E-03

MASS FLUX(LB/FT2-SEC)  =  0.0100                STOCHIOMETRIC COEFFICIENTS

AF= 0.15E 11   SF= 0.00   AEF= 85.0             R1   R2   R3   P1   P2   P3

AR= 0.10E-29   SR= 0.00   AER=  0.0            1.0  1.0  0.0  2.0  0.0  0.0

FWR1  FWR2  FWR3  FWP1  FWP2  FWP3              EXPONENTS ON THE COMP. OF THE RATE EQUATION

12.0  44.0   0.0  28.0   0.0   0.0              R4   R5   R6   P4   P5   P6

                                               0.0  0.0  0.0  0.0  0.0  0.0
```

Table F-1. Conversion of Pyrolysis Reactions in Mole Percent for a Mass Flux of 0.01 lb/ft^2-sec

Char Thickness = 0.25 inches, Porosity = 0.8

Reaction	Conversion, Mole Percent 500°F	1000°F	1500°F	2000°F	2500°F	3000°F	Ref
$CH_4 = 1/2\ C_2H_6 + H_2$	0	0	0	0	20.3	100	(2)
$CH_4 = C + 2\ H_2$	0	0	0	2.6	6.6	12.4	(3)
$CH_4 = 1/2\ C_2H_2 + 3/2\ H_2$	0	0	0	0	4.2	7.4	(2)
$C_2H_6 = (H_2, CH_4, C_2H_4, C)$	0	0	15.8	100	100	100	(2)
$C_2H_4 = (C_2H_2, C_2H_6, CH_4, H_2)$	0	0	8.9	87.9	100	100	(2)
$C_2H_2 = (CH_2, TrC_4H_2 - 900°K)$	0	0	0	0	1.8	6.7	(2)
$C_3H_8 = (C_3H_6, C_3H_4, CH_4, H_2)$	0	0	31.1	100	100	100	(2)
$C_3H_6 = (H_2, CH_4, C_2H_4,$ etc.)	0	0	2.7	100	100	100	(2)
$C_3H_6 + H_2 = CH_4 + C_2H_4$	0	0	0	1 0	15.2	60.9	(2)
Cyclobutane = 2 C_2H_4	0	1.2	100	100	100	100	(2)
Methylcyclobutane = $C_2H_4 + C_3H_8$	0	1.1	100	100	100	100	(2)
t-butanol = isobutene + H_2O	0	0	29.0	100	100	100	(2)
Cyclopentene = Cyclopentadiene + H_2	0	0	70.1	100	100	100	(2)
$n\text{-}C_4H_{10} = CH_4 + C_3H_6$	0	1.6	100	100	100	100	(2)
Isobutene = Products	0	0	1.4	97.3	100	100	(2)
$C_6H_6 = 3\ C_2H_2$	0	0	0	35.7	99.3	100	(2)
$C_6H_6 = 1/2\ C_{12}H_{10} + 1/2\ H_2$	0	0	54.2	97.0	99.5	99.8	(2)

Table F-1. Conversion of Pyrolysis Reactions (Continued).

Reaction	Conversion, Mole Percent 500°F	1000°F	1500°F	2000°F	2500°F	3000°F	Ref
$CH_3CHO = CH_4 + CO$	0	0	0	0	7.4	90.5	(2)
$CH_2O = H_2 + CH_3$	0	0	0	8.1	59.3	98.6	(2)
$CH_4 + H = H_2 + CH_3$	100	100	100	100	100	100	(2)
$CH_2N_2 = CH_2 + N_2$	0	100	100	100	100	100	(2)
$C_2H_6 + H = C_2H_5 + H_2$	100	100	100	100	100	100	(2)
$C_2H_4 + H_2 = C_2H_6$	0	0	0	1.2	11.6	44 7	(2)

Table F-2. Conversion of Hydrogen, Oxygen and Hydrogen-Oxygen Reactions in Mole Percent for a Mass Flux of 0.01 lb/ft^2-sec.
Char Thickness = 0.25 inches, Porosity = 0.8

Reaction	Conversion, Mole Percent						Ref.
	500°F	1000°F	1500°F	2000°F	2500°F	3000°F	
$H_2 + M = 2H + M$	0	0	0	0	0	0	(2)
$O_2 + M = 2O + M$	0	0	0	0	0	0	(2)
$2\ O_2 = O_3 + O$	0	0	0	0	0	3.5	(2)
$O_3 + M = O + O_2 + M$	0	0	0	0	100	100	(2)
$O + M = O^+ + e^- + M$	0	0	0	0	0	0	(2)
$H + O_2 = OH + O$	0	0	0	0	0	0	(2)
$O + H_2 = OH + H$	0	0	0	0	0	0	(2)
$O + H_2O = 2\ OH$	100	100	100	100	100	100	(2)
$H_2O + M = OH + H + M$	0	0	0	0	0	0	(2)
$H_2O + H = H_2 + OH$	100	100	100	100	100	100	(2)
$H_2 + O_2 = 2\ OH$	0	0	0	0	0	4.7	(2)
$OH + M = O + H + M$	0	0	0	0	0	0	(2)
$H_2 + O = H_2O$	100	100	100	100	100	100	(2)
$H + O_2 + M = HO_2 + M$	100	100	100	100	100	100	(2)

Table F-3. Conversion of Nitrogen and Ammonia Reactions in Mole Percent for a Mass Flux of 0.01 lb/ft^2-sec.
Char Thickness = 0.25 inches, Porosity = 0.8

Reaction	Conversion, Mole Percent						Ref
	500°F	1000°F	1500°F	2000°F	2500°F	3000°F	
$N_2 + M = 2N + M$	0	0	0	0	0	0	(2)
$2\ NO = NO_2 + N$	0	0	0	0	0	1.3	(2)
$2\ NO = N_2 + O_2$	0	0	0	0	0	1.1	(2)
$NO + M = N + O + M$	0	0	0	0	0	0	(2)
$NO_2 + M = NO + O + M$	0	0	0	0	100	100	(2)
$N_2O + M = N_2 + O + M$	0	0	0	0	0	3.5	(2)
$N_2O = N_2 + 1/2\ O_2$	0	0	0	47.0	100	100	(2)
$N_2O + O = N_2 + O_2$	3.4	62.0	90.0	95.7	97.4	98.1	(2)
$N_2O + O = 2\ NO$	0	71.5	99.1	100	100	100	(2)
$NO + O = O_2 + N$	0	0	0	0	0	0	(2)
$NO + N = N_2 + O$	100	100	100	100	100	100	(2)
$NO + O_2 = NO_2 + O$	0	0	0	0.7	7.4	30.3	(2)
$NO + N_2 = N_2O + N$	0	0	0	0	0	0	(2)
$NO + N_2O = NO_2 + N_2$	0	0	0.6	27.8	85.6	95.0	(2)
$NO_2 + O_2 = N_2 + O_2 + O$	0	0	0	0	0	0	(2)
$NO_2 + O_2 = NO + O_3$	0	0	0.9	54.1	100	100	(2)
$NO_3 + M = NO_2 + O + M$	0	0	0	0	0	0	(2)

Table F-3. Conversion of Nitrogen and Ammonia Reactions (Continued).

Reactions	Conversion, Mole Percent 500°F	1000°F	1500°F	2000°F	2500°F	3000°F	Ref
$H + N_2O = N_2 + OH$	98.4	100	100	100	100	100	(2)
$NH_3(g) + C(s) = HCN(s) + H_2$	0	0	0	0	0	0	(2)
$NH_3 = 1/2\ N_2 + 3/2\ H_2$	0	0	0	0	0	0.6	(2)
$NH_3 + 5/2\ O = 3/2\ H_2O + NO$	100	100	100	100	100	100	(2)
$N + M = N^+ + e^- + M$	0	0	0	0	0	0	(2)
$N + NO = N_2 + O^+ + e^-$	0	0	0	0	0	0	(2)
$N_2^+ + e^- = 2N$	100	100	100	100	100	100	(2)
$N_2^+ + N = N_2 + N^+$	0	0	0	0	0	0	(2)
$O_2^+ + e^- = 2O$	100	100	100	100	100	100	(2)

Table F-4. Conversion of Carbon, Hydrocarbon and Oxygen Reactions in Mole Percent for a Mass Flux of 0.01 lb/ft^2-sec.

Char Thickness = 0.25 inches, Porosity = 0.8

Reactions	Conversion, Mole Percent 500°F	1000°F	1500°F	2000°F	2500°F	3000°F	Ref.
$C(s) + CO_2(g) = 2\ CO$	0	0	0	55.6	100	100	(2)
$CO_2 + M = CO + O + M$	0	0	0	0	4.9	100	(2)
$CH_4 + O_2 = (CO,\ CO_2,\ H_2O,$ etc)		0	20.2	59.3	78.0	100	(2)
$CH_4 + O_2 = (CO,\ CO_2,\ H_2O,$ etc)		57.6	86.5	93.2	95.5	97.8	(2)
$CH_4 + O + M = CO,\ CO_2\ H_2O,$ etc)		0	0	0	0	0	(2)
$C_3O_2 = C(s) + 2\ CO$	0	7.0	100	100	100	100	(2)
$CO + OH = H + CO_2$	100	100	100	100	100	100	(2)
$CH_4 + OH = CH_3 + H_2O$	100	100	100	100	100	100	(2)

REFERENCES

1. Pike, Ralph W., G. C. April and E. G. del Valle, "Non-Equilibrium Flow and the Kinetics of Chemical Reactions in the Char Zone," NASA-CR-66455 (July 15, 1967).

2. Pike, Ralph W., "Evaluation of the Literature for Chemical Reactions and Reaction Rates for the Decomposition Products from Charring Ablators," Langley Working Paper 181, NASA, Langley Research Center, Hampton, Virginia (January 21, 1966).

3. Happel, J. and L. Kramer, "Acetylene and Hydrogen from the Pyrolysis of Methane," Industrial and Engineering Chemistry, 59 (1), 39 (January 1967).

G. METHODS FOR ESTIMATING PYROLYSIS PRODUCT COMPOSITIONS (1)

Three methods were used to determine accurately the typical pyrolysis product composition entering the char zone. These were:

(1) Analysis of the gases evolved during the thermal degradation of nylon-phenolic resins reported in the literature (1, 2, 3, 4, 5).

(2) Calculation of the heat of pyrolysis using heats of formation data for the reactants and reported pyrolysis products followed by a comparison with experimentally determined heats of pyrolysis.

(3) Qualitative inspection of the molecular structure of the plastic materials to determine possible decomposition products based on the relative strength or weakness of bond energies.

Each technique will be discussed in the following sections.

Products of Nylon-Phenolic Resin Thermal Degradation by Pyrolysis Gas Chromatography

The most direct method of determining the products of degradation is analysis by pyrolysis gas chromatography. This has been done by Sykes (2, 7) in which the hot degradation products were injected directly into the gas chromatograph. However there is a certain amount of condensation of heavy molecular weight species which remain unidentified and a possible source of error. The method has, however, reduced the total amount of unidentified liquid phase species from fifty percent obtained with the more conventional methods, to seventeen percent (by weight). Also the kind and concentration of the species are more precisely determined. These analyses form the basis for quantitatively selecting a pyrolysis product composition. The remaining methods are used to make adjustments to the analytically determined composition, especially with regard to the species which could logically make up the unidentified portion of the pyrolysis product stream.

A Comparison of the Experimental and Calculated Heat of Pyrolysis Based on the Heats of Formation of the Analytically Determined Gases

The pyrolysis products are obtained by the thermal degradation of virgin plastic materials such as nylon, phenolic resin and composites of these polymers.

$$\begin{matrix}\text{Virgin}\\ \text{Plastics}\end{matrix}\begin{bmatrix}\text{Nylon, Phenolic Resin}\\ \text{and Composites}\end{bmatrix}\xrightarrow[\Delta]{}\begin{matrix}\text{Gaseous}\\ \text{Products}\end{matrix}+\text{Char} \tag{G-1}$$

The heat of reaction is the heat of pyrolysis, ΔH_{pyr}, and is calculated knowing the heats of formation of the products (char plus gases) and reactants (nylon and phenolic resin), along with sensible enthalpy corrections from the reference temperature of 25°C.

$$\Delta H_{pyr} = \sum_{i=1}^{K+1} \left[x_{pi}\ \Delta H_{f_{pi}} + \int_{T=25°C}^{T_p} x_{pi}\ C_{ppi}\ dT \right] - \sum_{j=1}^{M} \left[x_{rj}\ \Delta H_{f_{ri}} + \int_{T=25°C}^{T_r} x_{rj}\ C_{prj}\ dT \right] \qquad \text{(G-2)}$$

For nylon-phenolic resin composites, the temperature, T_r, where degradation starts is approximately 250°C and the final temperature attained by the products leaving, T_p, is 1000°C. Mean molal heat capacities evaluated at a weighted average temperature of 700°C based on mass loss rates from differential thermal analyses, and heats of formation at 25°C are tabulated in Table G-1. Values of the heats of pyrolysis of nylon, phenolic resin and their composites were reported by Sykes (2) and Nelson (3). Heats of formation of the reactants are calculated from experimental heats of combustion data presented in Table G-2 and G-3, respectively. Details of the experimental procedure and apparatus are contained in the original reference (1).

The combustion of nylon or phenolic resin forming carbon dioxide and water is represented by the following expression:

$$\begin{matrix}\text{Nylon or}\\ \text{Phenolic Resin}\end{matrix} + O_2 \longrightarrow CO_2 + H_2O \qquad \text{(G-3)}$$

The heat of formation of nylon (or phenolic resin) is then simply:

$$\Delta H_{f\ Nylon} = \Delta H_C - \sum_{i=1}^{K+1} x_{pi}\ \Delta H_{f_{pi}} \qquad \text{(G-4)}$$

Table G-1. Heats of Formation and Heat Capacities of Various Pyrolysis Products. (8)

Species	ΔH_f, BTU/lb	$^{**}C_{P_{mean}}$ BTU/lb-°F	M_w
Phenol	-415.3	0.3*	94.1
MethylPhenol	-511.6	0.3	108.1
DimethylPhenol	-570.0	0.3*	122.2
TrimethylPhenol	-600.0	0.3*	136.1
Benzene	456.3	0.3*	78.1
Toluene	226.6	0.3*	93.1
Hydrogen	0.0	3.5	2.0
Methane	-2013.8	0.7	16.0
Carbon Monoxide	-1697.1	0.25	28.0
Carbon Dioxide	-3850.2	0.35	44.0
Water	-5780.0	0.5	18.0
Ammonia	-1160.5	0.67	17.0
Butylamine	-384.1		73.1
Acetone	-2214.7	0.44	42.1
Methylamine	-387.8		31.1
Formaldehyde	-1697.9	0.41	30.0
Ethylene	804.3	0.63	28.0
Ethane	-1212.0	0.6	30.0
Acetylene	3752.3	0.6	26.0
Butane	-923.2	0.7	58.1
Butene	9.7	0.74	56.1
Cyclohexane	-629.1	0.44	84.2
Cyclopentane	-475.0	0.47	70.1
EthylBenzene	120.3		106.2
Hydrogen Cyanide	2080.0	0.4	27.0
Methyl Cyclohexane	-676.8	0.46	98.2
Methyl Cyclopentane	-545.1	0.5	84.2
Pentane	-871.2	0.6	72.2
Propane	-1012.2	0.6*	44.1
Xylene	76.3	0.3*	106.2
Amorphous Carbon	390.0	0.3	12.0

Note: * Estimated heat capacity by analogy with homolog(s).
** Mean heat capacity calculated over a temperature range from 250°-1000°C .

Table G-2. Heat of Formation of Nylon-66 from the Experimental Heat of Combustion Data.

<u>Reaction</u>: $(C_{12}H_{22}N_2O_2)_n + O_2 = 12n\ CO_2 + 11n\ H_2O + 2n\ NO_2$

<u>Basis</u>: 1 gram of nylon (Molecular weight of monomer = 226)

$\frac{\text{1 gram nylon}}{\text{226 gr/gr mole}}$ = 0.00442 gm moles

gm moles CO_2 = 0.00442 x 12 = 0.053

gm moles H_2O = 0.00442 x 11 = 0.049

gm moles NO_2 = 0.00442 x 2 = 0.009

ΔH_{fCO_2} = -94,052 cal/gm mole (0.053) = -5004 cal/gm

ΔH_{fH_2O} = -57,800 cal/gm mole (0.049) = -2815 cal/gm

ΔH_{fNO_2} = + 8090 cal/gm mole (0.009) = 72 cal/gm

$\Sigma \Delta H_{fprod}$ = -7747 cal/gm

ΔH_C = -7214 cal/gm (Experimental)- Reference (1)

$\Delta H_{fR} = \Sigma \Delta H_{fprod} - \Delta H_C$

= -7747 - (-7214)

= -533 cal/gm (-959 BTU/lb)

Table G-3. Heat of Formation of Phenolic Resin from the Experimental Heat of Combustion Data.

Reaction:

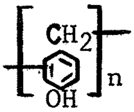

$+ O_2 = 7n\ CO_2 + 3n\ H_2O$

Basis: 1 gram phenolic resin (Molecular weight of monomer = 106)

$$\frac{\text{1 gram phenolic resin}}{\text{106 gram/gram moles}} = 0.00943 \text{ gm moles}$$

gm moles CO_2 = $0.00943 \times 7 = 0.0660$

gm moles H_2O = $0.00943 \times 3 = 0.0283$

ΔH_{fCO_2} = -94,052 cal/gm mole (0.0660) = -6207 cal/gm

ΔH_{fH_2O} = -57,800 cal/gm mole (0.0283) = -1636 cal/gm

$\Sigma \Delta H_{fprod}$ = -7843 cal/gm

ΔH_C = -7386 cal/gm (Experimental) - Reference (1)

$\Delta H_{f_R} = \Sigma \Delta H_{fprod} - \Delta H_C$

$= -7843 - (-7386)$

$= -457$ cal/gm (-823 BTU/lb)

Therefore, for a known composition of the various species in a nylon-phenolic resin composite, the heat of formation of the composite is:

$$\Delta H_{f\ \mathrm{Composite}} = \sum_{j=1}^{M} \Delta H_{f_j} \quad ; \quad j = \text{nylon, phenolic resin, etc.} \qquad \text{(G-5)}$$

Now all of the pertinent data are available to evaluate the heat of pyrolysis. In doing so, a selected composition determined by some analytical or numerical method is postulated to be valid. If the calculated value of the heat of pyrolysis is approximately equal (to ± 10% of the desired value, for example), the composition is judged a representative composition. If, on the other hand, a mismatch is obtained for the heat of pyrolysis value, the composition proposed as a valid set of values is either in error or incomplete.

Correction of the mismatch is made using any similar logic to that listed below:

(1) Inspect the literature data over a wide range of conditions by several authors, when available.

(2) Select those pyrolysis products which always appear in the analyses.

(3) If various fractional analyses are presented, weight each composition according to the size of each fraction. For example if gases are collected for fractions corresponding to a ten percent

weight loss of initial virgin plastic, twenty percent weight loss and fifty percent weight loss, each fractional composition should be weighted according to the size of sample (percent weight loss) to calculate an average composition.

(4) Superimpose these results and construct an overall species listing.

(5) Average values of species that appear within a reasonable range of values.

(6) Use the species that appear in only one analysis to make minor adjustments to the composition being corrected.

(7) Continue the evaluation until an energy-balance-calculated heat of pyrolysis matches the literature value. Now based on the best possible literature composition, decide whether the corrections made to obtain a match are logical and reasonable. If so, the procedure is ended; if not, repeat the procedure with other more reasonable species.

When no previous analytical data are readily available, an analysis using the kinetic theory approach is suggested to arrive at pyrolysis products which are reasonable. A great deal of chemical engineering judgement is necessary to decide whether a set of proposed pyrolysis gases are representative or just an arbitrary combination of some fictitious system.

Either procedure requires a detailed literature survey of available analytical results and some background regarding the particular system under study. Used in connection with analytical data, it becomes a powerful method for establishing the correct composition of the pyrolysis products.

Pyrolysis Product Composition by Relative Strength or Weakness of Bond Energies

The thermal degradation of char forming ablative materials is a complex process. As a result, little quantitative data indicating the decomposition mechanism have been reported. The high resistivity of the char layer to aerodynamic stresses and high temperatures has been known for many years. This ability is attributed, in part, to the highly crosslinked nature of the aromatic polymers such as phenolic resin. The already strong C-C bonds are reinforced by resonance effects resulting from the crosslinked structure. Therefore, during thermal degradation, these C-C bonds remain intact, and, the weaker bonds (C-H, C-O, C-N, etc.) break producing the pyrolysis gas products. It is the purpose of this section to indicate the origin of likely pyrolysis products based on the bond energies of the polymers. A qualitative discussion for nylon and phenolic resin and composites of these is presented in the following paragraphs.

Decomposition of Phenolic Resin: Parker (6) indicated a possible mechanism for the thermal degradation of phenolic novalac resins. Emphasis was placed on the final char structure, however, a great deal of information regarding the origin of some pyrolysis products was also reported. Representing the phenolic novalac polymer as shown below,

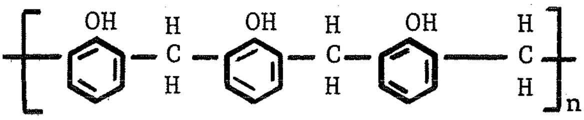
(G-6)

Parker pointed out the place where cleavage was most likely to be initiated was at the methylene bridge (-CH_2-) linkage. This resulted in the formation of a variety of free radicals including those of phenol, the cresols and many shorter polymeric units of the novalac resin which undergo still further degradation. A schematic diagram of the proposed mechanism is reproduced in Figure G-1. In addition to the above mentioned products, water, hydrogen, carbon monoxide and methane are also shown to be formed.

Decomposition of Nylon-66 (Hexamethylenediamine-Adipic Acid): The nylon-66 polymer is formed by the polymerization of one monomer of adipic acid with one monomer of hexamethylenediamine in alternating steps.

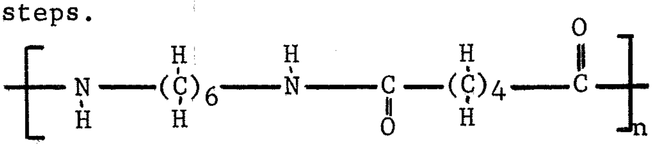

$$\left[-\underset{H}{N}-(\overset{H}{\underset{H}{C}})_6-\overset{H}{N}-\underset{\overset{\|}{O}}{C}-(\overset{H}{\underset{H}{C}})_4-\overset{\overset{O}{\|}}{C}-\right]_n$$

(G-7)

Inspection of the bond energies between atoms of the CHON system listed in Table G-4, neglecting considerations of resonance and electronegativity effects that exist in the polymer, indicates that the most logical place for cleavage to occur is at the C-N bond. This essentially separates the polymer into shorter chain polymers and monomer units. From this point cleavage of bonds within the monomer structure can occur forming such species as

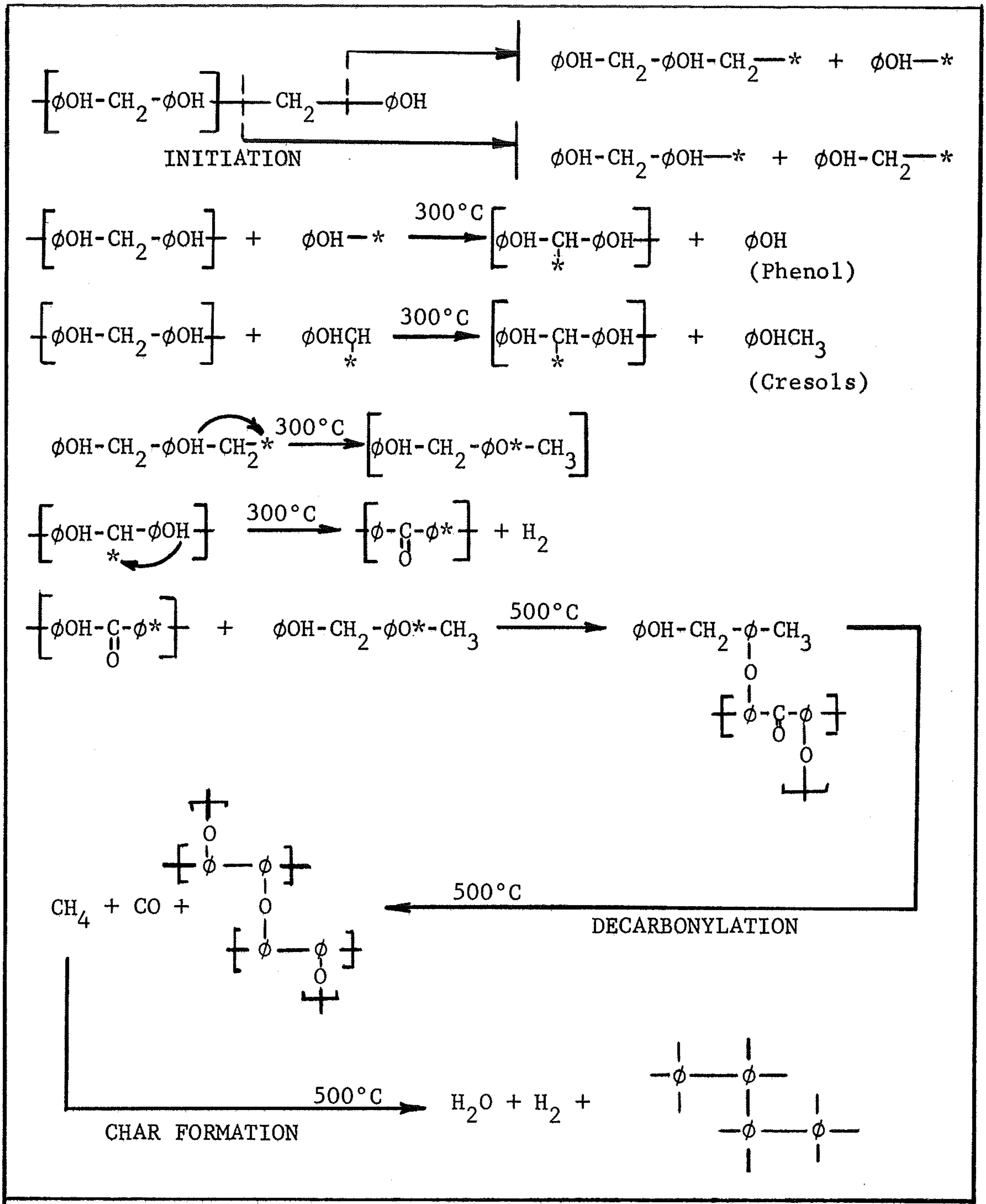

Figure G-1. Mechanism of Phenolic Novalac Degradation to Char.

Table G-4. Bond Energies Between Atoms in the CHON System (7).

Bond	Bond Energies, Kcal/gram
H - H	104
H - C	99
H - N	84
H - O	110
C - C	80
C - N	62
C - O	81
N - N	32
O - O	33
C = C	142
C ≡ C	186

NH_3, CO, CO_2, H_2O, H_2, CH_4, C_2H_6, etc. In fact, reported experimental data shows that only about seven percent (by weight) of nylon-66 is degraded to residue (2,3). The remaining ninety-three percent forms gaseous products. From this analysis, it is evident that the char structure of a charring nylon-phenolic resin composite is primarily composed of the phenolic degradation to carbon, while a major portion of the pyrolysis gases are formed from the nylon-66.

Decomposition of Nylon-Phenolic Resin Composites: Combining of these two polymers with subsequent thermal degradation would necessarily result in all of the above mentioned products with relative quantities based on the weight fraction of each polymer in the composite. A detailed listing of various pyrolysis products identified by gas chromatographic and/or mass spectrographic analyses is presented in Table G-5. Many of the species may only exist in small quantities, however, the large number forms a very good reference of typical products which may be formed when nylon-phenolic resins undergo thermal decomposition.

Comparison of the Methods with Various Analytically Determined Pyrolysis Product Compositions and Heats of Pyrolysis

To illustrate the use of the above discussed methods, two works reporting pyrolysis gas compositions and heats of pyrolysis values will be compared. These are the analyses by Sykes and Nelson (2,3) and by Freidman (5).

Table G-5. Various Species Identified as Pyrolysis Gas Products by Gas Chromatographic and/or Mass Spectrographic Analysis of Thermally Degraded Nylon-Phenolic Resin Composites.

Hydrogen
Nitrogen
Oxygen
Methane
Carbon Monoxide

Carbon Dioxide
Water
Ethylene
Ethane
Propadiene

Propylene
Propane
Butadiene
Butene
Butane

Isoprene
Cyclopentene
Cyclopentadiene
Cyclopentanone
Pentadiene

Pentene
Pentane
Benzene
Cyclohexane
Hexadiene

Hexene
Hexane
Toluene
Dimethyl Benzene
Dimethyl Phenol

Hexadiene
Methyl Phenol
Phenol
2-Propanol
Acetone

Benzaldehyde
Formaldehyde
Ammonia
Acetylene
Hydrogen Cyanide

Methanol
Propyne
Ethanol
Diacetylene
Vinylacetylene

Acrolein
Propanol
Isopropanol
2-Pentene-4-yne
Isopentanes

n-Butanol
Phenyl Acetylene
Styrene
Xylenes
4-Ethyl-1-Cyclohexane

Methyl Phenyl Acetylene
Methyl Styrene
C9 Aromatics
C10 Aromatics
Dimethyl Styrene

Identification of Pyrolysis Products from the Thermal Decomposition of Phenolic Resin and Nylon-Phenolic Resin Composites: Sykes (2,7) reported typical pyrolysis gas compositions for eighty-three percent of the total decomposition products evolved during the thermal degradation of nylon-phenolic resin composites. His techniques included differential thermal analysis, thermogravimetric analysis and pyrolysis gas chromatography of the hot gases evolved during rapid heating of the composite materials. The remaining seventeen percent was reported as an unidentified, dark tarry substance. The compositions from this research are presented in Tables G-6 and G-7. Also shown are the comparisons of the heat of pyrolysis calculations with the experimental values of Sykes (2). A very good agreement is obtained in Table G-6 indicating a high reliability in the reported analysis. The unidentified portion of the pyrolysis products was taken as phenol for calculating the heat of pyrolysis. In an earlier work, the results were somewhat poorer as indicated by the larger difference in the calculated and experimental heat of pyrolysis values. This was probable caused by either improper curing of the specimen resulting in the higher water content or an inaccurate analysis of the evolved pyrolysis products.

As a third example the pyrolysis products reported by Freidman (5) are compared in Table G-8. In this case the composition was determined from near room temperature samples analysed by gas chromatography. The absence of the higher molecular weight species such as phenol and the cresols is evident. This resulted in a much poorer comparison between the calculated and experimental heat of

Table G-6. Comparison of the Experimental Heat of Pyrolysis with Calculated Values Based on Heats of Formation of the Reported Pyrolysis Gas Components (7).

Component Name	Weight Fraction by: Flash	Weight Fraction by: 50°C Inc.	Average Weight Fraction, x_i	$x_i\ \Delta H_{f_{pi}}$ BTU/lb	$x_i\ C_{P_{mean}}\ \Delta T$ BTU/lb
Phenol	0.124	0.112	0.118	- 49	34
Methylphenol	0.067	0.061	0.064	- 33	18
Dimethylphenol	0.049	0.052	0.051	- 29	14
Trimethylphenol	0.040	0.042	0.041	- 25	12
Benzene	0.004	0.001	0.003	2	2
Toluene	0.000	0.002	0.001	1	1
Cyclopentanone	0.019	0.039	0.029	- 18	9
Hydrogen	0.010	0.010	0.010	0	34
Methane	0.010	0.010	0.010	- 20	10
Carb. Monoxide	0.025	0.016	0.021	- 18	6
Carb. Dioxide	0.087	0.047	0.067	- 36	5
Water	0.059	0.066	0.062	-258	23
Ammonia	0.002	0.001	0.002	- 2	2
Unidentified*	0.173	0.173	0.173	- 72	51
Carbon Residue	-	-	0.340	133	99
			1.000	-742	320

Reactants	Weight Fraction, x_j	$x_j \Delta H_{r_j}$ BTU/lb	$x_j\ C_{P_{mean}} \Delta T$ BTU/lb	
Nylon	0.4	-384	250	ΔH_{pyr}(Calculated) = 213 BTU/lb
Phenolic Resin	0.6	-501		ΔH_{pyr}(Experimental) = ~ 200 BTU/lb Ref. (2)
	1.0	-885	250	

* Unidentified materials considered phenol in calculation of ΔH_{pyr}.

Table G-7. Comparison of the Experimental Heat of Pyrolysis with Calculated Values Based on the Heats of Formation of Reported Pyrolysis Products (2).

Component Name	Pyrolysis Gas Analysis		Average Weight Fraction, x_i	$x_i\ \Delta H_{fi}$ BTU/1b	$x_i\ C_{Pmean}\ \Delta T$ BTU/1b
	Moles	Pounds			
Carb. Dioxide	1.6	70.4	0.019	- 74	6
Carb. Monoxide	5.5	154.1	0.042	- 71	10
Benzene	0.2	15.6	0.004	2	2
Toluene	0.3	32.4	0.009	1	5
Phenol	7.1	668.2	0.181	- 75	52
Methylphenol	1.8	219.9	0.060	- 34	17
Methane	10.0	160.0	0.043	- 87	29
Water	23.4	421.0	0.114	-661	55
Hydrogen	50.1	100.2	0.027	0	91
Unidentified*	-	-	0.150	- 62	43
Carbon Residue	-	-	0.350	137	101
			1.000	-924	411

Reactant	$x_j \Delta H_{fr_j}$ BTU/1b	$x_j\ C_{Pmean} \Delta T$ BTU/1b
Phenolic Resin (Only)	-823	200

ΔH_{pyr}(Calculated) = 110 BTU/1b

ΔH_{pyr}(Experimental) = ~ 146 BTU/1b
Ref (2)

* Unidentified Materials considered phenol in calculation of ΔH_{pyr}.

Table G-8. Comparison of the Experimental Heat of Pyrolysis with Calculated Values Based on Heats of Formation of the Reported Pyrolysis Gas Components (5).

Component Name	Pyrolysis Gas Analysis		Average Weight Fraction, x_i	$x_i \Delta H_{f_i}$ BTU/1b	$x_i C_{P_{mean}} \Delta T$ BTU/1b
	Moles	Pounds			
Hydrogen	23.9	47.8	0.011	0	37
Methane	4.1	65.6	0.015	- 31	11
Ammonia	4.1	69.7	0.016	- 19	10
Water	15.3	275.7	0.064	-371	31
Acetylene	10.9	283.4	0.066	248	38
Hydrogen Cyanide	3.5	94.5	0.022	46	13
Carbon Monoxide	10.9	305.2	0.071	-121	17
Nitrogen	0.1	2.8	0.001	0	2
Ethylene	14.0	392.0	0.091	73	53
Ethane	0.2	6.0	0.001	- 2	1
Carbon Dioxide	2.2	96.8	0.023	- 87	7
Diacetylene	0.9	45.0	0.011	45	6
Acetone	0.7	40.7	0.010	- 21	6
Benzene	0.9	70.2	0.016	8	10
Toluene	0.5	46.2	0.011	2	6
Xylene	0.3	31.8	0.007	1	5
Isopropanol	1.3	78.0	0.018	- 10	7
Propane	1.5	63.0	0.015	- 7	5
Carbon Residue	-	2270.9	0.529	206	127
			1.000	- 40	392

Reactants	$x_j \Delta H_{f_j}$ BTU/1b	$x_j C_{P_{mean}} \Delta T$ BTU/1b	x_j	ΔH_{pyr}(Calculated) = 987 BTU/1b
Nylon	-384	250	0.4	ΔH_{pyr}(Experimental) = 200-500 BTU/1b
Phenolic Resin	-501		0.6	Ref (5)
	-885	250	1.0	

pyrolysis as would be expected if important species were omitted from the composition. The inclusion of phenol and similar high molecular weight species which are liquids at room temperature where the particular samples were collected should be included. The quantity of each species added to correct the composition to a more representative value can only be determined by investigating the literature for the specific conditions of the experiment and subsequent analysis. If no such information is available, comparison with an analogous system (similar composite materials, for example) is a logical approach.

Conclusion

As a result of these methods applied to several reported pyrolysis gas compositions in the literature (1), it was concluded that the composition in Table G-9 best represented the products evolved when nylon-phenolic resin thermally degrades. It is this composition that is used as the simulated pyrolysis product stream in this research.

Table G-9. Most Representative Composition of the Pyrolysis Products Evolved During the Thermal Degradation of Nylon-Phenolic Resins.

Component	Pyrolysis Product Composition	
	Mole %	Weight%
Hydrogen	33.4	3.6
*Water	48.9	47.8
Methane	6.7	5.8
*Phenol	4.7	24.1
Carbon Monoxide	3.7	5.7
*Dimethylphenol	1.2	8.7
Carbon Dioxide	1.1	2.5
*Toluene	0.2	1.2
*Benzene	0.1	0.6
	100.0	100.0

* Liquids at room temperature.

REFERENCES

1. April, Gary C., E. G. del Valle, Simon Hacker and R. W. Pike, "Comparison of Methods for Determining the Composition of Pyrolysis Products from the Degradation of Nylon-Phenolic Resin Ablative Composites," NASA-RFL-9, Louisiana State University, Baton Rouge, Louisiana (March 1969).

2. Sykes, G. F., "Decomposition Characteristics of a Char Forming Phenolic Polymer Used for Ablative Composites," NASA TN-D-3810 (February 1967).

3. Nelson, J. B., "Determination of Kinetic Parameters of Six Ablative Polymers by Thermogravimetric Analysis," NASA TN-D-3919 (April 1967).

4. Ladacki, M., J. V. Hamilton and S. N. Conz, "Heat of Pyrolysis of Resin in Silica-Phenolic Ablator," AIAA Journal, 4 (10), 1798-1832 (1966).

5. Freidman, H. L., "Pyrolysis of Plastics in a High Vacuum Arc Image Furnace," Journal of Applied Polymer Science, 9, 1005 (1965).

6. Parker, J. A. and E. L. Winkler, "The Effects of Molecular Structure on the Thermochemical Properties of Phenolics and Related Polymers," NASA TR-R-276 (1967).

7. Sykes, G. F., Private Communication to R. W. Pike (March 14, 1968).

8. Perry, J. H., Ed., Chemical Engineers' Handbook , 3rd. Edition, McGraw-Hill Book Co., New York, 236-243 (1950).

H. MIMIC SOLUTIONS OF THE FROZEN FLOW, VARIABLE PROPERTIES ENERGY EQUATION

The purpose of obtaining MIMIC solutions to the frozen flow, variable properties energy equation was to provide a method of stepwise checking the fourth order Runge-Kutta analysis in the TEMPRE System. MIMIC is an analog-digital simulator program which permits the integration of functions with built-in numerical integration formulae. A fourth order Runge-Kutta technique is used by MIMIC, and is a direct method of comparing solutions or portions of solutions in each program. It essentially provided a rapid means of determining the capability of the TEMPRE System for calculating the correct solution to the differential energy equation.

MIMIC solutions were calculated for two forms of the frozen flow energy equation. In the first, the following form of the second order differential equation was solved.

$$W_p \bar{C}_p \epsilon \frac{dT}{dz} = \frac{d}{dz}\left(k_e \frac{dT}{dz}\right) \qquad \text{(H-1)}$$

A second solution to the energy equation after differentiating the conductive heat transfer term, followed by rearrangement, was also calculated.

$$\frac{d^2T}{dz^2} = \frac{dT}{dz}\left(\frac{W\epsilon\bar{C}_p}{k_e} - \frac{dT}{dz}\frac{\left(\frac{dk_e}{dT}\right)}{k_e}\right) \qquad \text{(H-2)}$$

This second equation was identical to the form used in the TEMPRE System. The solutions to these two equations were obtained to determine whether the calculation of the term, $\frac{dk_e}{dT}$, by interpolation from a table of k_e versus T data was being performed correctly. It also proved to be a very fast and easy technique for defining the incremental temperature necessary in the interpolation routine.

A comparison of the temperature distributions for the frozen flow of pyrolysis products in a one-quarter inch thick char between 500°F and 2000°F is presented in Table H-1. Very good agreement is obtained for a step size of one hundred units in the fourth order Runge-Kutta method (TEMPRE). The slight differences in the temperatures are attributed to round-off or truncation errors. Based on comparisons like these, the numerical integration method in the TEMPRE System was proven to give an accurate solution to the energy equation.

Copies of the MIMIC programs for solution of each form of the differential energy equation are provided in Listings H-1 and H-2 with typical input and output data.

Table H-1. Comparison of the Runge-Kutta Solution for Frozen Flow Variable Physical Properties with Two Solutions Obtained Using MIMIC (Analog-Digital Simulator)

Dimensionless Char Distance (z/L)	Temperature (°F) MIMIC (a) Solution	MIMIC (b) Solution	Runge-Kutta Solution
0.0	500.00	500.00	500.00
0.2	626.52	627.11	625.48
0.4	821.89	821.95	819.45
0.6	1105.76	1104.90	1102.78
0.8	1492.95	1494.89	1492.83
1.0	2000.00	2000.00	2000.00

Conditions: $W = 0.05$ lb/ft^2-sec $\epsilon = 0.8$ $L = 0.0208$ ft $(dT/dz)_o = 24172$ °F/ft

Gas Composition (mole/mole gas):

$CO = 0.245$, $CO_2 = 0.046$, $N_2 = 0.073$, $CH_4 = 0.570$, $C_6H_6 = 0.068$

(a) solution of equation (H-1)

(b) solution of equation (H-2)

Listing H-1. MIMIC Program for Solving the Differential Energy Equation (H-1).

```
               CON(DT,DTMIN,DTMAX)
               CON(AK,BK)
               CON(A1,B1,C1,D1)
               CON(A2,B2,C2,D2)
               CON(A3,B3,C3,D3)
               CON(A4,B4,C4,D4)
               CON(A5,B5,C5,D5)
               CON(MF1,MF2,MF3,MF4,MF5)
               PAR(B,A)
               PAR(TI,DTI)
TP             (TA&460.0)/1.8
T2             TP*TP
T3             TP*T2
CP1            A1&B1*TP&C1*T2&D1*T3
CP2            A2&B2*TP&C2*T2&D2*T3
CP3            A3&B3*TP&C3*T2&D3*T3
CP4            A4&B4*TP&C4*T2&D4*T3
CP5            A5&B5*TP&C5*T2&D5*T3
K              AK&BK*TP
KE             K*30.48/(252.0*1.8)
CPK            MF1*CP1&MF2*CP2&MF3*CP3&MF4*CP4&MF5*CP5
CP             CPK*454.0/(252.0*25.4*1.8)
DTP            INT(A*CP*DTP/KE-B*DTP*DTP/(K*1.8),DTI)
TA             INT(DTP,TI)
               HDR(CP,KE,TEMP,DTP,DIST)
               OUT(CP,KE,TA,DTP,T)
               FIN(T,.0208)
               END
```

Listing H-1. MIMIC Program. (a) Input Data

```
.25         1.           1.
.01         .0005        .0005
5.25    F-04 2.835   E-06 .04
6.726       4.001    E-04 1.283  E-06 -5.307 E-10
5.316       1.4285   E-02 -8.362 E-06 1.784  E-09
6.903       -3.75    E-04  1.93  E-06 -6.861 E-10
4.75        1.2      E-02 3.03   E-06 -2.63  E-09
-8.65       1.1578   E-01 -7.54  E-05 1.854  E-08
0.238       0.045        0.07         0.574        0.067
500.        10000.       40000.       25000.       2000.        2.
```

Listing H-2. MIMIC Program for Solving the Differential Energy Equation (H-2).

```
MIMIC PROGRAM FOR FROZEN FLOW IN ABLATOR                                TEMP 001
                  CON(LG,AXX,AXA)                                       TEMP 002
                  CON(DT,DTMIN,DTMAX)                                   TEMP 003
                  CON(AK,BK,A)                                          TEMP 004
CONSTANTS IN HEAT CAPACITY FQUATION - CP=A&B*T&C*T*T&D*T*T*T            TEMP 005
                  CON(A1,B1,C1,D1)                                      TEMP 006
                  CON(A2,B2,C2,D2)                                      TEMP 007
                  CON(A3,B3,C3,D3)                                      TEMP 008
                  CON(A4,B4,C4,D4)                                      TEMP 009
                  CON(A5,B5,C5,D5)                                      TEMP 010
MOLE FRACTIONS FOR FIVE COMPONFNTS                                      TEMP 011
                  CON(MF1,MF2,MF3,MF4,MF5)                              TEMP 012
PAPAMETERS                                                              TEMP 013
                  PAR(TI,DTSL,DTSH,DTI,TD,TOL)                          TEMP 014
SETS LOGICAL VARIABLES                                                  TEMP 015
         FW       FSW(T,TRUE,TRUE,FALSE)                                TEMP 016
         FA       FSW(T-LG-(AXX-1.)*LGA,FALSE,TRUE,TRUE)                TEMP 017
         FD       FSW(T-AXX*LGA,FALSE,TRUE,TRUE)                        TEMP 018
         FC       FSW(T-LG-(AXA-1.)*LGA,FALSE,TRUE,TRUE)                TEMP 019
         FF       FSW(T-LG-(AXX-1.)*LGA-DTMIN,FALSE,TRUE,TRUE)          TEMP 020
         FE       NOT(AND(FA,FF))                                       TEMP 021
         FY       AND(FA,FC,NOT(FW))                                    TEMP 022
COMPUTES INITIAL CONSTANTS                                              TEMP 023
 FW      BBB      454.0/(252.*25.4*1.8)                                 TEMP 024
 FW      CA       BBB*(A1*MF1&A2*MF2&A3*MF3&A4*MF4&A5*MF5)              TEMP 025
 FW      CB       BBB*(B1*MF1&B2*MF2&B3*MF3&B4*MF4&B5*MF5)              TEMP 026
 FW      CC       BBB*(C1*MF1&C2*MF2&C3*MF3&C4*MF4&C5*MF5)              TEMP 027
 FW      CD       BBB*(D1*MF1&D2*MF2&D3*MF3&D4*MF4&D5*MF5)              TEMP 028
 FW      TB       (TI&460.0)/1.8                                        TEMP 029
 FW      TZZ      DTI*(AK&BK*TB)*30.48/(252.0*1.8)                      TEMP 030
 FW      TH       TD&TOL                                                TEMP 031
 FW      TL       TD-TOL                                                TEMP 032
 FW      LGA      LG&.01                                                TEMP 033
SETS CONSTANTS FOR ITEPATION PURPOSFS                                   TEMP 034
```

```
 FC       AXA         AXA&1.                                                      TEMP 035
 FD       AXX         AXX&1.                                                      TEMP 036
TESTS FOR HIGH OR LOW RESULT                                                      TEMP 037
 FE       HIGH        FSW(TA-TH,TRUE,TRUE,FALSE)                                  TEMP 038
 FE       LOW         FSW(TA-TL,FALSE,TRUE,TRUE)                                  TEMP 039
TESTS FOR FINISH                                                                  TEMP 040
 FA       RH          LSW(HIGH,1.,0.)                                             TEMP 041
 FA       RG          LSW(LOW,1.,0.)                                              TEMP 042
 FA                   FIN(RH*RG,.5)                                               TEMP 043
RESETS HIGH AND LOW LIMITS, COMPUTES INITIAL SLOPE FOR NEXT ITERATION             TEMP 044
 FY       DTSH        LSW(HIGH,DTSH,DTI)                                          TEMP 045
 FY       DTSL        LSW(LOW,DTSL,DTI)                                           TEMP 046
 FY       DTI         (DTSH&DTSL)/2.                                              TEMP 047
 FY       TZ          DTI*(AK&BK*TB)*30.48/(252.0*1.8)                            TEMP 048
CALCULATES HEAT CAPACITY AND THERMAL CONDUCTIVITY                                  TEMP 049
          TP          (TA&460.0)/1.8                                              TEMP 050
          T2          TP*TP                                                       TEMP 051
          T3          TP*T2                                                       TEMP 052
          CP          CA&CB*TP&CC*T2&CD*T3                                        TEMP 053
          K           AK&BK*TP                                                    TEMP 054
          KE          K*30.48/(252.0*1.8)                                         TEMP 055
SOLUTION OF DIFFERENTIAL EQUATION                                                 TEMP 056
          DTK         INT(A*CP*DTP/12.,LSW(FW,TZZ,TZ),TRUE,FE)                    TEMP 057
          DTP         DTK/KE                                                      TEMP 058
          TA          INT(DTP/12.,TI,TRUE,FE)                                     TEMP 059
CALCULATES DISTANCE THROUGH CHAR ZONE                                             TEMP 060
          DIST        T-(AXX-1.)*LGA                                              TEMP 061
OUTPUT                                                                            TEMP 062
                      HDR(DIST,TEMP,SLOPE)                                        TEMP 063
                      OUT(DIST,TA,DTI)                                            TEMP 064
                      END                                                         TEMP 065
```

Listing H-2. MIMIC Program. (a) Input Data

```
5.0     E-05 5.0    E-05 5.0    E-05
5.25    E-04 2.835  E-06
6.726       4.001   E-04 1.283  E-06 -5.307 E-10
5.316       1.4285  E-02 -8.362 E-06 1.784  E-09
6.903       -3.75   E-04  1.93  E-06 -6.861 E-10
4.75        1.2     E-02 3.03   E-06 -2.63  E-09
-8.65       1.1578  E-01 -7.54  E-05 1.854  E-08
0.238       0.045       0.07        0.574     0.067
2.835   E-06 4.0    E-02
500.0       25000.0
2.835   E-06 4.0    E-02
500.0       24000.0
2.835   E-06 4.0    E-02
500.0       23000.0
```

VITA

Gary Charles April was born in [redacted] on [redacted] [redacted]. He completed his secondary education at DeLaSalle High School of that city in June of 1958. He then attended Louisiana State University at New Orleans during the initial two years of its opening and transferred to the main campus at Baton Rouge in 1960. In June of 1962 he was awarded the Bachelor of Science degree in Chemical Engineering. After graduation he was employed with the Nylon Intermediates Research and Development Group of the E. I. DuPont DeNemours Company at Orange, Texas. Three and one half years later, he enrolled in the graduate school of Louisiana State University while on an educational leave of absence. He received the Master of Science degree in Chemical Engineering in January of 1968 and is presently pursuing a Doctor of Philosophy degree in the same curriculum. His immediate plan upon graduation is to accept a position on the Chemical Engineering faculty at the University of Alabama, Tuscaloosa, Alabama.